WHEAT FIBER FROM A RESIDUE TO A REINFORCING MATERIAL

by

MOHAMMED T. ALBAHTTITI

B. S., American University of Sharjah, United Arab Emirates, 2010

A THESIS

Submitted in partial fulfillment of the requirements for the degree

MASTER OF SCIENCE

Department of Civil Engineering
College of Engineering

KANSAS STATE UNIVERSITY
Manhattan, Kansas

2012

Approved by:

Major Professor
Hayder A. Rasheed

Abstract

Throughout history natural fiber was used as one of the main building materials all over the world. Because the use of such materials has decreased in the last century, not much research has been conducted to investigate their performance as a reinforcing material in cement and concrete. In order to investigate one of the most common natural fibers, wheat fibers, as a reinforcing material, 156 mortar specimens and 99 concrete specimens were tested. The specimens were tested in either uniaxial compression or flexure. The uniaxial compression test included 2 in (50.8 mm) mortar cubes and 4x8 in (101.6 x 203.2 mm) concrete cylinders. As for the flexure test, they were either 40x40x160 mm cementitious matrix prisms or 6x6x21 in (152.4x152.4x533.4 mm) concrete prisms. Several wheat fibers percentages were studied and compared with polypropylene fiber as a benchmarking alternative. The average increase in the uniaxial compression strength for cementitious matrix cubes reinforced with 0.5% long wheat fiber exceeded that of their counterparts reinforced with polypropylene fiber by 15%. Whereas for concrete cylinders reinforced with 0.75% long wheat fiber, their strength exceeded that of their counterparts reinforced with polypropylene fiber by 5% and that of the control by 7%. The flexural strength of cementitious matrix prisms reinforced with 0.75% long wheat fiber exceeded that of their counterparts reinforced with polypropylene fiber by 27%. Meanwhile, concrete prisms reinforced with both long wheat fiber and polypropylene fiber showed deterioration in strength of up to 17%. Finally, ABAQUS models were developed for concrete cylinders and prisms to simulate the effect of inclusion of the wheat fibers.

"بسم الله الرحمن الرحيم"

In the name of the God, the most gracious and merciful

Table of Contents

List of Figures

List of Tables

Acknowledgements

First of all I am thankful to Allah, the Creator, the Most Gracious and Most Merciful. One of the greatest minds of the 19th century, Charles Darwin, once said “We must, however, acknowledge, as it seems to me, that man with all his noble qualities... still bears in his bodily frame the indelible stamp of his lowly origin.” In order to avoid showing this indelible stamp, I would like to thank my advisors Dr. Hayder Rasheed, for his relentless support and for his guidance through my masters, Dr. Dunja Perić, for her support and questions which opened my mind to different possibilities in approaching a problem, and Dr. Lawrence Davis, for his support and for being my teacher when it came to the biochemistry of the wheat fibers. I also would like to thank all the members of the Department of Civil Engineering, staff and professors, in Kansas State University for their help and support. The National Science Foundation for their financial support and all those who helped me with this research.

From the deepest corners of my myogenic muscular which pumps blood throughout my blood vessels, heart, to all of my family members, friends who’s with me or beyond the seas and my roommates, I say in the language of every one of you:

Shúkraan (شُكْرًا)

Thank you

Xièxiè (谢谢)

Hvala

Merci

Danke

Śukriyā (शुक्रिया)

Takk fyrir

Grazie

Spasibo (спасибо)

Muchas Gracias

Teşekkür Ederim

Hontōni arigatō (本当にありがとう)

Finally all I can do trying to repay you is to wish that you *live long and prosper*.

Dedication

This thesis is dedicated to ***my parents*** *who have always given me the encouragement to complete my graduate studies and continuously supporting me in any decision I make as well as for their love and sacrifice.*

CHAPTER 1 - Introduction

1.1 Background

The use of synthetic fibers in concrete was first introduced in 1978 by the FORTA Corporation of Grove City, Pennsylvania, USA (Macdonald 2009). Since then, the study of concrete reinforced with fibers has become a topic of interest for researchers all over the world. Synthetic fibers have been proven to reduce micro-cracks at early ages, increase the flexural load of materials and structures, increase the high temperature performance and toughness (AÏTCIN 1998), but due to their higher cost, the increase in the unit weight of the structural elements and their negative environmental impact, the use of natural fibers is an attractive alternative. Different types of fibers such as steel, glass, and carbon have been studied with the intent of improving the weaknesses of the concrete. Although natural fibers have been traditionally used for centuries in construction all over the world (Castro 1981), their engineering behavior has not been thoroughly assessed as a building material. Berhane (1994) found that some of the hydration products of Portland cement cause the fibers to become brittle, while another study indicated that the fibers showed deterioration in concrete mixes (Kosa 1991). Regardless of these weaknesses of the natural fibers this study aims to assess the increase in the strength and stiffness of cementitious matrices reinforced with wheat fibers. One possible resolution to the issue of degradation of the wheat fibers is to dip these fibers in resin prior to mixing if assessment of benefits is proven positive. Though there are many types of natural fibers that can be used as reinforcing materials, this study concerns one of the most abundant natural fibers, wheat fiber. This fiber is especially abundant in the state of Kansas, in the American Midwest, one of the largest wheat producing areas in the world.

1.2 Objectives

In this research there have been two major studies the initial study and the secondary study. In the initial study, small cementitious matrix samples were casted with wheat and polypropylene fibers. In order to verify the advantages of wheat fibers when compared to other synthetic fibers, 156 specimens were tested in direct compression and flexure. Several percentages and sizes of fibers were tested in the range of 0.5% to 5% by volume of the specimens in order to determine the best amount and length of fibers that will lead to highest strength and initial stiffness increase. As for the secondary study, the percentages of fibers that have been proven to yield the best result from the initial study will be used to cast concrete samples. Two types of specimens will be used in the secondary study, 72 specimens of the 4x8 in (101.6 x 203.2 mm) cylinders and 27 samples of the 6x6x21 in (152.4 x 152.4 x 533.4 mm) prisms. These samples will be tested direct compression and flexure according to the ASTM C39 and C78 standards in order to verify the advantages of wheat fibers in concrete.

1.3 Scope

CHAPTER 1 -Introduction: This chapter presents a brief background information about the use of Fibers especially natural fibers as a construction material, the objectives of the study and the scope of each chapter.

CHAPTER 2 -Literature Review: Contains a brief review on the previous studies related to the research conducted. Several relevant publications on the use of natural fibers in concrete and cement matrices are highlighted in this section of the thesis.

CHAPTER 3 -Fiber Reinforced Cementitious Matrix: This chapter presents the initial study of this research. This initial study of the use of wheat fibers with different sizes and percentages in cementitious matrices in compared with polypropylene fiber.

CHAPTER 4 -Fiber Reinforced Concrete: This chapter presents the secondary study of this research. This secondary study depends on the initial study to determine the optimal size and amount of fiber to reinforce concrete specimens in term of load capacity and stiffness.

CHAPTER 5 -Finite Element Modeling and Simulation: In this chapter the results from Chapter 4 is used to simulate the fibers in the concrete using a commercial software, ABAQUS.

CHAPTER 6 -Discussion, Conclusions and Recommendations: Discussion of the results of the previous chapters is presented along with some conclusions and recommendation for future work.

CHAPTER 2 - Literature Review

Since the start the human have been on hunt to build better homes. They started using rocks, woods and mud to build their houses, with the use of mud came the need to enforce a stronger bond with the use of fibers from natural resources. Since then the use fibers have been developing to use steel reinforcement and later on to the use of Fiber Reinforced Polymers (FRP). Recently, the world trend changed toward more green and environmental friendly materials. One of these materials is the wheat fibers derived from wheat straws, which is considered one of the most abundant materials in the American Midwest. Looking at the previous researches led the author to believe that not enough research was conducted to study the use of natural fibers in concrete and that is due to the fact that natural fibers tend to dissolve or lose structure due to the high alkalinity of the concrete. Recently there have been some researches on the use of natural material in cement and concrete structures.

According to Savastano *et al.* (2006) in their paper titled “Mechanical behavior of cement-based materials reinforced with sisal fibers” they describe how the high alkalinity of these cement based matrices cause hydrolysis of the cellulose of the fibers. They also described that at one month age the sisal fibers in blast furnace slag (BFS) based cement matrices showed an increase in the flexural strength of 120% over that of the control. They also studied the toughness of the specimens reinforced with sisal fibers and came to a conclusion that the initial and the final toughness range between 0.7 to 1 MPa in which they label acceptable.

In his research, Soroushian and Marikunte (1990) showed that the excessive use of softwood and hardwood kraft fibers lead to deterioration in the compressive strength in cement based matrices and that due to the entrapped air in the fibers. He also showed that flexural strength increased and the cracking delayed as the amount of fibers increased in the flexural specimens.

In his dissertation “Durability of Pulp Fiber-Cement Composites”, Benjamin J. Mohr (2005), he studies the durability of the pulp fibers in cement matrices subjected to wet/dry cycling. In chapter two of his dissertation he refer to the work on workability of pulp matrices done by Soroushian and Marikunte (1990) in which it was concluded that the hardwood kraft fibers with 1% fiber mass decreased in flow more than that of the softwood kraft fibers, while at 2% there was no difference. Also the work done by Naik *et al.* (2004) on concrete with low amounts of fibers showed a significant drop in the slump, from 235 mm to 170 mm when using 0.8% by mass fibers. As for the setting time which was studied by Soroushian and Marikunte (1990 through 1994), there was no deterioration in the initial setting time but the final setting time was delayed for the softwood and the hardwood reinforced specimens. In the terms of heat of hydration Bilba *et al.* (2003) and Hofstrand *et al.* (1984) showed that the use of wood fibers that contains high dosage of lignin cause a reduction in the heat of hydration thus delaying the setting time. Meanwhile, the effect of the various types fibers on the various types of shrinkage were studied by many researchers, like; Balaguru (1994) studied different kinds of fibers and their ability to counter the plastic shrinkage in concrete slaps. He showed that the polypropylene fibers were much more effective in preventing the cracking that results from the plastic shrinkage and that due to the small aspect ratio of the pulp fibers when compared to the polypropylene fibers. As for Soroushian (2000) in his research concluded that a small percentage of 0.2% by volume of pulp fibers is capable reducing the plastic shrinkage cracks' width from 0.14 mm to 0.02 mm and delays the appearance of the first drying shrinkage's crack by about three days.

As for the compressive strength Lin *et al.* (1994) showed that 4% by mass plup fibers reinforced cement pastes deteriorated about 50% in the strength when compared to the control. Soroushian and Marikunte (1990) reported that the 1% of hardwood kraft fibers by mass exhibited a reduction of about 13% when compared to the control, and at 2% of the same fibers it increased to 26% reduction and similar results for the softwood kraft fibers. On the other hand, El-Ashkar (2002) reported that the softwood kraft fibers did not affect the mortar compressive strength up to 1.2% of fibers by volume fraction and up to 1% for the concrete compressive strength. In a study by Soroushian and Ravanbakhsh (1999), it was reported that the cellulose fibers reinforced high early strength concrete exhibited results higher than both control and polypropylene reinforced specimens. They also concluded that the addition of calcium chloride improve d the cellulose fibers behavior in cement matrices. Some researchers like de Gutierrez *et al.* (2004) were able to compensate for the reduction in the compressive strength by using slag and silica fumes as cementitious materials.

For the flexural strength, Khorami *et al.* (2011) reported an increase in the maximum flexural strength of about 25% exhibited by specimens reinforced by 4% by mass wheat fibers and contains 5% silica fumes and an increase of about 7% for the same amount of fibers without the silica when compared to the control specimen. Li *et al.* (2004) reported a reduction of up to

15% in the flexural strength, from 7.31MPa to 6.15 MPa, for concrete reinforced with wheat fibers.

In Mohr (2005) dissertation he discussed that the use of supplementary cementitious materials (SCM) like; silica fumes, slag and others has proven to minimize the natural fibers degradation due to the fact that these lower the pH of the concrete mix. Also Ziraba *et al.* (1985) concluded the same by replacing 45% cement by using rice-husk ash thus lowering the pH by about 20%.

As for the finite element modeling of concrete structures, Concrete Damaged Plasticity (CDP) is one of the most recent and commonly applied hypotheses. Concrete Damaged Plasticity is a modification of the Drucker-Prager strength hypothesis according to models proposed Lubliner *et al.* (1989) and Lee *et al.* (1998). In the meridional plane the CDP model mimic the behavior of the hyperbolic curve of the Drucker-Prager as described by Kmiecik *et al.* (2011) (see Figure 2-1).

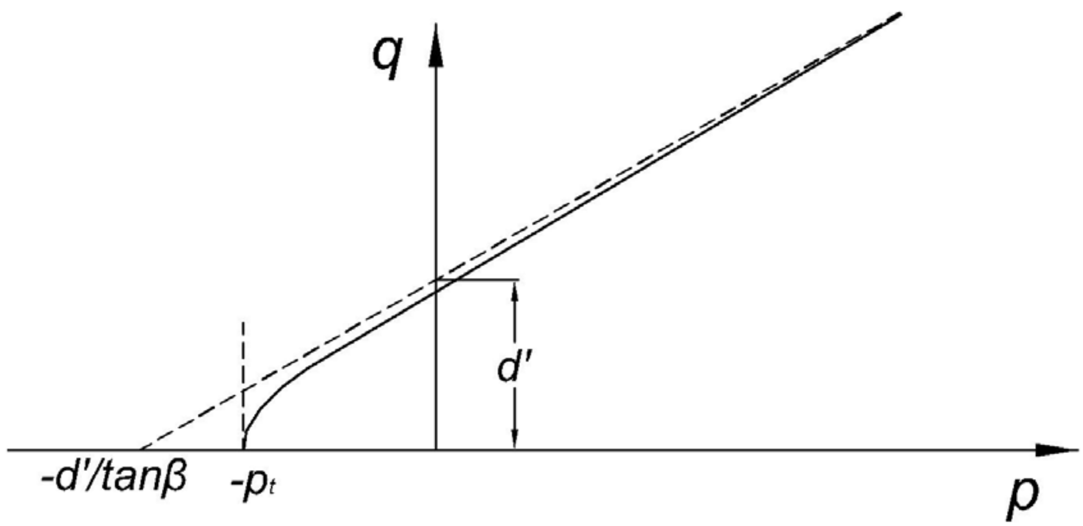

Figure 2-1: A Reproduction of the Hyperbolic Surface of Plastic Potential in Meridional Plane from ABAQUS User Manual.

For the concrete the yield surface in the deviatoric plane correspond to a default value of Kc=2/3 as shown below.

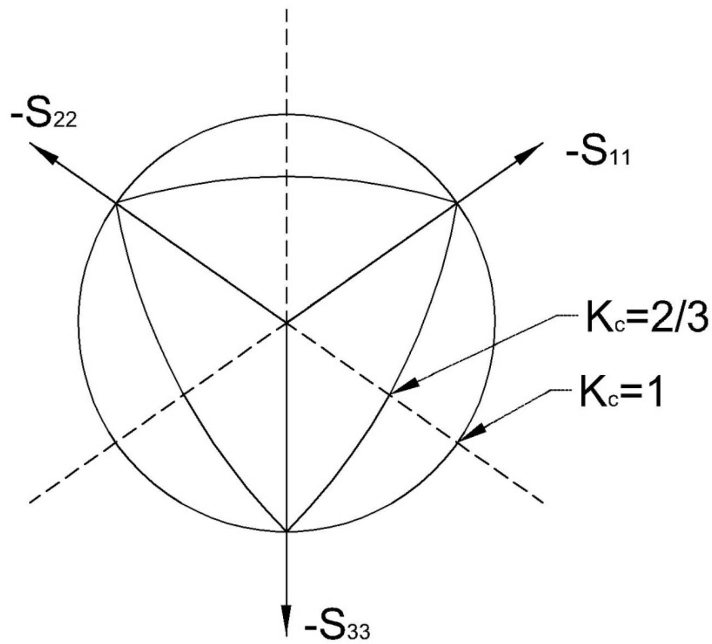

Figure 2-2: A Reproduction of the the Yield Surfaces in the Deviatoric Plane from ABAQUS User Manual.

Meanwhile the response of concrete to uniaxial loading in tension (f'_t) was assumed according to a model suggested by Coronado *et al.* (2006). This model is bilinear model based on behavior of the concrete softening under uniaxial tension (see Figure 2-3 for a reproduction of the model). In which w_{ch} the width of the crack is calculated based on Equation 2-1 and G_f which is the fracture energy (N/m) calculated based on Equation 2-2.

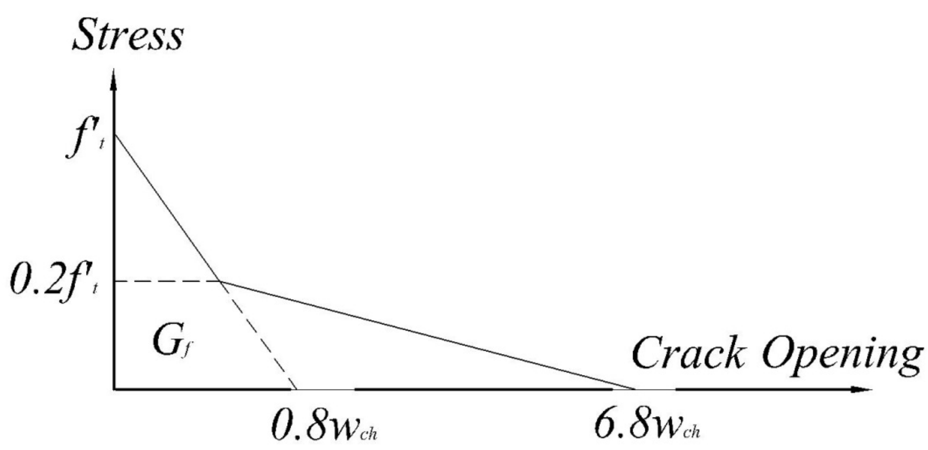

Figure 2-3: A Reproduction of the Concrete Softening under Uniaxial Tension from Coronado *et al.* (2006).

$$w_{ch} = \frac{G_f}{f_t'} \qquad Equation\ 2-1$$

$$G_f = 2.5\alpha_0 \left(\frac{f_c'}{0.051}\right)^{0.46} \left(1 + \frac{d_a}{11.27}\right)^{0.22} \left(\frac{w}{c}\right)^{-0.30} \qquad Equation\ 2-2$$

Where α_0 is 1.44 for crushed aggregates and d_a is the diameter of the aggregate in millimeters and *w/c* is the water cement ratio. As for the response of concrete to uniaxial loading in Compression (f'_c), it was calculated from the cyclic loading of concrete cylinders.

CHAPTER 3 - Fiber Reinforced Cementitious Matrix

This chapter is intended to address the use of natural fibers derived from wheat straws for reinforcing cementitious matrix specimens in compare with polypropylene fibers. In order to study the properties of the cementitious matrix reinforced with wheat fibers, 156 specimens were tested in uniaxial compression and flexure. The wheat fibers were prepared in two sizes and different volume fractions of these sizes are studied in this chapter to determine the optimal amount and size of the fiber for the study in the next chapter.

3.1 Materials

This research studied cementitious matrix with type I cement, Midwest crushed aggregate, Ottawa sand, long and short wheat fibers and polypropylene fibers (ProCon-F) which meets the requirements of ASTM C-1116. The following materials (Table 3-1) were utilized in this study of the cementitious matrix specimens:

Table 3-1: Materials Specifications.

Materials	**Specification**
Cement	Type I Cement
Sand	Ottawa Sand that meets the requirement of ASTM C87, C109, C348, C359, C593, C778.
Long Wheat Fibers	Nominal Length: 20-30 mm (**Error! Reference source not found.**, c) Average Diameter: 2-3 mm
Short (Fine) Wheat Fibers	Nominal Length: less than 5 mm (**Error! Reference source not found.**, b) Average Diameter: 0.01-0.02 mm
Polypropylene Fibers	Length of 19 mm (**Error! Reference source not**

	found., a)
	Diameter: 0.012 mm

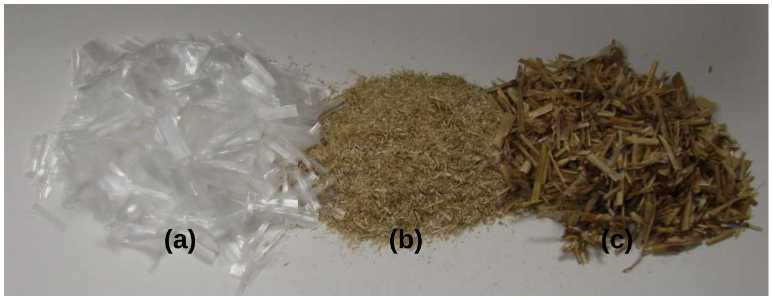

Figure 3-1: (a) Polypropylene Fibers, (b) Short Wheat Fibers, (c) Long Wheat Fibers.

3.2 Mixing Proportions

Table 3-2 represents the mixing proportions of the control cementitious matrix mixes according to the ASTM C109 (American Standard ASTM 2011) for three cubes and C348 (American Standard ASTM 2008) for three prisms which had a 0.485 water to cement ratio (w/c) and 0.364 cement to sand ration (c/s):

Table 3-2: Control Mix for Three Specimens.

Material	Quantities for Three Cubes (cm^3)	Quantities for Three Prisms (cm^3)
Cement	79.4	155
Sand	259.4	506.6
Water	121	195.3

The mixing was performed by mixing the cement, sand and the fibers for 30 seconds and then adding the water slowly and mixing for 2 minutes and the reason that the water is added the last is to avoid clustering the fibers in the mixture. The amount of water in the mixes containing fibers needed to be adjusted to accommodate for the reduction in workability due to the added fibers. This adjustment was accomplished by adding 3 mL for each gram of fibers added. That was concluded based on the absorption of the fibers, after weighting the dry fibers and the wet fibers (soaked in water then compressed to get rid of the excess water). Also the fibers were measured by volume of the specimen due to the substantial variability of the wheat fibers.

Therefore, Table 3-3 represents the adjusted amount of water for each percentage of fibers, the volume of fiber required for three specimens of cubes and prisms, and the number of specimens that were cast for each type of the three fibers. These volumes fraction of fibers, between 0.5% and 5%, were decided based on what El-Ashkar (2002) concluded in his study, that the addition 2% or more of softwood kraft fibers lead to a reduction in mortar compressive. Also Coutts (1987) in his research showed that 6% of mass fraction of Eucalyptus wood fibers produced the highest strength.

Table 3-3: Adjusted Water for Each Percentage of Fiber.

Volume % Fiber	Adjusted Water, mL	Wheat Fibers Volume, mm^3/3 Cubes	Wheat Fibers Volume, mm^3/3 Prisms
0%	121	0	0
0.5%	130	1970	3840
0.75%	134.3	2950	5760
1.0%	138.7	3930	7680
2.0%	156.4	7870	15360
3.0%	174.1	11800	23040
5.0%	209.5	19650	38400

3.3 Specimens and Casting

Due to the availability of 4 molds for prisms and 4 for cubes, each batch contained 12 of each cubes and prisms.

Table 3-4: Number of Specimen Per Each Percentage.

Volume % Fiber	No. of Cube Specimens	No. of Prism Specimens
0%	18	21
0.5%	9	12
0.75%	9	12
1.0%	18	21
2.0%	6	6

3.0%	9	9
5.0%	3	3

According to Table 3-4, the total number of specimens is 156, consisting of 84 prisms and 72 cubes. These specimens were divided into six batches according to the mixing date as shown in Figure 3-2 due to the limitation of the number of molds available to the researcher. Because of this different control specimens were made to assure accuracy and avoid the variability of the cementitious matrices. Batch 5 is contains 6 prisms and not 6 cubes due to the fact that some of the cubes showed huge amount of honeycombing and these cubes were discarded.

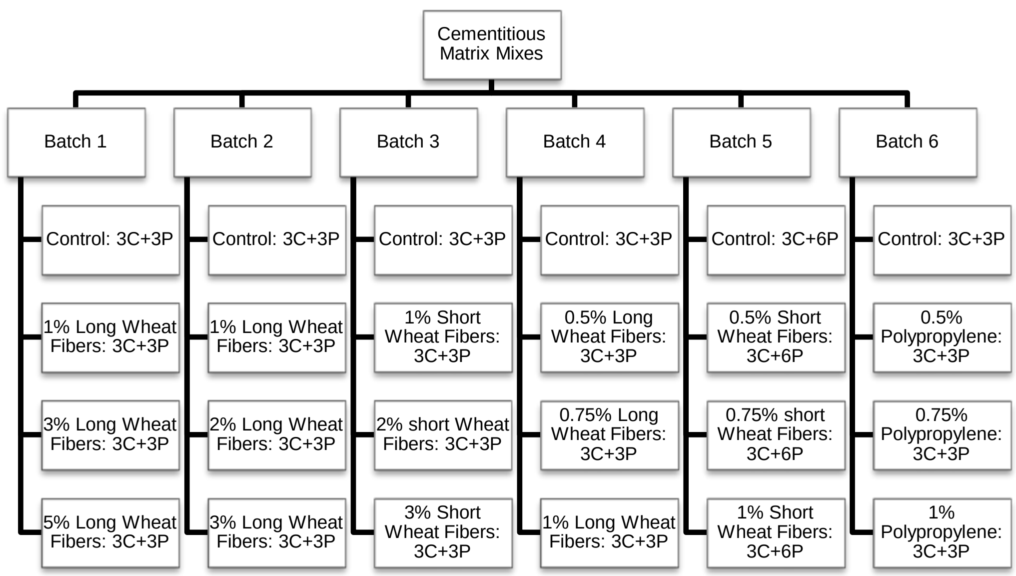

Figure 3-2: Cementitious Matrix Mix Batches for the Different Types of Fibers (C: represents the cubes, P: represents the prisms).

3.4 Testing

For the different cementitious matrix specimens two types of testing were conducted on them. On the 2 in (50.8 mm) cubes the uniaxial compression test and on the 160 x 40 x 40 mm prisms the three point flexural test was performed. In these two destructive tests the load deflection curves were recorded using the MTS compression machine.

3.4.1 Uniaxial Compression Testing:

Uniaxial compression tests on 2 in (50.8 mm) cubes were conducted in the load control mode with a rate of 550 lb/sec (2500 N/s) in accordance with the ASTM C109 and the EN 196-1:2005 (European standard EN 2005). The load control was initiated after applying 50 lb (228 N) of initial force to guarantee full contact between the machine and the specimen (Figure 3-3).

Figure 3-3: Test Setup for a Cube Reinforced with 0.5% Short Wheat Fiber.

3.4.2 Three Point Flexure:

Three point flexure tests were conducted on 160 x 40 x 40 mm prisms in the displacement control mode with a rate of 0.4 mm/sec in accordance with the ASTM C348 and the EN 196-1:2005 (European standard EN 2005) with a span length of 100 mm as shown in Figure 3-4.

Figure 3-4: Test Setup for a Prism Reinforced with 0.75% Short Wheat Fiber.

3.5 Results

3.5.1 Cubes Results:

The full load-deflection curves were generated (Figure 3-5 to Figure 3-9) due to the fact that an MTS compression machine was used. But since the load cell is trying to engage the specimen, the graphs showed some anomaly in the early stages of loading. Other machines were used to confirm the peak load of the specimen and it yielded very close results. As for the calculation of the stiffness, it was conducted over the linear portion of the rising part of the curves. The following graphs represent the load-deflection curves for the different percentages of different fibers.

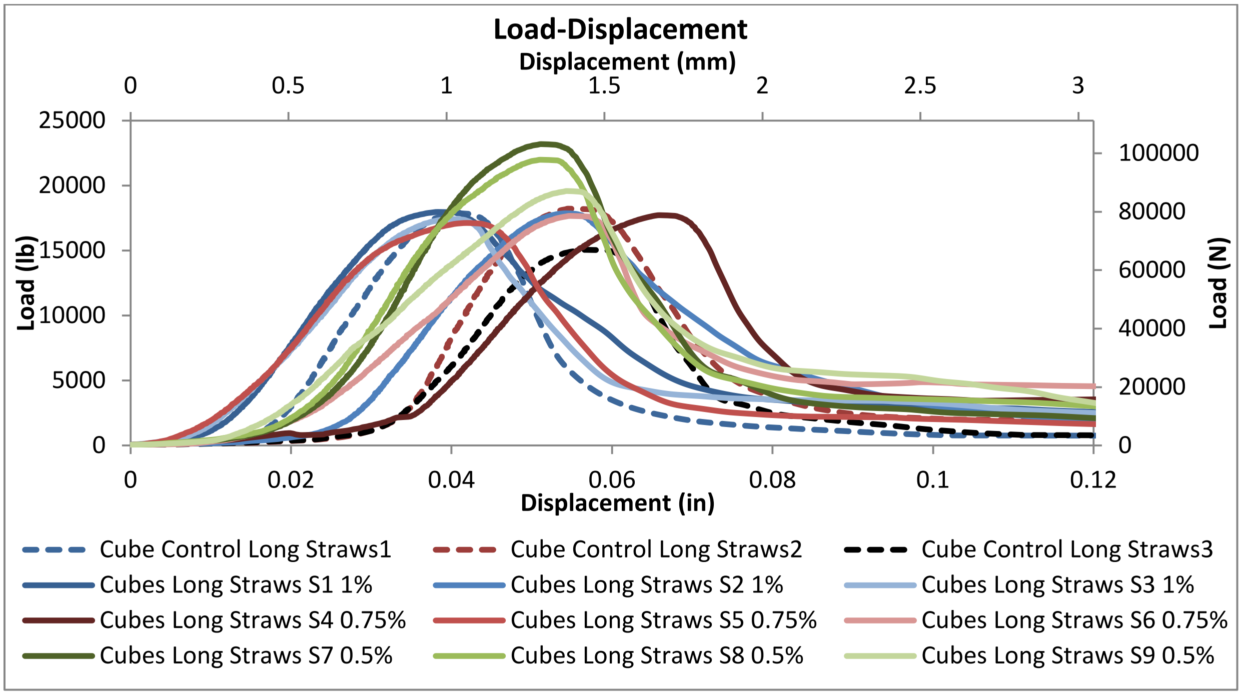

Figure 3-5: Cubes Specimens with 0.5% to 1% Long Wheat Fibers Compared to the Control Specimens.

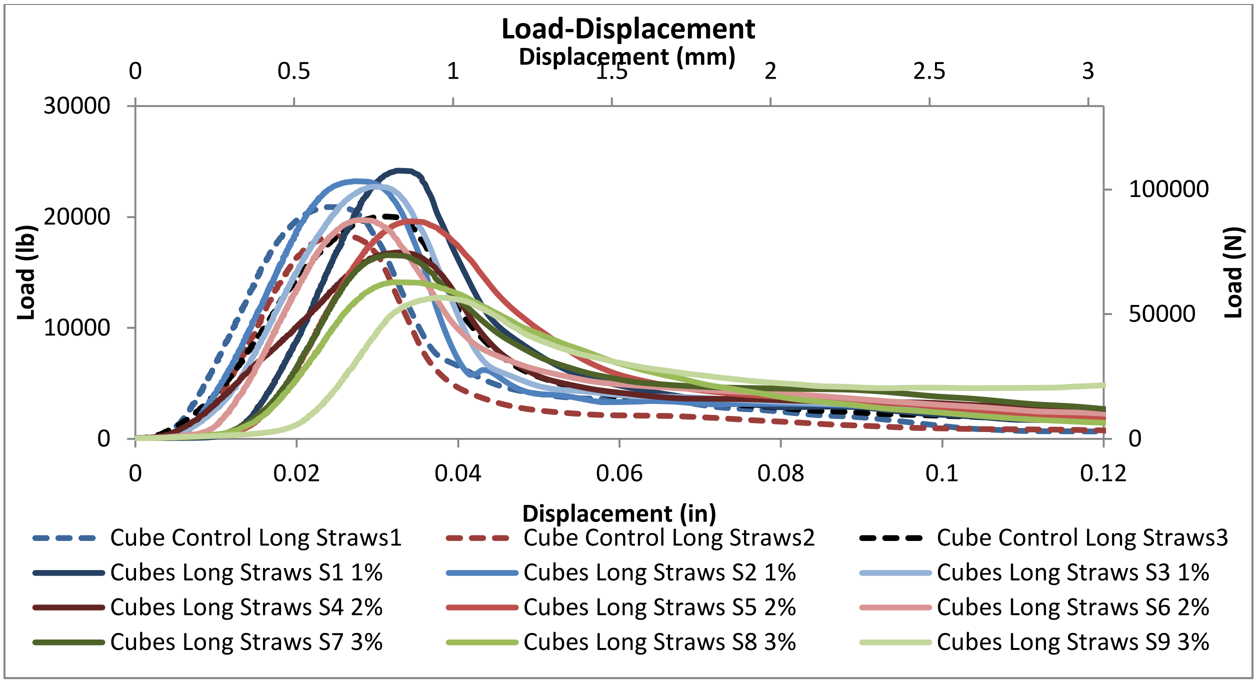

Figure 3-6: Cubes Specimens with 1% to 3% Long Wheat Fibers Compared to the Control Specimens.

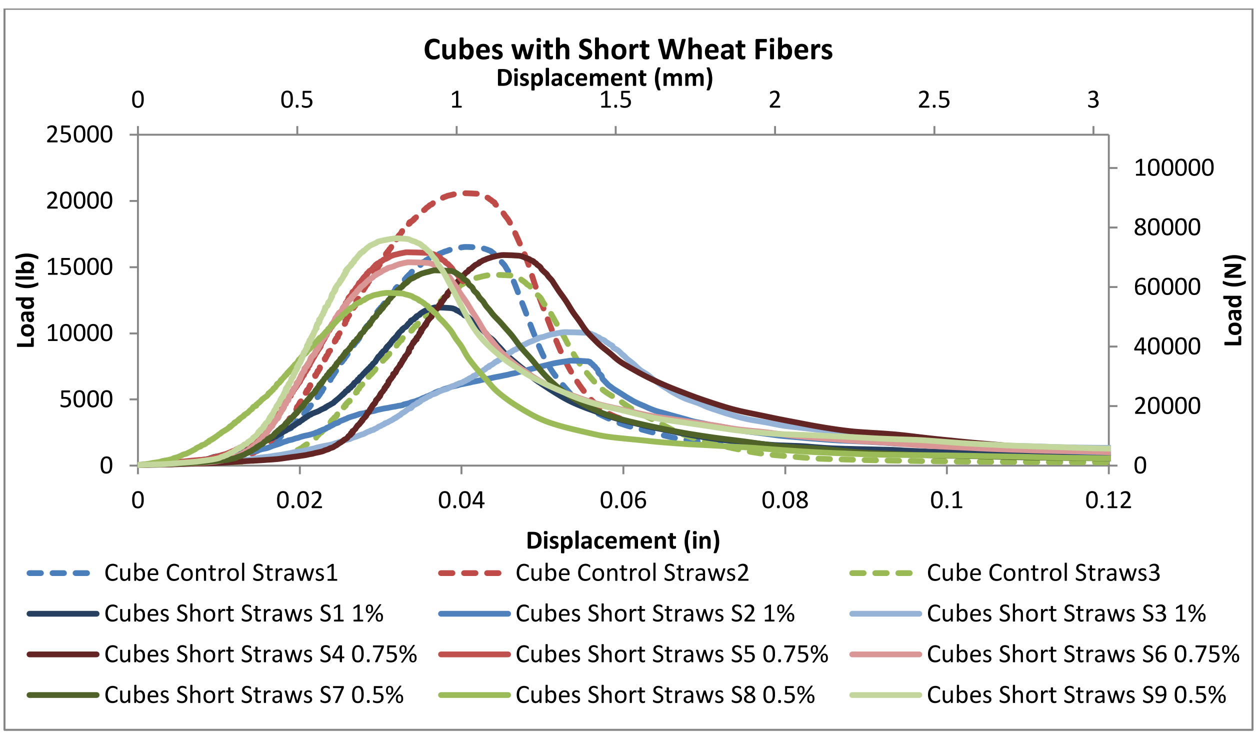

Figure 3-7: Cubes Specimens with 0.5% to 1% Short Wheat Fibers Compared to the Control Specimens.

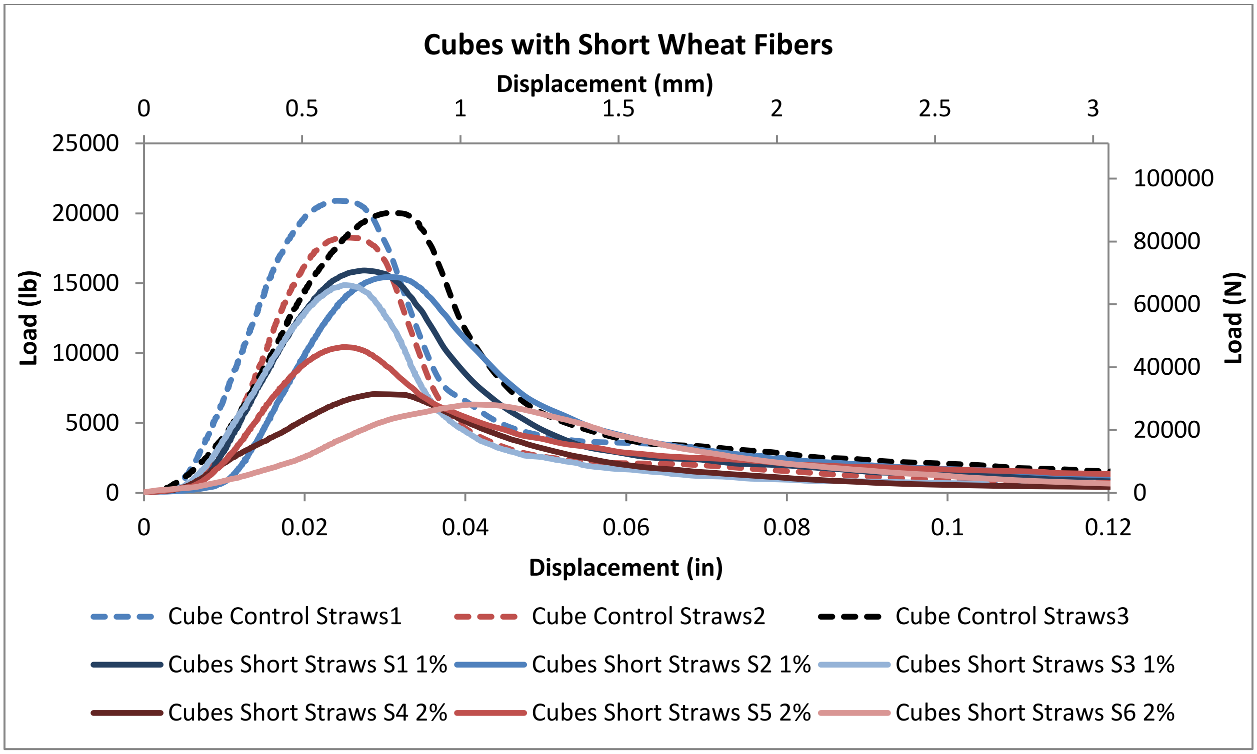

Figure 3-8: Cubes Specimens with 1% to 3% Short Wheat Fibers Compared to the Control Specimens.

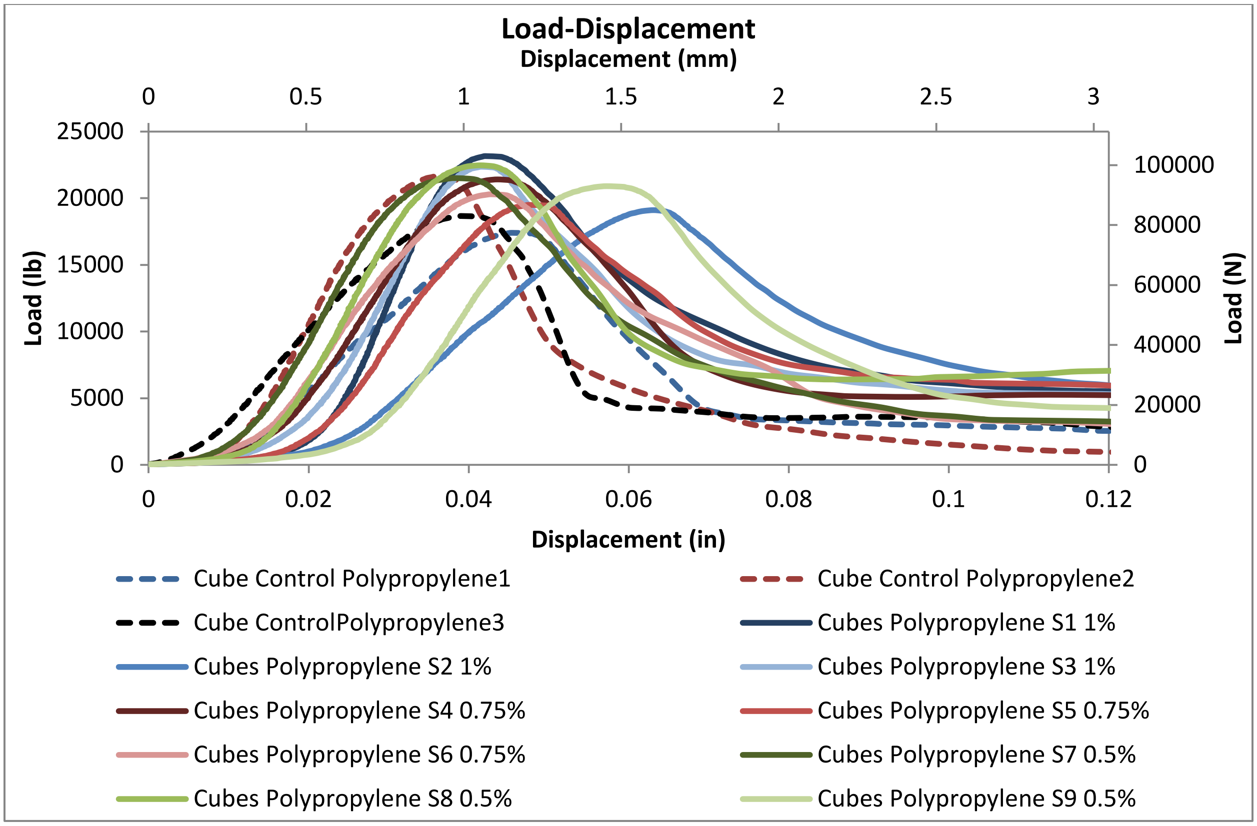

Figure 3-9: Cubes Specimens with 0.5% to 1% Polypropylene Fibers Compared to the Control Specimens.

Based on the measured peak loads and calculated stiffness, the following graphs were developed (Figure 3-10 and Figure 3-11) in order to present maximum, minimum, and average increasing or decreasing trends with the increasing amount of fibers. In these figures, the lines are connecting the average peak loads or stiffness in uniaxial compression, while the vertical lines with the tick marks represent the maximum, minimum, and middle values.

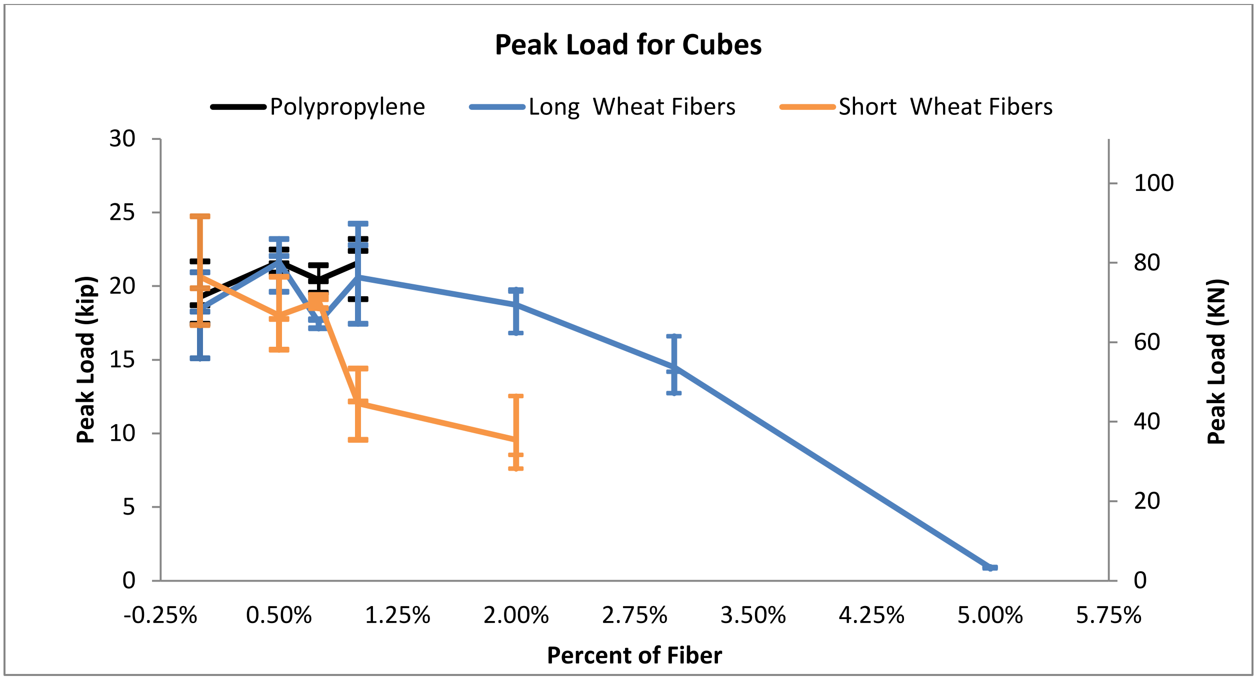

Figure 3-10: Peak Loads for Cubes Containing Different Percentages of Different Fibers.

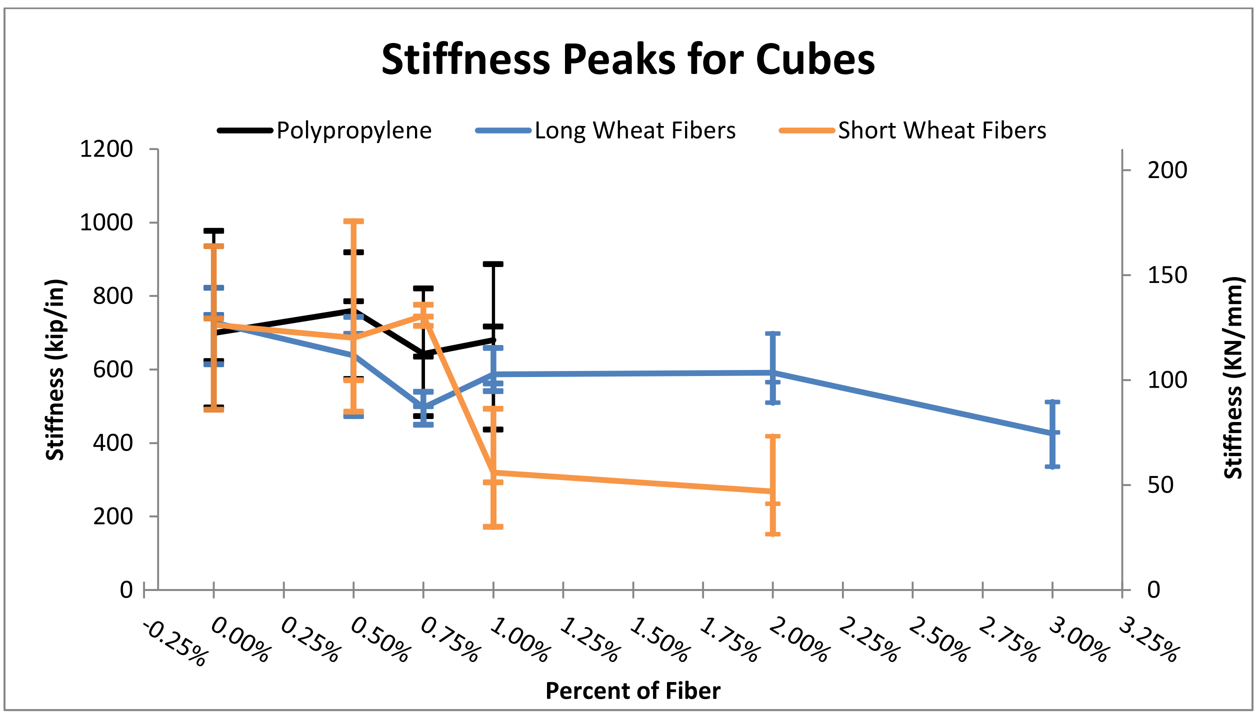

Figure 3-11: Stiffness Peaks for Cubes with Different Percentages of Different Fibers.

It is difficult to compare these different types of fibers due to the fact that they have different control specimens. Consequently peak load and stiffness results were normalized by dividing the peak load or the stiffness of each specimen by the average load or stiffness of its control specimen (Figure 3-12 and Figure 3-13). In these figures, the lines are connecting the average peak load or stiffness increase relative to the average of its control in uniaxial compression, while the vertical lines with the tick marks represent the maximum, minimum, and middle values in term of relative uniaxial compression peak load or stiffness. Table 3-5 represents the average increase in both load and stiffness for the cubes with the different percentages and different fibers.

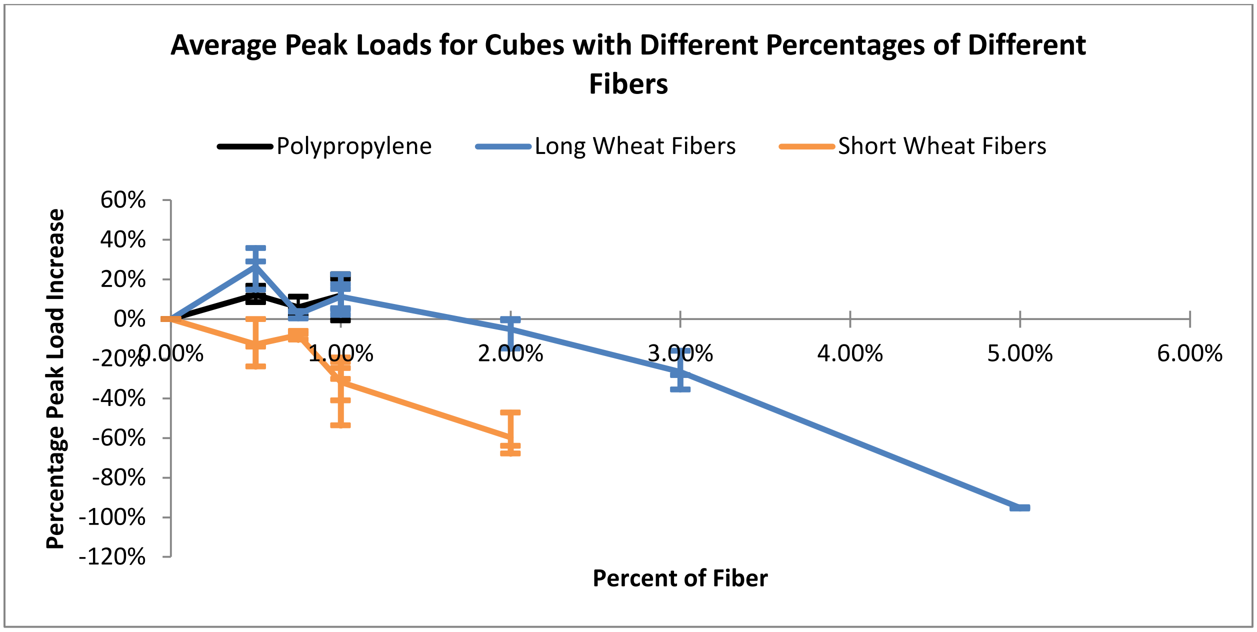

Figure 3-12: Average Peak Loads for Cubes with Different Percentages of Different Fibers.

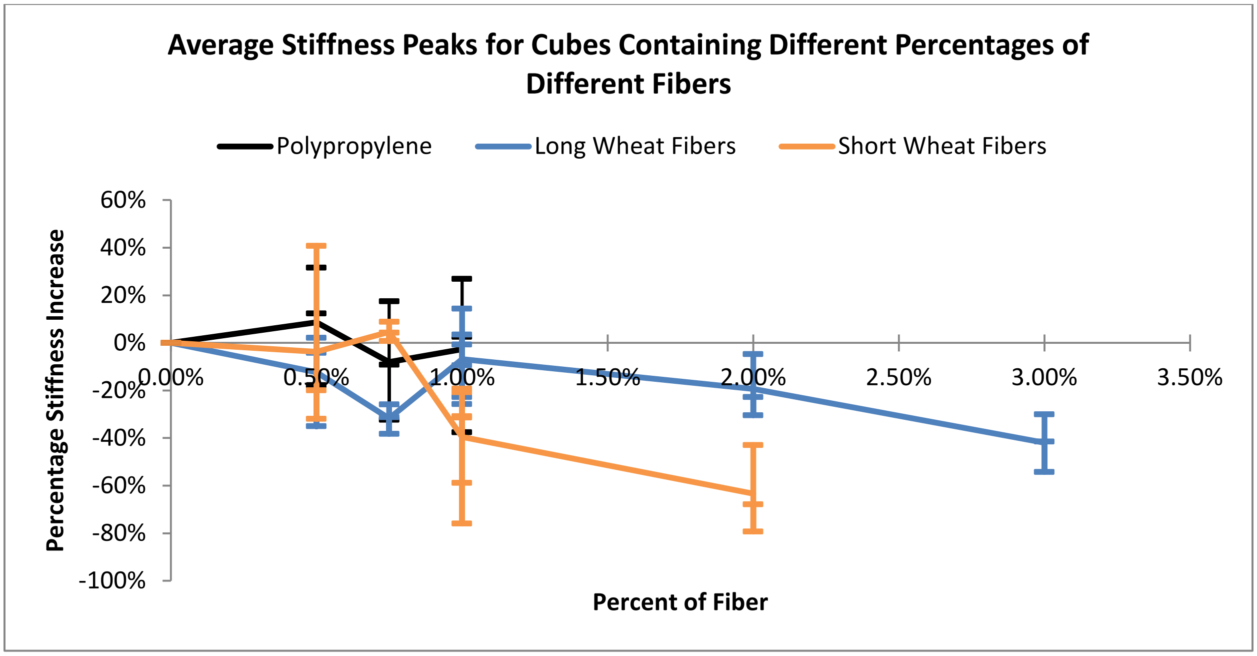

Figure 3-13: Average Stiffness Peaks for Cubes with Different Percentages of Different Fibers.

Table 3-5: Average Increase in the Load and Stiffness for Cubes with Different Amount of Different Fibers.

Volume % Fiber	Long Wheat Fibers		Short Wheat Fibers		Polypropylene Fibers	
	Avg. Load Increase	Avg. Stiffness Increase	Avg. Load Increase	Avg. Stiffness Increase	Avg. Load Increase	Avg. Stiffness Increase
0%	0%	0%	0%	0	0%	0%
0.50%	27%	-12%	-13%	0%	12%	9%
0.75%	3%	-32%	-8%	-4%	6%	-8%
1%	11%	-7%	-32%	5%	11%	-3%
2%	-5%	-19%	-60%	-40%	-	-
3%	-27%	-42%	-	-	-	-
5%	-95%	-	-	-	-	-

The following Figure shows some of the cubes with the different percentages of fibers.

Figure 3-14: Cubes with Different Wheat Fibers Percentages.

3.5.2 Prisms Results:

The load-deflection curves were also generated (Figure 3-16 to Figure 3-20) due to the fact that an MTS compression machine was used (setup shown in Figure 3-4). As for the calculation of the stiffness, it was conducted over the linear portion of the rising part of the curve as shown in Figure 3-15. The following graphs represent the load-deflection curves for the different percentages of different fibers.

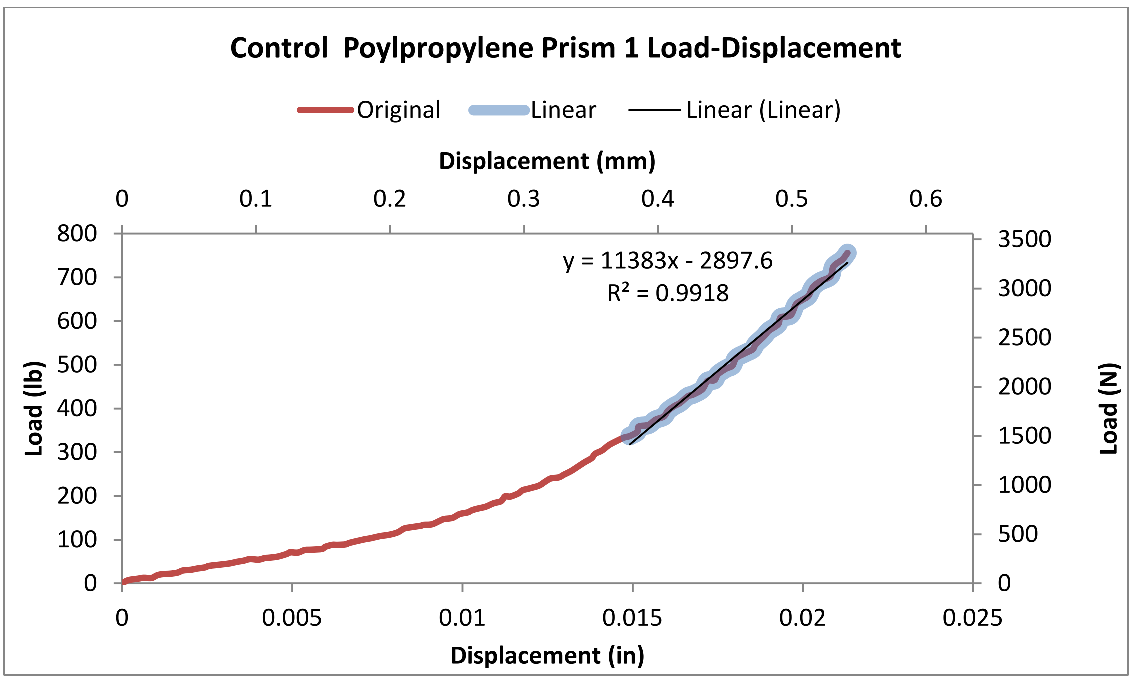

Figure 3-15: Load-Deflection Curve for Control Polypropylene Prism Indicating the Linear Portion Used in the Calculation of the Stiffness.

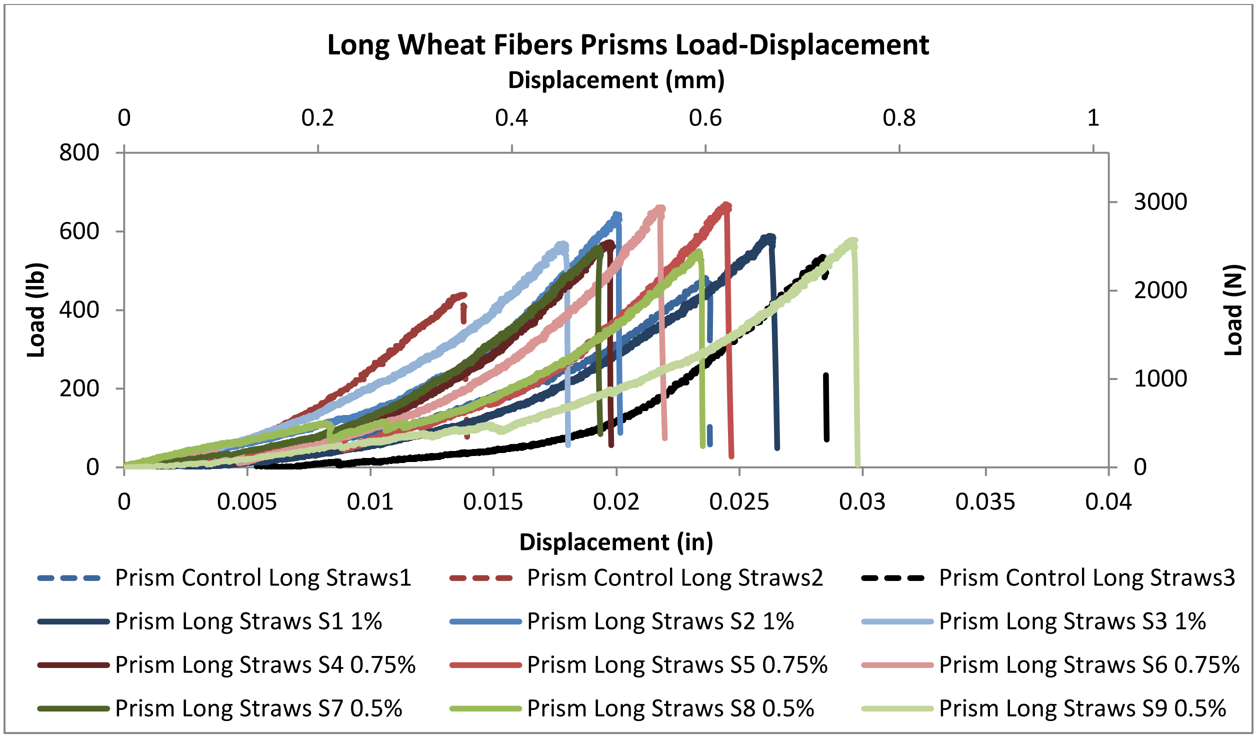

Figure 3-16: Prisms Specimens with 0.5% to 1% Long Wheat Fibers Compared to the Control Specimens.

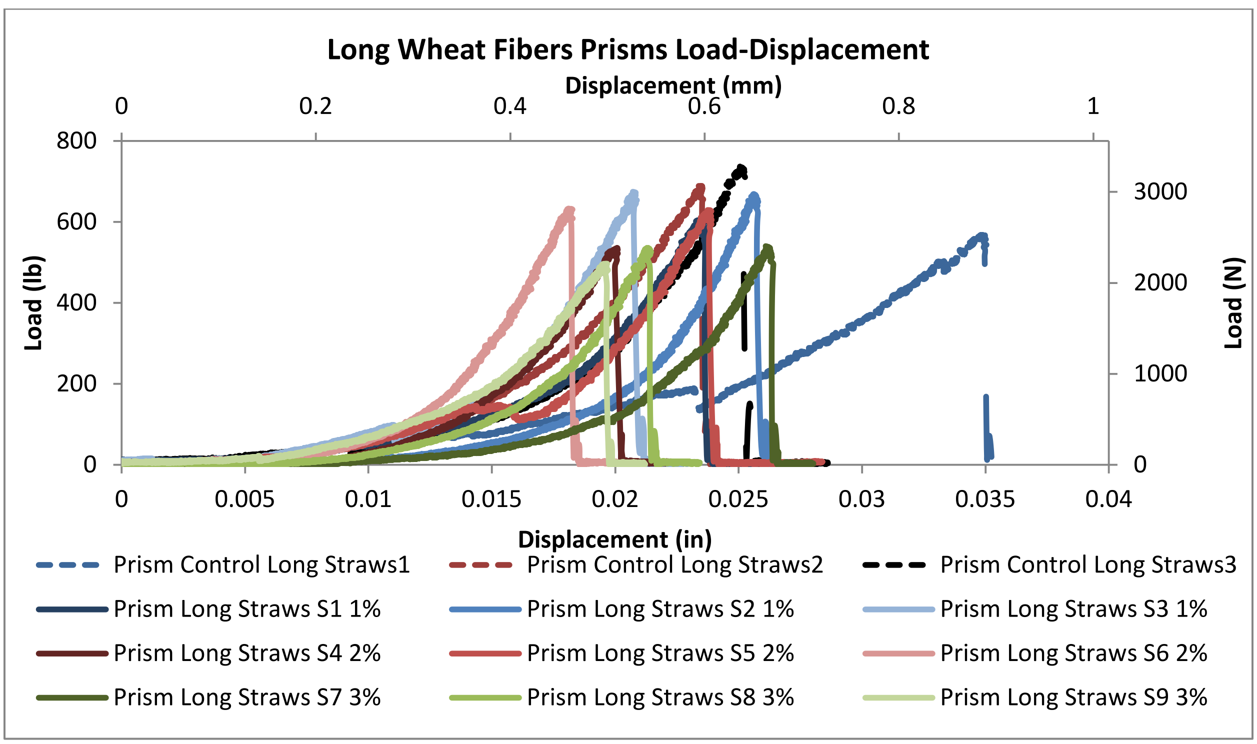

Figure 3-17: Prisms Specimens with 1% to 3% Long Wheat Fibers Compared to the Control Specimens.

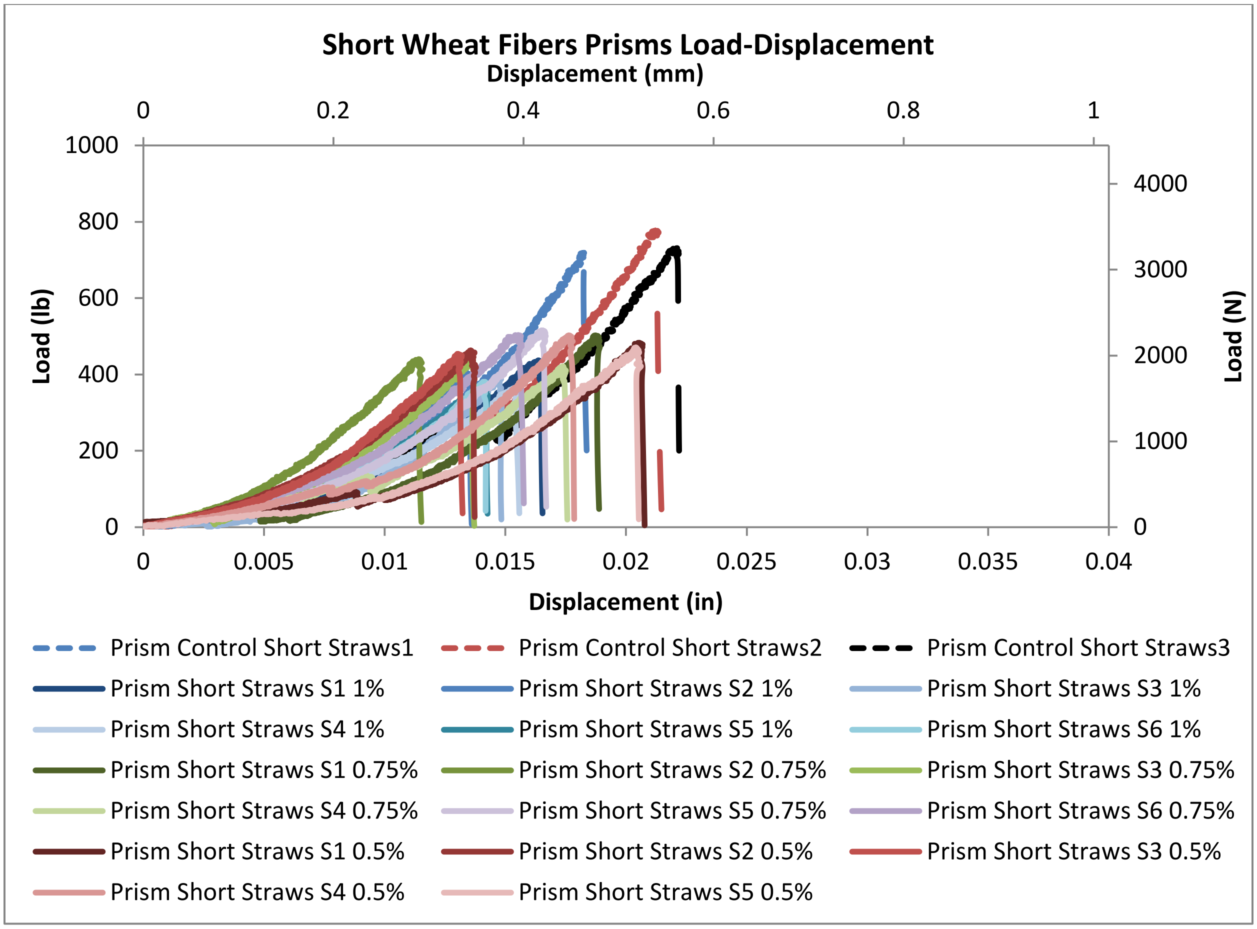

Figure 3-18: Prisms Specimens with 0.5% to 1% Short Wheat Fibers Compared to the Control Specimens.

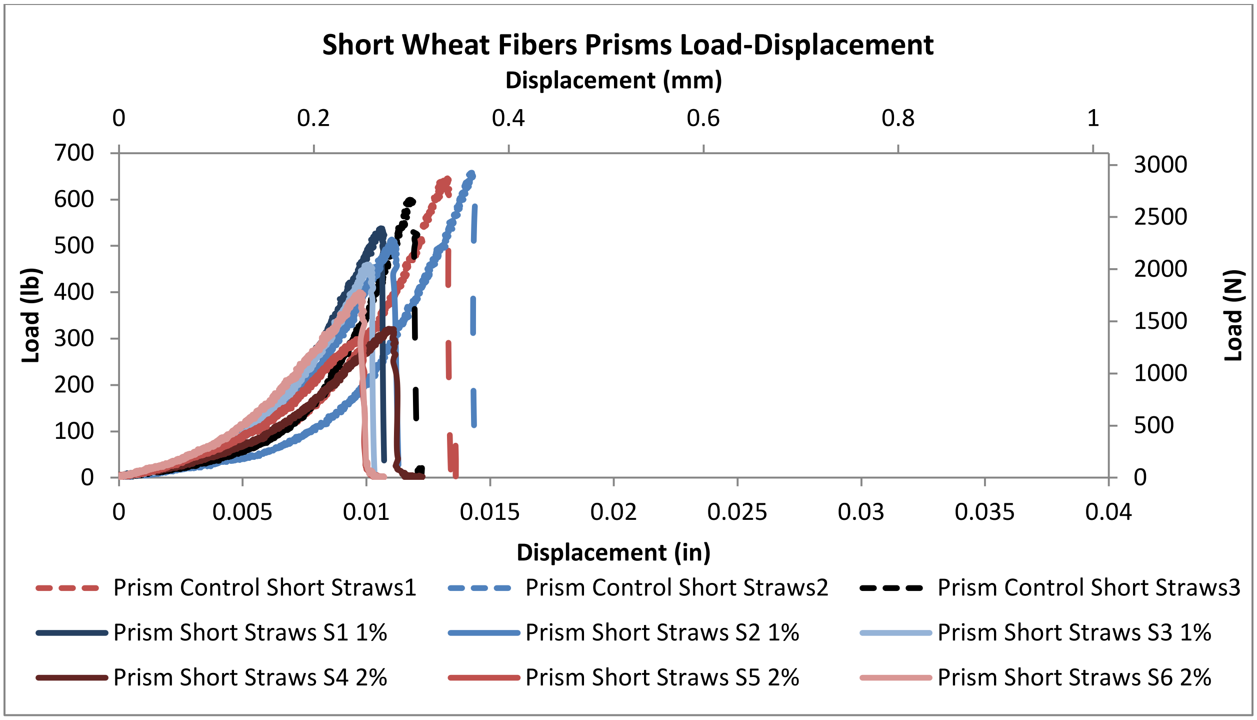

Figure 3-19: Prisms Specimens with 1% to 3% Short Wheat Fibers Compared to the Control Specimens.

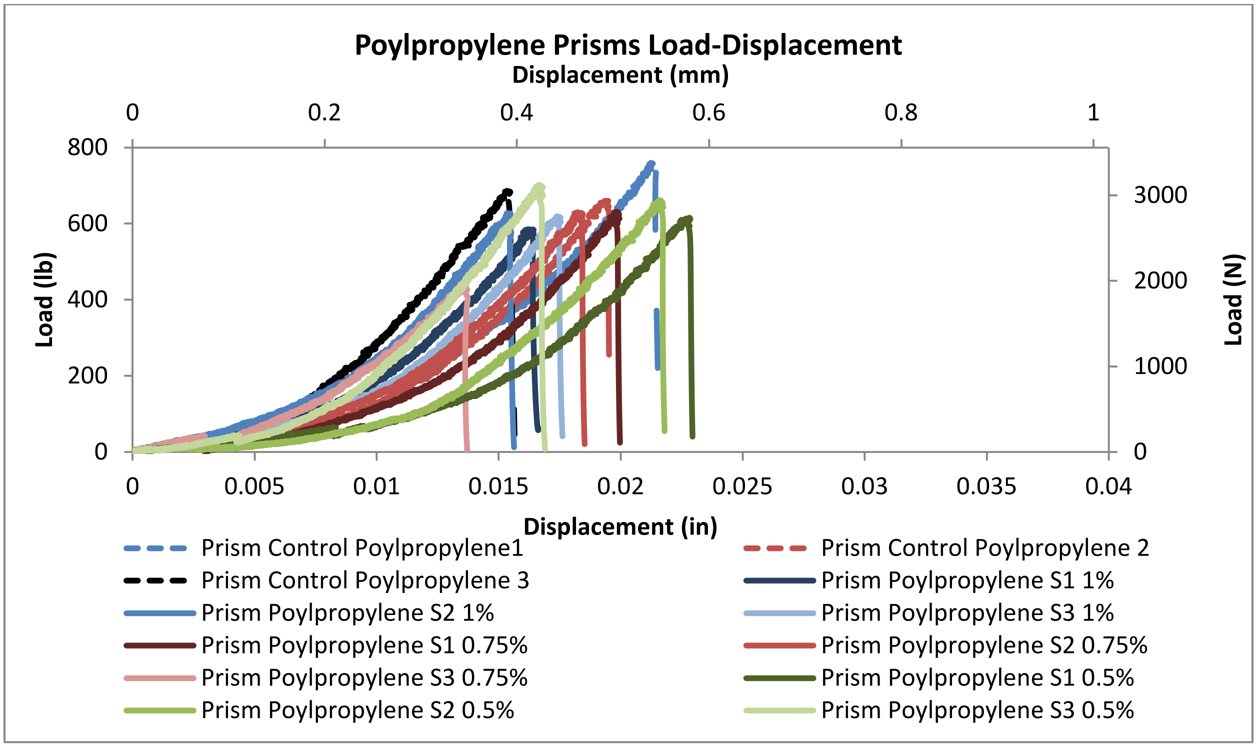

Figure 3-20: Prisms Specimens with 1% to 3% Polypropylene Fibers Compared to the Control Specimens.

The following graphs (Figure 3-21 and Figure 3-22), developed from the peak loads and the calculated stiffnesses for all three types of fibers, present the peak load and stiffness benefits of the different fibers. In these figures, the lines are connecting the average peak load or stiffness in three-point flexure, while the vertical lines with the tick marks represent the maximum, minimum, and middle values. As for the crack angle which was taken as the angle between the crack direction and the minor principal stress direction for all prisms Table **Error! No text of specified style in document.**-1 in the Appendix shows the values for the different prisms.

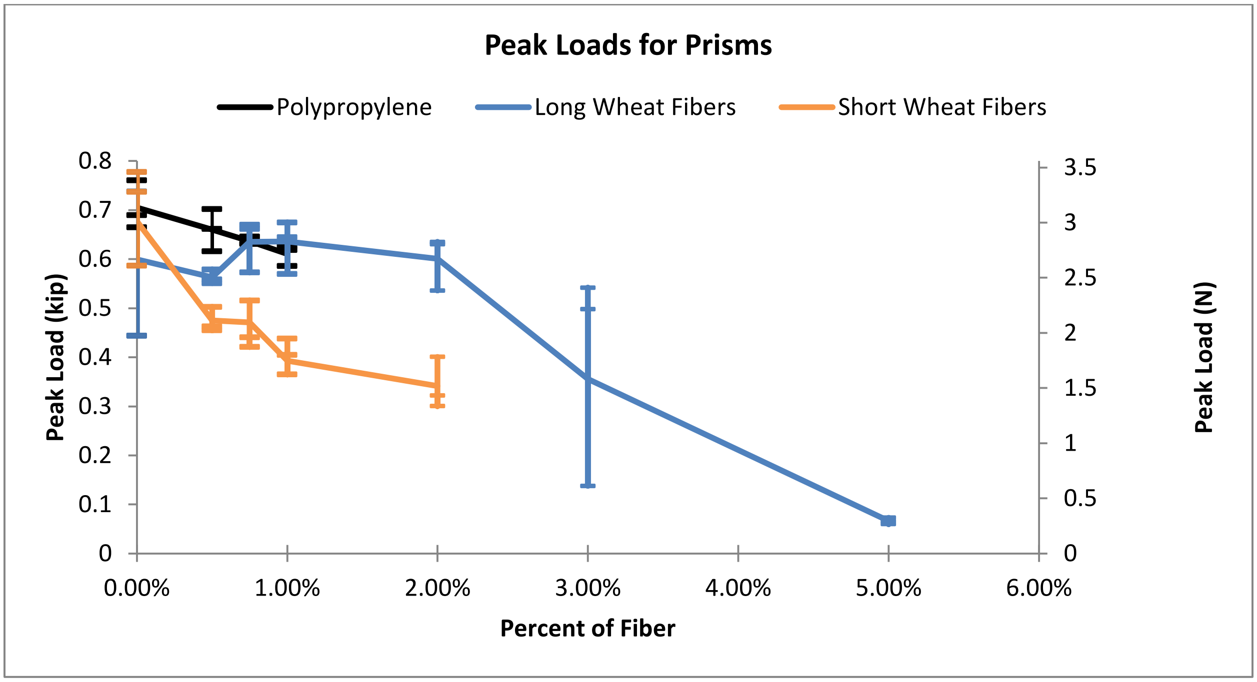

Figure 3-21: Peak Loads for Prisms Containing Different Percentages of Different Fibers.

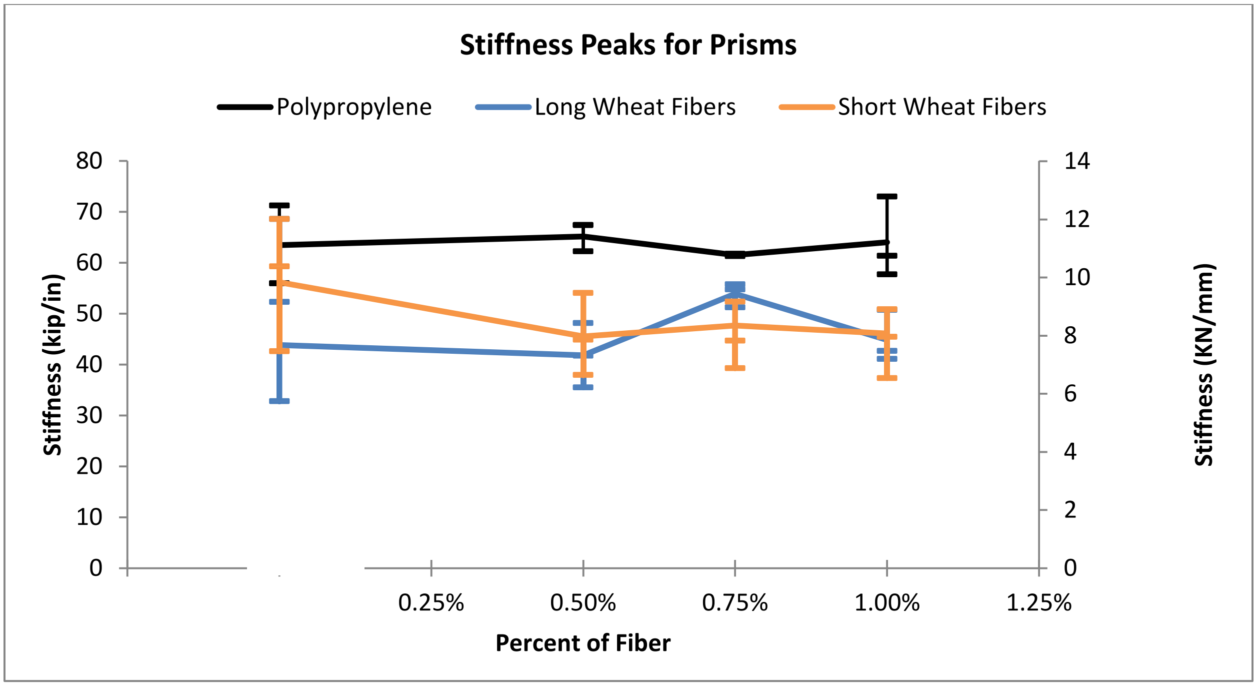

Figure 3-22: Stiffness Peaks for Prisms Containing Different Percentages of Different Fibers.

Similar to Figure 3-12 and Figure 3-13, Figure 3-23 and Figure 3-24 represent the percentages of peak load and stiffness increases in comparison with the average values of the corresponding control specimens. In these figures, the lines are connecting the average peak load or stiffness increase relative to the average of its control in three-point flexure, while the vertical lines with the tick marks represent the maximum, minimum, and middle values in term of relative flexural peak load or stiffness. Table 3-6 represents the average increase in both load and stiffness for the prisms with the different percentages and different fibers.

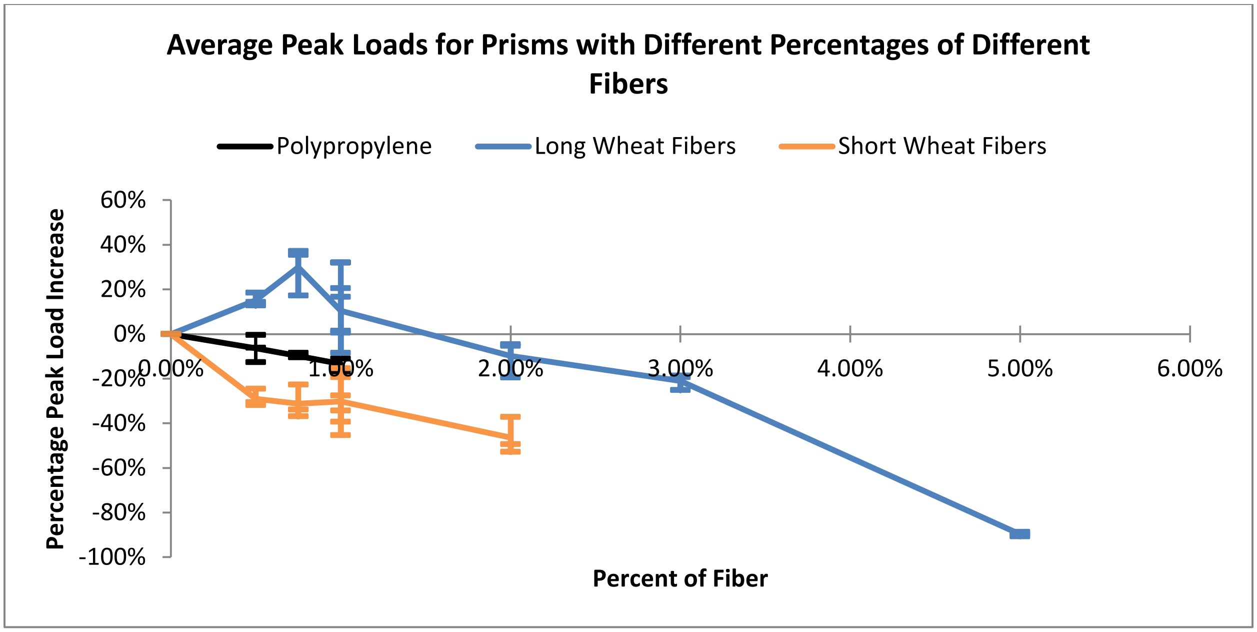

Figure 3-23: Average Peak Loads for Prisms with Different Percentages of Different Fibers.

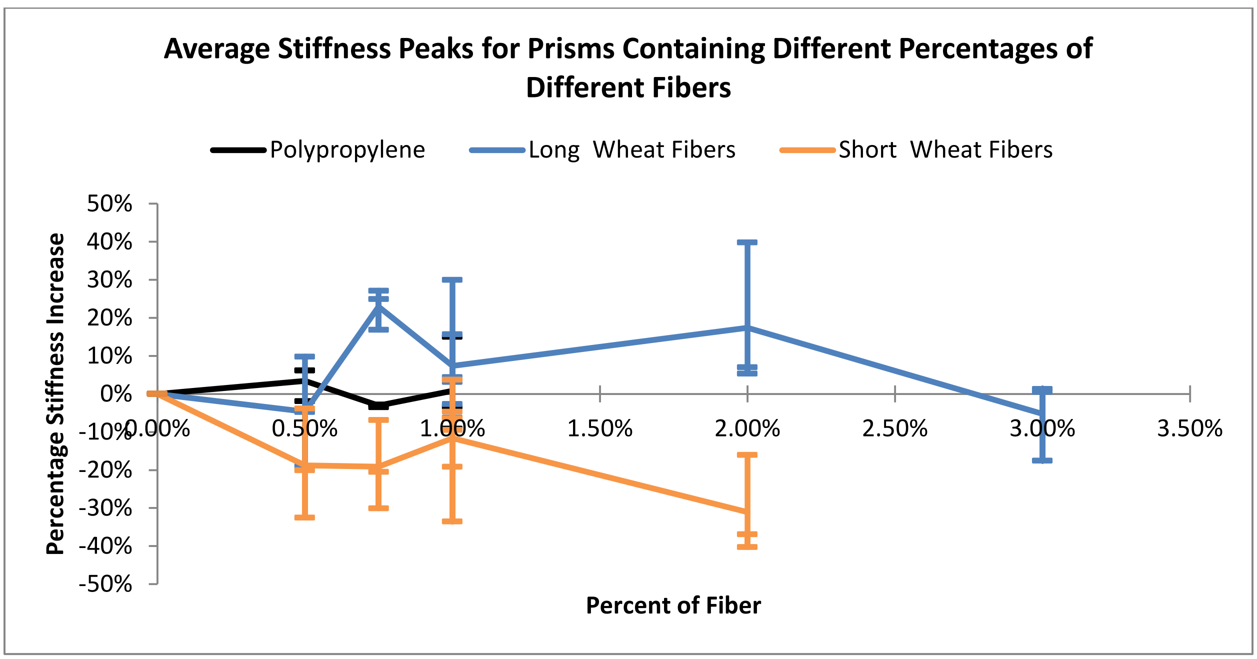

Figure 3-24: Average Stiffness Peaks for Prisms with Different Percentages of Different Fibers.

Table 3-6: Average Increase in the Load and Stiffness for Prisms with Different Amount of Different Fibers.

Volume % Fiber	Long Wheat Fibers		Short Wheat Fibers		Polypropylene Fibers	
	Avg. Load Increase	Avg. Stiffness Increase	Avg. Load Increase	Avg. Stiffness Increase	Avg. Load Increase	Avg. Stiffness Increase
0%	0%	0%	0%	0	0%	0%
0.50%	15%	-5%	-29%	0%	-6%	3%
0.75%	30%	23%	-31%	-19%	-10%	-3%
1%	10%	7%	-30%	-19%	-13%	1%
2%	-10%	17%	-46%	-12%	-	-
3%	-21%	-5%	-	-	-	-
5%	-90%	-	-	-	-	-

As for the cracking, Figure 3-25 represents the difference in cracking between the control prism and the prism with different percentages of wheat fibers. Cracks in the prisms with wheat fibers are inclined which indicate that these cracks are shear cracks, while the control prisms have flexural cracks, straight cracks.

Figure 3-25: Prisms with Wheat Fibers.

CHAPTER 4 - Fiber Reinforced Concrete

This chapter is intended to address the use of wheat fibers as a reinforcing material for concrete specimens in compare with polypropylene fibers. In order to study the properties of the reinforced concrete, 99 specimens were tested in uniaxial compression and flexure. The wheat fibers percentages and size were concluded from the initial study in CHAPTER 3 -.

4.1 Materials

In this part of the research only long wheat fibers will be studied in compare with the polypropylene fibers ranging from 0.5-1% fraction volumes (Figure 3-1). The properties for these fibers are given in Table 4-1.

Table 4-1: Material Properties

Materials	**Specification**
Cement	Type I Cement
Long Wheat Fibers	Nominal Length: 20-30 mm (**Error! Reference source not found.**, c) Average Diameter: 2-3 mm
Polypropylene Fibers	Length of 19 mm (**Error! Reference source not found.**, a) Diameter: 0.012 mm

As for the fine aggregate and coarse aggregate (aggregate 12mm or less) the following figures represent the sieve analysis that was conducted on both of the sand and rock. As for the absorption for the fine aggregate it was 1.76% and 1.58% for the coarse aggregate which was conducted over an oven dried aggregate and collected for five samples.

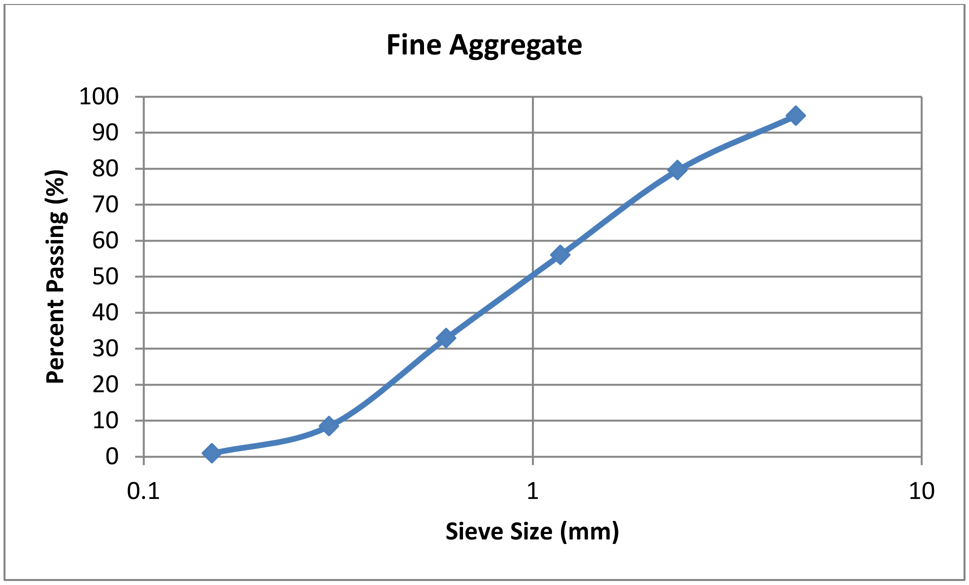

Figure 4-1: Fine Aggregate Sieve Analysis

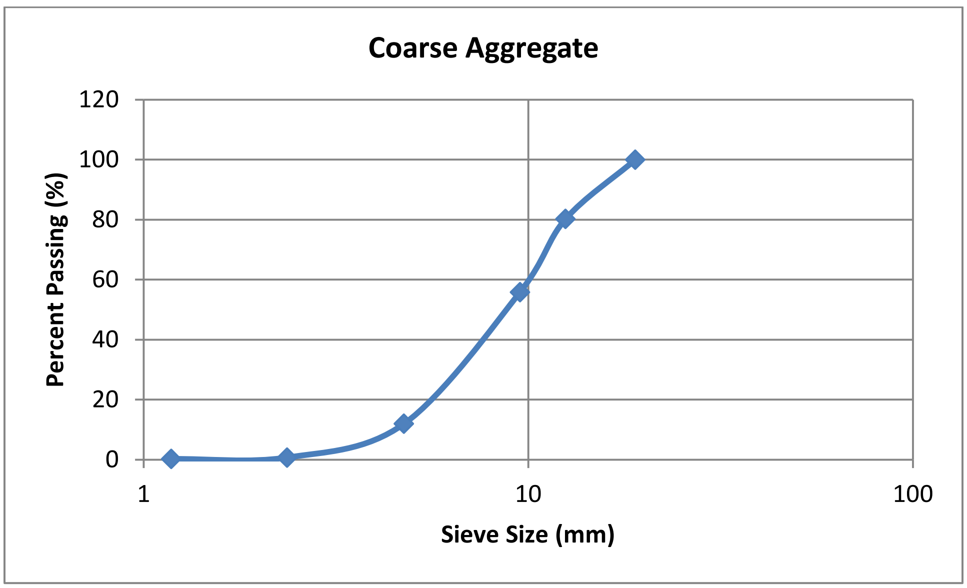

Figure 4-2: Coarse Aggregate Sieve Analysis

4.2 Mixing Proportions

Table 4-2 represents the mixing proportions of the control concrete mixes according to the ASTM C192 (American Standard ASTM 2007) for 10 cylinders and 6 prisms which had a 0.45 water to cement ratio (w/c), 0.385 cement to sand (fine aggregate) ration (c/s) and 0.374 cement to rock (coarse aggregate) ratio (c/r):

Table 4-2: Control Mix for Cylinder and Prism Specimens.

Material	Quantities for 4x8 in Cylinder (gram)	Quantities for 6x6x21 in Prism (gram)
Cement	8649.71	30354.99
Water	3894.24	13666.30
Coarse Aggregate (SSD)	23147.01	81231.33
Fine Aggregate (SSD)	22458.21	78814.10

The mixing was performed by mixing the cement, sand, rock and the fibers for 30 seconds and then adding the water slowly and mixing for 2 minutes and the reason that the water is added the last is to avoid clustering the fibers in the mixture. The amount of water in the mixes containing fibers needed to be adjusted to accommodate for the reduction in workability due to the added fibers. This adjustment was accomplished by adding 3 mL for each gram of fibers added. That was concluded based on the absorption of the fibers, after weighting the dry fibers and the wet fibers (soaked in water then compressed to get rid of the excess water). Also the fibers were measured by volume of the specimen due to the substantial variability of the wheat fibers. Therefore, Table 4-3 represents the adjusted amount of water for each percentage of fibers, the volume of fiber required for cylinders and prisms specimens, and the number of specimens that were cast for each type of fiber. These volumes fraction of fibers, between 0.5% and 1%, were decided based on the previous study on the cementitious matrix in CHAPTER 3 - CHAPTER 3 -.

Table 4-3: Adjusted Water for Each Percentage of Fiber.

Volume % Fiber	Adjusted Water for Cylinders (gram)	Adjusted Water for Prisms (gram)	Wheat Fibers Volume for Cylinder (cm^3)	Wheat Fibers Volume for Prism (cm^3)
0%	0	0	0	0
0.5%	6.2	449.28	5.99	41.29
0.75%	27.8	511.22	9.27	61.94
1.0%	36.9	573.16	12.4	82.59

4.3 Specimens and Casting

All the specimen were casted in accordance with the ASTM standards for casting concrete in laboratories and slump and air content tests were performed and the results are reported in Table 4-4.

Table 4-4: Slump and Air Content of the Concrete Mixes

Type	Slump (mm)	Air content (%)
Control	0	5
0.5% Wheat Fibers	6.35	2.8
0.75% Wheat Fibers	19.05	2.6
1% Wheat Fibers	44.45	2.7
0.5% Polypropylene	0	6
0.75% Polypropylene	0	4.8
1% Polypropylene	0	3.9

Due to the availability of 9 molds for prisms and 72 for cylinders, all the cylinders were casted as one batch, while the prisms were divided into batches as shown in Figure 4-3.

Table 4-5: Number of Specimen Per Each Percentage.

Volume % Fiber	No. of Cylinder Specimens	No. of Prism Specimens
0%	10	9
0.5%	22	6
0.75%	20	6
1.0%	20	6

According to Table 4-5, the total number of specimens is 99, consisting of 27 prisms and 72 cylinders. These specimens were divided into four batches according to the mixing date as shown in Figure 4-3 due to the limitation of the number of molds available to the researcher. Because of this different control specimens were made to assure accuracy and avoid the variability of the concrete mixes. Batch 1 contains all the cylinders, 10 for each percentage except for the 0.5% of both fibers due to the fact that some of these cylinders were made for cyclic loading.

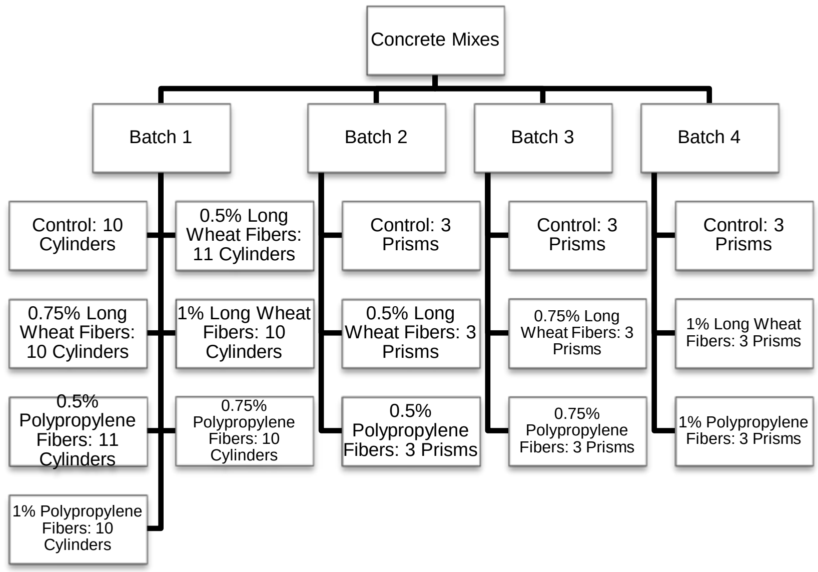

Figure 4-3: Concrete Mix Batches for the Different Types of Fibers.

4.4 Testing

In this portion of the research, two mechanisms of testing were implemented. The first mechanism is the monotonic testing which included the uniaxial compression and the four point bending. As for the second mechanism the cyclic testing, it included only uniaxial compression.

4.4.1 Monotonic Testing:

4.4.1.1 Uniaxial Compression Testing:

Uniaxial compression was performed over 4x8 in (101.6x 203.2 mm) cylinders according to the ASTM C39 (American Standard ASTM 2010). In order to insure perfect contact between the cylinders and the load-cell, sulfur capping or neoprene pads were used. Figure 4-4 represents the cylinder setup in the compression machine.

Figure 4-4: Cyliner Setup for Uniaxial Compression Testing.

4.4.1.2 Four Point Flexure:

Four Point Flexure was performed over 6x6x21 in (152.4x152.4x533.4 mm) prisms according to the ASTM C78 (American Standard ASTM 2010). On each prism two strain gages were installed in the bottom of the mid-span of the prism according to Vishay's Technical note on mounting gages on concrete structures, Application Note TT-611. Also two LVDTs were placed on the top of the mid-span of each prism. Figure 4-5 represents the prism setup in the compression machine with the LVDTs and the strain gages.

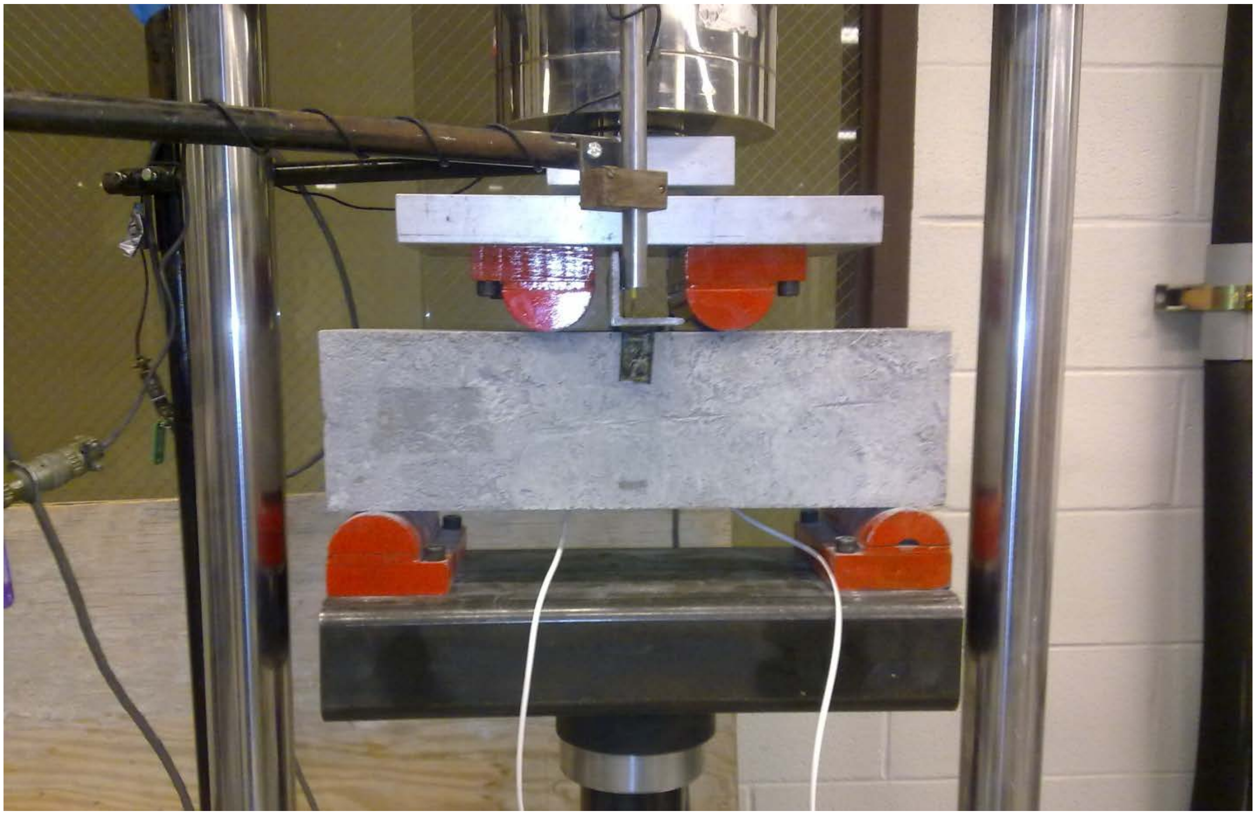

Figure 4-5: Prism Setup for Four Point Flexural Testing.

4.4.2 Cyclic Testing:

In order to determine the modulus of elasticity and the hardening function, the inelastic strain that develop for the concrete specimen with and without fibers cyclic loading was performed. For each type and percentages of fiber one cylinder was tested under cyclic loading after 28 days of curing. Each of these cylinders had two strain gages mounted on the mid-height of the cylinder 180^o from each other. Nine cycles was performed on each cylinder; three on 0.4f'_c (159692 N), three on 0.5 f'_c (199503 N) and three on 0.6 f'_c (239092 N). The f'_c was determined from averaging the control cylinders under monotonic loading.

4.5 Results

4.5.1 Cylinder Results:

4.5.1.1 Monotonic Testing Result:

Since the development of the load capacity of the concrete was studied after 7, 14 and 28 day of curing for the different percentages of the long wheat fibers and the polypropylene fibers.

Figure 4-6 represent the peak load increase for all the specimens (63 cylinders) over the curing period, while Figure 4-7 represent the average peak load development for the different percentages of fibers over the same curing period. The exact values of the peak loads and the averages are presented in Table 4-6.

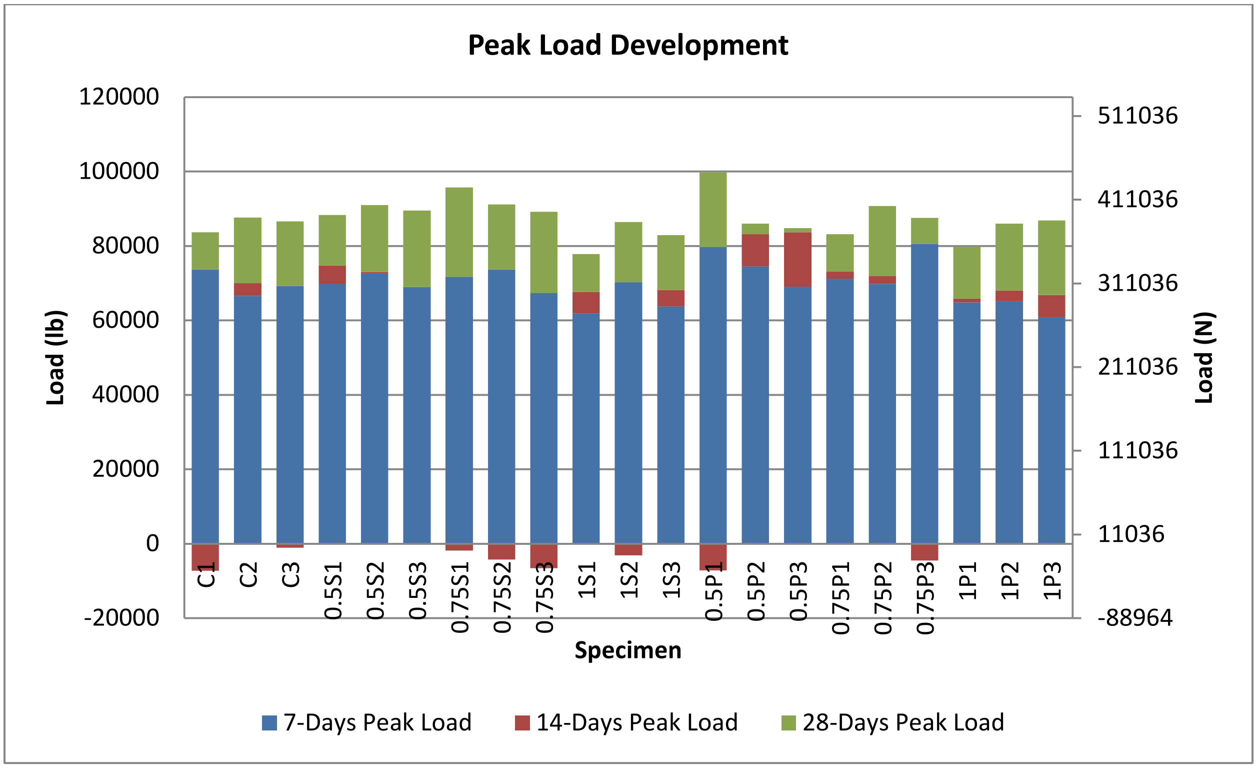

Figure 4-6: Development of the Load Capacity for the Concrete Cylinders.

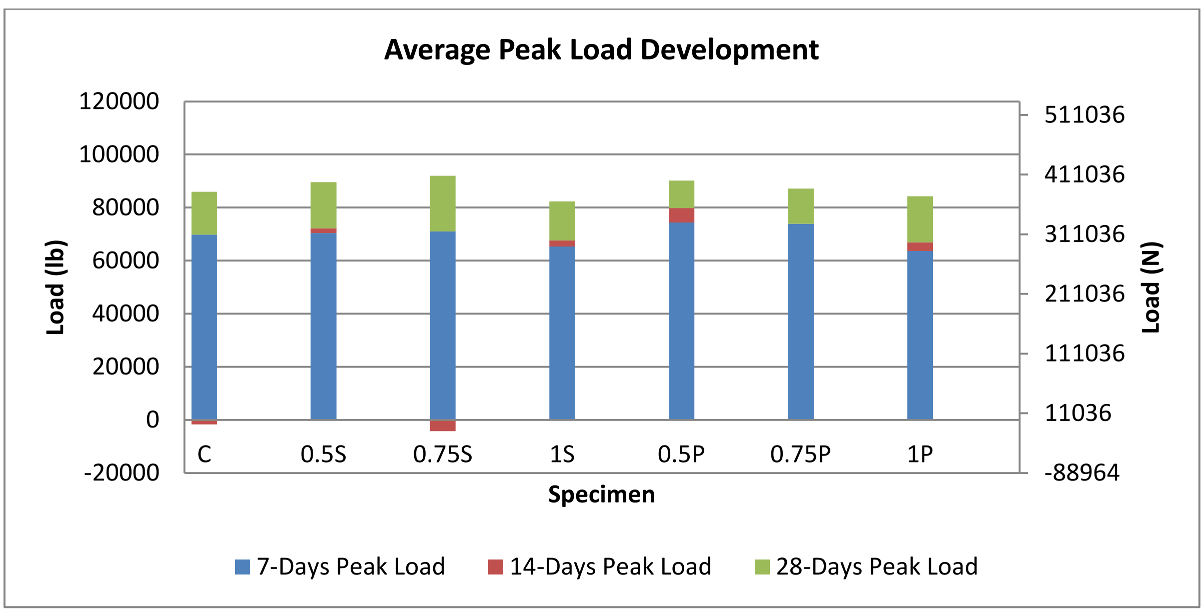

Figure 4-7: Development of the Average Load Capacity for the Concrete Cylinders.

Table 4-6: Peak Load Development for the Concrete Cylinders.

Specimen	*7-Day Peak Load (N)*	*Average (N)*	*14-Day Peak Load (N)*	*Average (N)*	*28-Day Peak Load (N)*	*Average (N)*
C1	327871		295406		372316	
C2	296166	310680	311153	303220	389709	382377
C3	308003		303102		385105	
0.5S1	309989		332238		392711	
0.5S2	322753	313205	324653	321162	404721	398487
0.5S3	306874		306594		398027	
0.75S1	318902		310575		425828	
0.75S2	327879	315515	308907	296689	405567	409333
0.75S3	299766		270585		396603	
1S1	275363		300477		345960	
1S2	312462	290345	298631	300796	384326	366274
1S3	283209		303280		368535	
0.5P1	354437		322607		443732	
0.5P2	331039	330889	369936	354961	382347	401029
0.5P3	307191		372338		377009	
0.75P1	316621		325343		369714	
0.75P2	310523	328570	320050	327953	403476	387470
0.75P3	358565		338465		389219	
1P1	288420		292871		354901	
1P2	289998	283053	302368	297527	382503	374607
1P3	270740		297341		386417	

The full load-deflection curves were generated for cylinders cured for 7 days (Figure 4-8 to Figure 4-11) due to the fact that an MTS compression machine was used. Figure 4-12 to Figure 4-15 represent the curves for the cylinders tested after 14 days of curing. As for the 28 days curing, Figure 4-16 through Figure 4-19 shows the load-displacement curves. But since the load cell is trying to engage the specimen, the graphs showed some anomaly in the early stages of loading. Other machines were used to confirm the peak load of the specimen and it yielded very close results. As for the calculation of the stiffness, it was conducted over the linear portion of the rising part of the curves as demonstrated in Figure 3-15. The following graphs represent the load-deflection curves for the different percentages of different fibers.

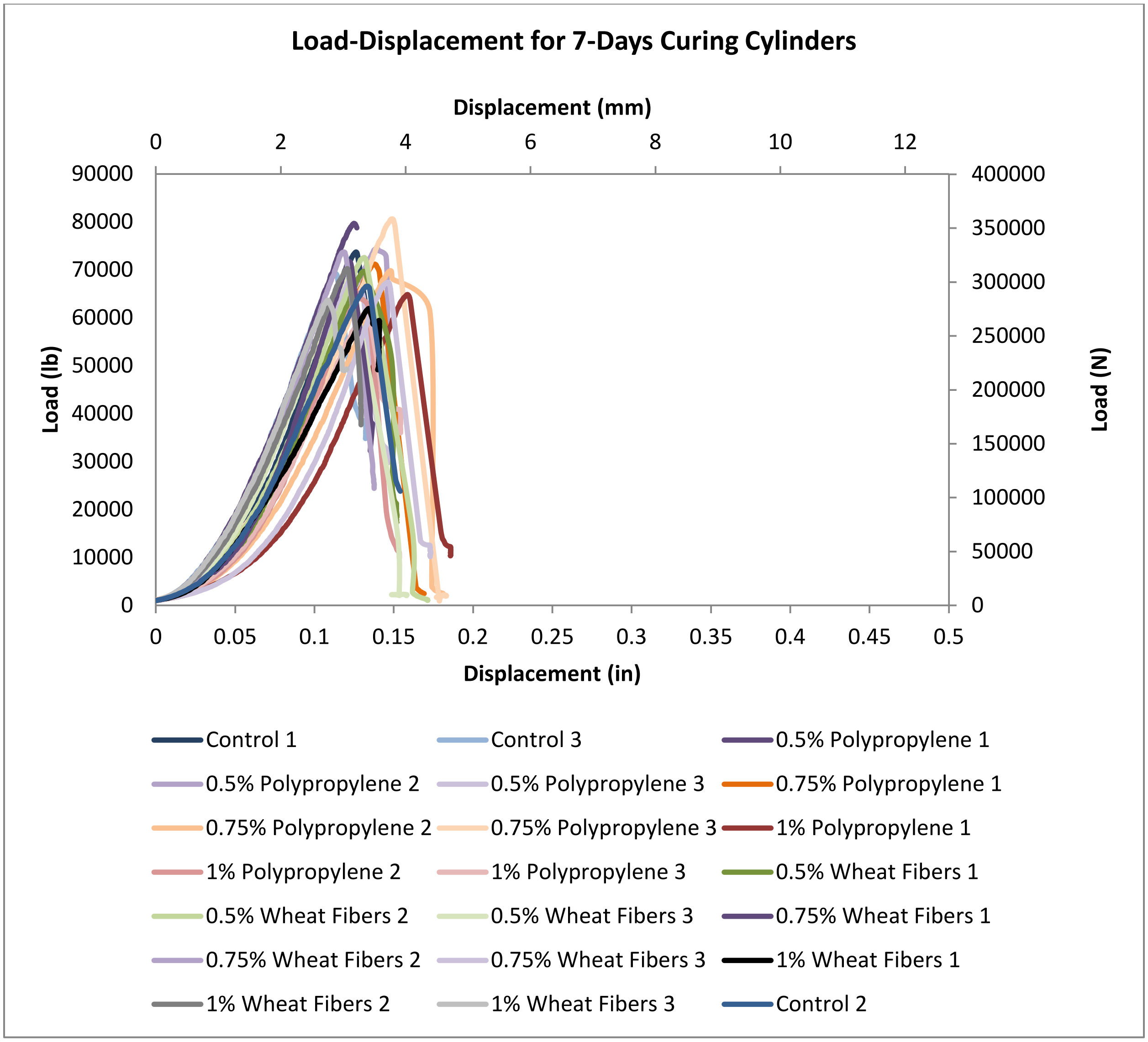

Figure 4-8: All Concrete Cylinders Tested After 7-Days Curing.

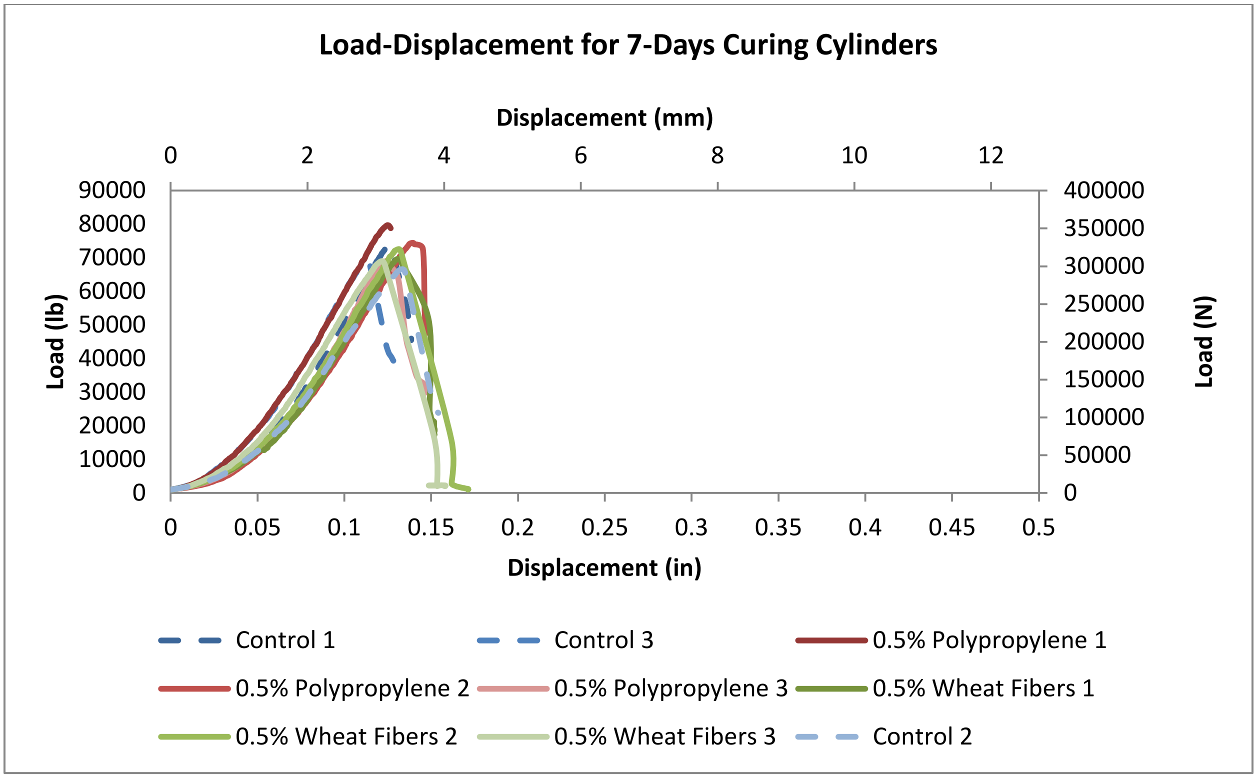

Figure 4-9: Cylinders with 0.5% Fiber vs. Control Tested After 7-Days Curing.

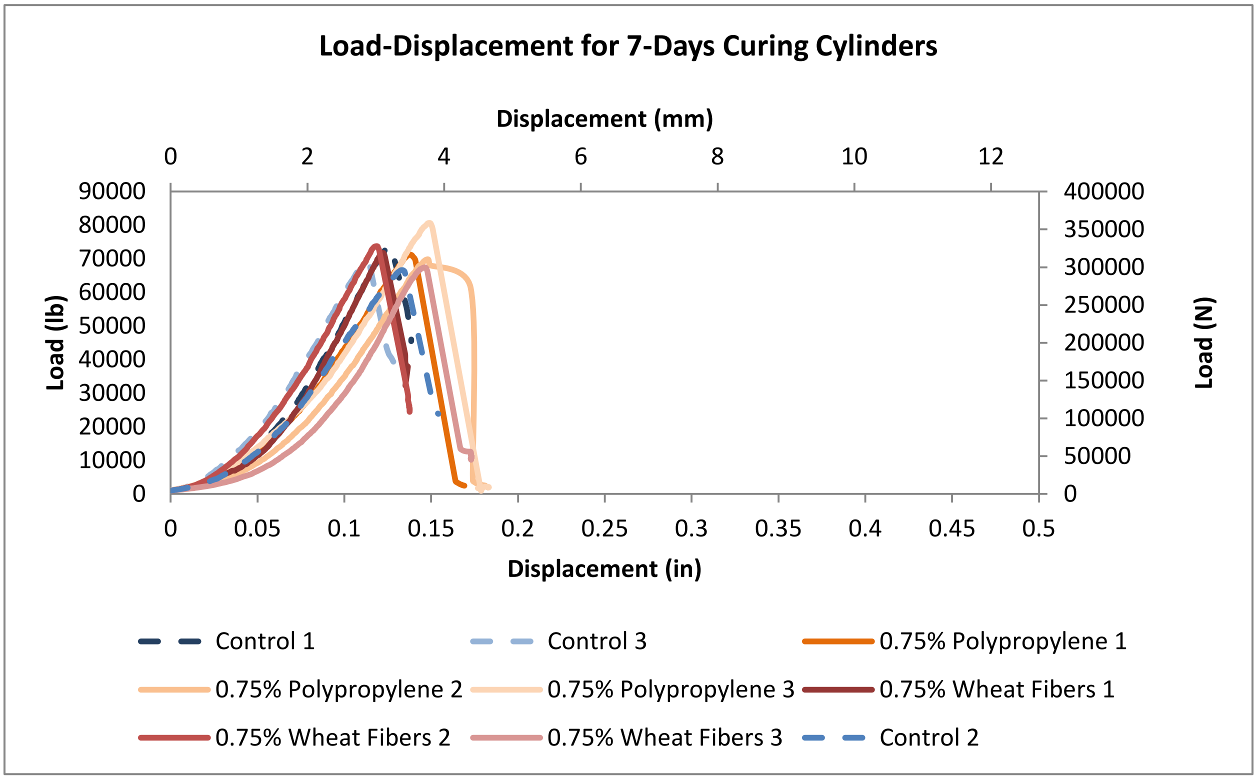

Figure 4-10: Cylinders with 0.75% Fiber vs. Control Tested After 7-Days Curing.

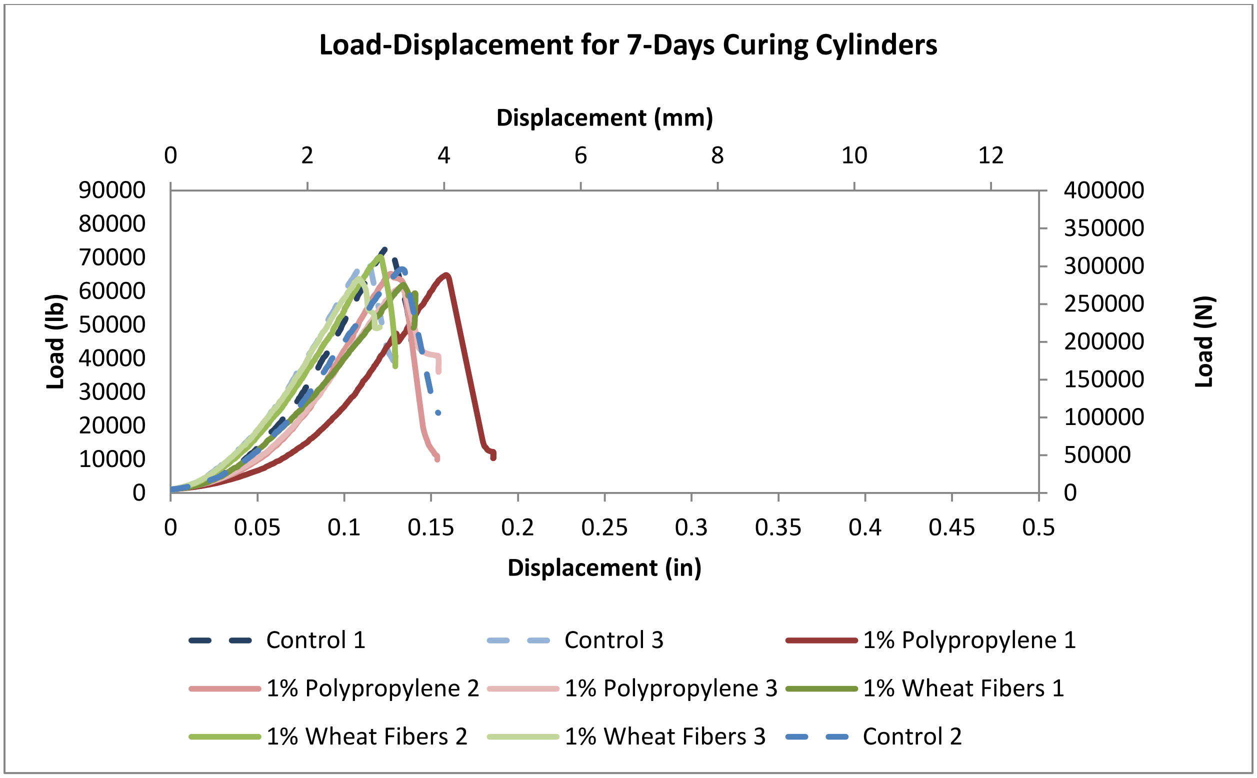

Figure 4-11: Cylinders with 1% Fiber vs. Control Tested After 7-Days Curing.

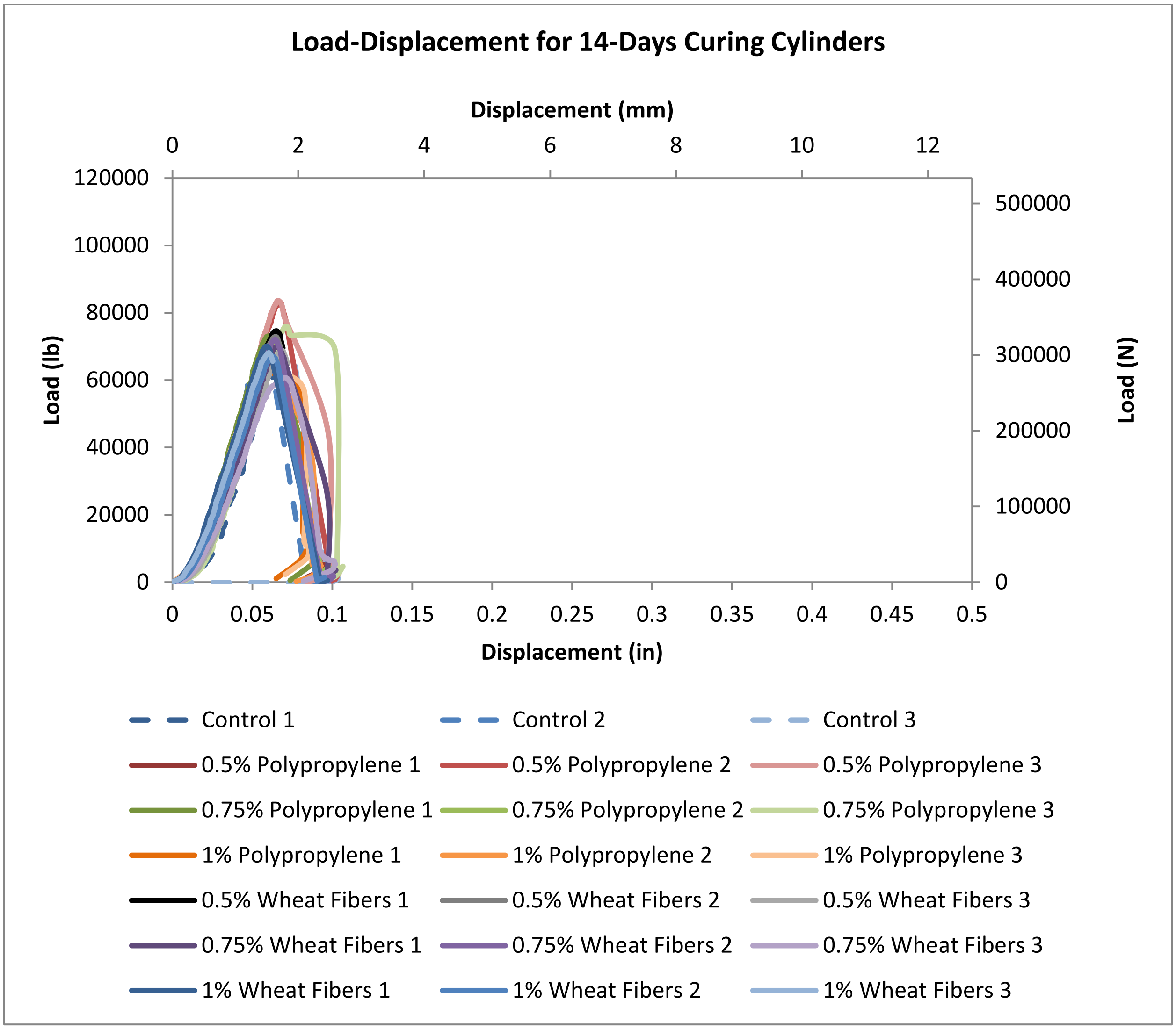

Figure 4-12: All Concrete Cylinders Tested After 14-Days Curing.

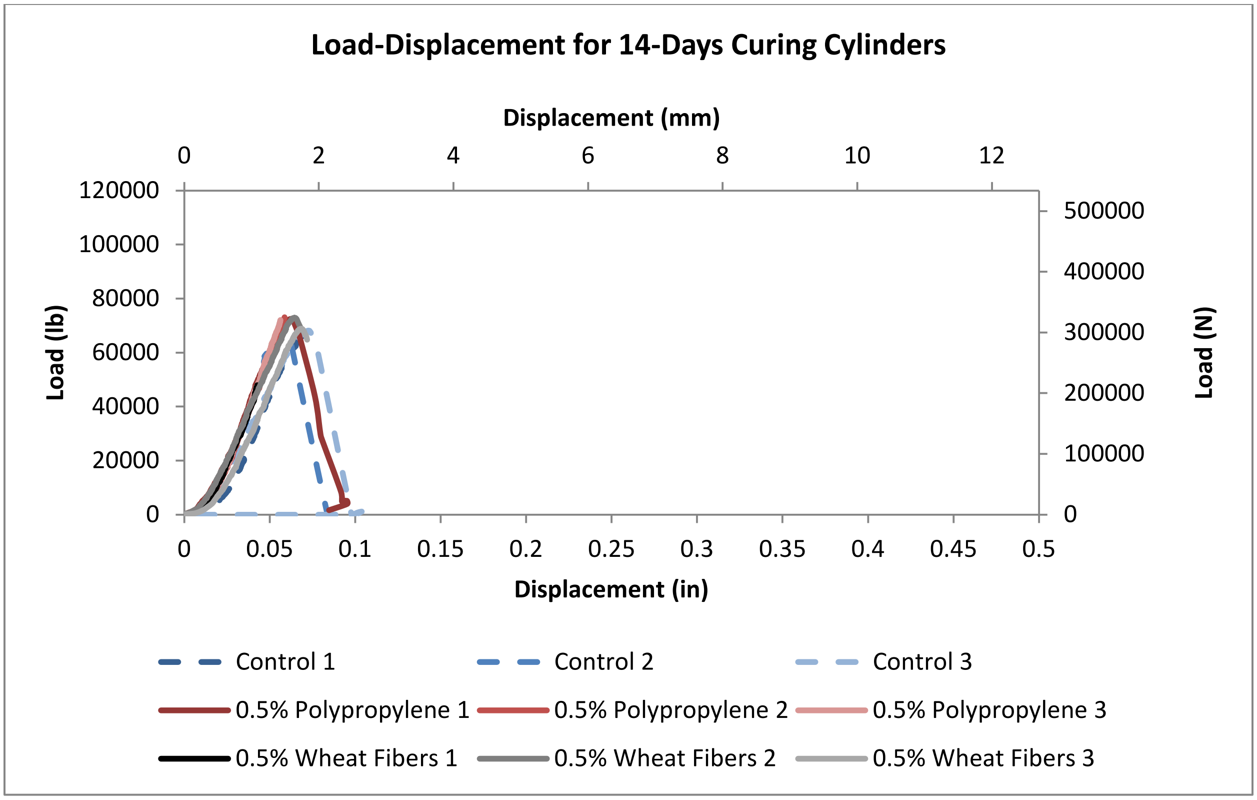

Figure 4-13: Cylinders with 0.5% Fiber vs. Control Tested After 14-Days Curing.

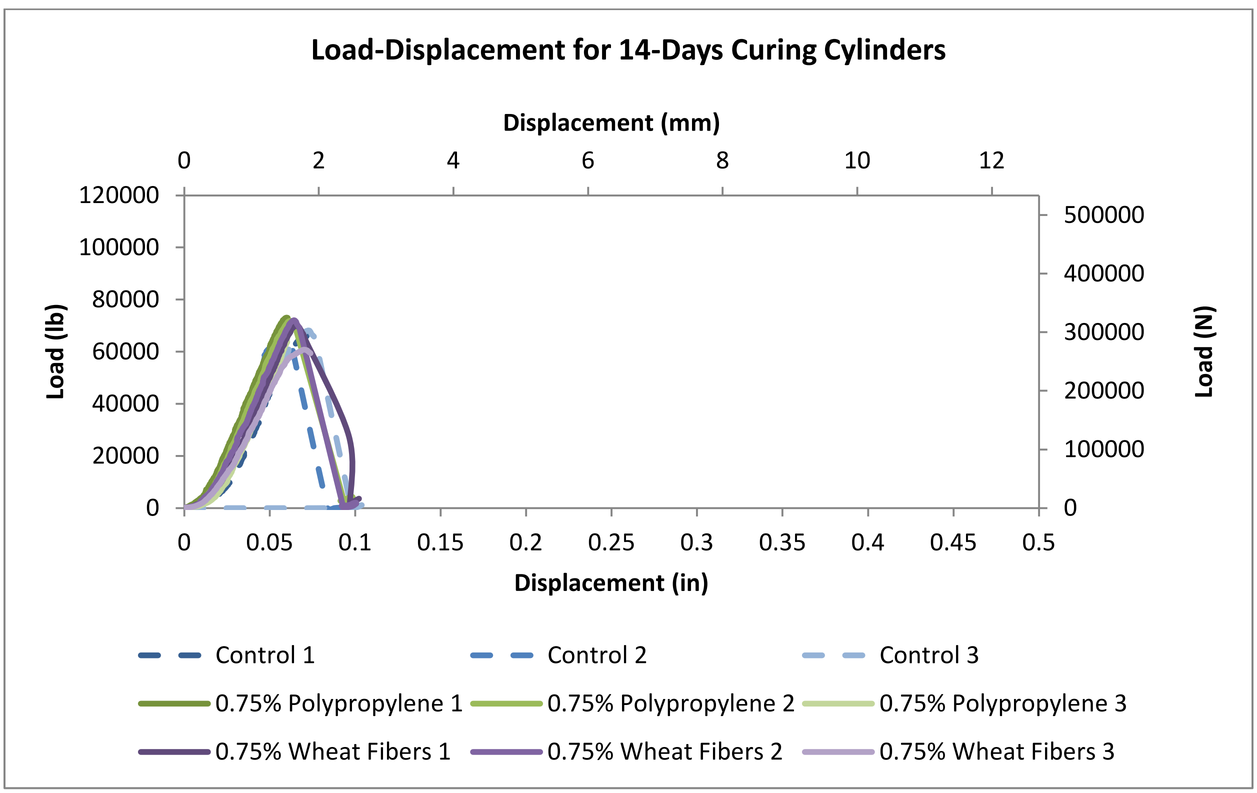

Figure 4-14: Cylinders with 0.75% Fiber vs. Control Tested After 14-Days Curing.

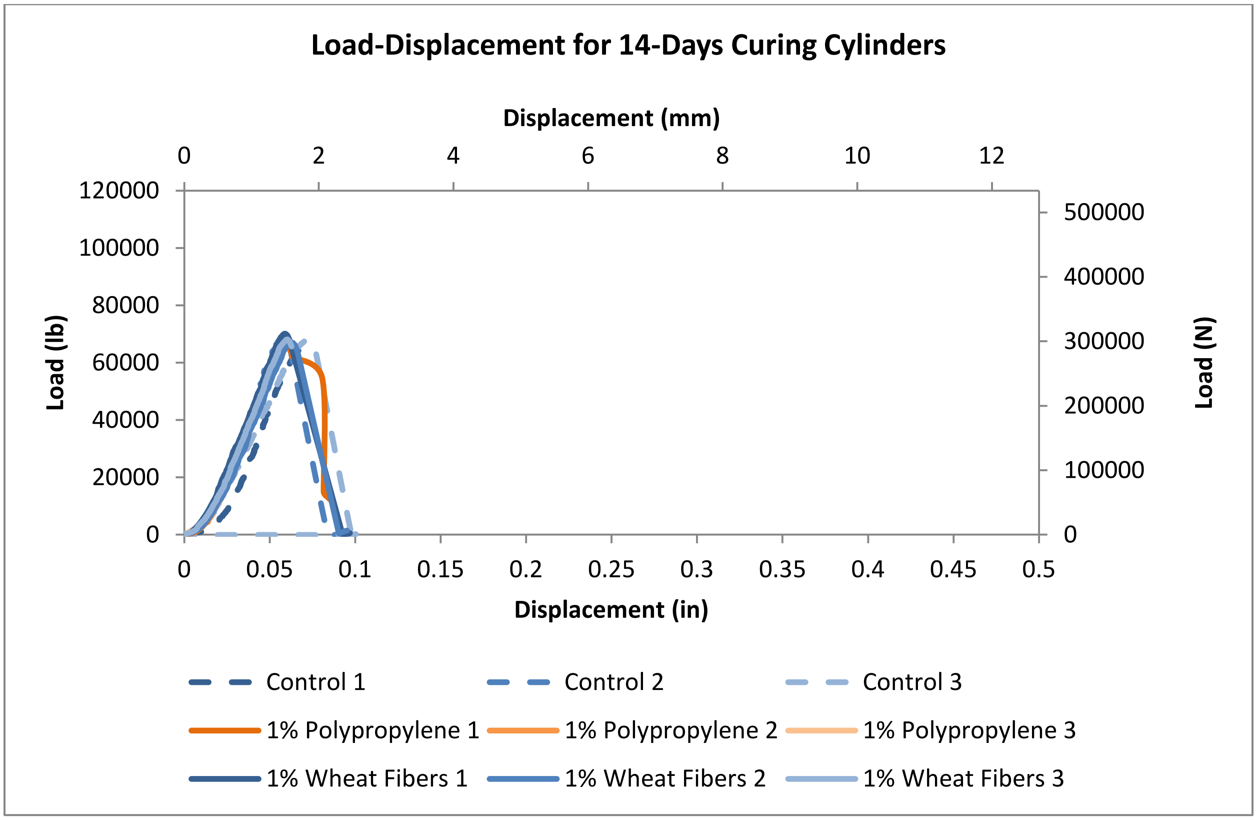

Figure 4-15: Cylinders with 1% Fiber vs. Control Tested After 14-Days Curing.

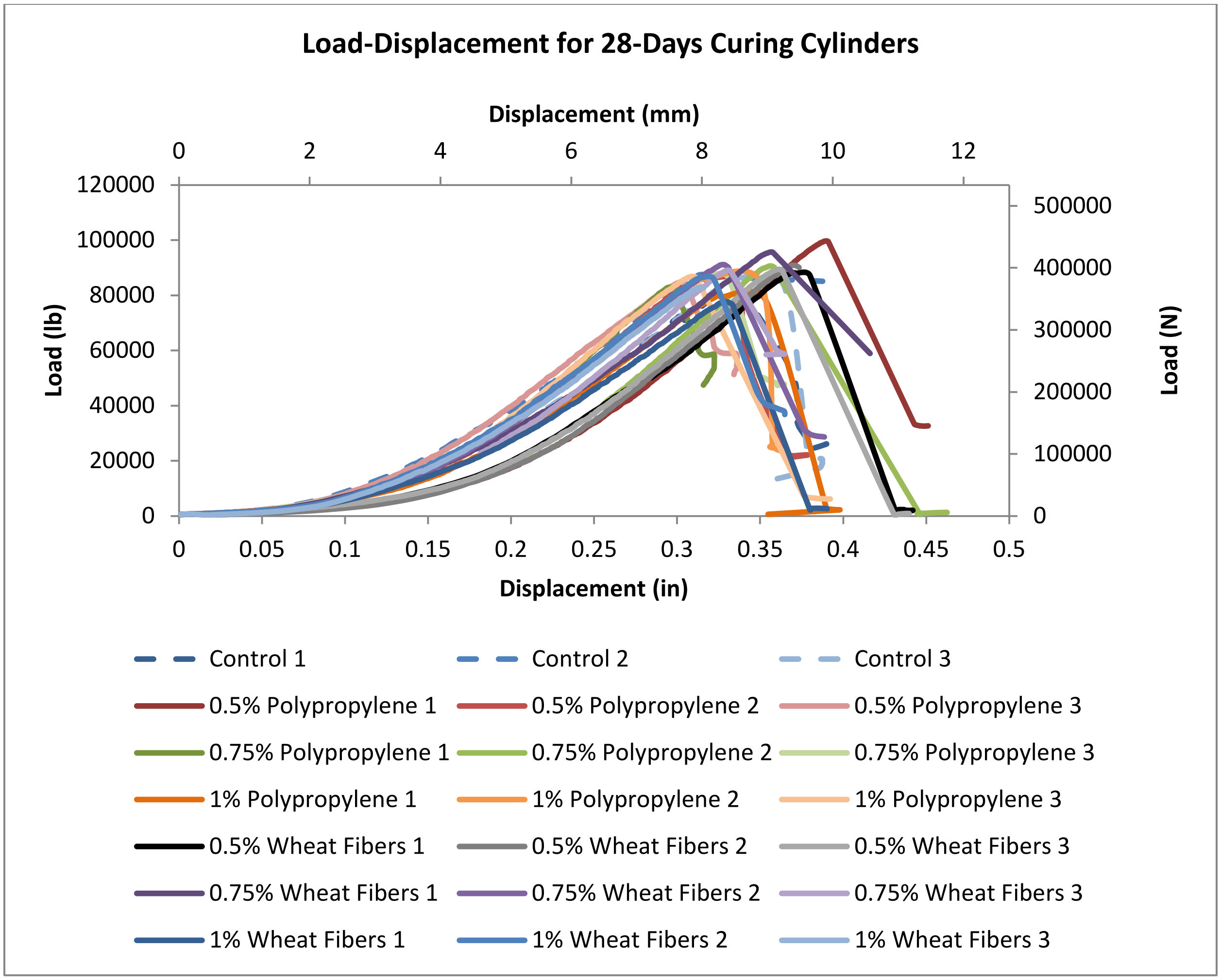

Figure 4-16: All Concrete Cylinders Tested After 28-Days Curing.

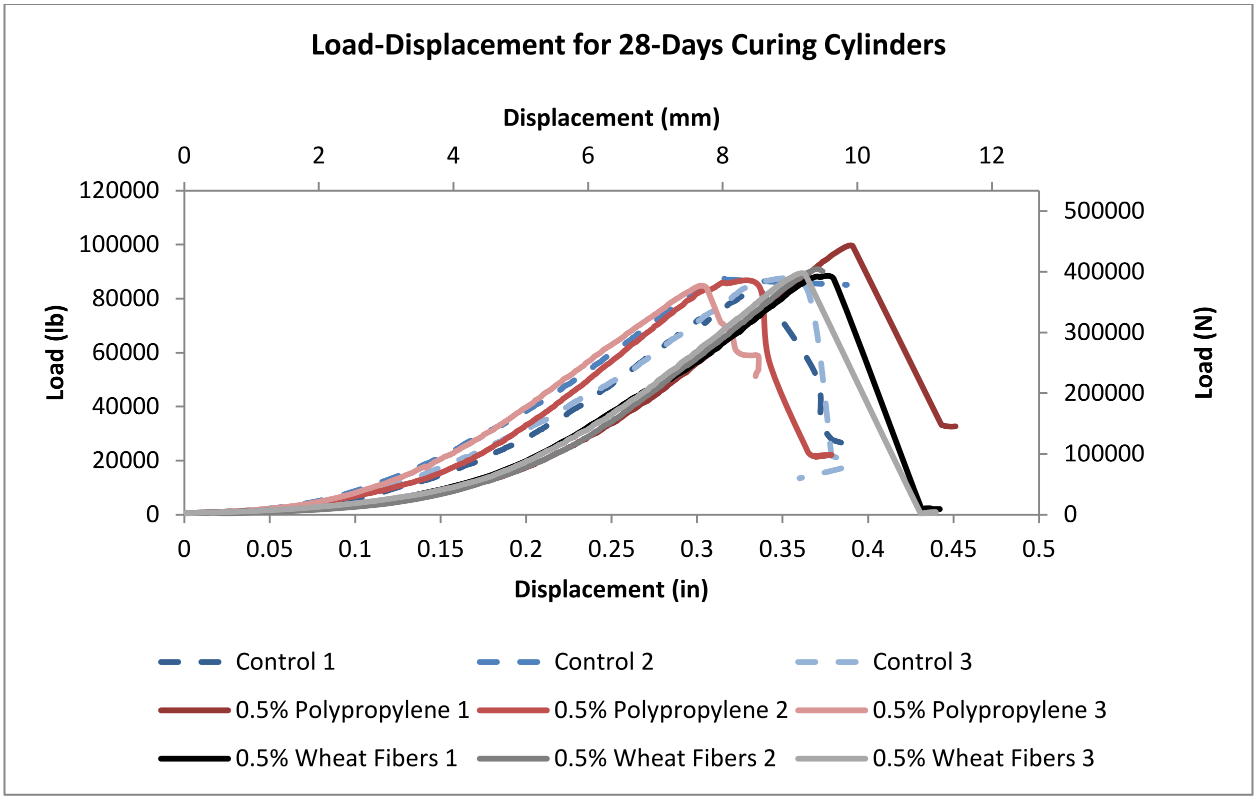

Figure 4-17: Cylinders with 0.5% Fiber vs. Control Tested After 28-Days Curing.

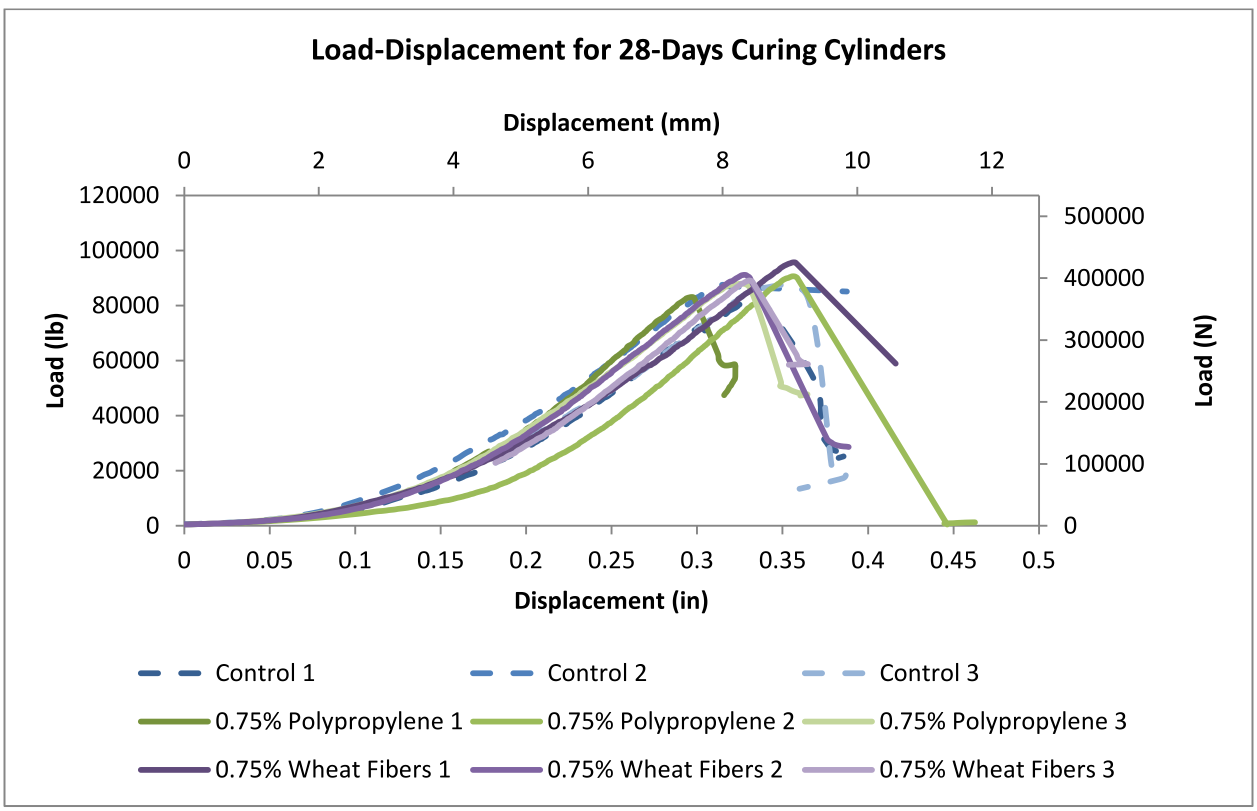

Figure 4-18: Cylinders with 0.75% Fiber vs. Control Tested After 28-Days Curing.

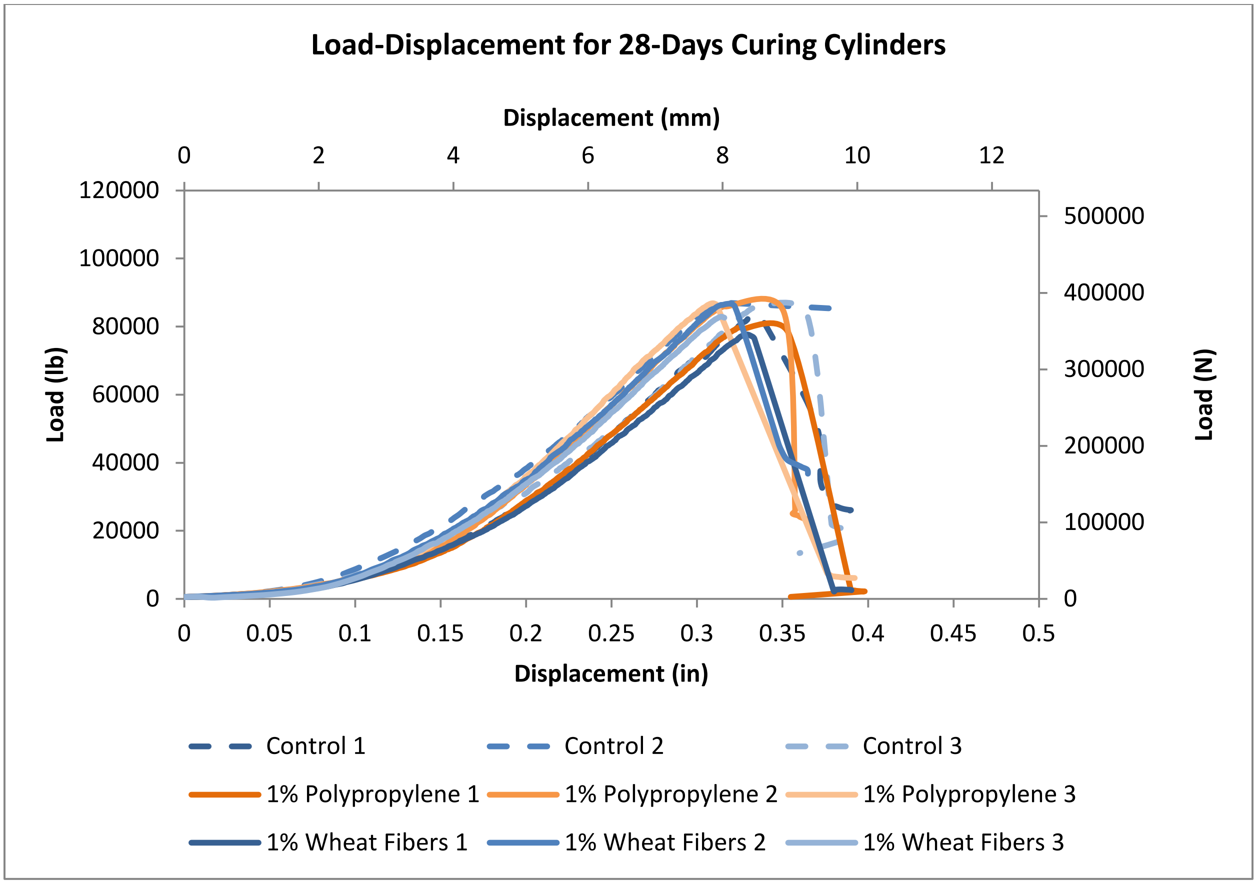

Figure 4-19: Cylinders with 1% Fiber vs. Control Tested After 28-Days Curing.

Similar to what was done in CHAPTER 3 -, the following graphs were developed (Figure 4-20 and Figure 4-21) in order to present maximum, minimum, and average increasing or decreasing trends with the increasing amount of fibers based on the measured peak loads and calculated stiffness for the 28 day cured cylinders. In these figures, the lines are connecting the average peak loads or stiffness in uniaxial compression, while the vertical lines with the tick marks represent the maximum, minimum, and middle values.

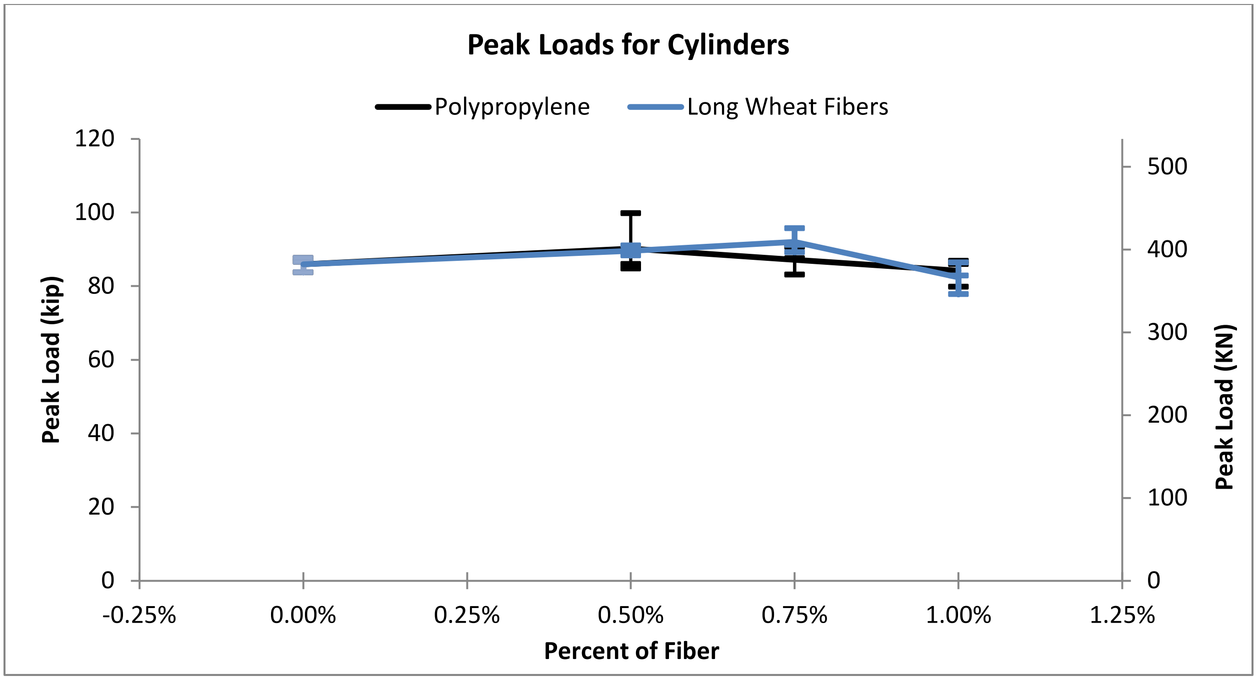

Figure 4-20: Peak Loads at 28 Days for Cylinders Containing Different Percentages of Different Fibers.

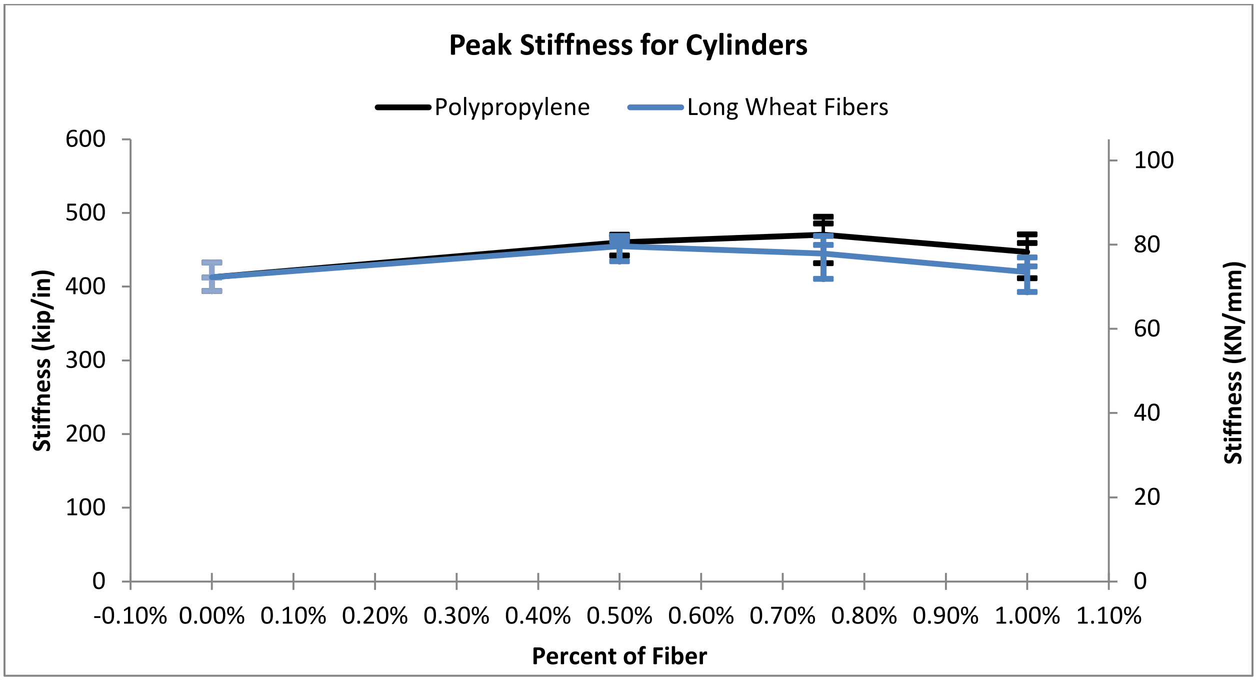

Figure 4-21: Stiffness Peaks at 28 Days for Cylinders with Different Percentages of Different Fibers.

Since these cylinders all share the same control specimens, it can be seen that the trend is clear but to be consistent with what have been presented in CHAPTER 3 -, the peak load and stiffness results were normalized by dividing the peak load or the stiffness of each specimen by the average load or stiffness of the control specimens (Figure 4-22 and Figure 4-23). In these figures, the lines are connecting the average peak load or stiffness increase relative to the average of its control in uniaxial compression, while the vertical lines with the tick marks represent the maximum, minimum, and middle values in term of relative uniaxial compression peak load or stiffness. Table 4-7 represents the average increase in both load and stiffness for the cylinders with the different percentages and different fibers.

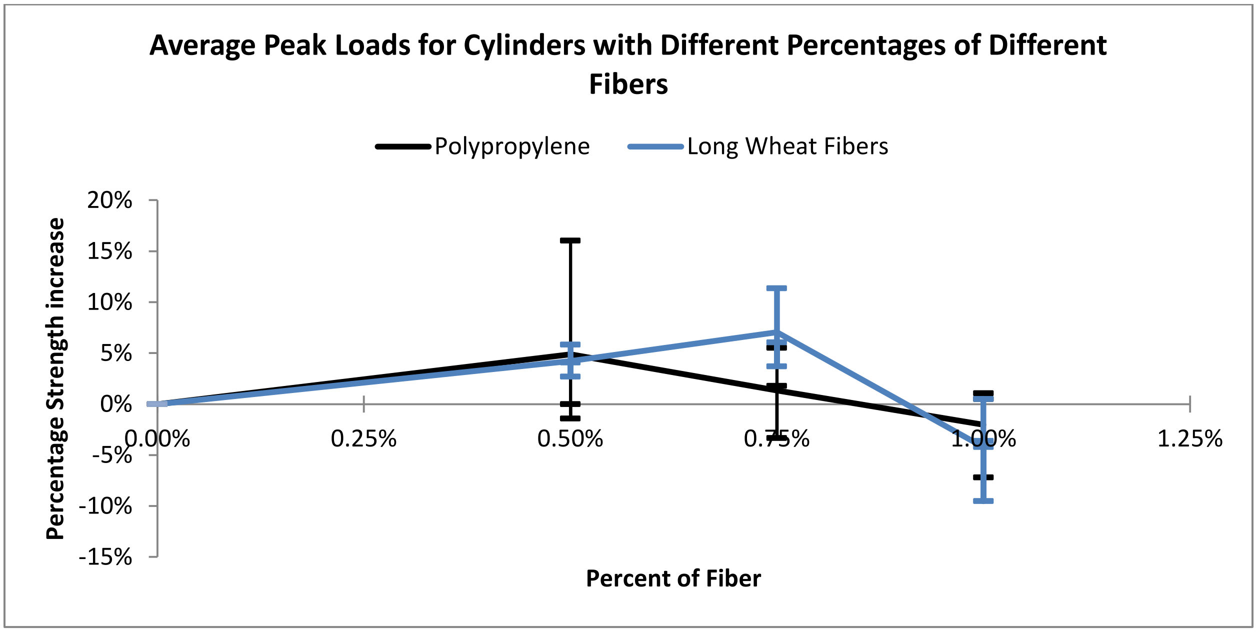

Figure 4-22: Average Peak Loads at 28 Days for Cylinders with Different Percentages of Different Fibers.

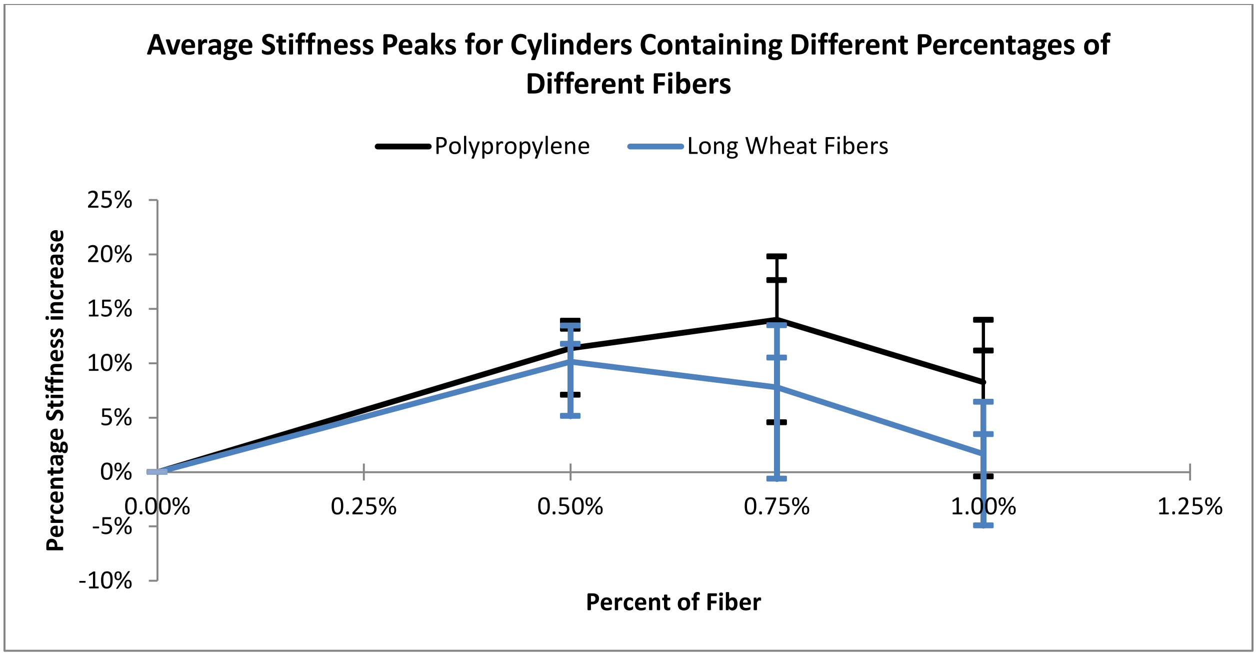

Figure 4-23: Average Stiffness Peaks at 28 Days for Cylinders with Different Percentages of Different Fibers.

Table 4-7: Average Increase in the Load and Stiffness for Cylinders with Different Amount of Different Fibers.

Volume % Fiber	**Long Wheat Fibers**		**Polypropylene Fibers**	
	Avg. Load Increase	Avg. Stiffness Increase	Avg. Load Increase	Avg. Stiffness Increase
0%	0%	0%	0%	0%
0.50%	4%	10%	5%	11%
0.75%	7%	8%	1%	14%
1%	-4%	2%	-2%	8%

4.5.1.2 Cyclic Testing Result:

The full load-Strain curves were generated for cylinders cured for 28 days due to the fact that strain gages were mounted on each cylinder that was tested in cyclic loading. Figure 4-25, Figure 4-27, Figure 4-29, Figure 4-31, Figure 4-33, Figure 4-35 and Figure 4-37 represent the cycles with the failure curve for the cylinders tested in cyclic then failed in monotonic loading. As for the cycles only, Figure 4-24, Figure 4-26, Figure 4-28, Figure 4-30, Figure 4-32, Figure 4-34 and Figure 4-36 shows the load-strain curves for three cycles at each of the three load levels. As for the calculation of the stiffness, it was conducted over the linear portion of the rising part of the first cycle.

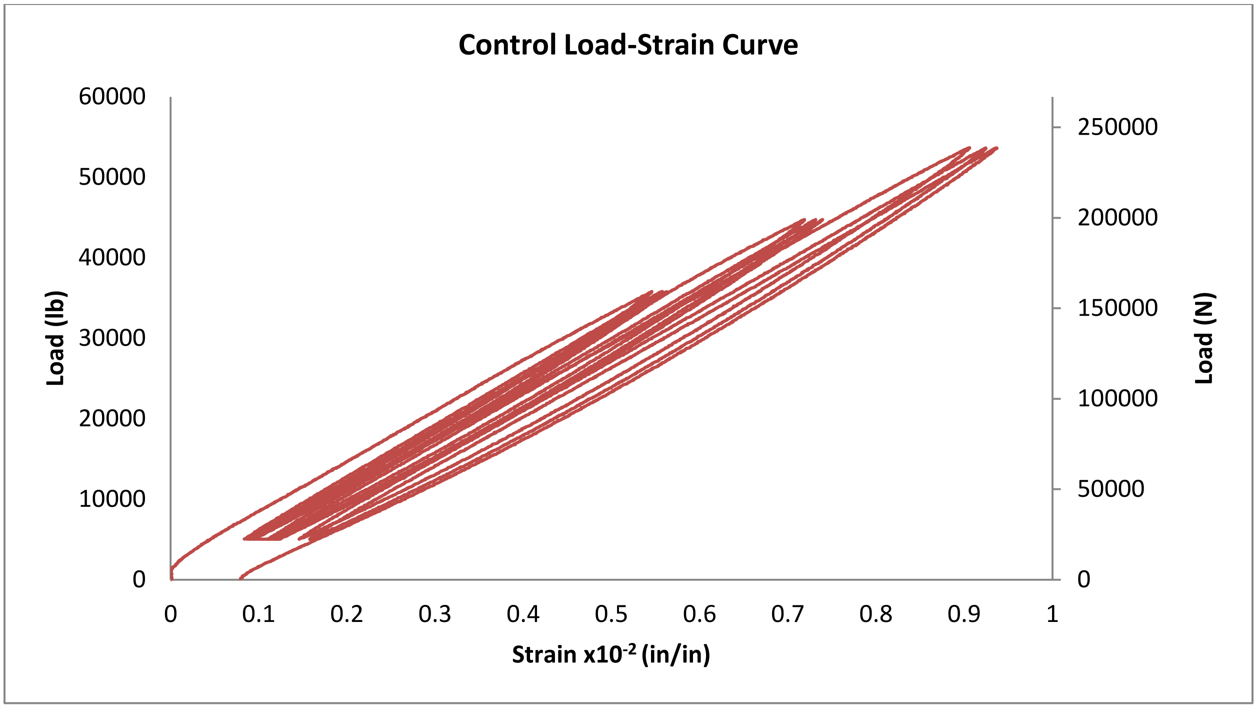

Figure 4-24: Cycles for the Control Cylinder.

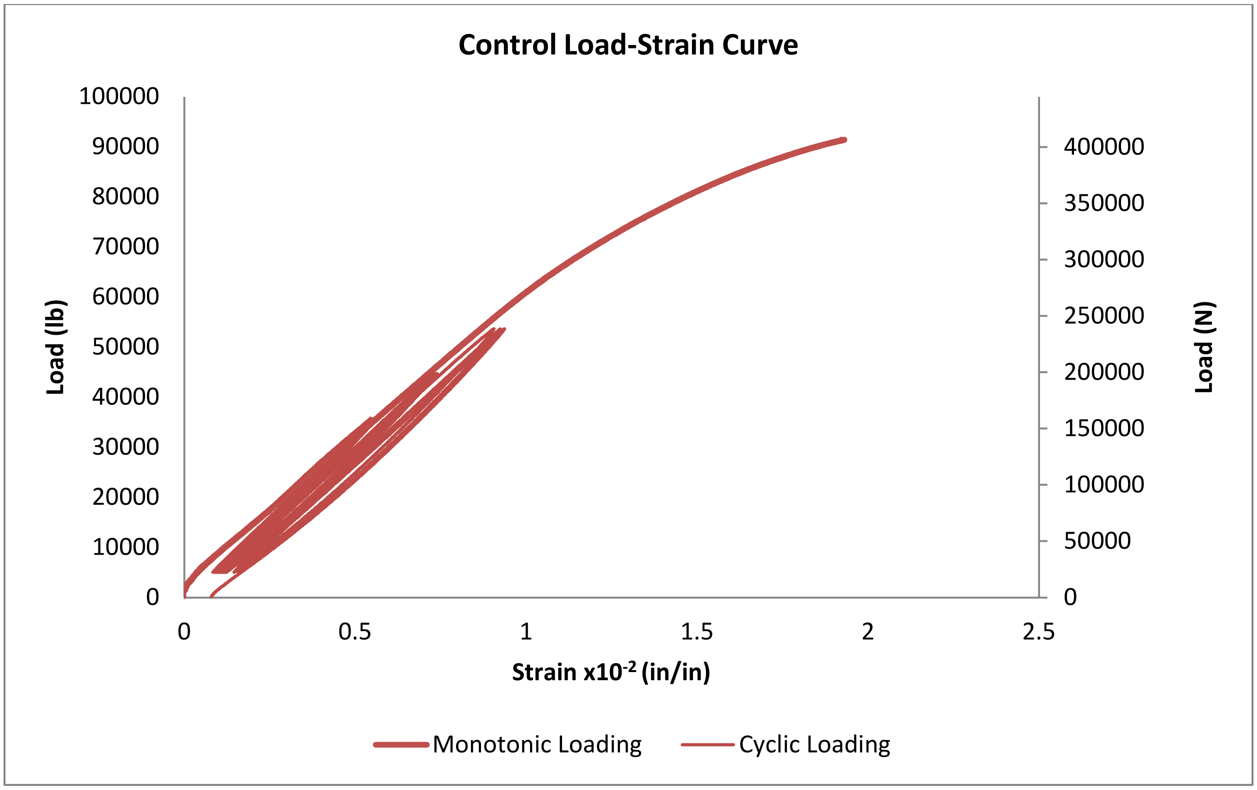

Figure 4-25: Cyclic with the Failure Curve for the Control Cylinder.

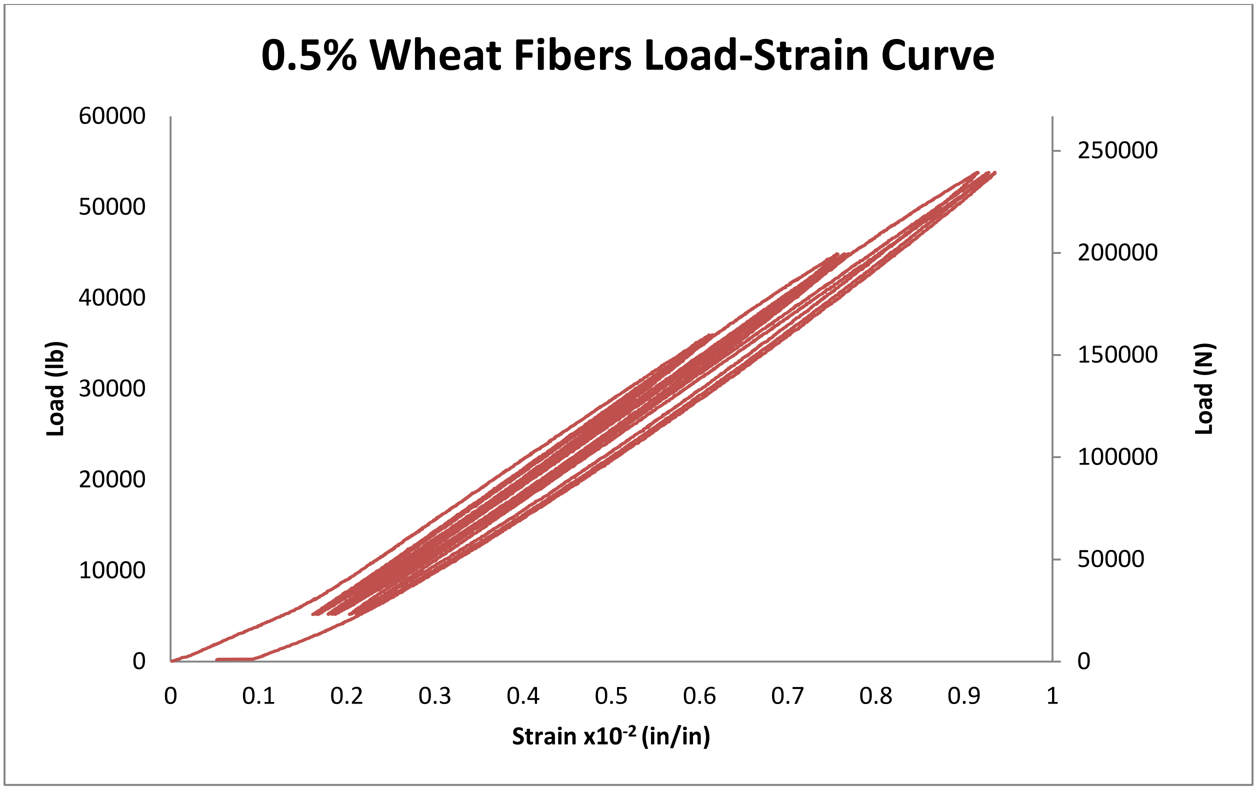

Figure 4-26: Cycles for the 0.5% Wheat Reinforced Cylinder.

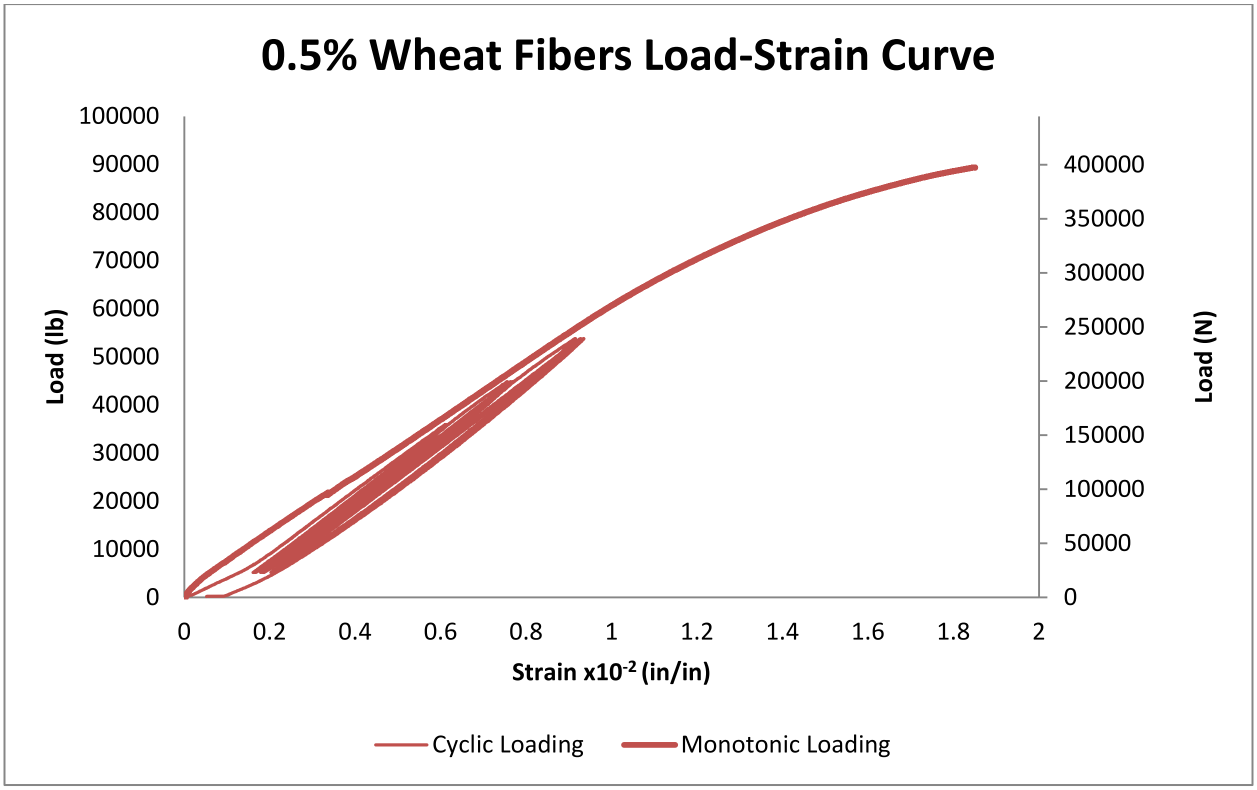

Figure 4-27: Cyclic with the Failure Curve for the 0.5% Wheat Reinforced Cylinder.

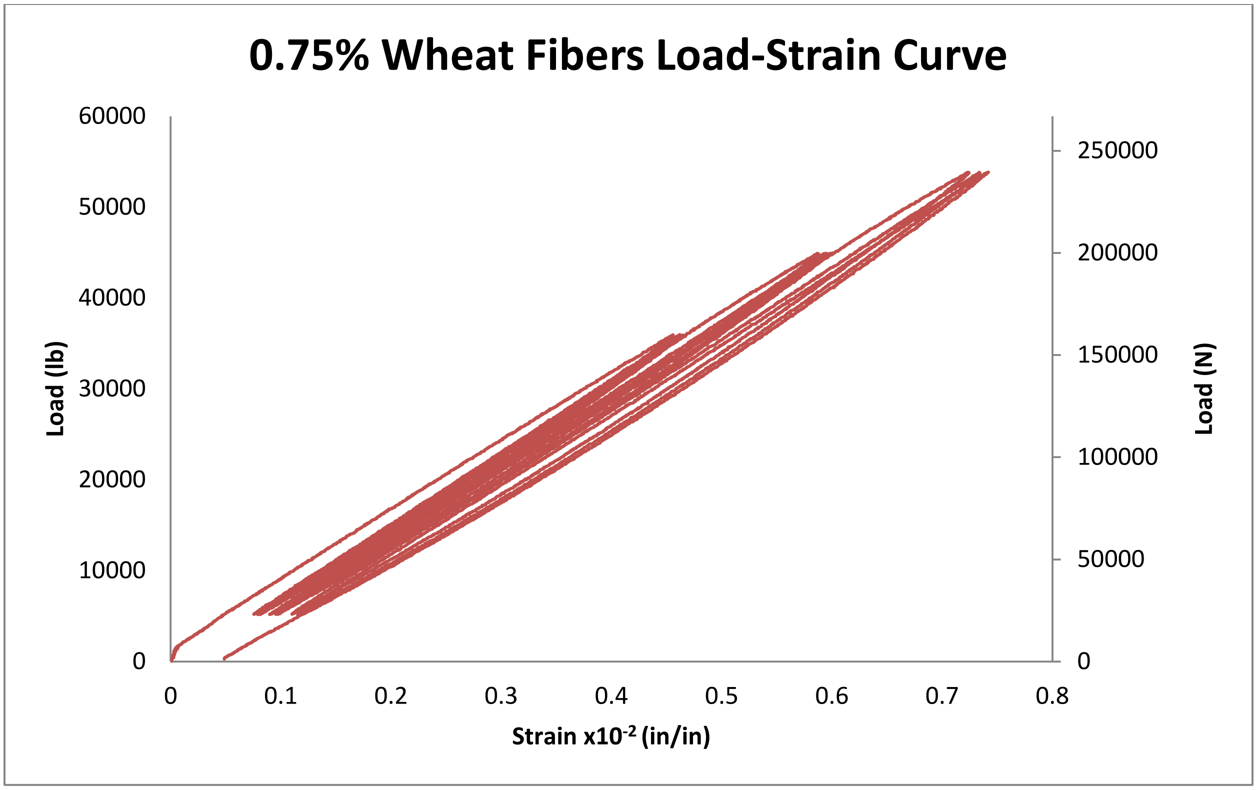

Figure 4-28: Cycles for the 0.75% Wheat Reinforced Cylinder.

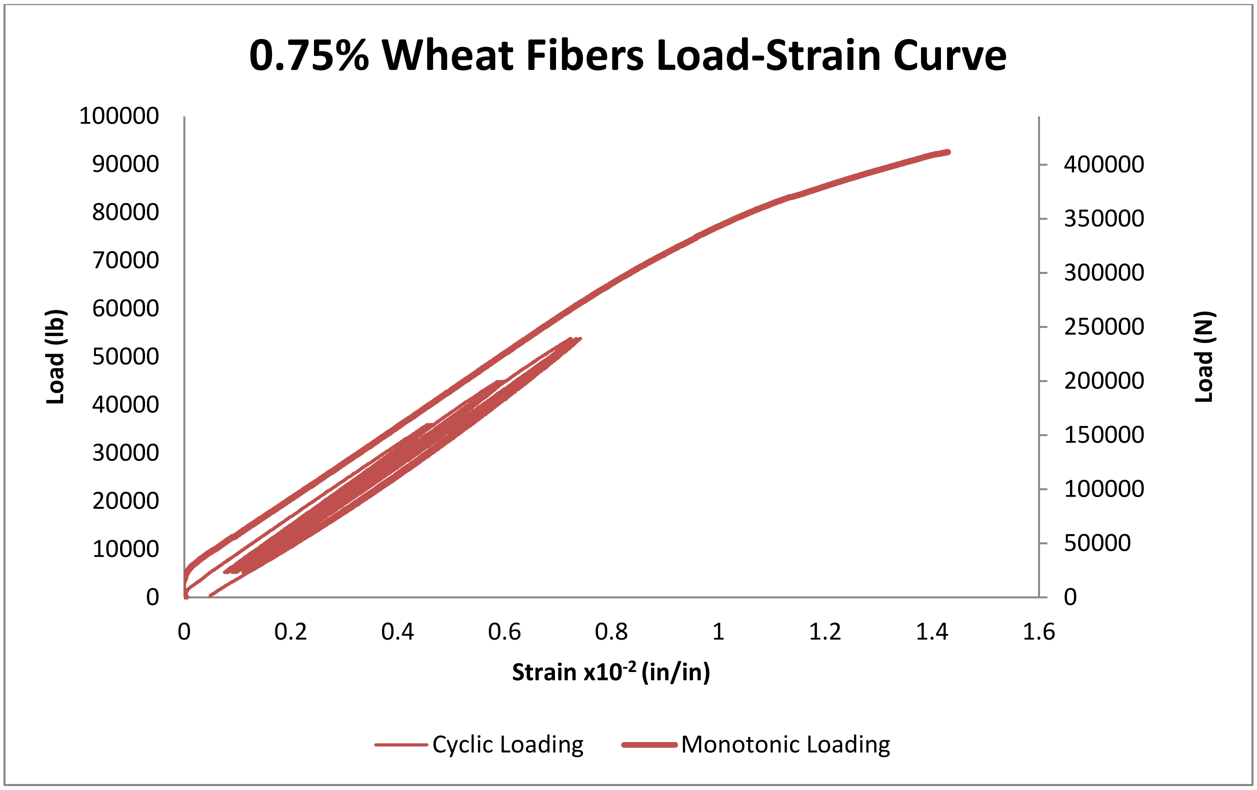

Figure 4-29: Cyclic with the Failure Curve for the 0.75% Wheat Reinforced Cylinder.

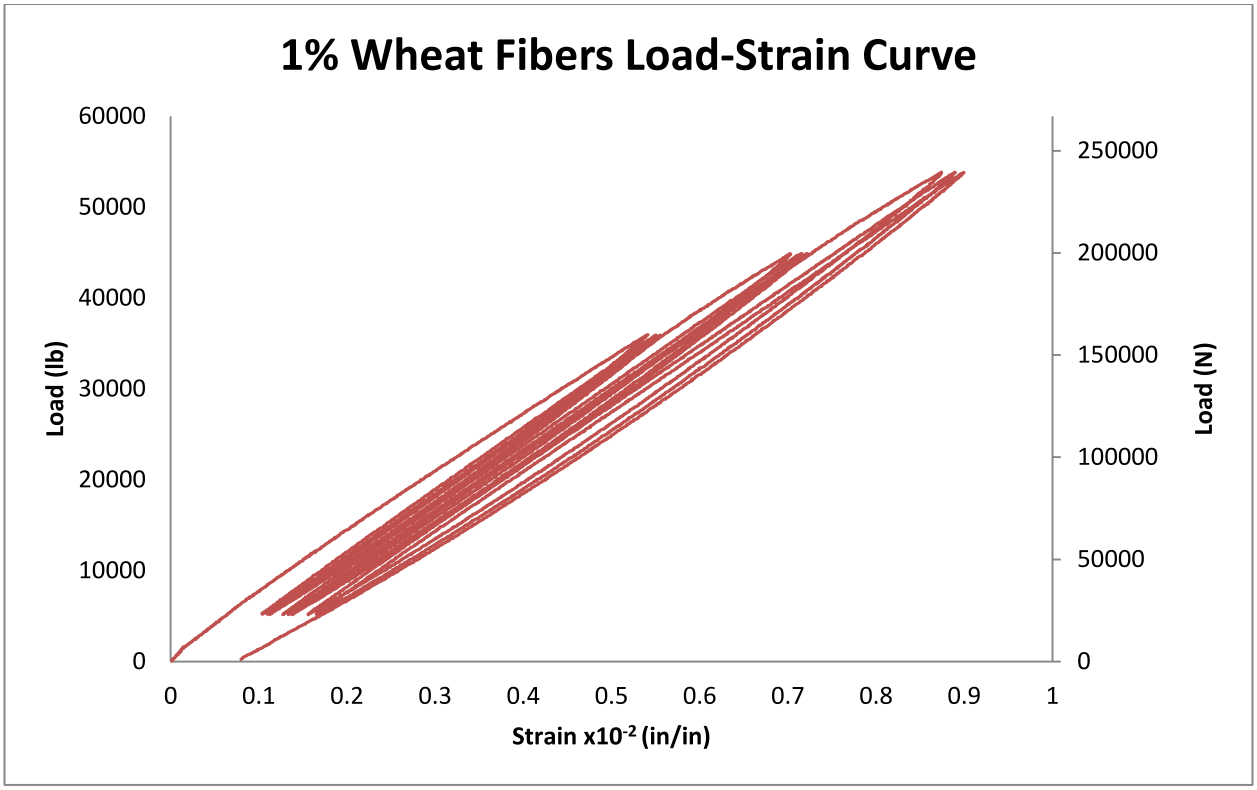

Figure 4-30: Cycles for the 1% Wheat Reinforced Cylinder.

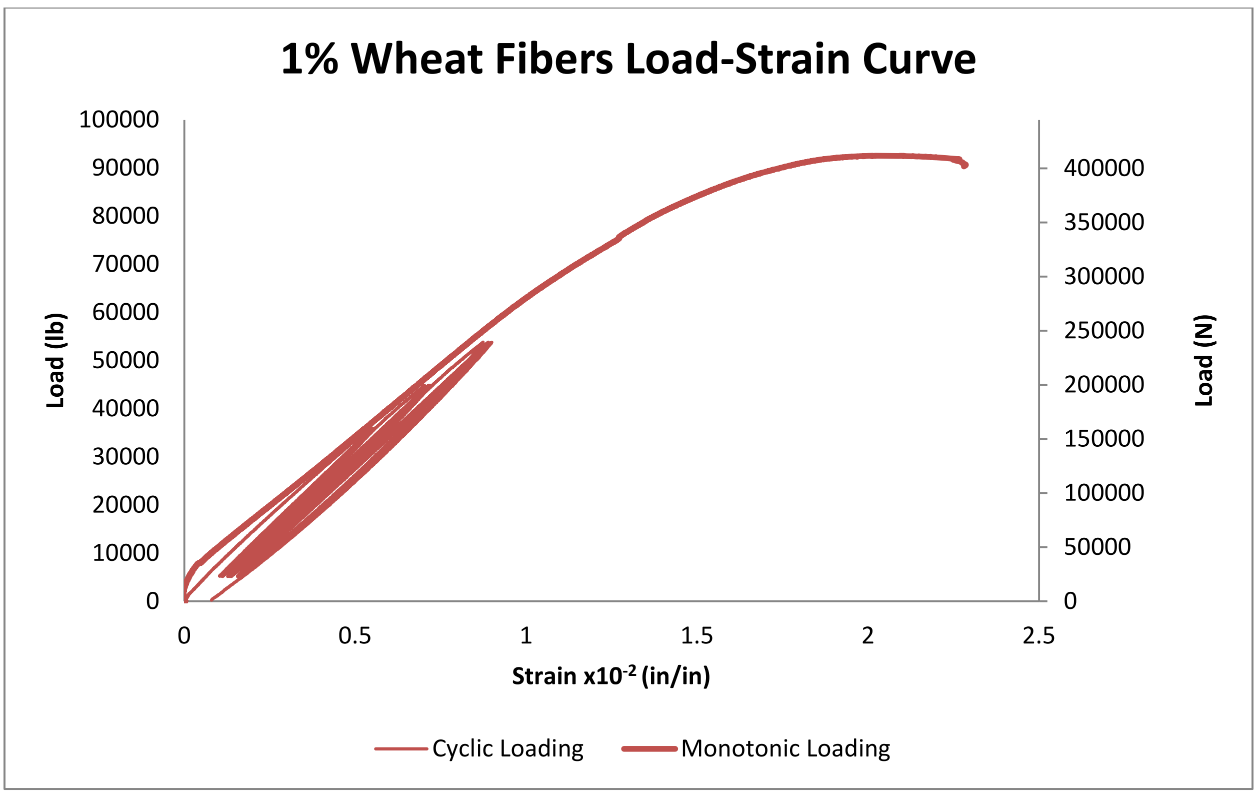

Figure 4-31: Cyclic with the Failure Curve for the 1% Wheat Reinforced Cylinder.

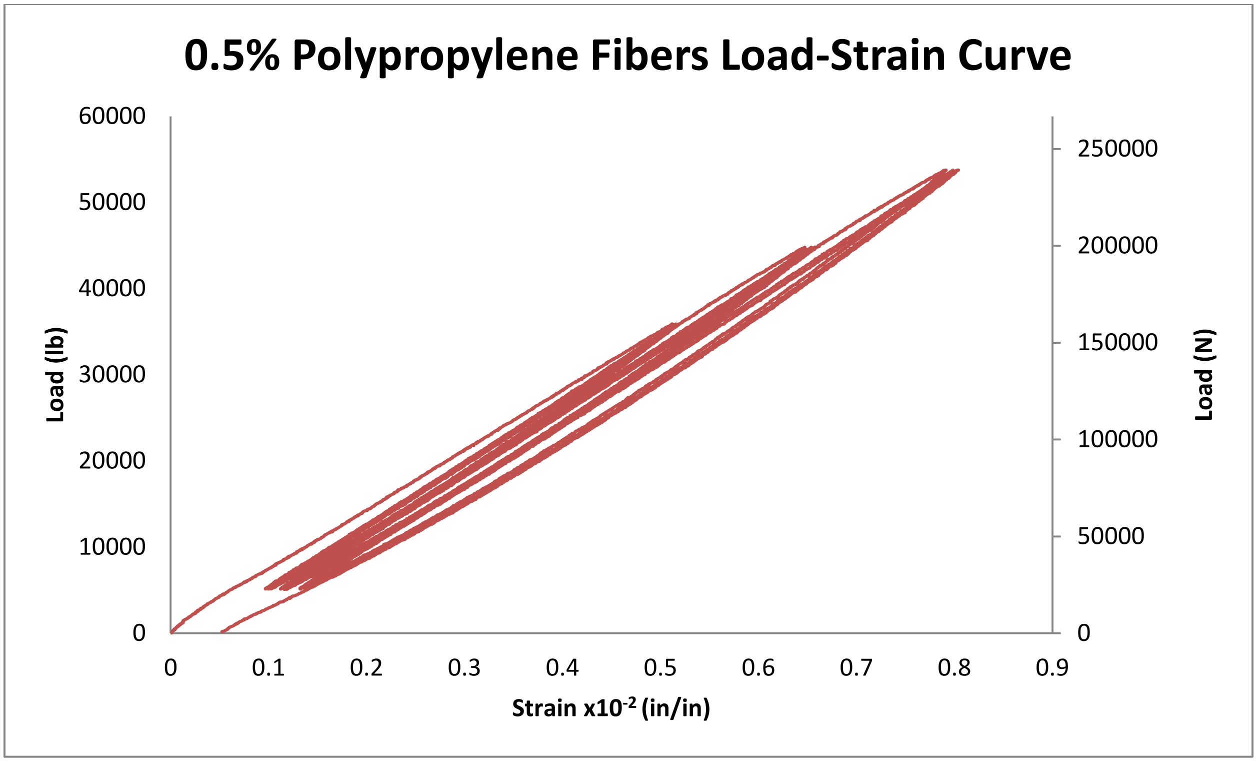

Figure 4-32: Cycles for the 0.5% Polypropylene Reinforced Cylinder.

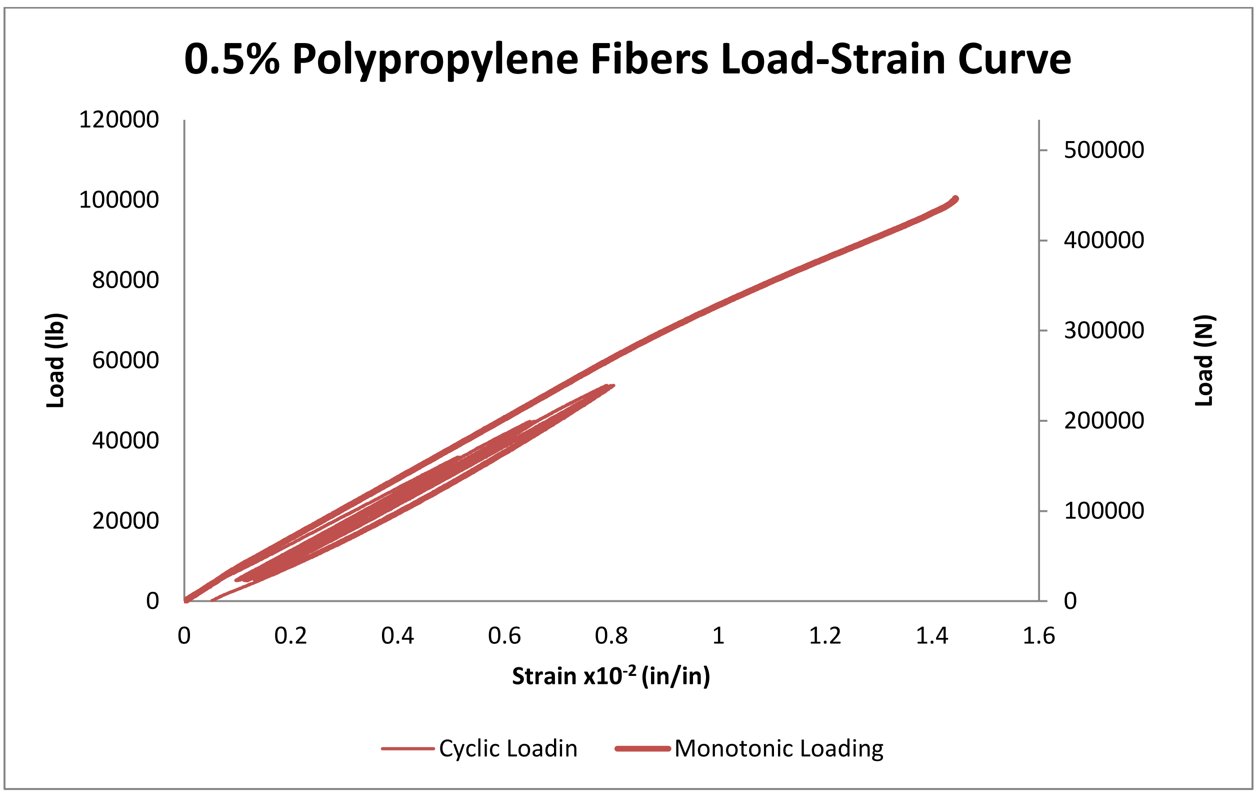

Figure 4-33: Cyclic with the Failure Curve for the 0.5% Polypropylene Reinforced Cylinder.

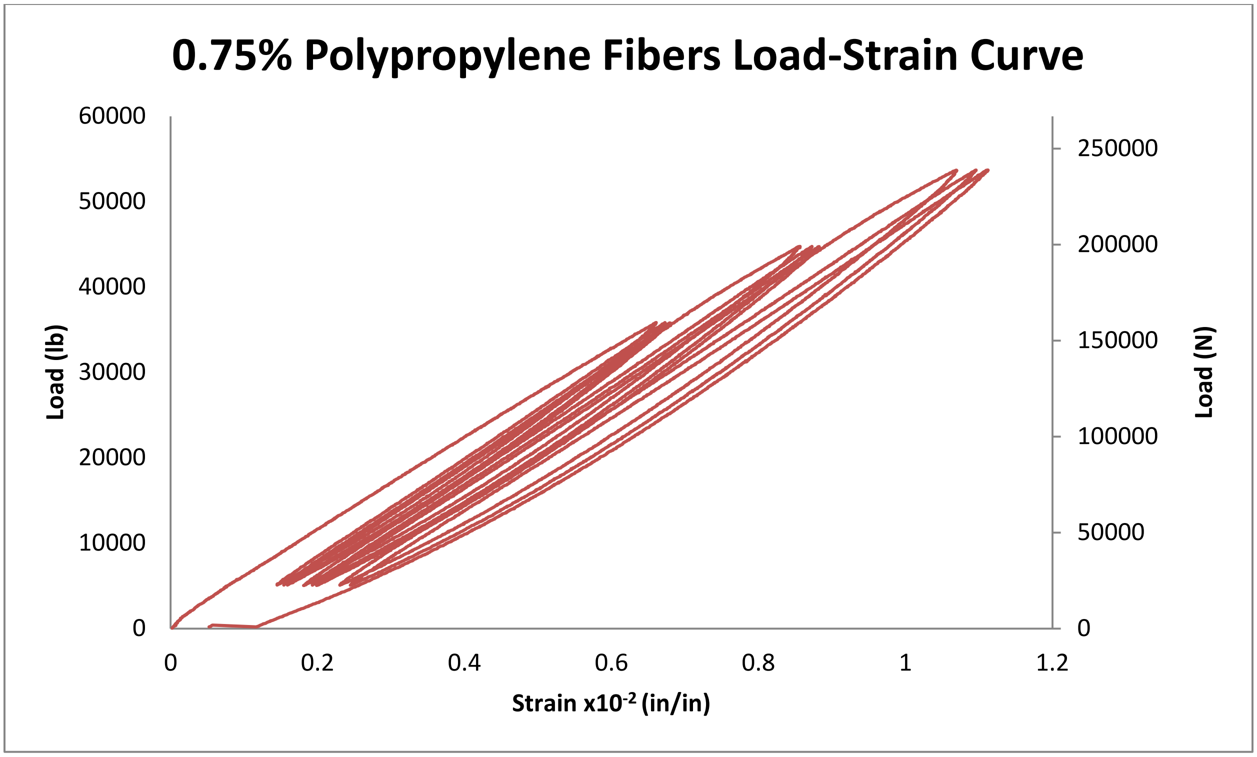

Figure 4-34: Cycles for the 0.75% Polypropylene Reinforced Cylinder.

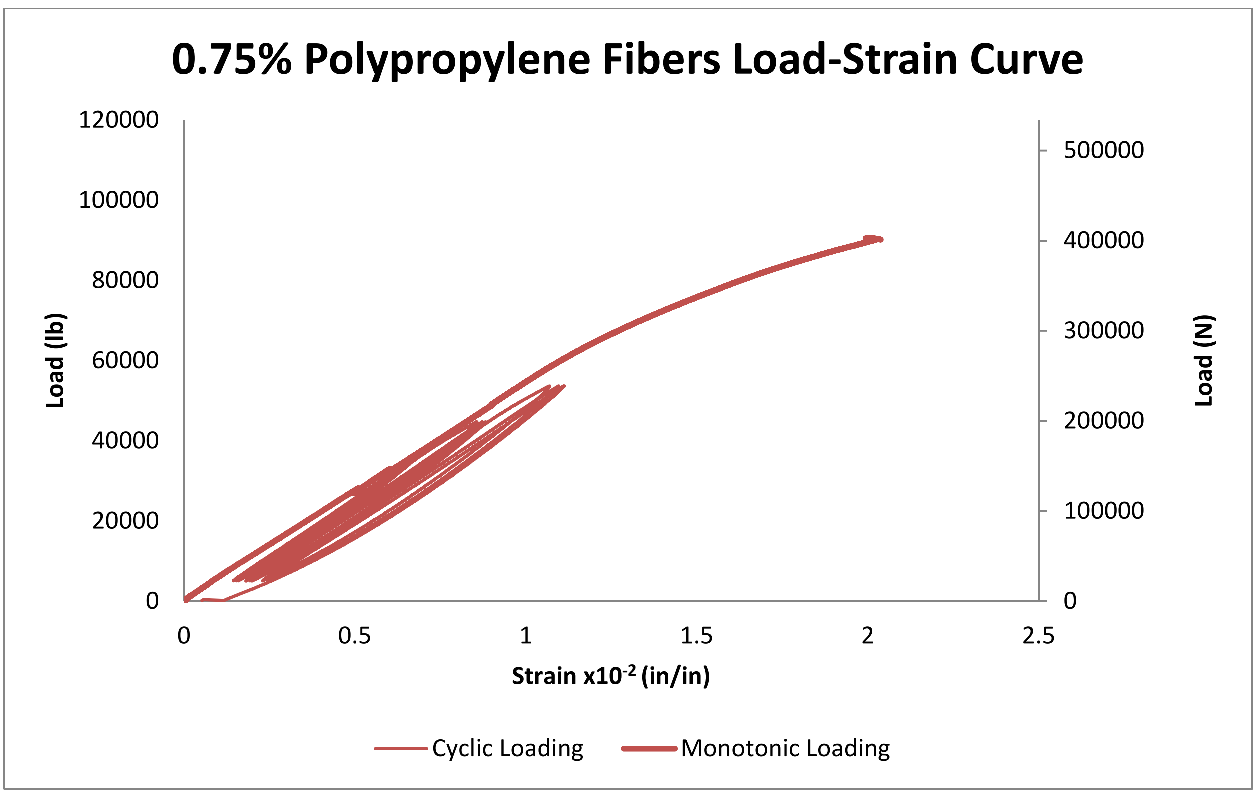

Figure 4-35: Cyclic with the Failure Curve for the 0.75% Polypropylene Reinforced Cylinder.

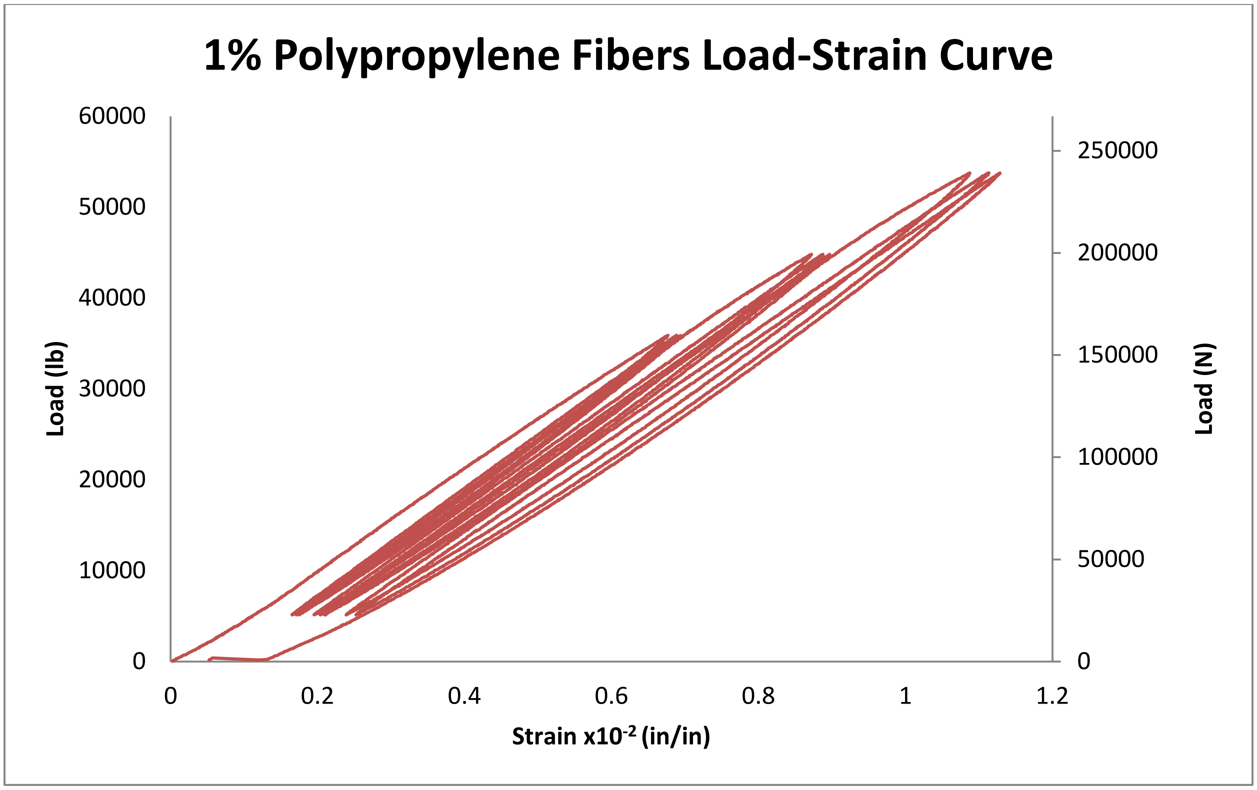

Figure 4-36: Cycles for the 1% Polypropylene Reinforced Cylinder.

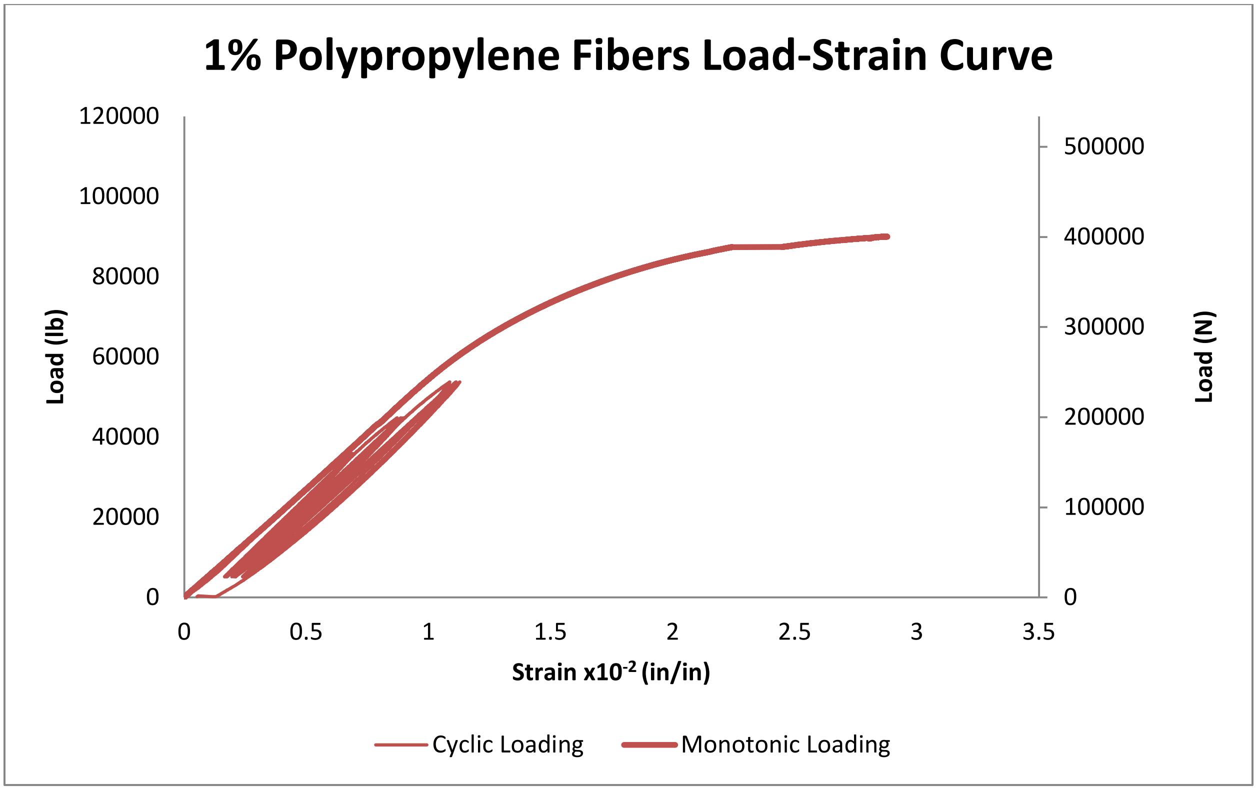

Figure 4-37: Cyclic with the Failure Curve for the 1% Polypropylene Reinforced Cylinder.

At each level of the cyclic load and based on each cycle the modulus of elasticity was calculated for all the specimens and the results are presented in Figure 4-38 versus the strain at the same cycle. Figure 4-39 represent the stiffness at each cycle strain level. Table 4-8 show a summary of the initial stiffness, initial modulus of elasticity and the ductility index for the cylinders reinforced with wheat fibers in cyclic loading.

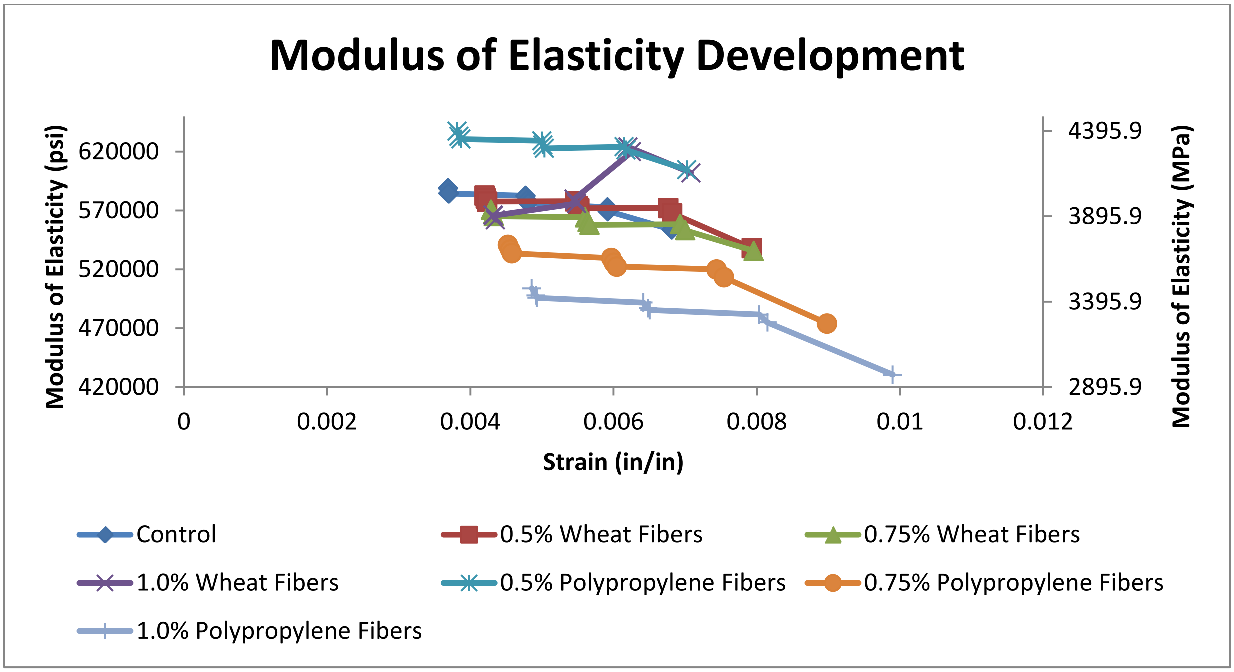

Figure 4-38: Modulus of Elasticity vs. Strain at Each Cycle.

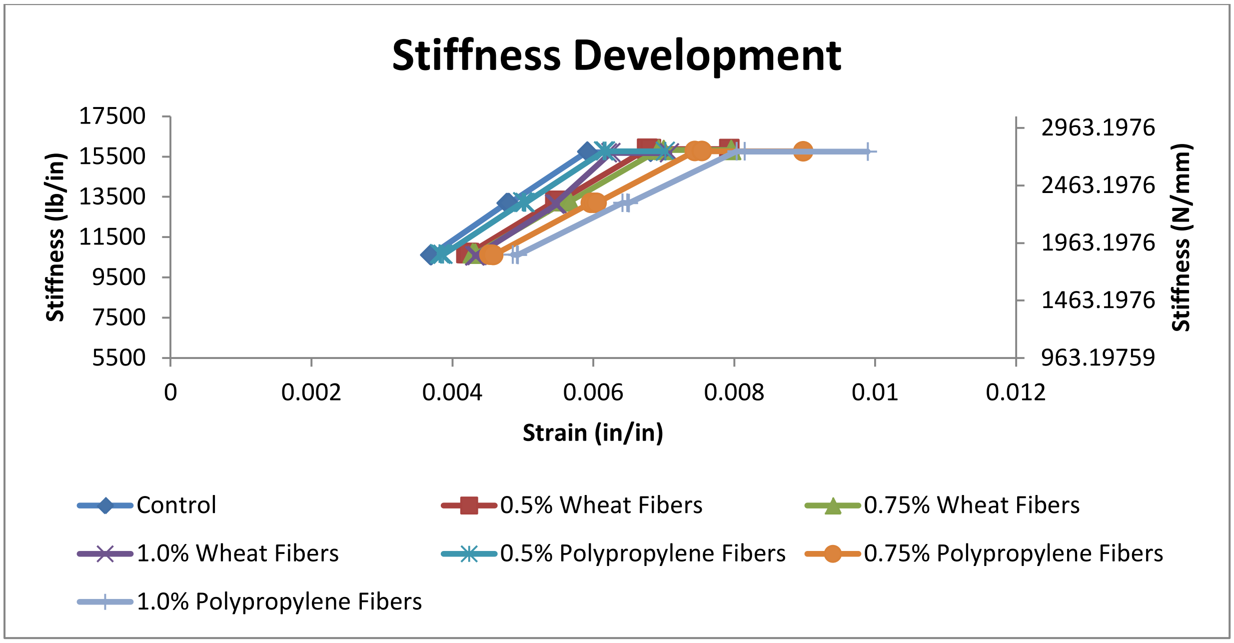

Figure 4-39: Stiffness vs. Strain at Each Cycle.

Table 4-8: Summary of Cyclic Cylinders Properties.

Sample	*Peak Load (N)*	*Initial Stiffness (N/mm)*	*Ductility Index*	*Initial Modulus of Elasticity (MPa)*
Control	406620.76	1858.68	1.7179	4061.12
0.5% Wheat Fibers	397564.91	1875.42	1.7508	4017.17
0.75% Wheat Fibers	411861.01	1870.95	1.9259	3934.21
1.0% Wheat Fibers	411698.31	1852.97	1.6729	3875.27
0.5% Polypropylene Fibers	451196.91	1869.28	1.9742	4394.07
0.75% Polypropylene Fibers	403288.73	1861.40	2.0025	3727.97
1.0% Polypropylene Fibers	400491.78	1860.94	2.1350	3474.20

4.5.2 Prisms Results:

The full load-deflection curves were generated for cylinders cured for 7 days (Figure 4-8 to Figure 4-11) due to the fact that an MTS compression machine was used. Figure 4-12 to Figure 4-15 represent the curves for the cylinders tested after 14 days of curing. As for the 28 days curing, Figure 4-16 through Figure 4-19 shows the load-displacement curves. But since the load cell is trying to engage the specimen, the graphs showed some anomaly in the early stages of loading. Other machines were used to confirm the peak load of the specimen and it yielded very close results. As for the calculation of the stiffness, it was conducted over the linear portion of the rising part of the curves as demonstrated in Figure 3-15. The following graphs represent the load-deflection curves for the different percentages of different fibers.

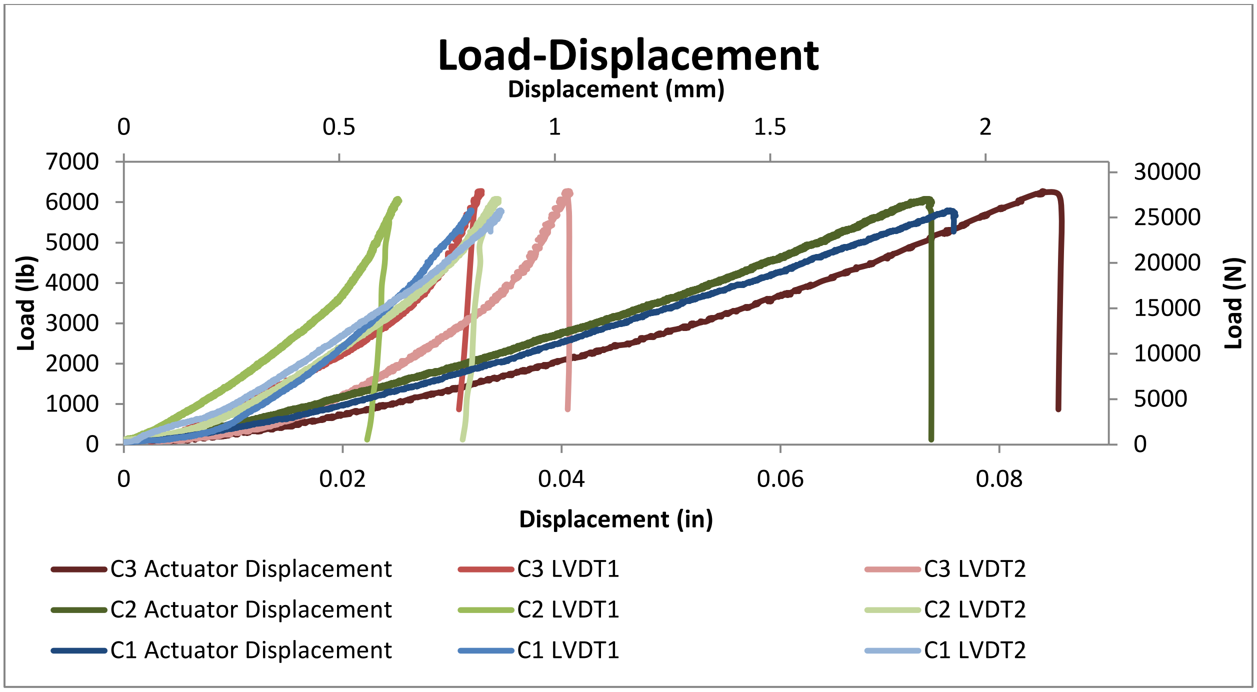

Figure 4-40: Batch 1, Load-Displacement Curves for the Control Specimens.

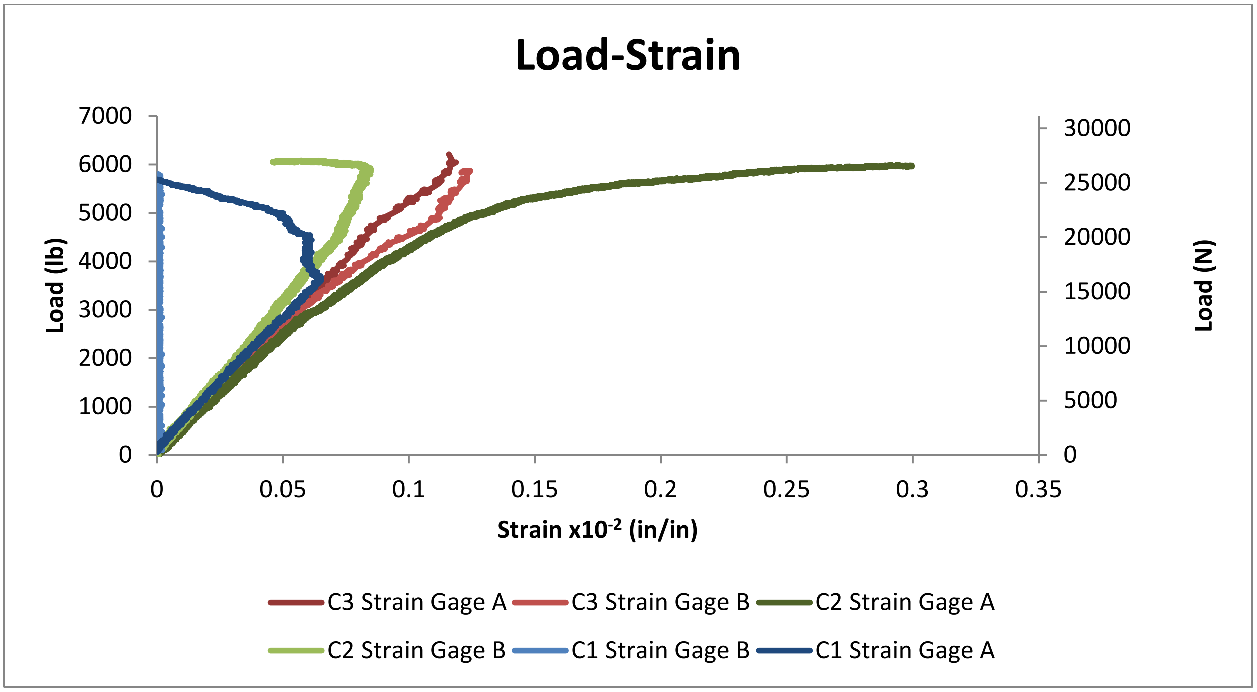

Figure 4-41: Batch 1, Load-Strain Curves for the Control Specimens.

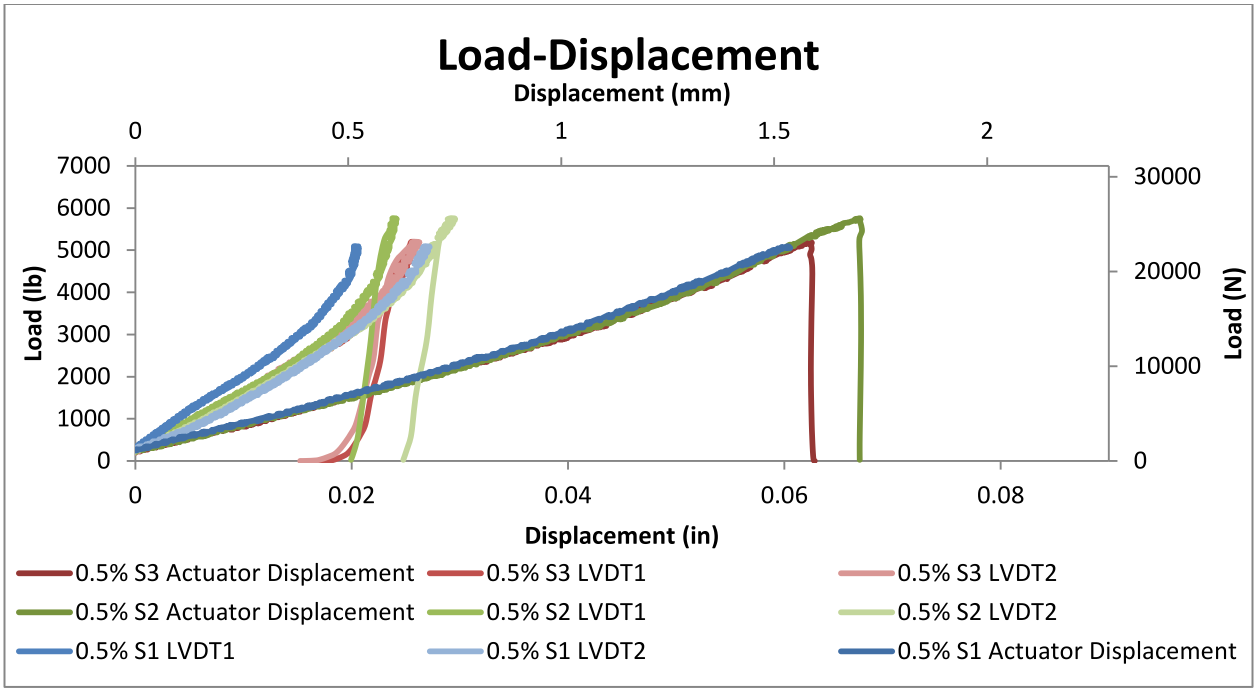

Figure 4-42: Batch 1, Load-Displacement Curves for the 0.5% Wheat Fibers Specimens.

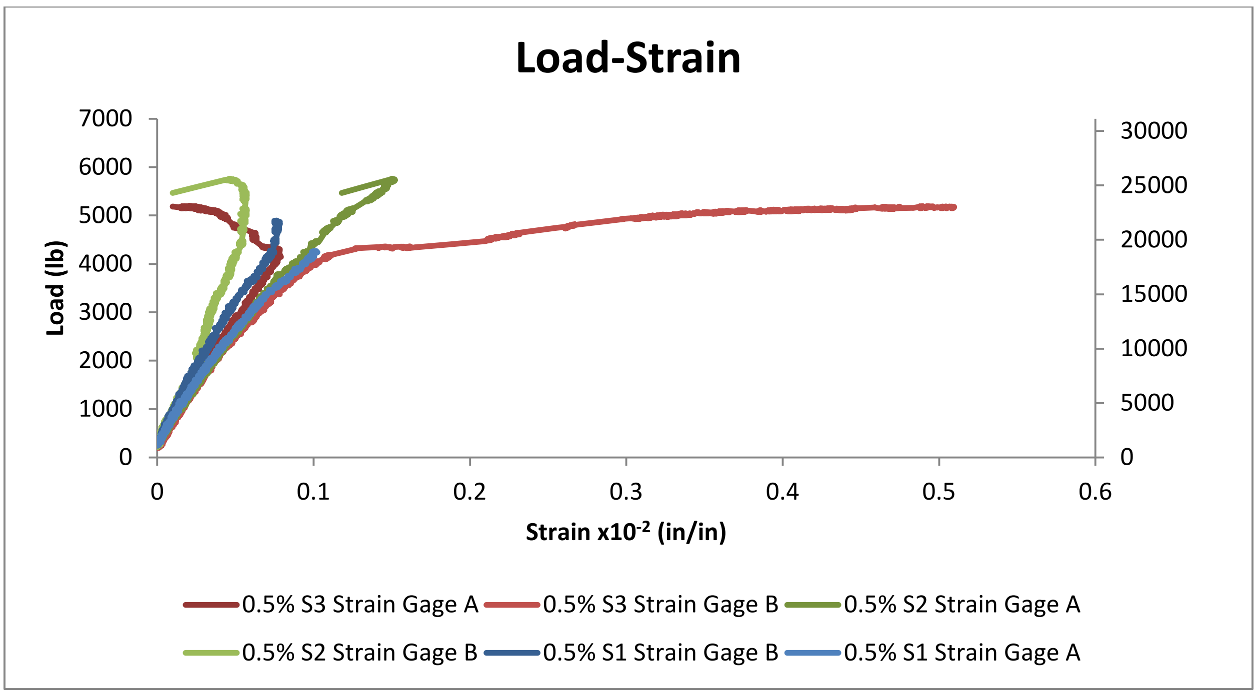

Figure 4-43: Batch 1, Load-Strain Curves for the 0.5% Wheat Fibers Specimens.

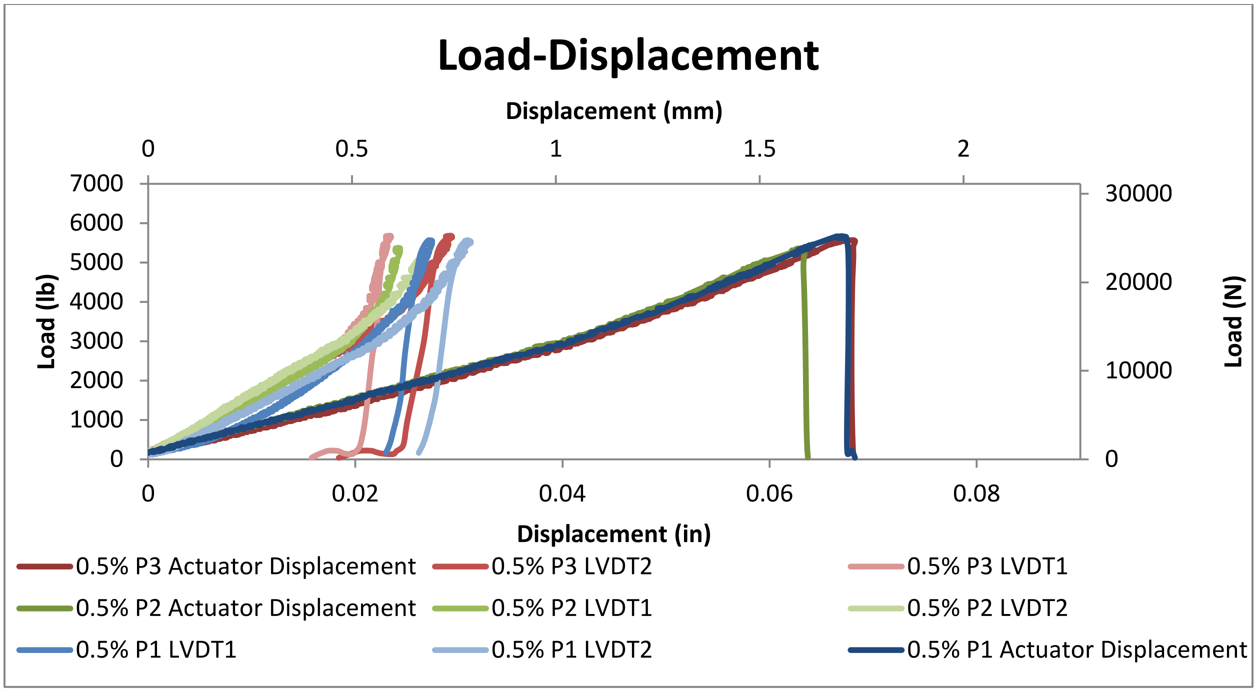

Figure 4-44: Batch 1, Load-Displacement Curves for the 0.5% Polypropylene Fibers Specimens.

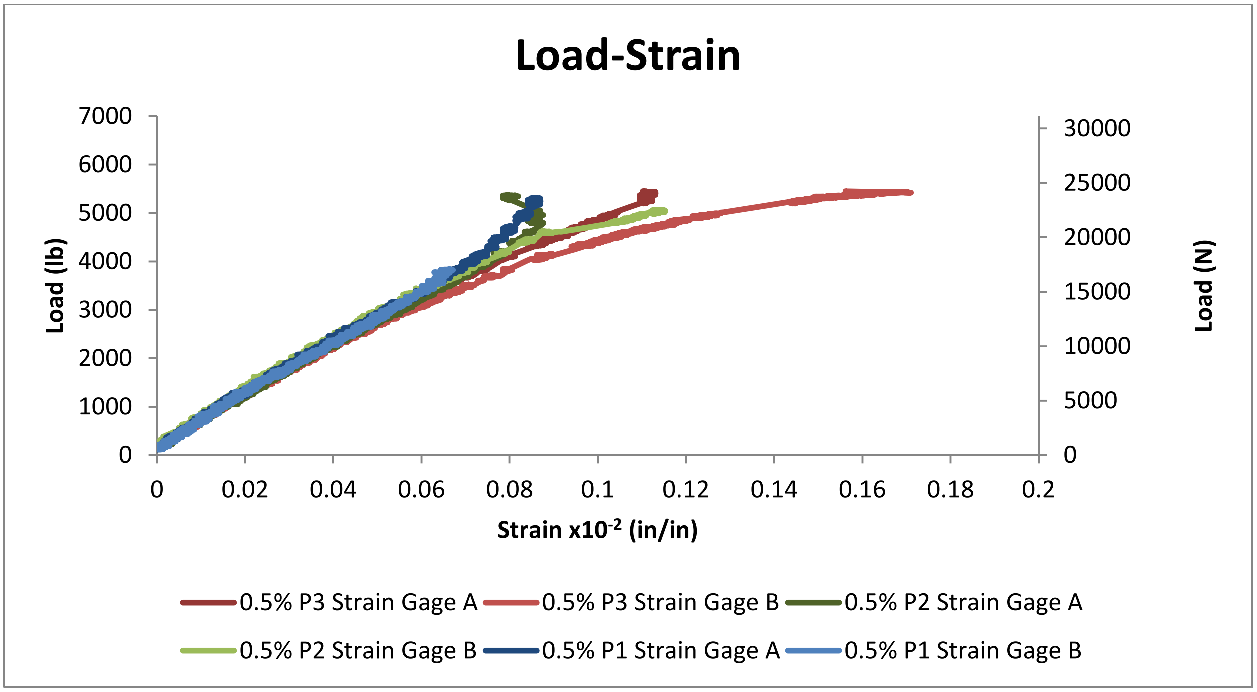

Figure 4-45: Batch 1, Load-Strain Curves for the 0.5% Polypropylene Fibers Specimens.

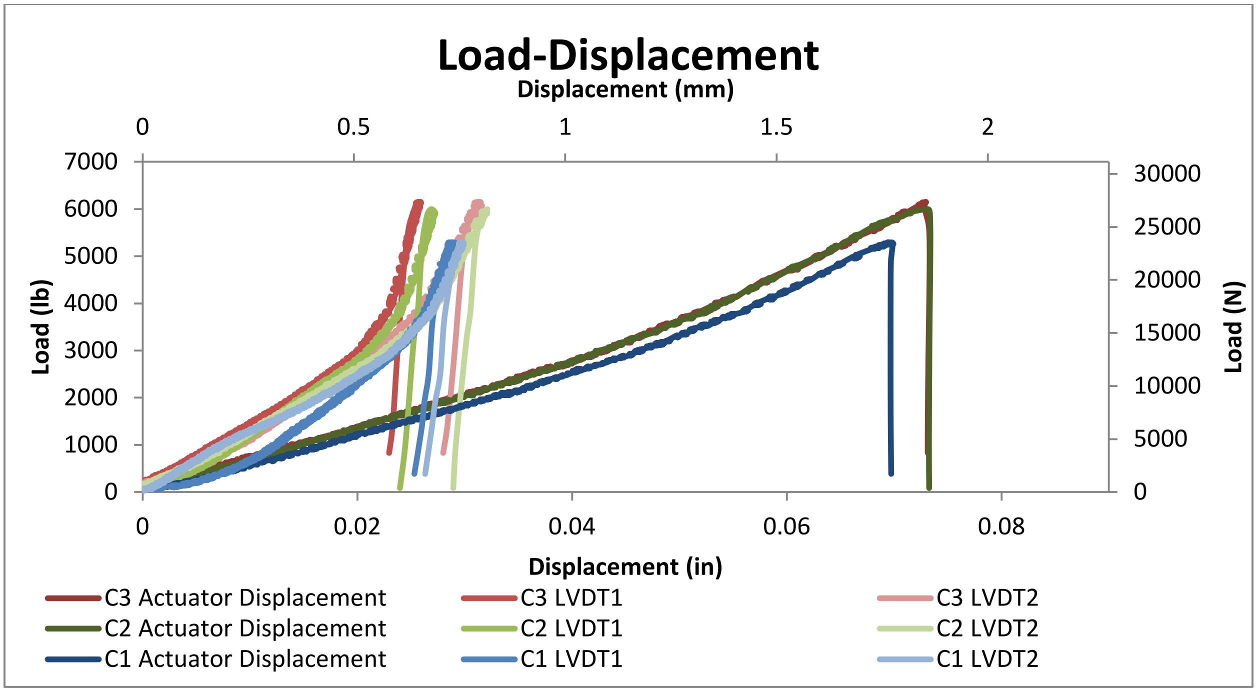

Figure 4-46: Batch 2, Load-Displacement Curves for the Control Specimens.

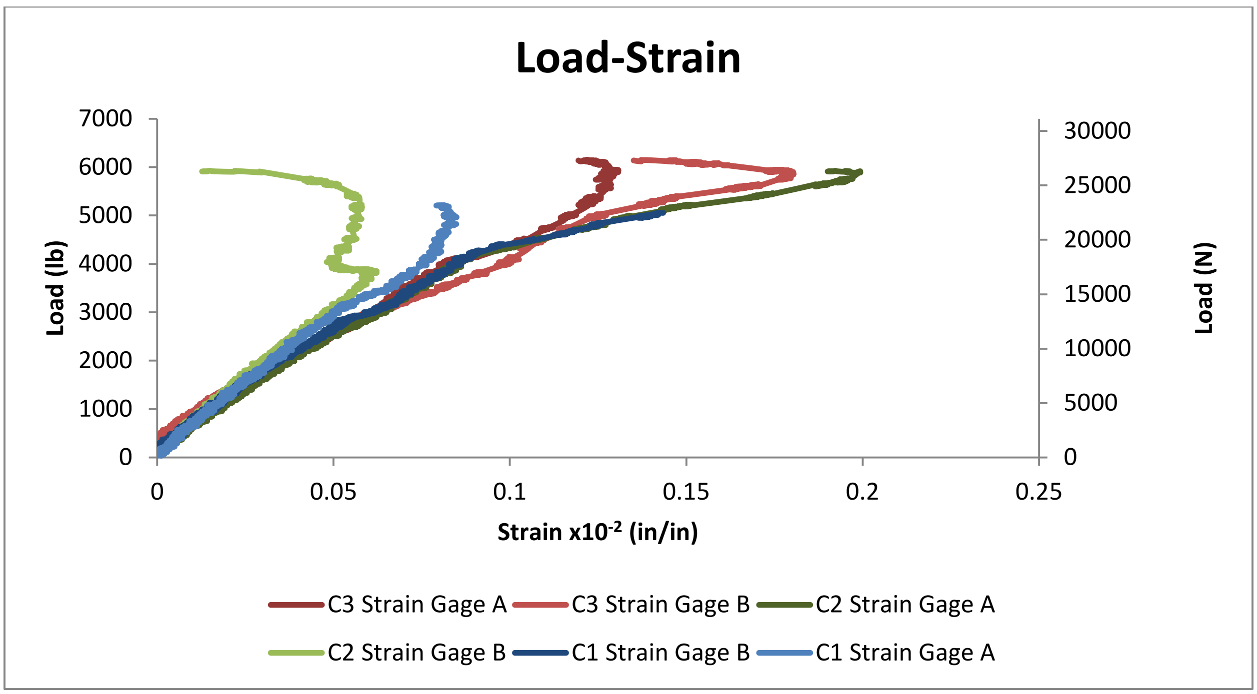

Figure 4-47: Batch 2, Load-Strain Curves for the Control Specimens.

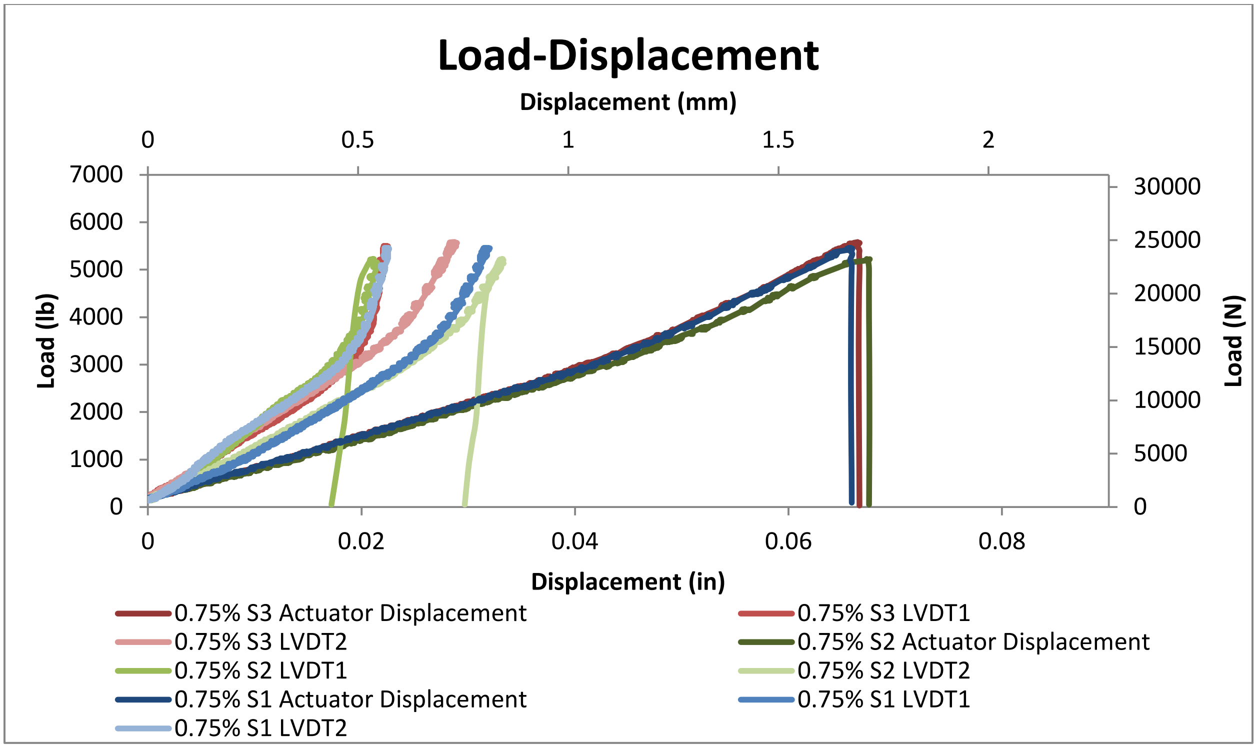

Figure 4-48: Batch 2, Load-Displacement Curves for the 0.5% Wheat Fibers Specimens.

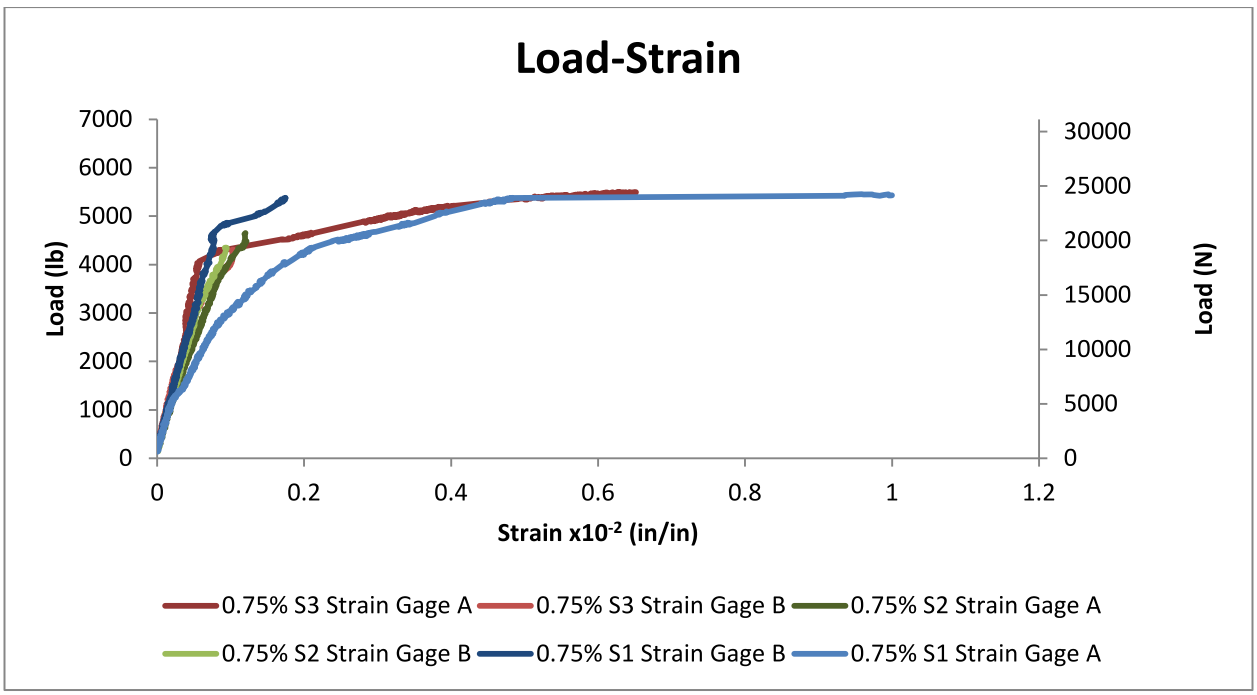

Figure 4-49: Batch 2, Load-Strain Curves for the 0.5% Wheat Fibers Specimens.

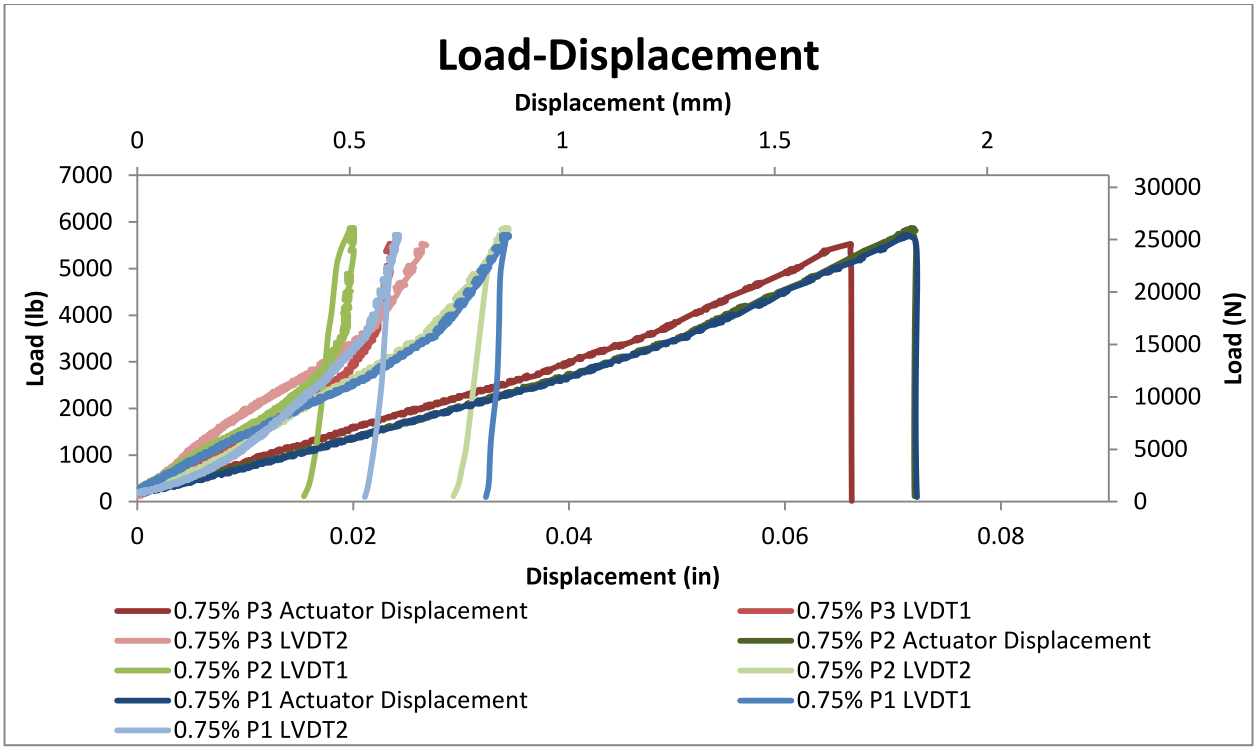

Figure 4-50: Batch 2, Load-Displacement Curves for the 0.75% Polypropylene Fibers Specimens.

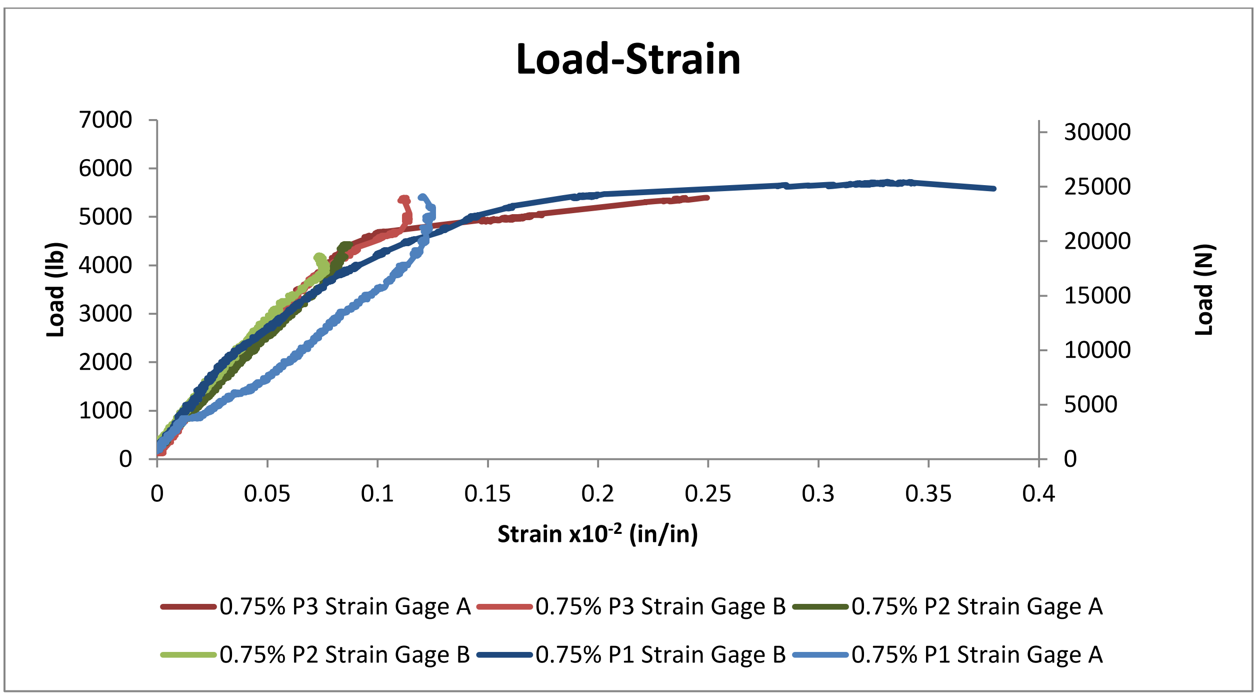

Figure 4-51: Batch 2, Load-Strain Curves for the 0.75% Polypropylene Fibers Specimens.

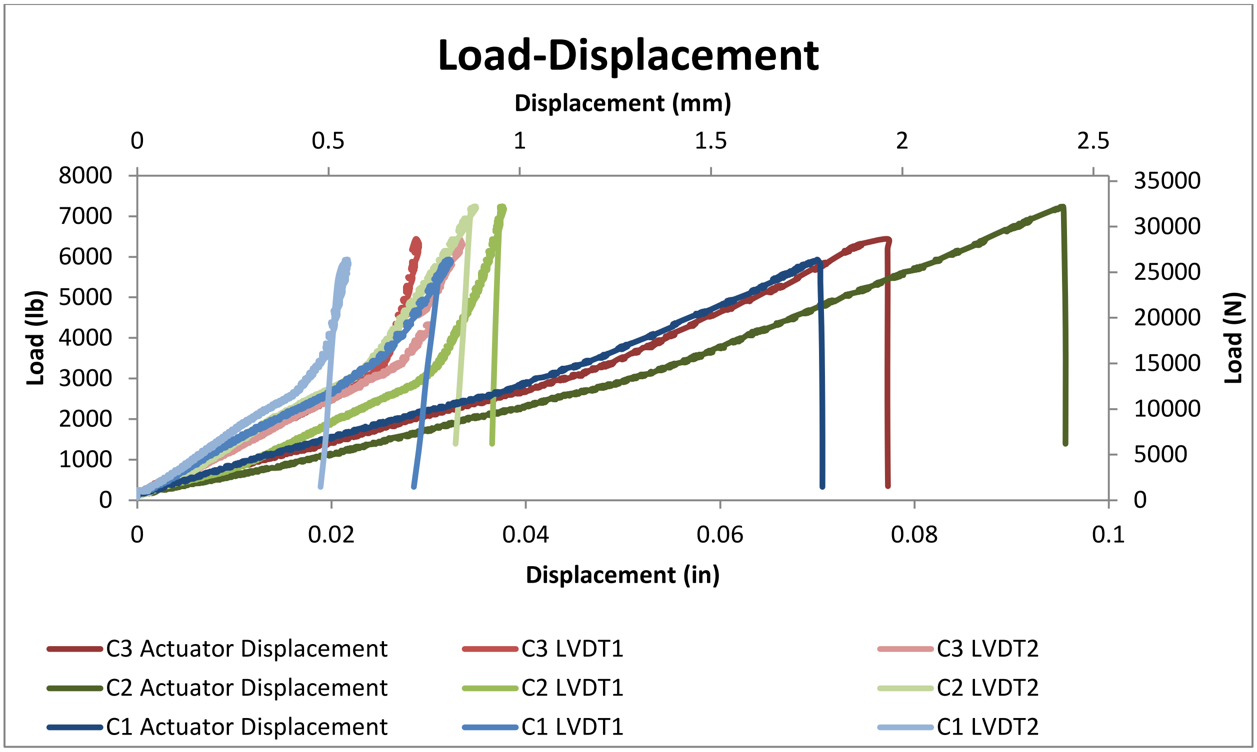

Figure 4-52: Batch 3, Load-Displacement Curves for the Control Specimens.

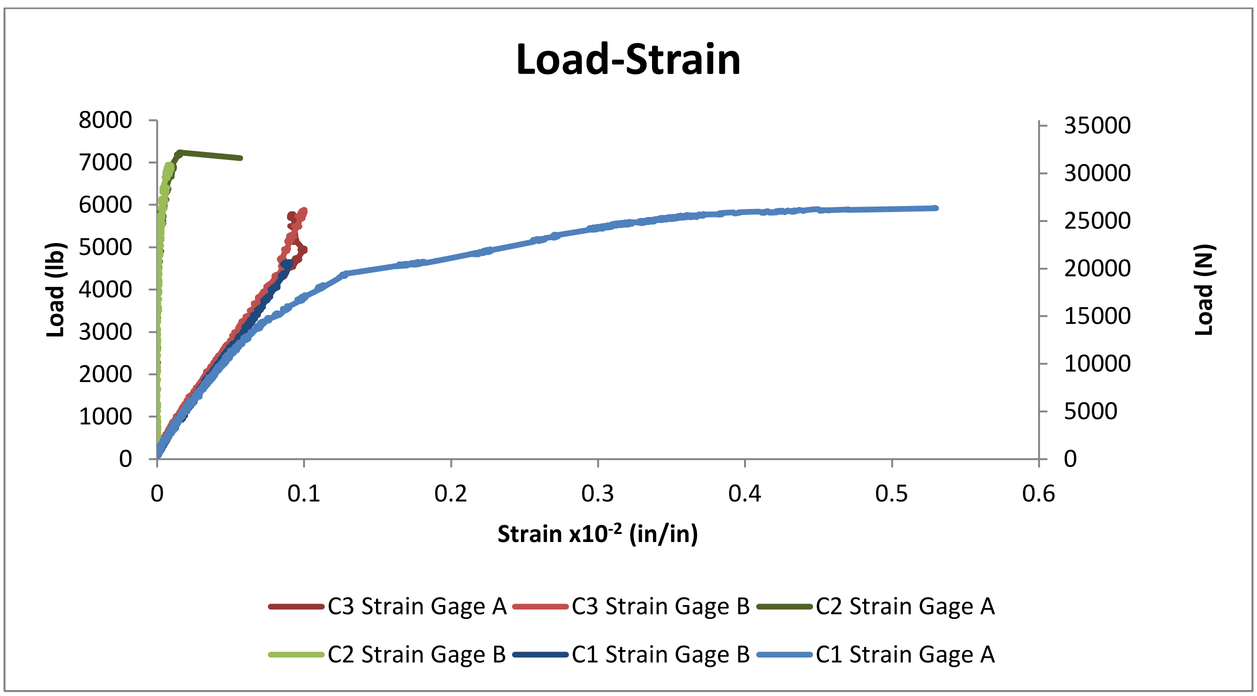

Figure 4-53: Batch 3, Load-Strain Curves for the Control Specimens.

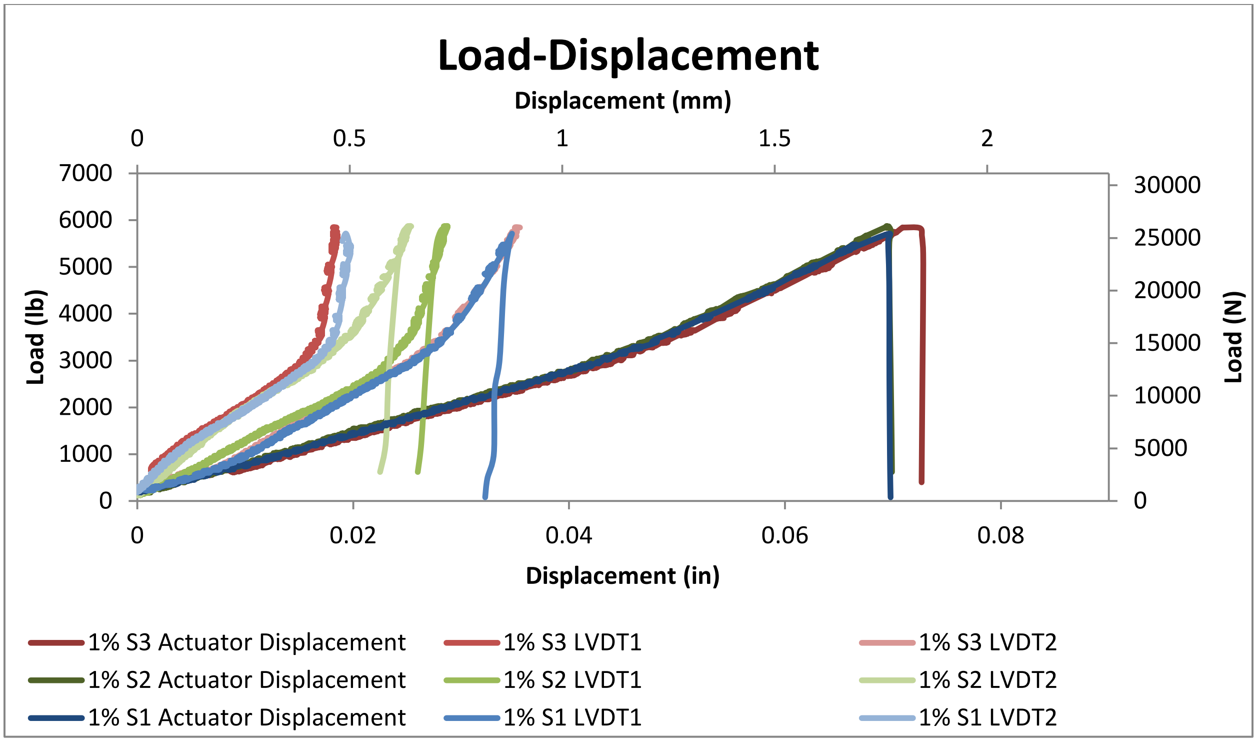

Figure 4-54: Batch 3, Load-Displacement Curves for the 1% Wheat Fibers Specimens.

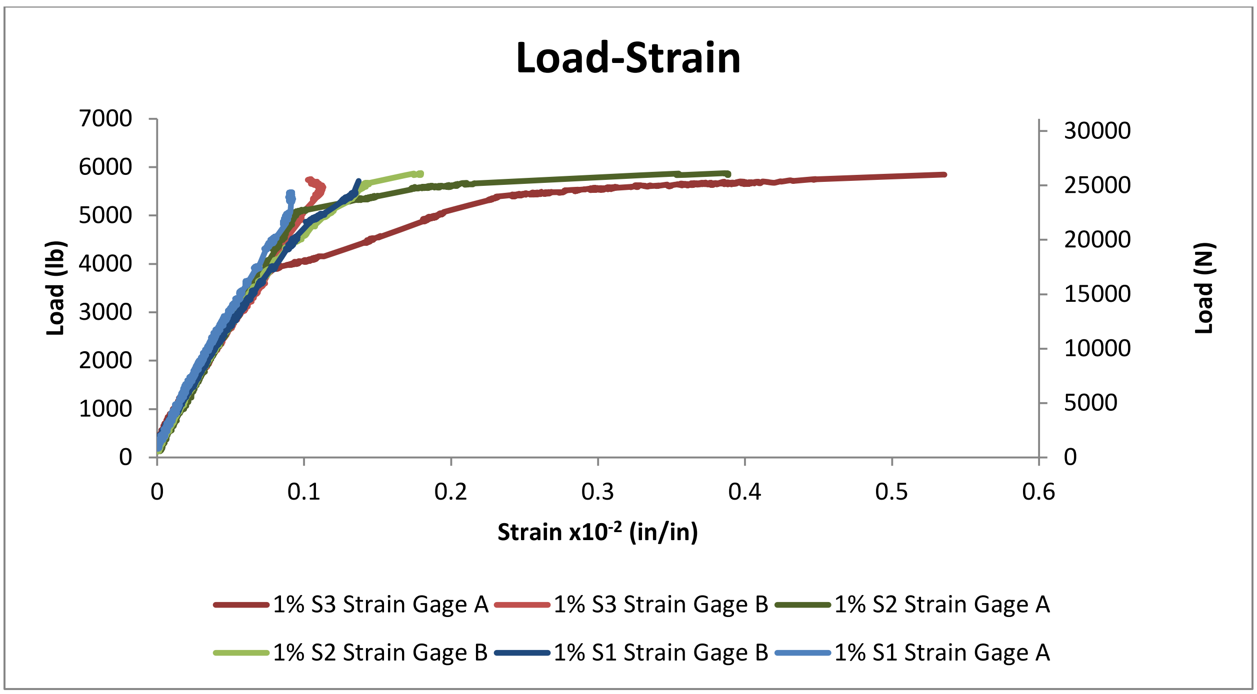

Figure 4-55: Batch 3, Load-Strain Curves for the 1% Wheat Fibers Specimens.

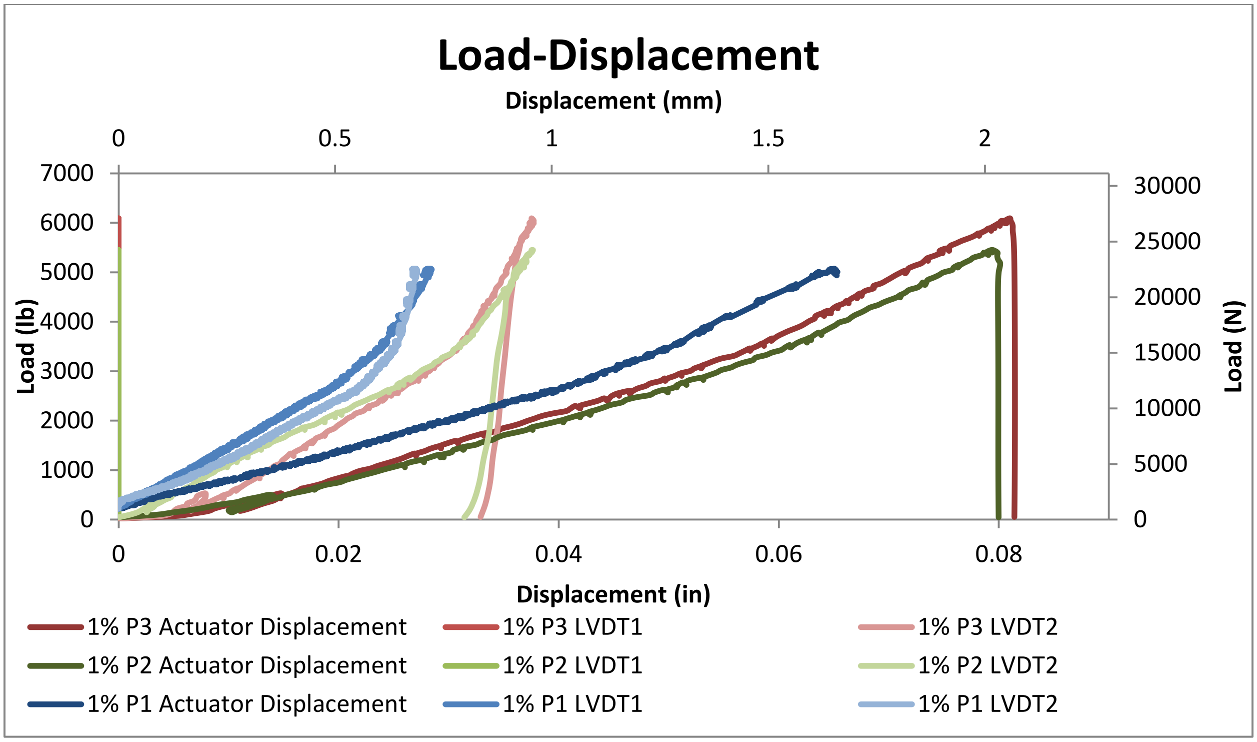

Figure 4-56: Batch 3, Load-Displacement Curves for the 1% Polypropylene Fibers Specimens.

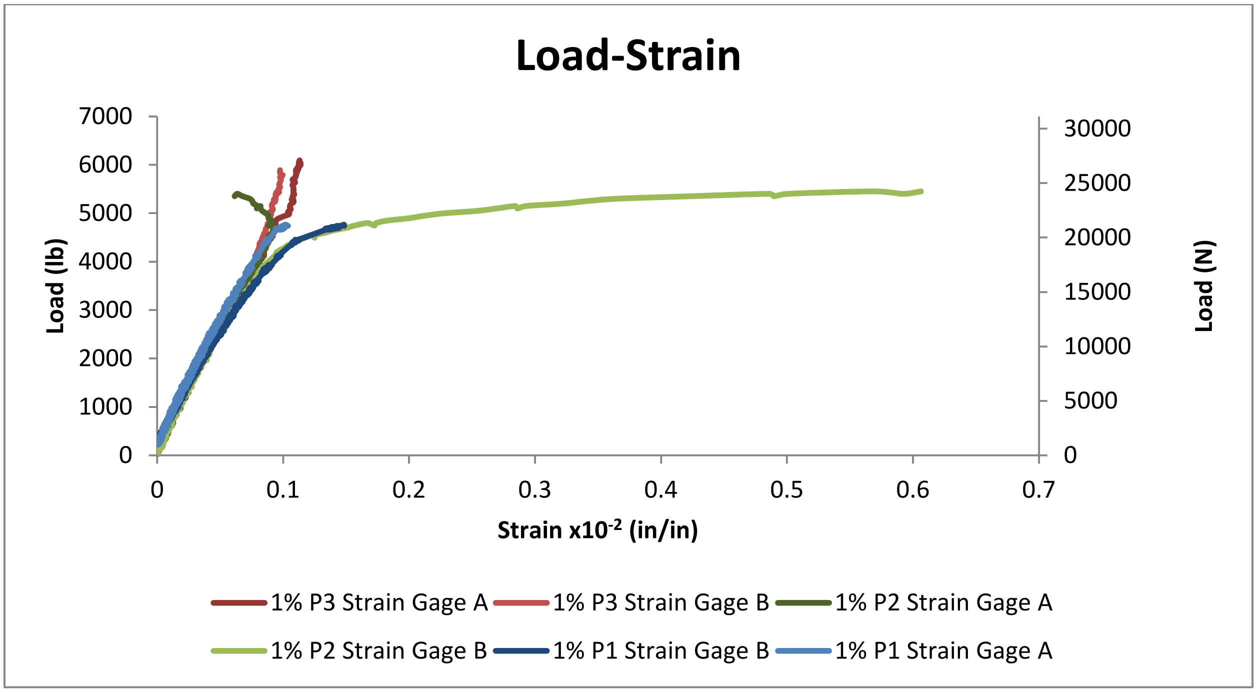

Figure 4-57: Batch 3, Load-Strain Curves for the 1% Polypropylene Fibers Specimens.

The following graphs (Figure 4-58 and Figure 3-22), developed from the peak loads and the calculated stiffnesses for the two types of fibers, present the peak load and stiffness benefits of the different fibers. In these figures, the lines are connecting the average peak load or stiffness in three-point flexure, while the vertical lines with the tick marks represent the maximum, minimum, and middle values.

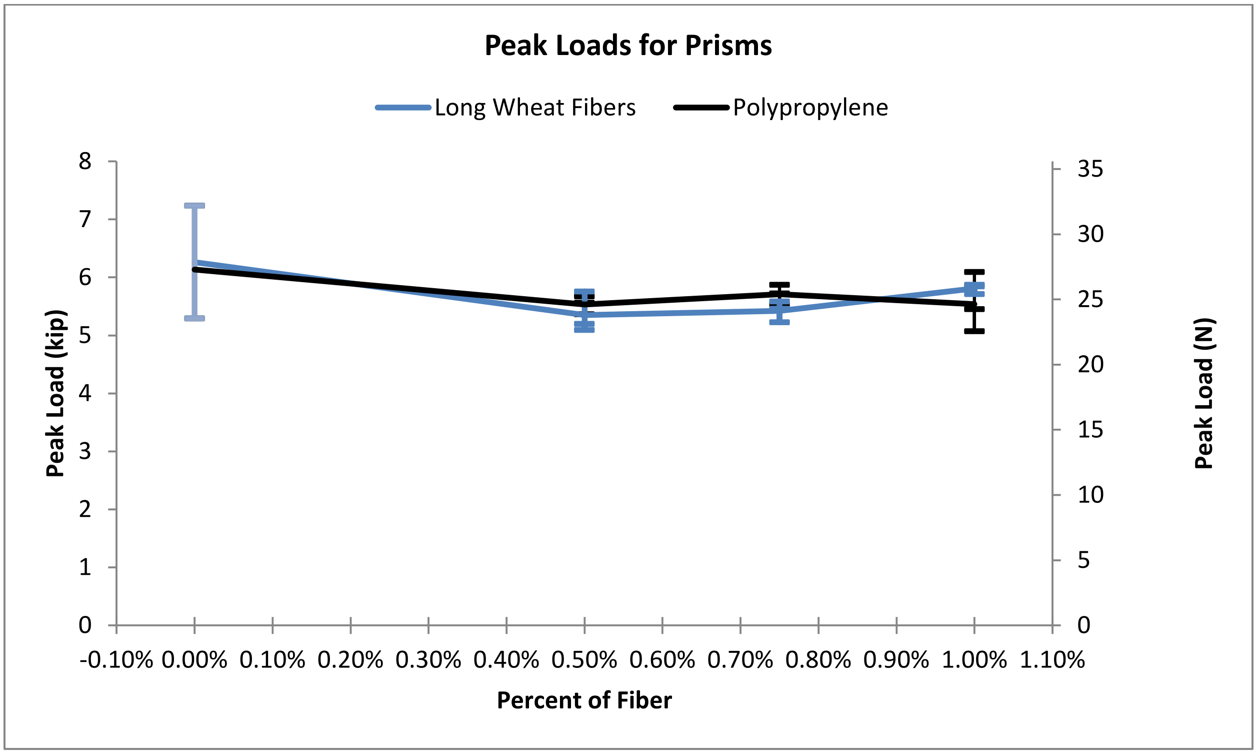

Figure 4-58: Peak Loads for Concrete Prisms Containing Different Percentages of Different Fibers.

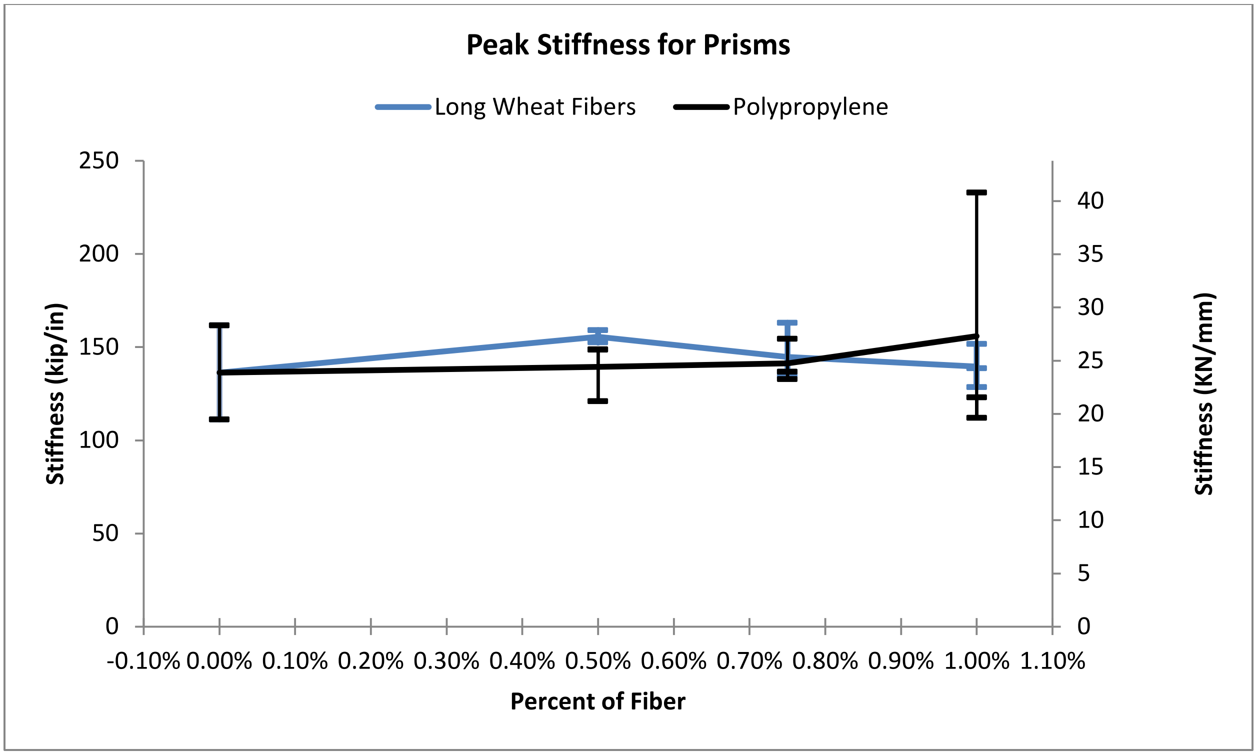

Figure 4-59: Stiffness Peaks for Concrete Prisms Containing Different Percentages of Different Fibers.

Similar to Figure 4-22 and Figure 4-23, Figure 4-60 and Figure 3-24 represent the percentages of peak load and stiffness increases in comparison with the average values of the corresponding control specimens. In these figures, the lines are connecting the average peak load or stiffness increase relative to the average of its control in four-point flexure, while the vertical lines with the tick marks represent the maximum, minimum, and middle values in term of relative flexural peak load or stiffness. Table 4-9 represents the average increase in both load and stiffness for the concrete prisms with the different percentages and different fibers.

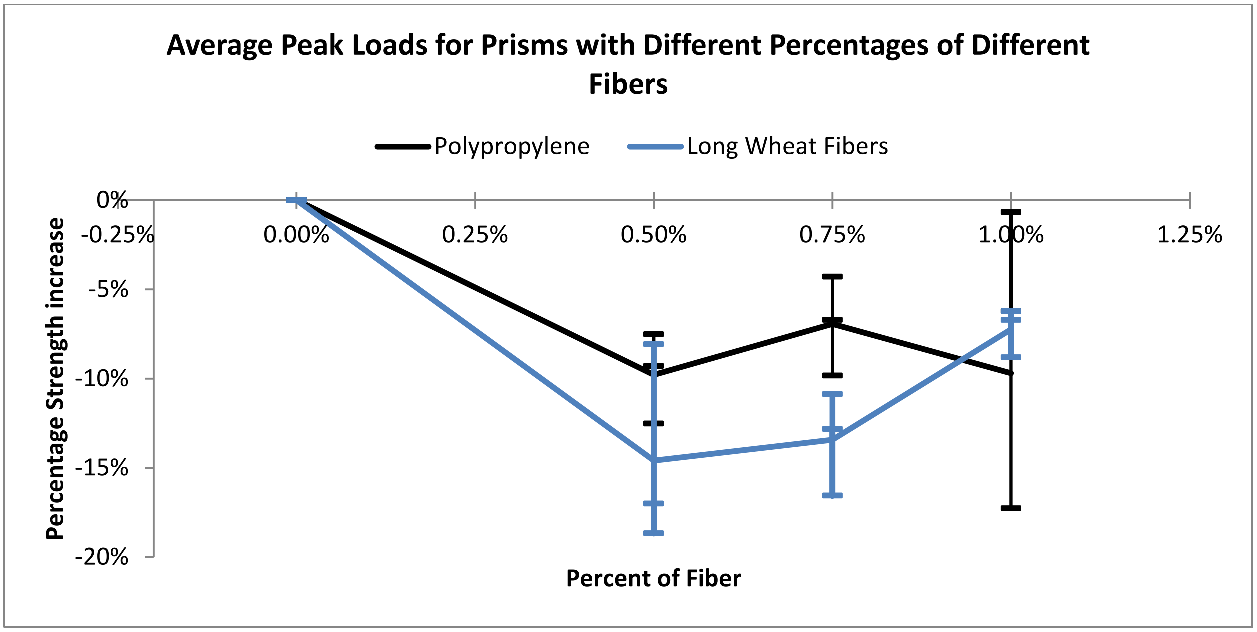

Figure 4-60: Average Peak Loads for Concrete Prisms with Different Percentages of Different Fibers.

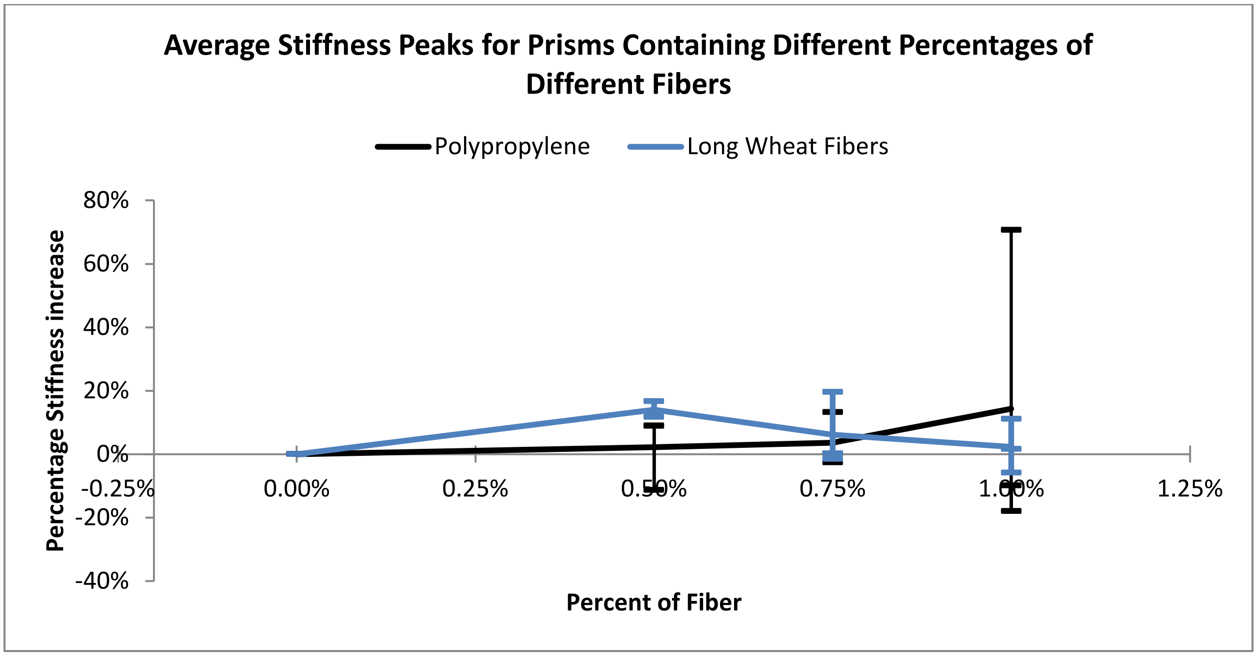

Figure 4-61: Average Stiffness Peaks for Concrete Prisms with Different Percentages of Different Fibers.

Table 4-9: Average Increase in the Load and Stiffness for Prisms with Different Amount of Different Fibers.

Volume % Fiber	**Long Wheat Fibers**		**Polypropylene Fibers**	
	Avg. Load Increase	Avg. Stiffness Increase	Avg. Load Increase	Avg. Stiffness Increase
0%	0%	0%	0%	0%
0.50%	-15%	14%	-10%	2%
0.75%	-13%	6%	-7%	4%
1%	-7%	2%	-10%	14%

CHAPTER 5 - Finite Element Modeling and Simulation

In this chapter a finite element modeling is performed for concrete cylinders and prisms similar to those tested in the previous chapter. Commercial finite element software, ABAQUS FEA, is used to simulate the control concrete specimen and the specimens with fibers.

5.1 Material Models

For the modeling of the concrete specimens two types of material properties had to be defined, elasticity and plasticity parameters. For the elasticity parameters, the Young's Modulus of Elasticity (E) and the Poisson's ratio (ν) are required. The Plasticity model that was selected was the *Concrete Damage Plasticity* which requires the following as defined by the ABAQUS user manual:

- Dilation Angle (ψ), in the *p–q* plane, and the units in degrees.
- Eccentricity, Flow potential eccentricity (ϵ). The eccentricity is a small positive number that defines the rate at which the hyperbolic flow potential approaches its asymptote.
- fb0/fc0, the ratio of initial equibiaxial compressive yield stress to initial uniaxial compressive yield stress.
- K or K_c, the ratio of the second stress invariant on the tensile meridian, $q_{(TM)}$, to that on the compressive meridian, $q_{(CM)}$, at initial yield for any given value of the pressure invariant p such that the maximum principal stress is negative, $\sigma_{max} < 0$. It must satisfy the condition $0.5 < K_c \leq 1$.
- Viscosity parameter (μ), used for the visco-plastic regularization of the concrete constitutive equations in ABAQUS/Standard analyses.
- Compressive Behavior, which consist of *Yield Stress* and *Inelastic Strain*.
- Tensile Behavior, which consist of *Yield Stress* and *Direct cracking displacement.*

In order to calculate the concrete compressive behavior the cyclic loading was performed concrete cylinders which was presented in CHAPTER 4 -. As for the concrete tensile behavior, a bilinear model suggested by Coronado *et al.* (2006) was used to calculate the tensile yield stress. The following table represents the materials parameters for the concrete control specimen calibrated to fit the experimental results in CHAPTER 4 -.

Table 5-1: Concrete Damage Plasticity Materials Parameter.

Young's Modulus of Elasticity (MPa)		4000	
Poisson's ratio		0.2	
Dilation Angle (^{o})		36	
Eccentricity		0.1	
fb0/fc0		1.16	
K		0.6666	
Viscosity parameter		0	
Compressive Behavior		Tensile Behavior	
Yield Stress (MPa)	Inelastic Strain (mm/mm)	Yield Stress (MPa)	Direct Cracking Displacement (mm)
32.9380913	0	4.647580015	0
35.68711245	5.01E-05	0.929516003	17.79231175
38.42588634	0.000353254	0	189.0433123
41.16120898	0.000784622		
43.90656272	0.00138962		
46.63870518	0.002224743		
49.39123902	0.003569561		

As for the wheat fiber material properties, only elastic properties were obtained from a paper by Wu *et al.* (2010). The modulus of elasticity (E) was 20.9 GPa and the Poisson's ratio (ν) was 0.25. The wheat fibers were assumed to have a constant length of 25 mm and a diameter of 2.5 mm. As for the steel supports, the modulus of elasticity that was used is 200 GPa with a poisson's ratio of 0.3.

5.2 Geometrical Model

5.2.1 Concrete Cylinders:

Similar to the experimental cylinders the geometrical cylinders have a diameter of 4 in (101.6 mm) and a length of 8 in (203.2 mm) as shown in Figure 5-1. As for the wheat fiber distribution Figure 5-2 through Figure 5-10 represent the fiber distribution, which was distributed in planes with an angle of 90^o from each others for the 0.5% fibers, 60^o for the 0.75% fibers and 36^o for the 1% fibers. The wheat fibers were attached to the concrete using the embedded region approach.

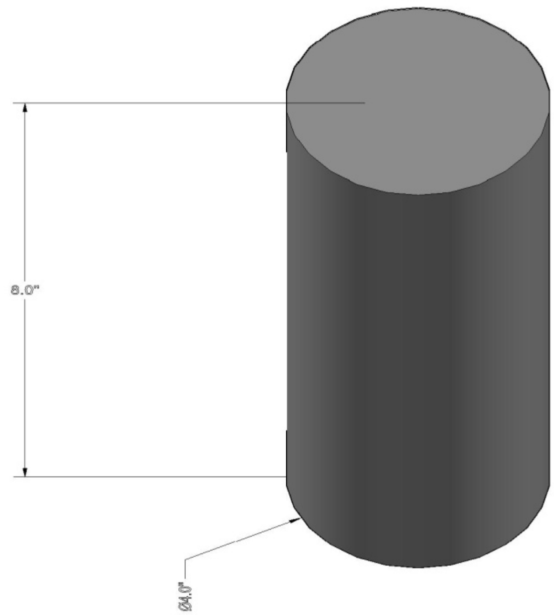

Figure 5-1: Cylinder Dimension in Inches.

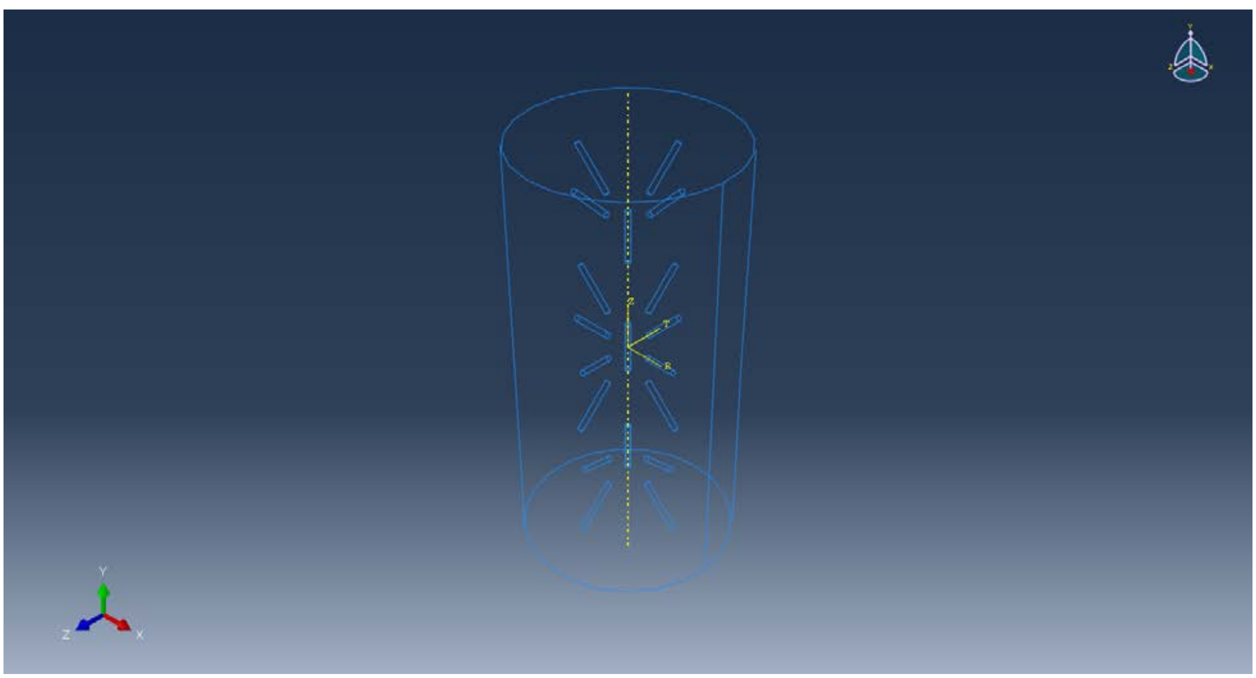

Figure 5-2: Isotropic View of Fiber Distribution for the 0.5% Wheat Fibers in Cylinders.

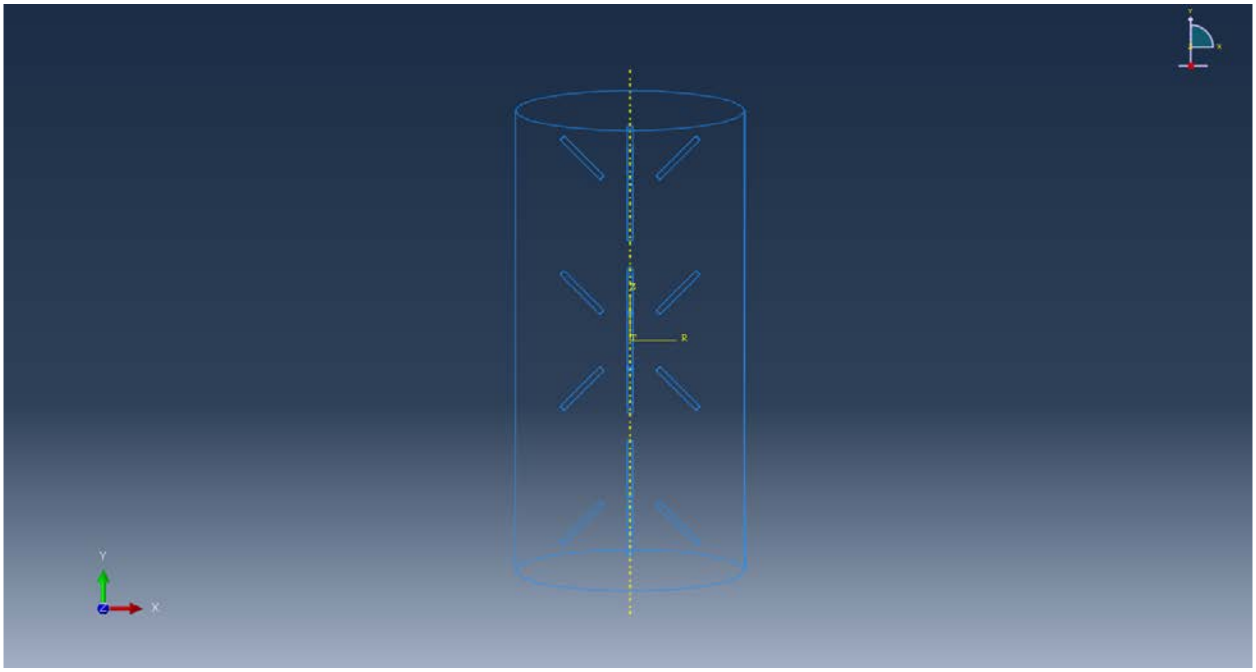

Figure 5-3: X-Y View of Fiber Distribution for the 0.5% Wheat Fibers in Cylinders.

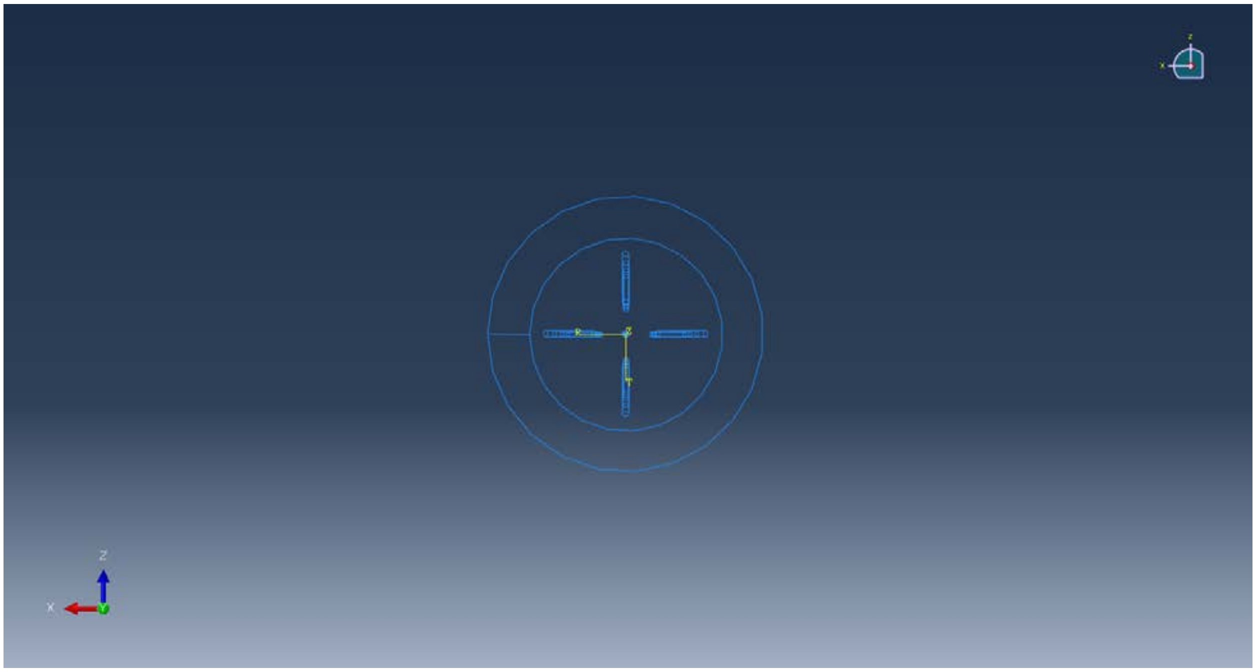

Figure 5-4: X-Z View of Fiber Distribution for the 0.5% Wheat Fibers in Cylinders.

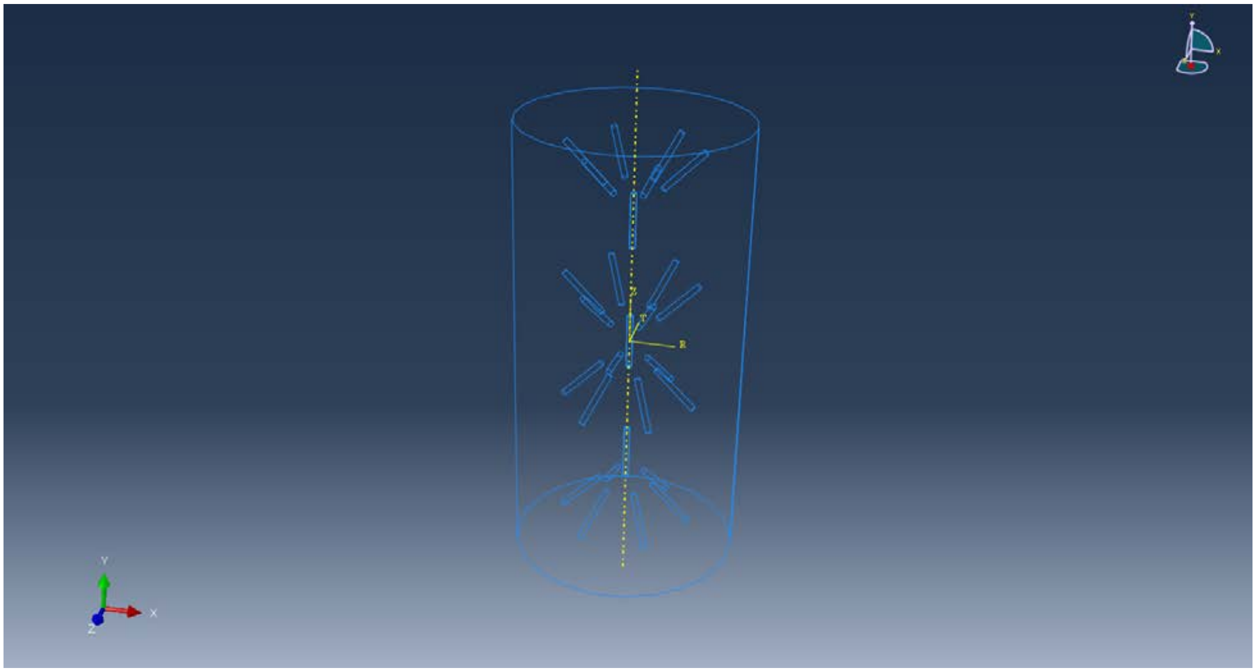

Figure 5-5: Isotropic View of Fiber Distribution for the 0.75% Wheat Fibers in Cylinders.

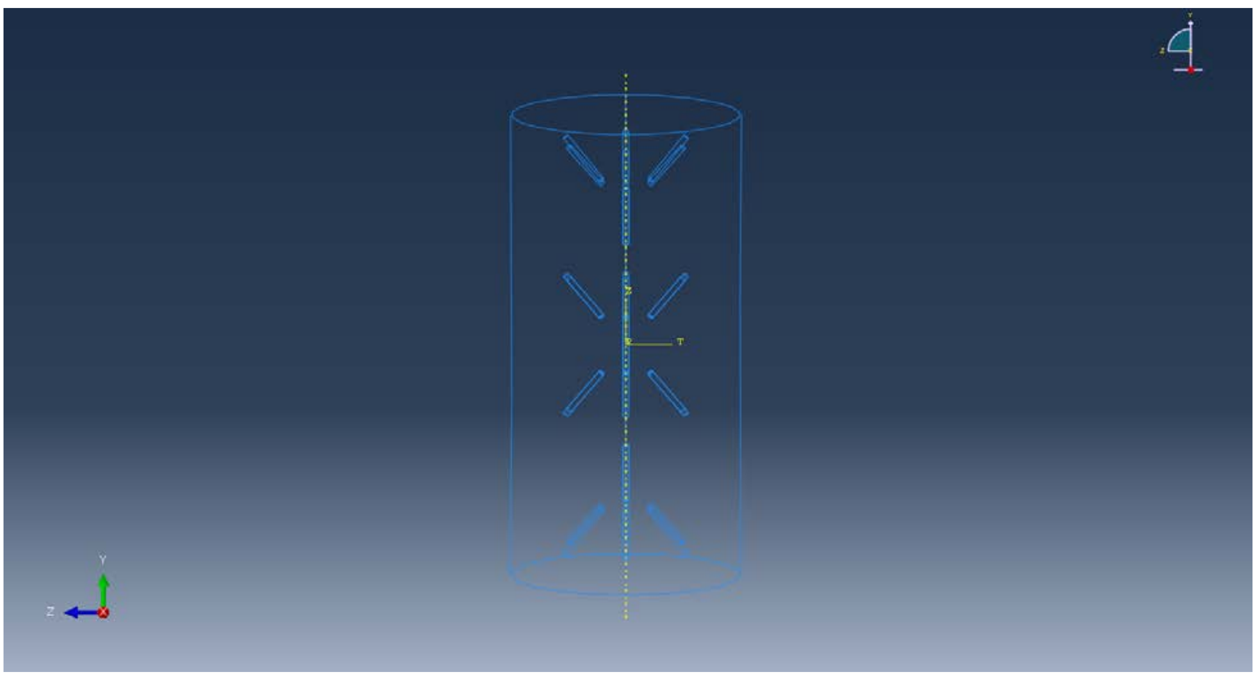

Figure 5-6: Y-Z View of Fiber Distribution for the 0.75% Wheat Fibers in Cylinders.

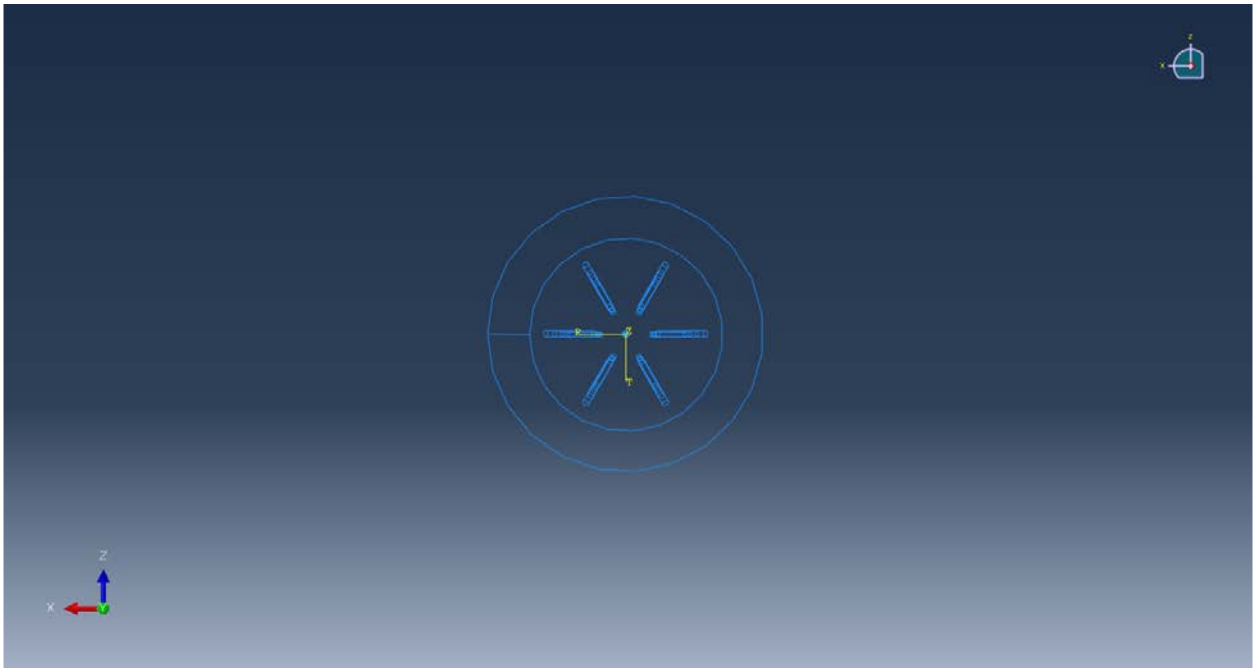

Figure 5-7: X-Z View of Fiber Distribution for the 0.75% Wheat Fibers in Cylinders.

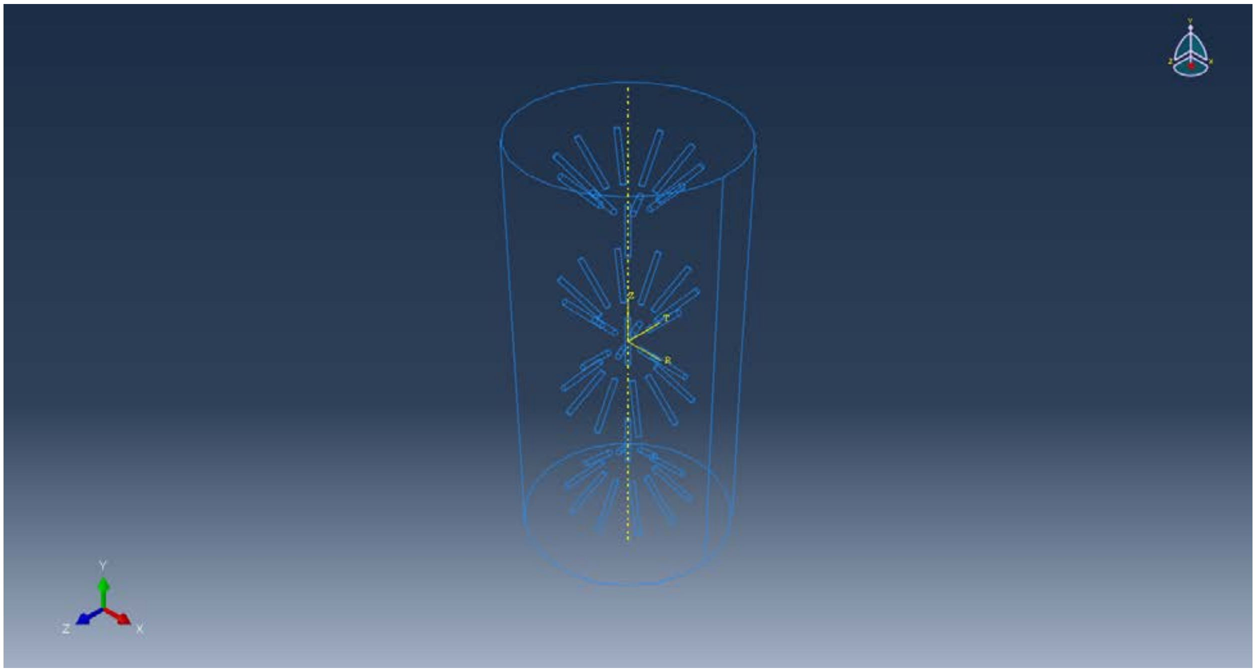

Figure 5-8: Isotropic View of Fiber Distribution for the 1% Wheat Fibers in Cylinders.

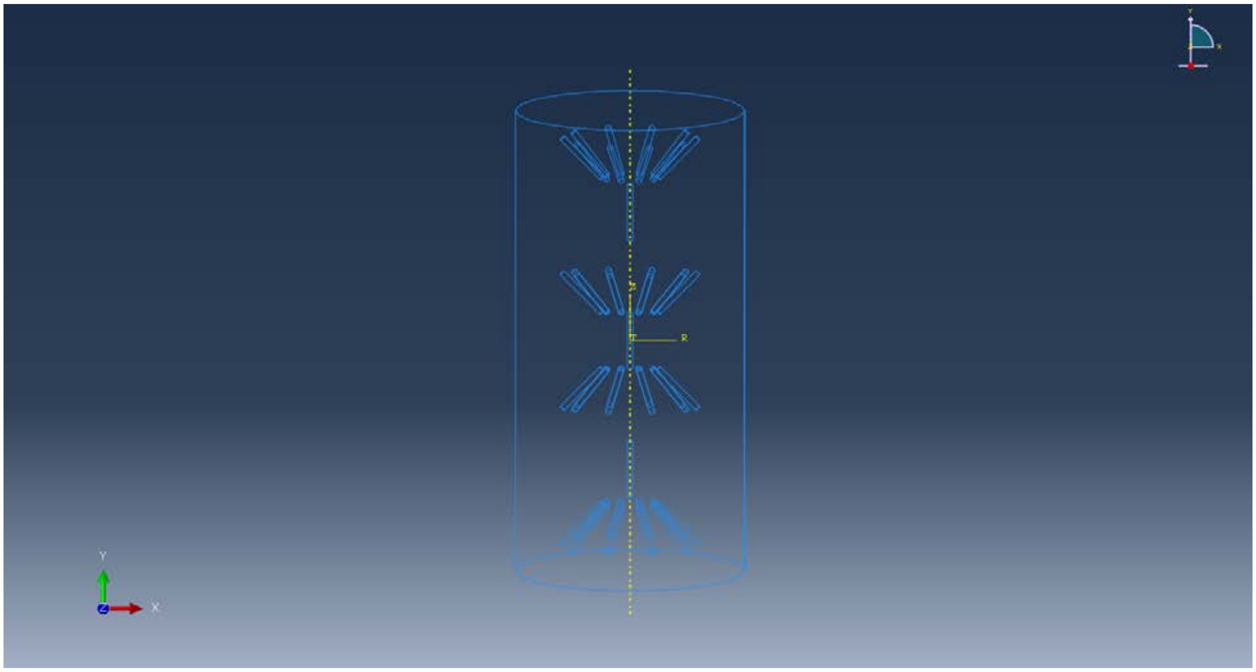

Figure 5-9: Y-Z View of Fiber Distribution for the 1% Wheat Fibers in Cylinders.

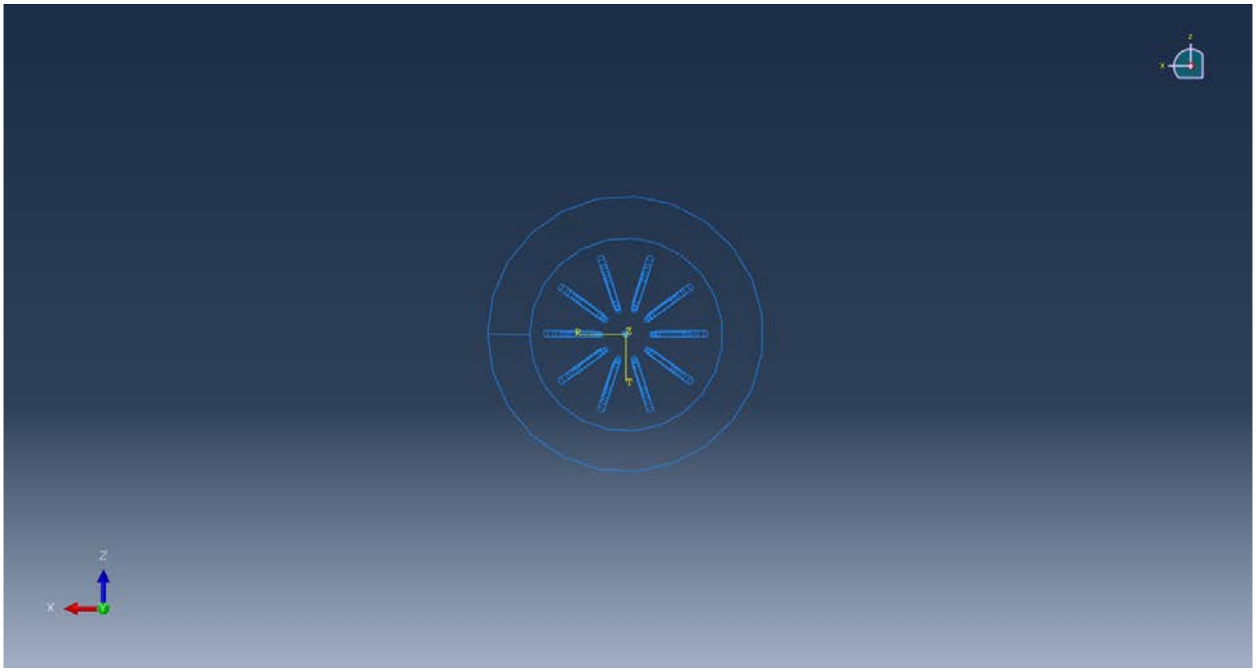

Figure 5-10: X-Z View of Fiber Distribution for the 1% Wheat Fibers in Cylinders.

5.2.2 Concrete Prisms:

Also similar to the experimental prisms the simulated prisms have a height and width of 6 in (152.4 mm) and a length of 21 in (533.4 mm) as shown in Figure 5-11. As for the fiber distribution Figure 5-12 through Figure 5-16 represent the wheat fiber distribution, which was distributed in planes with a spacing of 12.7 mm from each other's for the 0.5% fibers, 14.11 mm for the 0.75% fibers and 9 mm for the 1% fibers.

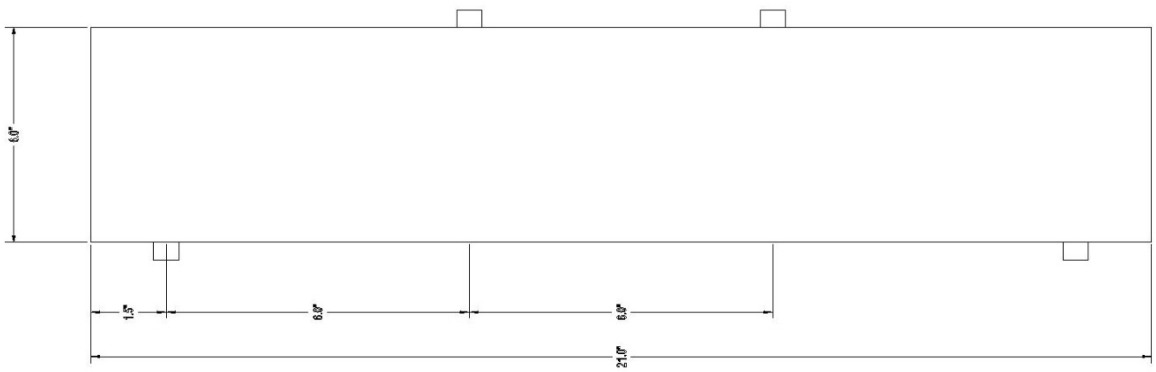

Figure 5-11: Prism Dimension in Inches.

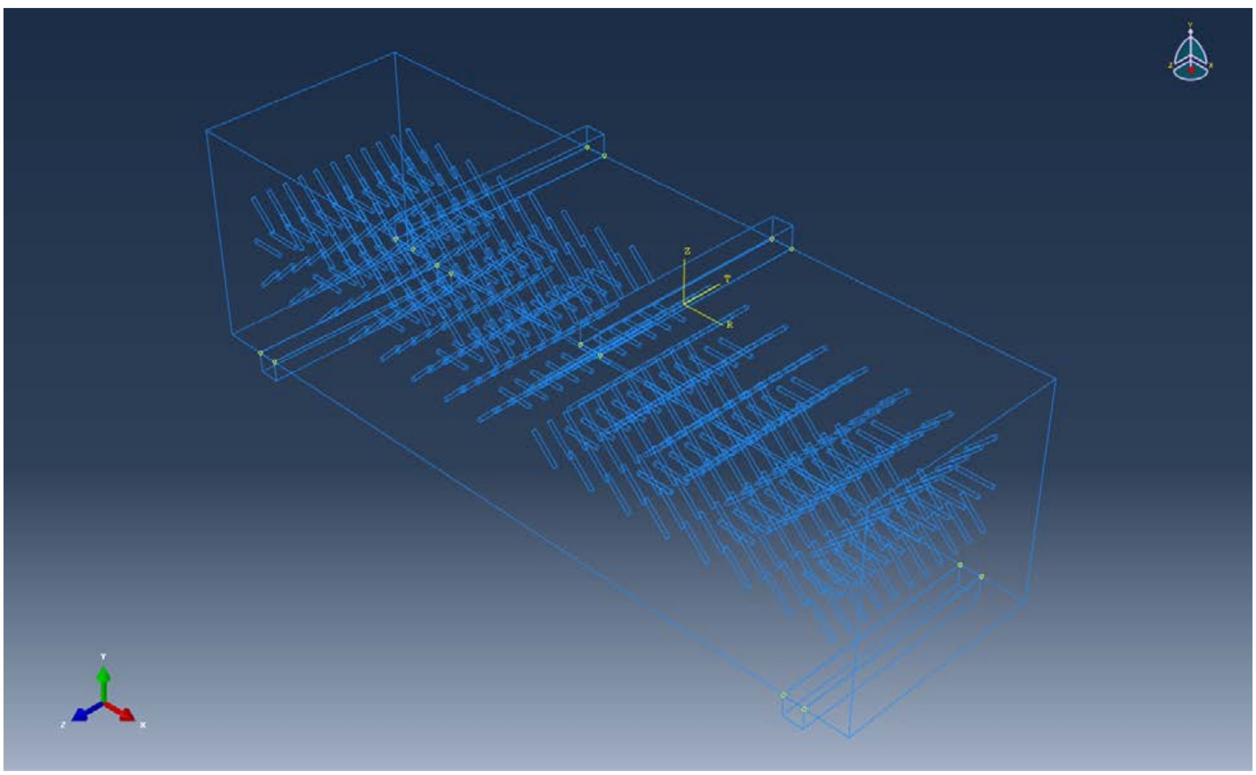

Figure 5-12: Isotropic View of 0.5% Wheat Fibers Distribution.

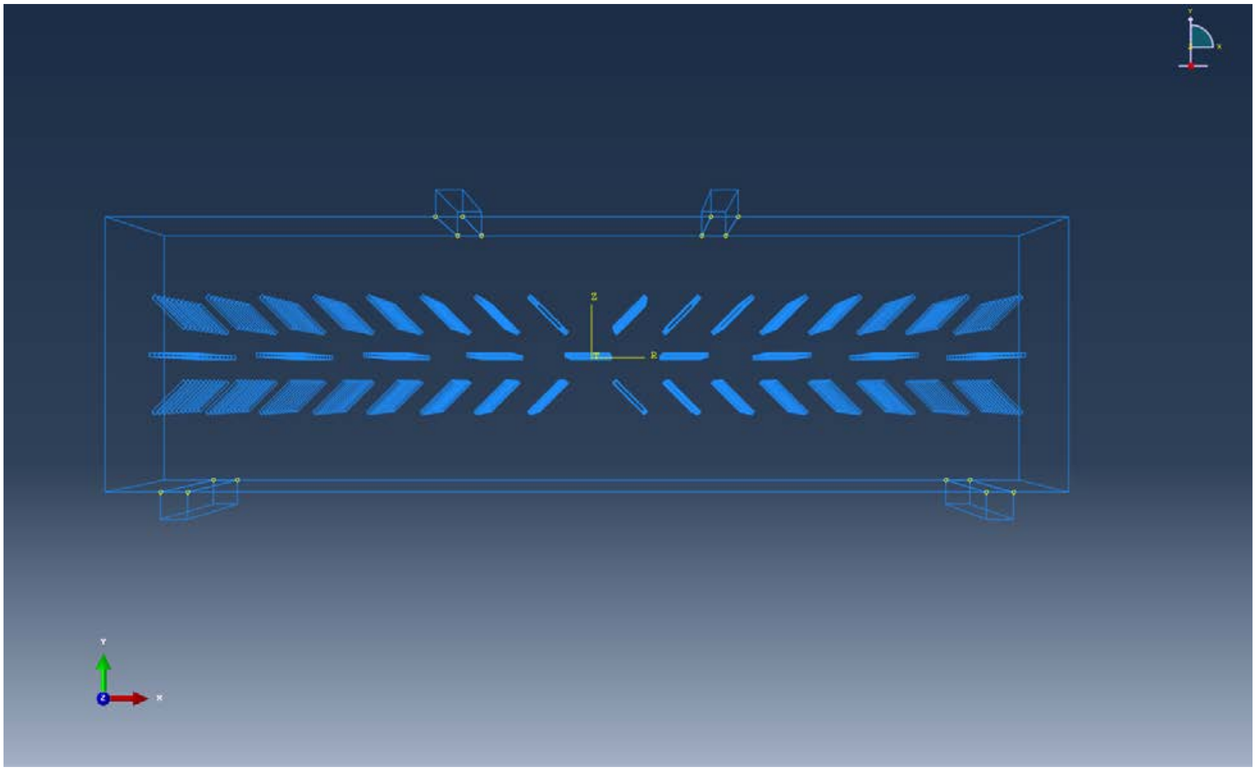

Figure 5-13: Front View of 0.5% Wheat Fibers Distribution.

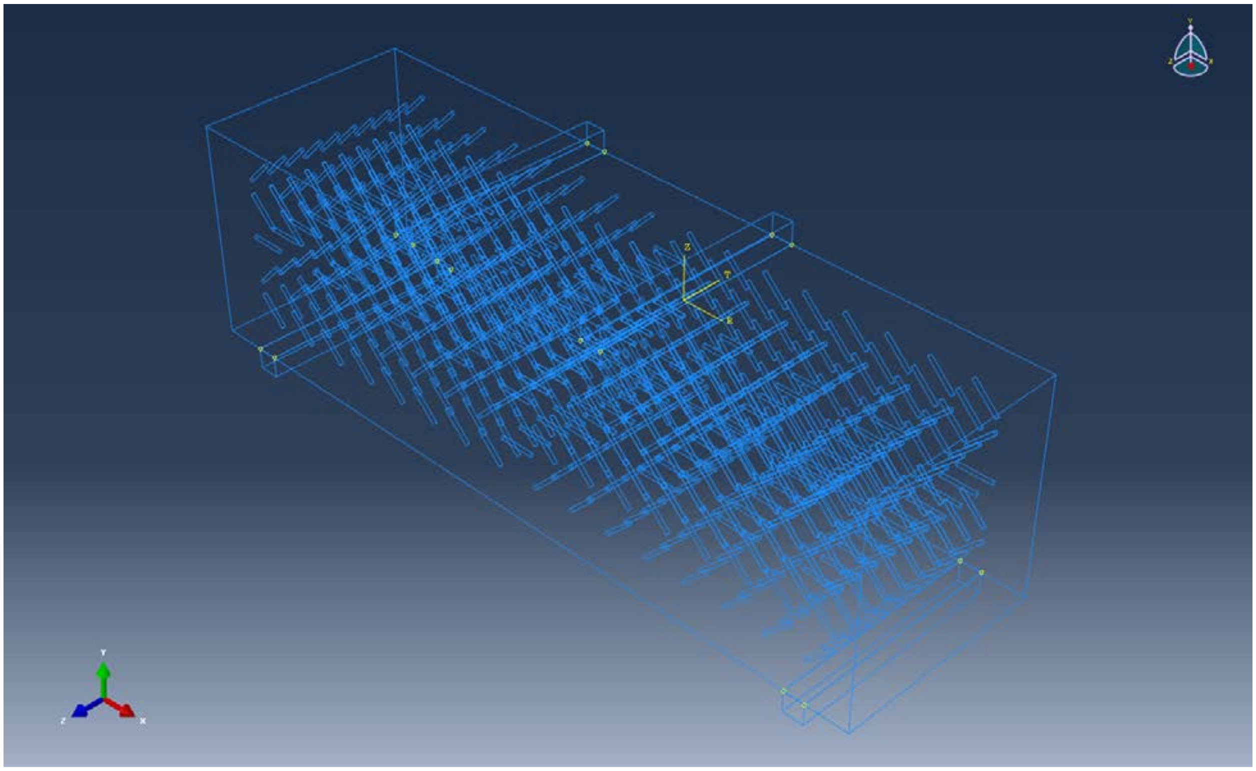

Figure 5-14: Isotropic View of 0.75% Wheat Fibers Distribution.

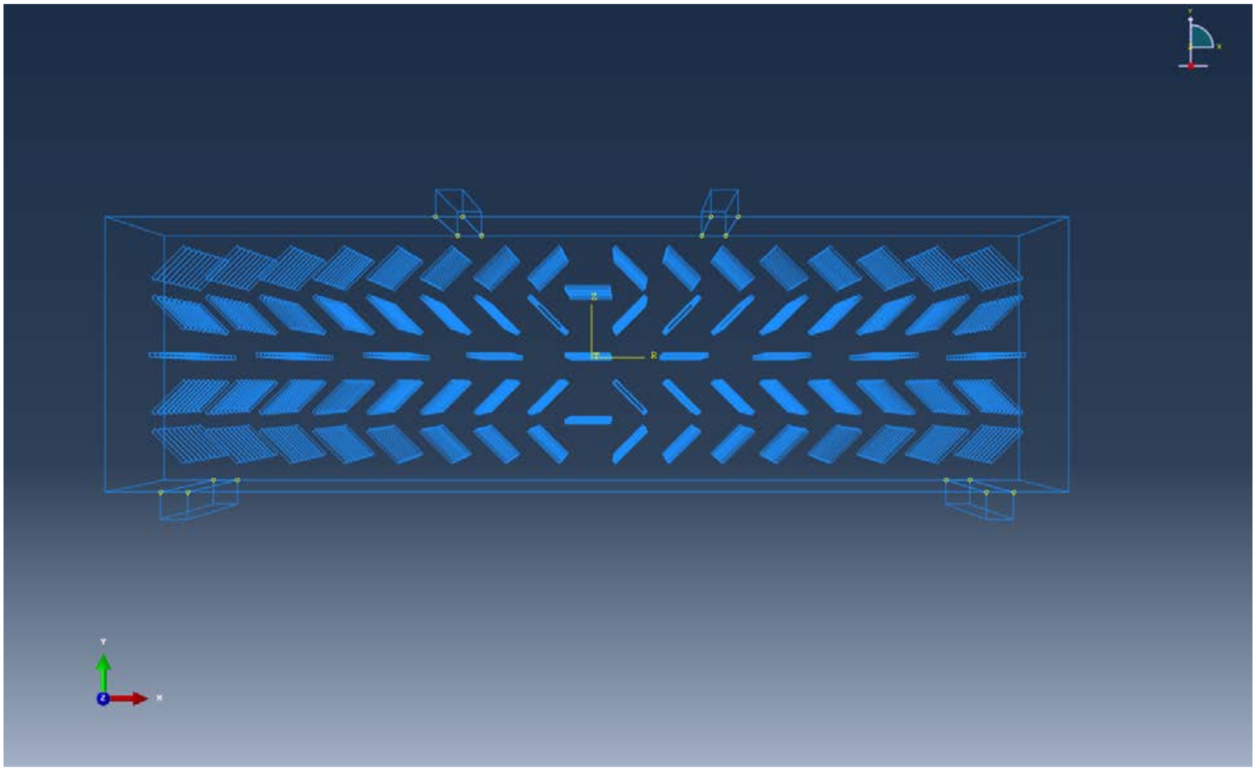

Figure 5-15: Front View of 0.75% and 1% Wheat Fibers Distribution.

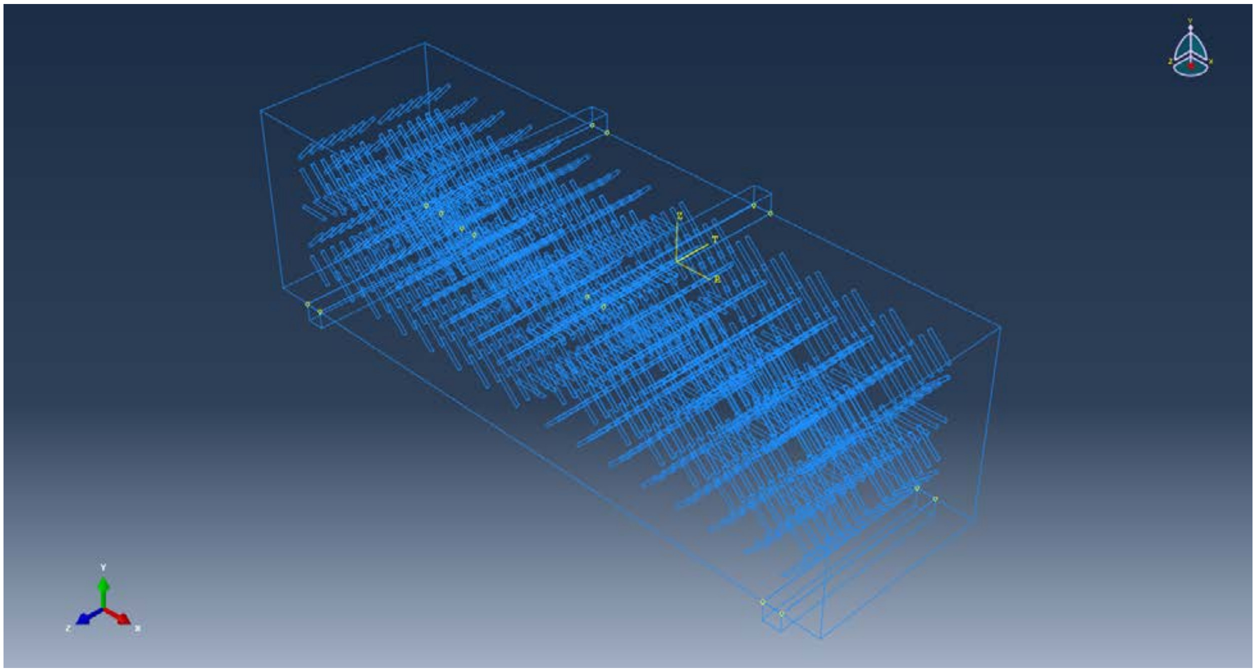

Figure 5-16: Isotropic View of 1% Wheat Fibers Distribution.

5.3 Model Setup

5.3.1 Concrete Cylinders:

A 3D model of the cylinder was developed in ABAQUS with two different boundaries to simulate a rough contacts and a smooth contact. The rough contact was simulated by preventing the top and the bottom surfaces of the cylinder from expanding in diameter, while the smooth contact was achieved by applying zero limitations to the expansion of the diameter (see Figure 5-17, Figure 5-18 and Figure 5-19).

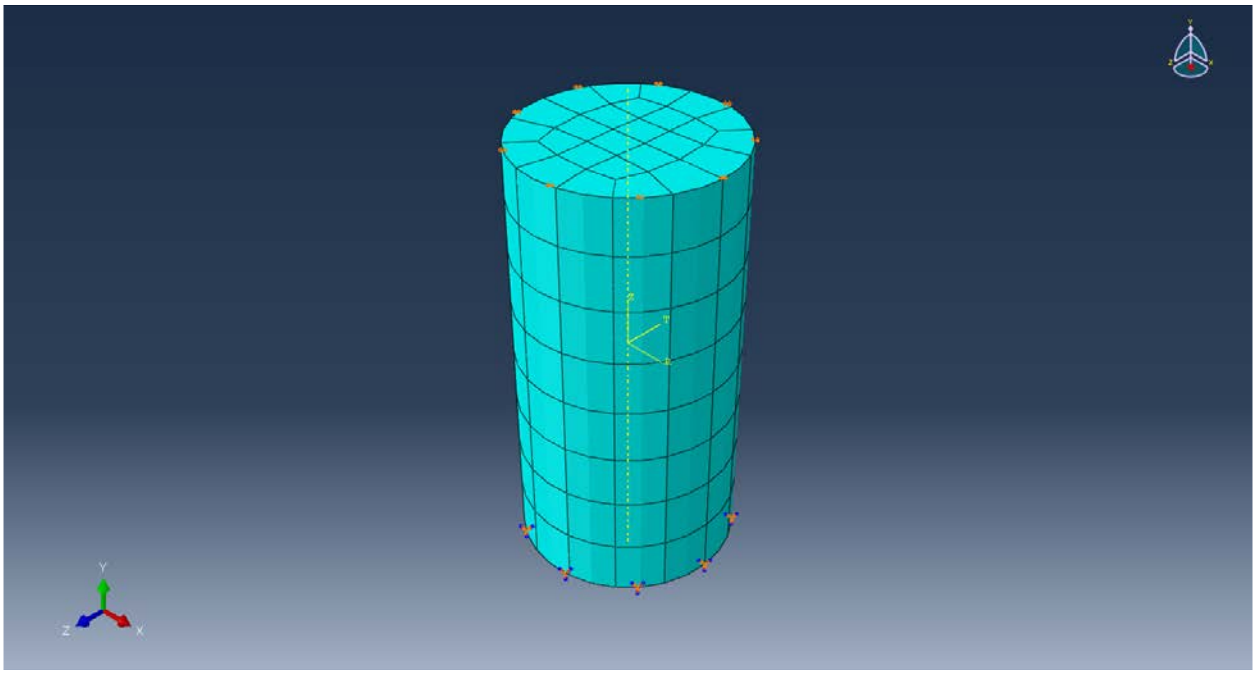

Figure 5-17: Cylinder Rough Boundaries.

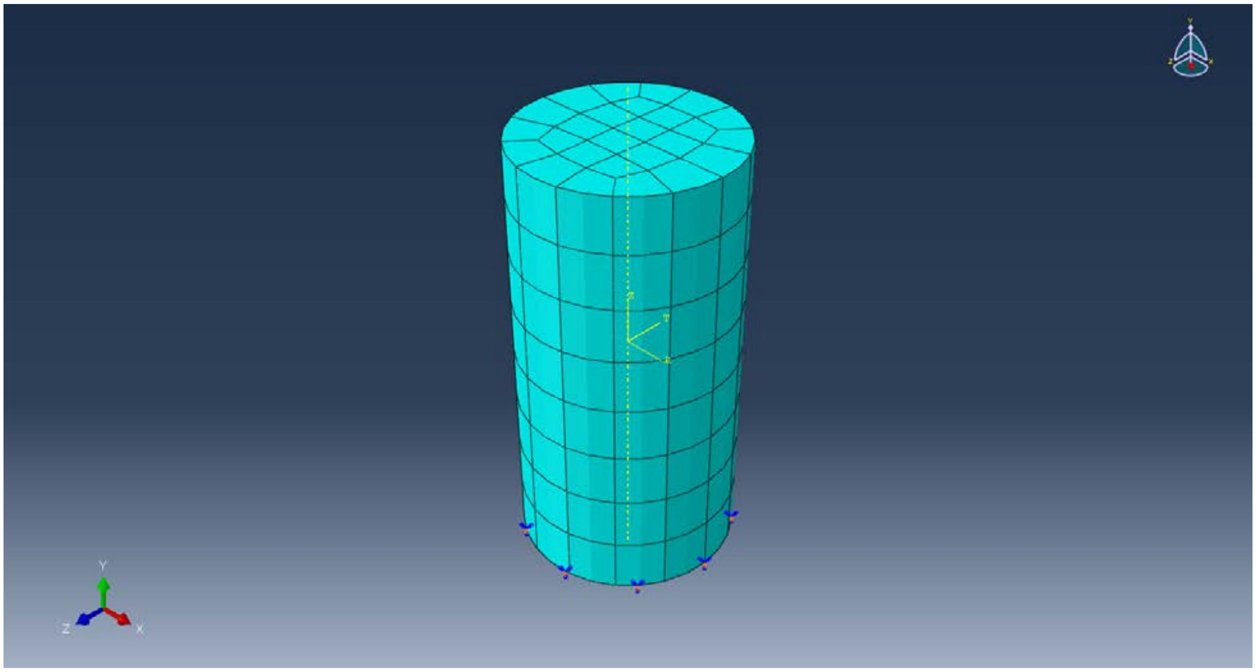

Figure 5-18: Cylinder Smooth Boundaries.

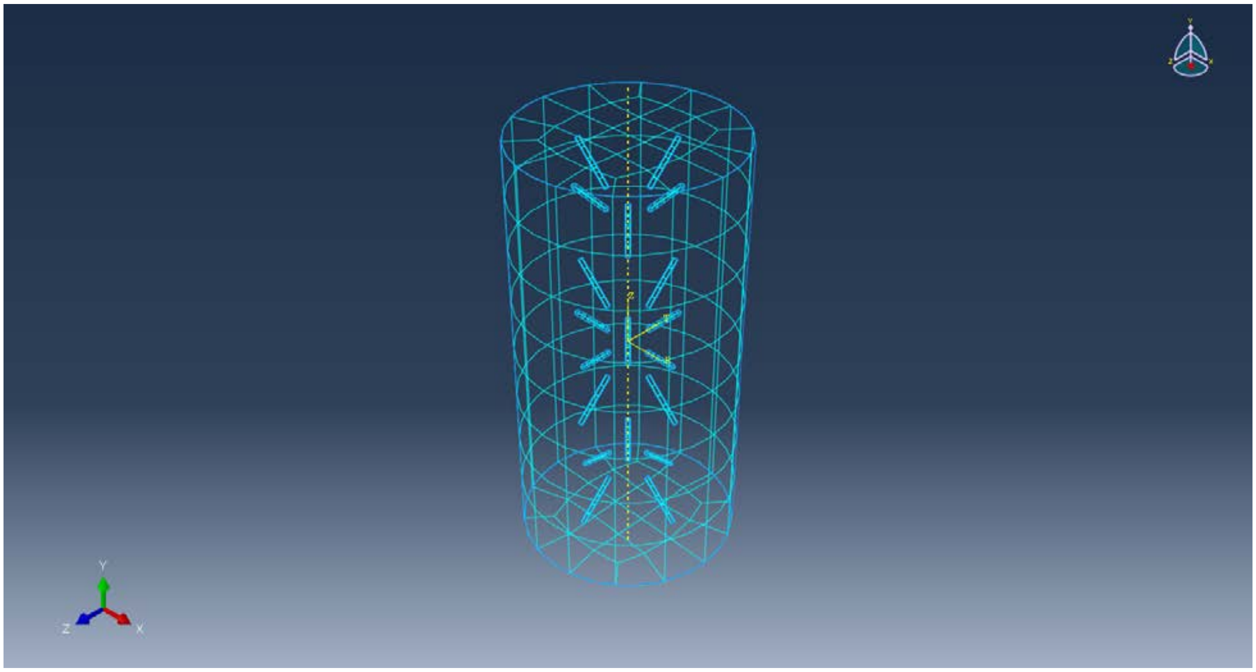

Figure 5-19: Cylinder See-Through Mesh.

5.3.2 Concrete Prisms:

As for the 3D model of the cylinder it was simulated with four steel plates, two for the supports and the other two for the loading, tied to the prism as shown in Figure 5-20. The support plates were pin and roller to simulate the simply support conditions. Finally the mesh was applied to the specimen as shown in Figure 5-21 and Figure 5-22.

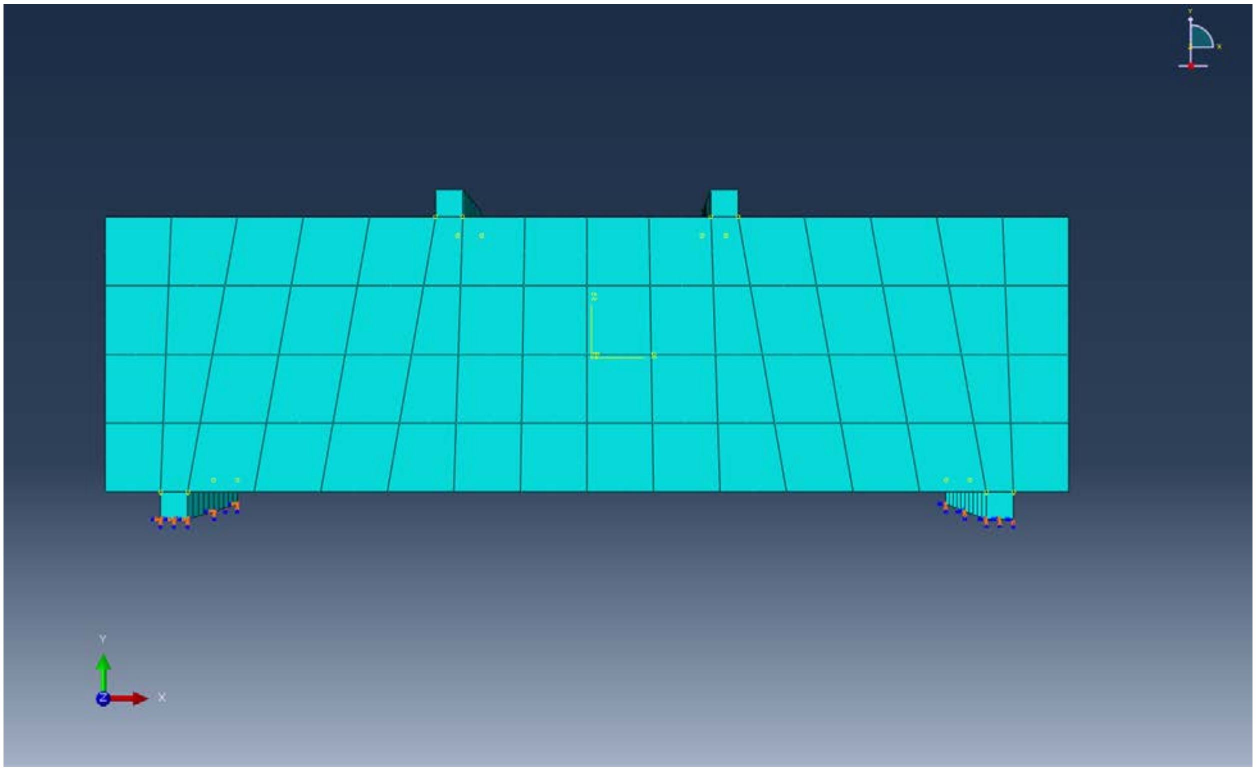

Figure 5-20: Prism Boundary Conditions.

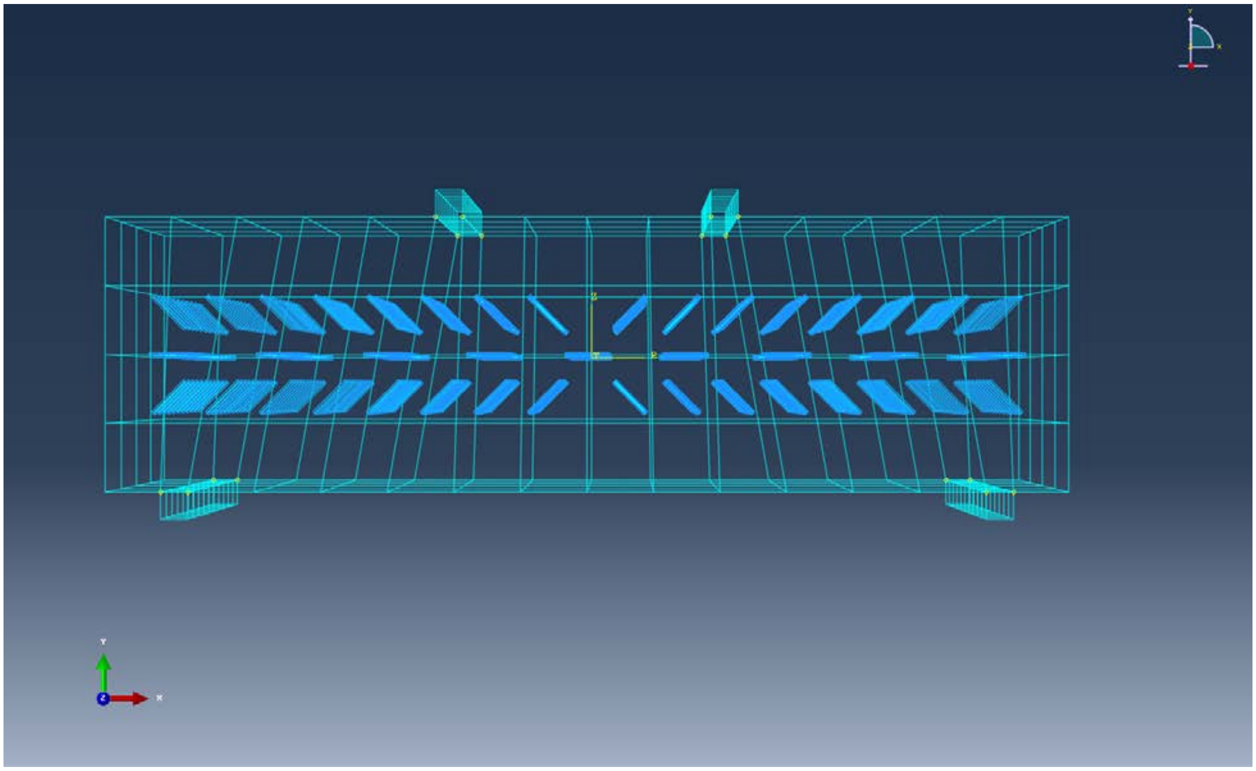

Figure 5-21: Prism See-Through Mesh.

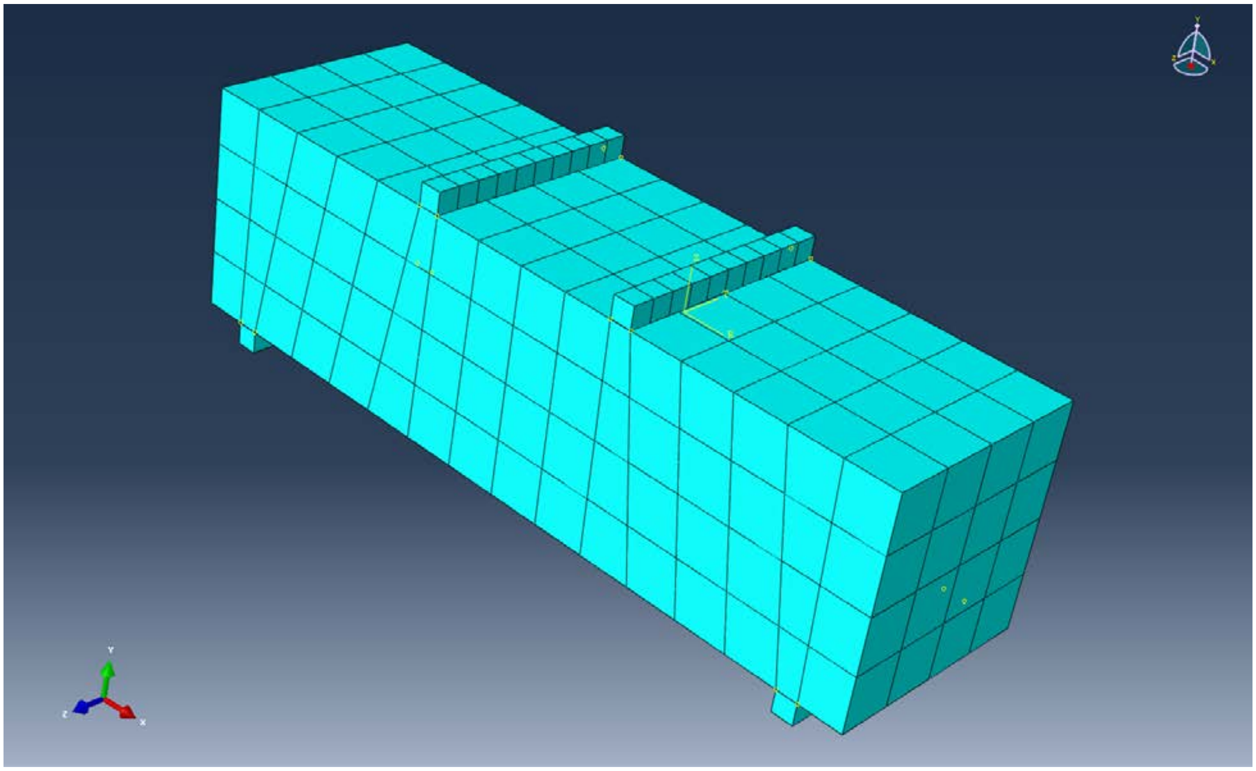

Figure 5-22: Isotropic View of the Mesh.

5.4 Results

5.4.1 Concrete Cylinders:

For the cylinders, the loading was applied as a pressure applied to the top surface till a load reaching that of the experimental cylinders. Figure 5-23 shows the results of the different cylinders modeled in ABAQUS with the different Percentages of wheat fibers. Figure 5-24 through Figure 5-27 represent the load versus strain curves for each percentage of fiber specimens from the experiment in compare with the simulation. Figure 5-28 through Figure 5-35 represents the cylinder contour strains obtained from the simulation for the different cylinders.

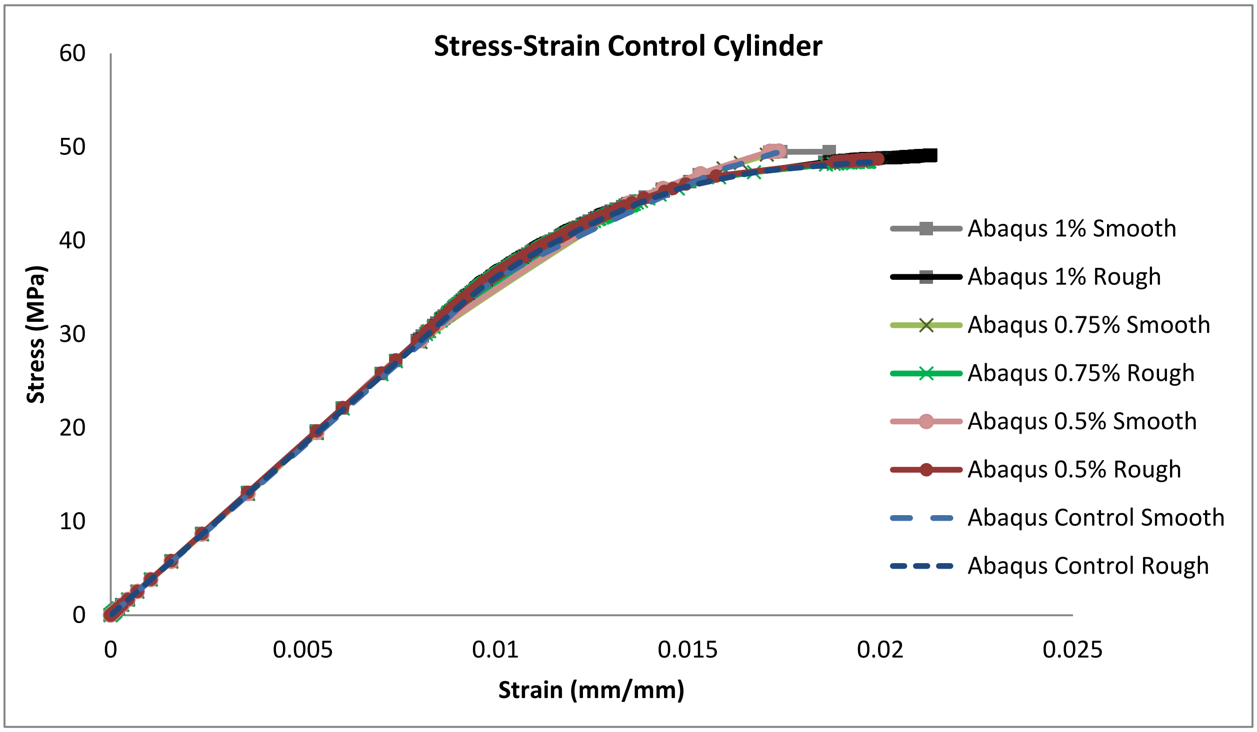

Figure 5-23: Stress-Strain for Simulations of Different Cylinders.

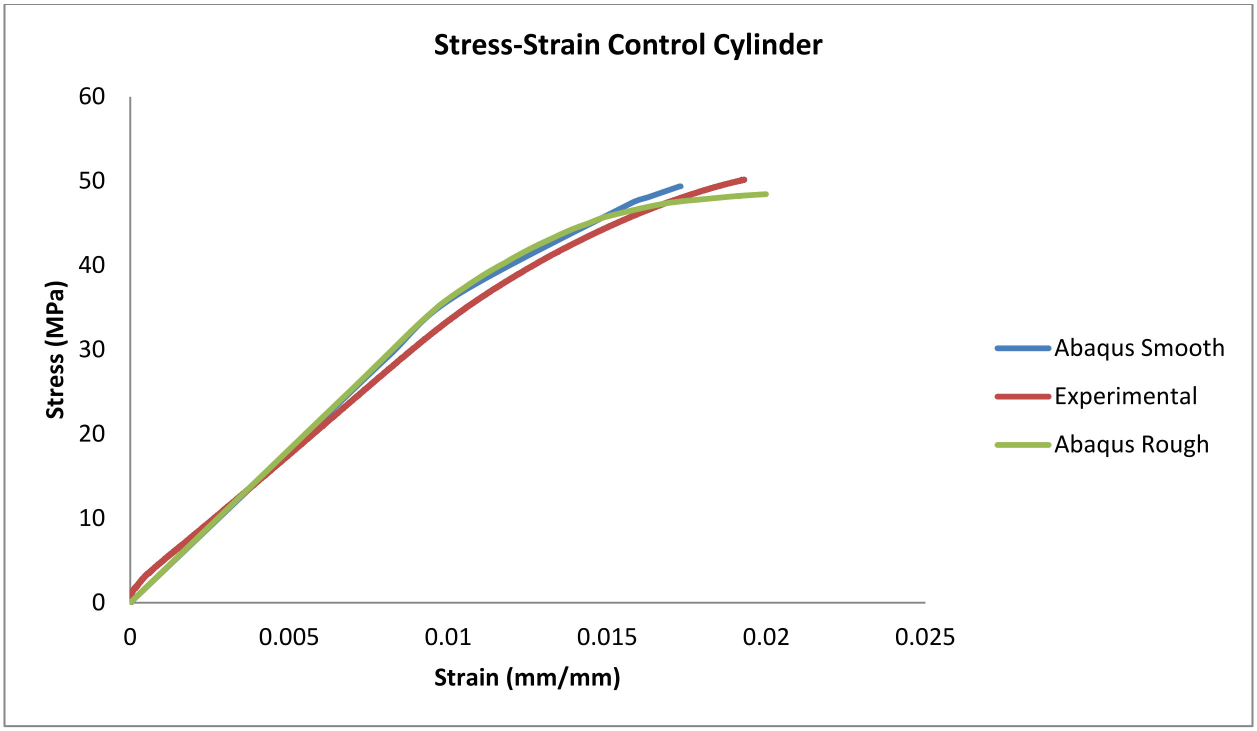

Figure 5-24: Abaqus Control Simulation vs. Experimental Results.

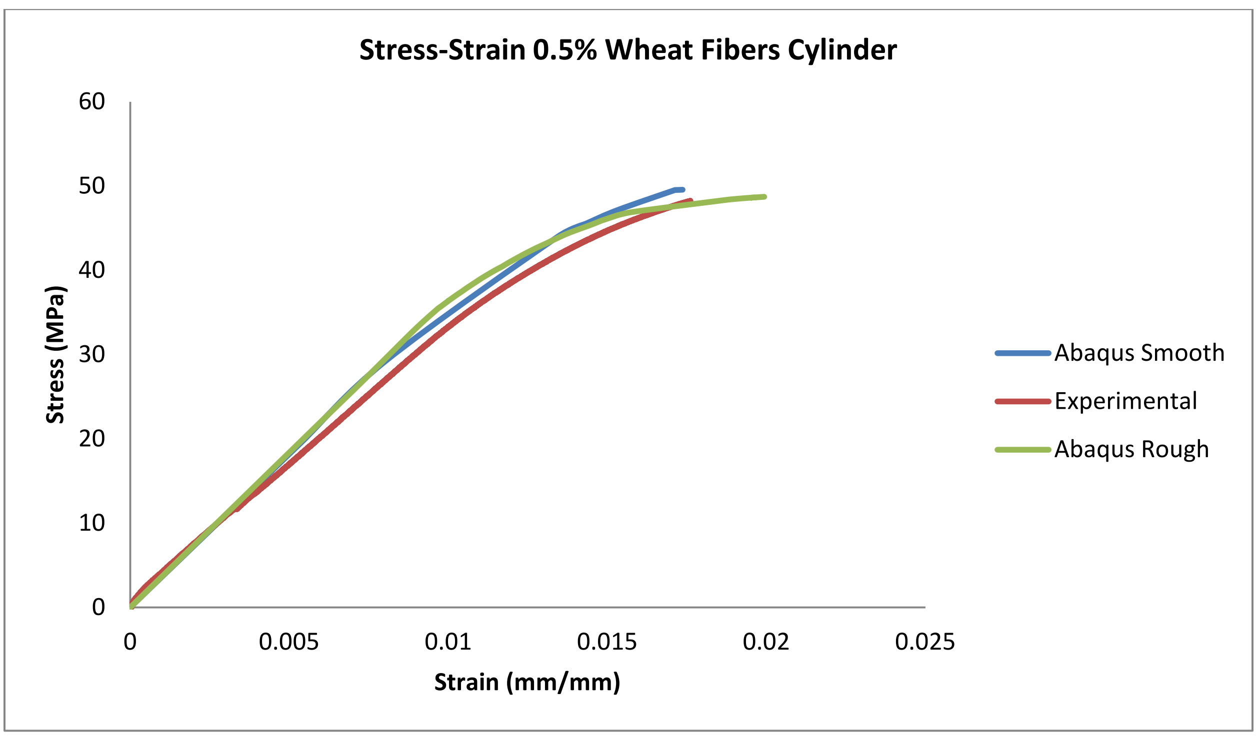

Figure 5-25: Abaqus Simulation for Cylinders with 0.5% Fibers vs. Experimental Results.

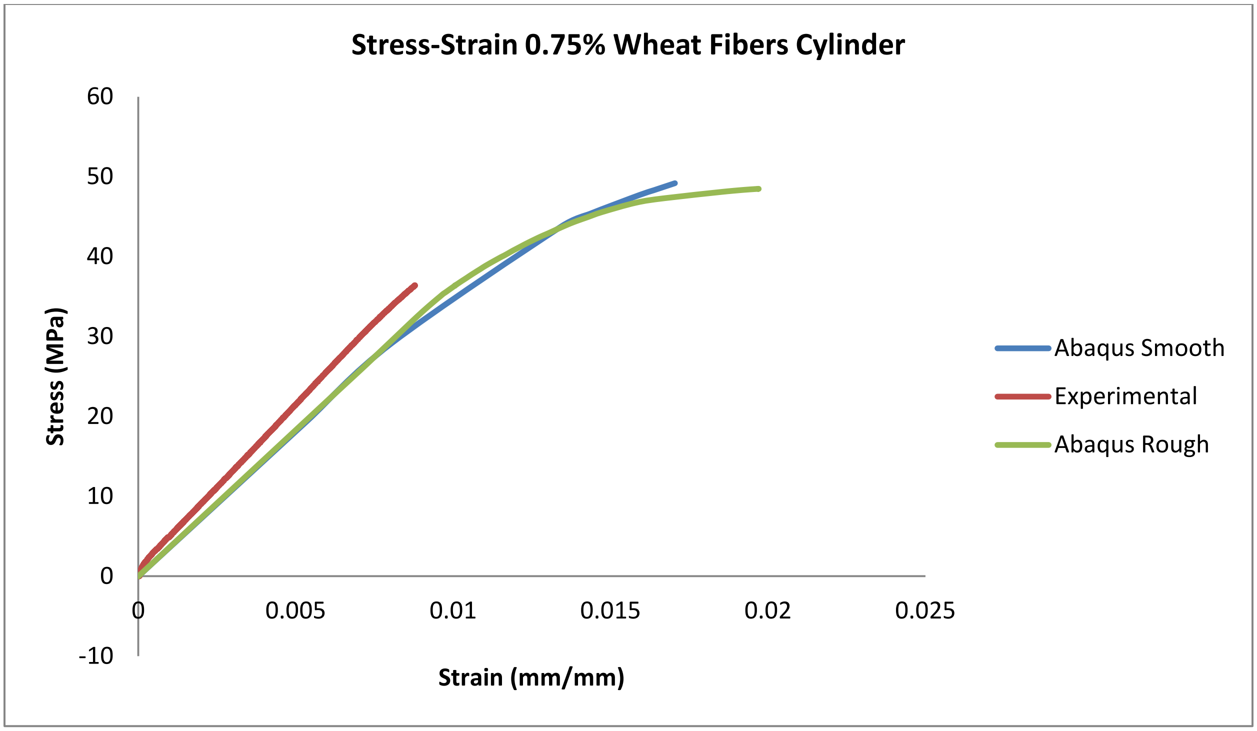

Figure 5-26: Abaqus Simulation for Cylinders with 0.75% Fibers vs. Experimental Results.

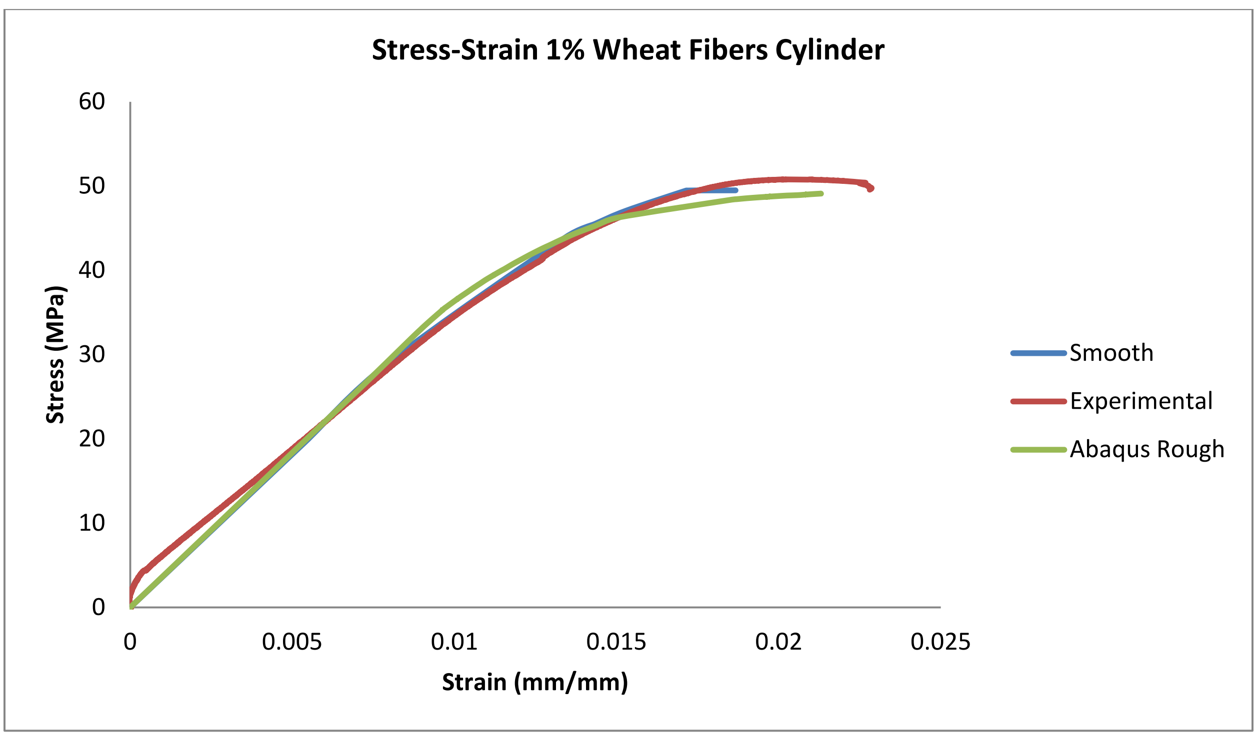

Figure 5-27: Abaqus Simulation for Cylinders with 1% Fibers vs. Experimental Results.

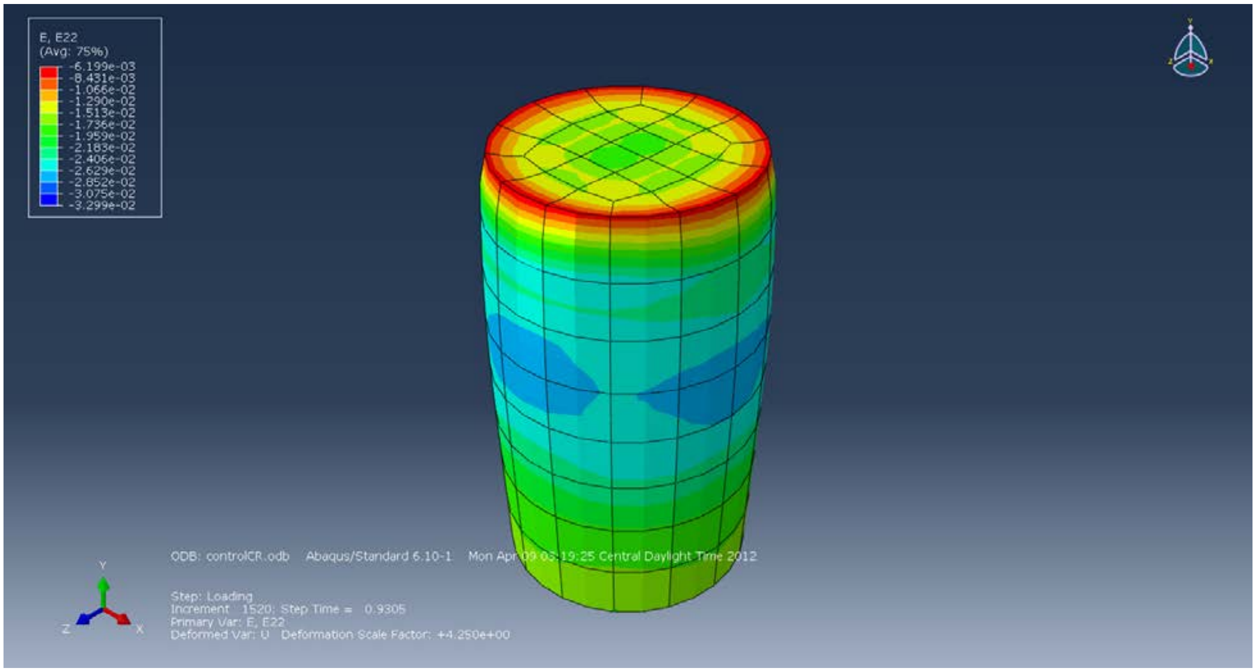

Figure 5-28: Vertical Strain (E22 in the Y-axis) for the Control Cylinder (Rough Boundaries).

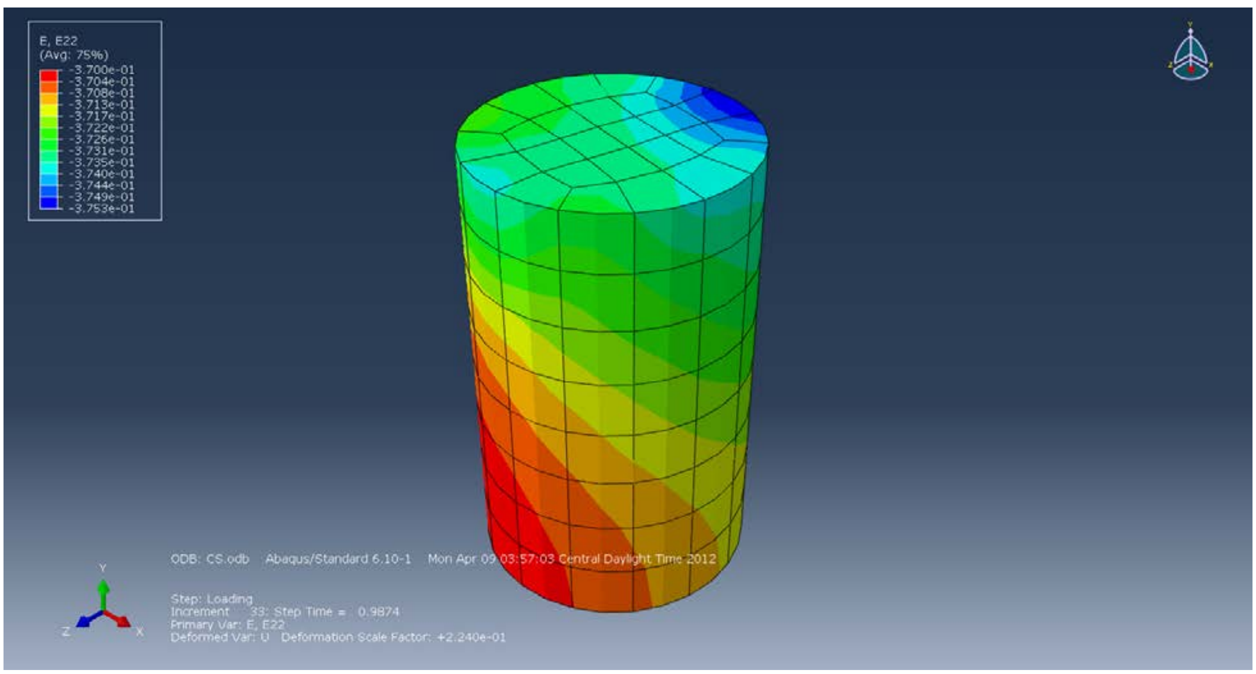

Figure 5-29: Vertical Strain (E22 in the Y-axis) for the Control Cylinder (Smooth Boundaries).

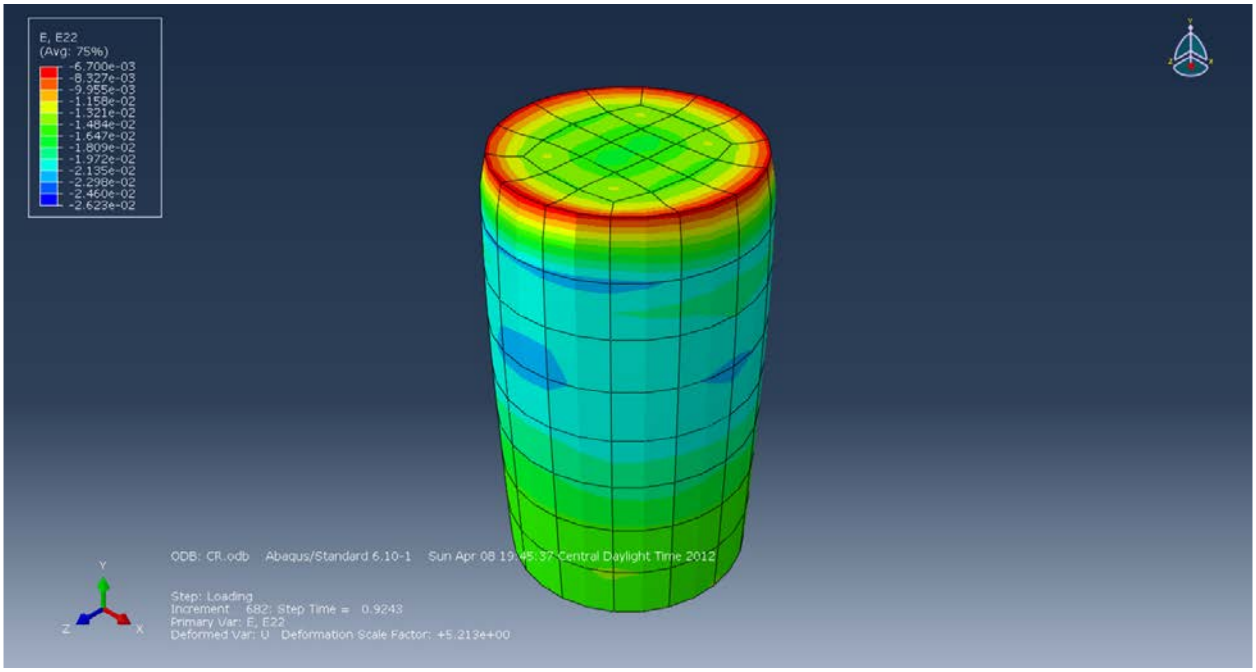

Figure 5-30: Vertical Strain (E22 in the Y-axis) for the Cylinder with 0.5% Wheat Fibers (Rough Boundaries).

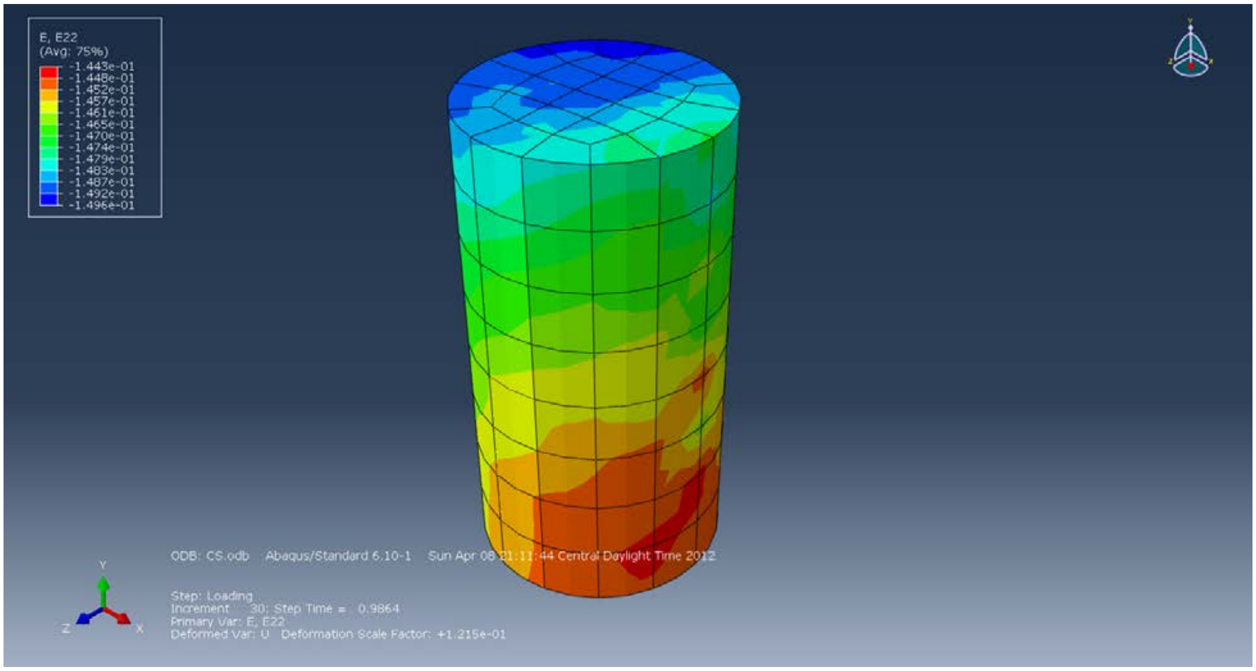

Figure 5-31: Vertical Strain (E22 in the Y-axis) for the Cylinder with 0.5% Wheat Fibers (Smooth Boundaries).

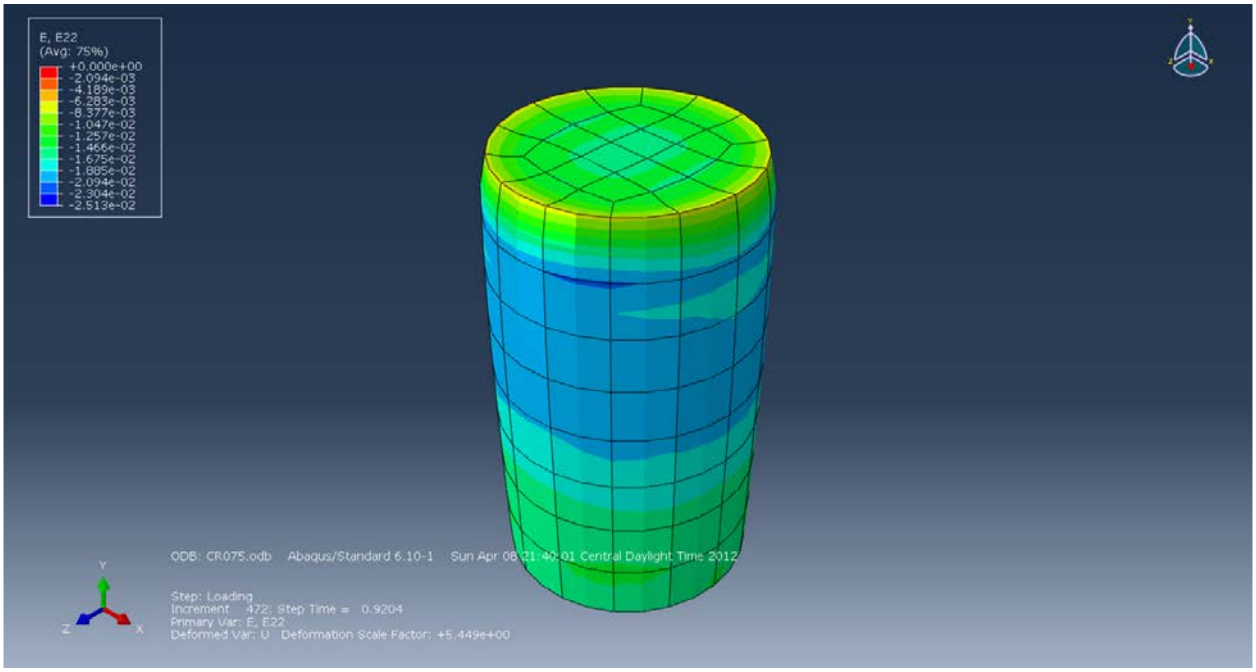

Figure 5-32: Vertical Strain (E22 in the Y-axis) for the Cylinder with 0.75% Wheat Fibers (Rough Boundaries).

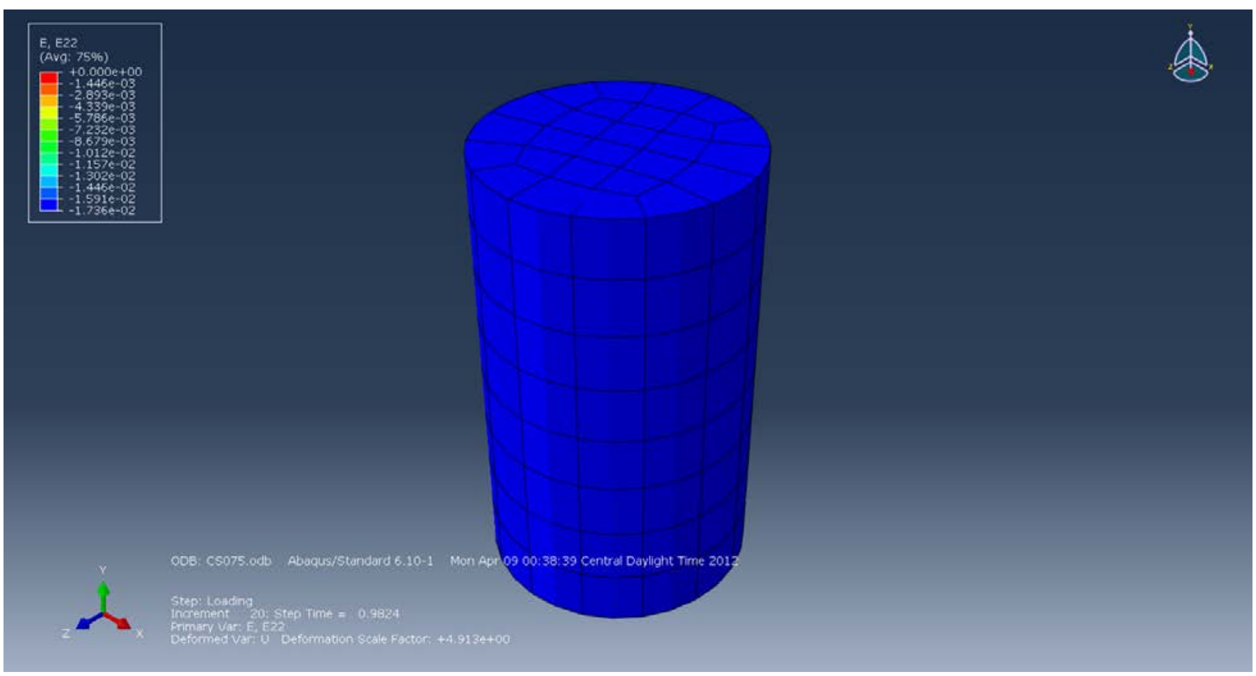

Figure 5-33: Vertical Strain (E22 in the Y-axis) for the Cylinder with 0.75% Wheat Fibers (Smooth Boundaries).

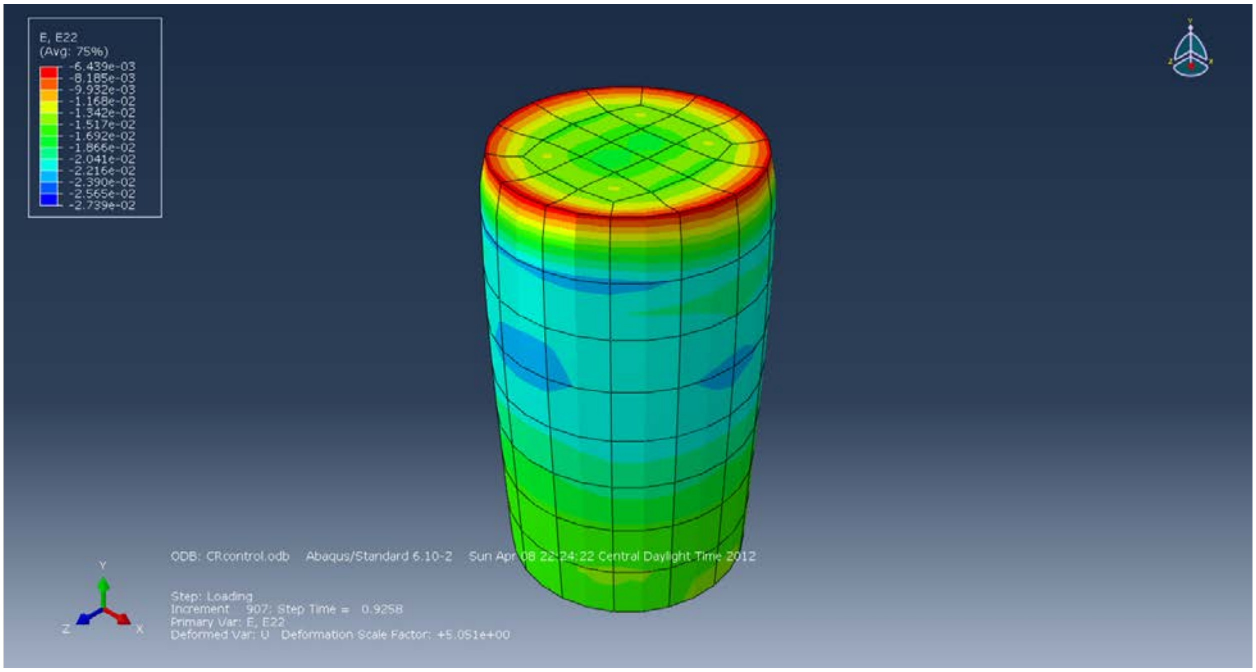

Figure 5-34: Vertical Strain (E22 in the Y-axis) for the Cylinder with 1% Wheat Fibers (Rough Boundaries).

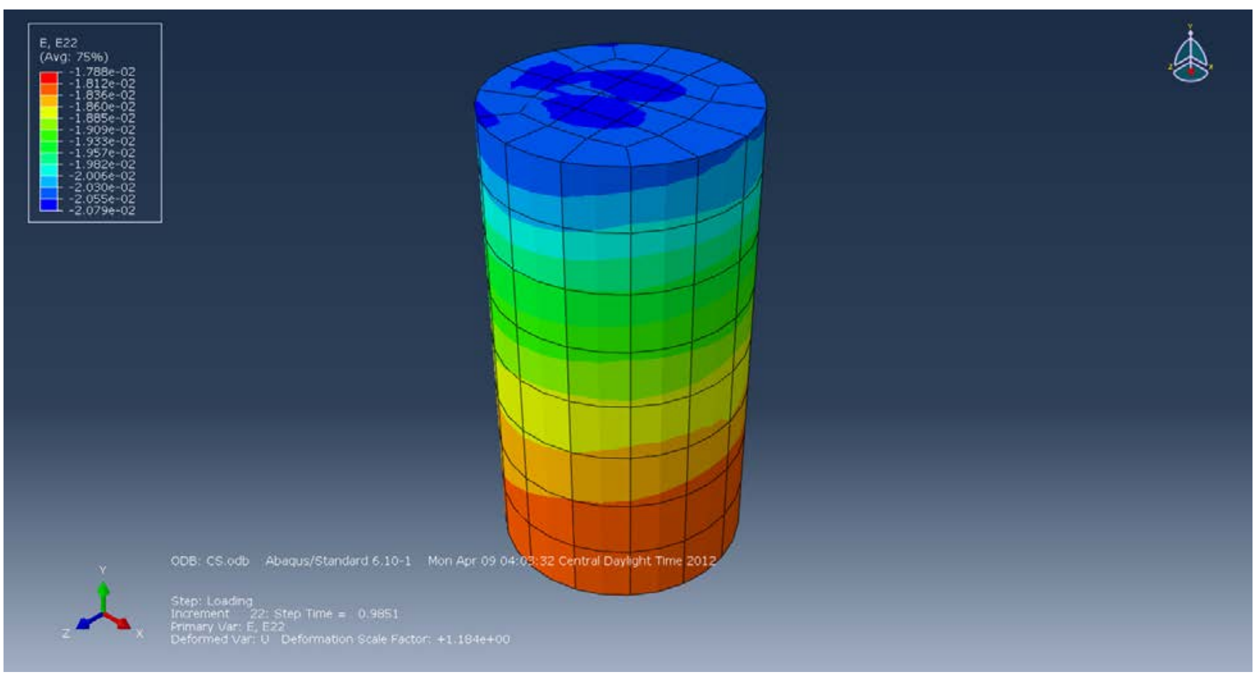

Figure 5-35: Vertical Strain (E22 in the Y-axis) for the Cylinder with 1% Wheat Fibers (Smooth Boundaries).

5.4.2 Concrete Prisms:

Meanwhile, the loading for the prisms was applied as a four point loading on the loading steel plates. Figure 5-36 shows the results of the different prisms modeled in ABAQUS with the different Percentages of wheat fibers. Figure 5-37 through Figure 5-42 represent the load versus strain curves for each percentage of fiber specimens from the experiment in compare with the simulation. Figure 5-43 through Figure 5-50 represents the prisms contour strains obtained from the simulation for the different specimens.

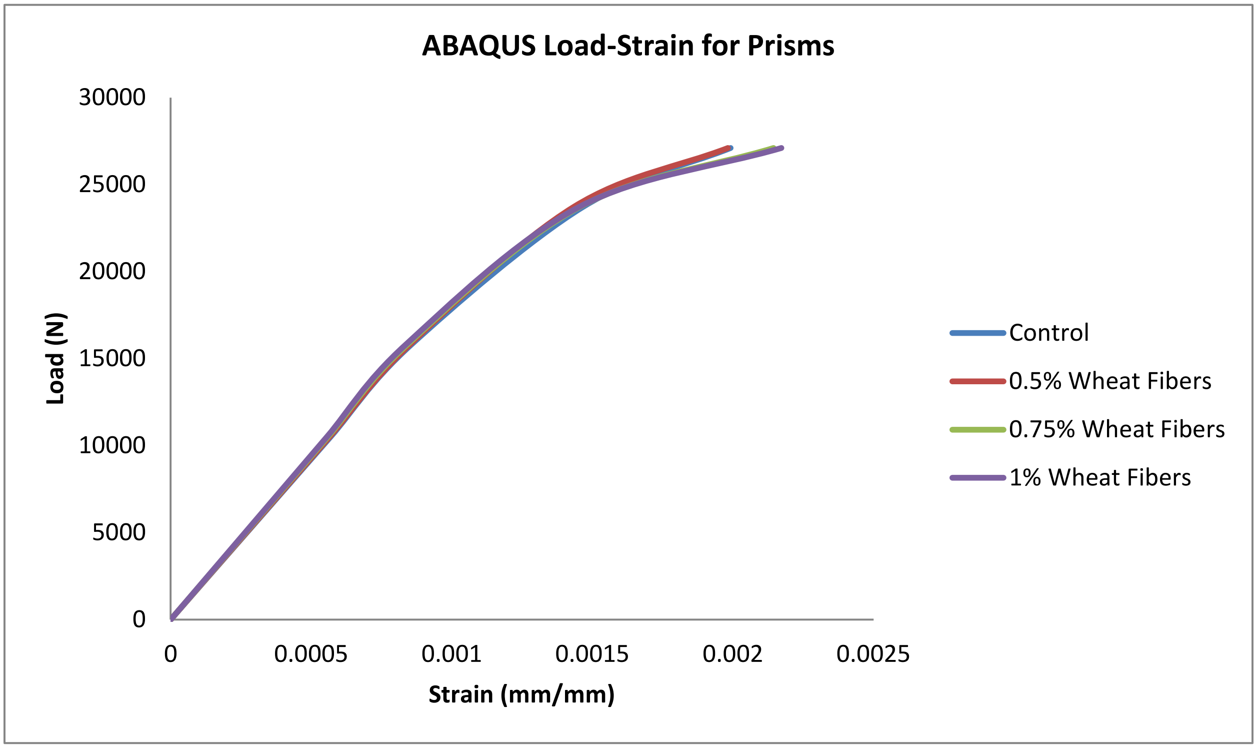

Figure 5-36: Load-Strain for Simulations of Different Prisms.

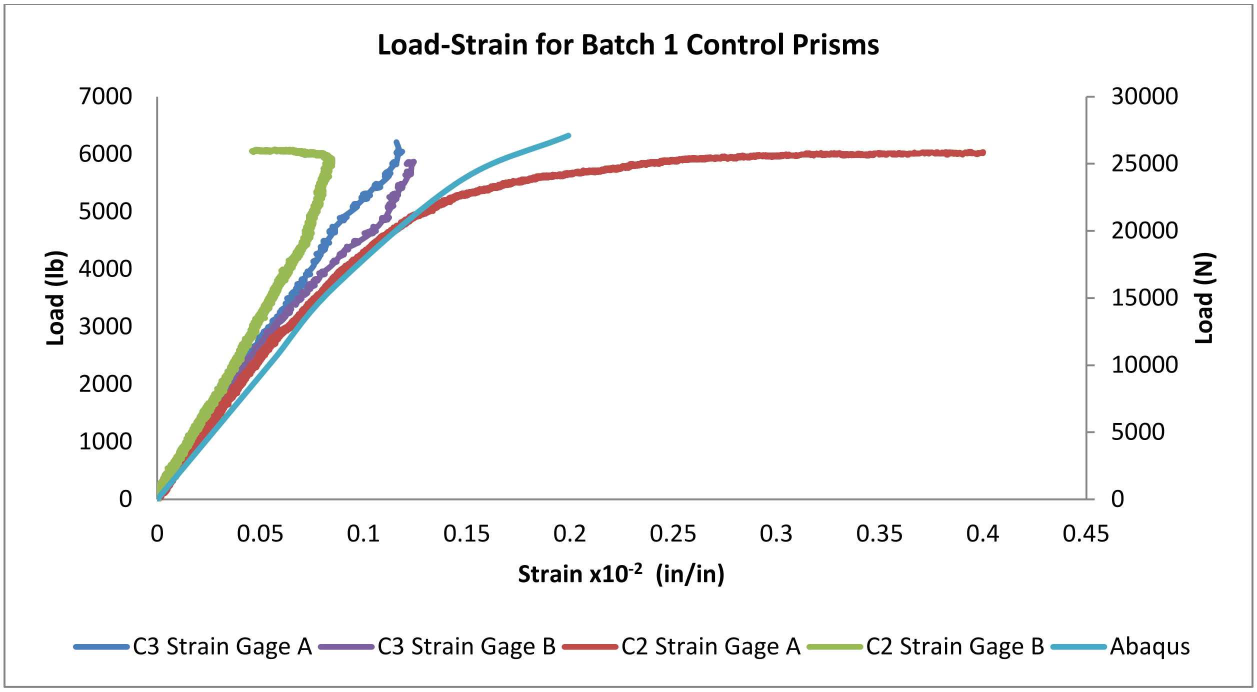

Figure 5-37: Abaqus Control Simulation vs. Experimental Results for Batch 1 Control Prisms.

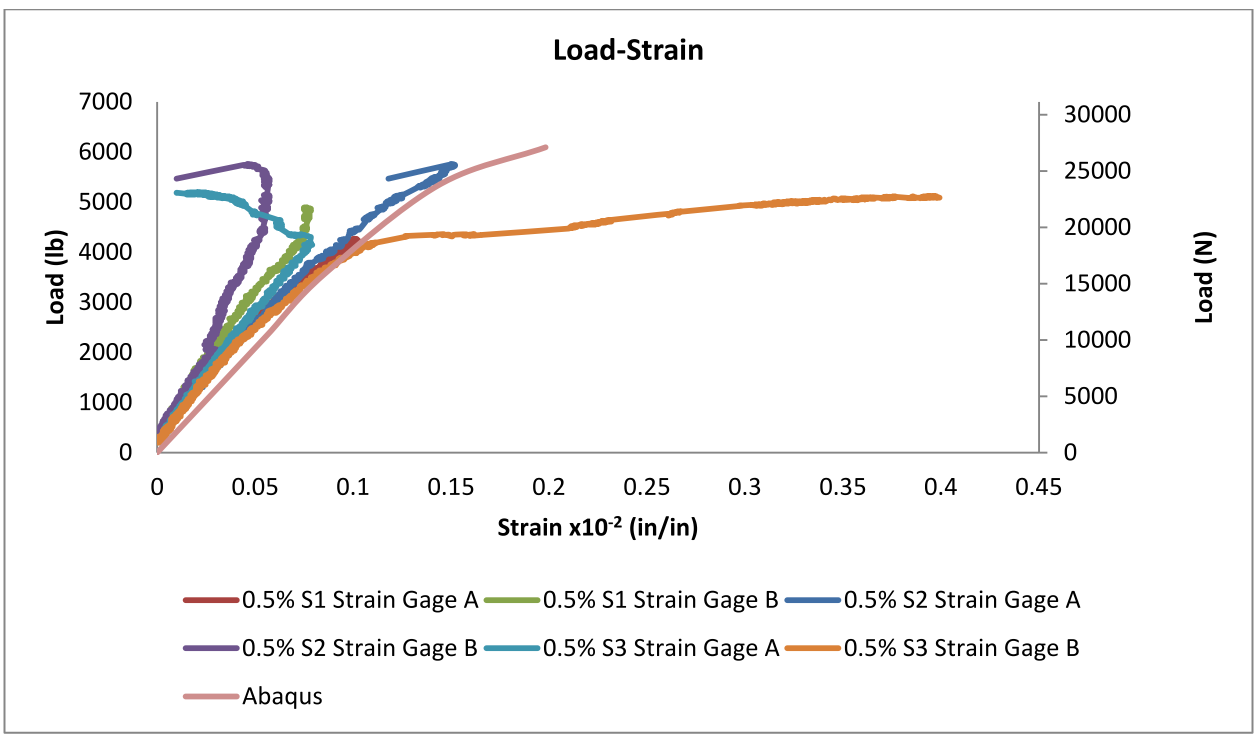

Figure 5-38: Abaqus Simulation vs. Experimental Results for Batch 1 Prisms with 0.5% Fibers.

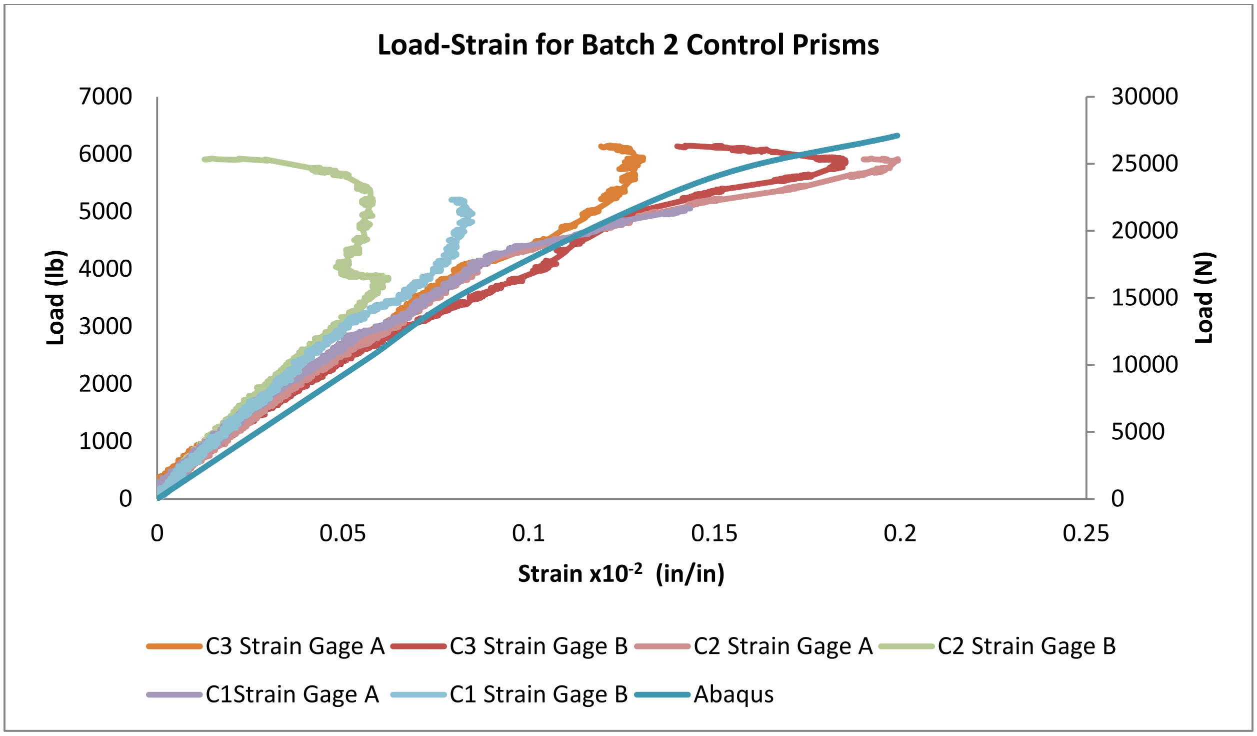

Figure 5-39: Abaqus Control Simulation vs. Experimental Results for Batch 2 Control Prisms.

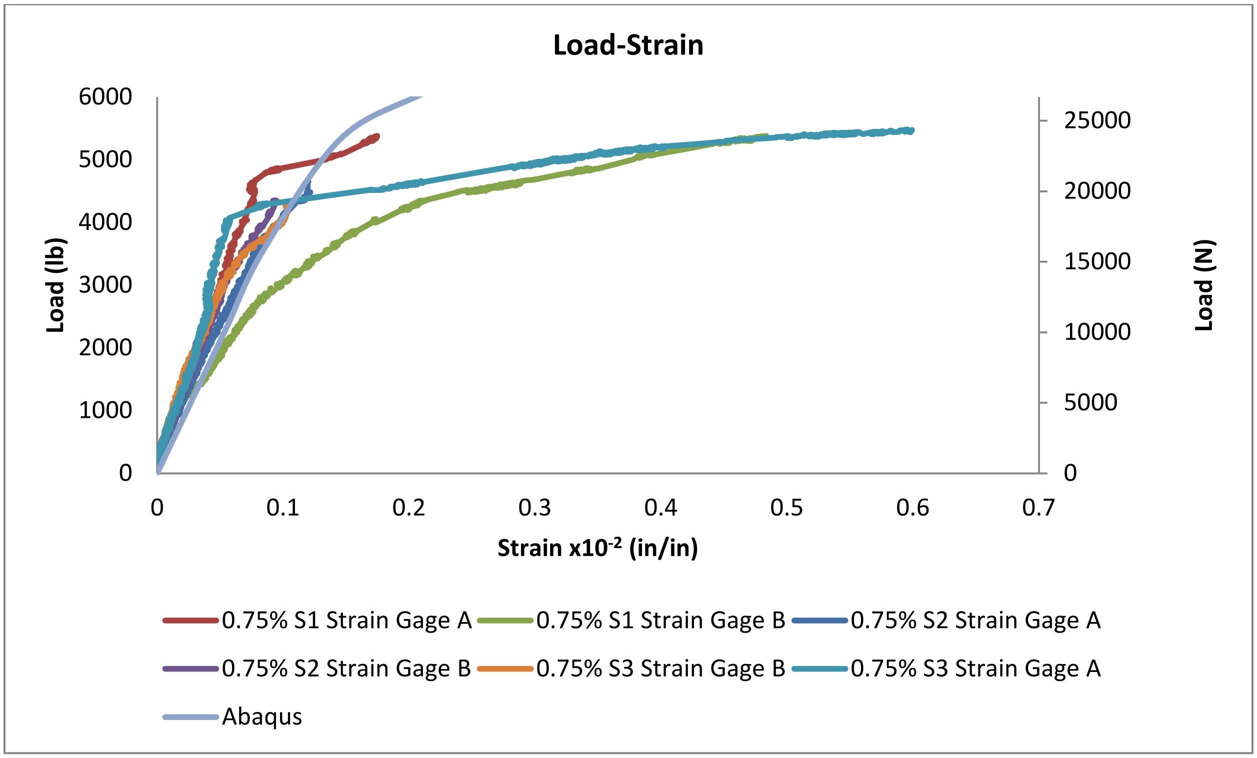

Figure 5-40: Abaqus Simulation vs. Experimental Results for Batch 2 Prisms with 0.75% Fibers.

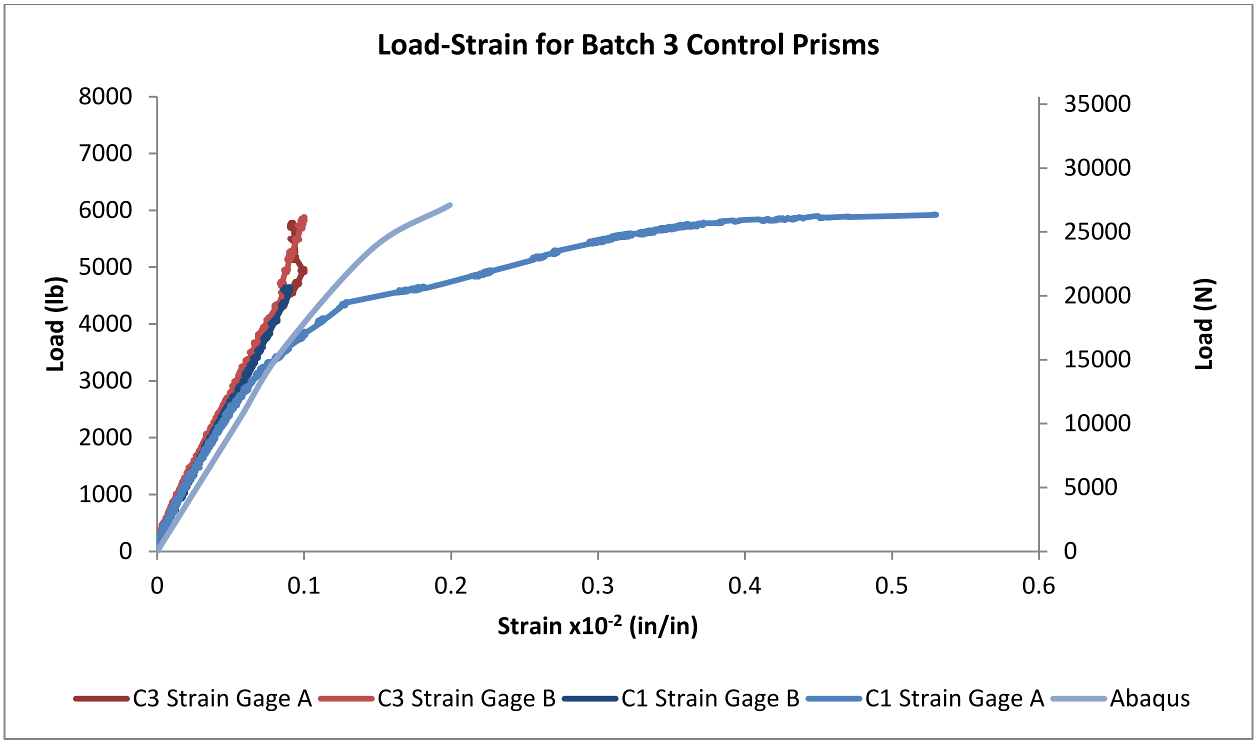

Figure 5-41: Abaqus Control Simulation vs. Experimental Results for Batch 3 Control Prisms.

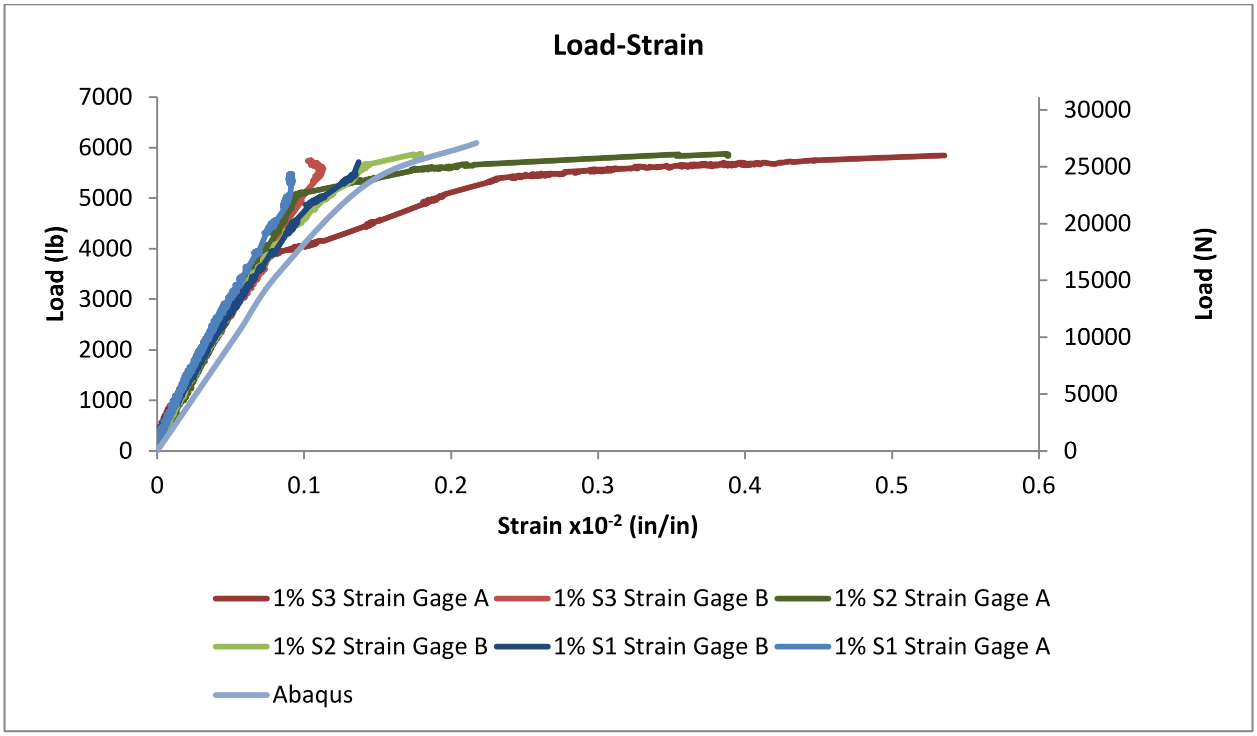

Figure 5-42: Abaqus Simulation vs. Experimental Results for Batch 3 Prisms with 1% Fibers.

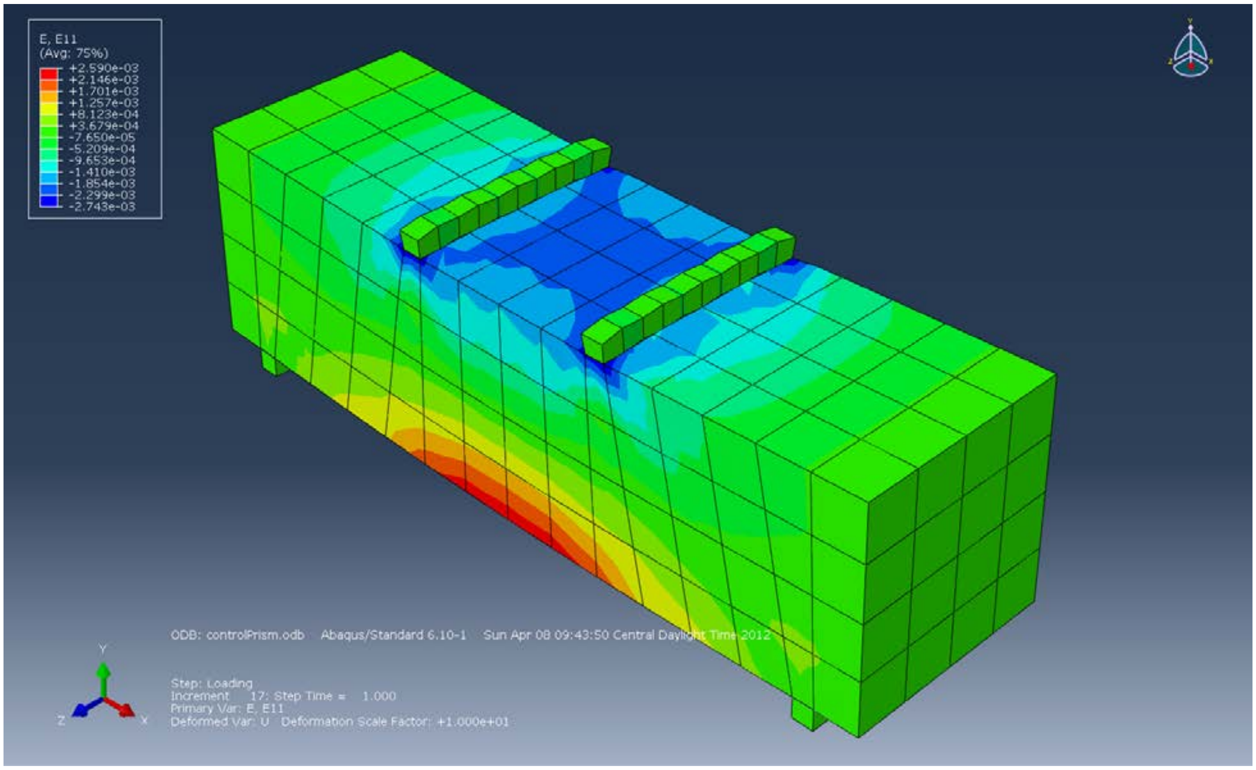

Figure 5-43: Strain in X-Direction (E11) for the Control Prism (Isotropic View).

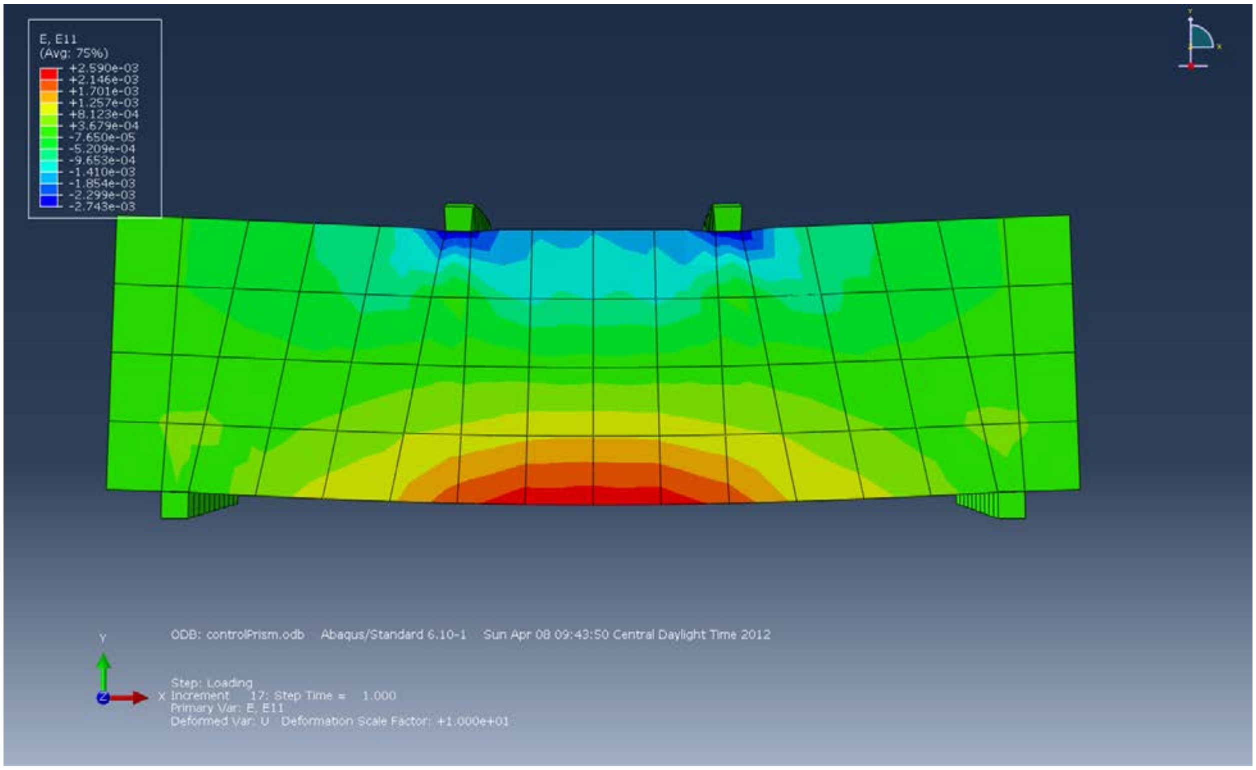

Figure 5-44: Strain in X-Direction (E11) for the Control Prism (Front View).

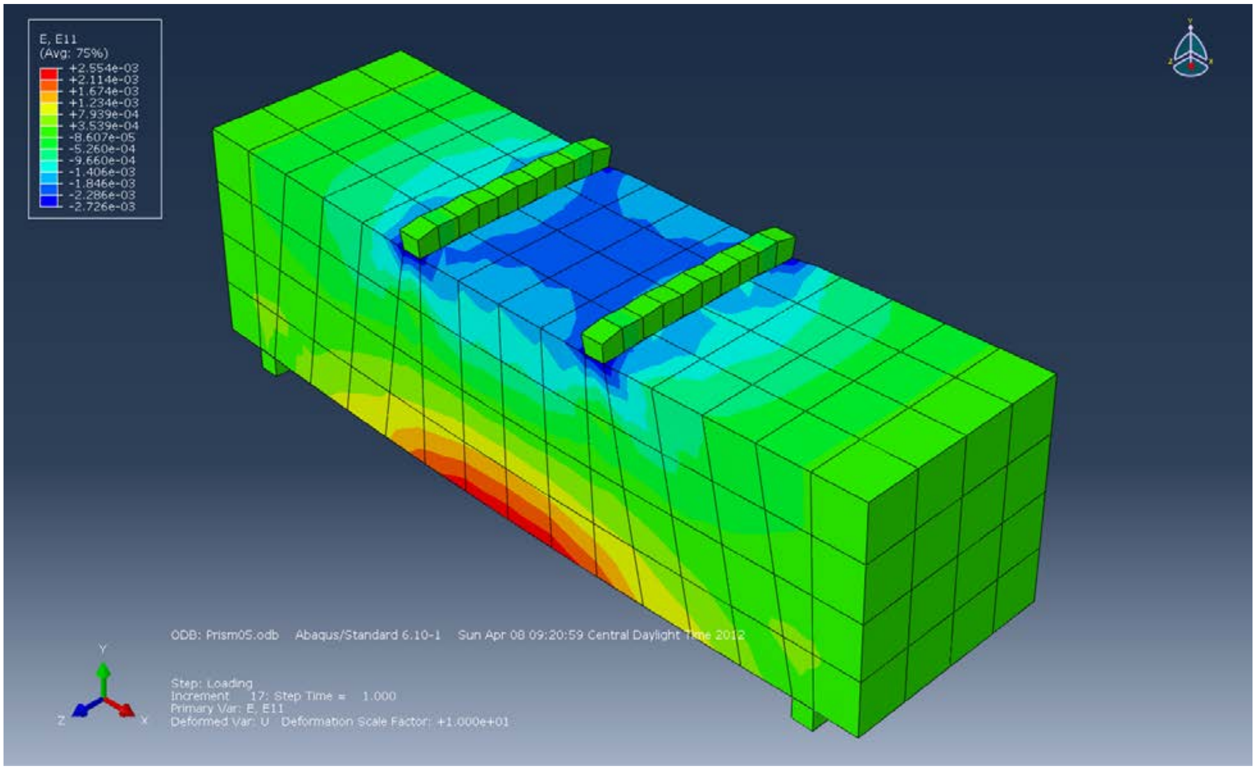

Figure 5-45: Strain in X-Direction (E11) for Prism with 0.5% Fibers (Isotropic View).

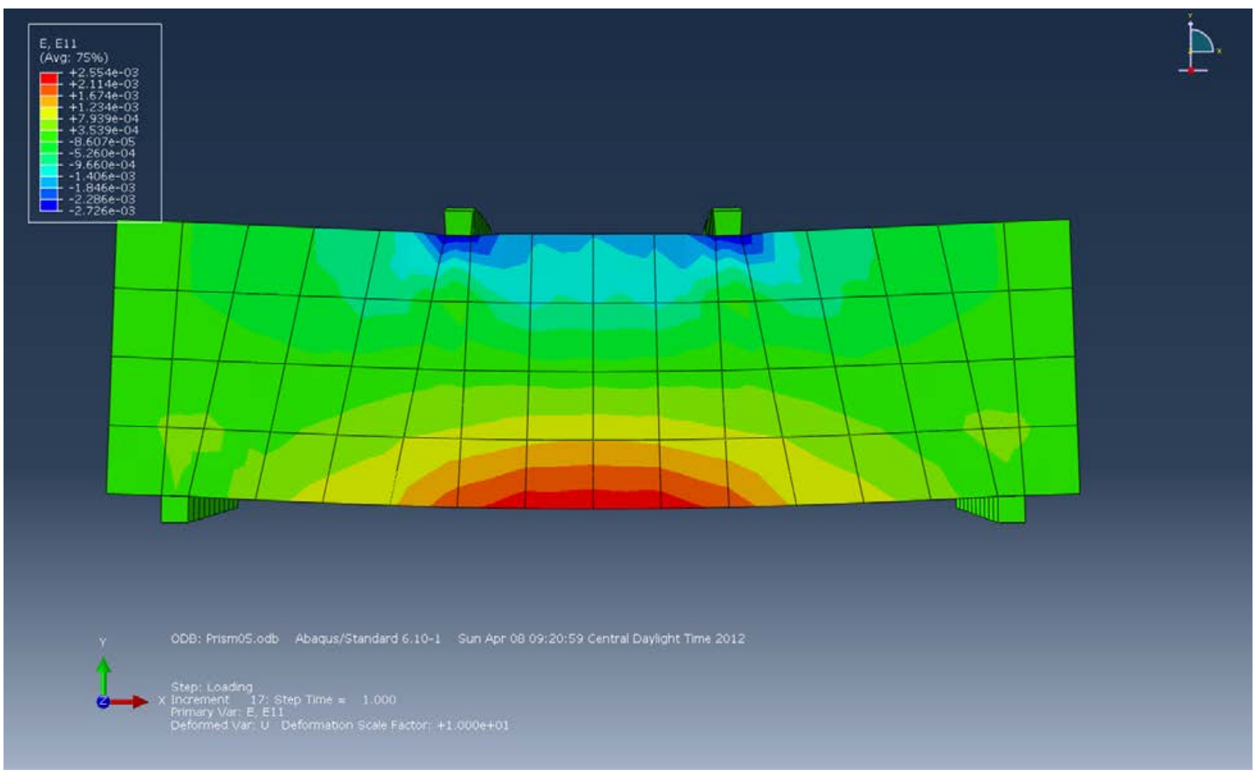

Figure 5-46: Strain in X-Direction (E11) for Prism with 0.5% Fibers (Front View).

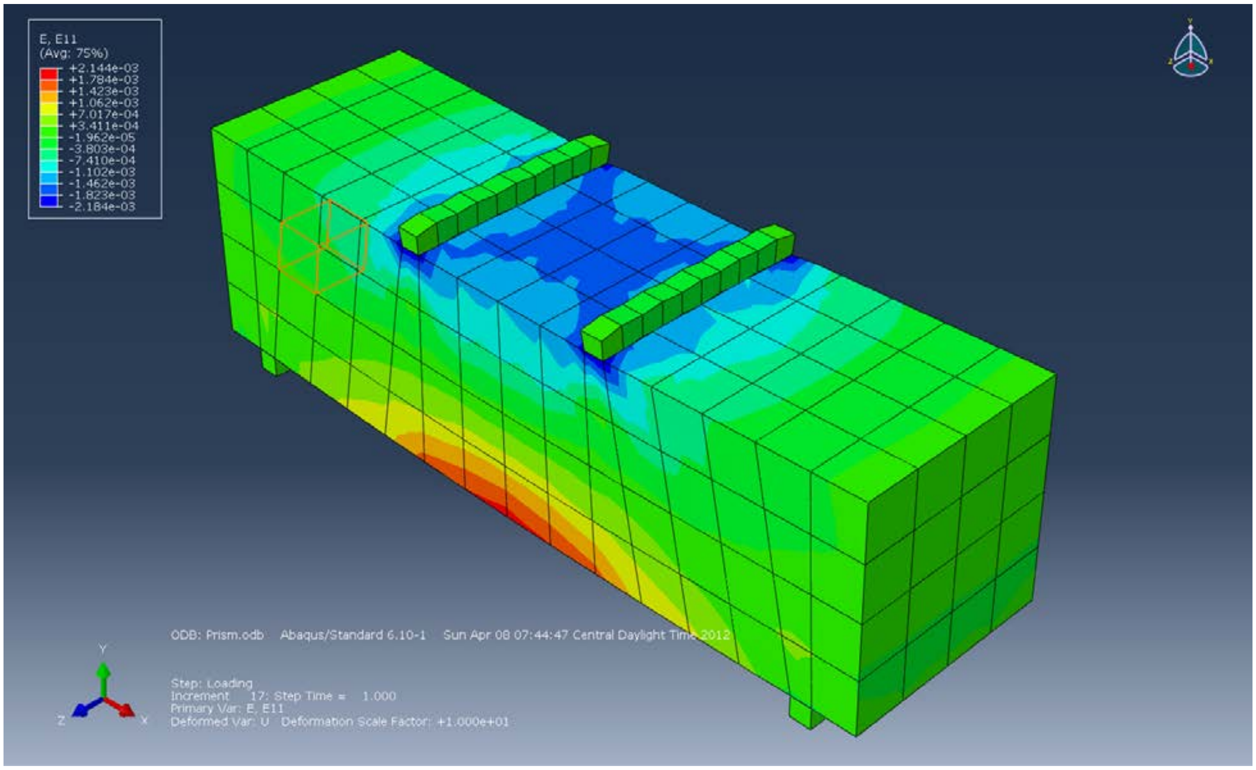

Figure 5-47: Strain in X-Direction (E11) for Prism with 0.75% Fibers (Isotropic View).

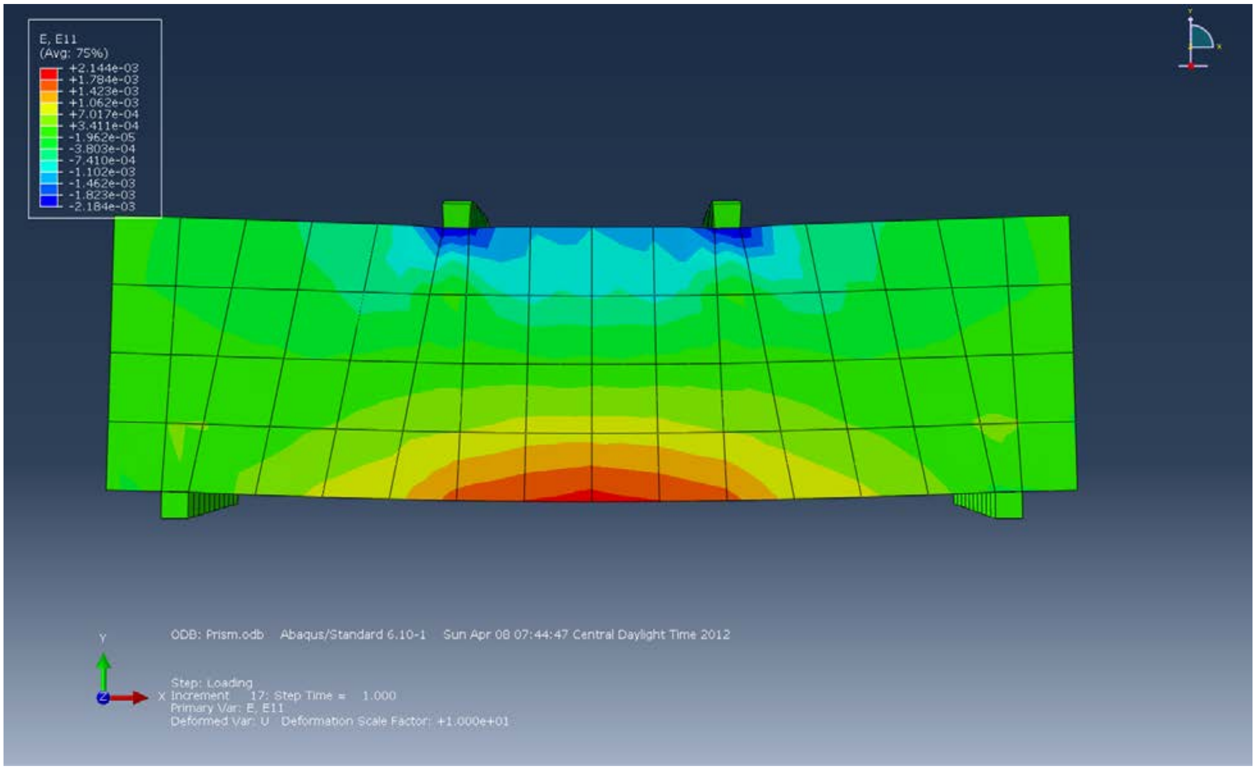

Figure 5-48: Strain in X-Direction (E11) for Prism with 0.75% Fibers (Front View).

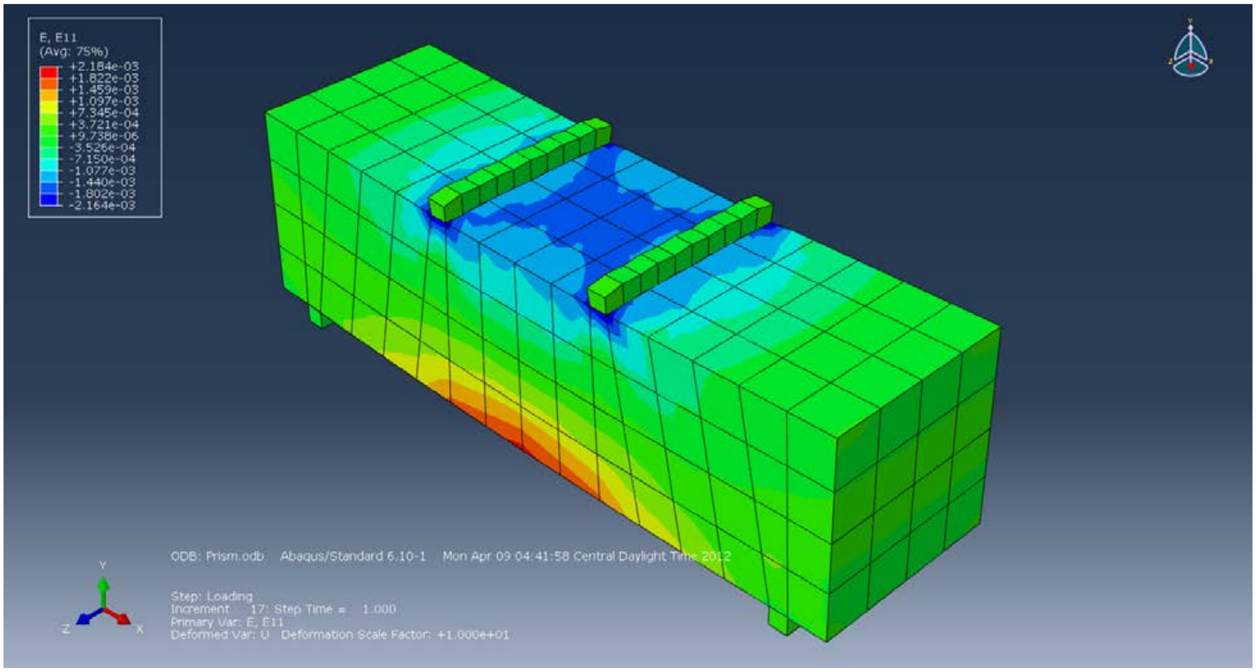

Figure 5-49: Strain in X-Direction (E11) for Prism with 1% Fibers (Isotropic View).

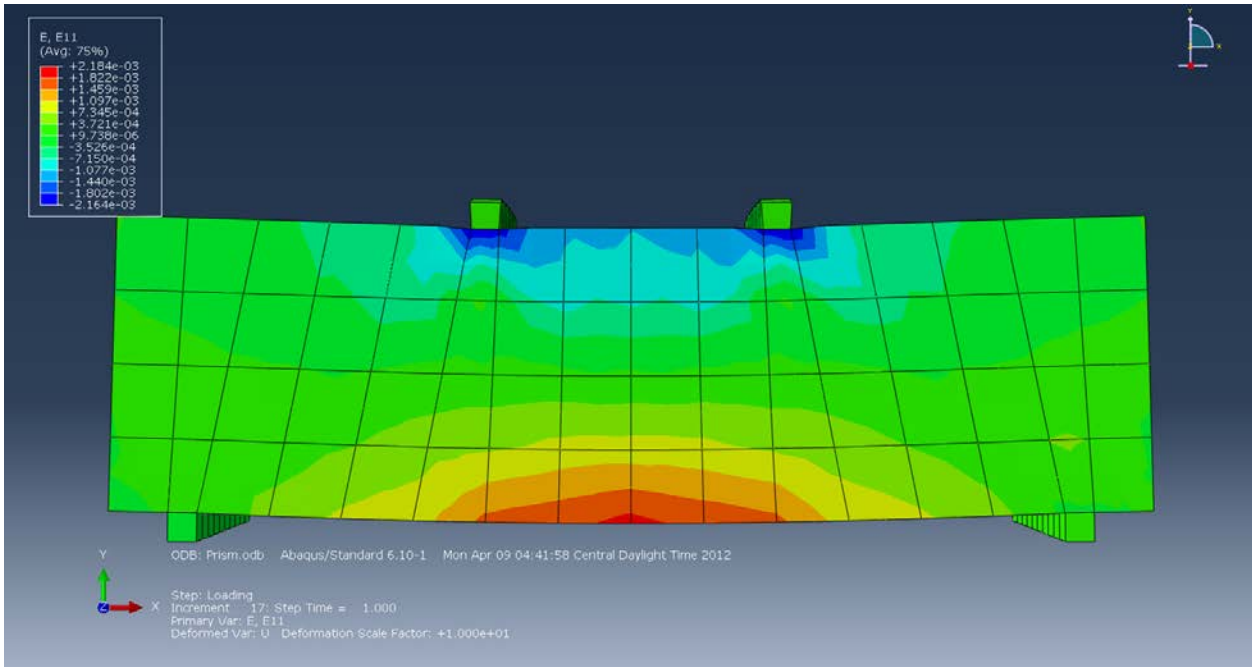

Figure 5-50: Strain in X-Direction (E11) for Prism with 1% Fibers (Front View).

CHAPTER 6 - Discussion, Conclusions and Recommendations

6.1 Discussion

6.1.1 Cementitious Matrix:

6.1.1.1 Uniaxial Compression (Cubes):

The peak load and stiffness values of the fiber-reinforced cementitious matrix specimens of the first batch (1, 3 and 5% of Long wheat fibers, 20-30 mm) were low when compared to those of the control group. This is attributed to excessive amounts of fibers in the mixes, which caused a weak location in the specimens due to the entrapped air in the cell walls of the fibers. In the second batch (1, 2 and 3% of Long wheat fibers) it was found that the uniaxial compression peak load for 1% wheat fiber was higher than that of the control specimens. The fourth batch (0.5, 0.75 and 1% of Long wheat fibers) containing lower percentages of the long wheat fibers exhibited an increase in uniaxial compression peak load with fiber percentages up to 0.5%. This increase in peak load can reach 30% over that of the control. At 0.5% of long wheat fibers there was an average reduction in stiffness of 12%, and at 1% the average reduction in stiffness was 7%. Batches three (1, 2 and 3% of Short wheat fibers) and five (0.5, 0.75 and 1% of Short wheat fibers), containing wheat fibers shorter than 5mm, were used to study the effects of fiber length on peak load. The uniaxial compression peak load of samples from these two batches dropped below that of the control specimens for all fiber percentages tested. Stiffness increase was observed in uniaxial compression at 0.75% of short wheat fibers. Both other types of fibers suffered a reduction in stiffness of up to 31% at 0.75%. In the case of the sixth batch (0.5, 0.75 and 1% of Polypropylene fibers), the polypropylene fibers produced a higher uniaxial compressive peak load at 0.5% and 1%, the average increase being 12% (Figure 3-12). At 0.5% of polypropylene fibers the stiffness experienced the highest increase (9%) over that of the control specimen, while the other types of fibers produced stiffness values close to those of their controls at the same percentage. Cubes reinforced by long wheat fibers demonstrated an average uniaxial compression peak load 17% higher than that of the cubes containing polypropylene fibers at 0.5% reinforcement (Figure 3-12). Cubes reinforced by short wheat fibers exhibited the highest average stiffness, 9% higher than that of the cubes containing polypropylene fibers at 0.75% reinforcement (Figure 3-12).

6.1.1.2 Three-Points Flexural (Prisms):

In the case of prisms, the measured flexural peak load for the first batch (1, 3 and 5% of Long wheat fibers, 20-30 mm) was slightly higher than that of the control for 1% of long wheat fibers and rather disappointing at higher percentages. This can be due to the excessive amount of fibers, which lead to weak locations in the prisms due to the entrapment of air in the fibers' cell walls causing premature failure. The flexural peak loads of the second (1, 2 and 3% of Long wheat fibers) and third batches (1, 2 and 3% of Short wheat fibers) were lower than those of their controls, while the stiffnesses of the samples containing 2% long wheat fibers were higher than those of the controls. Most of the specimens of the fourth batch (0.5, 0.75 and 1% of Long wheat fibers), containing 1% fibers or less, demonstrated peak loads higher than that of their controls. The curve showed an increasing trend up to 0.75% of long wheat fibers (Figure 3-23). Most of the specimens of the fifth (0.5, 0.75 and 1% of Short wheat fibers) and the sixth batches (0.5, 0.75 and 1% of Polypropylene fibers) had flexural peak load and stiffness values below those of the controls. Prisms reinforced by long wheat fibers showed an average flexural peak load 27% higher than that of the prisms containing polypropylene fibers at 0.75% reinforcement (Figure 3-23). Also, prisms reinforced by long wheat fibers showed the highest average stiffness, a full 28% higher than that of the prisms containing polypropylene fibers at 0.75% reinforcement (Figure 3-24). As for the crack angle, prisms with long wheat fibers and polypropylene fibers showed similar trend of an angle between 4 and 15 degrees, while it was between 3 and 18 degrees for specimens with short wheat fibers in compare with 0 to 1 degree for the control prisms.

6.1.2 Concrete:

6.1.2.1 Uniaxial Compression (Cylinders):

In the uniaxial compression tests that were performed at 7 days it can be noticed that 0.75% wheat fibers lead to an increase in the peak load of 1.56% (from 310680 N to 315515 N on average), while it was 6.5% increase over the control for the 0.5% polypropylene fiber (from 310680 N to 330889 N). As the 0.5% polypropylene continue to develop higher peak load at 14 days leading to 17.1% increase over the control (from 303220 N to 354961 N), the 0.75% wheat fiber deteriorated by 2.15% drop in the peak load over the control (from 303220 N to 296689 N) leaving the way to the 0.5% wheat fiber which increased by 5.92% in the peak load over the control (from 303220 N to 321162 N). Finally, at 28 days the 0.75% wheat fibers achieved the highest percentage increase in the peak load over the control at 28 days, which was 7.05% increase, exceeding that of their counterparts reinforced with polypropylene fiber by 5.72%. As for the 0.5% polypropylene fiber the increase was about 4.88% over the control which is slightly higher than that of the 0.5% wheat fibers (4.21%) as shown in Table 6-1.

Table 6-1: Percentage Increase in the Peak Load Over the Curing Period.

Curing	*Percentage Increase in the Peak Load*		
	7 Days	*14 Days*	*28 Days*
Control	0	0	0
0.5% Wheat Fiber	0.81	5.92	4.21
0.75% Wheat Fiber	1.56	-2.15	7.05
1% Wheat Fiber	-6.54	-0.79	-4.21
0.5% Polypropylene Fiber	6.50	17.06	4.88
0.75% Polypropylene Fiber	5.76	8.15	1.33
1% Polypropylene Fiber	-8.89	-1.88	-2.03

In terms of the stiffness the 0.5% wheat fibers showed an increase of 10% over the control at 28 days followed by 8% increase for the 0.75% wheat fiber. Meanwhile the 0.75% polypropylene fibers showed the highest increase in the stiffness over the control by 14%.

The cyclic loading on the cylinders indicated that plasticity start as early as 10000 lb (44482.22 N) in most cases of fibers and the control. Also it was noticed that the modulus of elasticity drops after each cycle due to the micro-cracking in the specimens except at 1% wheat fiber where it increased till the 8^{th} cycle (4303.88 MPa) above the control to drop later to a lower modulus (4151.27 MPa) but not as low as the starting (see Figure 4-38). It was also noticed that the 0.5% polypropylene achieved the highest modulus of elasticity but the wheat fibers with the 0.5% and the 0.75% achieved modules close to that of the control. Also the polypropylene modulus of elasticity dropped below that of the control and the wheat fibers for the 0.5% and the 0.75% polypropylene. Meanwhile the stiffness continued to increase for all the cylinders reaching a constant stiffness of 15827 lb/in (2759.71 N/mm) at the final cycles as shown in Figure 4-39. Although all specimen reached that constant stiffness, not all of them reached it at the same level of strain, like; the 0.75% and 1% polypropylene which had higher strains and all the percentages of wheat fibers had similar strain slightly higher than the control. Table 4-8 represents the peak load, initial stiffness, ductility index and the initial modulus of elasticity for the reinforced cylinders in compare with the control specimens. In that table the 0.75% wheat fibers achieved the highest ductility index of 1.9259 among the wheat fibers but the polypropylene fibers achieved a ductility index of 2.135 at 1% polypropylene, while the control cylinder had an index of 1.7179. This ductility index is calculated by dividing the strain at the peak load by the strain at the yielding load.

6.1.2.2 Four-Point Flexure (Prisms):

In the case of concrete prisms, the measured flexural peak loads for the first batch (control and 0.5% wheat and polypropylene fibers) were lower than that of the control for the 0.5% polypropylene fibers (10% reduction from the control) and rather disappointing for the 0.5% wheat fibers (15% reduction from the control) as shown in Figure 4-60. This can be due to the entrapment of air in the fibers' cell walls, which lead to weak locations in the prisms causing premature failure. The flexural peak loads of the second batch (control and 0.75% wheat and polypropylene fibers) were lower than those of their controls, while the stiffnesses of the samples containing 0.5% and 0.75% wheat fibers were higher than those of the polypropylene and the controls as shown in Figure 4-61. Most of the specimens of the fourth batch (control and 1% wheat and polypropylene fibers), containing 1% wheat fibers, demonstrated the lowest reduction in the peak loads (7% reduction from the control). Meanwhile the stiffness of the fourth batch was the highest for the polypropylene fibers and equal to that of 0.5% wheat fibers in batch 1. Finally, concrete prisms reinforced with both long wheat fiber and polypropylene fiber showed deterioration in strength of up to 17%.

6.1.3 Finite Element Modeling and Simulation:

From Figure 5-23 it can be seen that all the cylinders showed an exact trend till the plasticity started. After the plasticity develops in the cylinders it was noticed that the control and the 0.5% wheat fibers had very close results, while the other two percentages showed also close results to each other but different for that of the control. Meanwhile, Figure 5-24 through Figure 5-27 showed the results of the finite element analysis in compared to the experimental results. From these figures it can be seen that the results for all the cylinders were very close except for the 0.75% wheat fiber cylinder in which the finite element results were conservative in the prediction of the strain.

As for the concrete prisms simulations, Figure 5-36 represent the difference between the different percentages of wheat fibers reinforced prisms. In that figure it was a similar trend to the cylinders at which the 0.5% and the control gave very close results and the 0.75% and 1% wheat fibers gave similar trends. When compared to the experimental results Figure 5-37 through Figure 5-42, it was noticed that the result from the finite element analysis were conservative in all the cases at the early linear stage. The plastic stage in which most of the prisms had a higher simulated load when compared to the experimental load at the same strain. This can be due to the fact the fibers in some of these prisms and cylinders are not distributed in a uniform way as assumed by this simulation through the cross section. Also the dimensions of the fibers in the actual experimental is not exact and they have range as specified in the previous chapters, while the finite element analysis is based on an exact values and dimension.

6.2 Conclusions

Advancing the development of natural fibers as a reinforcing material in cement and concrete matrices is the goal of this study. The authors reach the following conclusions:

1. Cementitious matrix cubes reinforced with 0.5% of long (20-30 mm) wheat fibers and prisms containing 0.75% of the same fibers demonstrated the greatest increase in the peak load when compared to their respective control groups.
2. Cementitious matrix cubes containing 0.75% of short (less than 5 mm) wheat fibers and prisms containing 0.75% of long wheat fibers showed the highest stiffness values when compared to their respective control groups.
3. A non-uniform spatial distribution in the prisms containing high percentages (3% or greater) of long wheat fibers created weak locations within the prisms due to the fact that these wheat fibers entrap air in their cell walls, resulting in their premature failure.
4. Lignin leaching from the cell walls of the wheat fibers causes a delay in the setting time of the cementitious matrix at high percentages of both long and short wheat fibers. This conclusion is supported by discussion in references (Li 2004), (Wershaw 2003).
5. An increasing reduction in uniaxial compressive peak load results from exceeding a threshold of 1% volume fraction of both long and short wheat fibers.
6. The angle between the crack direction and the minor principal stress direction (vertical axis) of specimens (Figure 3-25) with both long wheat fibers and polypropylene fibers

was between 4 and 15 degrees, and was between 3 and 18 degrees in the case of specimens with short wheat fibers (Table Error! **No text of specified style in document.**-1). The crack angle of the control specimens was between 0 and 1 degree. Perić and Rasheed found that the presence of fibers changed the orientation of deformation bands, which can be interpreted as cracks in the case of strong discontinuity (Perić 2007)

7. Concrete cylinders reinforced with 0.75% wheat fibers (20-30 mm) achieved the highest percentage increase in the peak load over the control at 28 days, which was 7.05% increase, exceeding that of their counterparts reinforced with polypropylene fiber by 5.72%.
8. The stiffness of the Concrete cylinders reinforced with 0.5% wheat fibers (20-30 mm) showed an increase of 10% over the control at 28, while the 0.75% polypropylene fibers showed the highest increase in the stiffness over the control by 14% at 28 days.
9. The cyclic loading on the cylinders indicated that plasticity start as early as 10000 lb (44482.22 N) in most cases of fibers and the control.
10. The stiffness continued to increase for all the cylinders reaching a constant stiffness of 15827 lb/in (2759.71 N/mm) at the final cycles as shown in Figure 4-39.
11. The 0.75% wheat fibers (20-30 mm) achieved the highest ductility index of 1.9259 among the wheat fibers but the polypropylene fibers achieved a ductility index of 2.135 at 1% polypropylene.
12. Concrete prisms reinforced with both wheat fiber (20-30 mm) and polypropylene fiber showed deterioration in strength of up to 17%.
13. The stiffnesses of the concrete prisms containing 0.5% and 0.75% wheat fibers were higher than those of the polypropylene and the controls as shown in Figure 4-61.
14. The fibers affect only the plastic region of the concrete load-strain curves.
15. The finite element modeling proves that the fiber works only after the cracking starts.

6.3 Recommendations

1. Studying the use of the wheat fibers in reinforced concrete beam and slaps.
2. Studying wheat fibers laminates with natural epoxy.

3. Investigating the use of supplementary cementitious materials as way to reduce the degradation of the wheat fibers.

References

ABAQUS: Abaqus analysis user's manual, Version 6.10-2, 2010, Dassault Systèmes.

ASTM Standard C39/C39M- 10. (2010). Standard Test Method for Compressive Strength of Cylindrical Concrete Specimens. West Conshohocken, PA: ASTM International.

ASTM Standard C78/ C78M - 10. (2010). Standard Test Method for Flexural Strength of Concrete (Using Simple Beam with Third-Point Loading). West Conshohocken, PA: ASTM International.

ASTM Standard C109/ C109M - 11. (2011). Standard Test Method for Compressive Strength of Hydraulic Cement Mortars. West Conshohocken, PA: ASTM International.

ASTM Standard C192 / C192M - 07. (2007). Stan Standard Practice for Making and Curing Concrete Test Specimens in the Laboratory. West Conshohocken, PA: ASTM International.

ASTM Standard C348 - 08. (2008). Standard Test Method for Flexural Strength of Hydraulic Cement Mortars. West Conshohocken, PA: ASTM International.

ASTM Standard C1116 / C1116M – 10a. (2010). Standard Specification for Fiber-Reinforced Concrete. West Conshohocken, PA: ASTM International

AÏTCIN P.C., (1998), High-performance concretes, Construction and Building Materials, E&FN SPON, 591 pp.

Balaguru, P. (1994). Contribution of Fibers to Crack Reduction of Cement Composites During the Initial and Final Setting Period. *ACI Materials Journal, 91* (3), 280-288.

Berhane, Z. (1994, 07 01). Performance of Natural Fibre Reinforced Mortar Roofing Tiles. *Materials and Structures, 27*(6), 347-352.

Bilba, K., Arsene, M. A. & Ouensanga, A. (2003). Sugar cane bagasse fibre reinforced cement composites. Part I. Influence of the botanical components of bagasse on the setting of bagasse/cement composite. *Cement and Concrete Composites*, *25* (1), 91-96.

BS EN 196-1:2005. (2005). Methods of Testing Cement - Part 1: Determination of Strength. London: British Standards Institution.

Castro, J., & Naaman, A. E. (1981, January 1). Cement Mortar Reinforced with Natural Fibers. *ACI Materials Journal*, *78*(1), 69-78.

Coronado, C. A, Lopez, M. M. & (2006). Sensitivity analysis of reinforced concrete beams strengthened with FRP laminates. *Cement & Concrete Composites, 28* (1), 102-114.

Coutts RSP. Eucalyptus wood fiber-reinforced cement. *Journal of Materials Science Letters 1987;6*(8):955-957.

De Gutierrez, R., Diaz, L. & Delvasto, S. (2005). Effect of Pozzolans on the Performance of Fiber Reinforced Mortars. *Cement and Concrete Composites*, *27* (5), 593-598.

El-Ashkar NH. Wood pulp microfibers in cement-based composites: improving fiber distribution and characterizing composite behavior. Ph.D. Thesis, Georgia Institute of Technology, Atlanta, GA, 2002, p. 343.

Hofstrand, A. D., Moslemi, A. A. & Garcia, J. F. (1984). Curing Characteristics of Wood Particles from Nine Northern Rocky Mountain Species Mixed with Portland Cement. *Forest Products Journal, 34* (2), 57-61.

Khorami, M. & Ganjian, E. (2011). Comparing flexural behaviour of fibre–cement composites reinforced bagasse: Wheat and eucalyptus. *Construction and Building Materials, 25* (9), 3661-3667.

Kmiecik, P. & Kamiński, M. (2011). Modelling of reinforced concrete structures and composite structures with concrete strength degradation taken into consideration. *Archives of Civil and Mechanical Engineering*, *XI*, 623-636.

Kosa, K., Naaman, A. E., & Hansen, W. (1991, 5 1). Durability of Fiber Reinforced Mortar. *ACI Materials Journal, 88*(3), 310-319.

Lee, J., Fenves, G. L. & (1998). Plastic-Damage Model for Cyclic Loading of Concrete Structures. *Journal of Engineering Mechanics, 124* (8), 892-900.

Li, G., Yu, Y., Li, J., Li, C., & Wang, Y. (2004, July). Research on Adaptability Between Crop-Stalk Fibers and Cement. *Cement and Concrete Research, 34*(7), 1081-1085.

Lin, X., Silsbee, M., Roy, D., Kessler, K. & Blankenhorn, P. (1994). Approaches to Improve the Properties of Wood Fiber Reinforced Cementitious Composites. *Cement and Concrete Research, 24* (8), 1558-1566.

Lubliner, J., Oliver, J., Oller, S. & Oñate, E. (1989). A Plastic-Damage Model for Concrete. *International Journal of Solids and Structures, 25* (3), 229–326.

Naik, T. R., Friberg, T. S. & Chun, Y. (2004). Use of Pulp and Paper Mill Residual Solids in Production of Cellucrete. *Cement and Concrete Research, 34* 1229-1234.

MacDonald, C. N., Ballou, M. L., & Biddle, D. T. (2009). Case Histories Using Synthetic Fiber Reinforced Concrete. ECI Conference on Shotcrete for Underground Support XI, (p. P11). Davos, Switzerland.

Mohr B. J. (2005). Durability of Pulp Fiber Cement Composites. PhD thesis, Georgia Institute of Technology, Atlanta, GA.

Perić, D. & Rasheed, H. A. (2007). Localized failure of fiber reinforced elastic-plastic material subjected to plane strain loading. *International Journal for Numerical and Analytical Methods in Geomechanics, 31* , 893-916.

Savastano, H., Turner, A., Mercer, C. & Soboyejo, W. (2006). Mechanical behavior of cement-based materials reinforced with sisal fibers. *Journal of Materials Science, 41* (21), 6938–6948.

Soroushian P, Marikunte S. (1990). Reinforcement of cement-based materials with cellulose fibers. *Thin-section fiber reinforced concrete and ferrocement, SP-124*, Detroit: American Concrete Institute, 99-124.

Soroushian P, Marikunte S. (1991). Moisture sensitivity of cellulose fiber reinforced cement. *Durability of Concrete V.2, SP-126*, Detroit: American Concrete Institute, 821-835.

Soroushian, P. & Marikunte, S. (1992). Moisture Effects on Flexural Performance of Wood Fibercement Composites. *Journal of Materials in Civil Engineering, 4* (3), 277-291.

Soroushian, P., Marikunte, S. & Won, J. P. (1994). Wood fiber reinforced cement composites under wetting-drying and freezing-thawing cycles. *Journal of Materials in Civil Engineering, 6* (4), 595-611.

Soroushian, P., Shah, Z. & Won, J. (1995). Optimatization of wastepaper fiber-cement composites. *ACI Materials Journal, 92* (1), 82-97.

Soroushian, P., Ravanbakhsh, S. (1999). High-early-strength concrete: Mixture proportioning with processed cellulose fibers for durability. *ACI Materials Journal, 96* (5), 593-599.

Soroushian P. (2000). Reinforcing effects on processed cellulose fibers in mortar (stucco), thin sheet products, and concrete. *High-performance fiber-reinforced concrete thin sheet products, SP-190,* Detroit: American Concrete Institute, 203-214.

Wershaw, R. L., Rutherford, D. W., Leenheer, J. A., Kennedy, K. R., Cox, L. G., & Koci, D. R. (2003). Biogeochemical Processes That Produce Dissolved Organic Matter From Wheat Straw. 14 pages.

Wu, Y., Wang, S., Zhou, D., Xing, C., Zhang, Y. & Cai, Z. (2009). Evaluation of elastic modulus and hardness of crop stalks cell walls by nano-indentation. *Bioresource Technology, 101* (8), 2867-2871.

Ziraba, Y. N., Baluch, M. H. & Azad, A. K. (1985). Use of plasticized sulphur in sisal-fibre concrete. *Durability of Building Materials, 3,* 65-76.

APPENDIX A- Cementitious Matrix Results

Table **Error! No text of specified style in document.**-1 shows the peak loads and the cracking angle for the two types of cementitious matrix specimens that were tested in this research.

Table Error! No text of specified style in document.**-1: Peak Loads and the Angle of the Crack.**

Batch	Type	Cubes		Prisms		Angle of Crack
		Specimen	Maximum Load (N)	Specimen	Maximum Load (N)	
Batch 1: Long Wheat Fibers	Control	SP1	87852.38	SP1	2842.41	-
	Control	SP2	88497.37	SP2	2842.41	-
	Control	Sp3	71349.47	Sp3	2900.24	-
	1% Fibers	SP1	37565.23	SP1	2989.20	-
	1% Fibers	SP2	38210.22	SP2	2971.41	-
	1% Fibers	Sp3	42057.94	Sp3	2789.03	-
	3% Fibers	SP1	10697.97	SP1	613.85	-
	3% Fibers	SP2	9919.53	SP2	934.13	-
	3% Fibers	Sp3	7495.25	Sp3	925.23	-
	5% Fibers	SP1	4070.12	SP1	293.58	-
	5% Fibers	SP2	4092.36	SP2	266.89	-
	5% Fibers	Sp3	3647.54	Sp3	324.72	-
Batch 2: Long Wheat Fibers	Control	C1	93050.17	PLC1	2530.98	-
	Control	C2	81431.86	PLC2	3072.62	-
	Control	C3	89262.83	PLC3	3282.60	-
	1% Fibers	S1	107735.33	PLS1	2709.42	-
	1% Fibers	S2	103340.08	PLS2	2981.07	-
	1% Fibers	S3	101256.28	PLS3	3002.71	-

	2% Fibers	S4	74762.84	PLS4	2384.77	-
	2% Fibers	S5	87343.04	PLS5	2805.30	-
	2% Fibers	S6	87909.97	PLS6	2825.50	-
	3% Fibers	S7	73825.66	PLS7	2410.19	-
	3% Fibers	S8	63029.49	PLS8	2388.82	-
	3% Fibers	S9	56638.74	PLS9	2216.54	-
Batch 3: Short Wheat Fibers	Control	C1	93050.17	PSC1	2906.70	-
	Control	C2	81431.86	PSC2	2928.03	-
	Control	C3	89262.83	PSC3	2670.99	-
	1% Fibers	S1	70822.67	PSS1	2399.26	-
	1% Fibers	S2	68826.07	PSS2	2287.62	-
	1% Fibers	S3	66197.33	PSS3	2053.40	-
	2% Fibers	S4	31656.39	PSS4	1434.03	-
	2% Fibers	S5	46430.44	PSS5	1336.74	-
	2% Fibers	S6	28183.99	PSS6	1783.74	-
	3% Fibers	S7	-	PSS7	-	-
	3% Fibers	S8	-	PSS8	-	-
	3% Fibers	S9	-	PSS9	-	-
Batch 4: Long Wheat Fibers	Control	CL1	79578.68	PLC1	2179.63	0
	Control	CL2	81251.22	PLC2	1975.01	0
	Control	CL3	67092.53	PLC3	2384.25	0
	0.5% Fibers	L0.5% 1	103176.50	PL0.5% 1	2486.56	0
	0.5% Fibers	L0.5% 2	97980.98	PL0.5% 2	2450.97	14
	0.5% Fibers	L0.5% 3	87198.49	PL0.5% 3	2575.52	15
	0.75% Fibers	L0.75% 1	78933.69	PL0.75% 1	2548.83	14

	0.75% Fibers	L0.75% 2	76193.59	PL0.75% 2	2980.31	9
	0.75% Fibers	L0.75% 3	78711.28	PL0.75% 3	2944.72	6
	1% Fibers	L1% 1	80076.89	PL1% 1	2620.00	4
	1% Fibers	L1% 2	79494.17	PL1% 2	2869.10	14
	1% Fibers	L1% 3	77572.54	PL1% 3	2535.49	7
Batch 5: Short Wheat Fibers	Control	CF1	73569.14	PSC1	3202.72	0
	Control	CF2	91651.16	PSC2	3460.72	0
	Control	CF3	64290.15	PSC3	3278.34	0
	Control	CF4	-	PSC4	2611.11	0
	Control	CF5	-	PSC5	2646.69	0
	Control	CF6	-	PSC6	2869.10	0
	0.5% Fibers	Fn0.5% 1	65806.99	PFn0.5% 1	2152.94	0
	0.5% Fibers	Fn0.5% 2	58129.36	PFn0.5% 2	2059.53	4
	0.5% Fibers	Fn0.5% 3	76416.00	PFn0.5% 3	2023.94	6
	0.5% Fibers	Fn0.5% 4	-	PFn0.5% 4	2237.46	17
	0.5% Fibers	Fn0.5% 5	-	PFn0.5% 5	-	-
	0.5% Fibers	Fn0.5% 6	-	PFn0.5% 6	2095.11	10
	0.75% Fibers	Fn0.75% 1	70793.45	PFn0.75 % 1	2241.90	10
	0.75% Fibers	Fn0.75% 2	71852.12	PFn0.75 % 2	1957.22	11
	0.75%	Fn0.75%	68529.30	PFn0.75	1961.67	9

	Fibers	3		% 3		
	0.75% Fibers	Fn0.75% 4	-	PFn0.75 % 4	1872.70	3
	0.75% Fibers	Fn0.75% 5	-	PFn0.75 % 5	2295.28	7
	0.75% Fibers	Fn0.75% 6	-	PFn0.75 % 6	2246.35	7
	1% Fibers	Fn1% 1	53365.31	PFn1% 1	1948.32	10
	1% Fibers	Fn1% 2	35421.19	PFn1% 2	1801.53	17
	1% Fibers	Fn1% 3	45051.59	PFn1% 3	1748.15	3
	1% Fibers	Fn1% 4	-	PFn1% 4	1623.60	9
	1% Fibers	Fn1% 5	-	PFn1% 5	1668.08	5
	1% Fibers	Fn1% 6	-	PFn1% 6	1699.22	5
Batch 6: Polypropylene Fibers	Control	C1	77585.88	PPC1	3385.10	0
	Control	C2	96361.83	PPC2	2958.07	0
	Control	C3	83150.61	PPC3	3069.27	0
	0.5% Fibers	Poly 0.5% 1	95774.66	PP 0.5% 1	2740.10	8
	0.5% Fibers	Poly 0.5% 2	99982.68	PP 0.5% 2	2944.72	15
	0.5% Fibers	Poly 0.5% 3	93030.11	PP 0.5% 3	3122.65	14
	0.75% Fibers	Poly 0.75% 1	95258.67	PP 0.75% 1	2811.28	4
	0.75% Fibers	Poly 0.75% 2	86878.22	PP 0.75% 2	2806.83	7
	0.75% Fibers	Poly 0.75% 3	90374.52	PP 0.75% 3	2873.55	9
	1% Fibers	Poly 1% 1	103132.02	PP 1% 1	2606.66	4
	1% Fibers	Poly 1% 2	85023.31	PP 1% 2	2789.03	11

1% Fibers	Poly 1% 3	99564.54	PP 1% 3	2753.45	6

APPENDIX B- Finite Element Results

As for the other results for the finite element models, the following figures represent the sets of contour stresses, strains, displacements, and plastic strains. All units in the contour figures are SI Units.

Control Cylinders:

- Rough Boundaries:

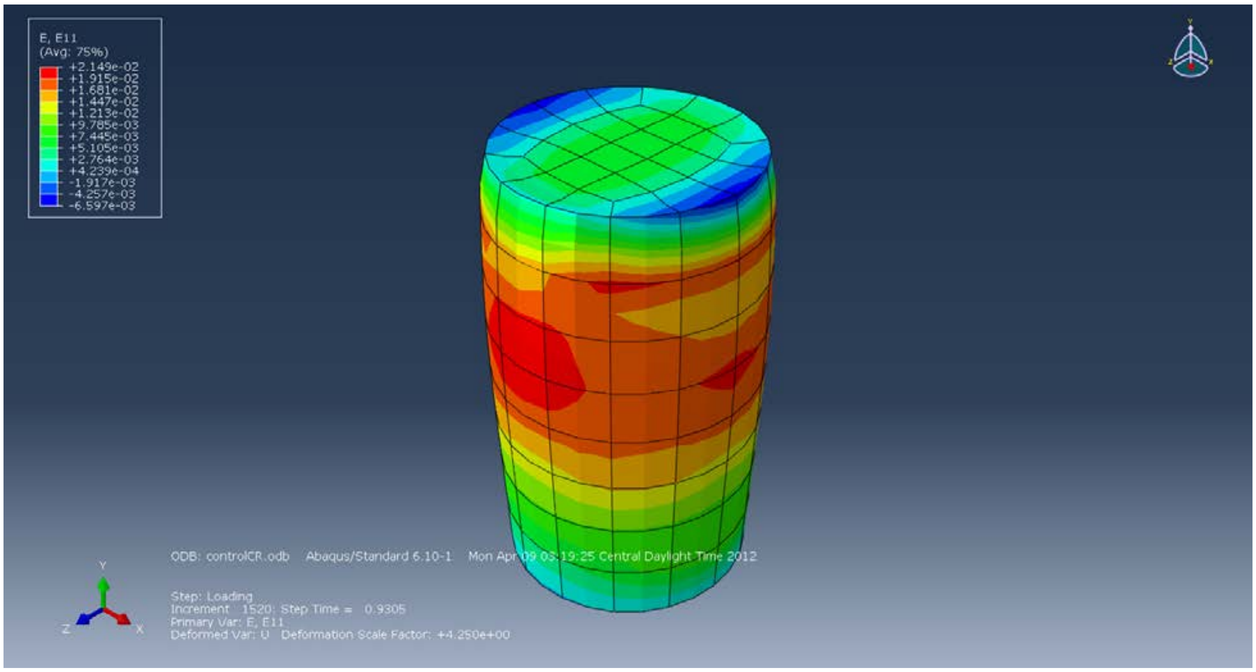

Figure B-1: Strain (E11) in the X-axis.

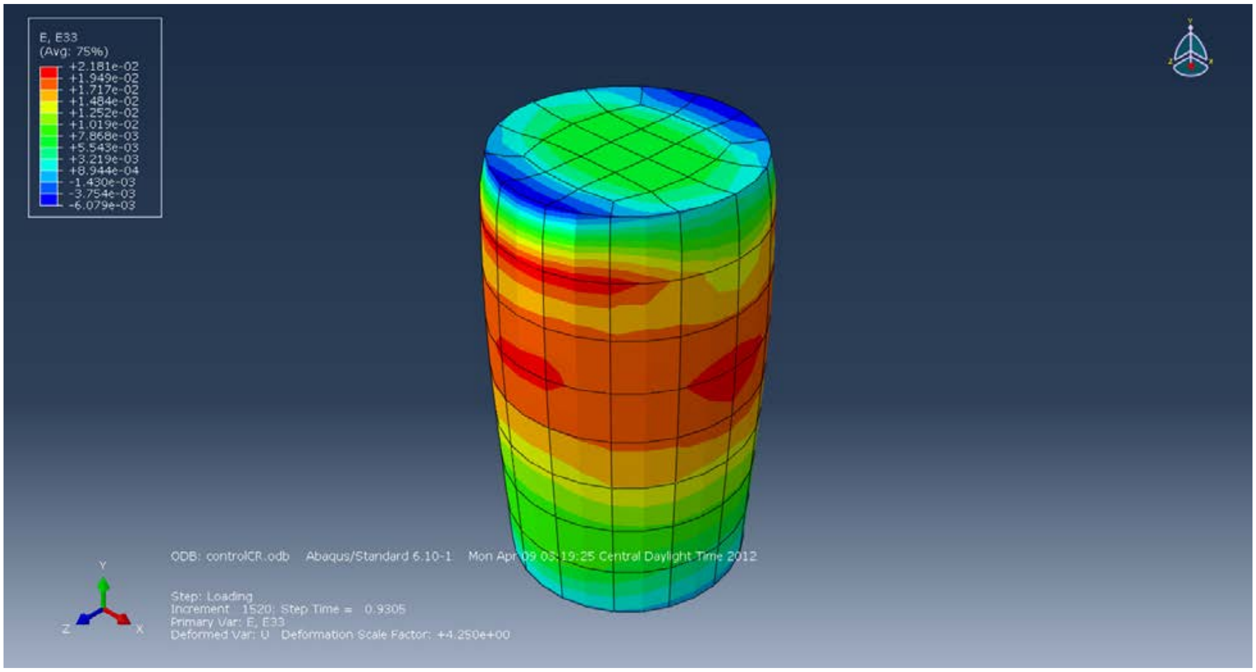

Figure B-2: Strain (E33) in the Z-axis.

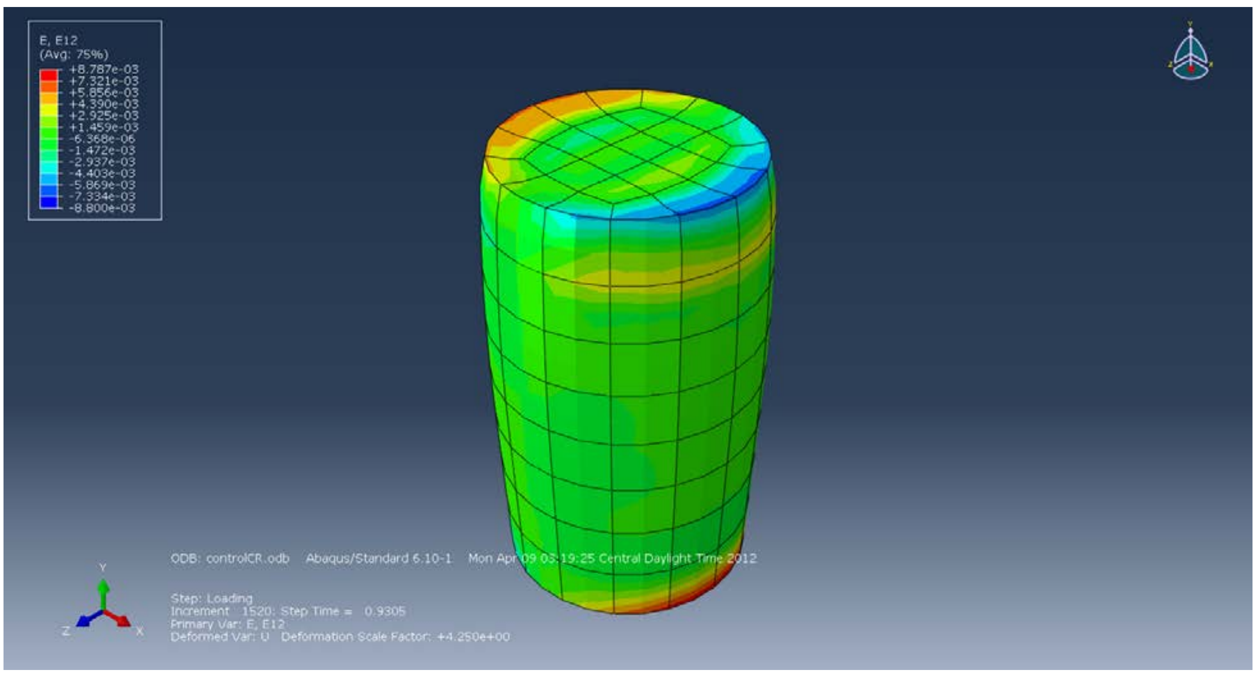

Figure B-3: Strain (E12) in the XY-Plane.

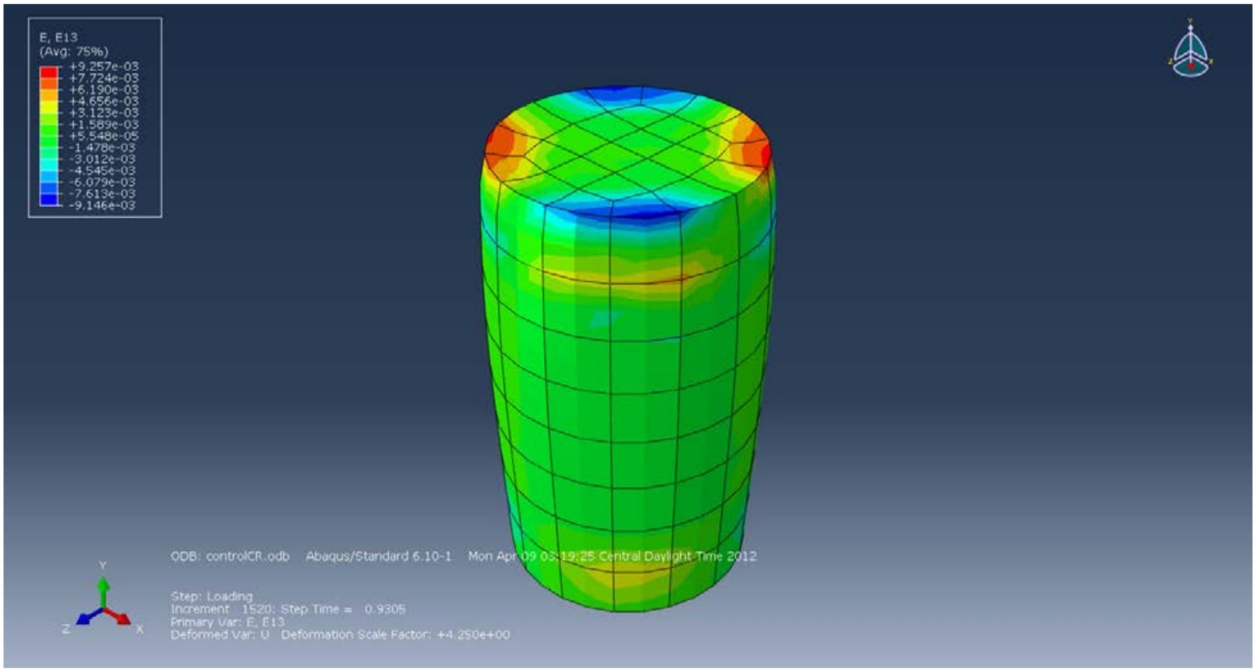

Figure B-4: Strain (E13) in the XZ-Plane.

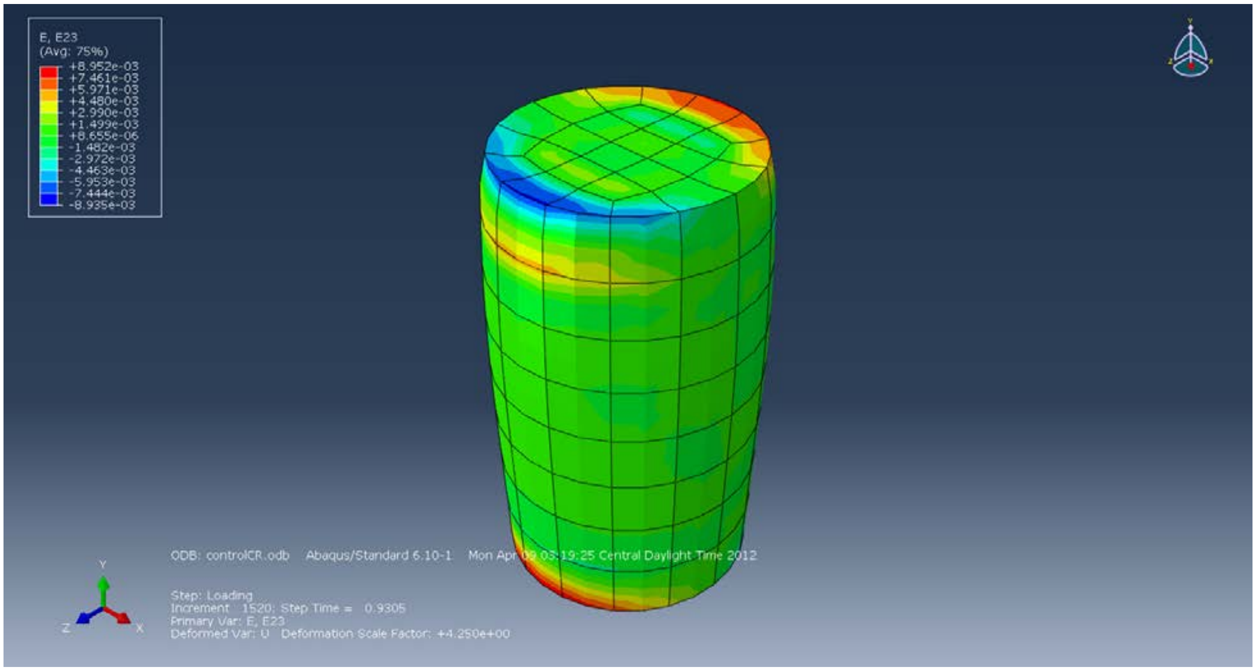

Figure B-5: Strain (E23) in the YZ-Plane.

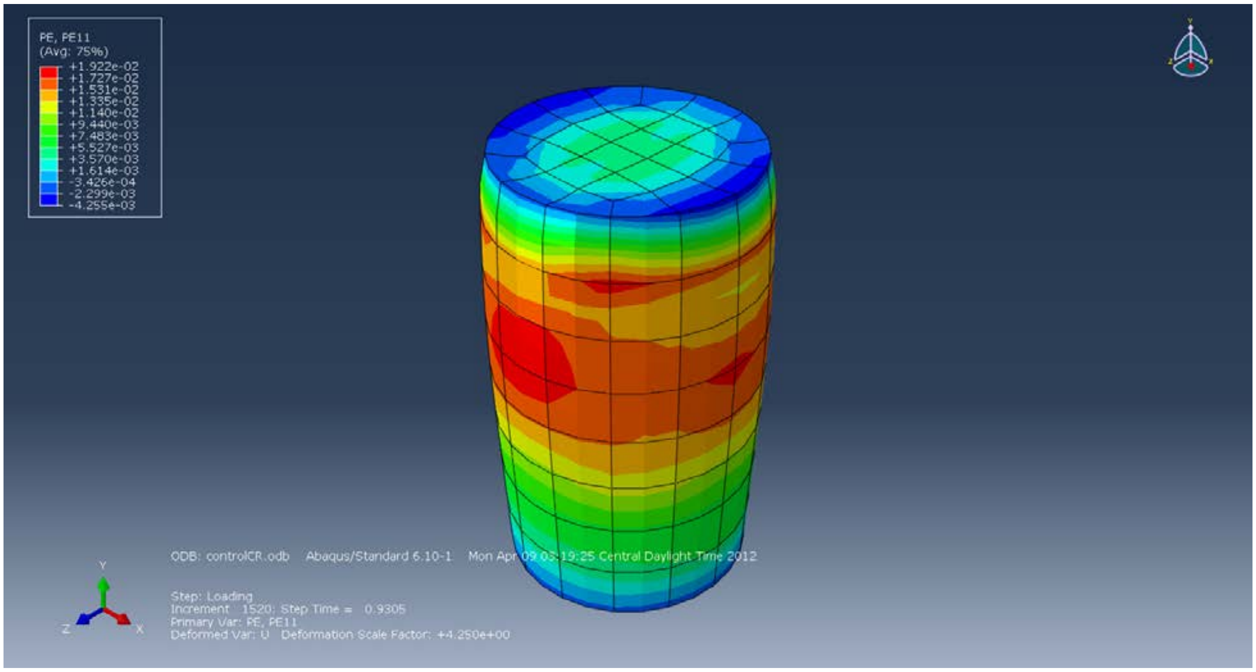

Figure B-6: Plastic Strain (PE11) in the X-axis.

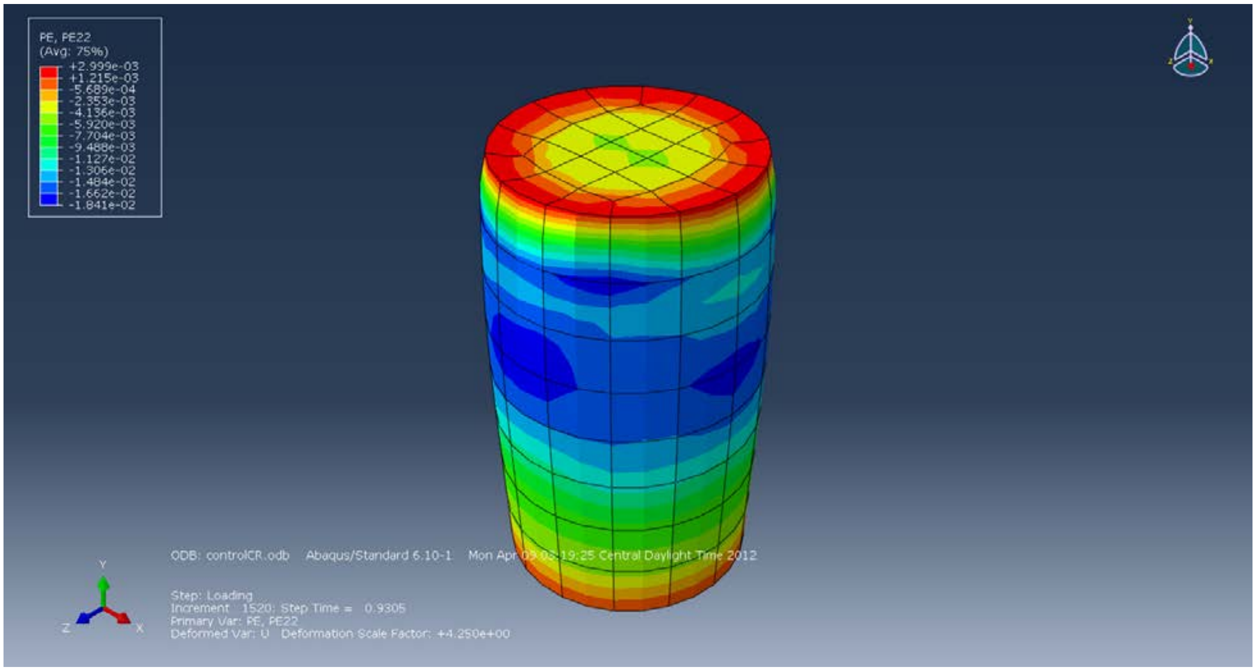

Figure B-7: Plastic Strain (PE22) in the Y-axis.

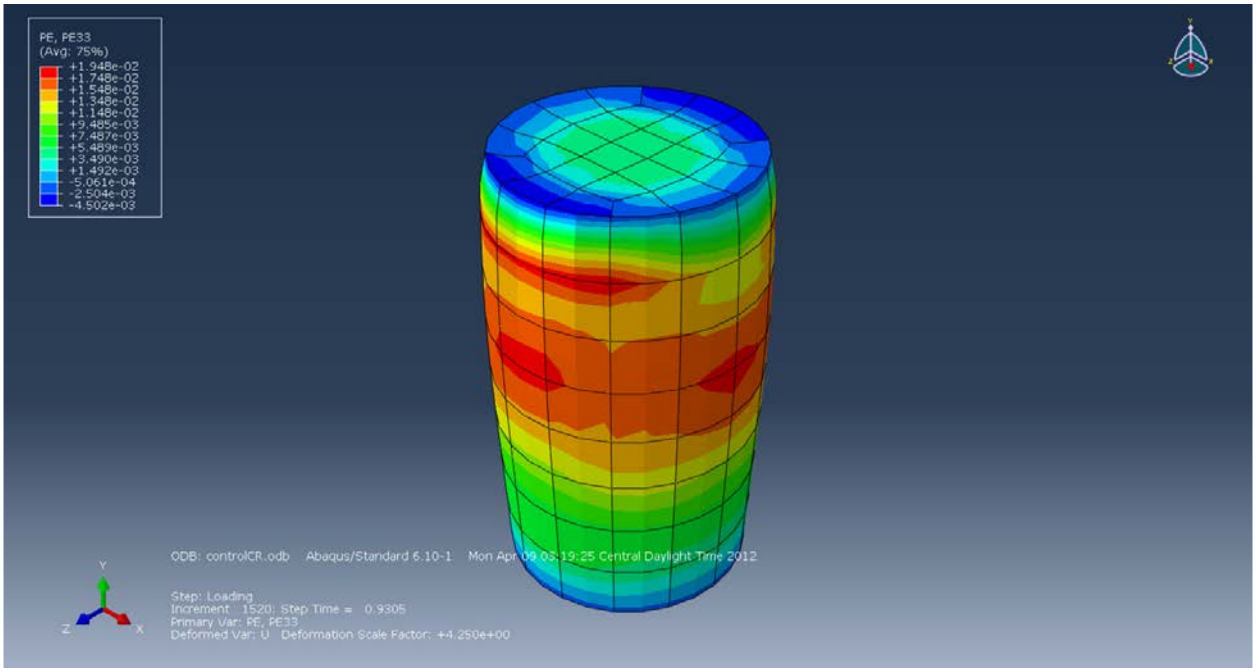

Figure B-8: Plastic Strain (PE33) in the Z-axis.

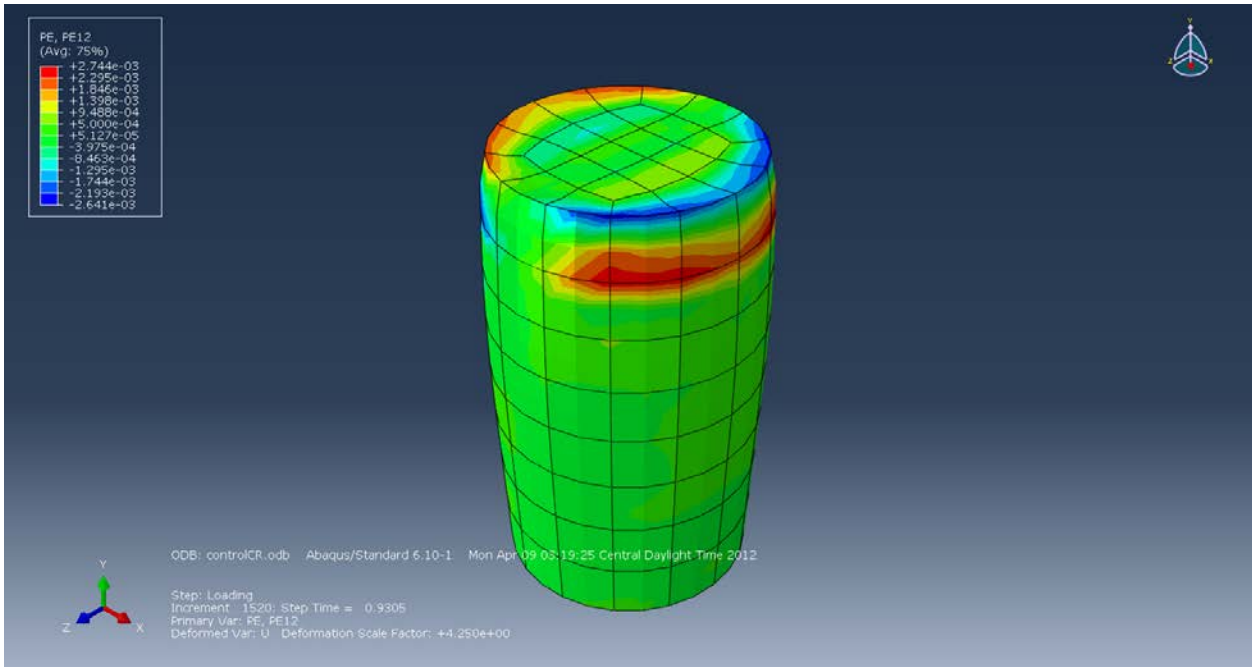

Figure B-9: Plastic Strain (PE12) in the XY-Plane.

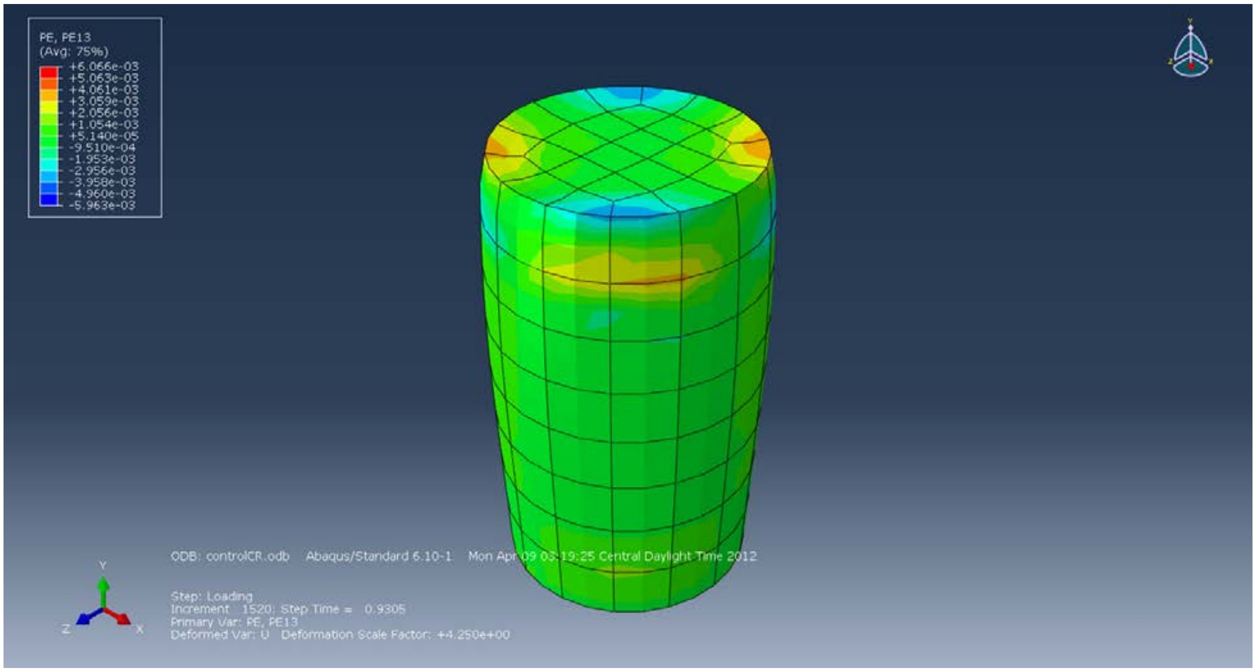

Figure B-10: Plastic Strain (PE13) in the XZ-Plane.

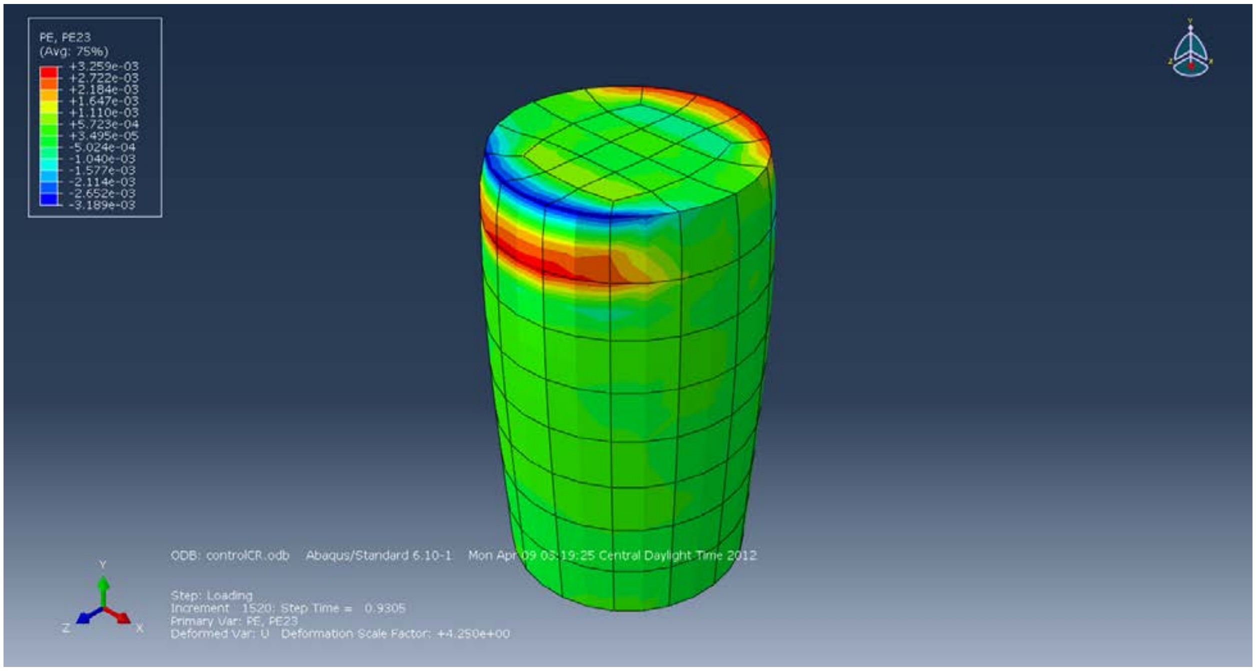

Figure B-11: Plastic Strain (PE23) in the YZ-Plane.

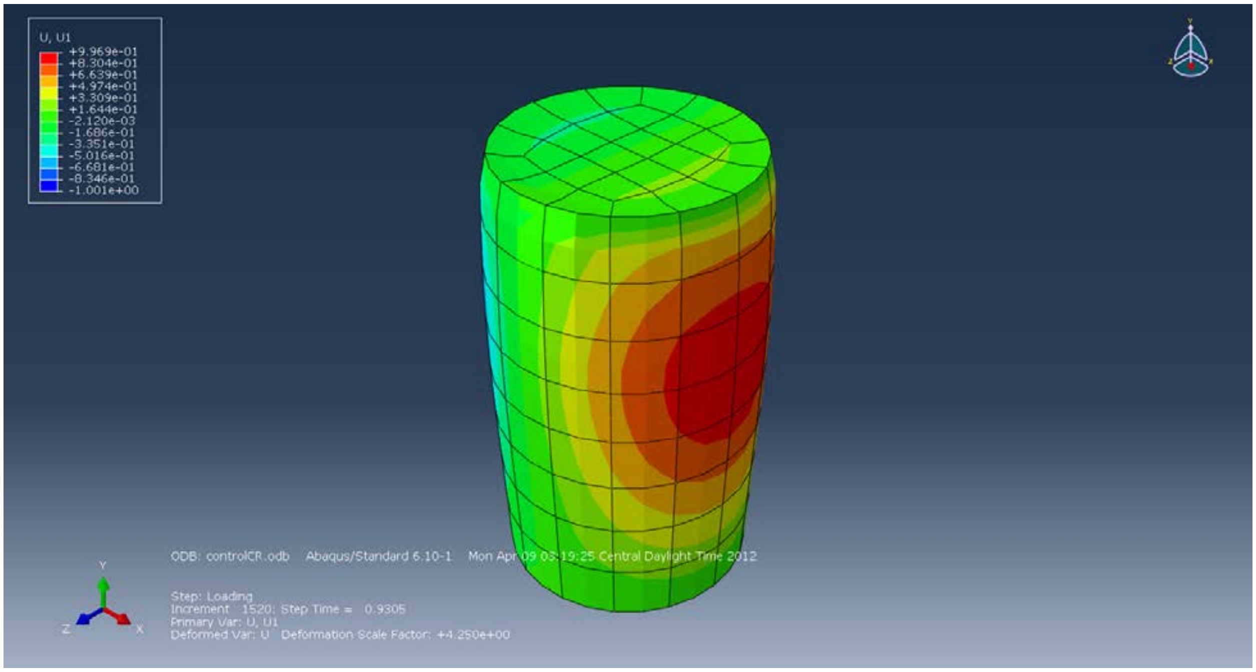

Figure B-12: Displacement (U1) in the X-axis (mm).

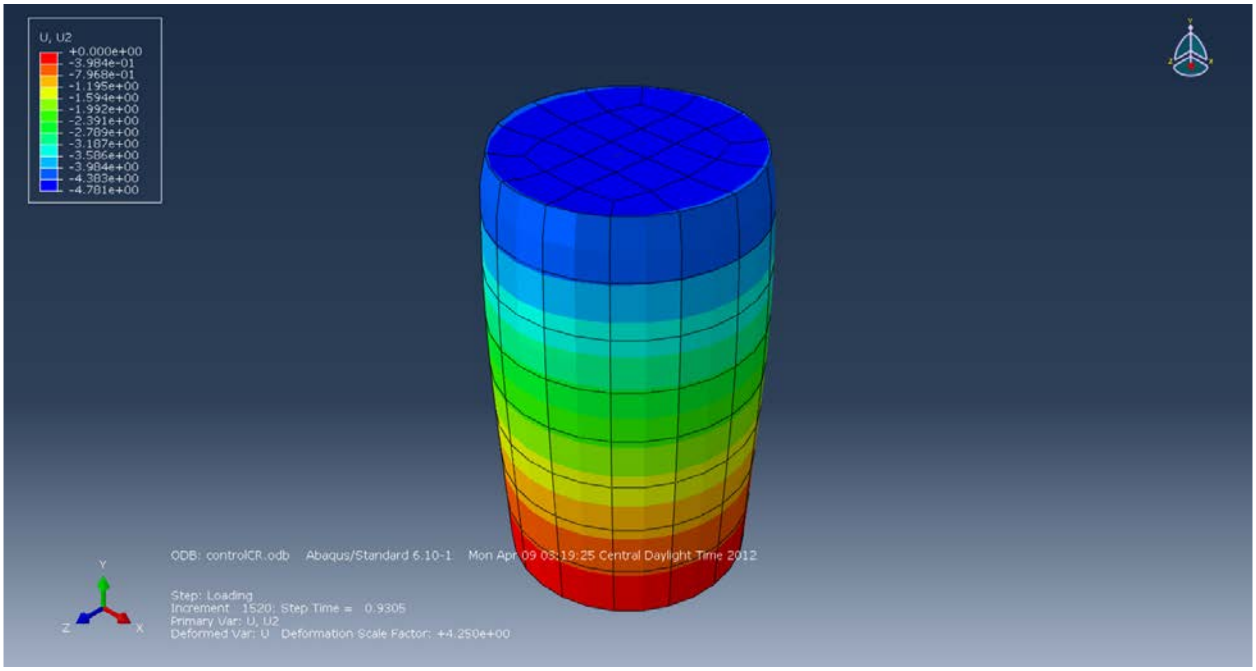

Figure B-13: Displacement (U2) in the Y-axis (mm).

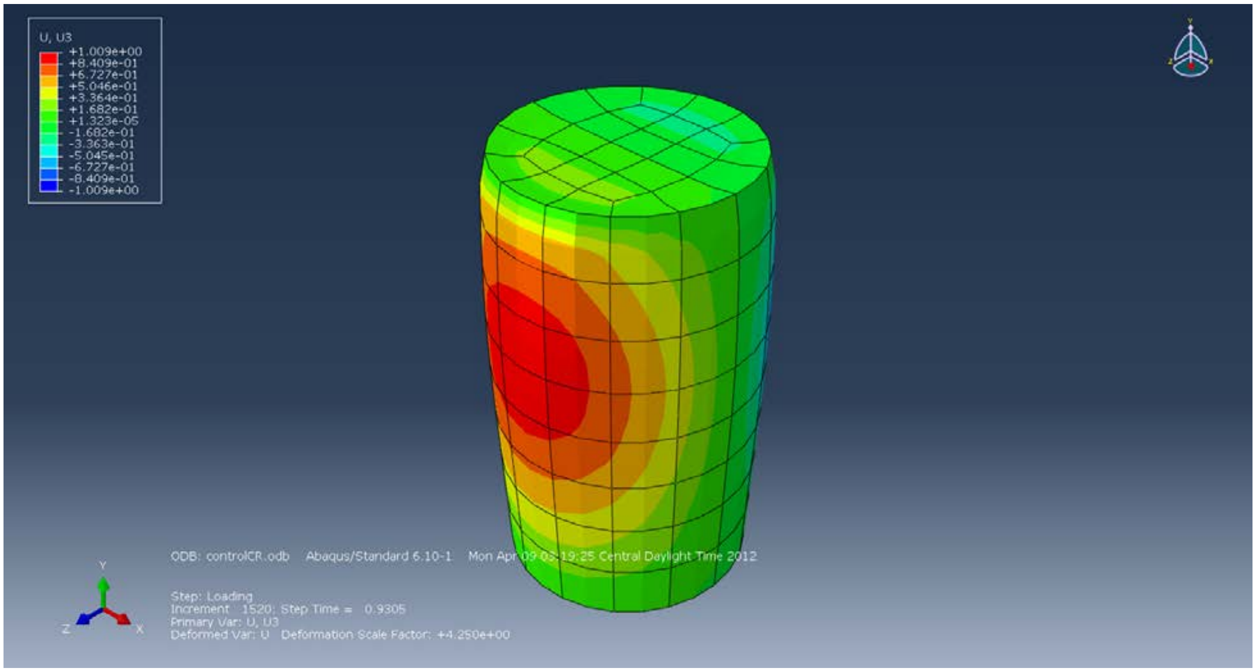

Figure B-14: Displacement (U3) in the Z-axis (mm).

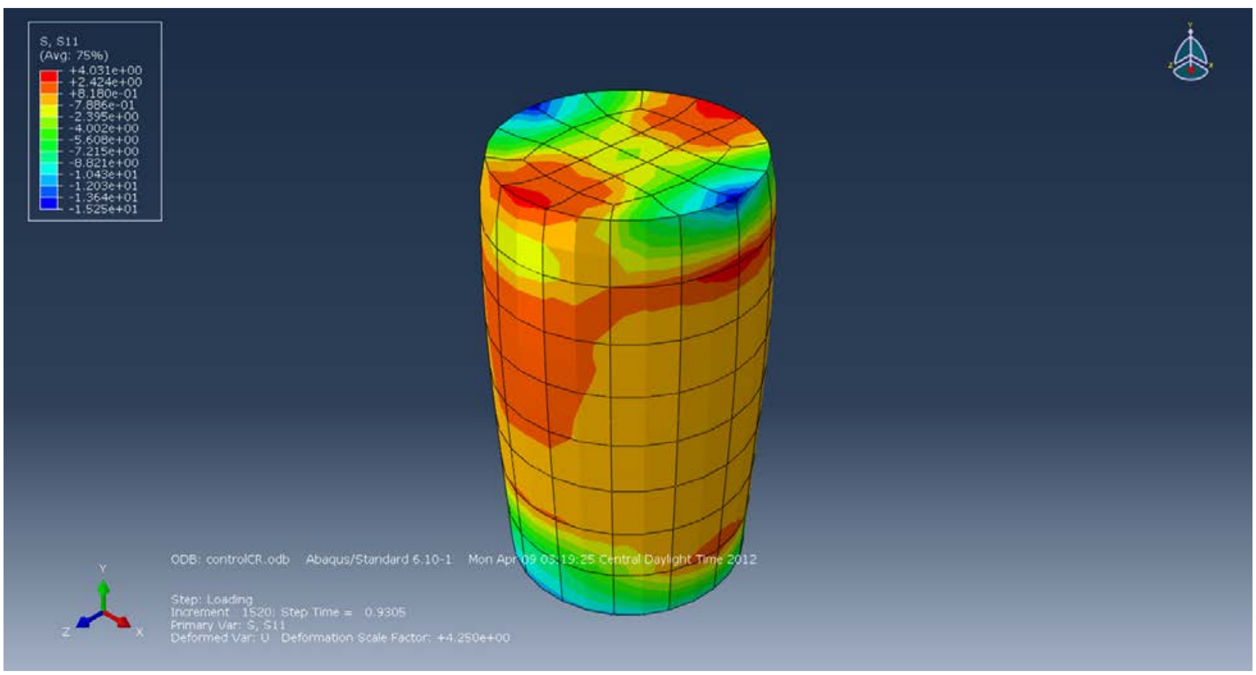

Figure B-15: Stress (S11) in the X-Direction (MPa).

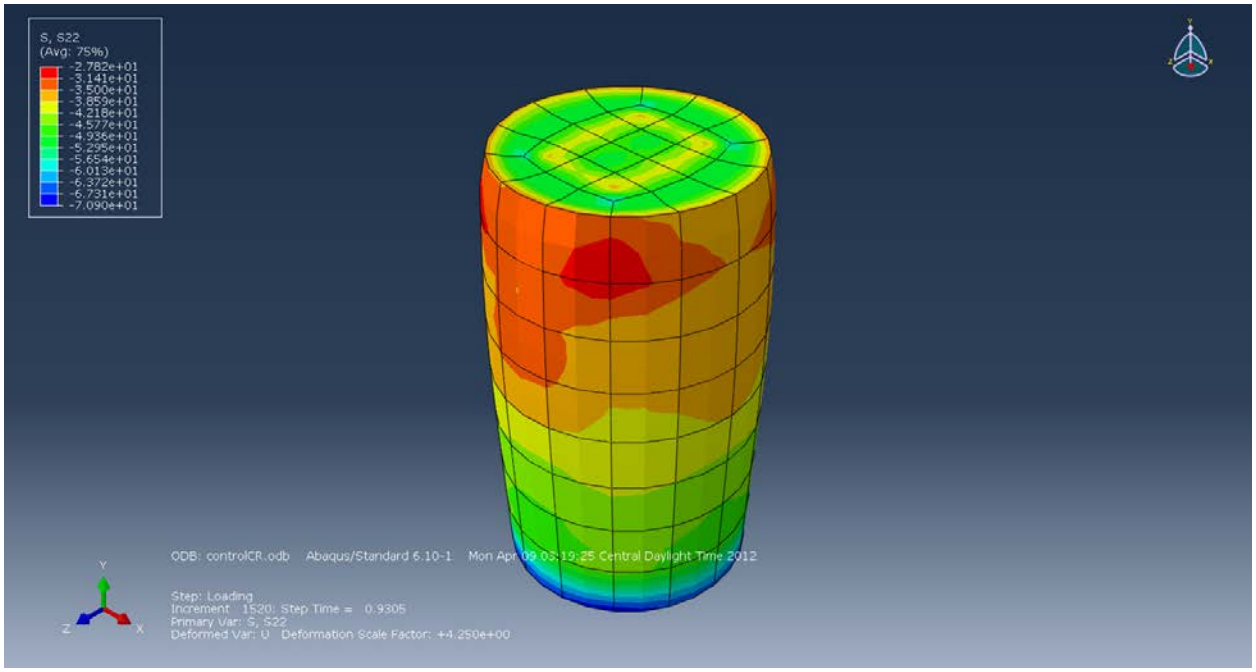

Figure B-16: Stress (S22) in the Y-Direction (MPa).

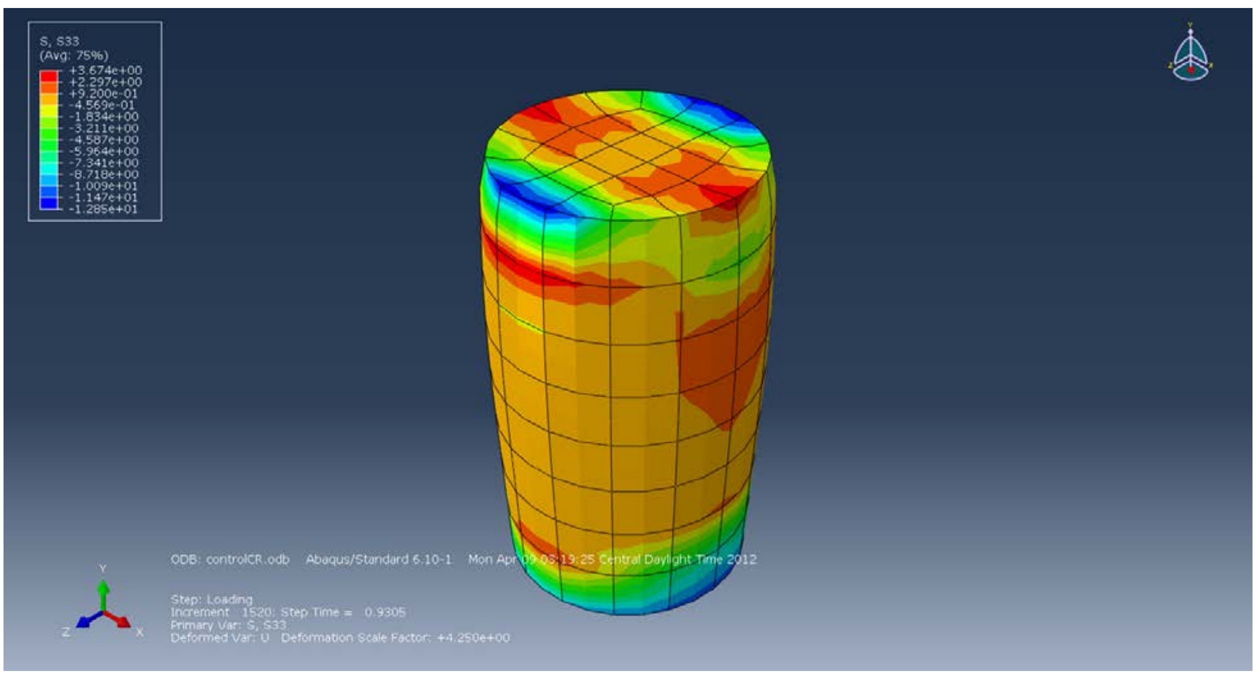

Figure B-17: Stress (S33) in the Z-Direction (MPa).

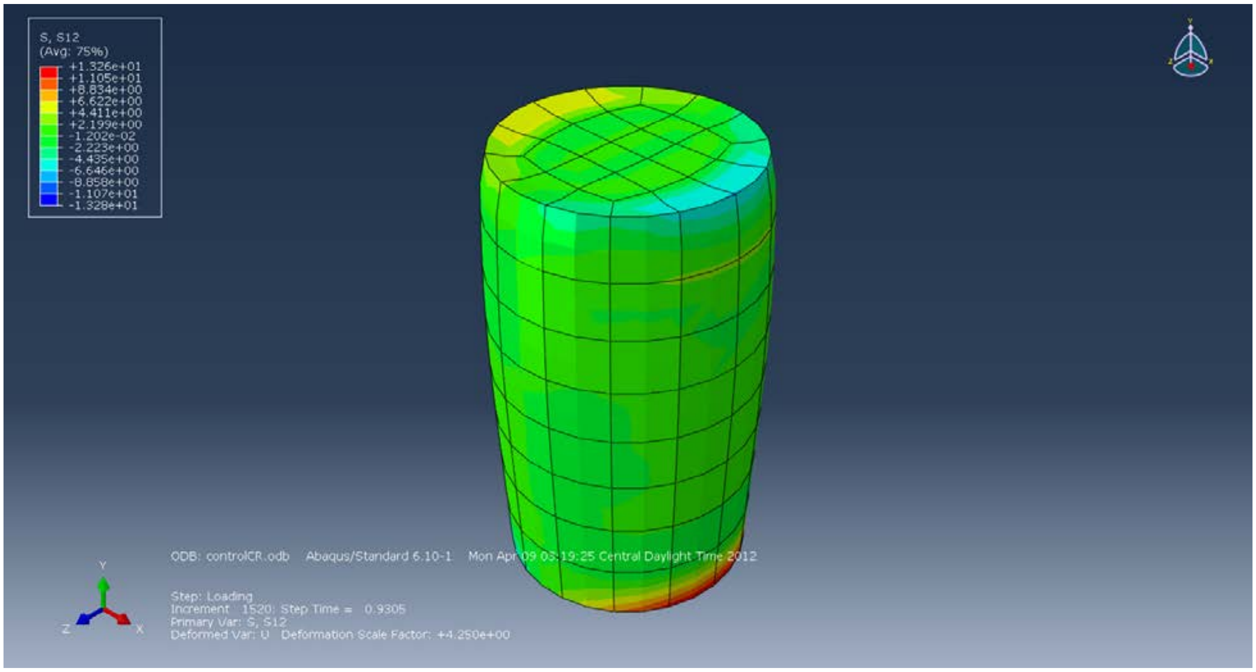

Figure B-18: Stress (S12) in the XY-Direction (MPa).

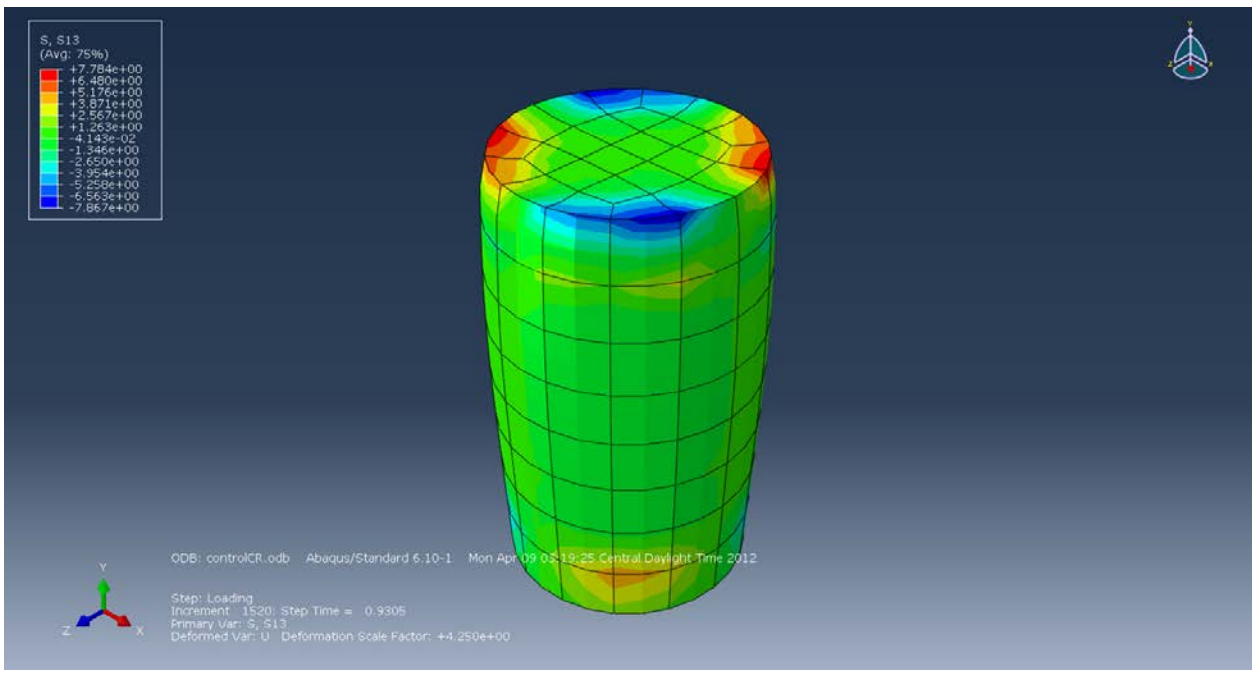

Figure B-19: Stress (S13) in the XZ-Direction (MPa).

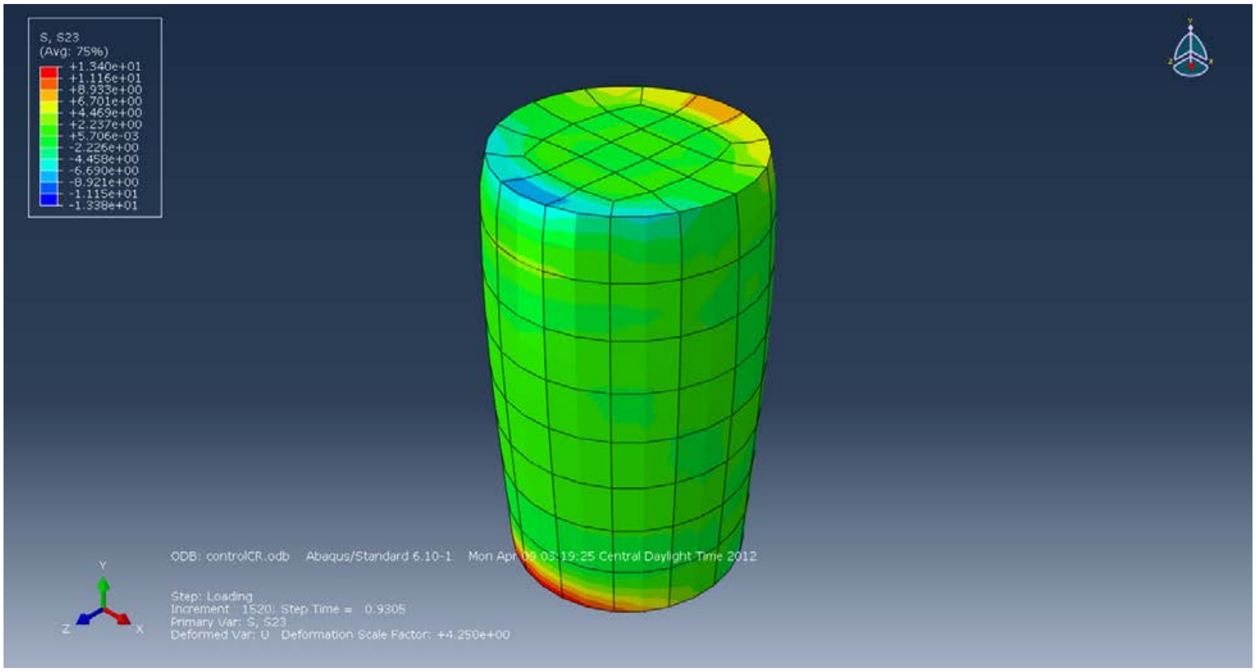

Figure B-20: Stress (S23) in the YZ-Direction (MPa).

- Smooth Boundaries:

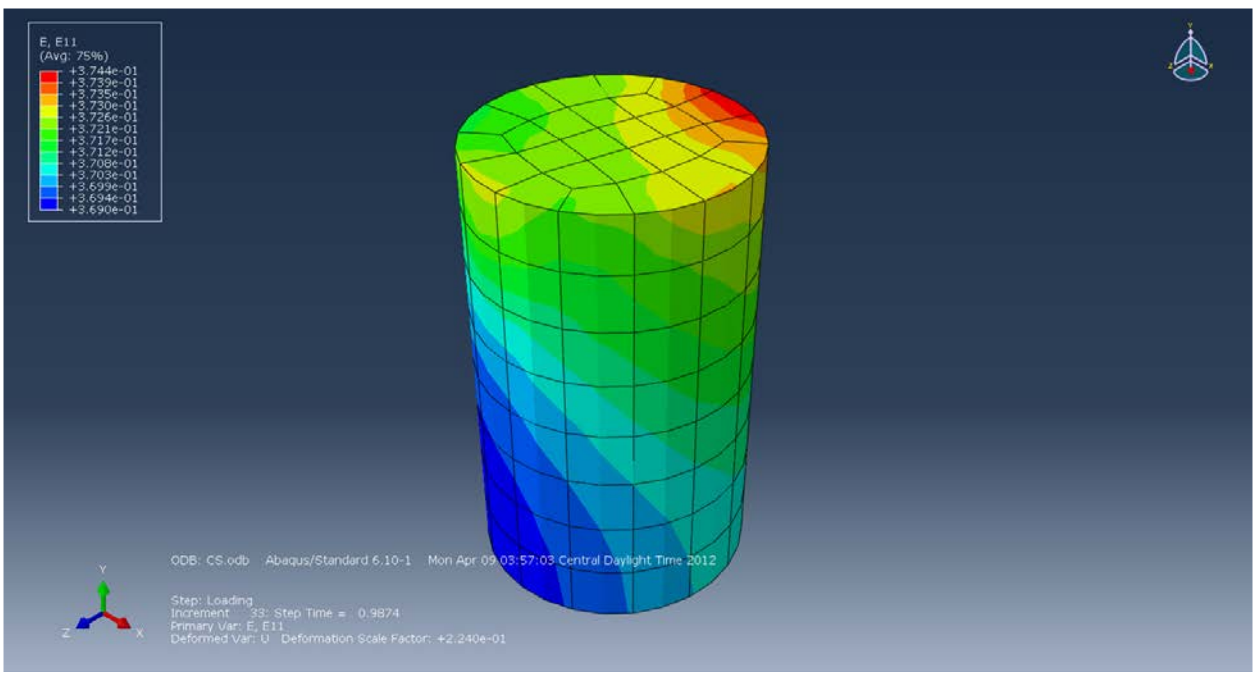

Figure B-21: Strain (E11) in the X-axis.

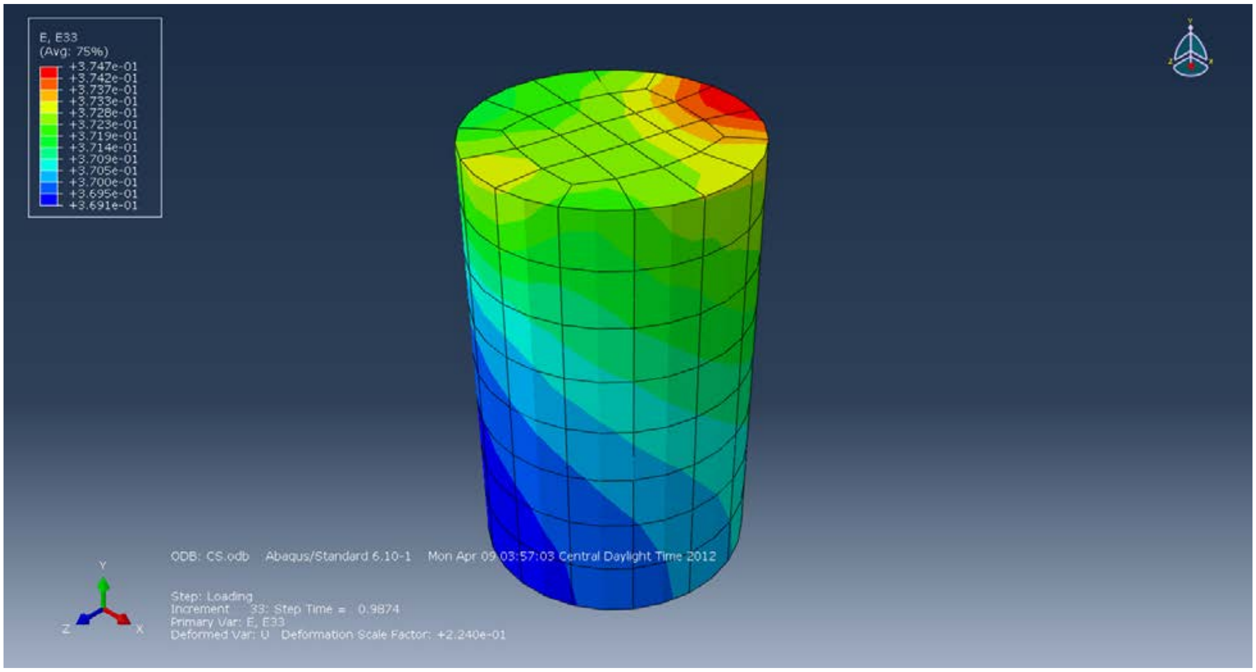

Figure B-22: Strain (E33) in the Z-axis.

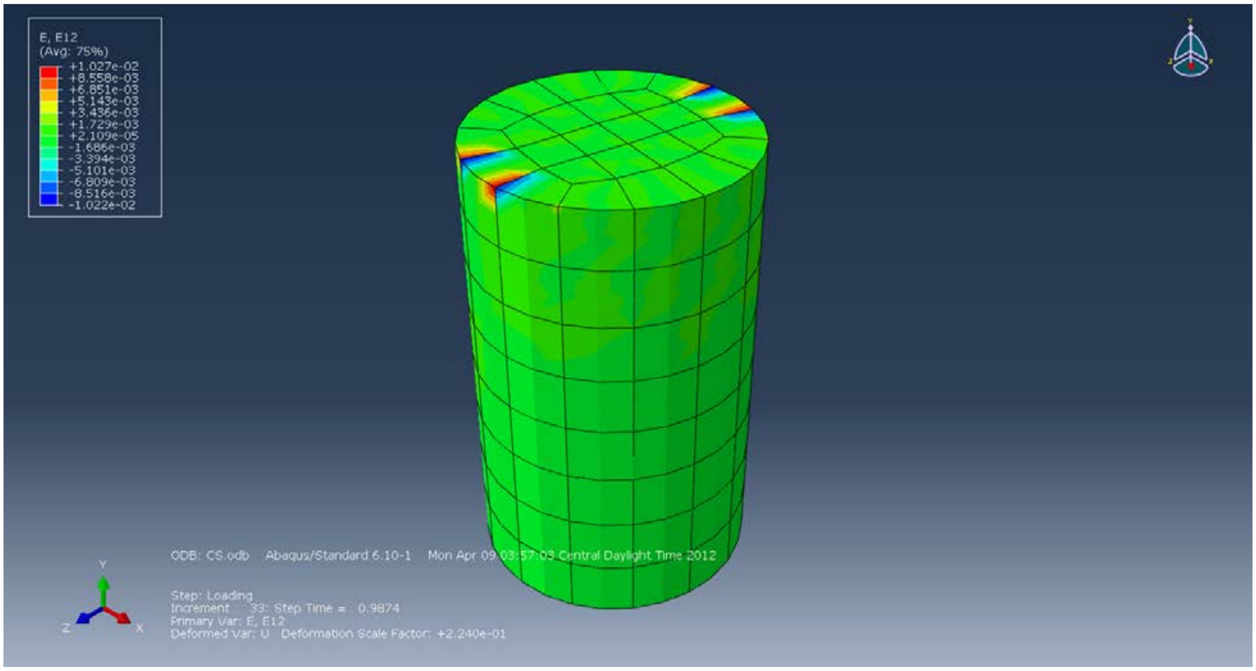

Figure B-23: Strain (E12) in the XY-Plane.

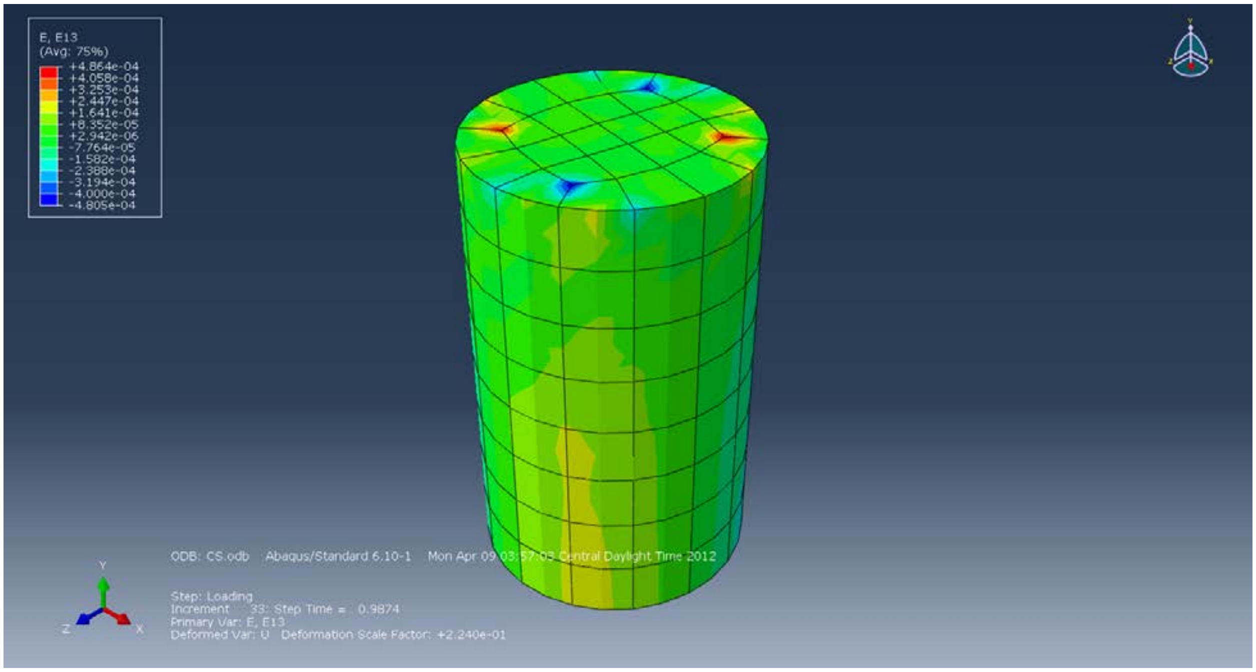

Figure B-24: Strain (E13) in the XZ-Plane.

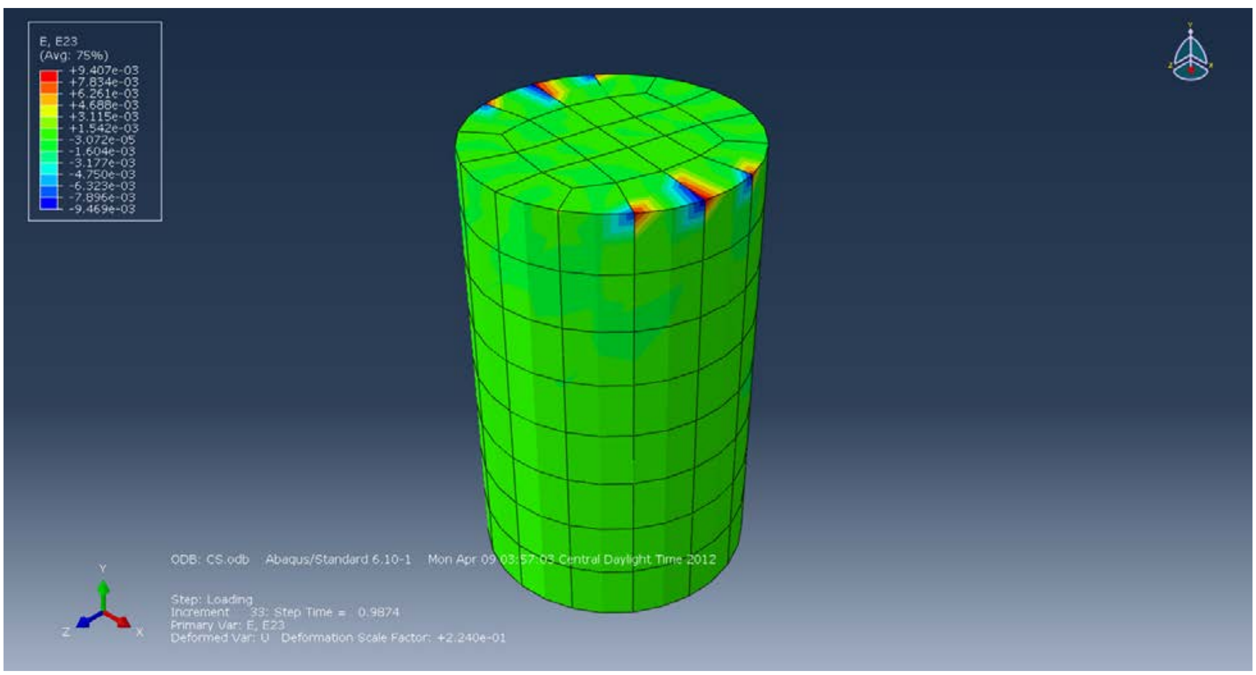

Figure B-25: Strain (E23) in the YZ-Plane.

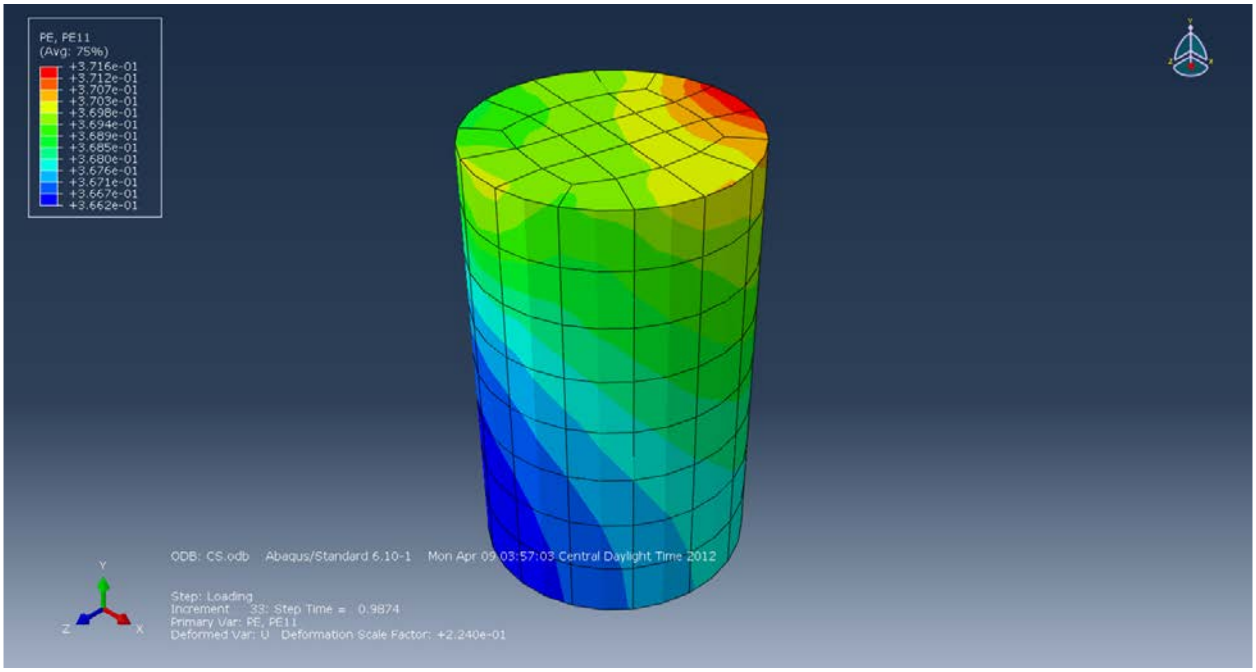

Figure B-26: Plastic Strain (PE11) in the X-axis.

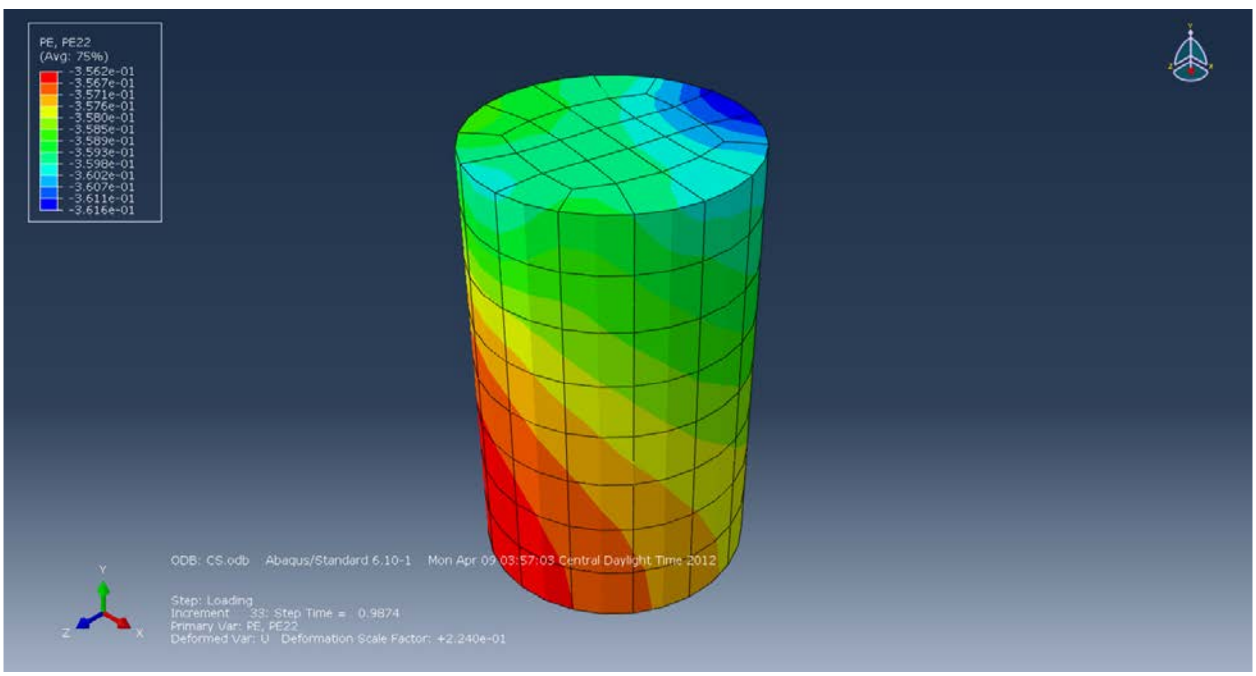

Figure B-27: Plastic Strain (PE22) in the Y-axis.

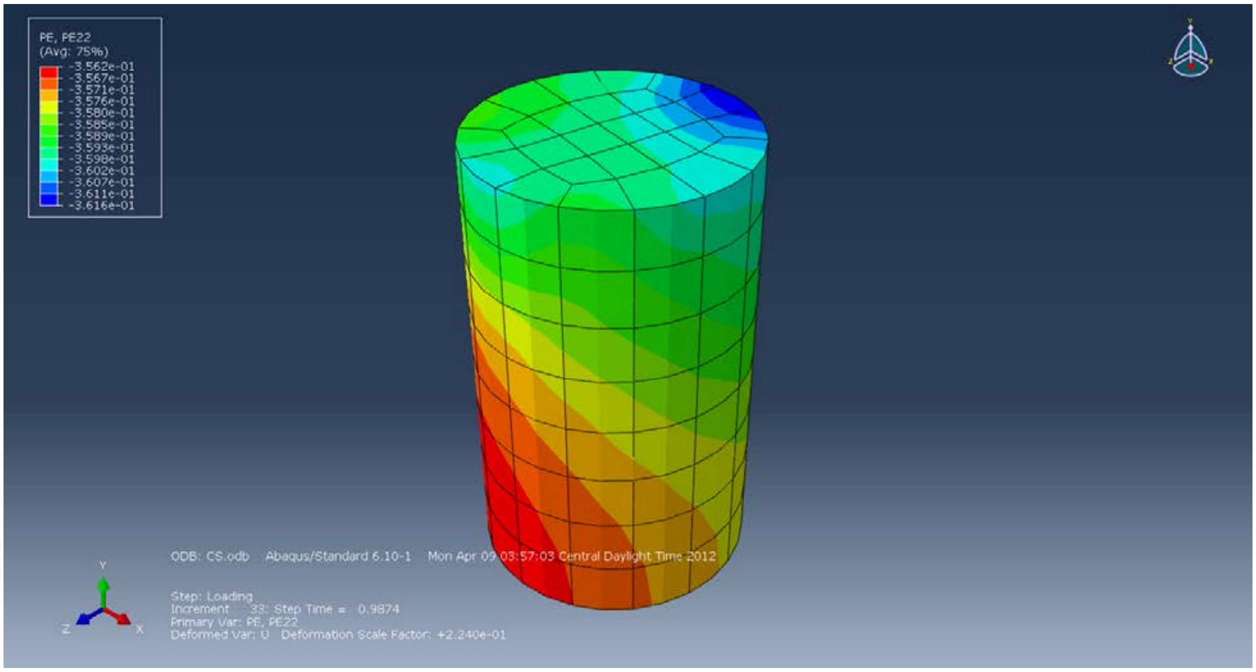

Figure B-28: Plastic Strain (PE33) in the Z-axis.

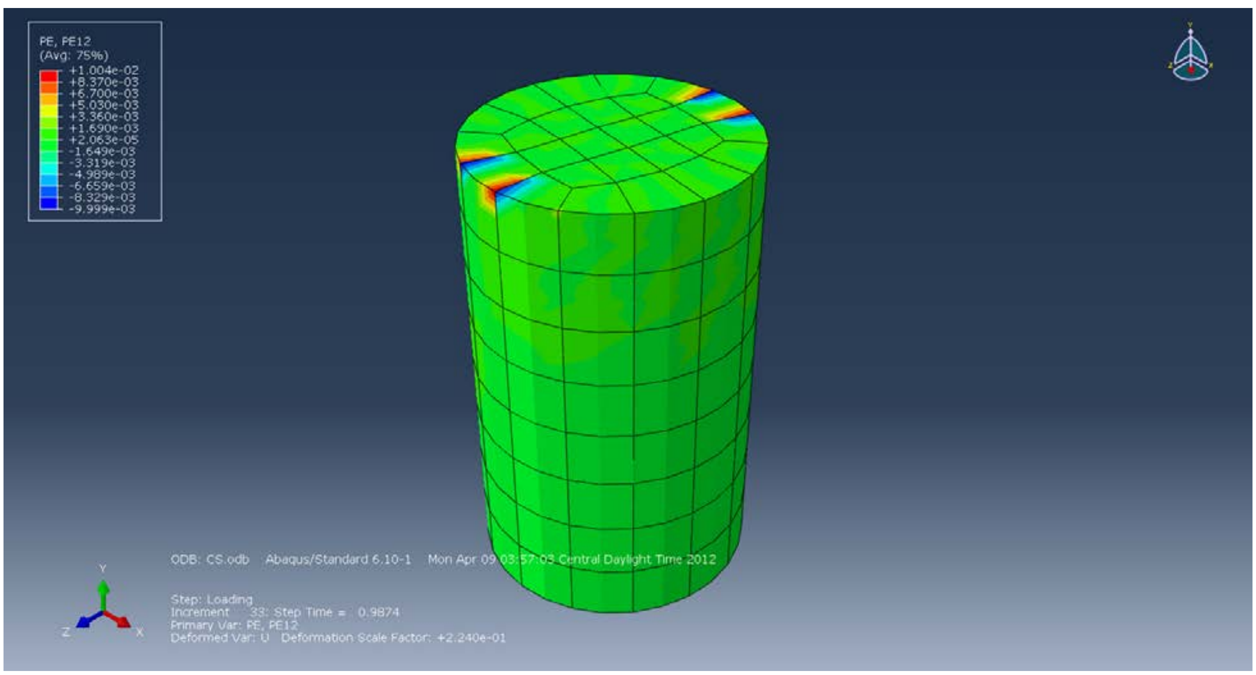

Figure B-29: Plastic Strain (PE12) in the XY-Plane.

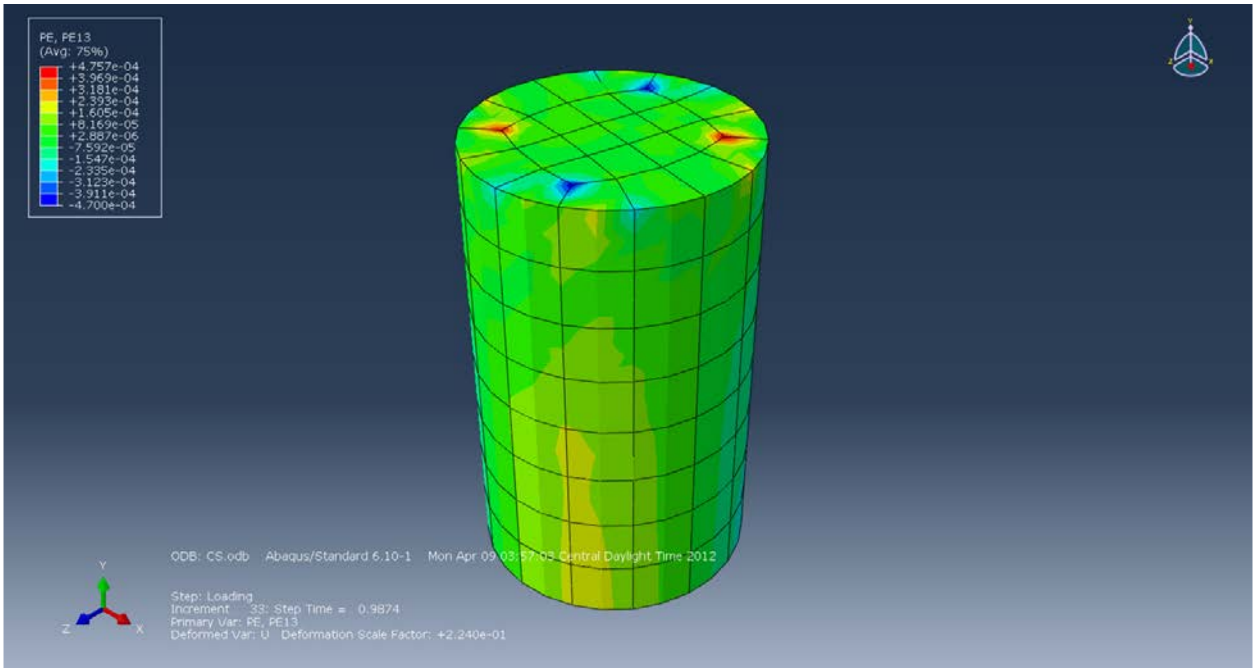

Figure B-30: Plastic Strain (PE13) in the XZ-Plane.

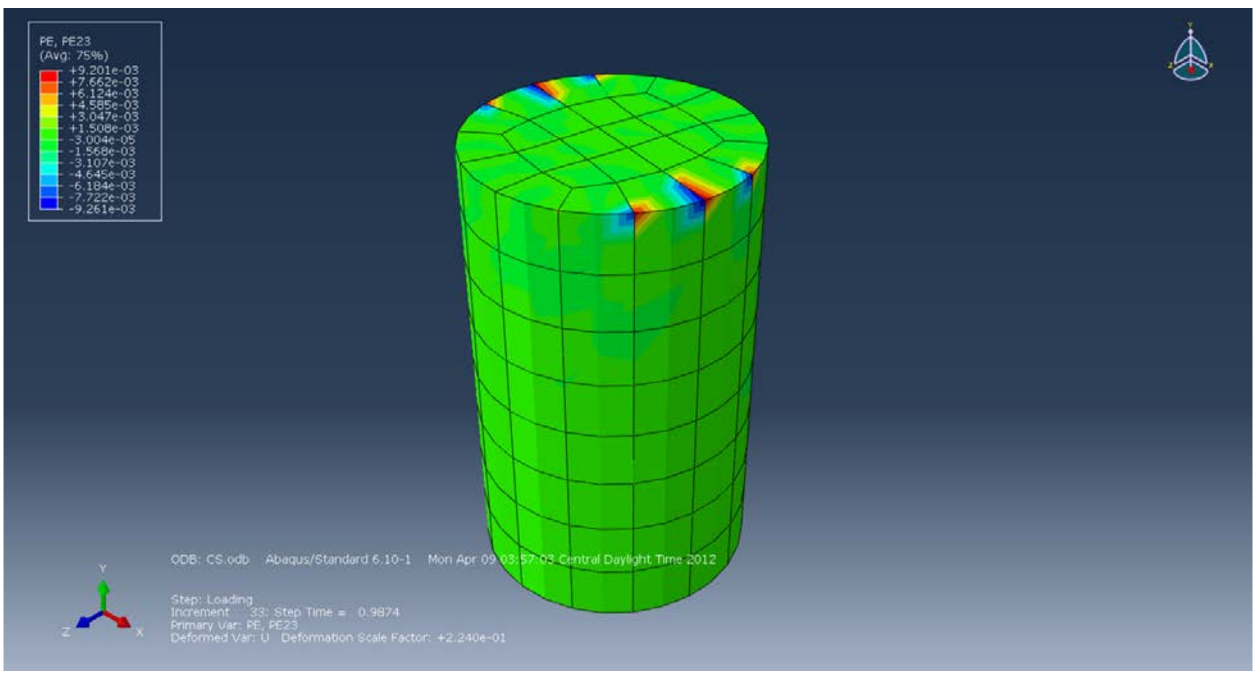

Figure B-31: Plastic Strain (PE23) in the YZ-Plane.

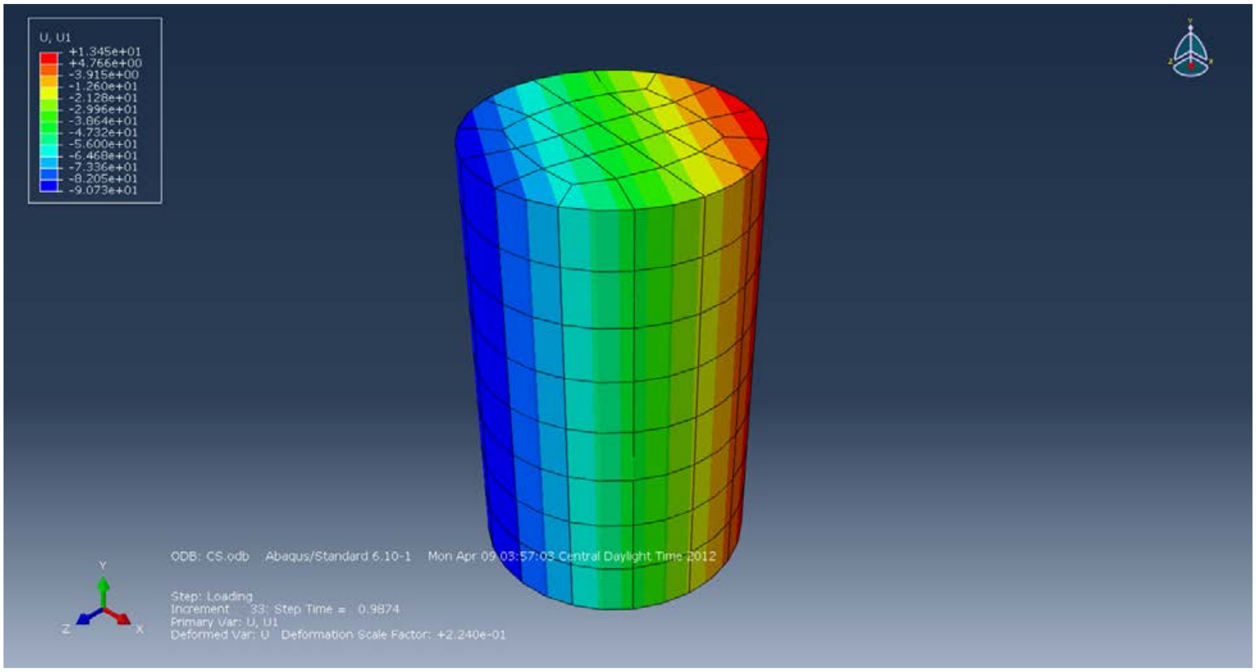

Figure B-32: Displacement (U1) in the X-axis (mm).

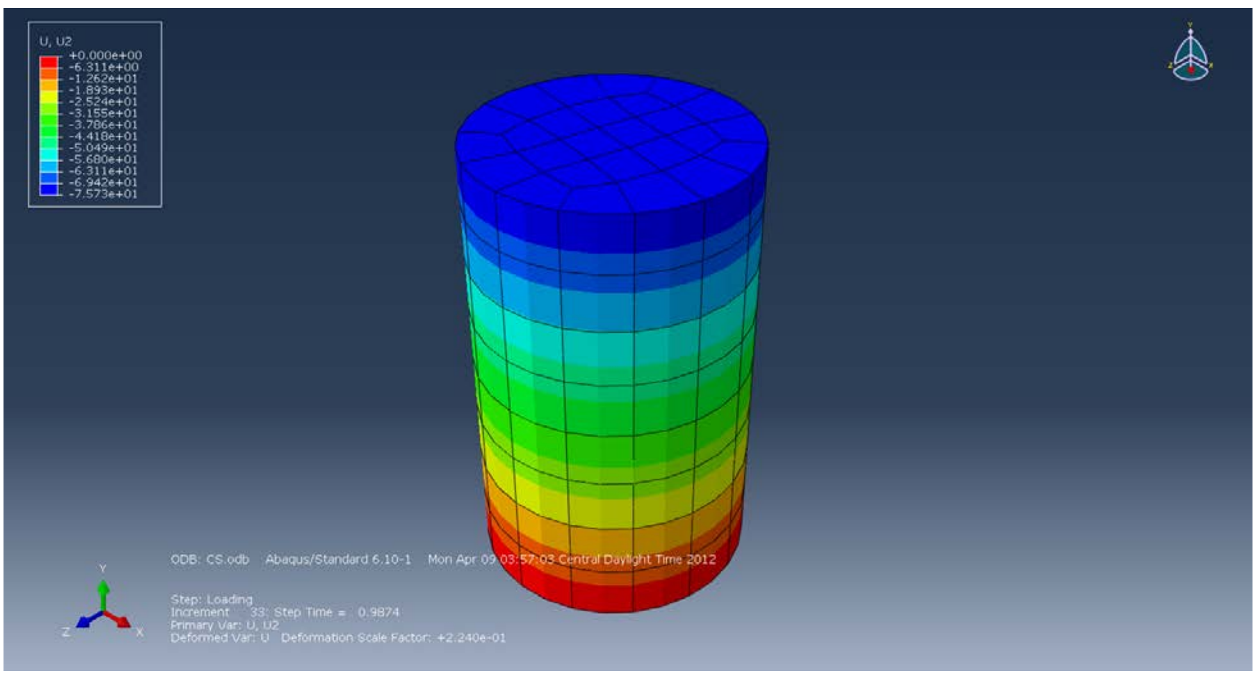

Figure B-33: Displacement (U2) in the Y-axis (mm).

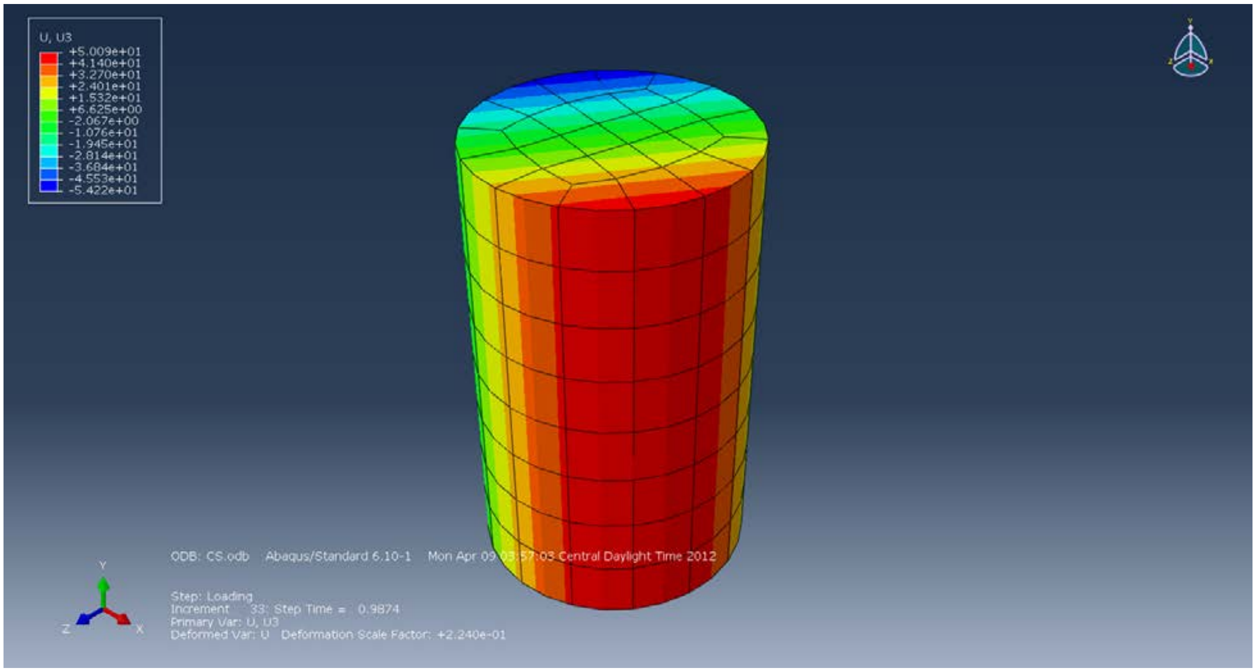

Figure B-34: Displacement (U3) in the Z-axis (mm).

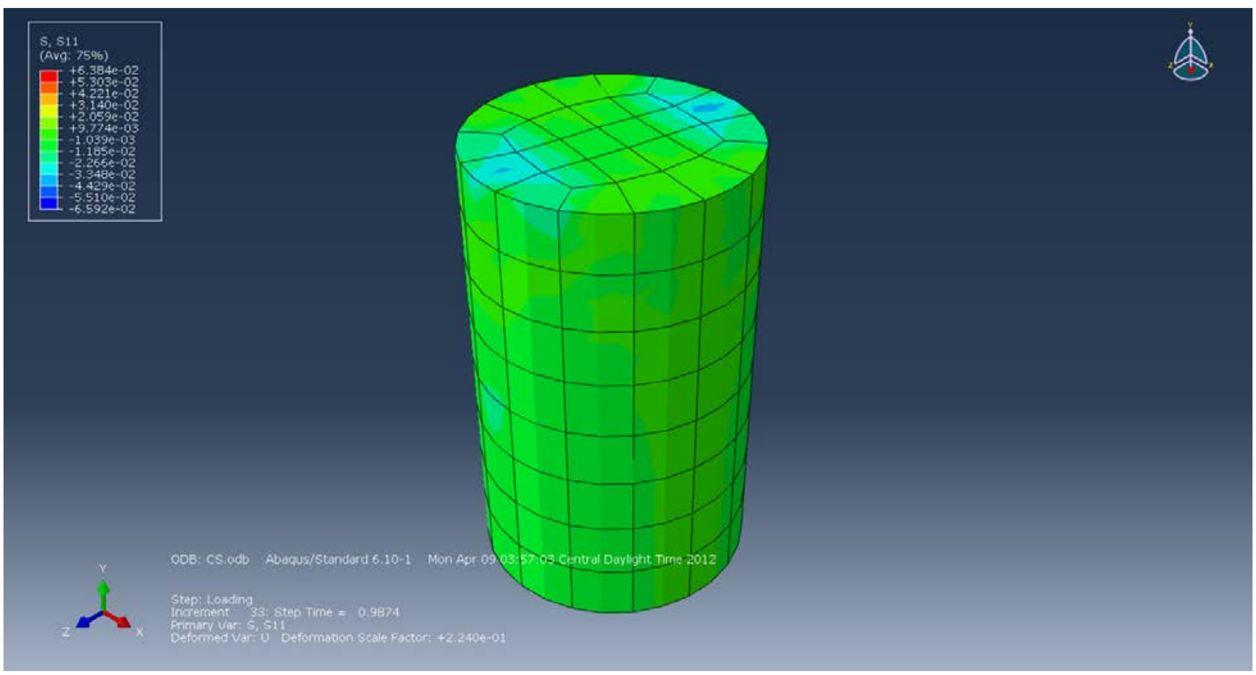

Figure B-35: Stress (S11) in the X-Direction (MPa).

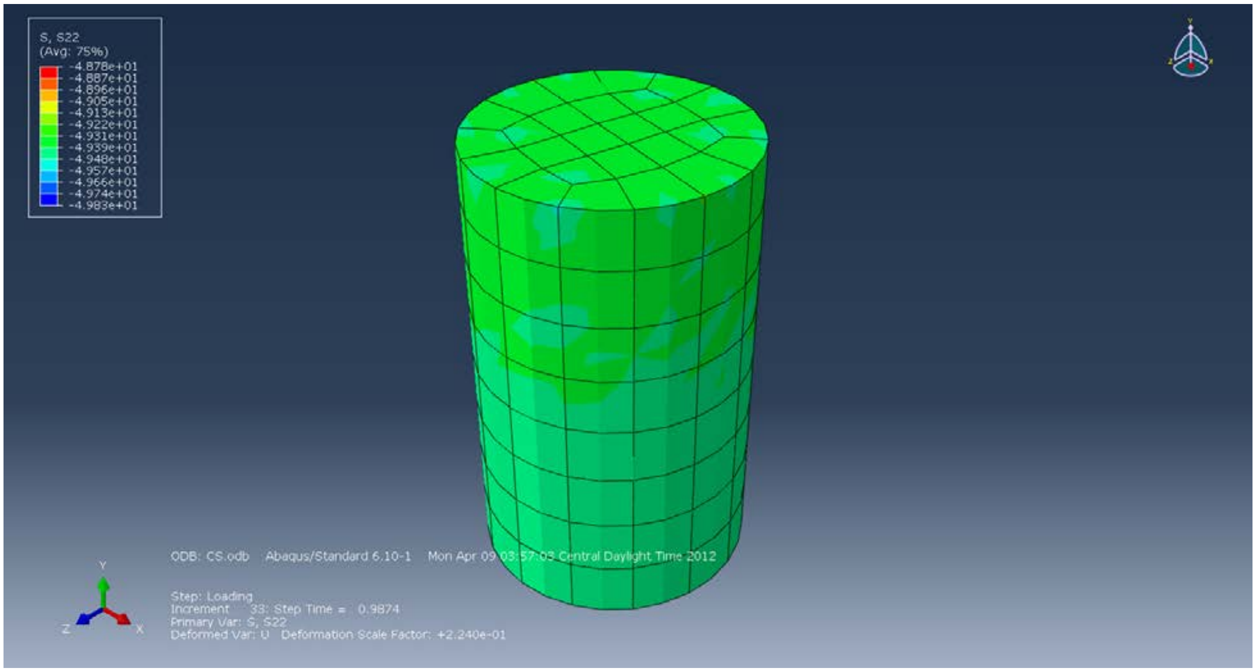

Figure B-36: Stress (S22) in the Y-Direction (MPa).

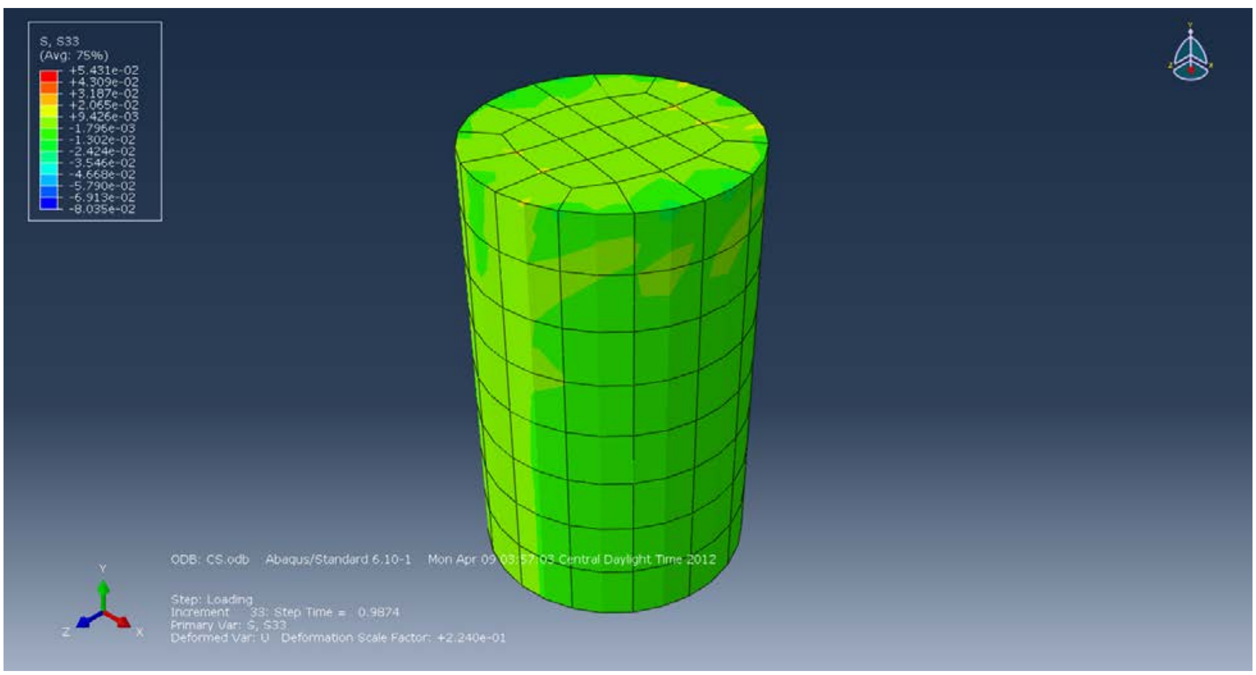

Figure B-37: Stress (S33) in the Z-Direction (MPa).

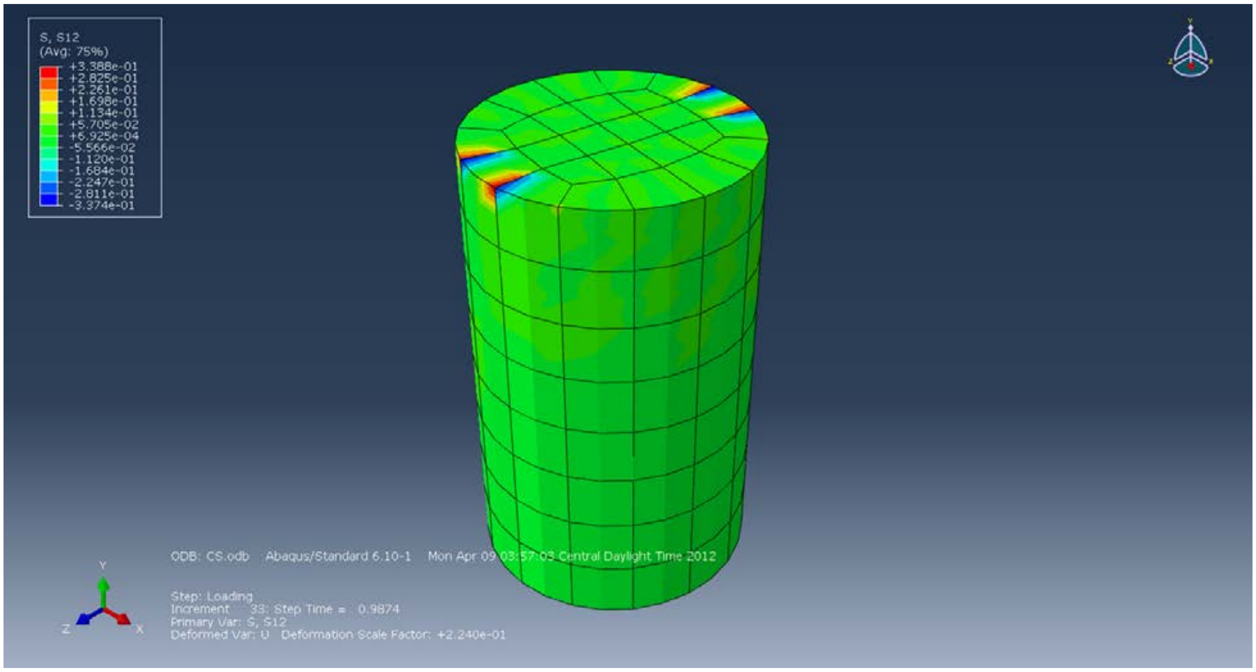

Figure B-38: Stress (S12) in the XY-Direction (MPa).

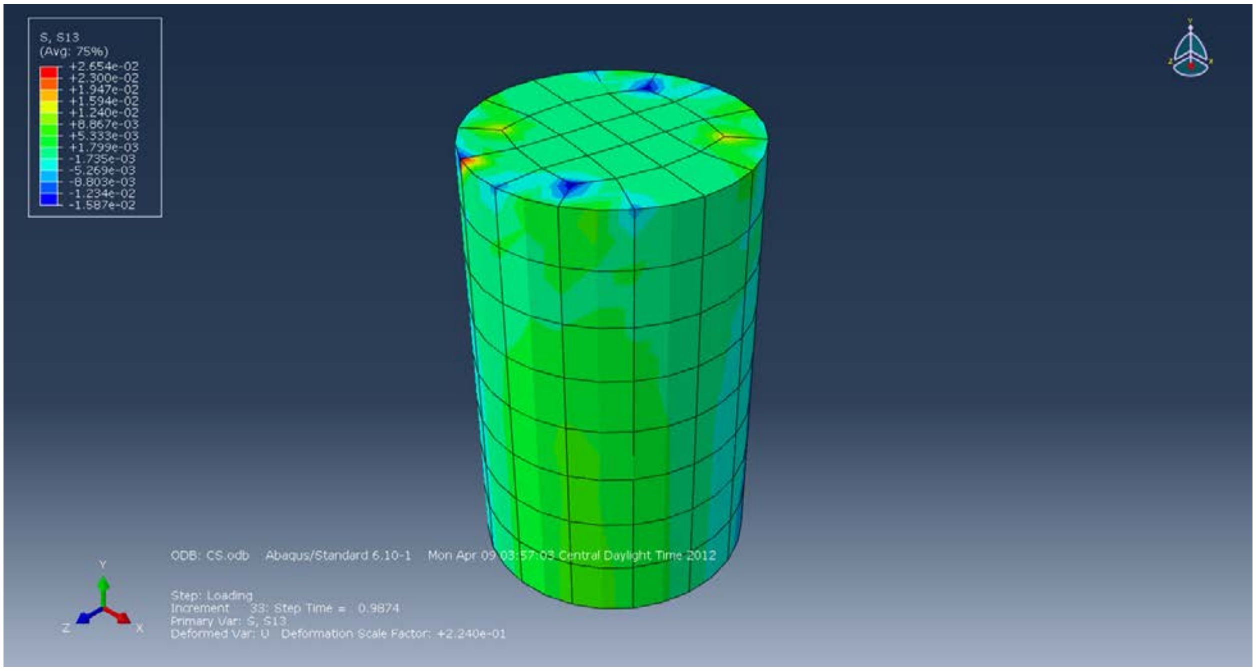

Figure B-39: Stress (S13) in the XZ-Direction (MPa).

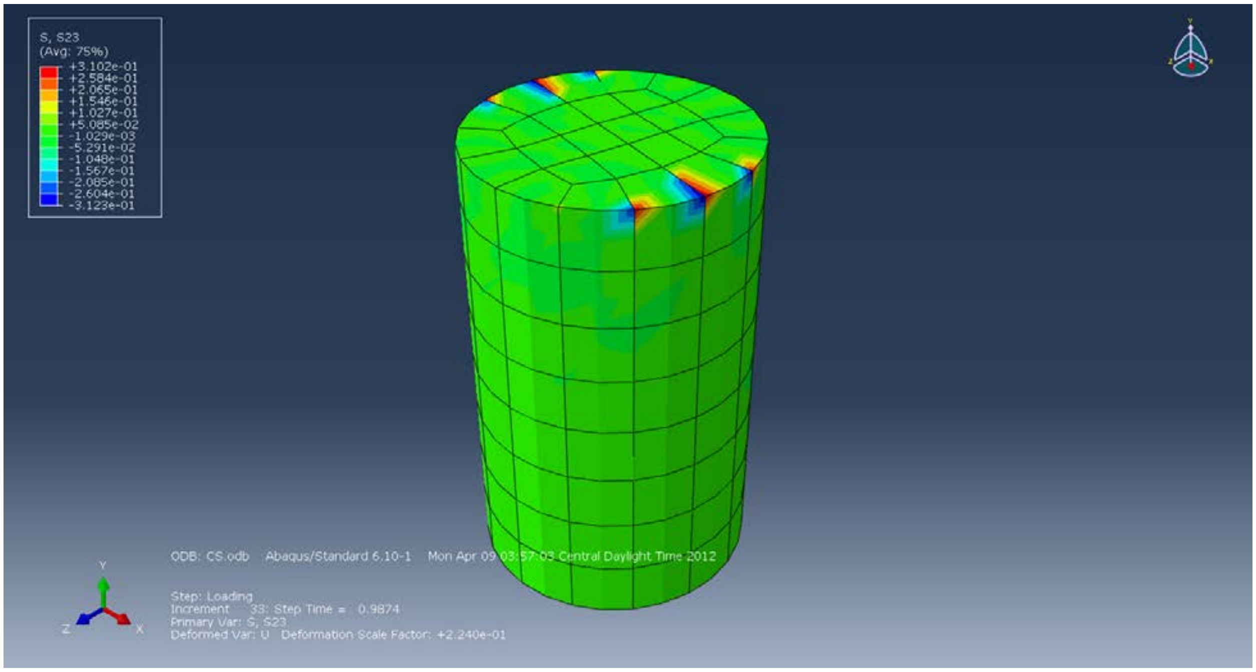

Figure B-40: Stress (S23) in the YZ-Direction (MPa).

Cylinders with 0.5% Wheat Fibers:

- Rough Boundaries:

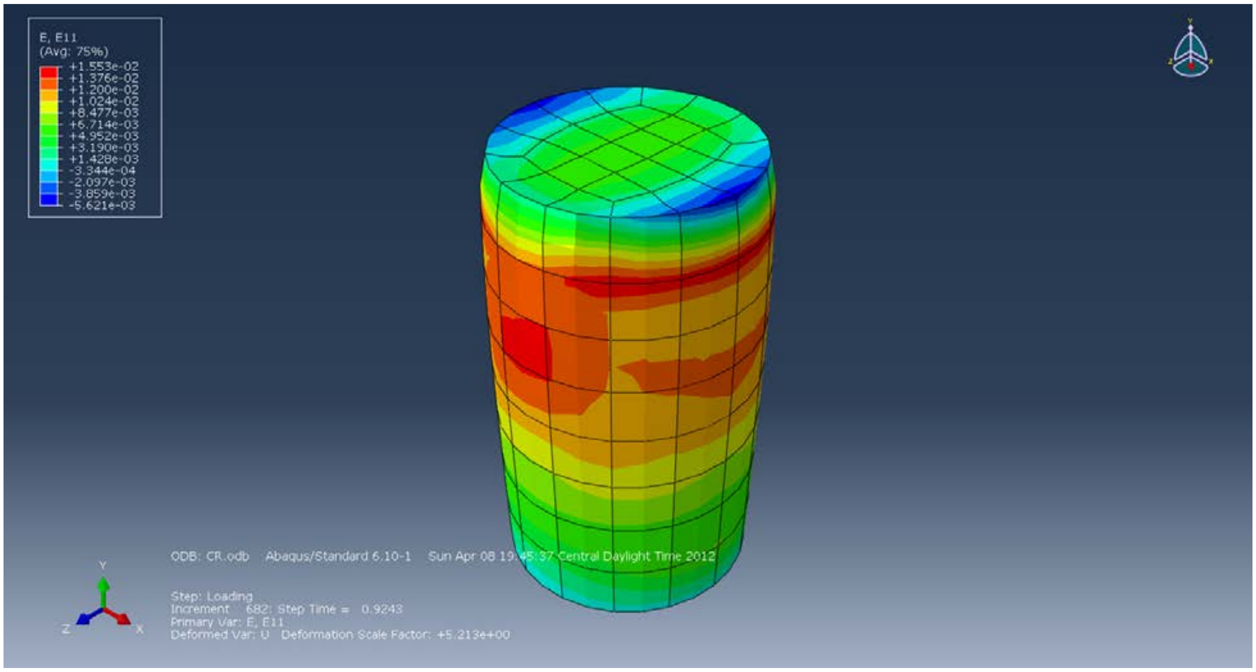

Figure B-41: Strain (E11) in the X-axis.

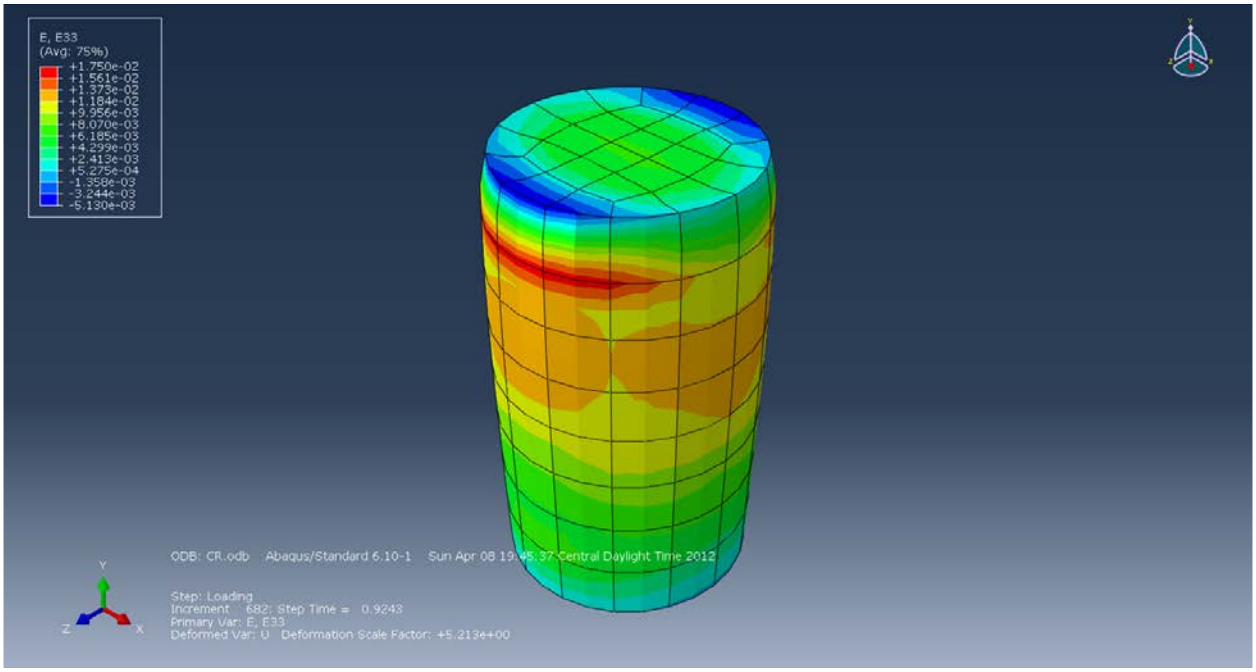

Figure B-42: Strain (E33) in the Z-axis.

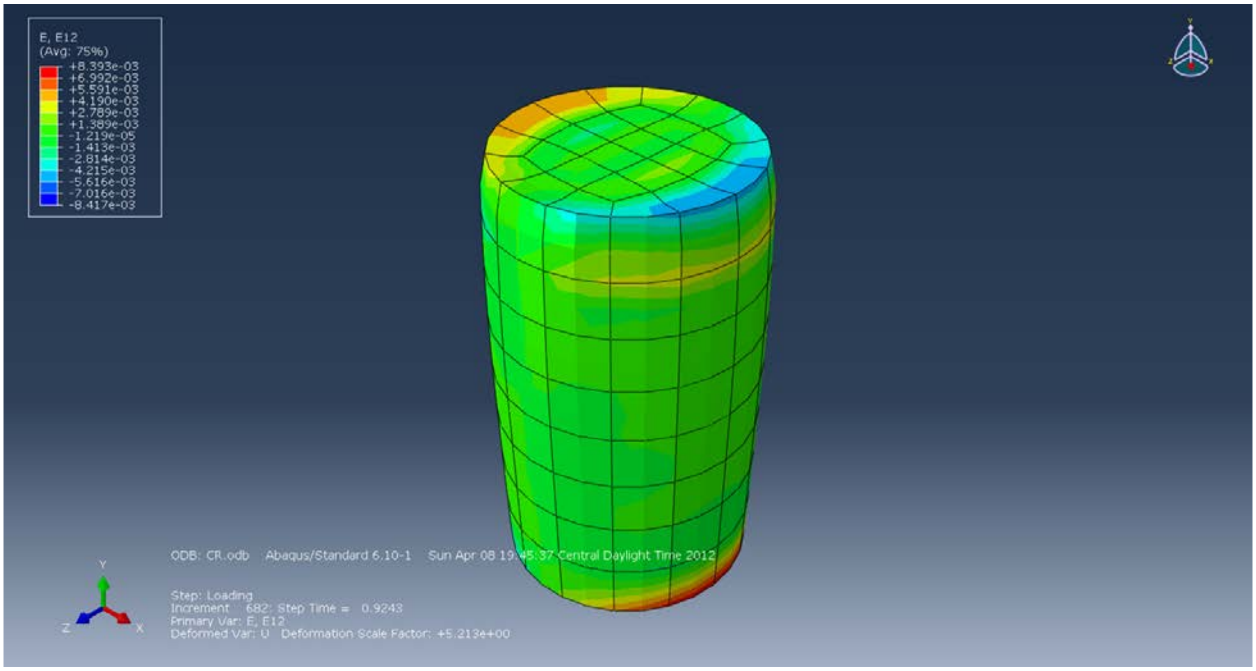

Figure B-43: Strain (E12) in the XY-Plane.

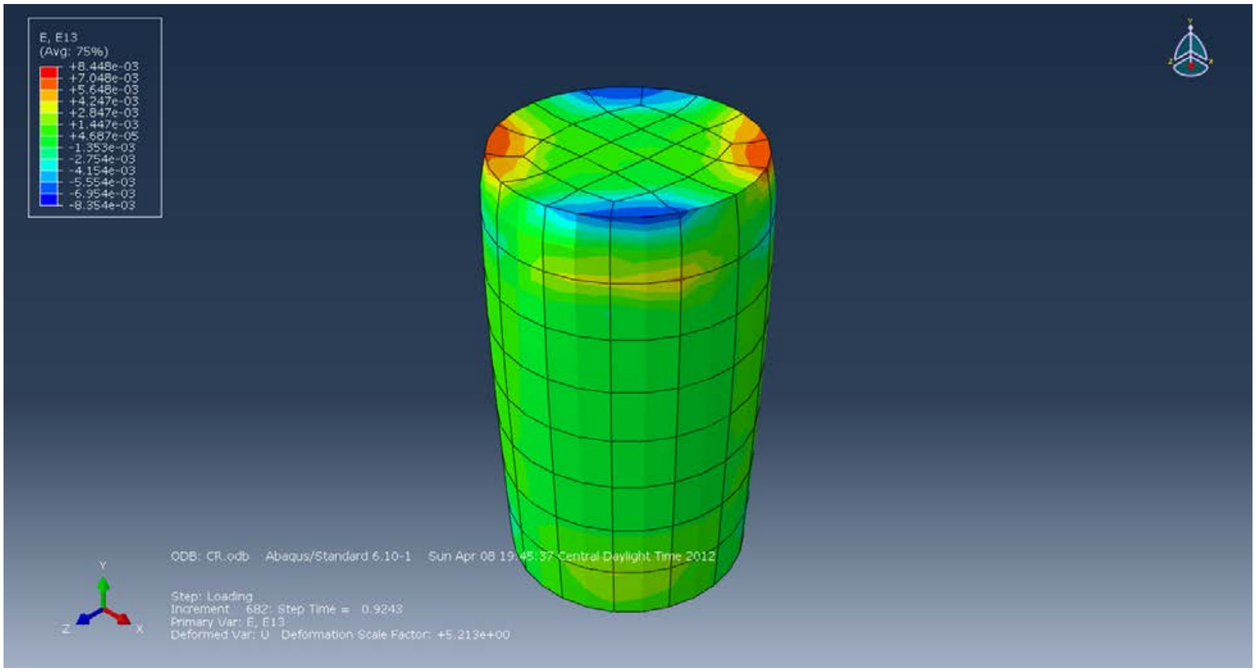

Figure B-44: Strain (E13) in the XZ-Plane.

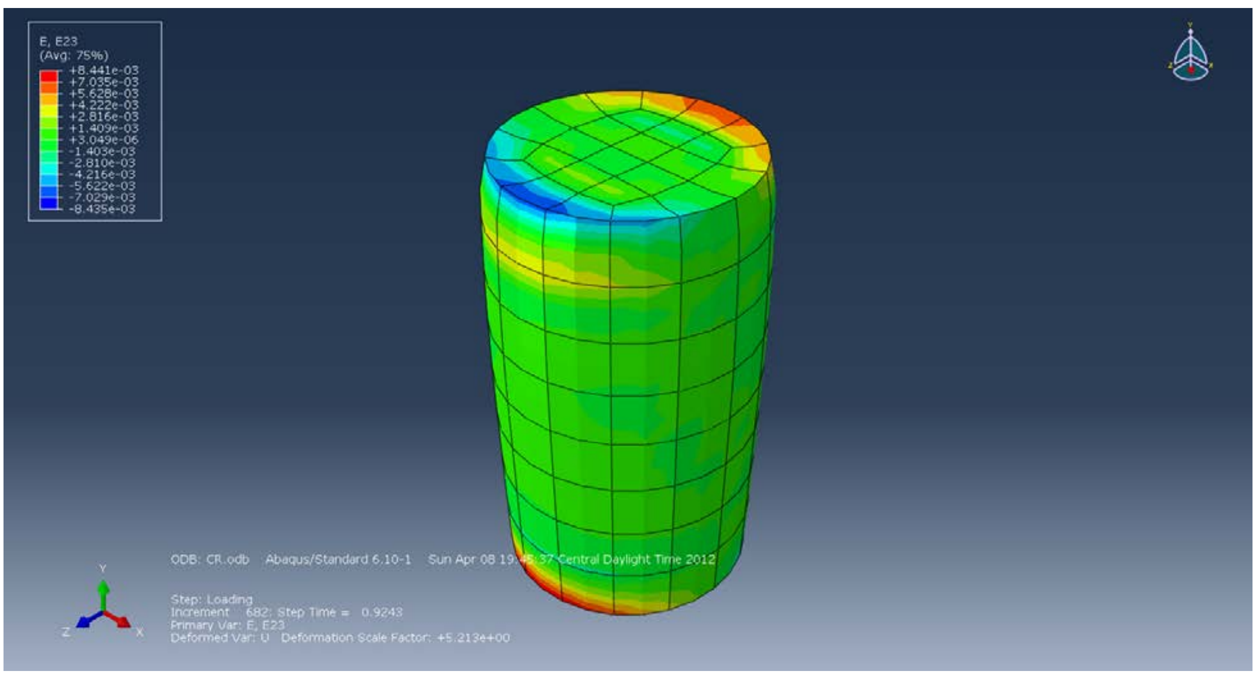

Figure B-45: Strain (E23) in the YZ-Plane.

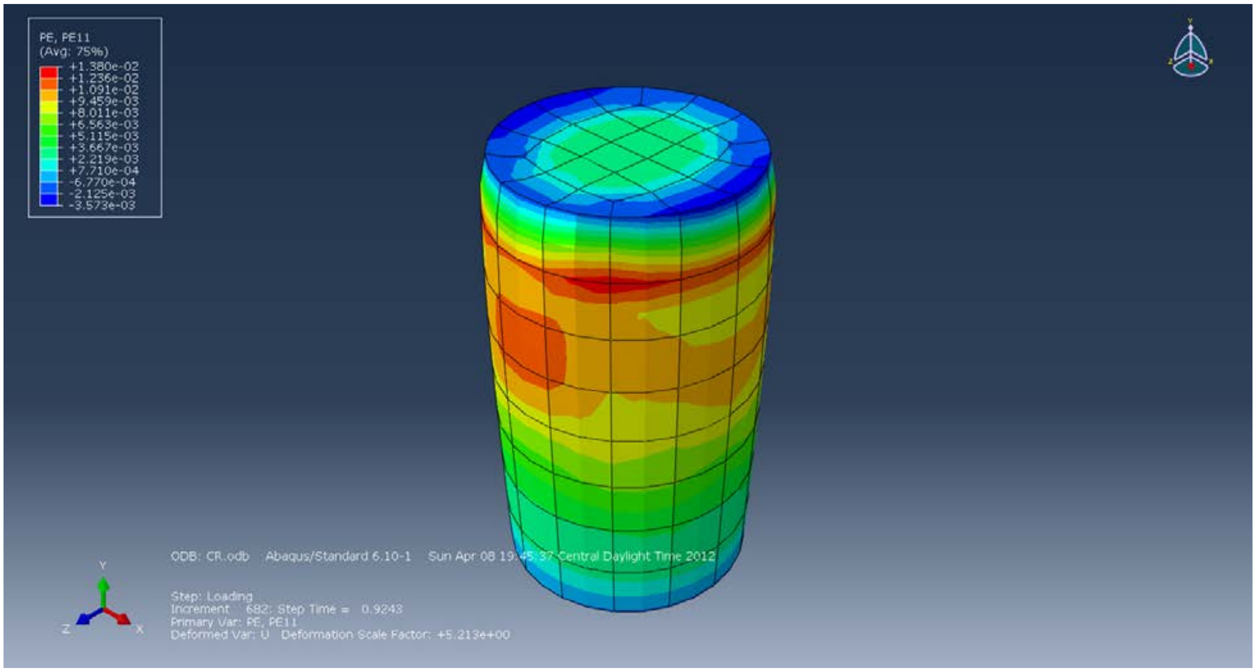

Figure B-46: Plastic Strain (PE11) in the X-axis.

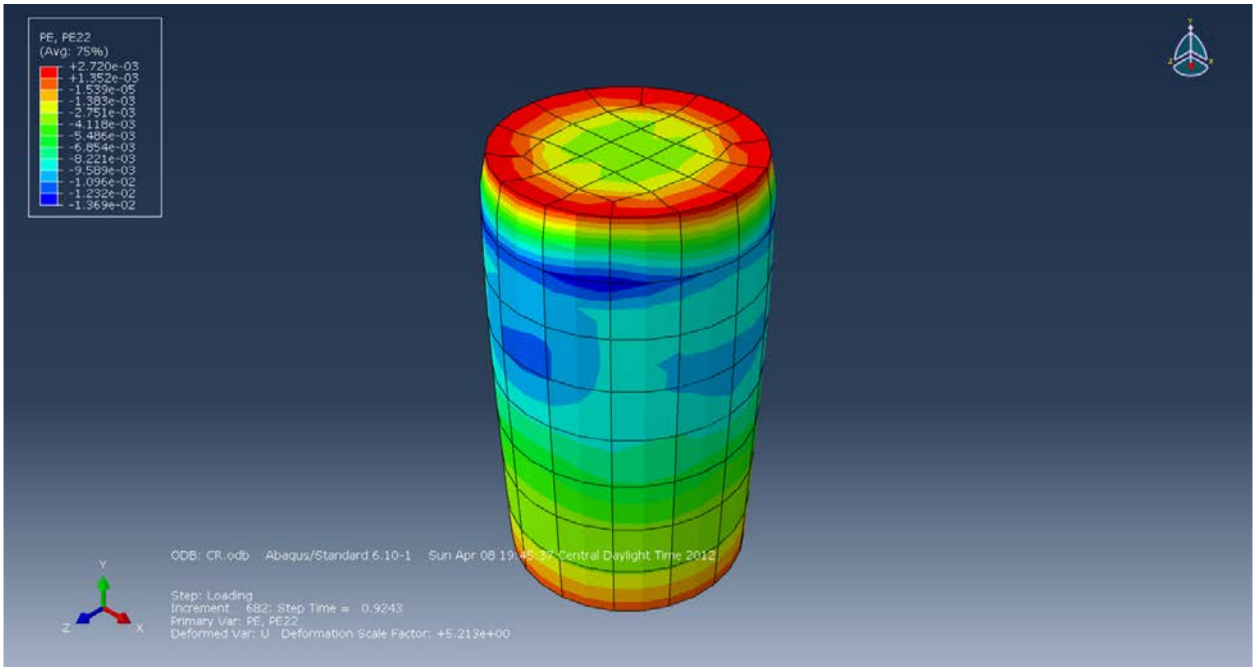

Figure B-47: Plastic Strain (PE22) in the Y-axis.

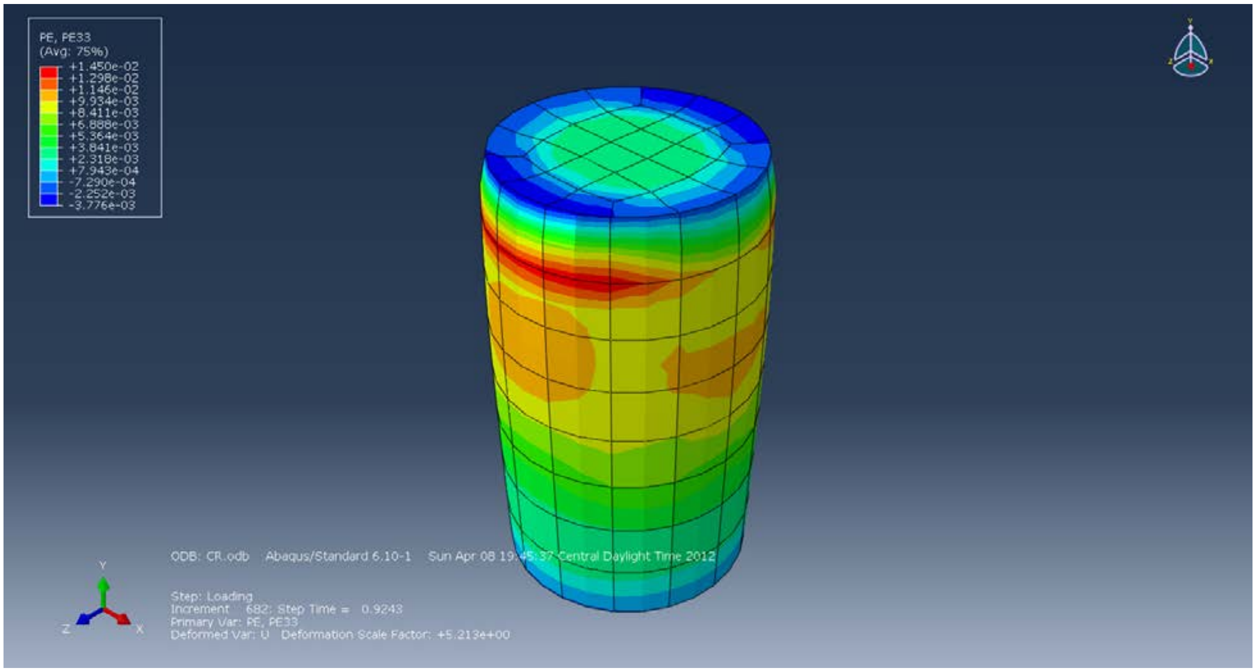

Figure B-48: Plastic Strain (PE33) in the Z-axis.

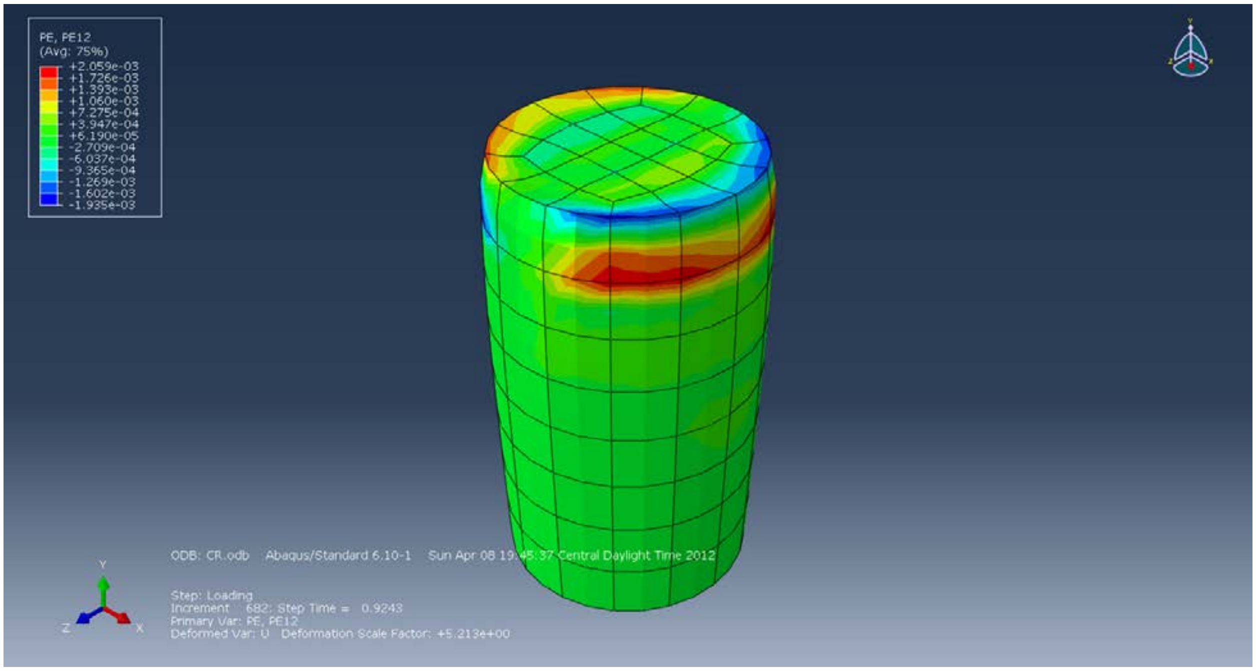

Figure B-49: Plastic Strain (PE12) in the XY-Plane.

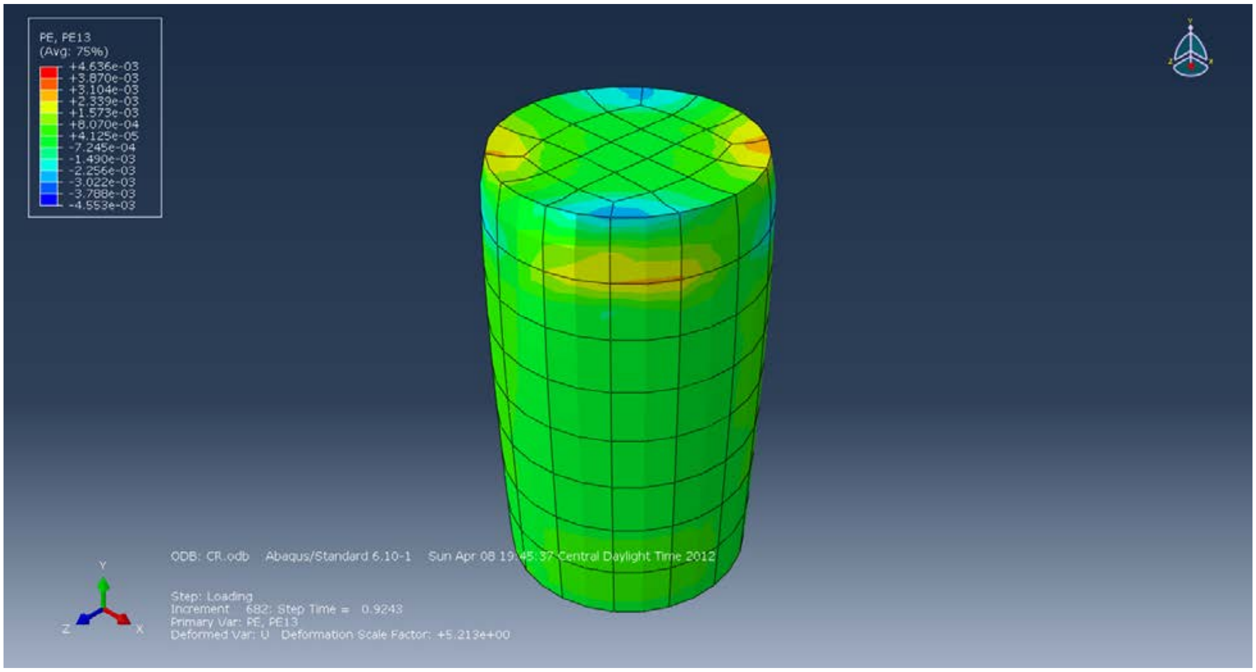

Figure B-50: Plastic Strain (PE13) in the XZ-Plane.

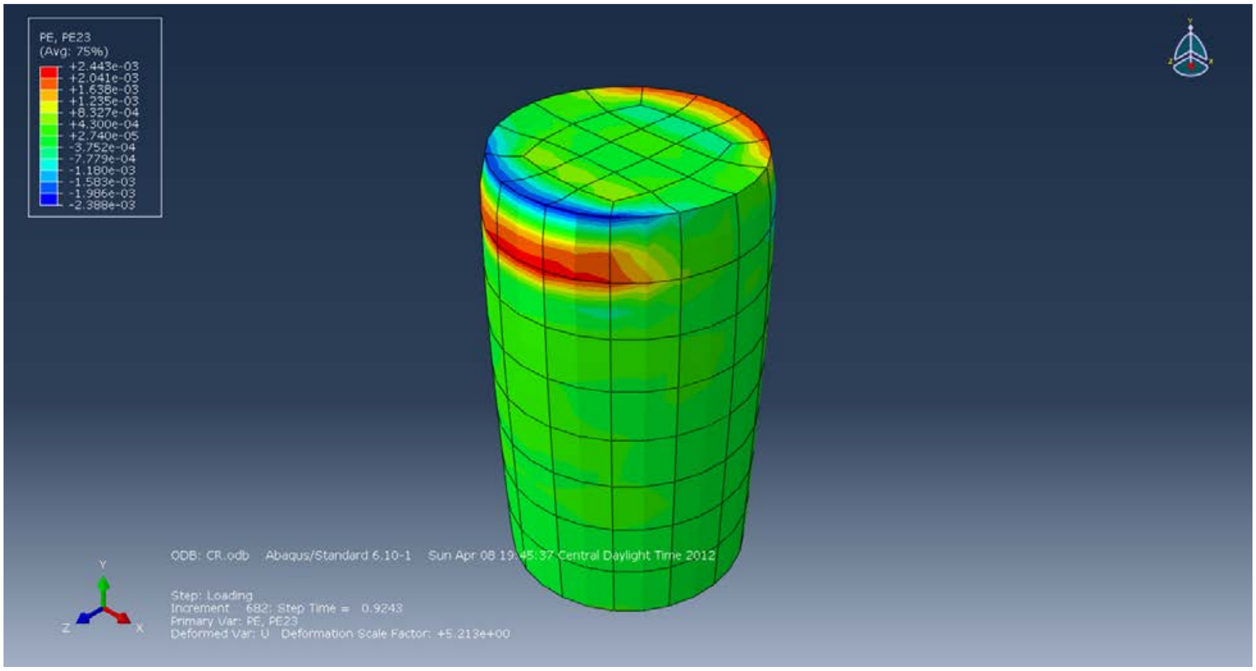

Figure B-51: Plastic Strain (PE23) in the YZ-Plane.

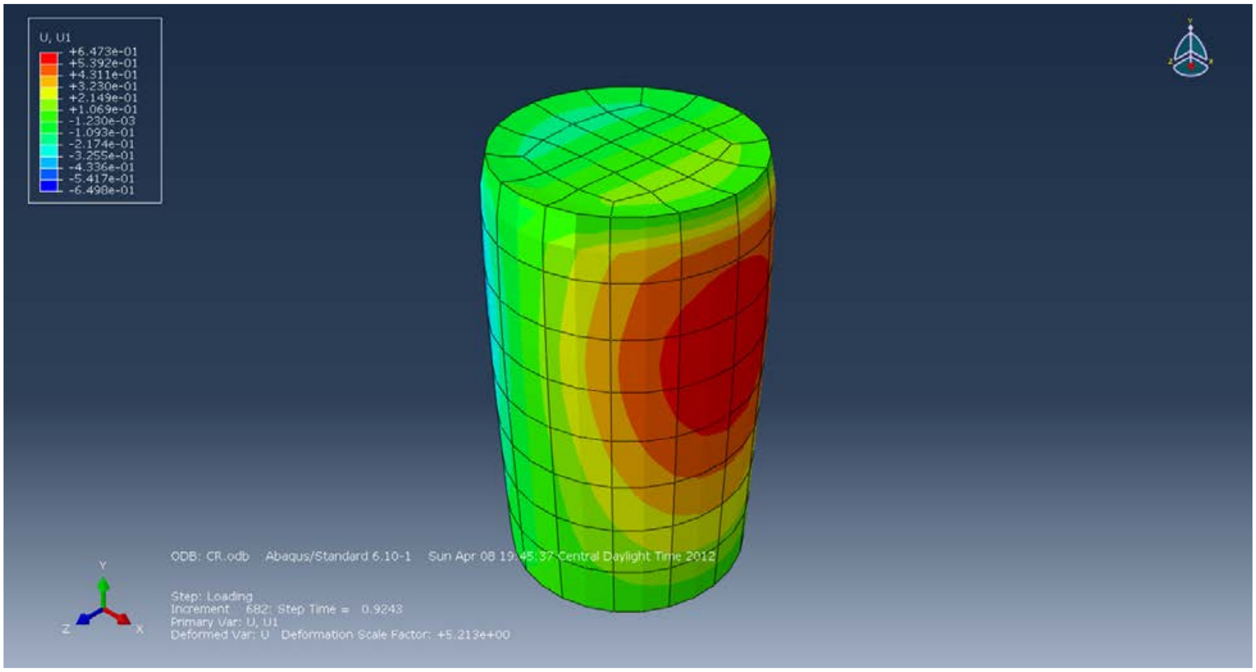

Figure B-52: Displacement (U1) in the X-axis (mm).

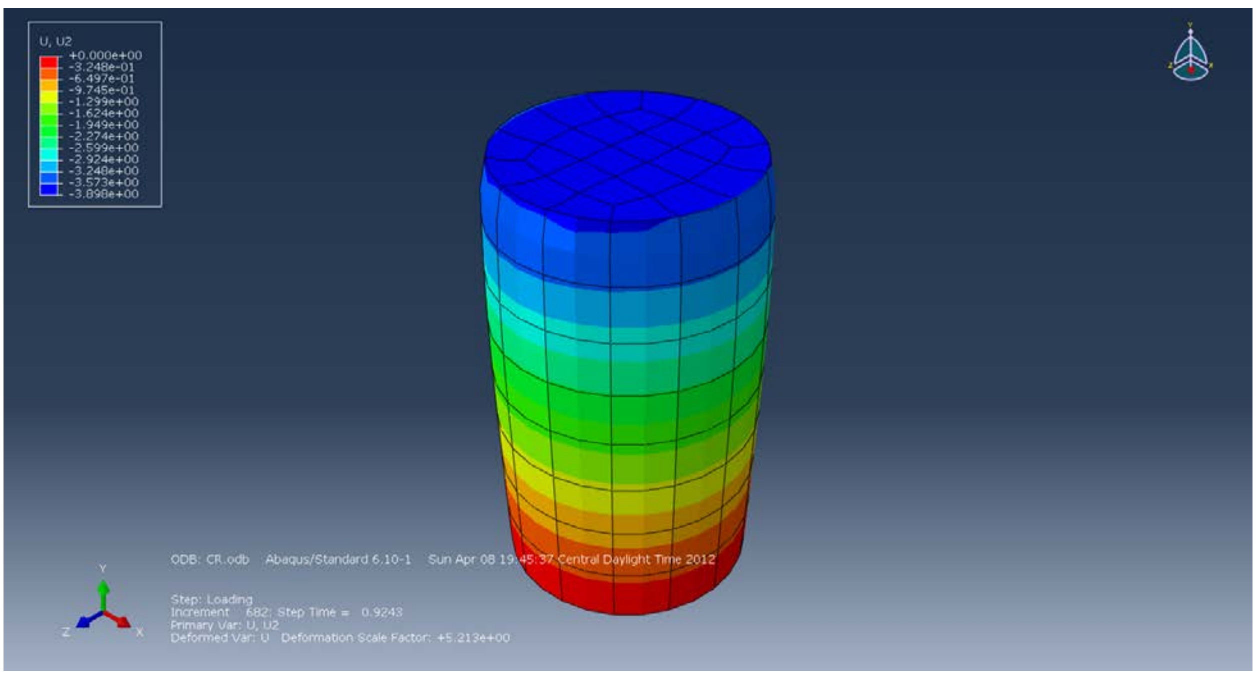

Figure B-53: Displacement (U2) in the Y-axis (mm).

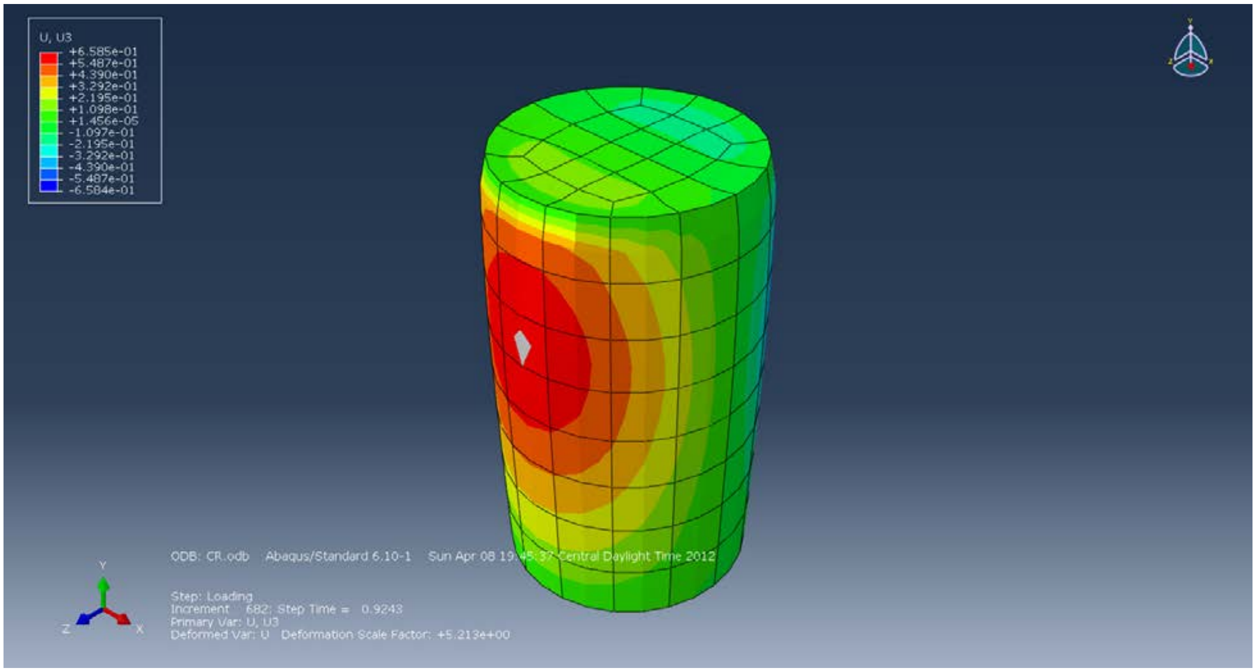

Figure B-54: Displacement (U3) in the Z-axis (mm).

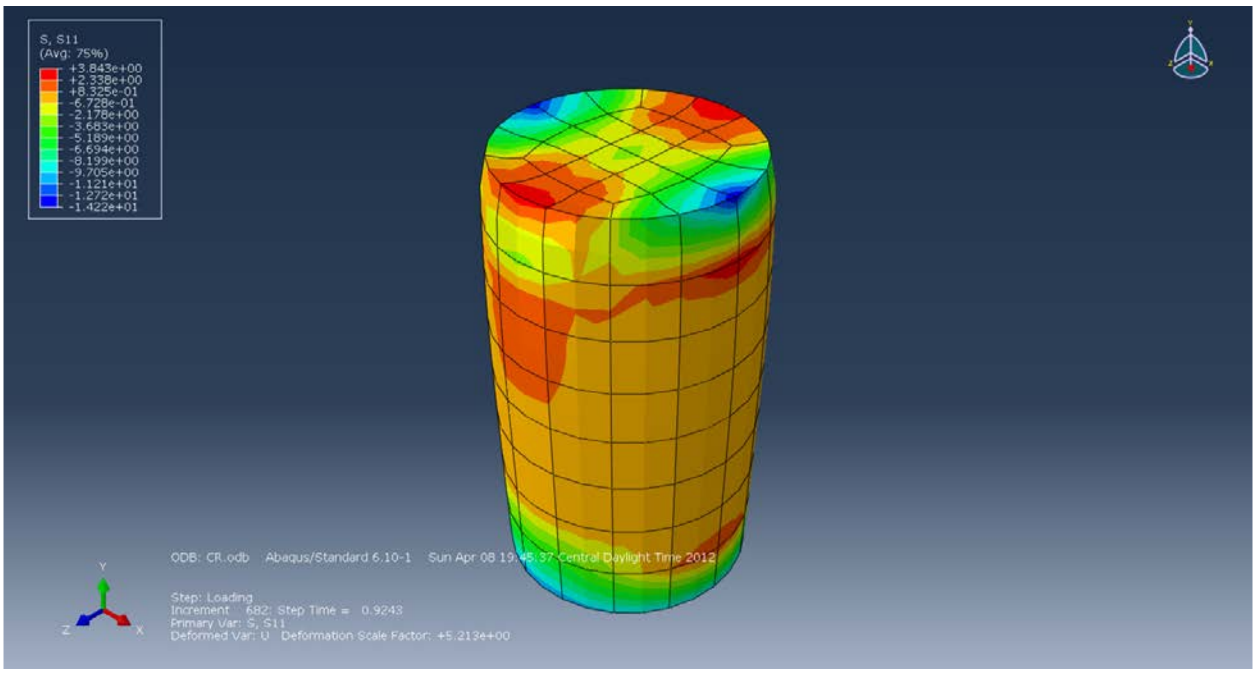

Figure B-55: Stress (S11) in the X-Direction (MPa).

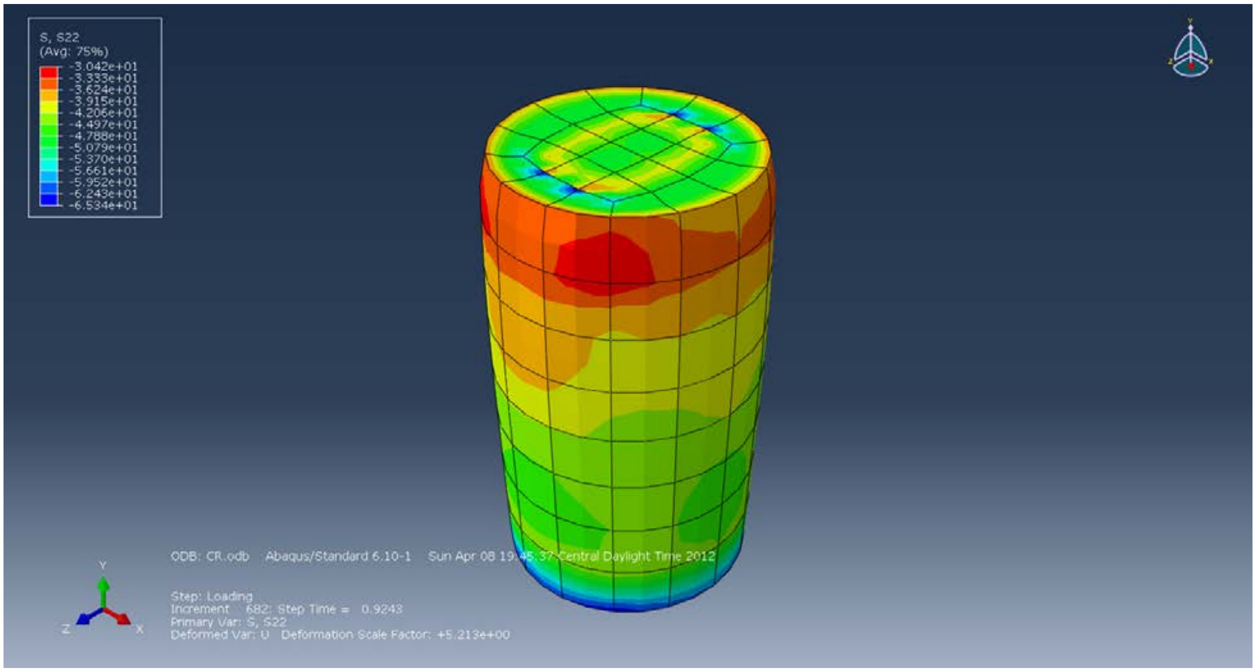

Figure B-56: Stress (S22) in the Y-Direction (MPa).

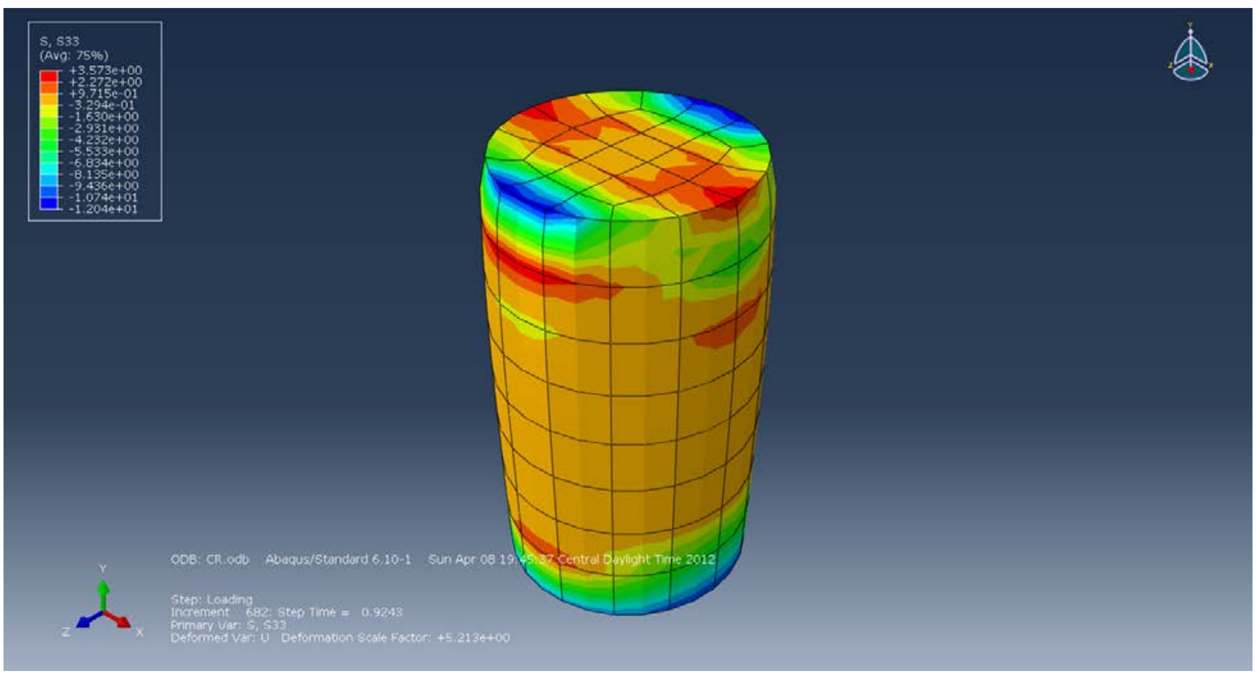

Figure B-57: Stress (S33) in the Z-Direction (MPa).

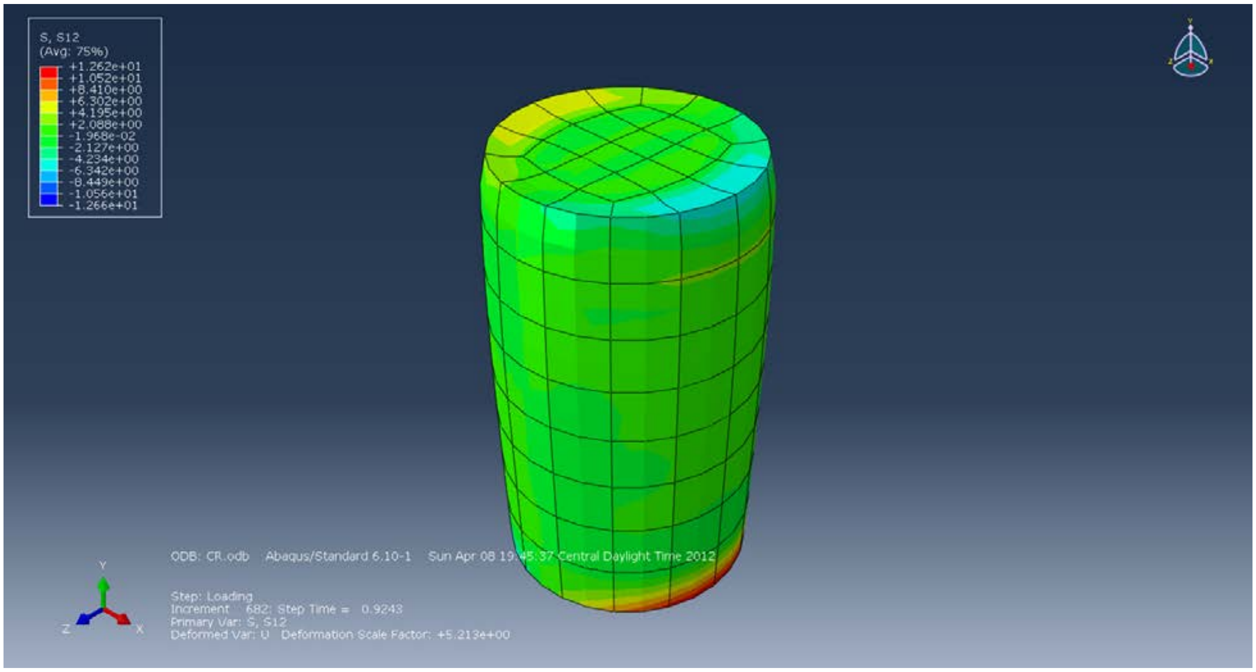

Figure B-58: Stress (S12) in the XY-Direction (MPa).

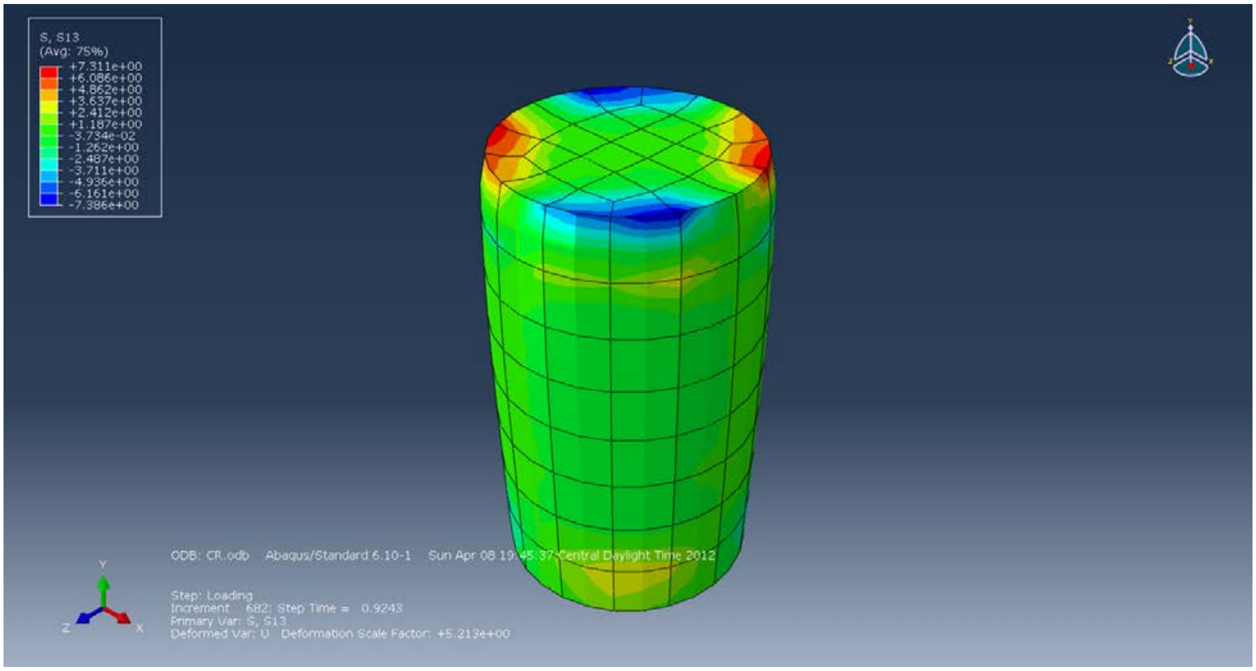

Figure B-59: Stress (S13) in the XZ-Direction (MPa).

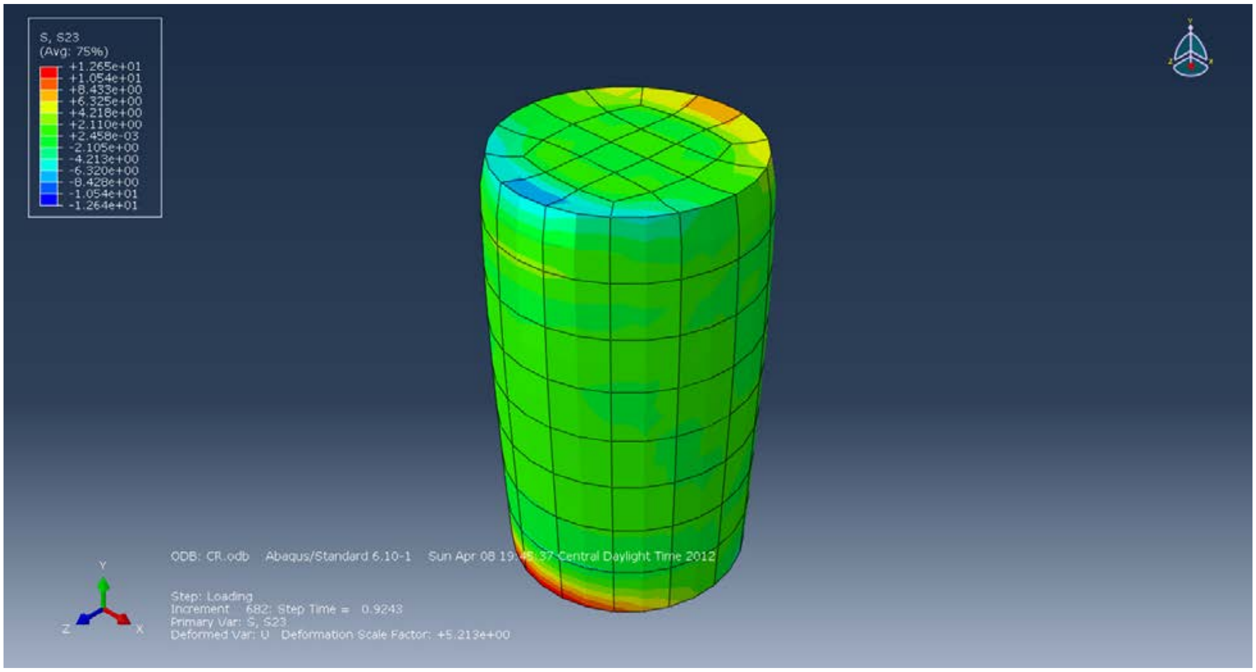

Figure B-60: Stress (S23) in the YZ-Direction (MPa).

- Smooth Boundaries:

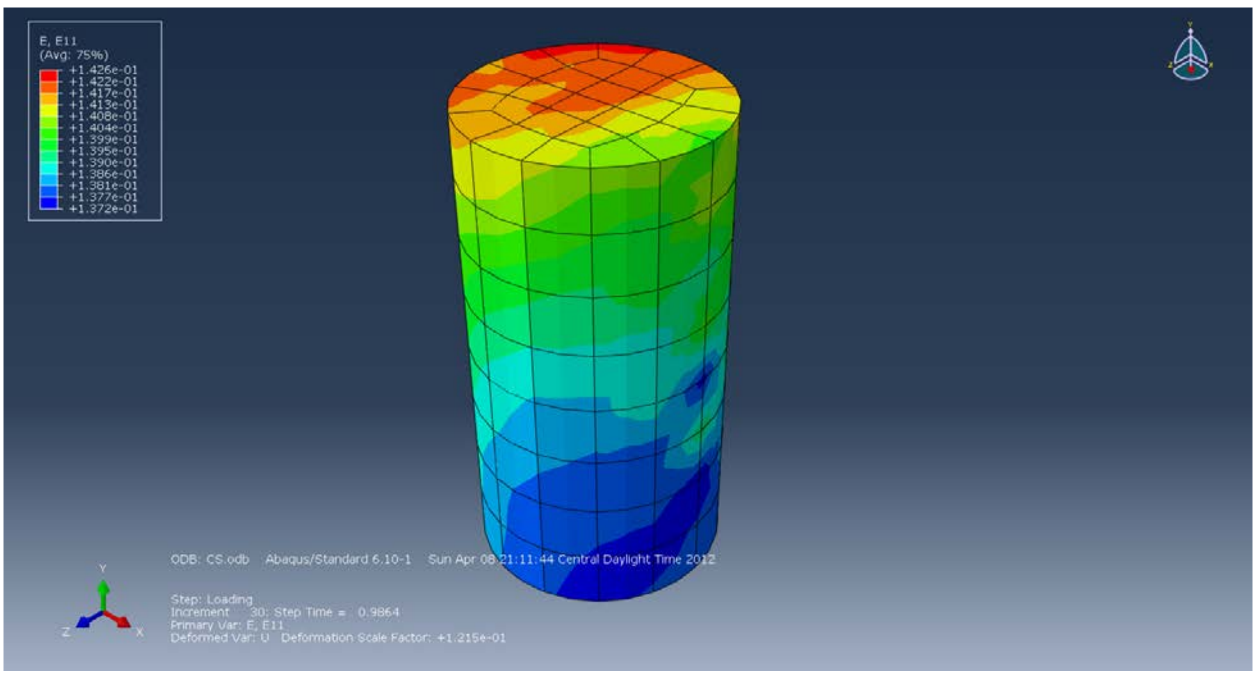

Figure B-61: Strain (E11) in the X-axis.

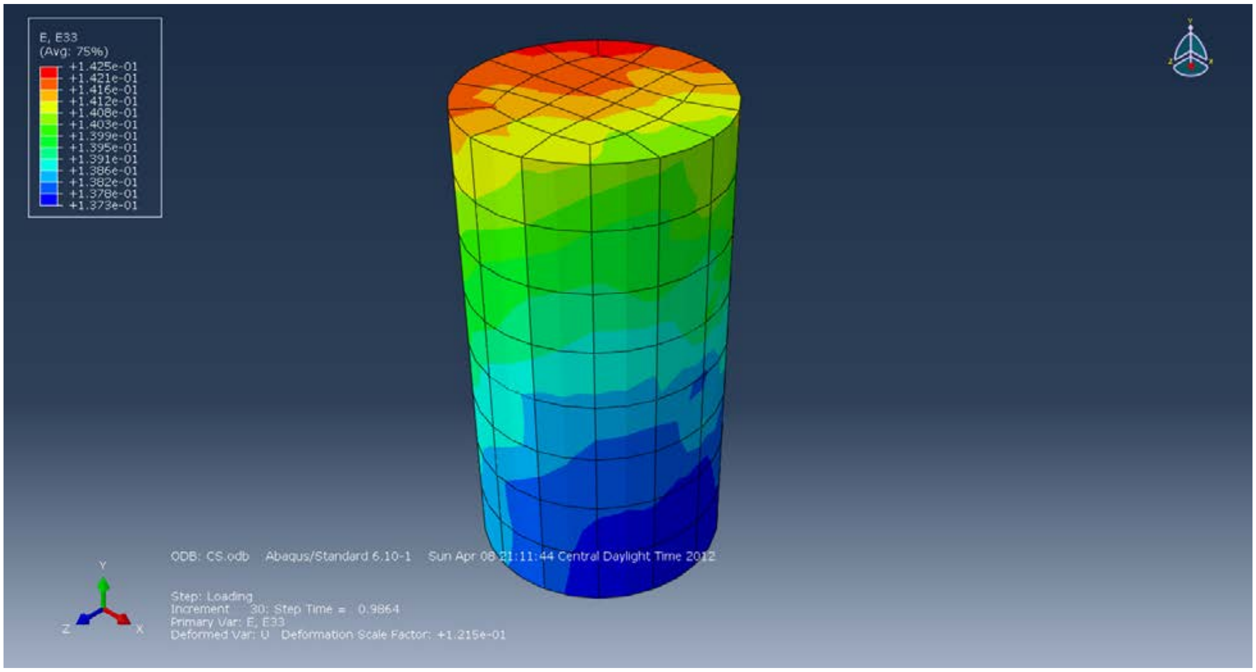

Figure B-62: Strain (E33) in the Z-axis.

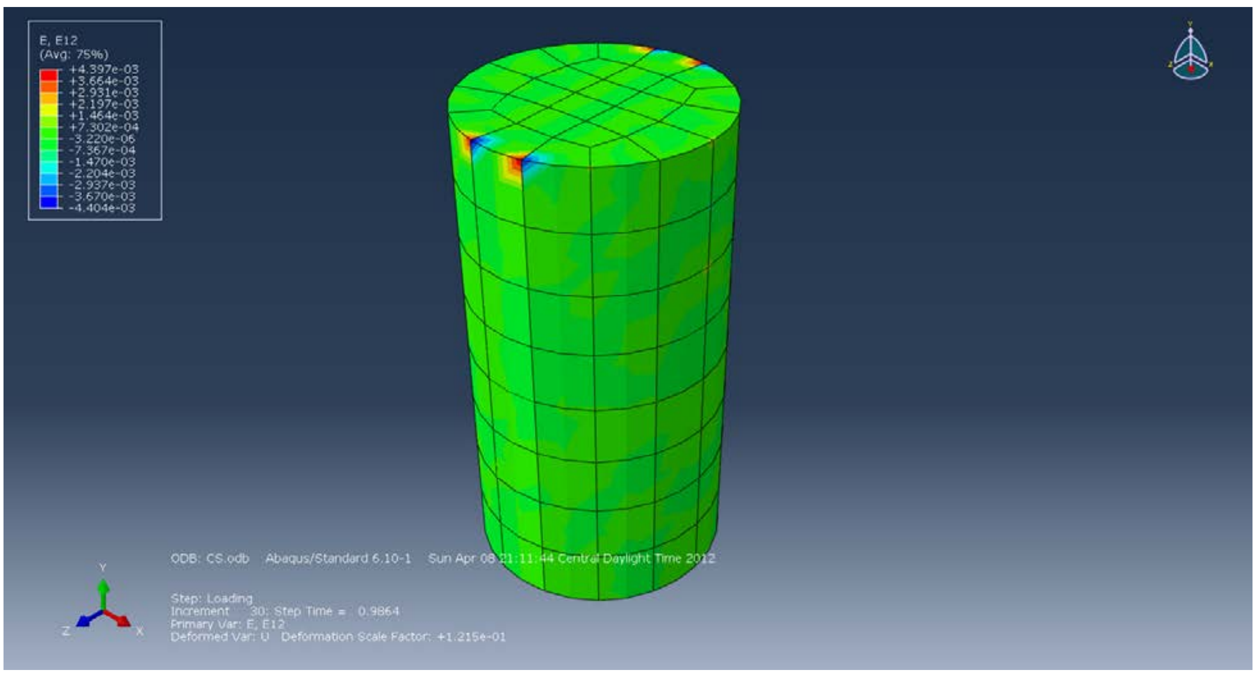

Figure B-63: Strain (E12) in the XY-Plane.

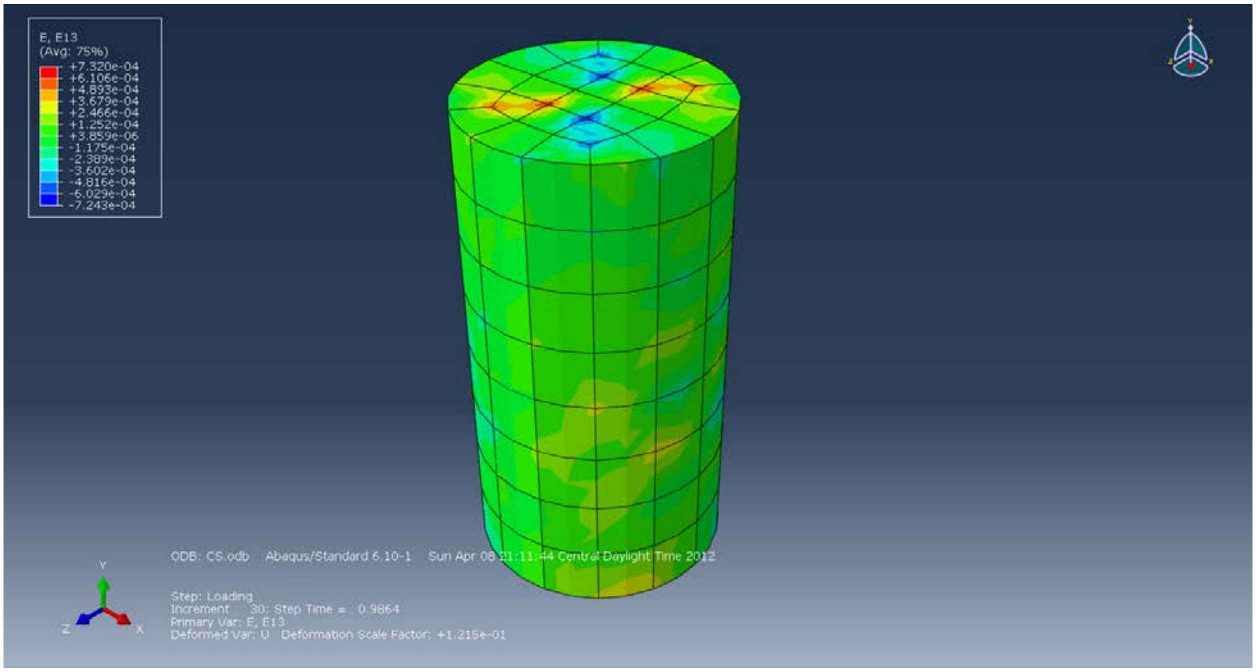

Figure B-64: Strain (E13) in the XZ-Plane.

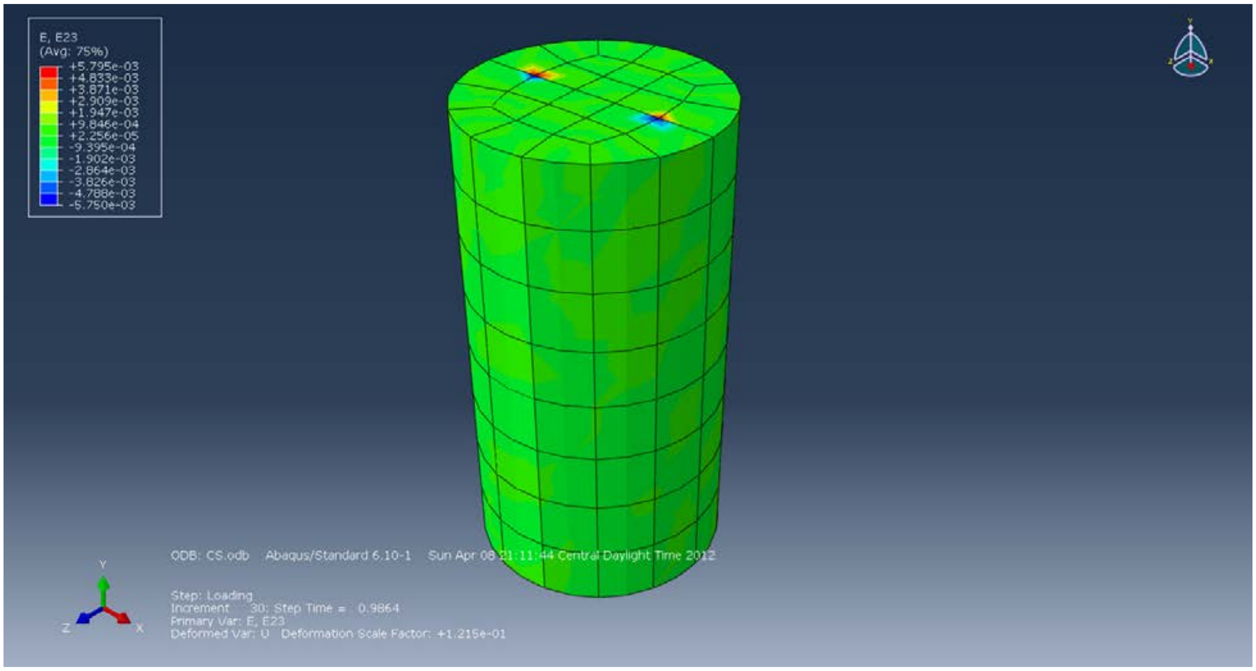

Figure B-65: Strain (E23) in the YZ-Plane.

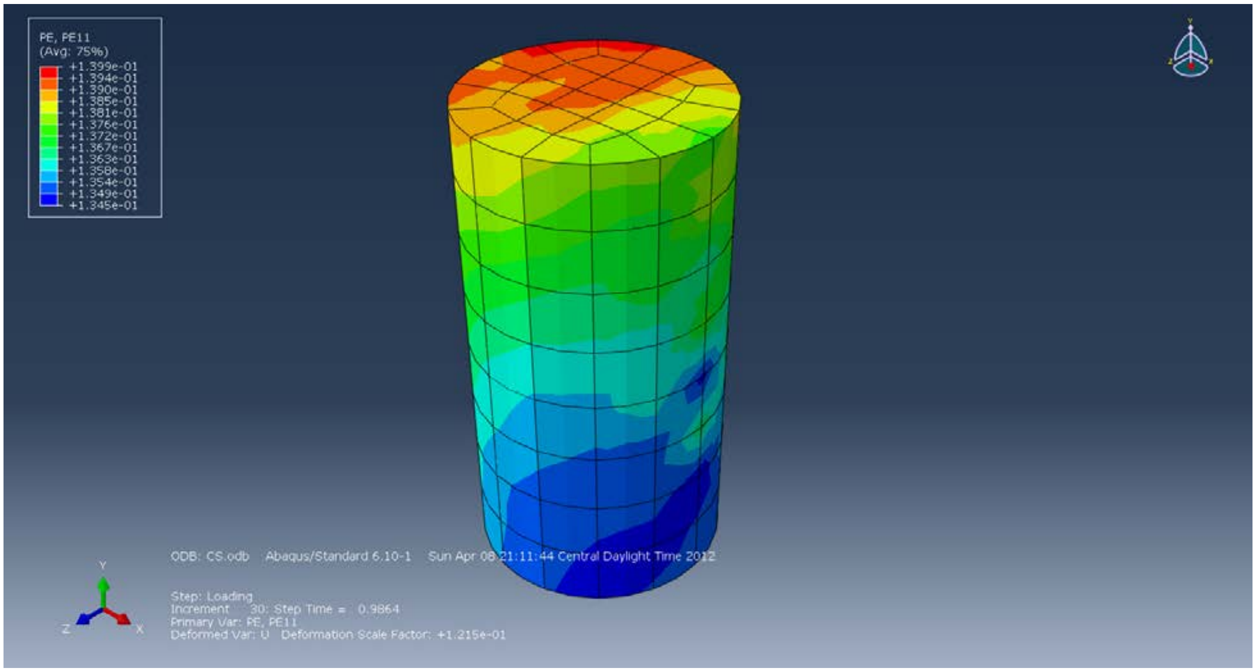

Figure B-66: Plastic Strain (PE11) in the X-axis.

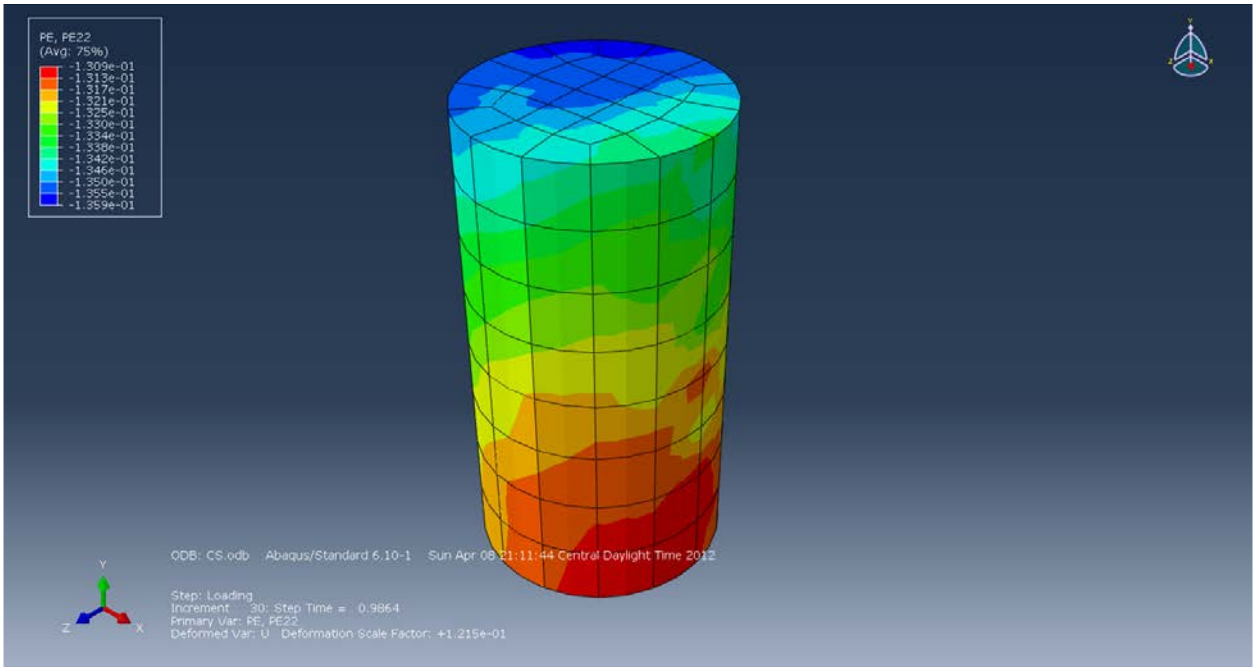

Figure B-67: Plastic Strain (PE22) in the Y-axis.

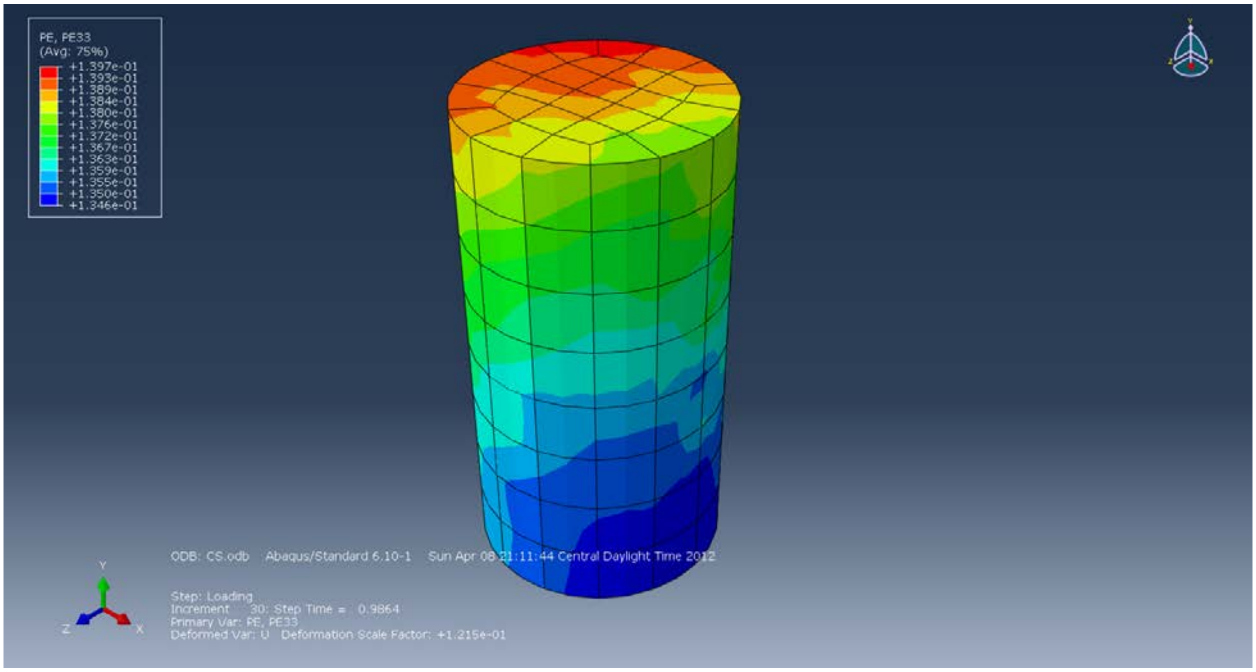

Figure B-68: Plastic Strain (PE33) in the Z-axis.

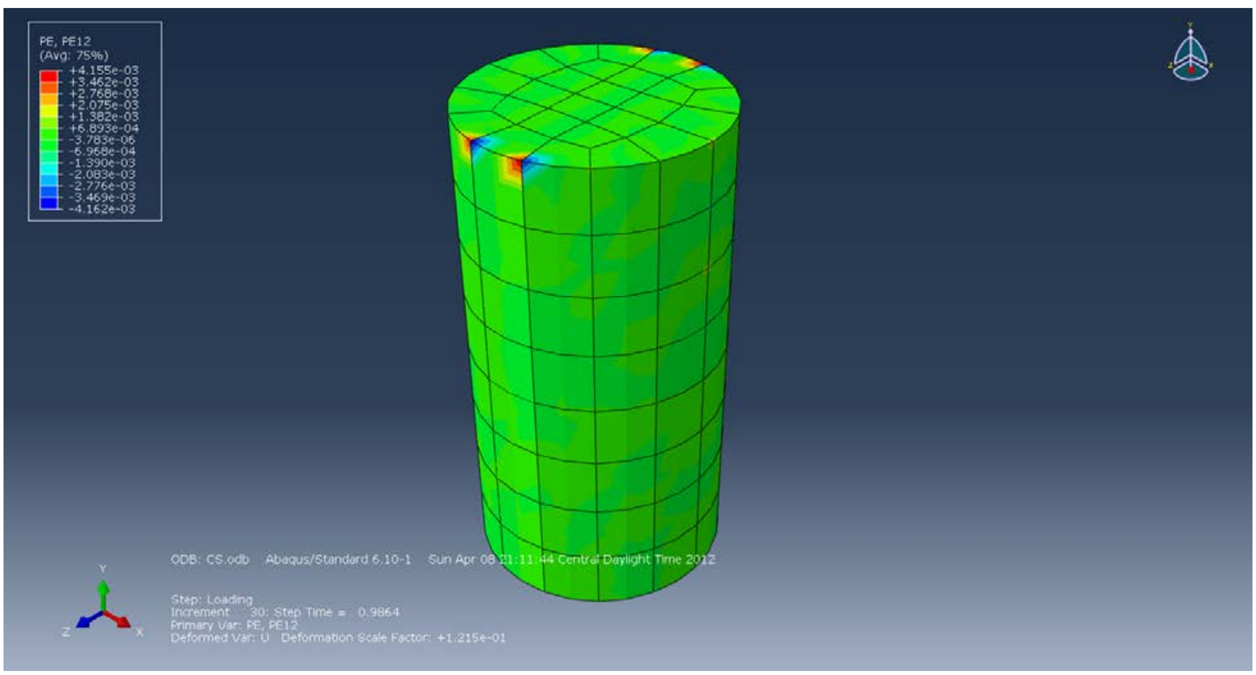

Figure B-69: Plastic Strain (PE12) in the XY-Plane.

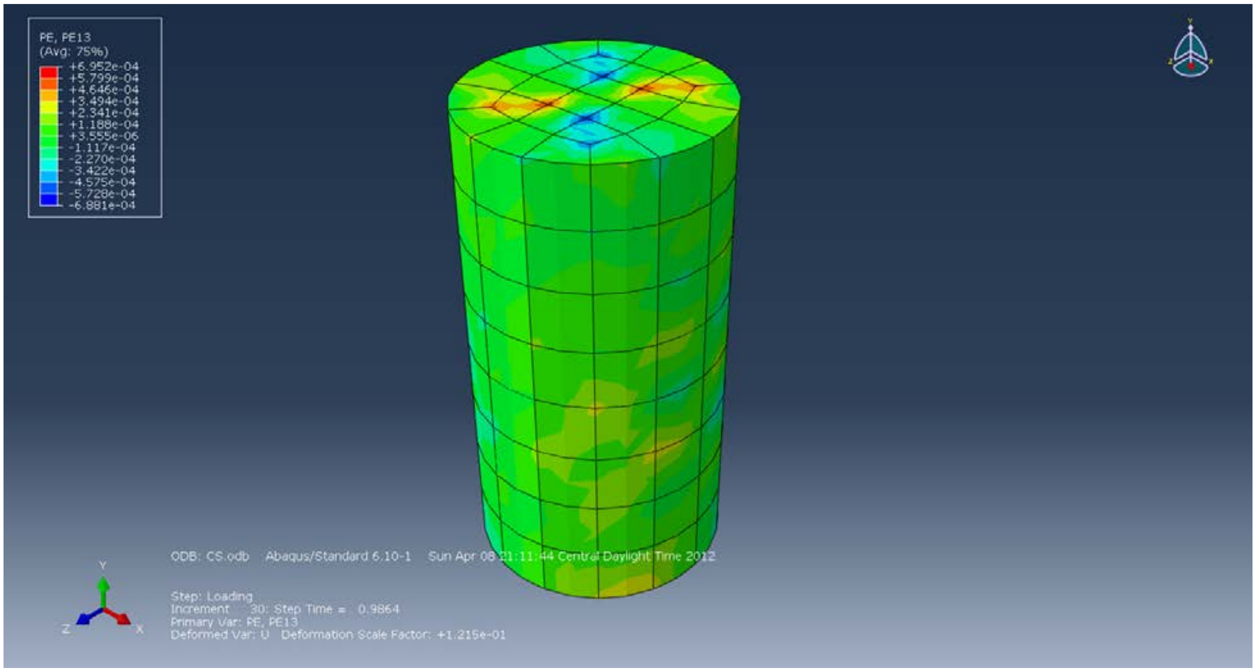

Figure B-70: Plastic Strain (PE13) in the XZ-Plane.

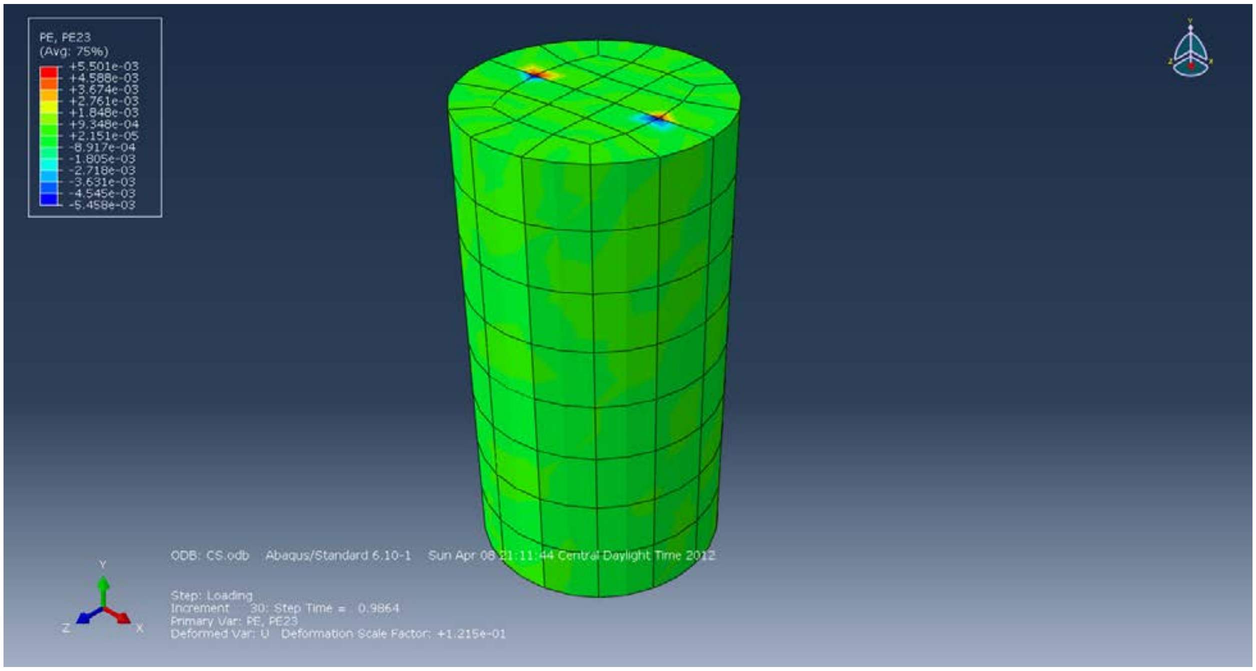

Figure B-71: Plastic Strain (PE23) in the YZ-Plane.

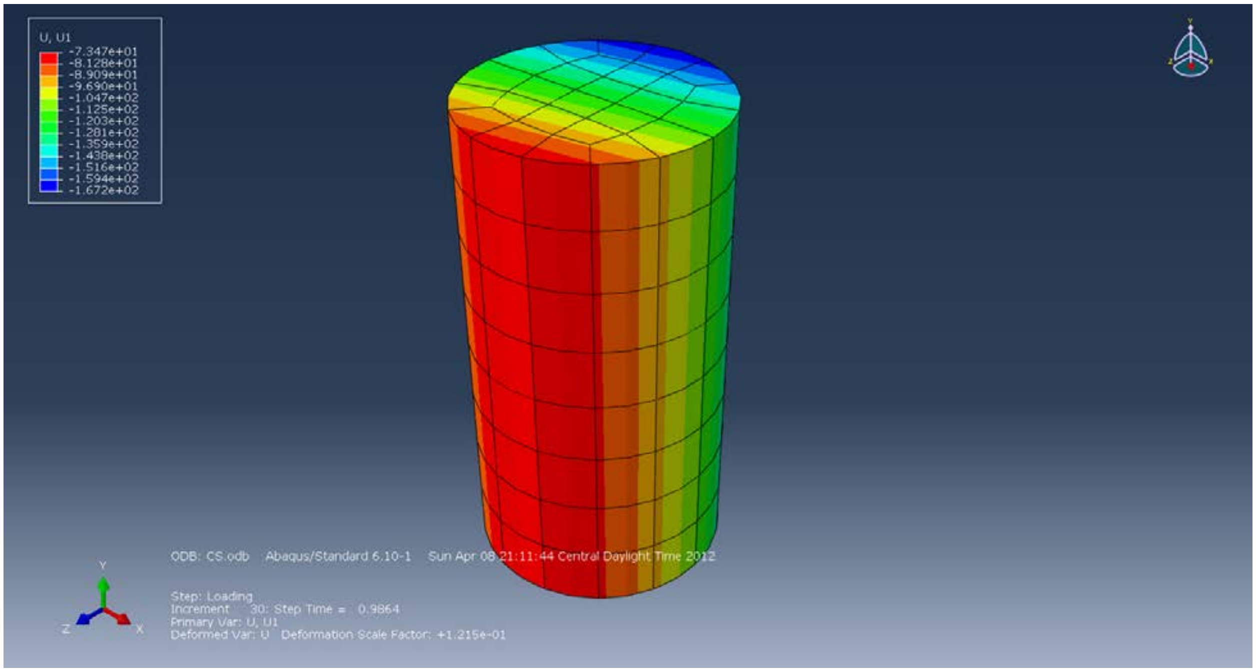

Figure B-72: Displacement (U1) in the X-axis (mm).

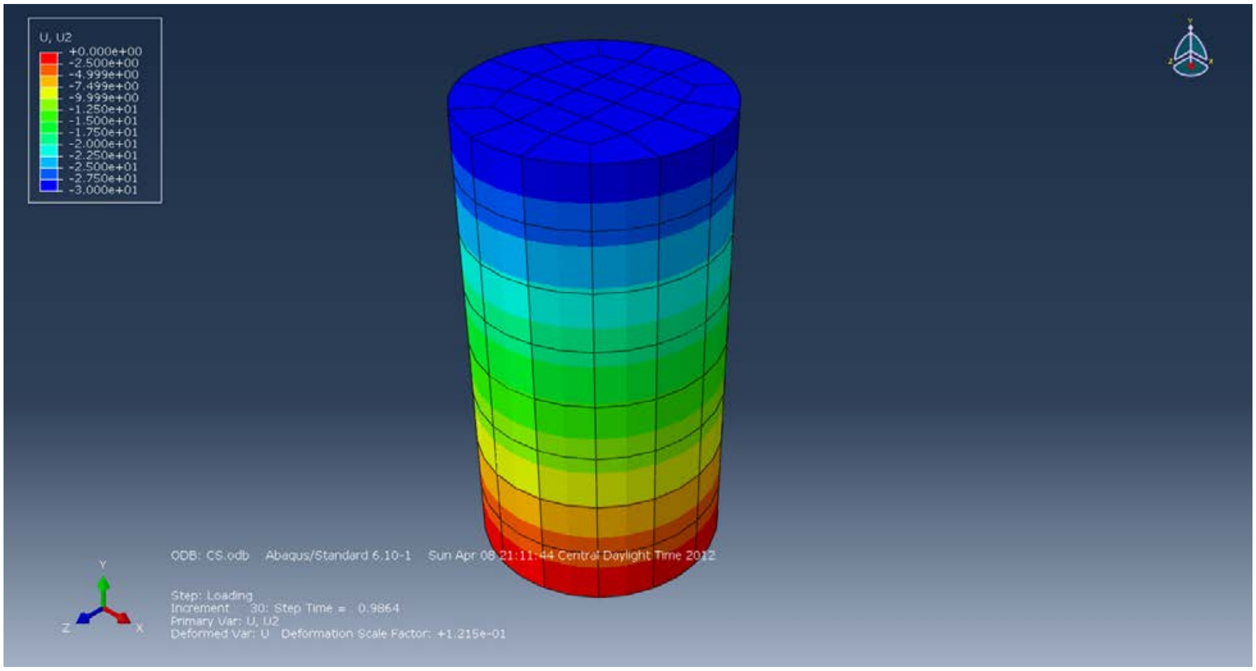

Figure B-73: Displacement (U2) in the Y-axis (mm).

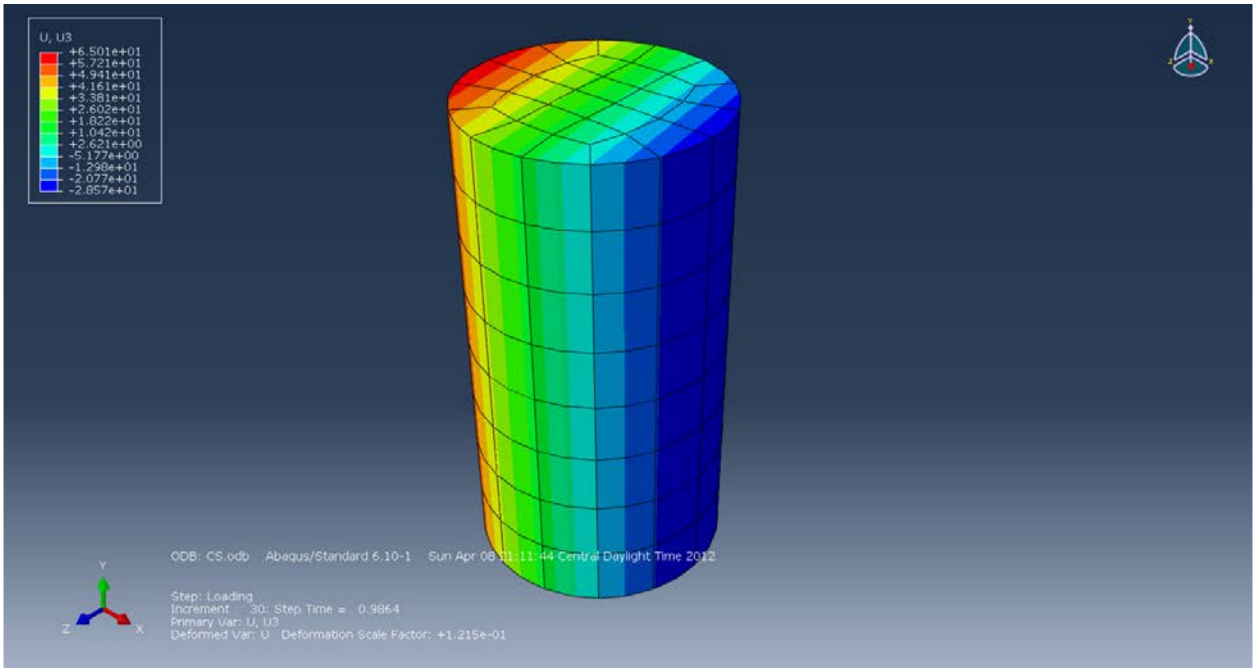

Figure B-74: Displacement (U3) in the Z-axis (mm).

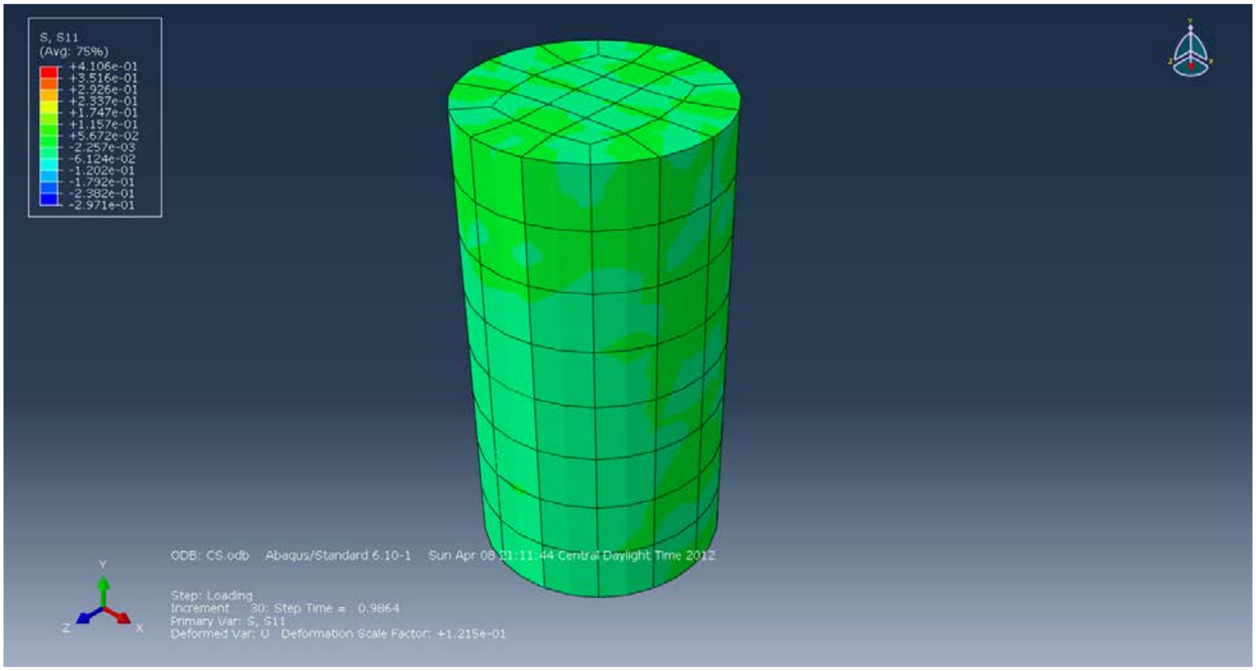

Figure B-75: Stress (S11) in the X-Direction (MPa).

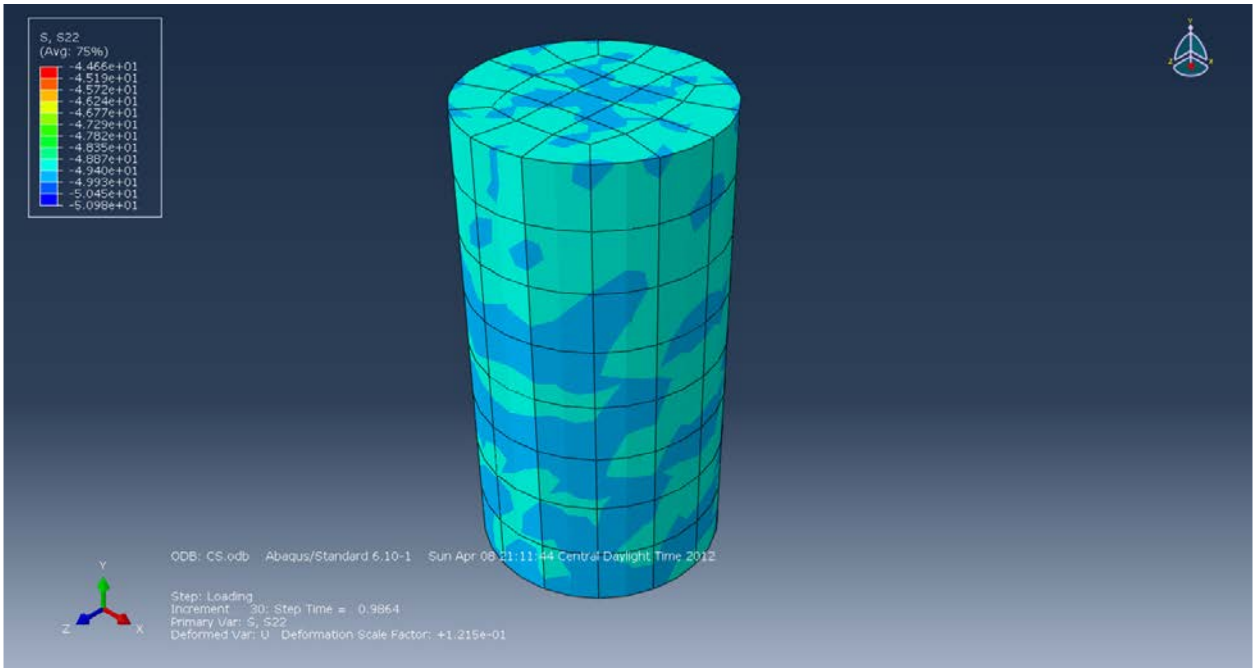

Figure B-76: Stress (S22) in the Y-Direction (MPa).

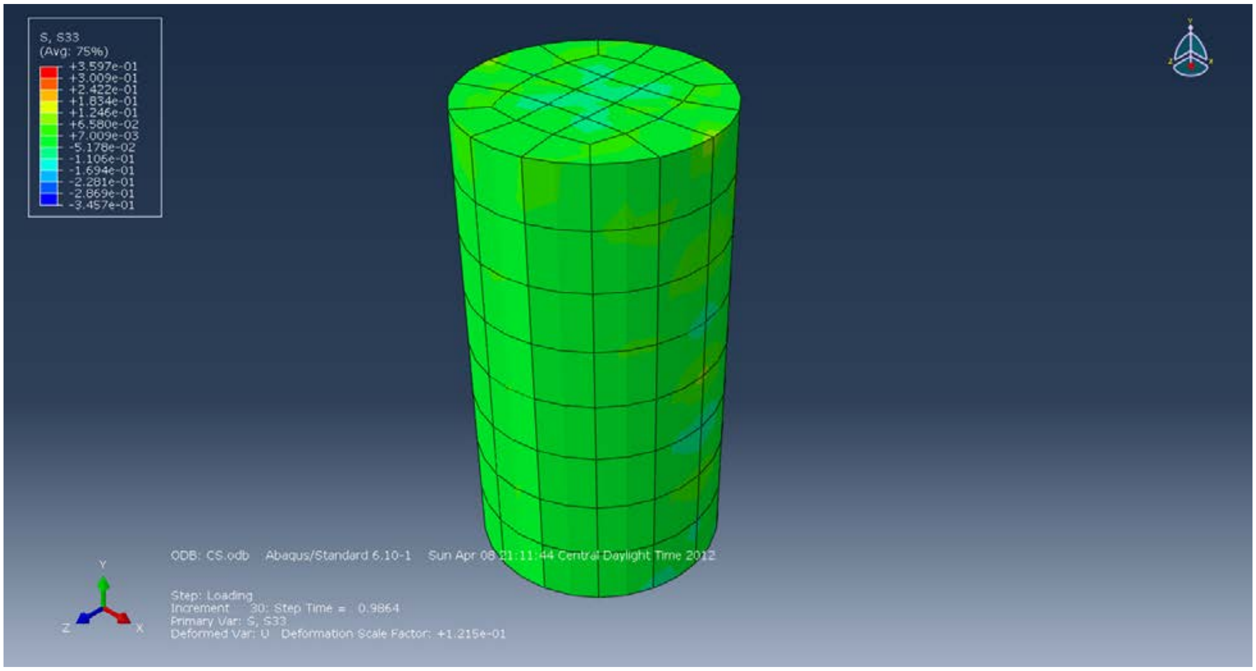

Figure B-77: Stress (S33) in the Z-Direction (MPa).

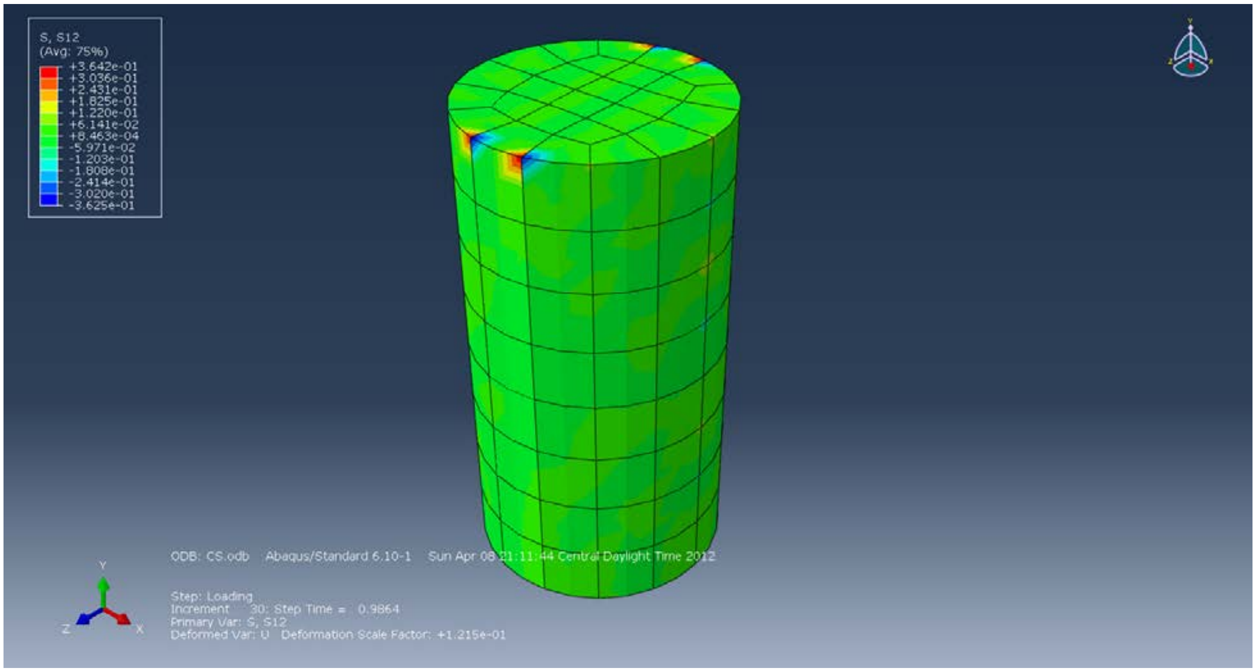

Figure B-78: Stress (S12) in the XY-Direction (MPa).

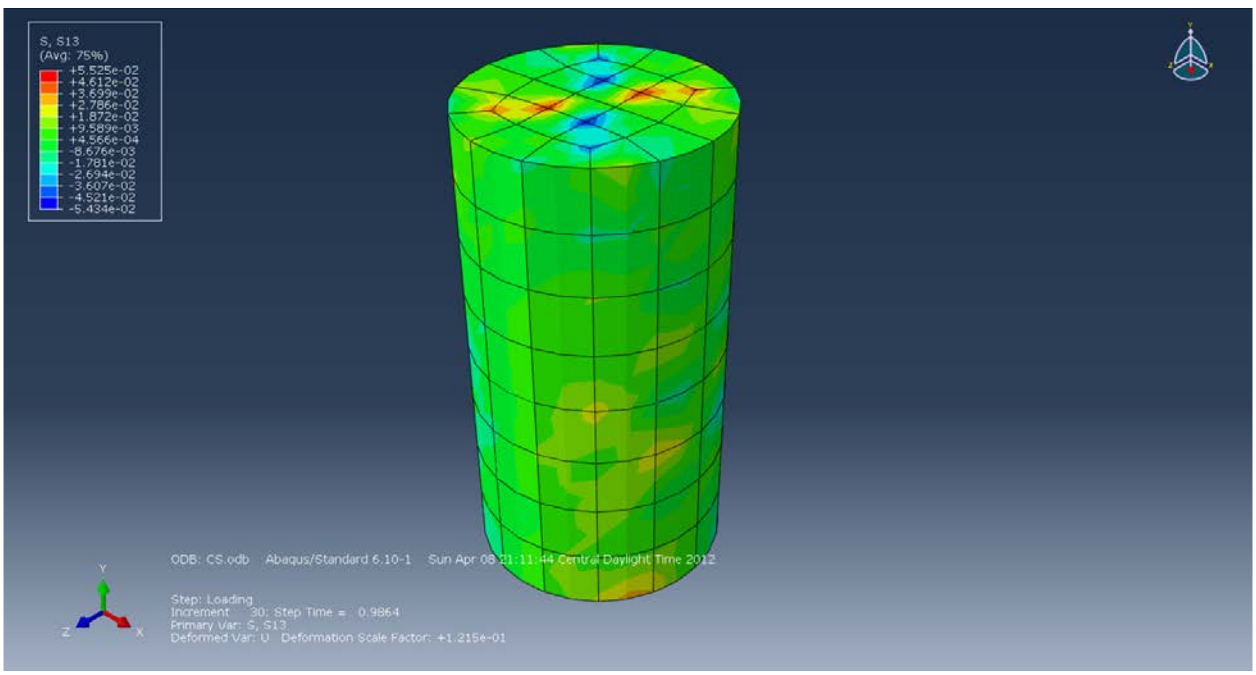

Figure B-79: Stress (S13) in the XZ-Direction (MPa).

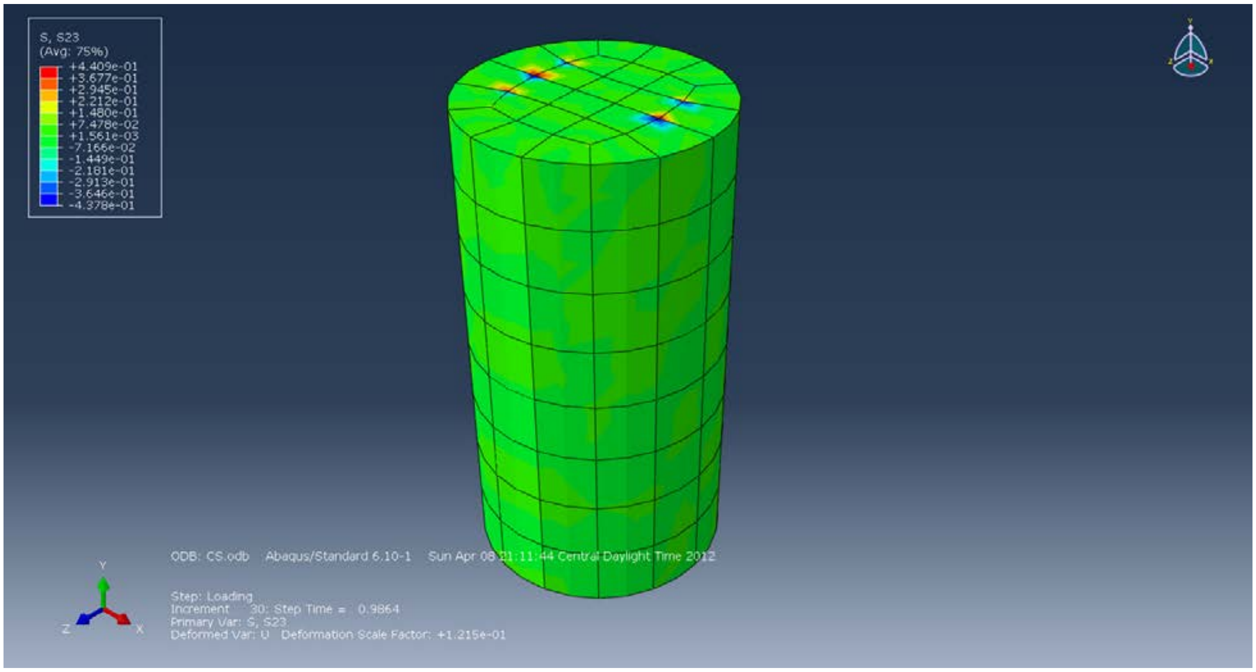

Figure B-80: Stress (S23) in the YZ-Direction (MPa).

Cylinders with 0.75% Wheat Fibers:

- Rough Boundaries:

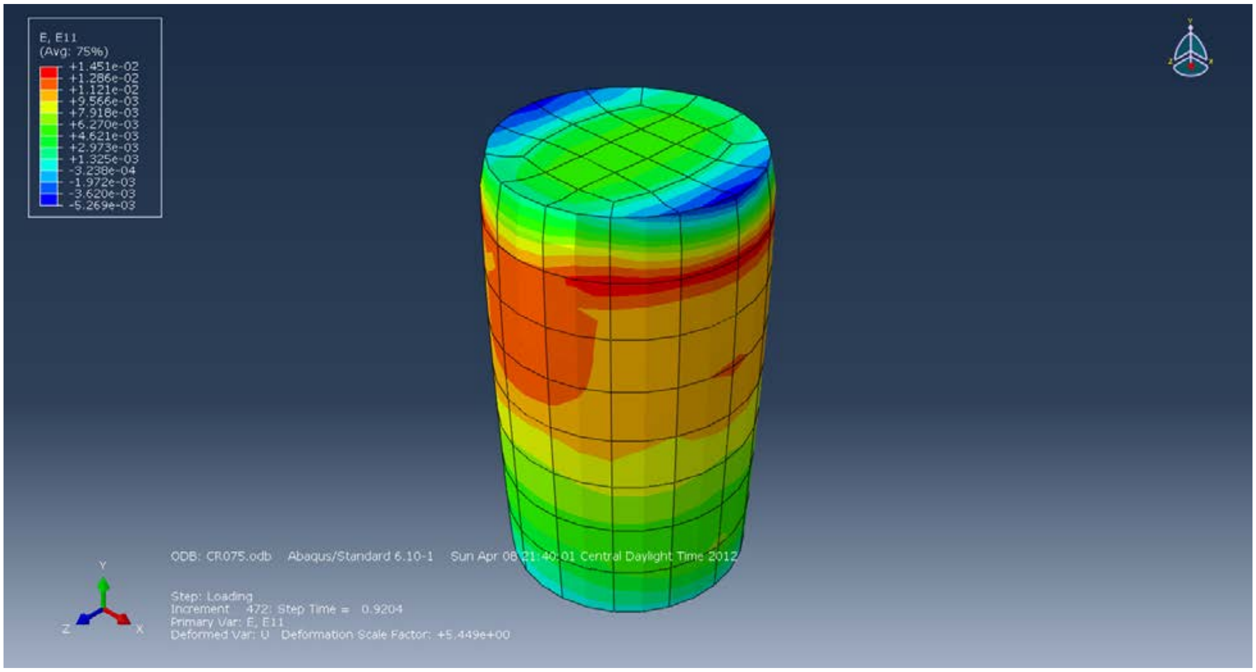

Figure B-81: Strain (E11) in the X-axis.

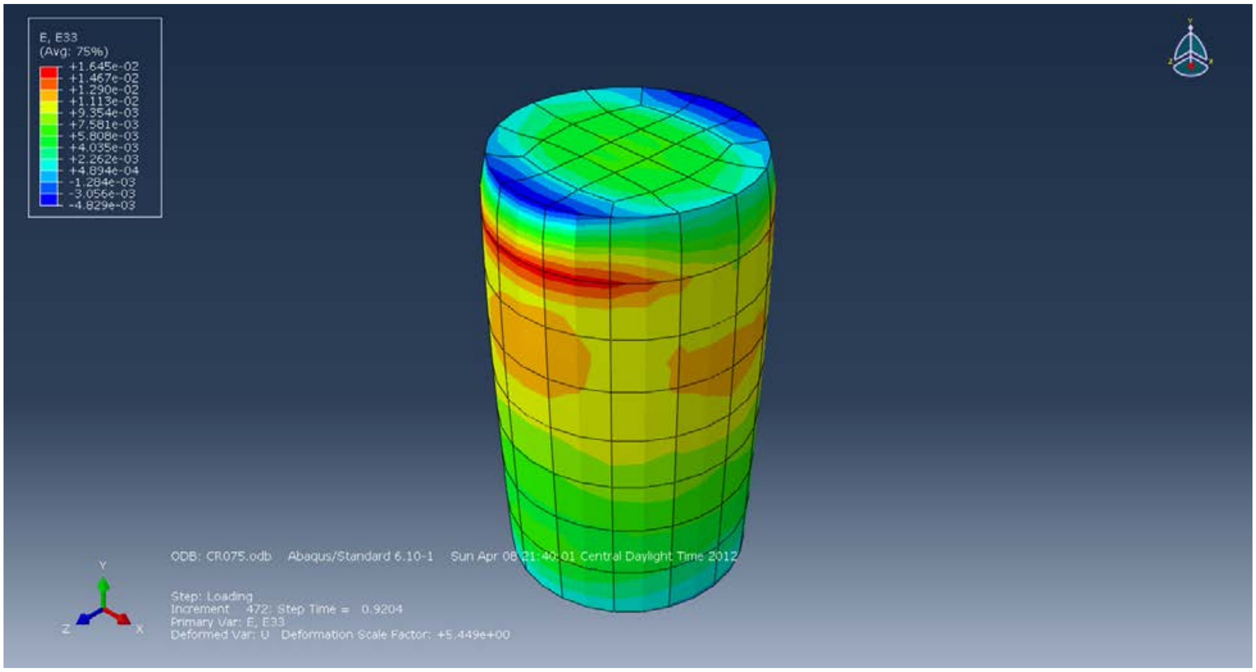

Figure B-82: Strain (E33) in the Z-axis.

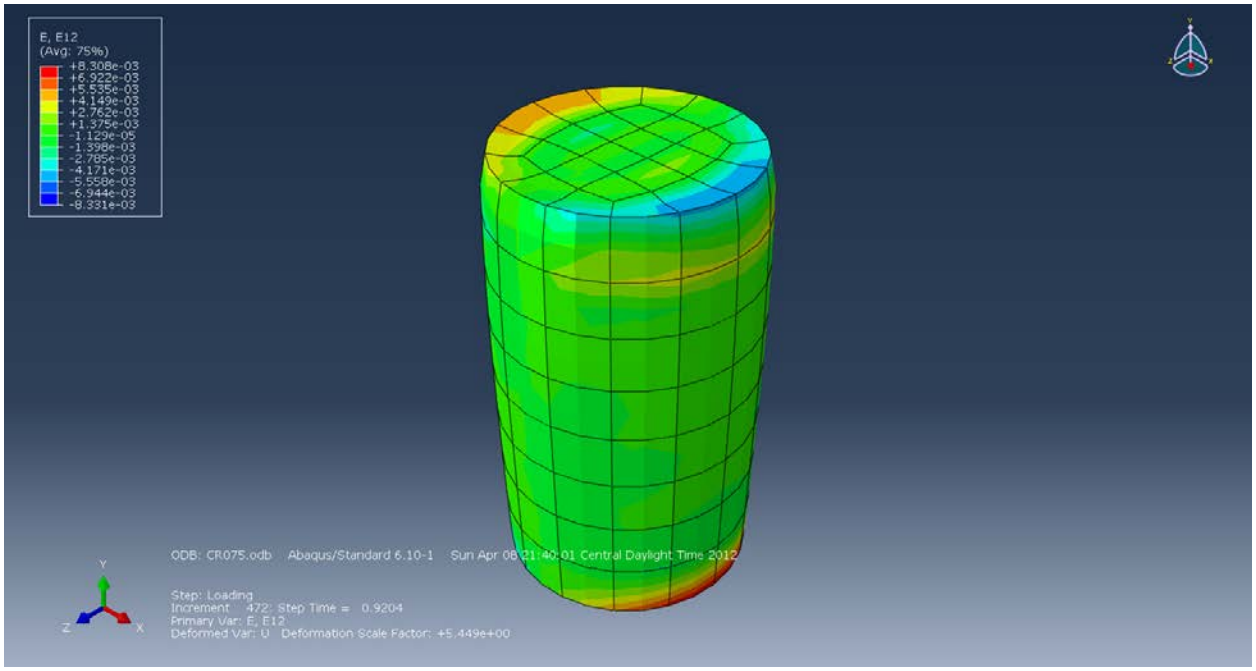

Figure B-83: Strain (E12) in the XY-Plane.

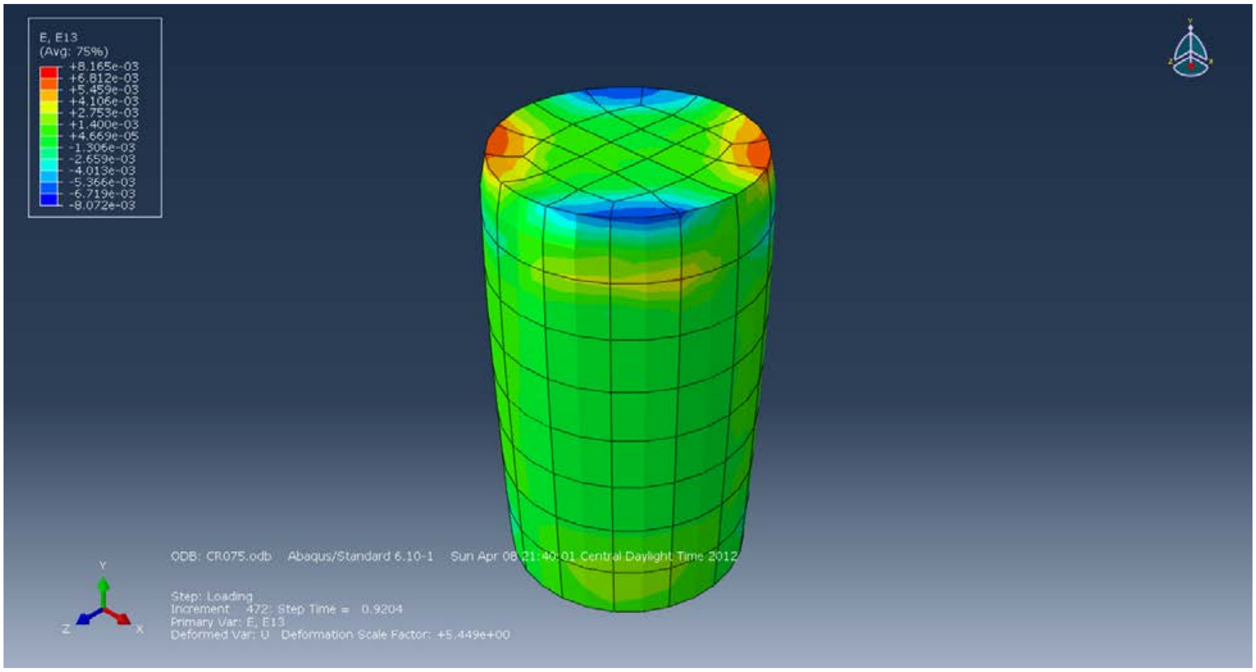

Figure B-84: Strain (E13) in the XZ-Plane.

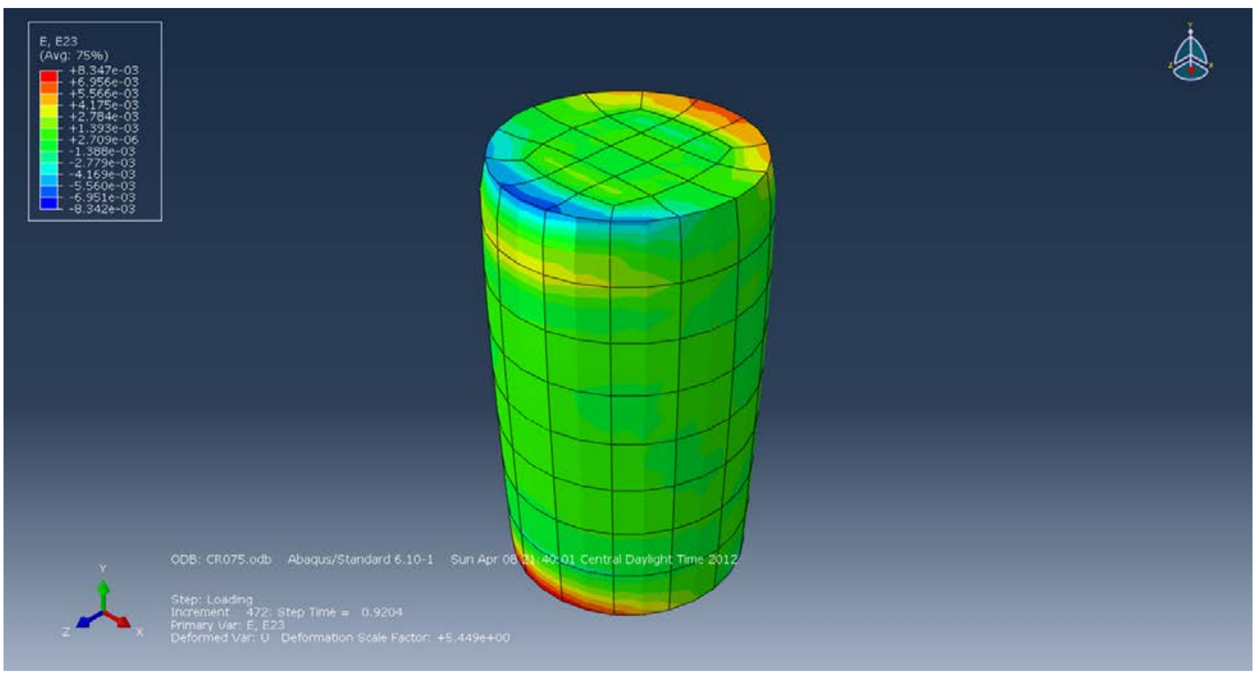

Figure B-85: Strain (E23) in the YZ-Plane.

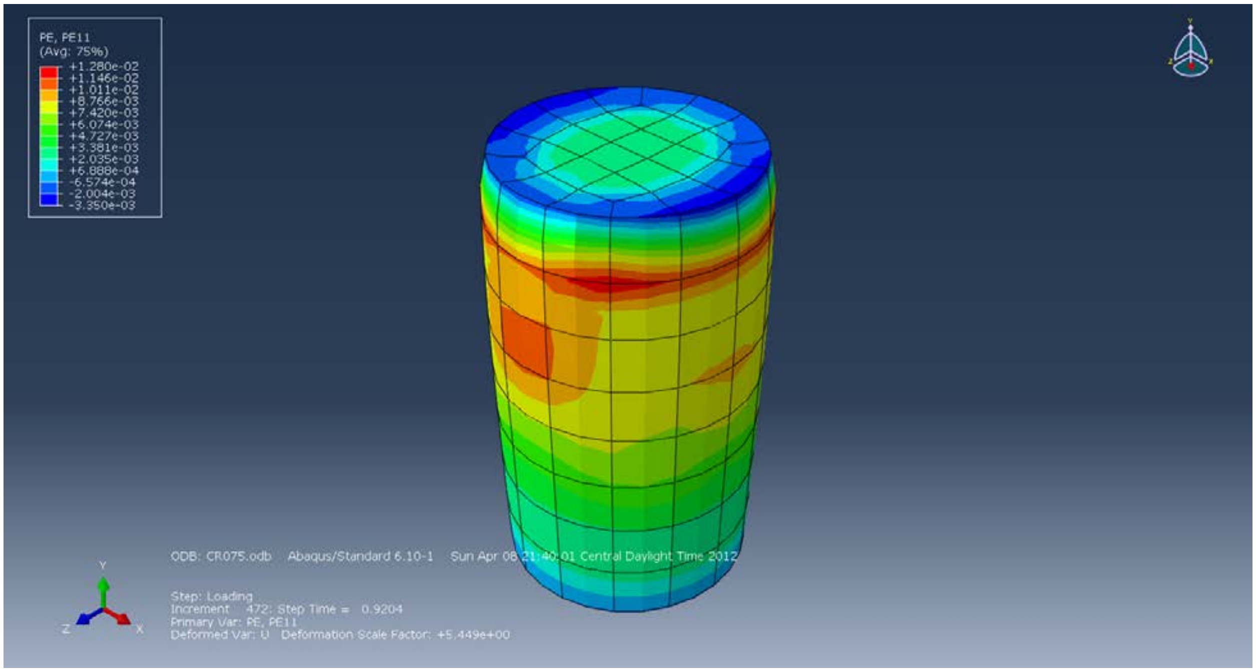

Figure B-86: Plastic Strain (PE11) in the X-axis.

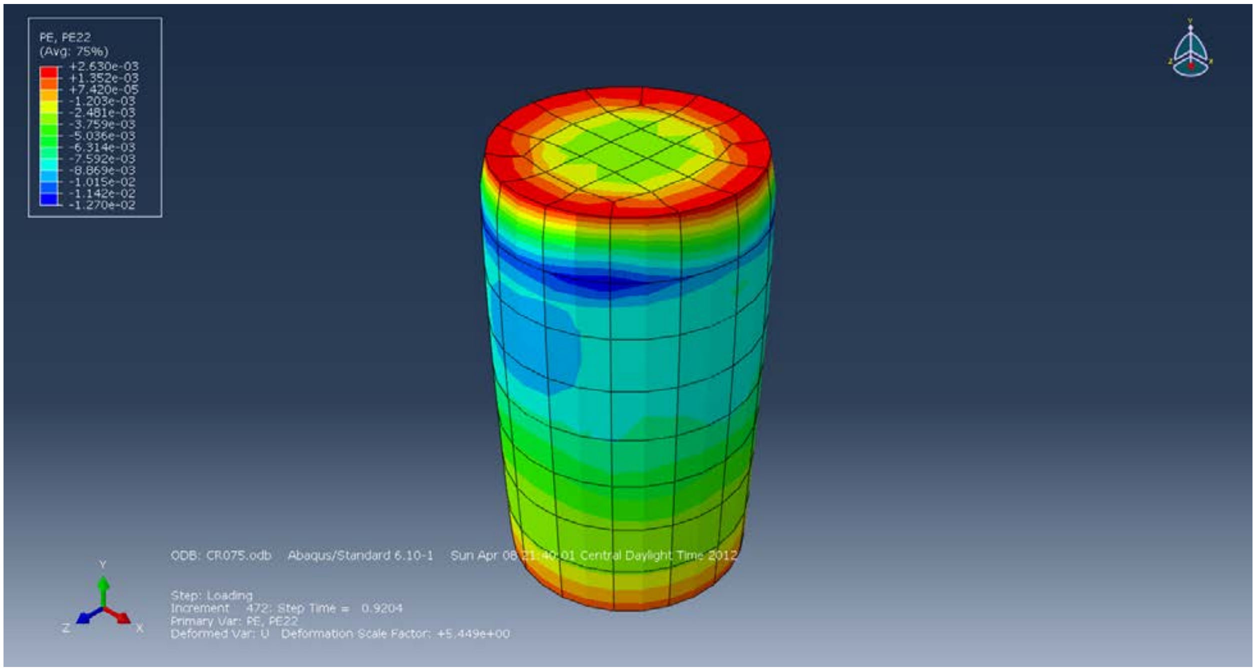

Figure B-87: Plastic Strain (PE22) in the Y-axis.

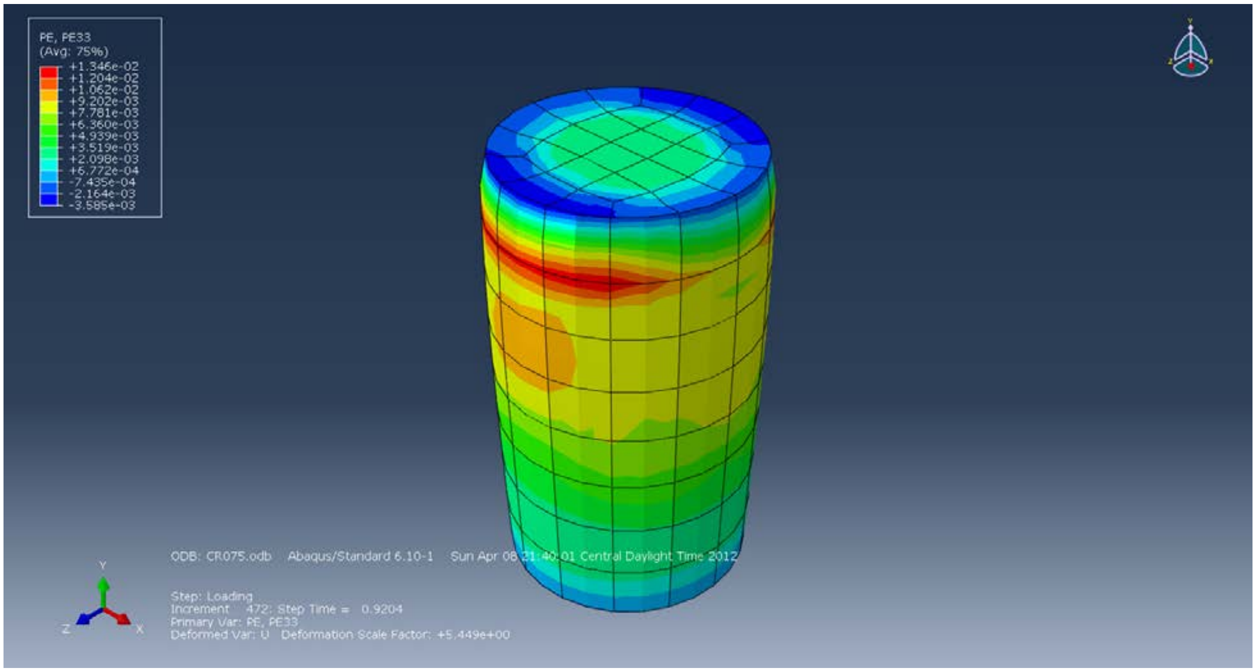

Figure B-88: Plastic Strain (PE33) in the Z-axis.

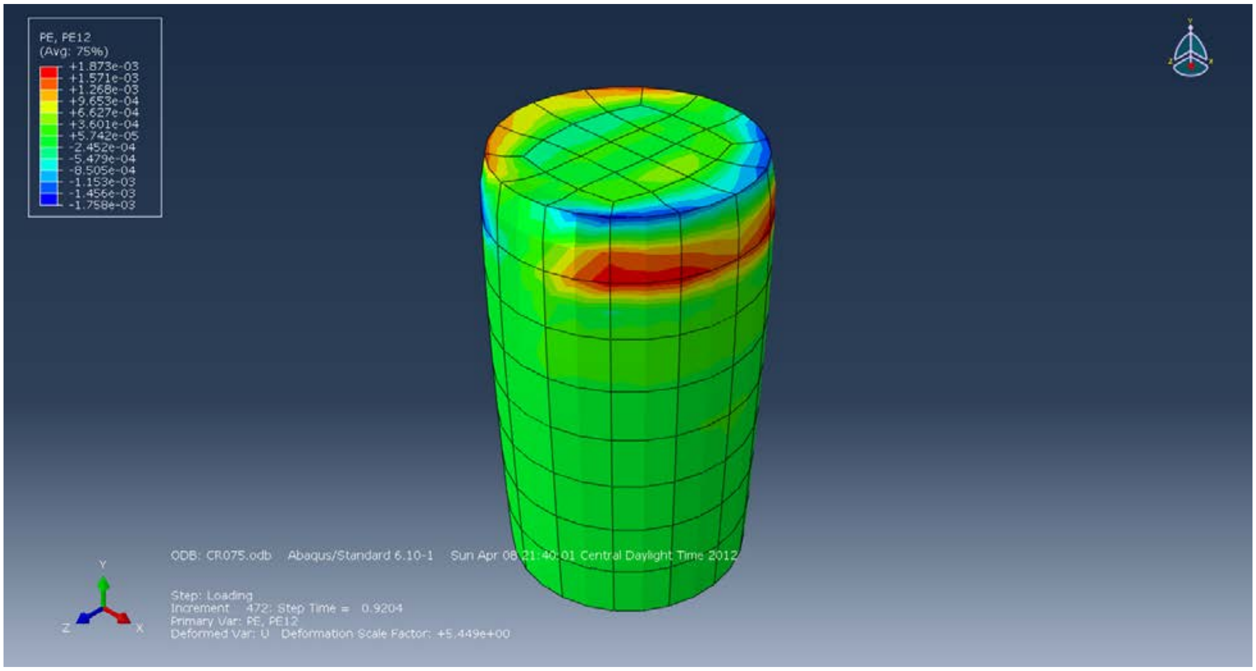

Figure B-89: Plastic Strain (PE12) in the XY-Plane.

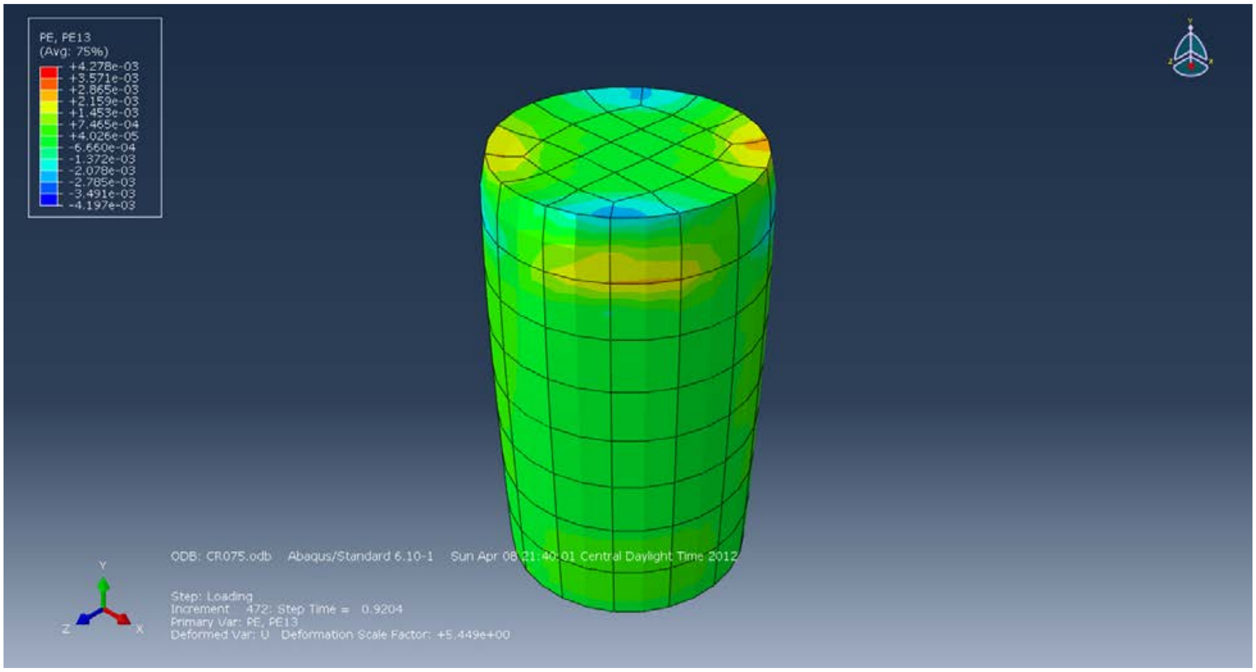

Figure B-90: Plastic Strain (PE13) in the XZ-Plane.

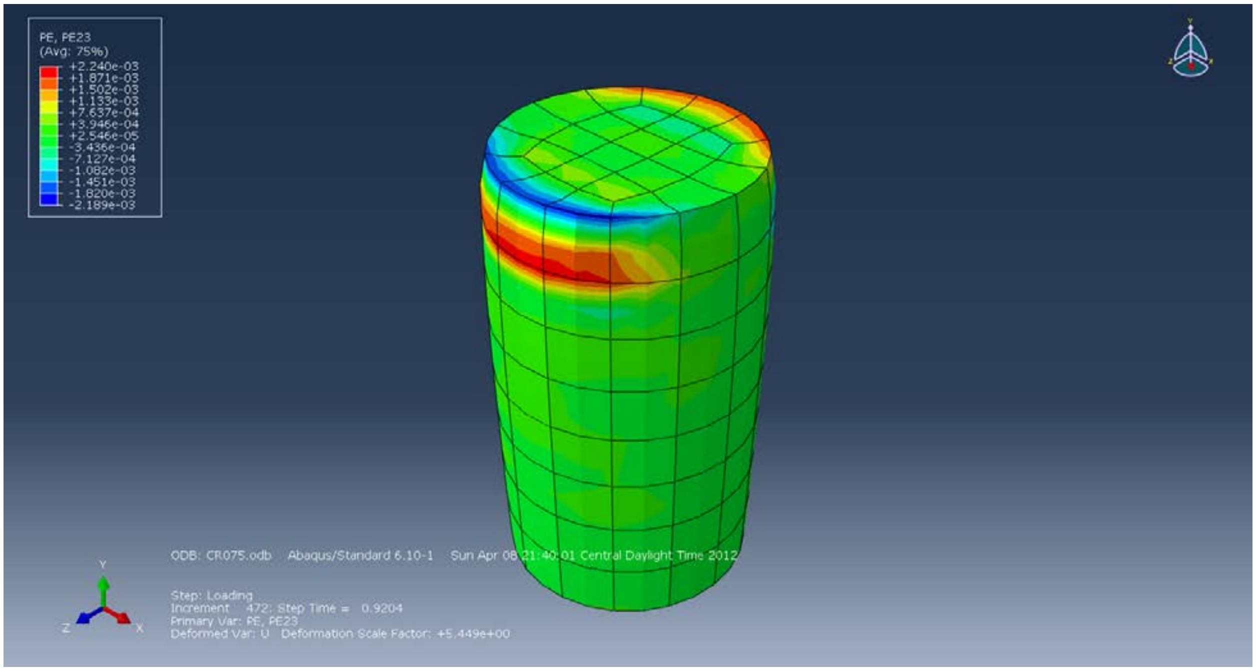

Figure B-91: Plastic Strain (PE23) in the YZ-Plane.

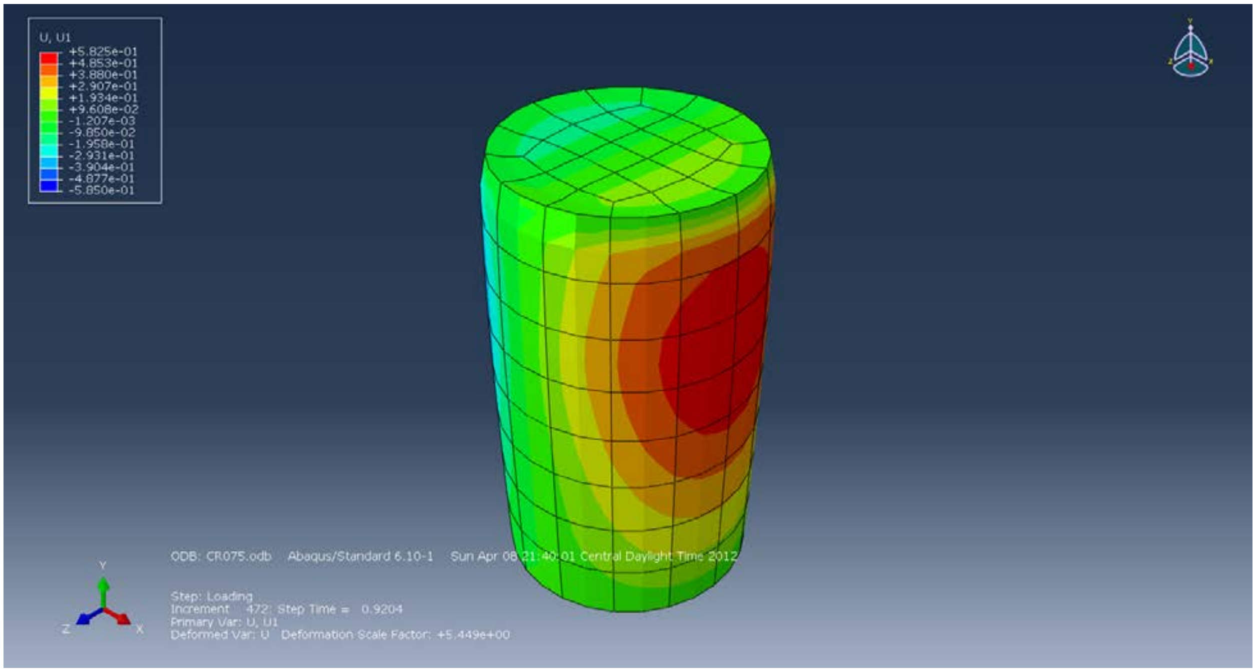

Figure B-92: Displacement (U1) in the X-axis (mm).

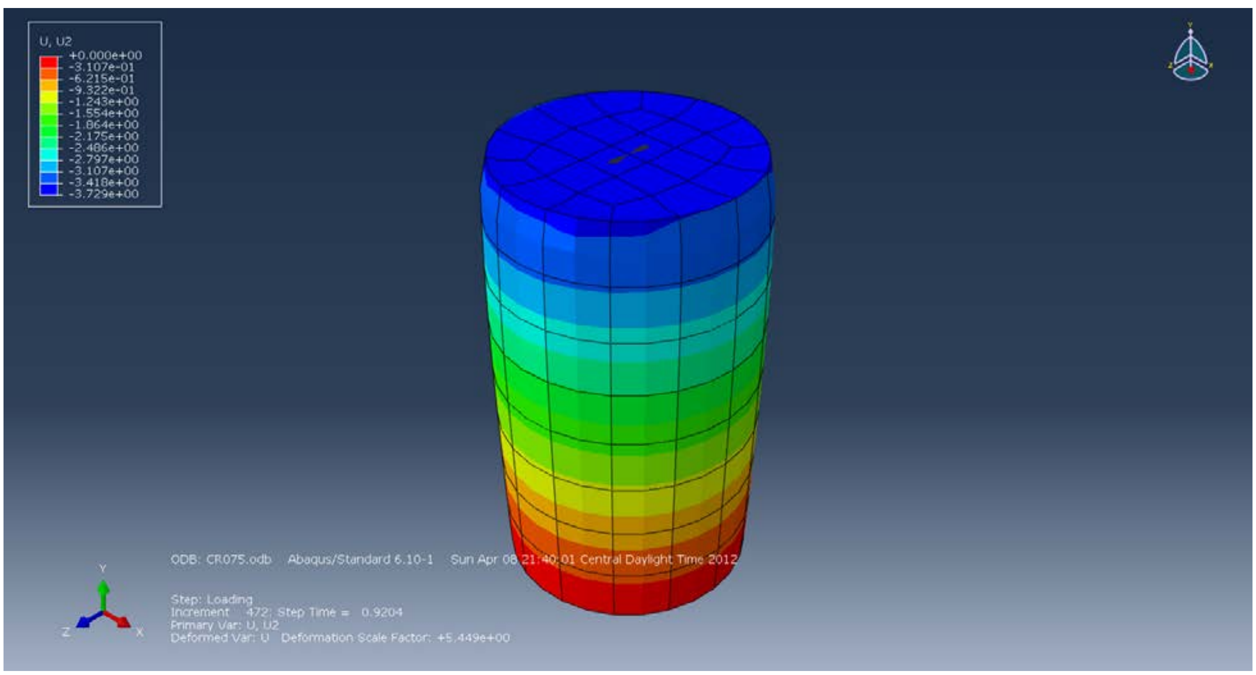

Figure B-93: Displacement (U2) in the Y-axis (mm).

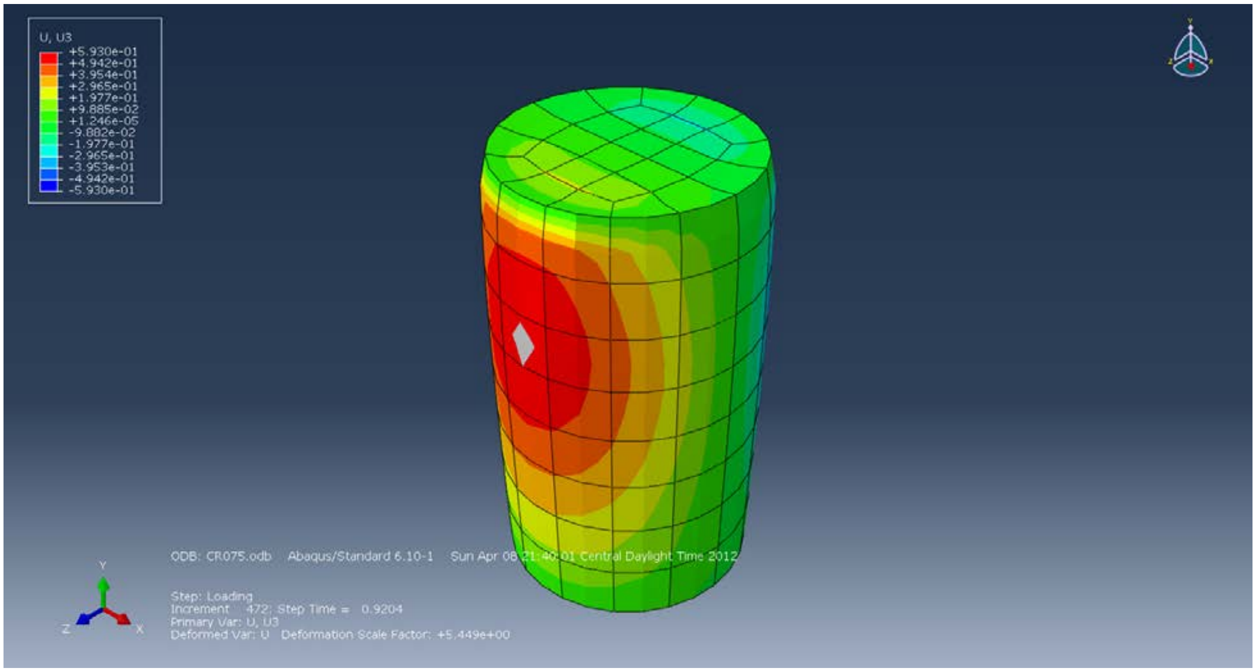

Figure B-94: Displacement (U3) in the Z-axis (mm).

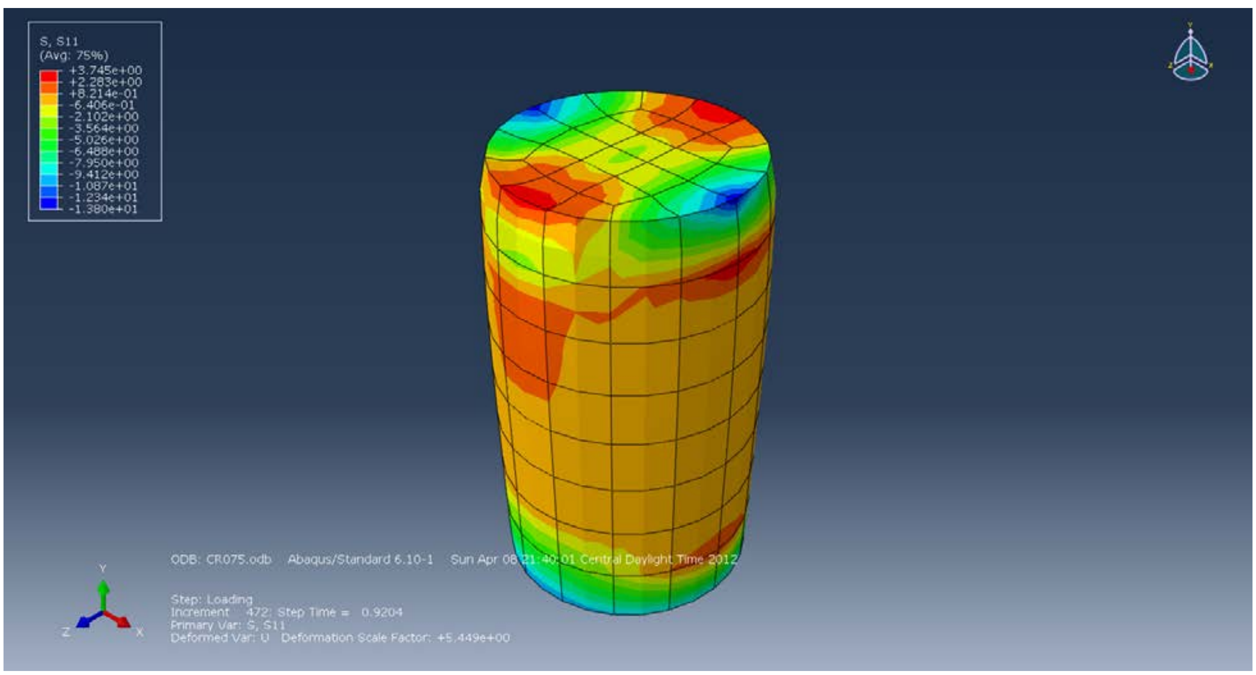

Figure B-95: Stress (S11) in the X-Direction (MPa).

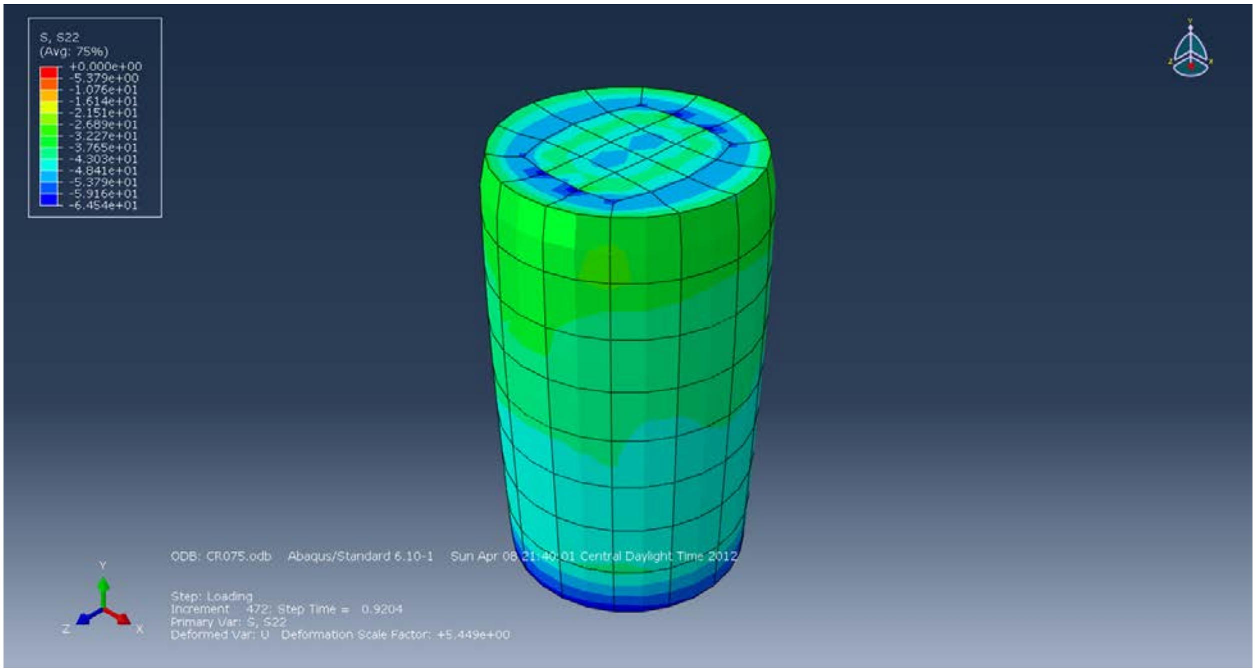

Figure B-96: Stress (S22) in the Y-Direction (MPa).

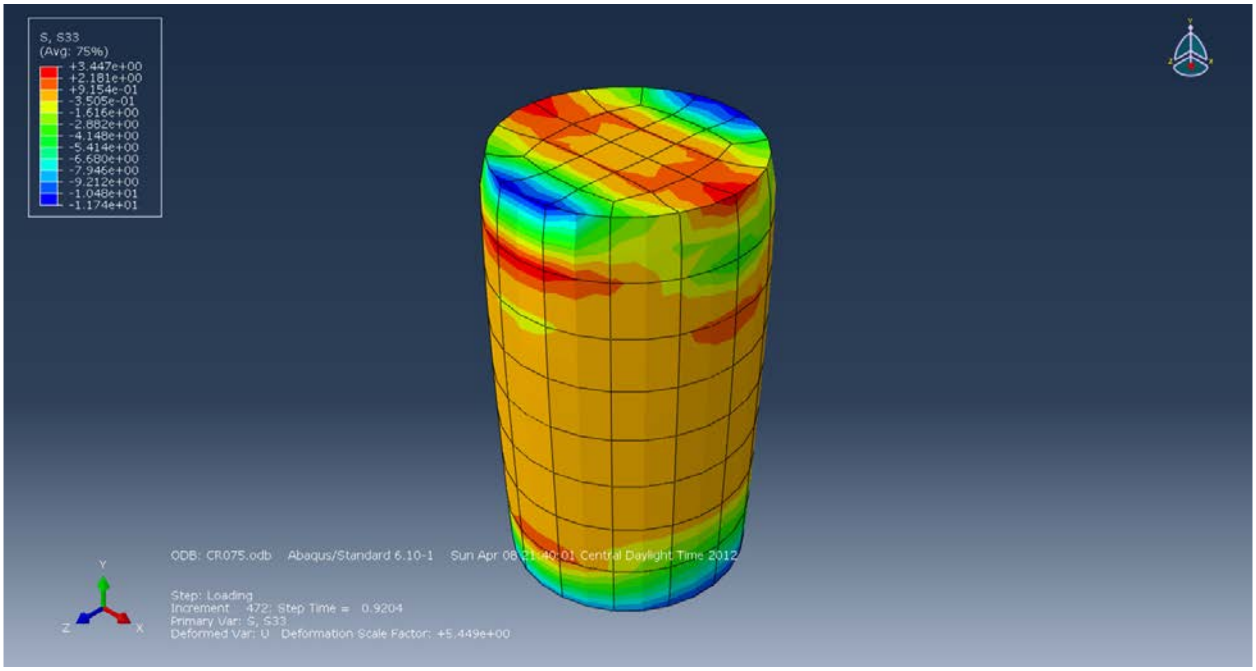

Figure B-97: Stress (S33) in the Z-Direction (MPa).

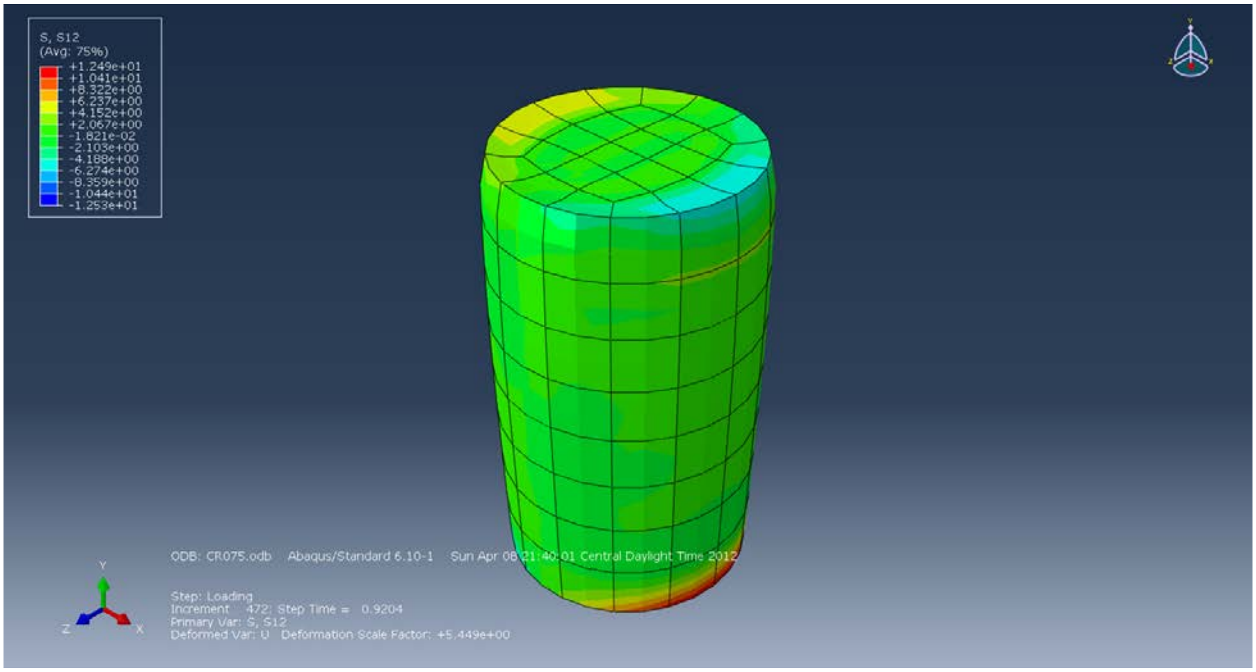

Figure B-98: Stress (S12) in the XY-Direction (MPa).

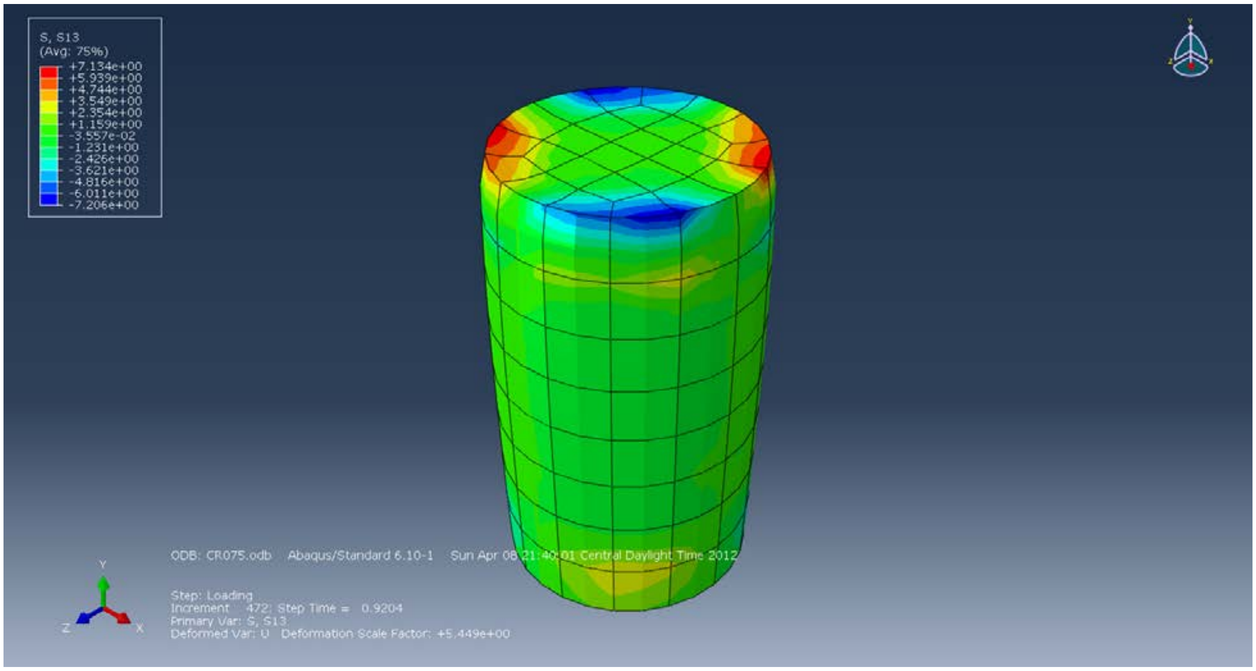

Figure B-99: Stress (S13) in the XZ-Direction (MPa).

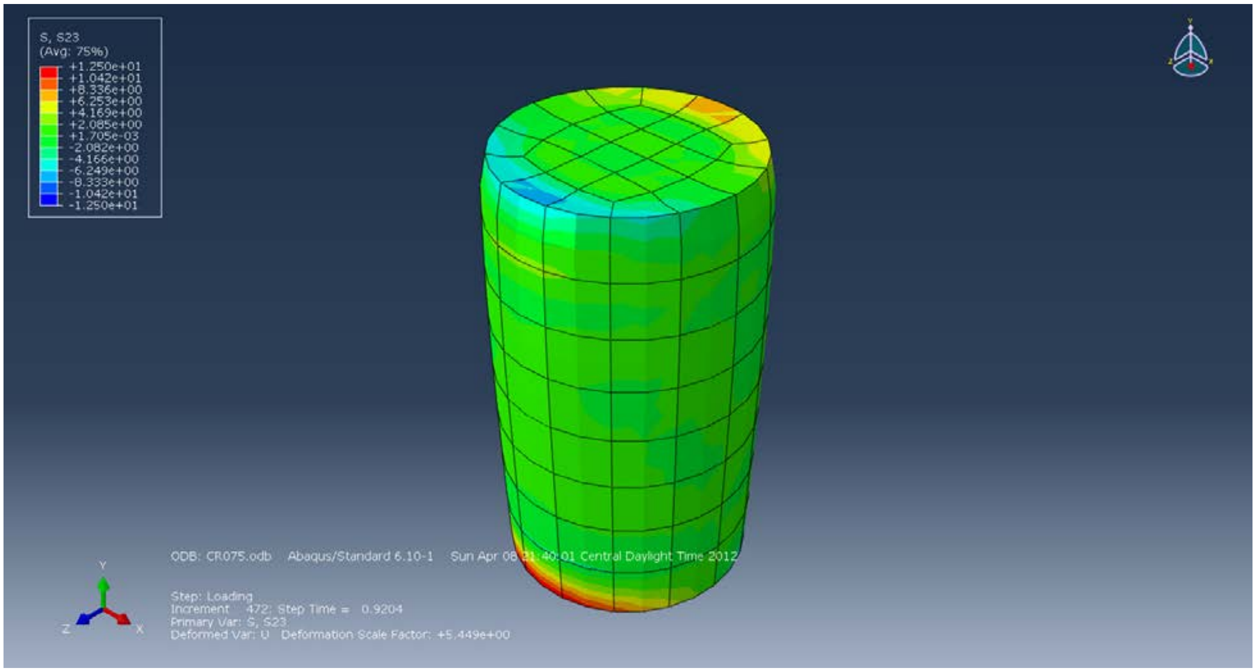

Figure B-100: Stress (S23) in the YZ-Direction (MPa).

- Smooth Boundaries:

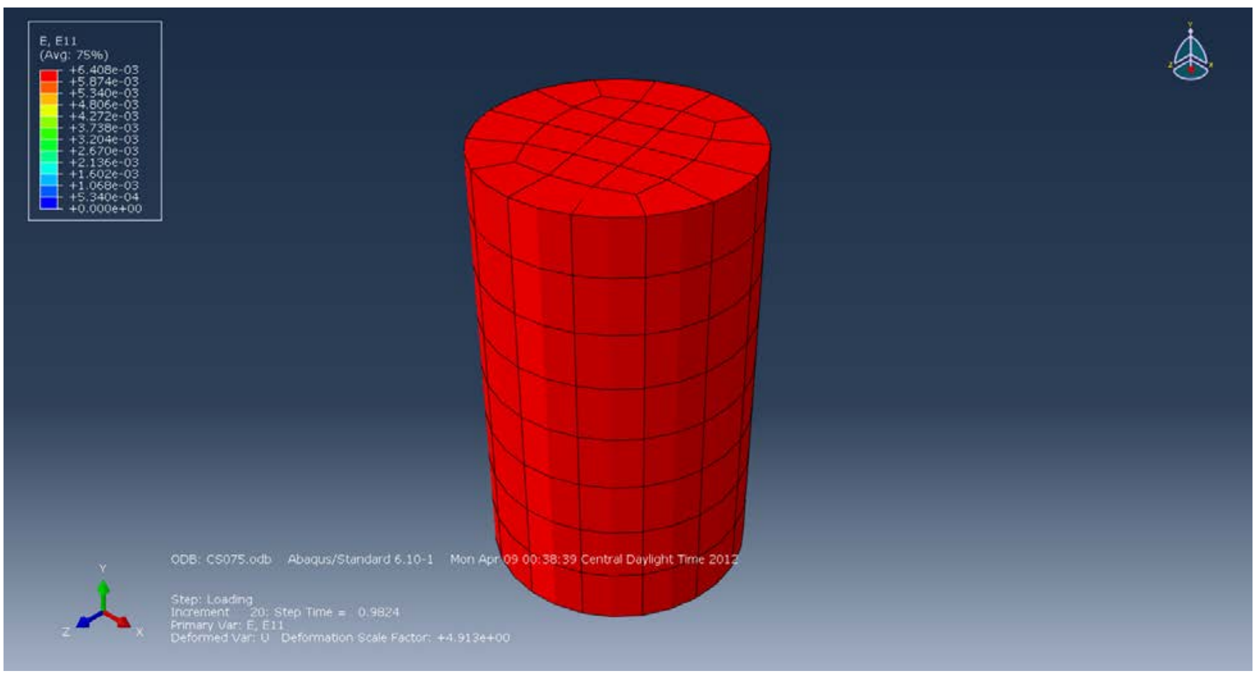

Figure B-101: Strain (E11) in the X-axis.

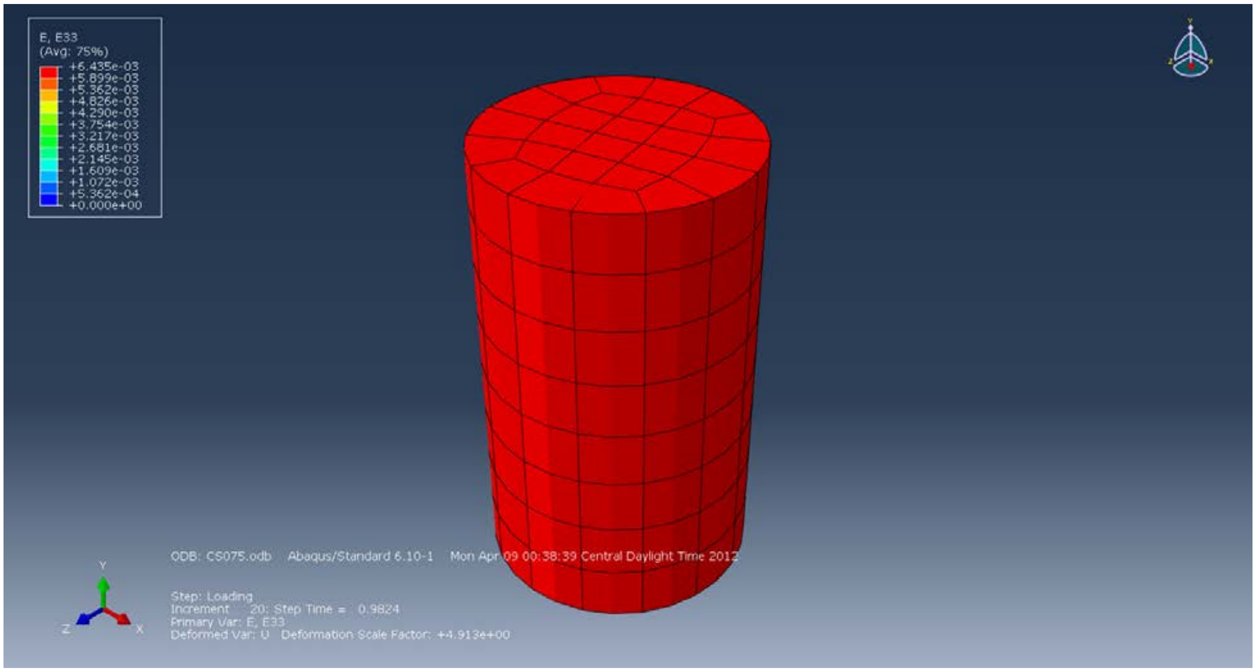

Figure B-102: Strain (E33) in the Z-axis.

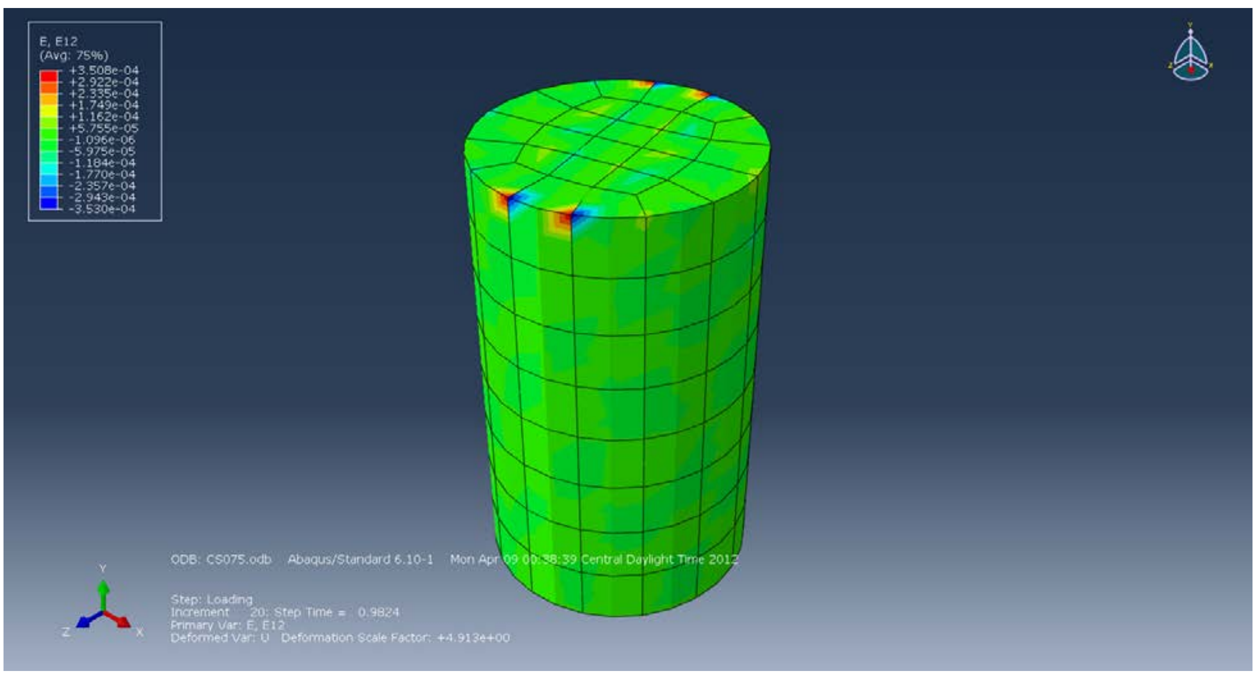

Figure B-103: Strain (E12) in the XY-Plane.

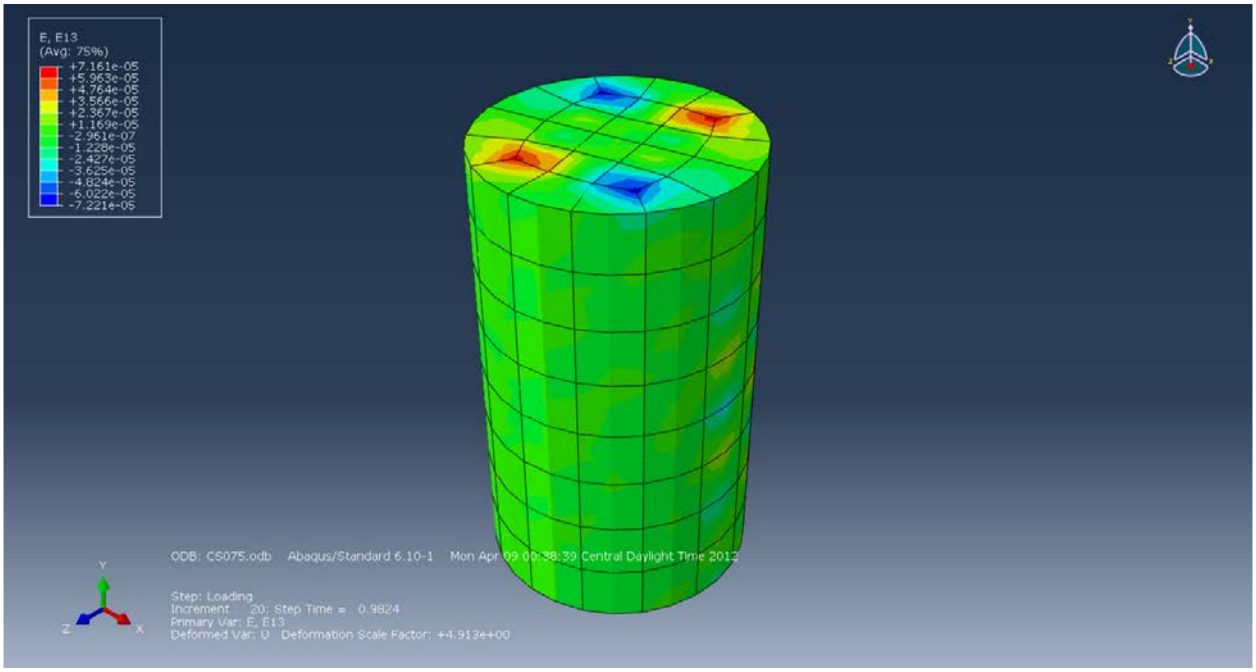

Figure B-104: Strain (E13) in the XZ-Plane.

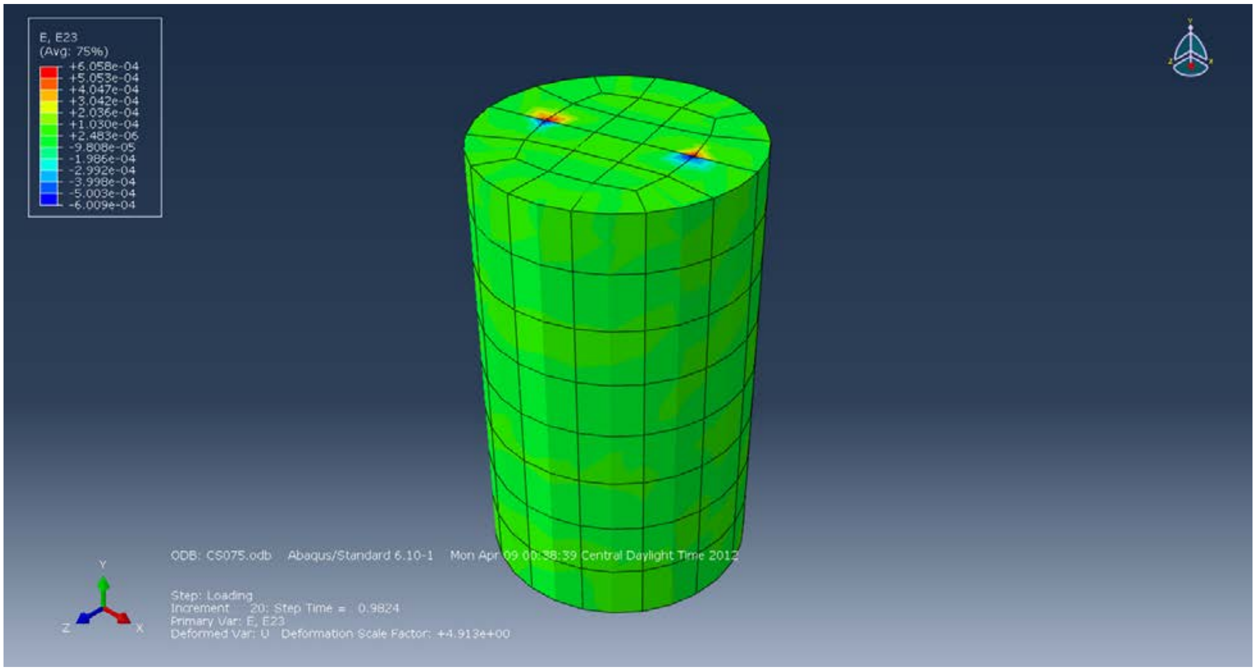

Figure B-105: Strain (E23) in the YZ-Plane.

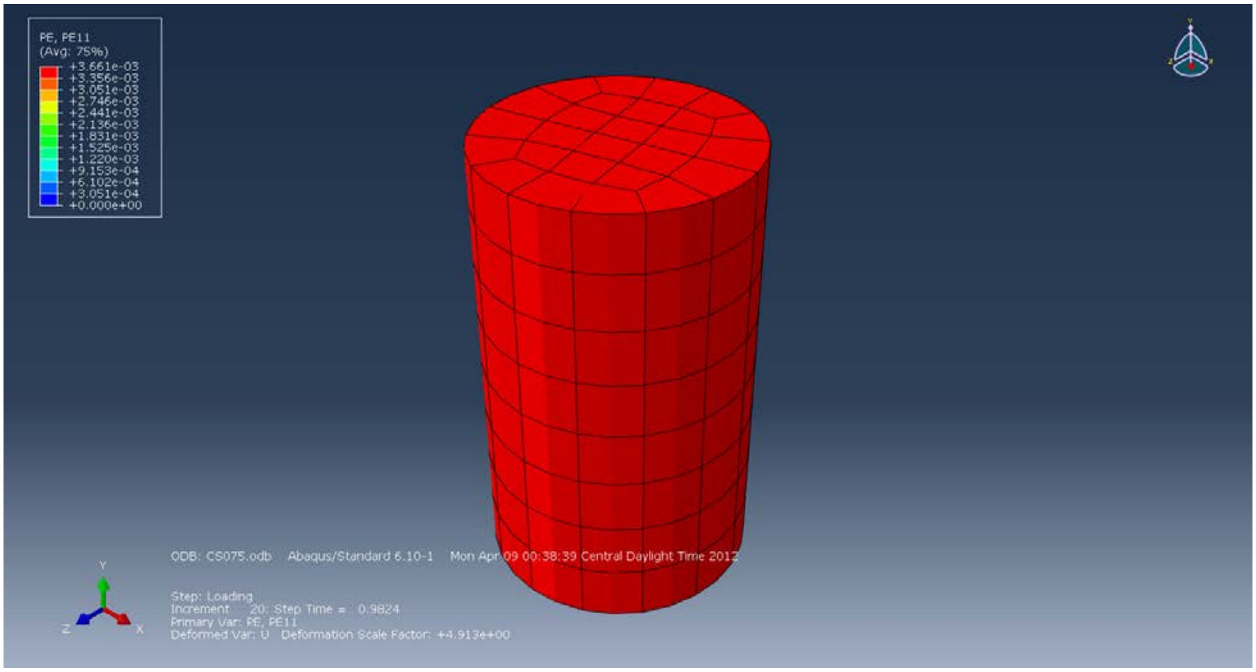

Figure B-106: Plastic Strain (PE11) in the X-axis.

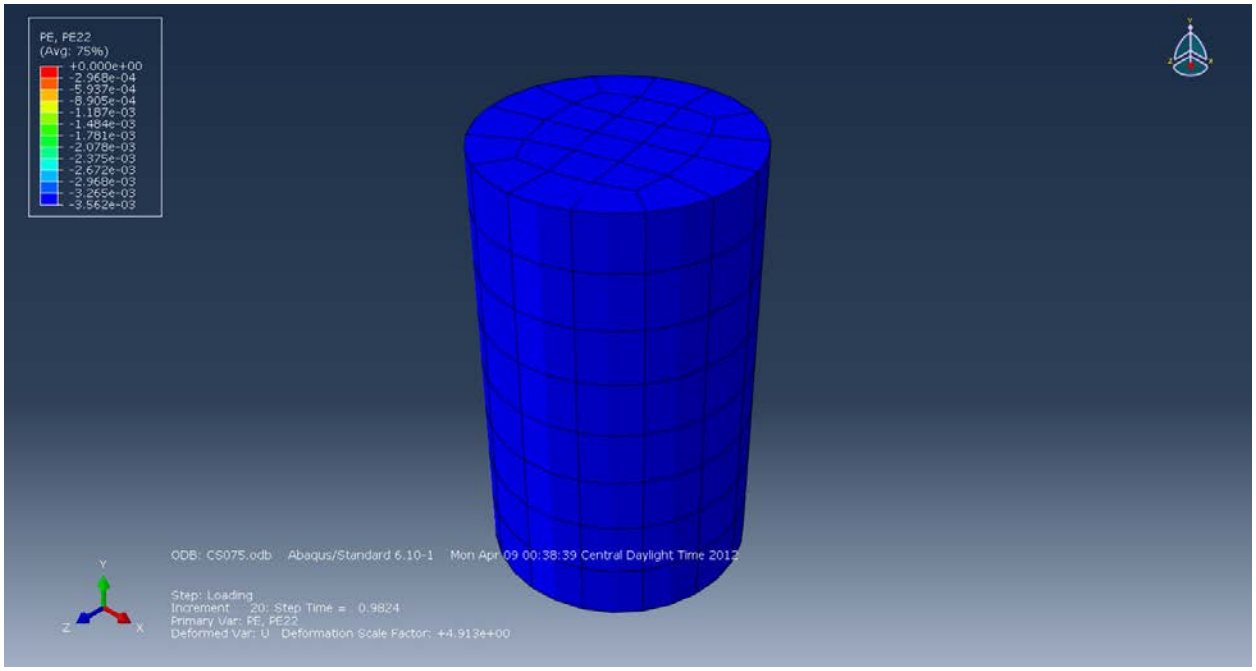

Figure B-107: Plastic Strain (PE22) in the Y-axis.

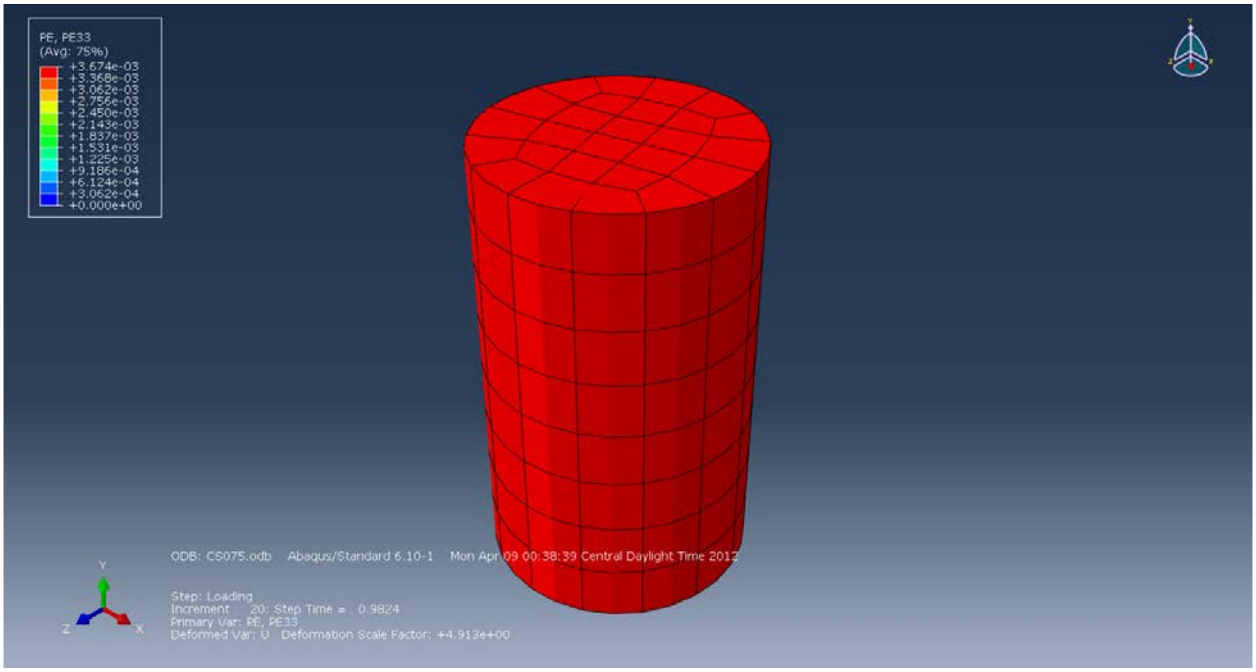

Figure B-108: Plastic Strain (PE33) in the Z-axis.

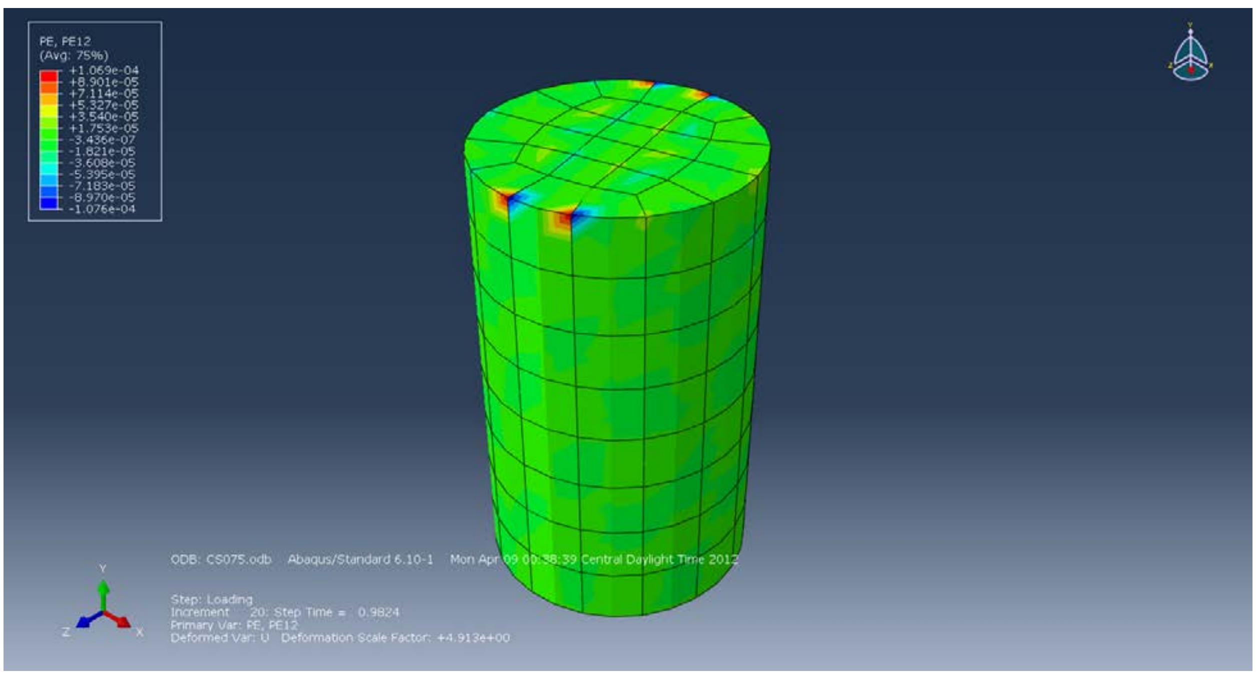

Figure B-109: Plastic Strain (PE12) in the XY-Plane.

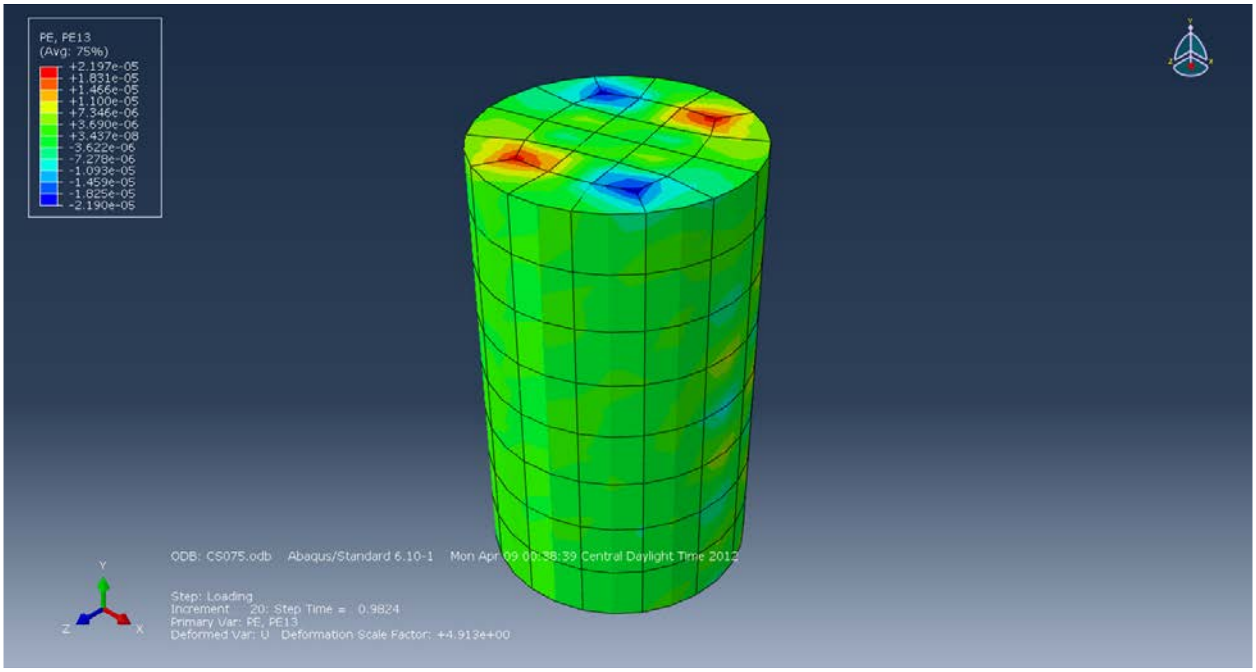

Figure B-110: Plastic Strain (PE13) in the XZ-Plane.

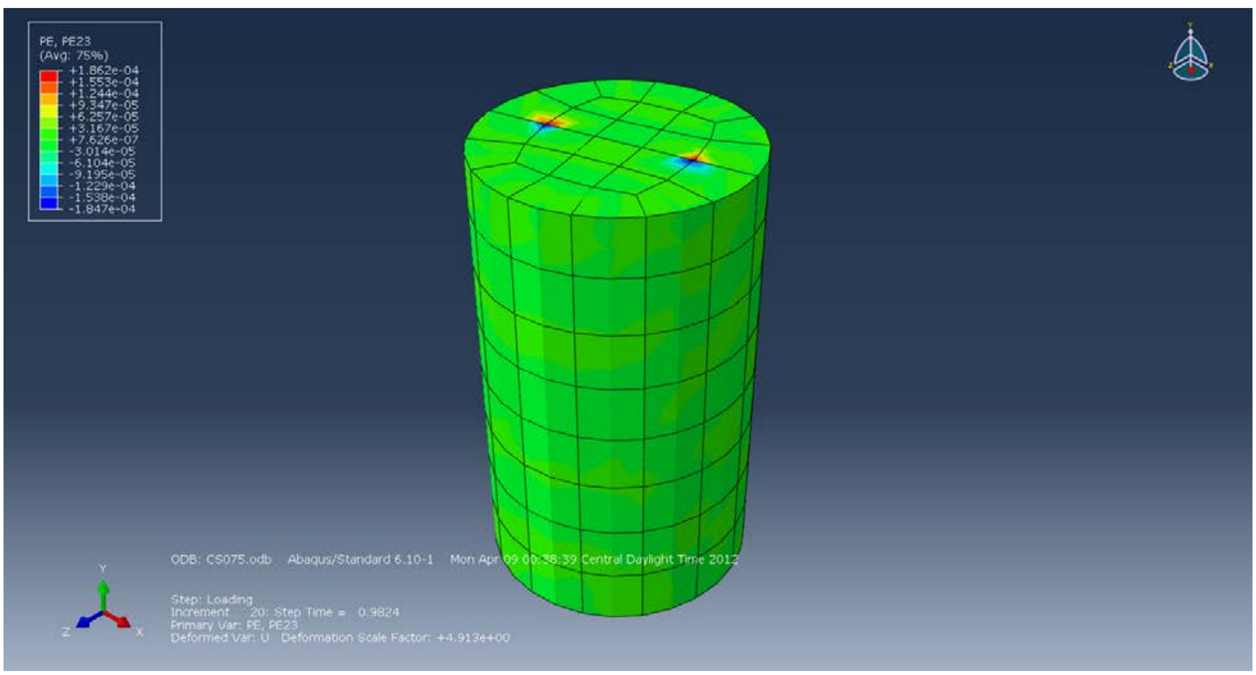

Figure B-111: Plastic Strain (PE23) in the YZ-Plane.

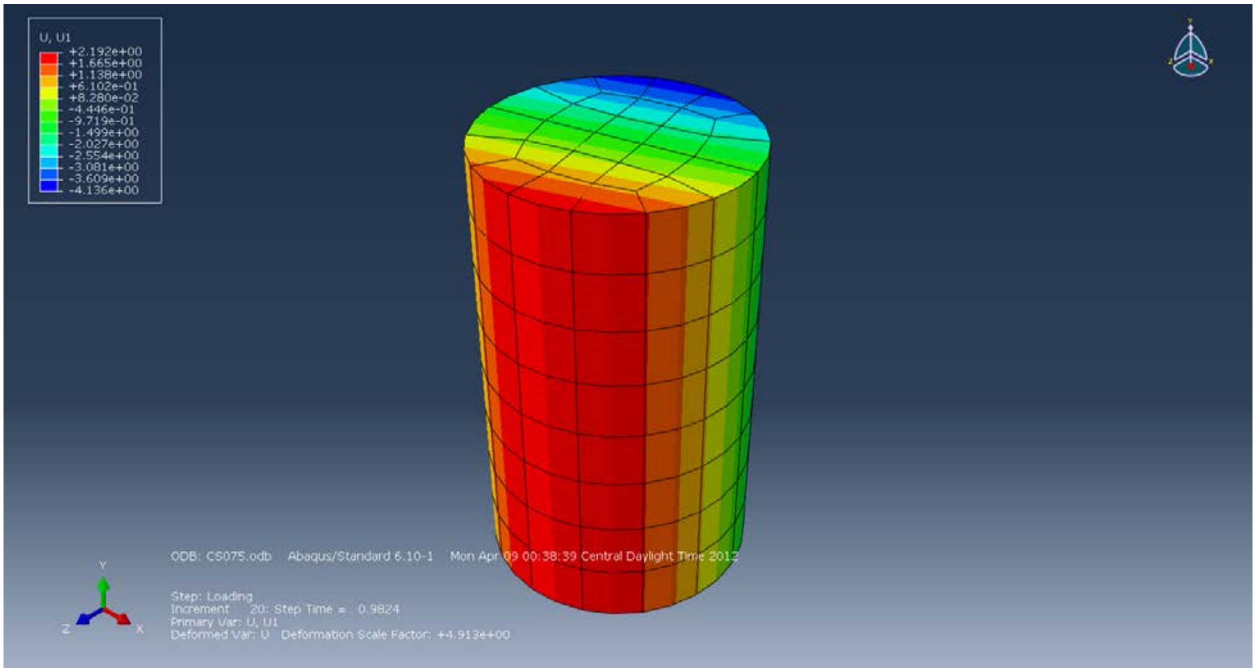

Figure B-112: Displacement (U1) in the X-axis (mm).

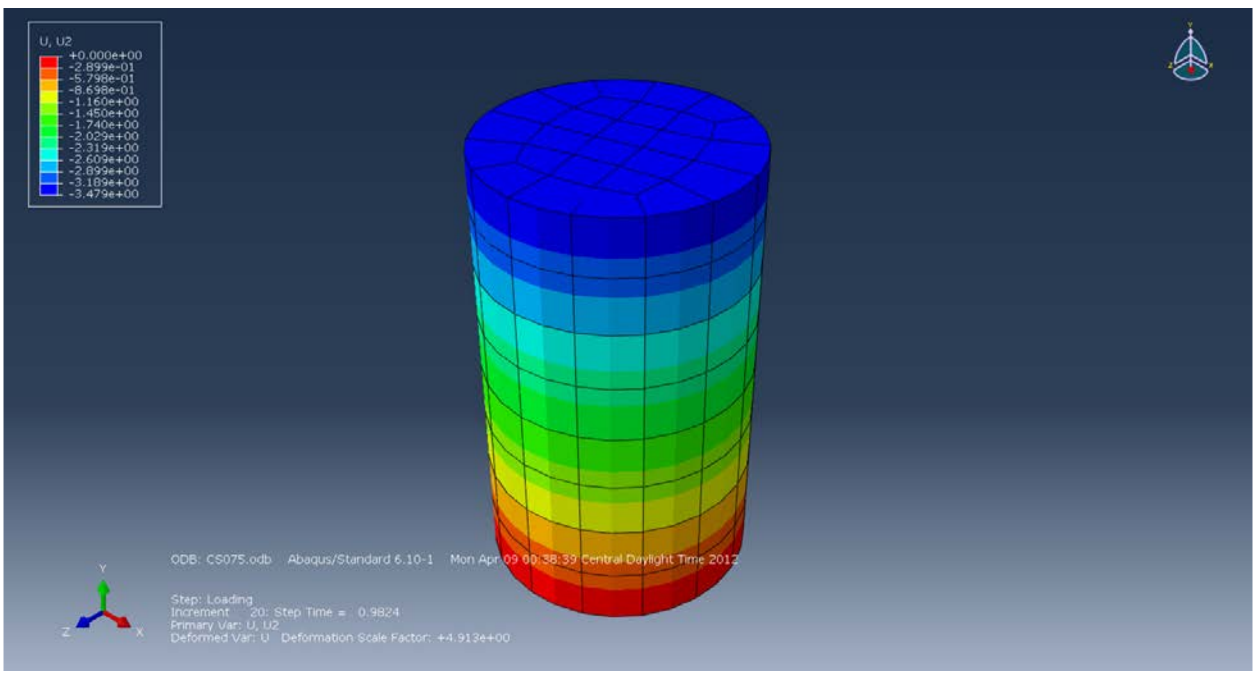

Figure B-113: Displacement (U2) in the Y-axis (mm).

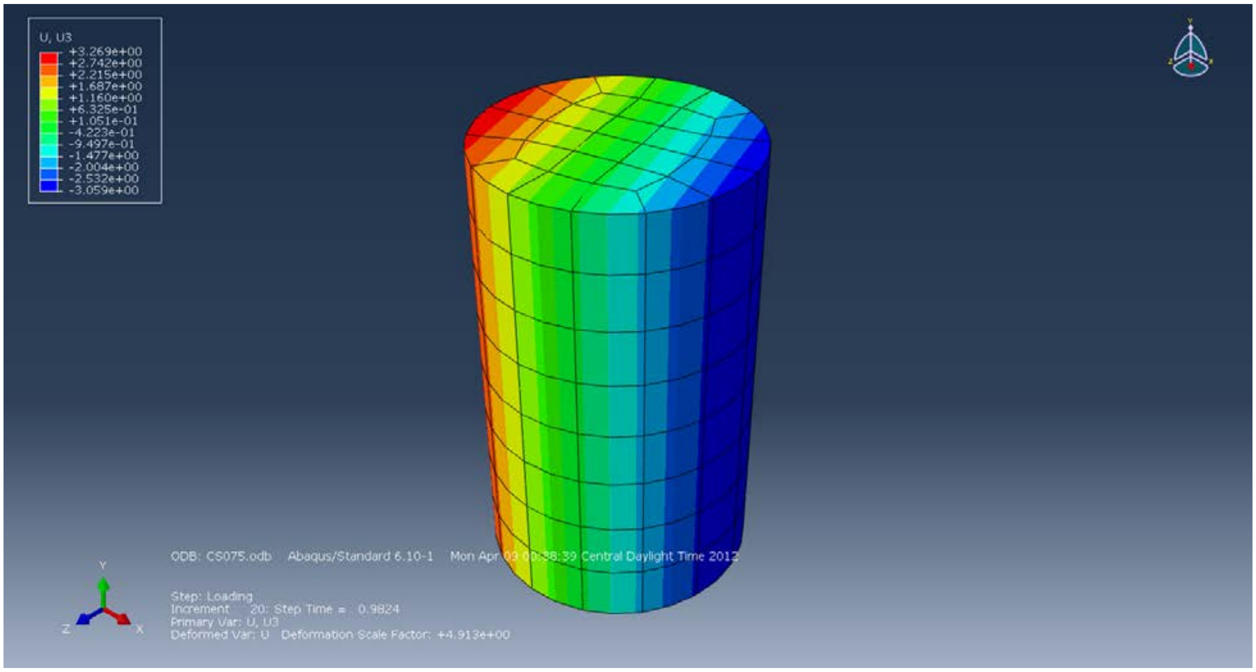

Figure B-114: Displacement (U3) in the Z-axis (mm).

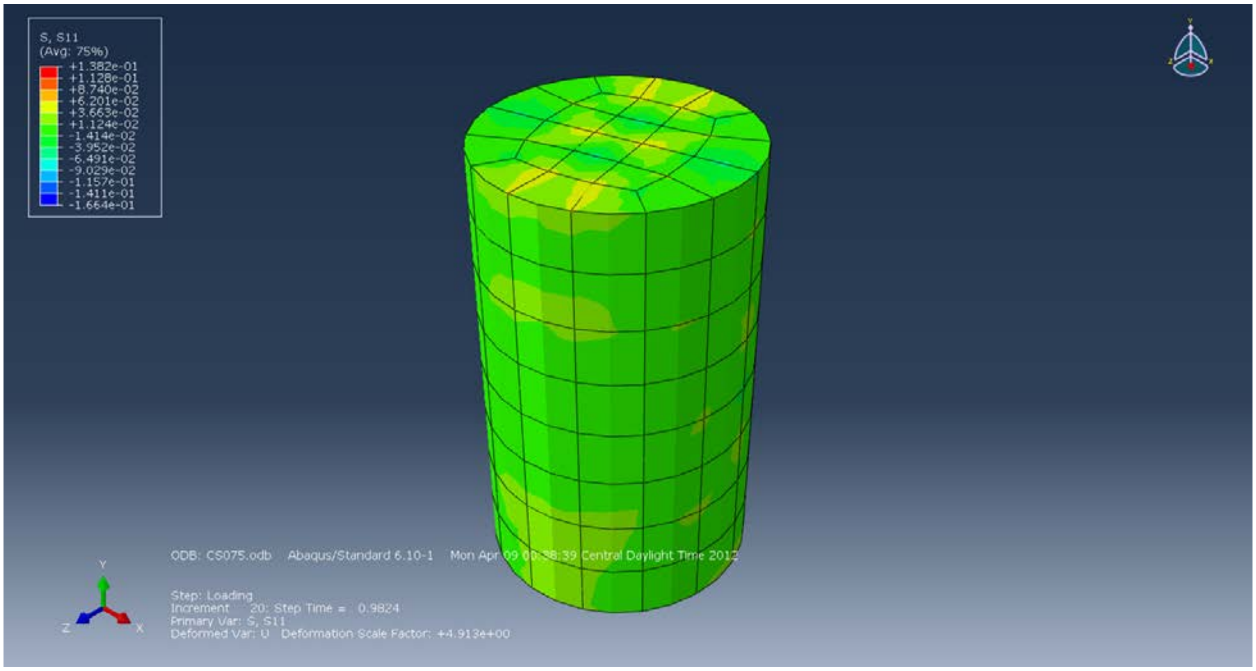

Figure B-115: Stress (S11) in the X-Direction (MPa).

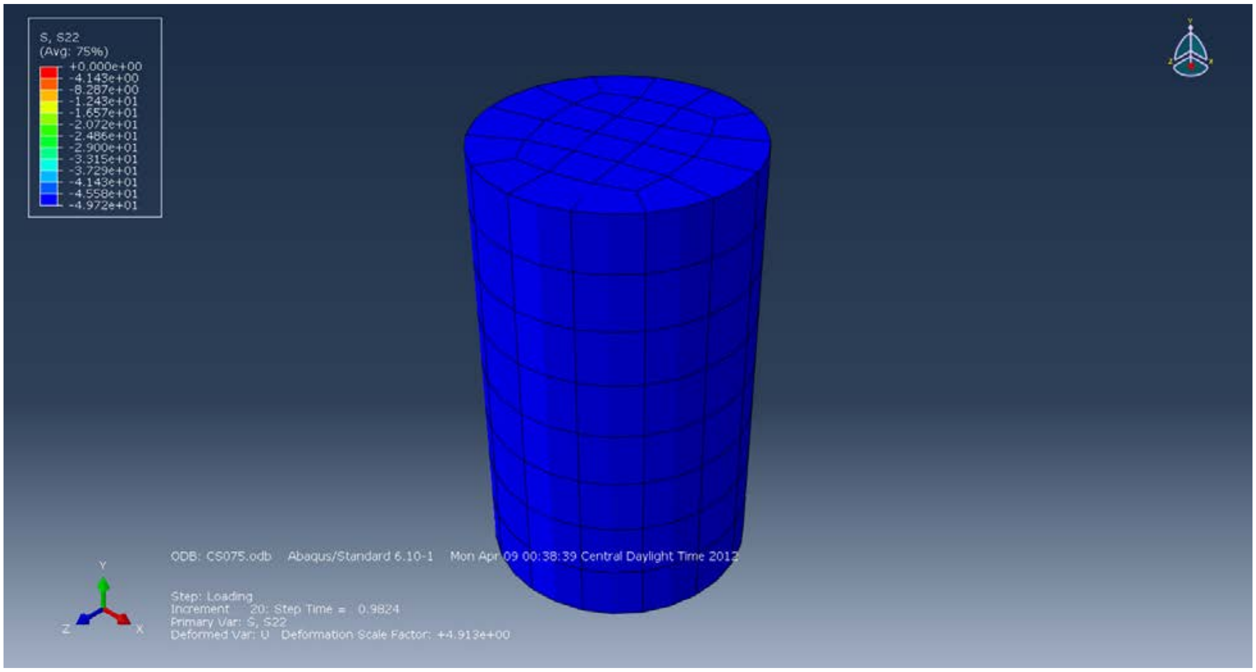

Figure B-116: Stress (S22) in the Y-Direction (MPa).

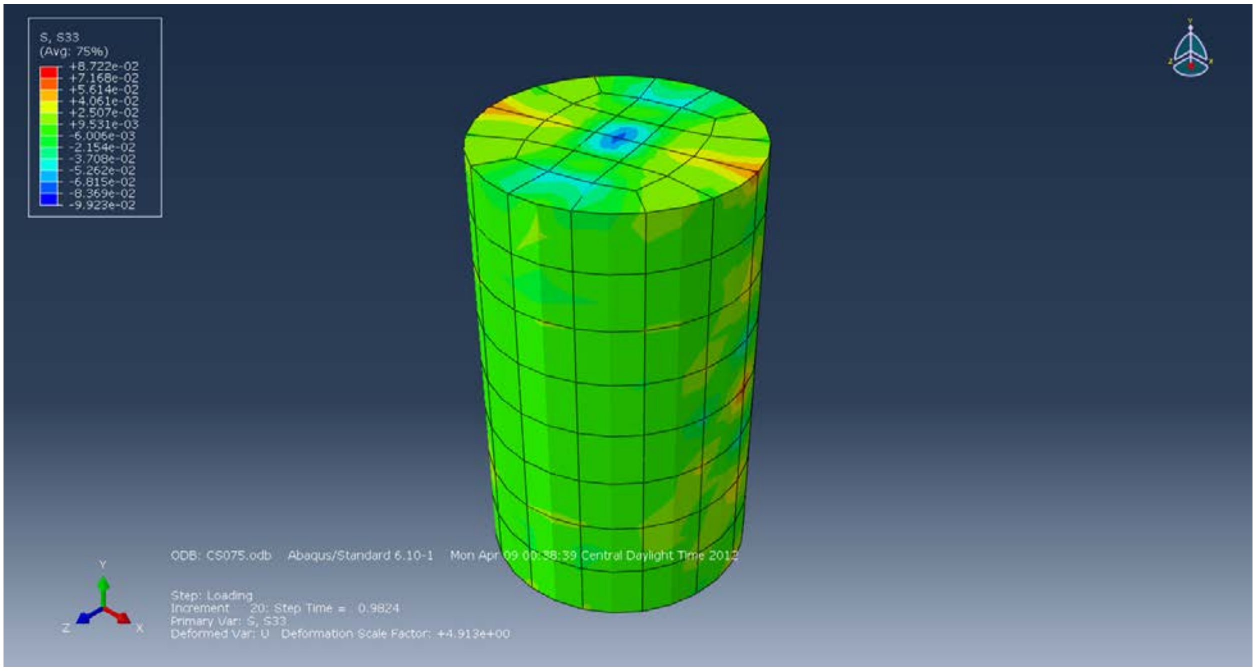

Figure B-117: Stress (S33) in the Z-Direction (MPa).

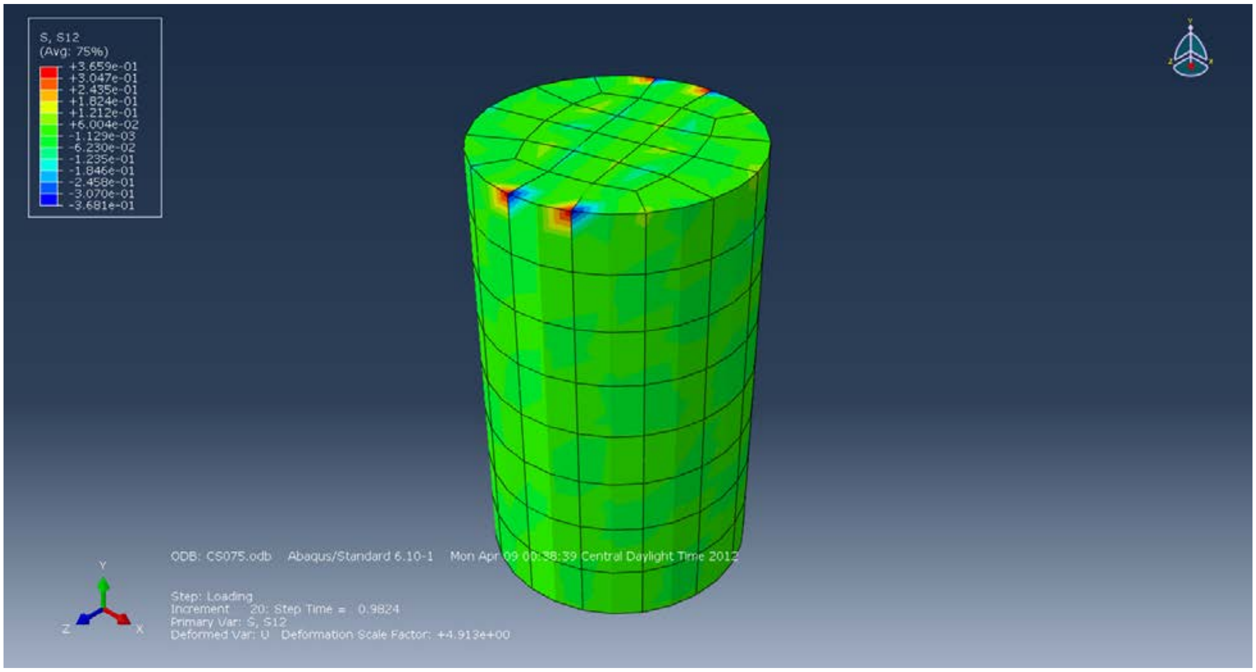

Figure B-118: Stress (S12) in the XY-Direction (MPa).

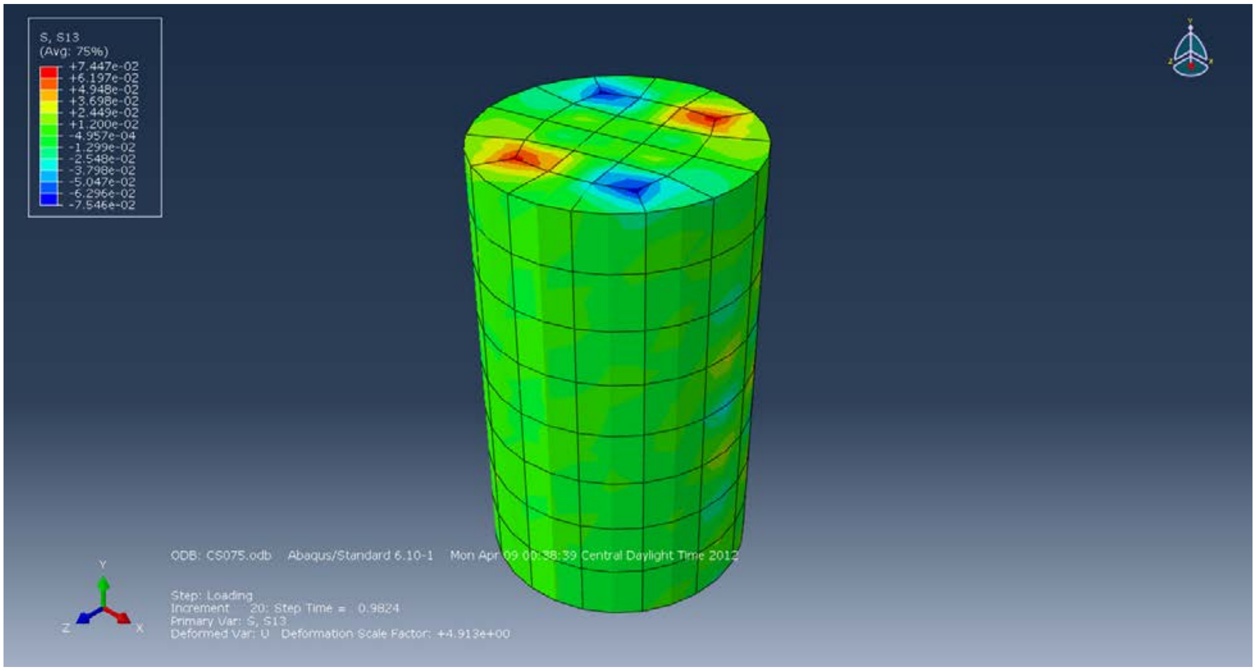

Figure B-119: Stress (S13) in the XZ-Direction (MPa).

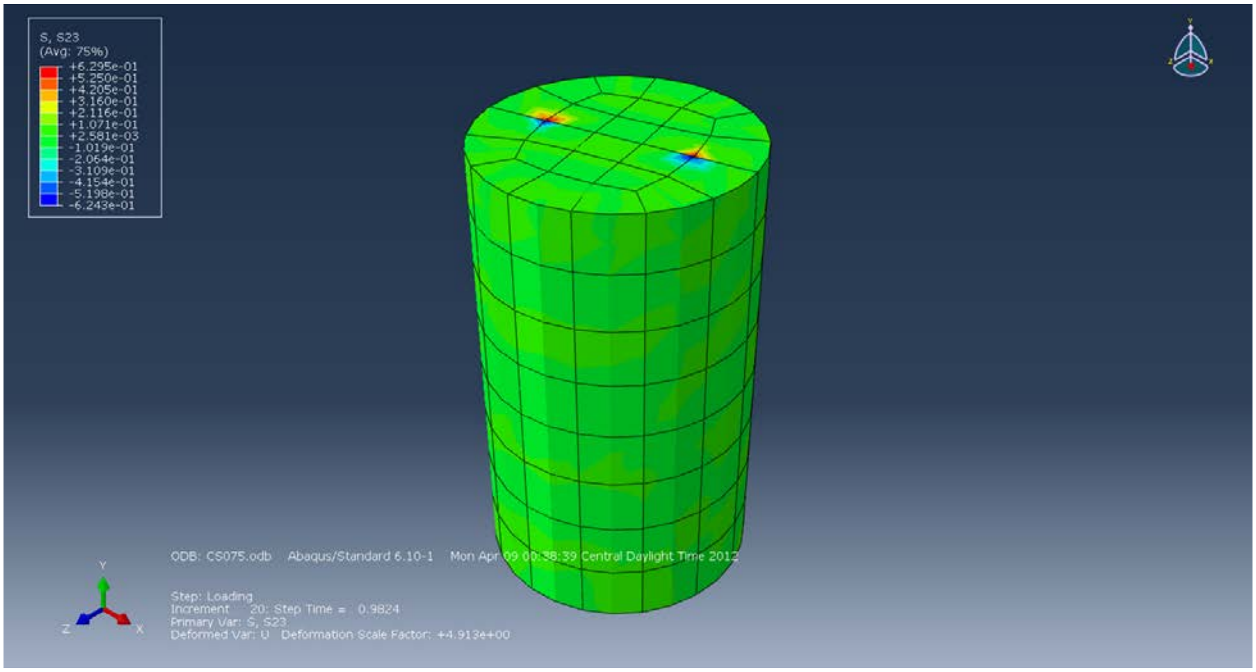

Figure B-120: Stress (S23) in the YZ-Direction (MPa).

Cylinders with 1% Wheat Fibers:

- Rough Boundaries:

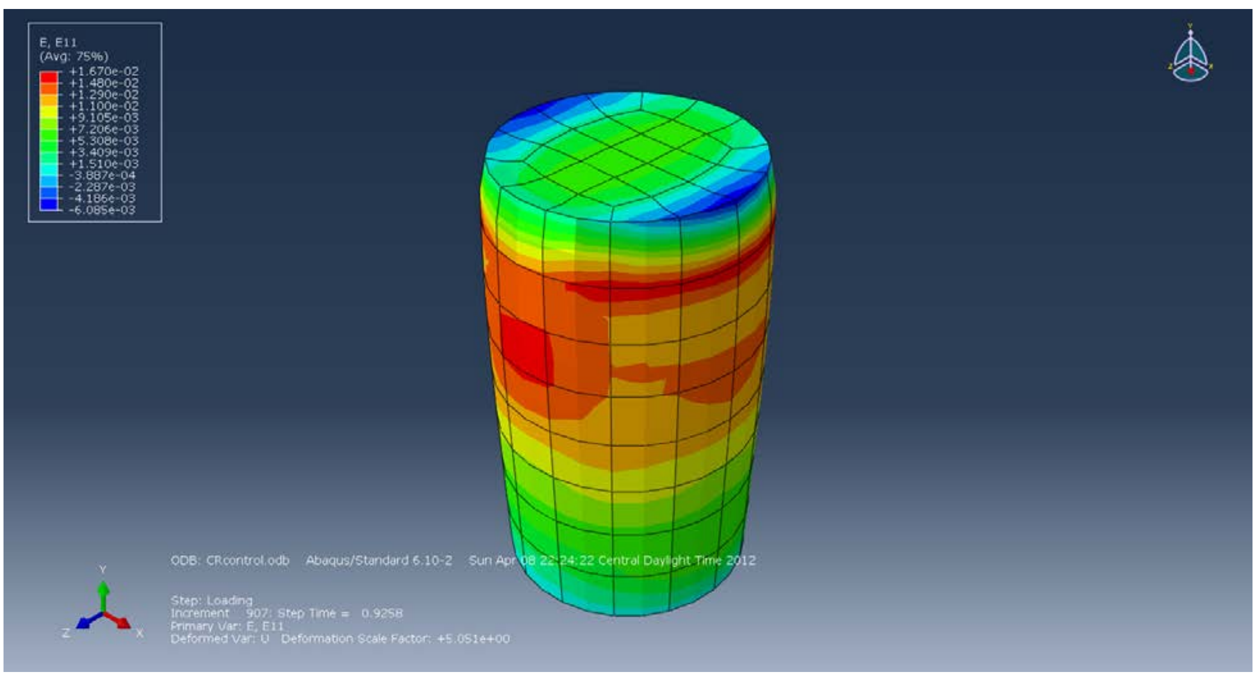

Figure B-121: Strain (E11) in the X-axis.

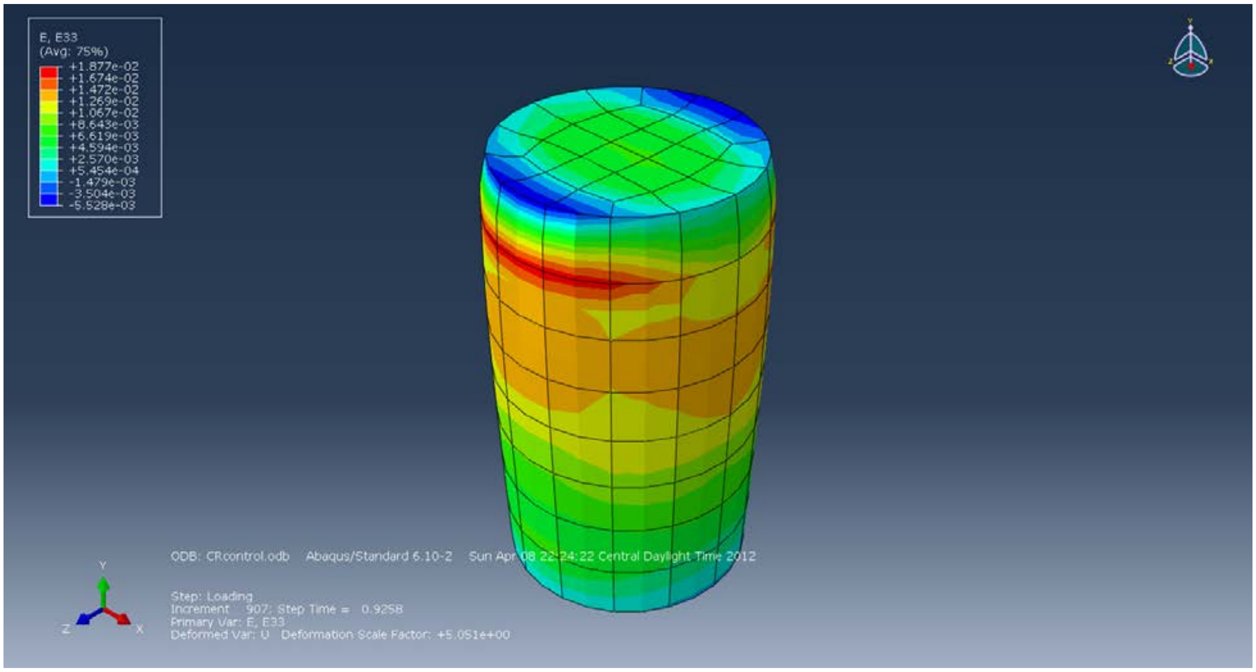

Figure B-122: Strain (E33) in the Z-axis.

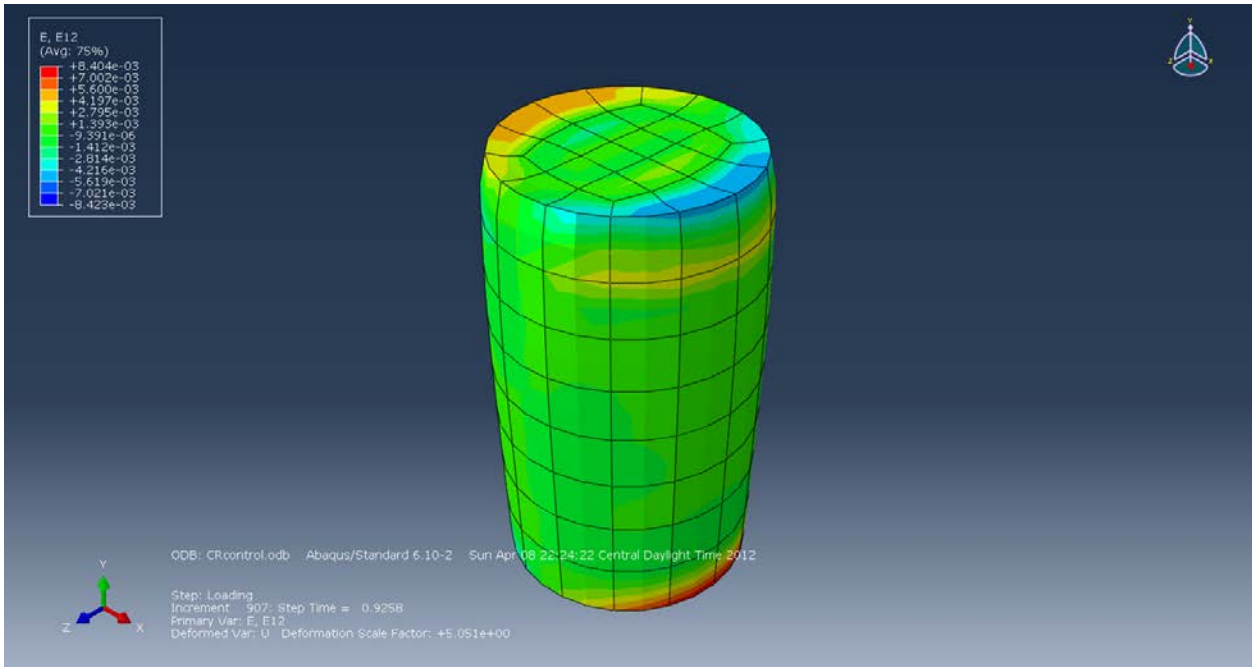

Figure B-123: Strain (E12) in the XY-Plane.

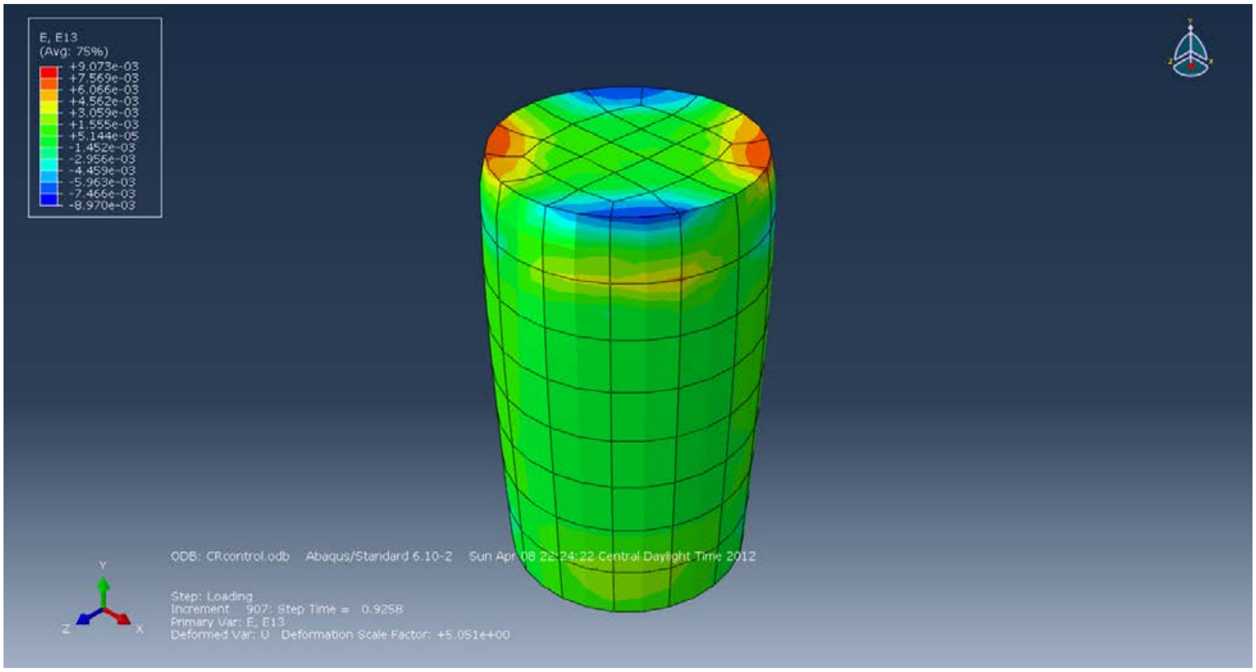

Figure B-124: Strain (E13) in the XZ-Plane.

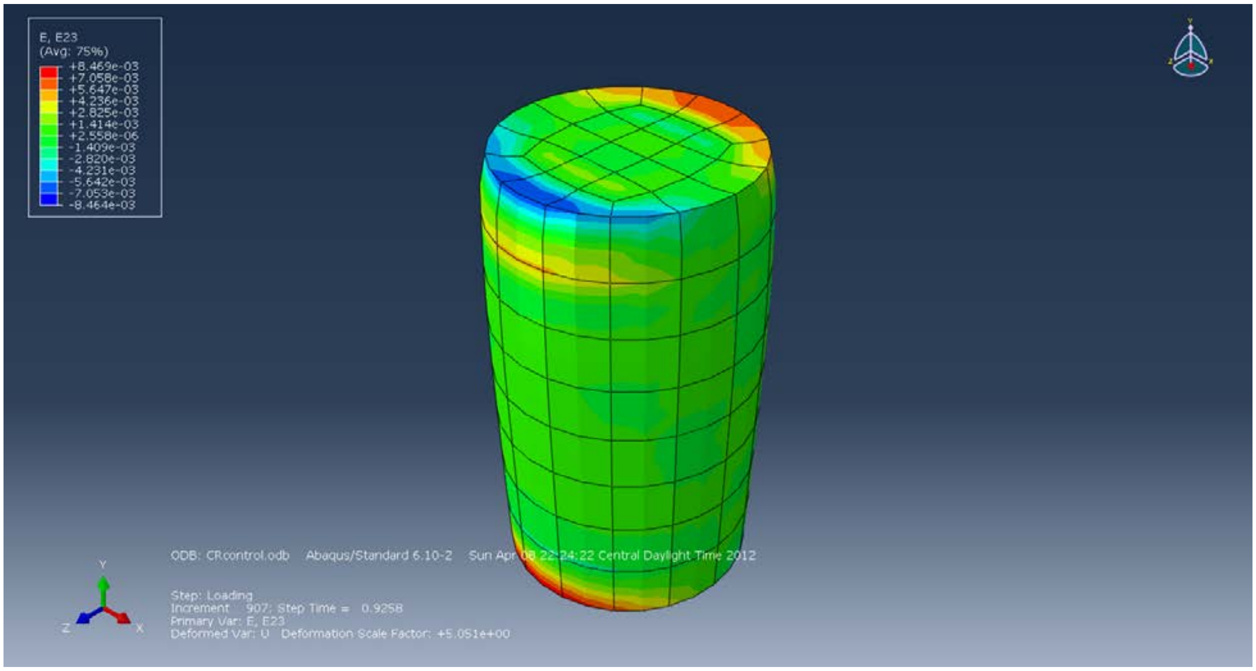

Figure B-125: Strain (E23) in the YZ-Plane.

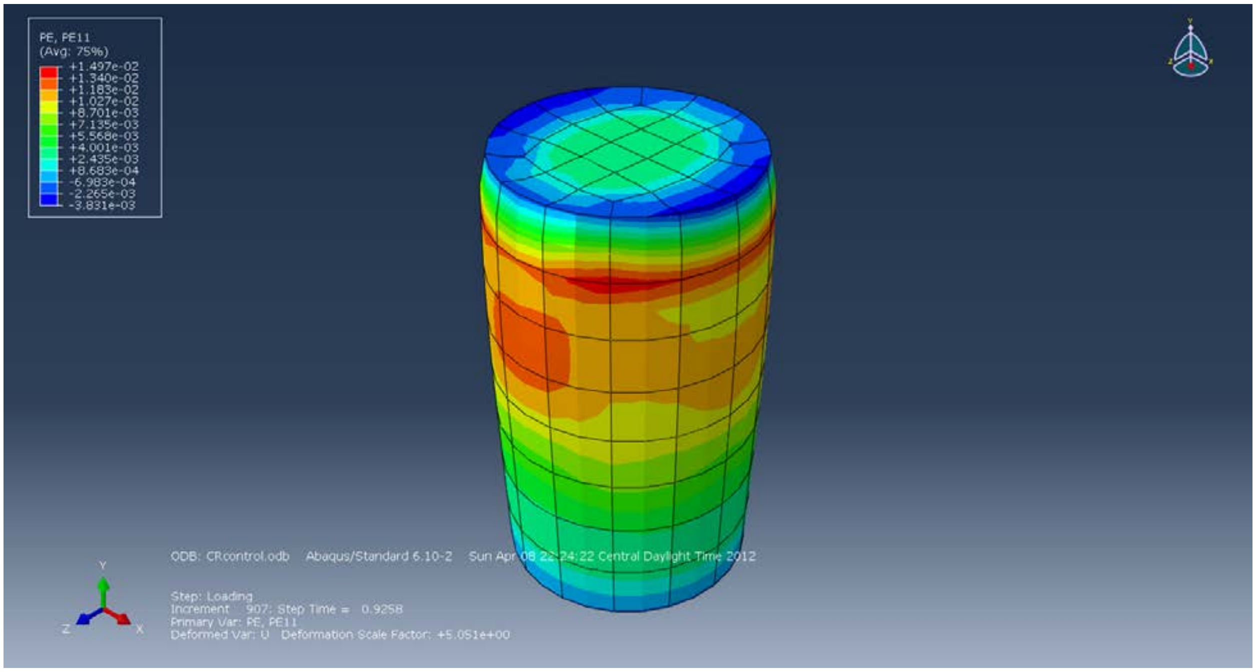

Figure B-126: Plastic Strain (PE11) in the X-axis.

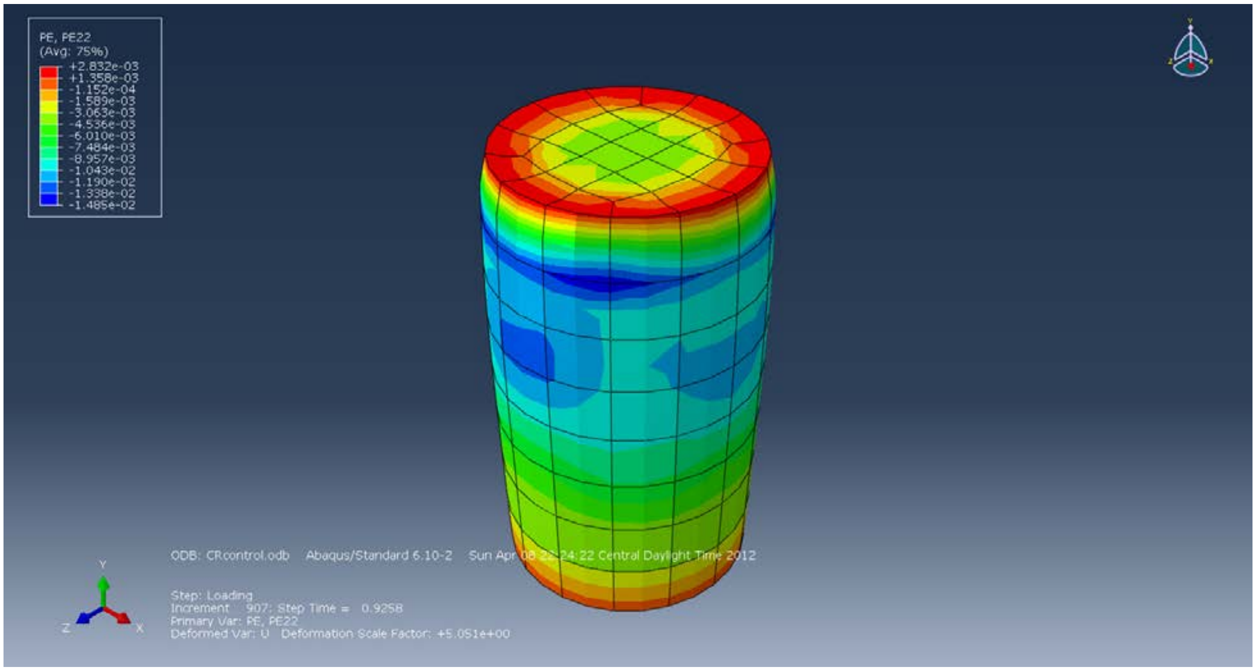

Figure B-127: Plastic Strain (PE22) in the Y-axis.

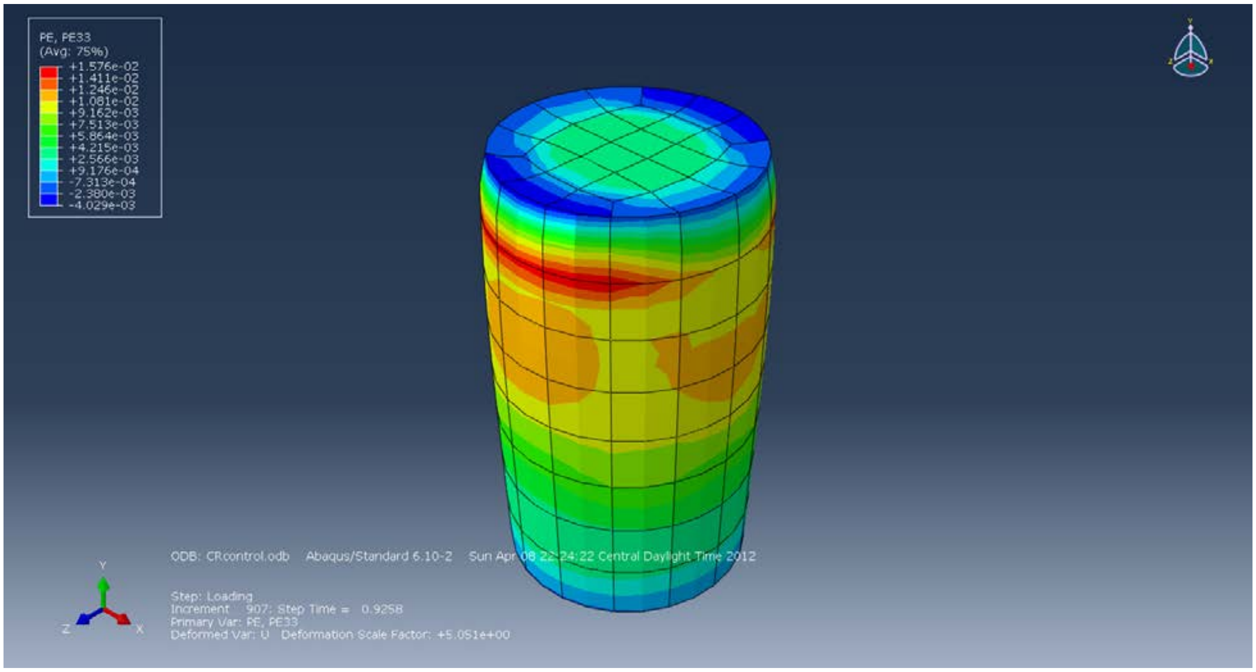

Figure B-128: Plastic Strain (PE33) in the Z-axis.

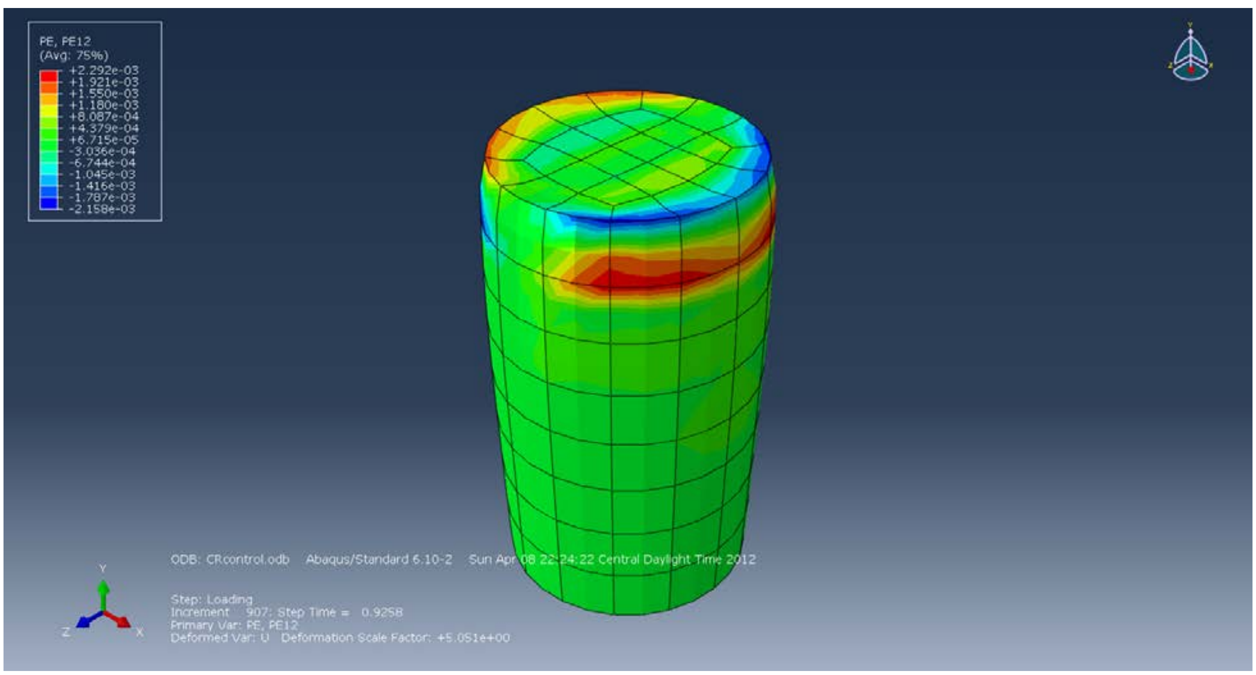

Figure B-129: Plastic Strain (PE12) in the XY-Plane.

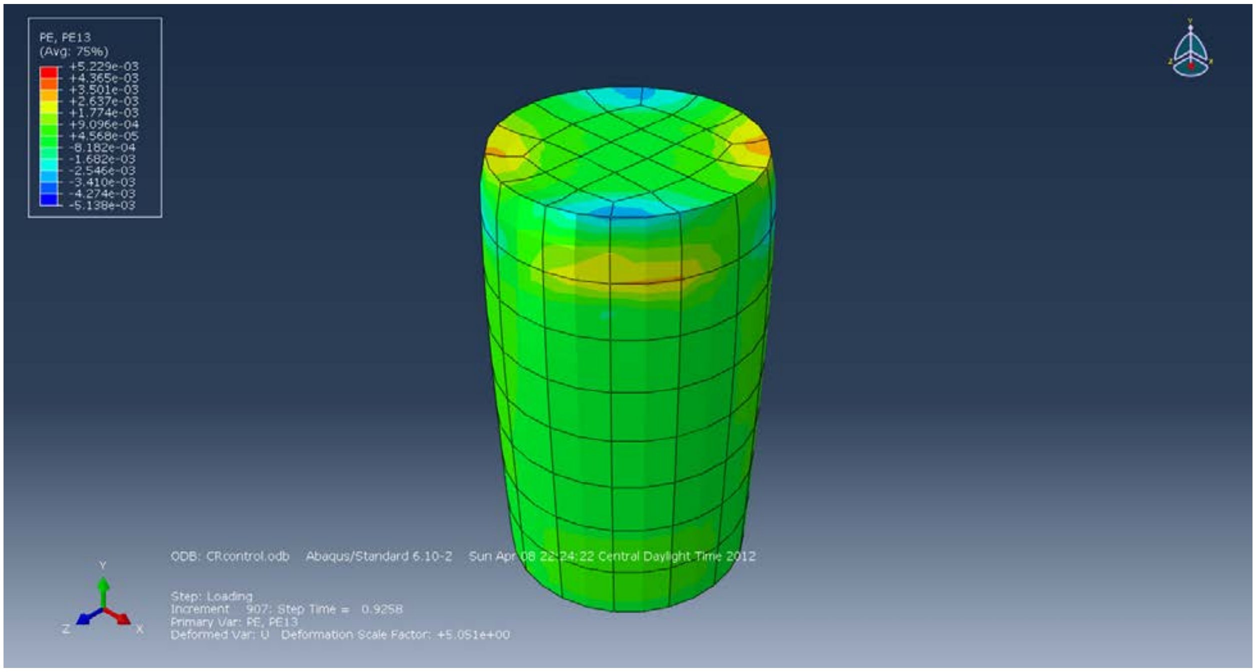

Figure B-130: Plastic Strain (PE13) in the XZ-Plane.

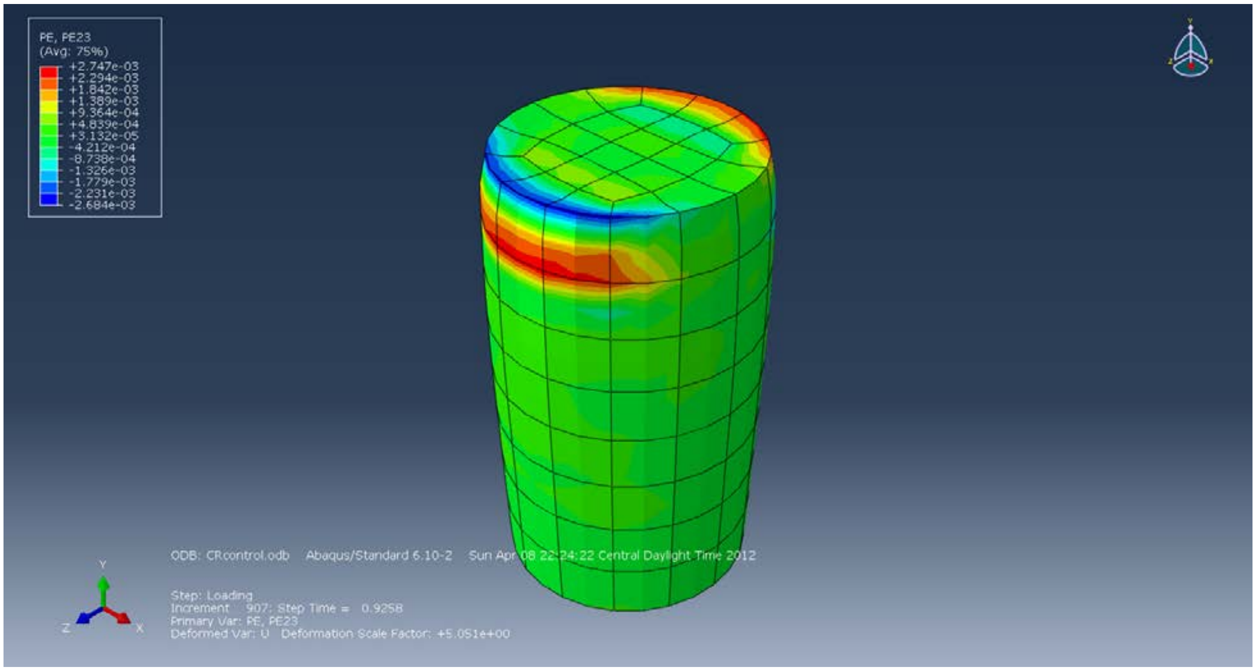

Figure B-131: Plastic Strain (PE23) in the YZ-Plane.

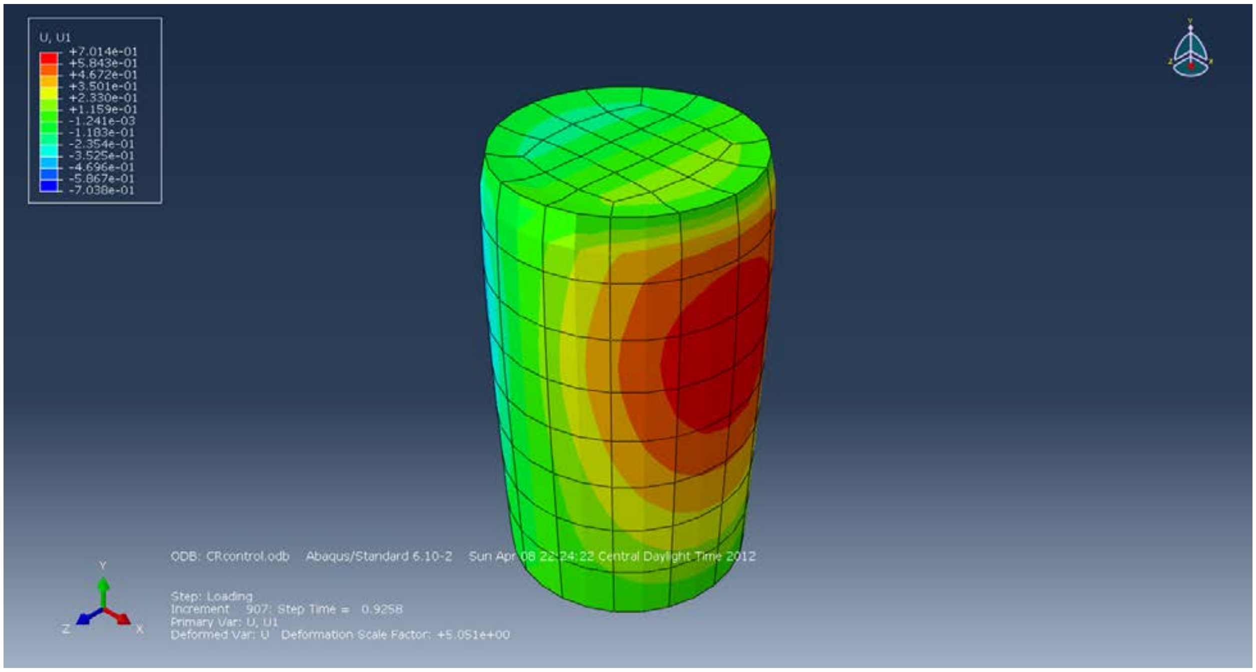

Figure B-132: Displacement (U1) in the X-axis (mm).

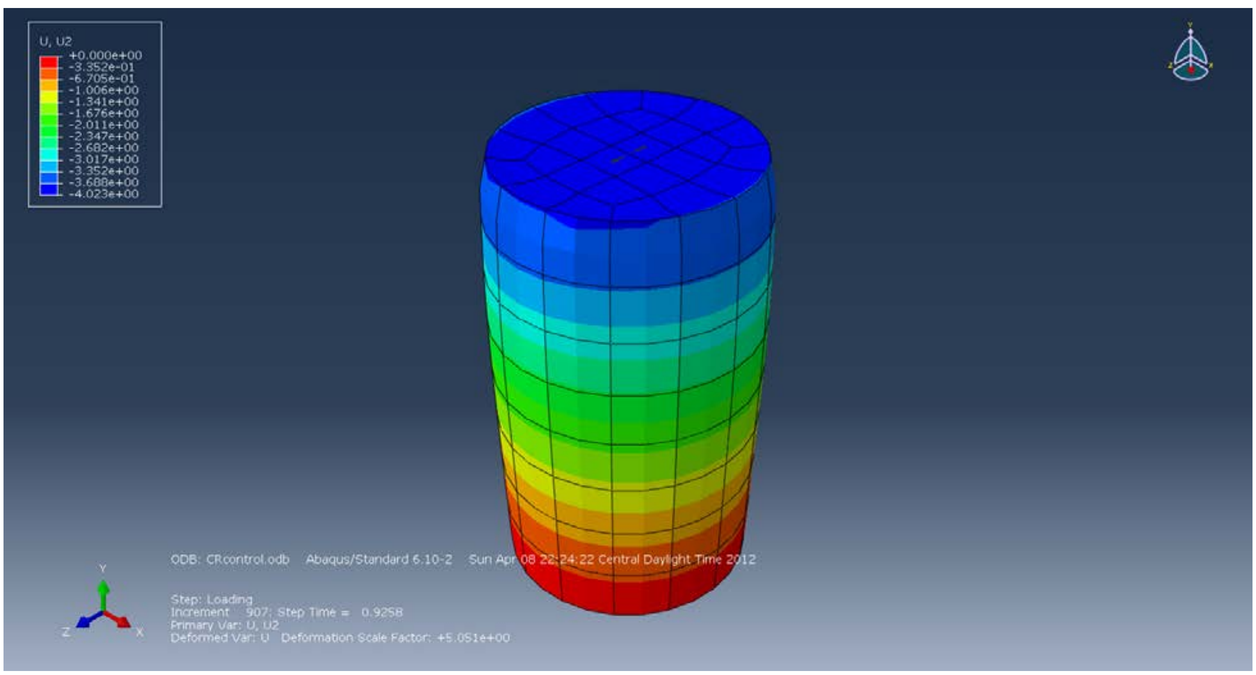

Figure B-133: Displacement (U2) in the Y-axis (mm).

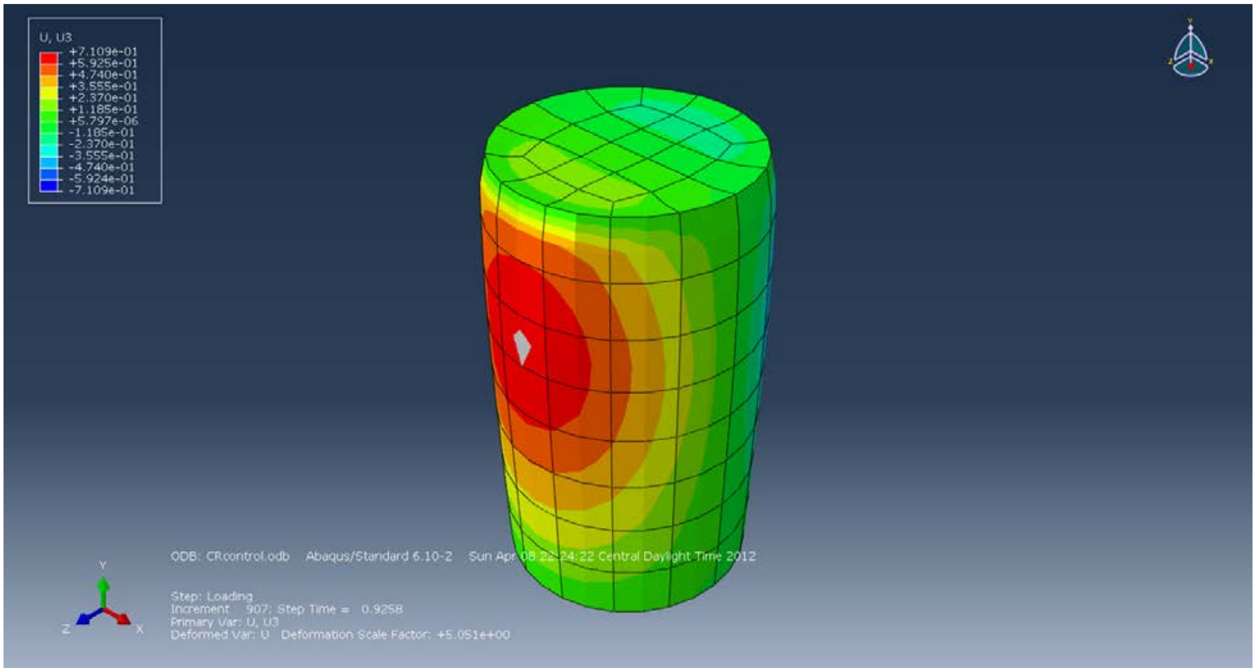

Figure B-134: Displacement (U3) in the Z-axis (mm).

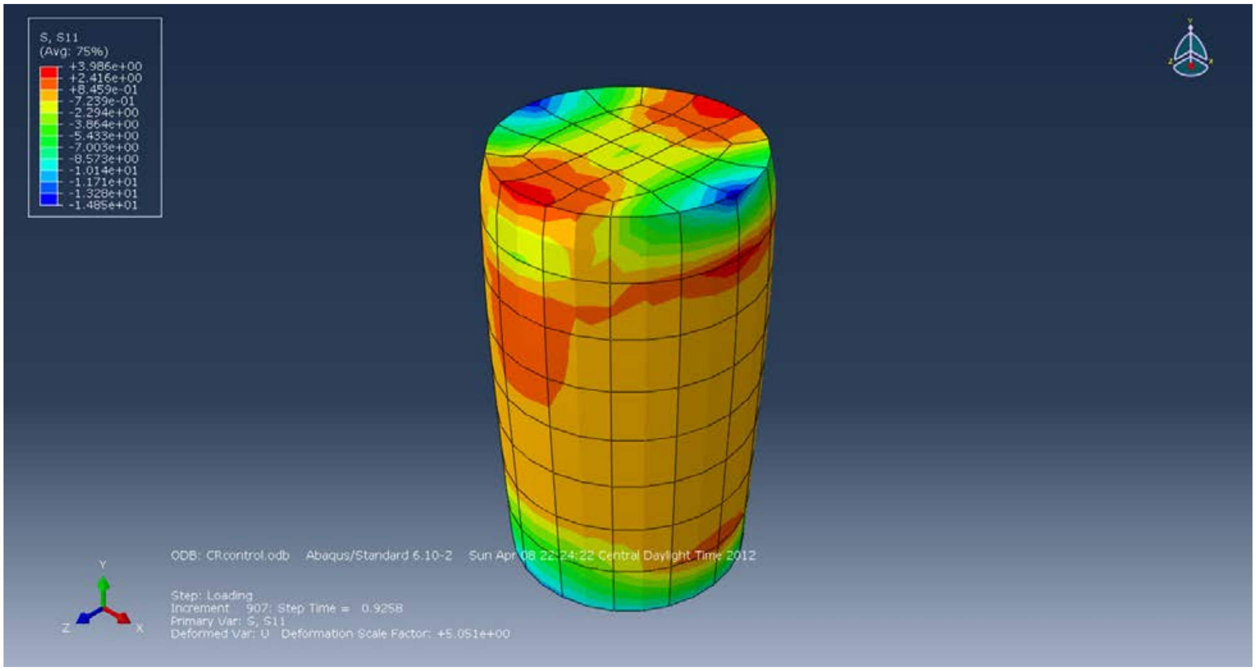

Figure B-135: Stress (S11) in the X-Direction (MPa).

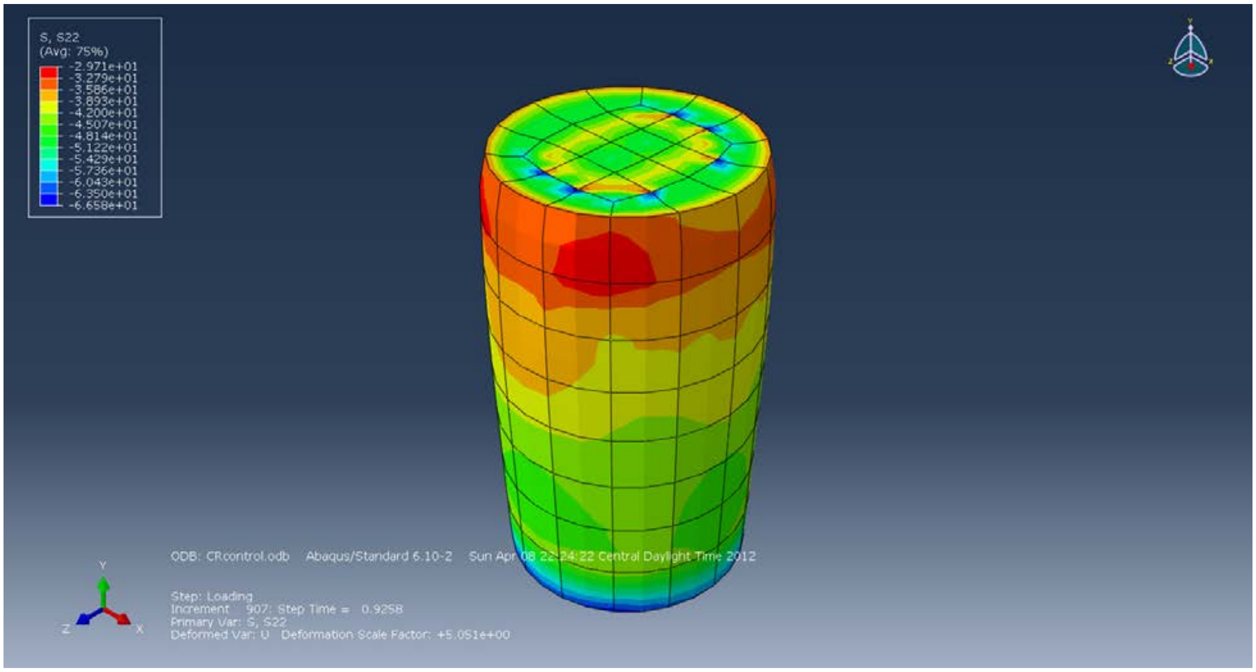

Figure B-136: Stress (S22) in the Y-Direction (MPa).

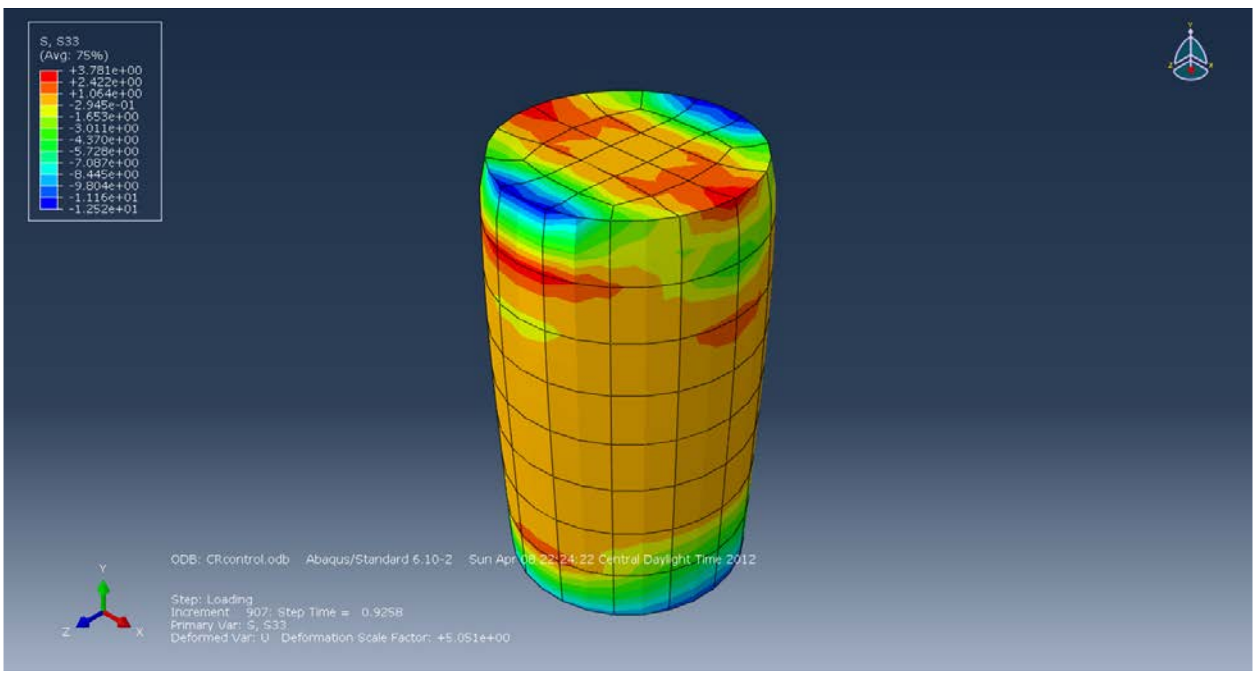

Figure B-137: Stress (S33) in the Z-Direction (MPa).

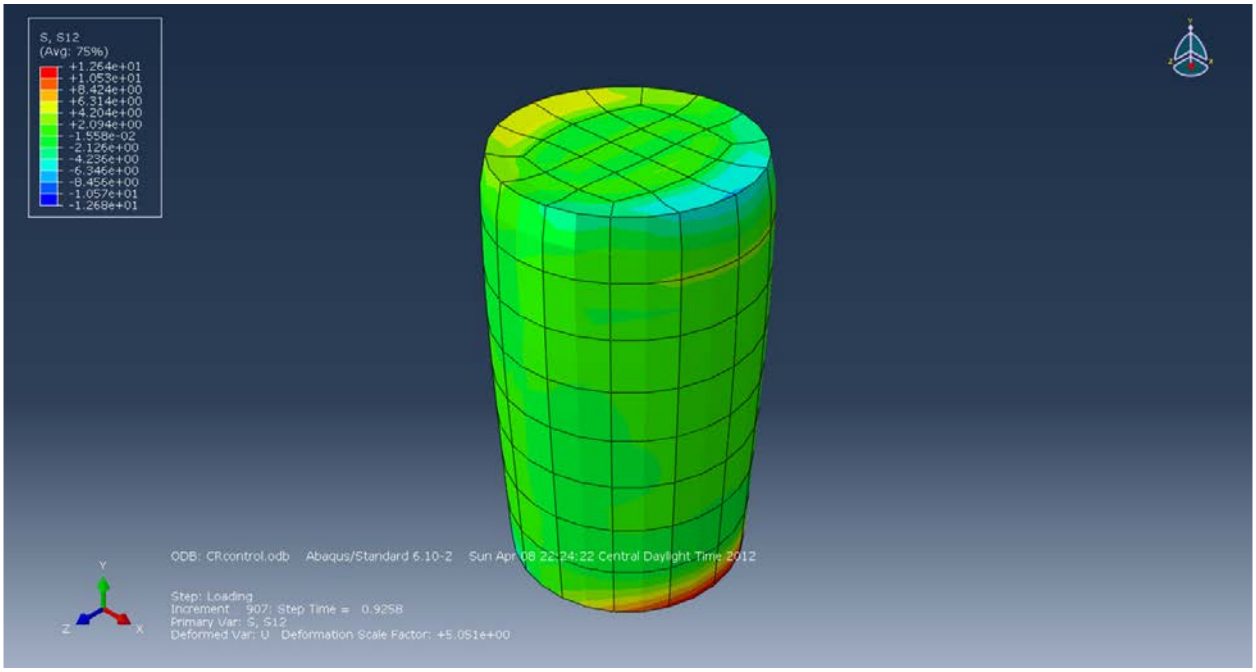

Figure B-138: Stress (S12) in the XY-Direction (MPa).

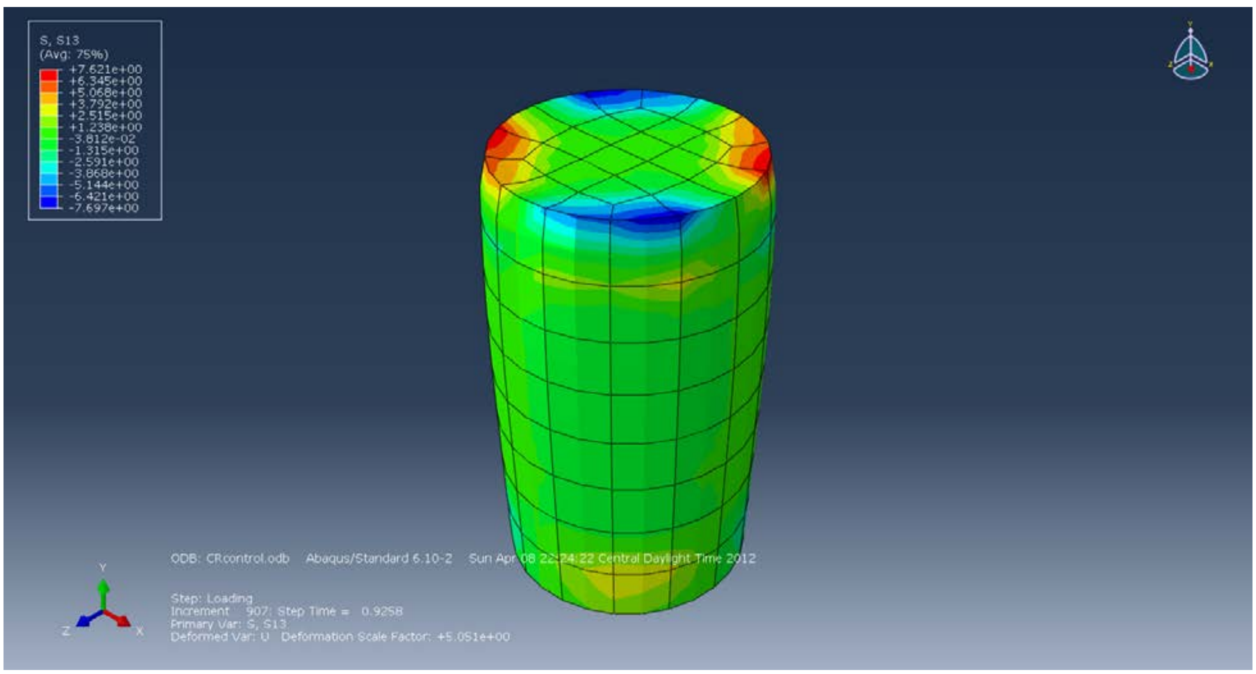

Figure B-139: Stress (S13) in the XZ-Direction (MPa).

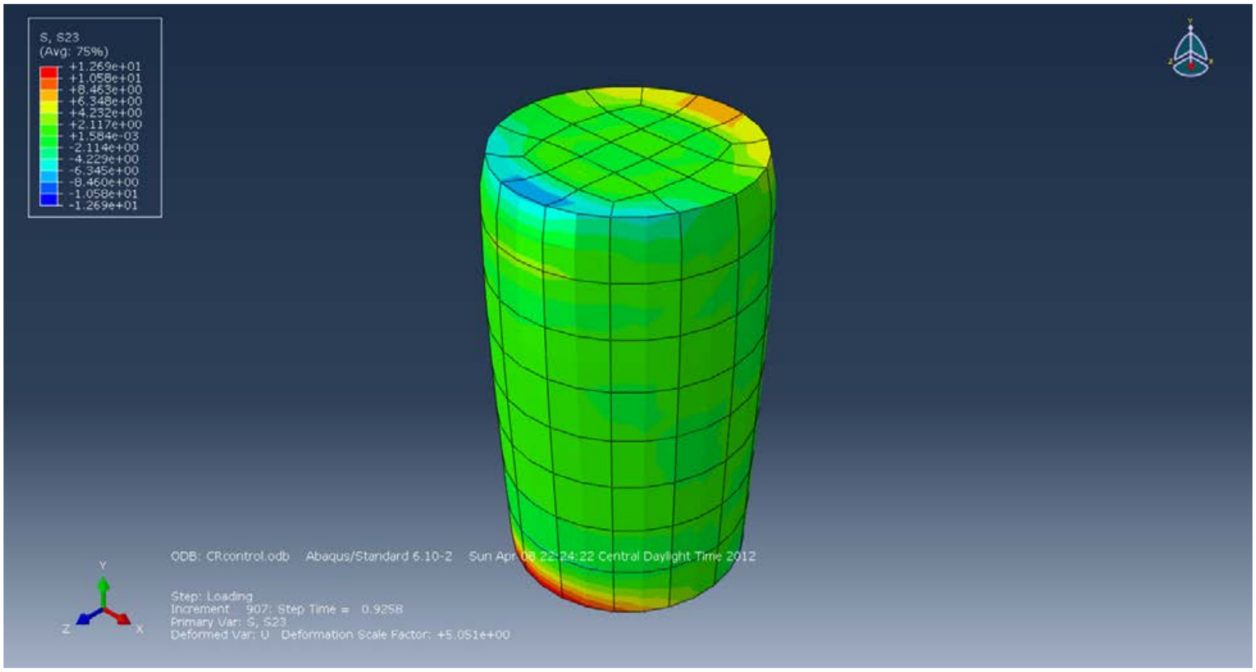

Figure B-140: Stress (S23) in the YZ-Direction (MPa).

- Smooth Boundaries:

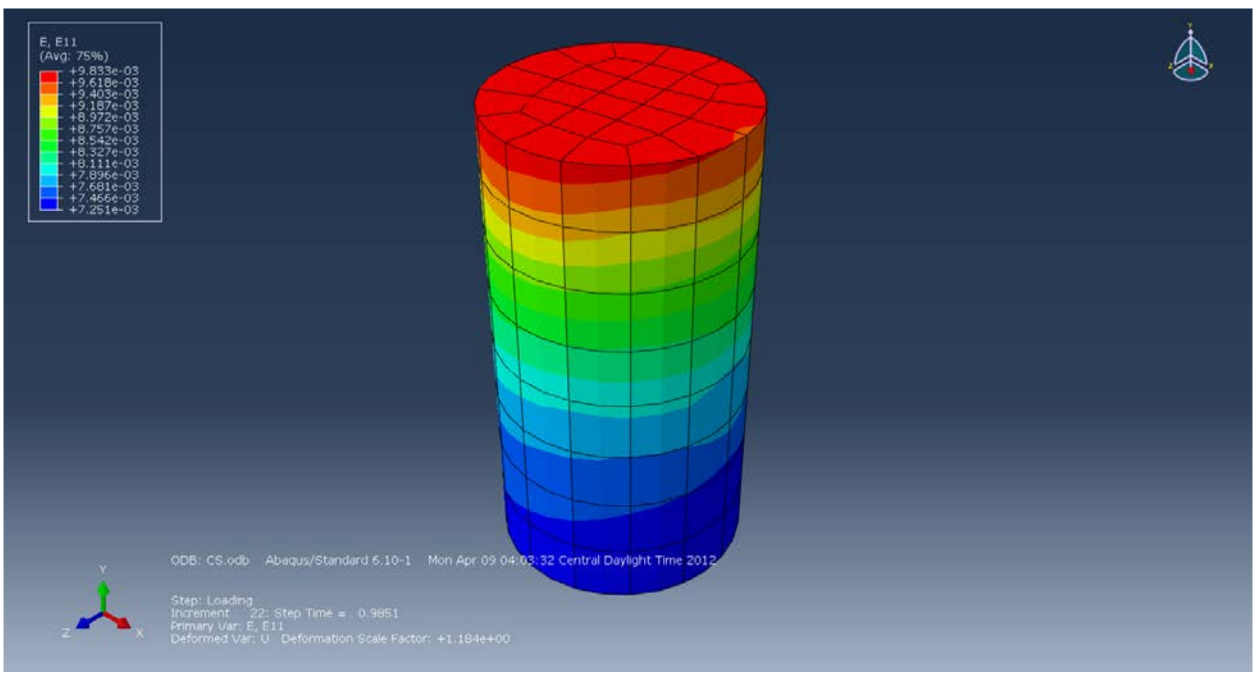

Figure B-141: Strain (E11) in the X-axis.

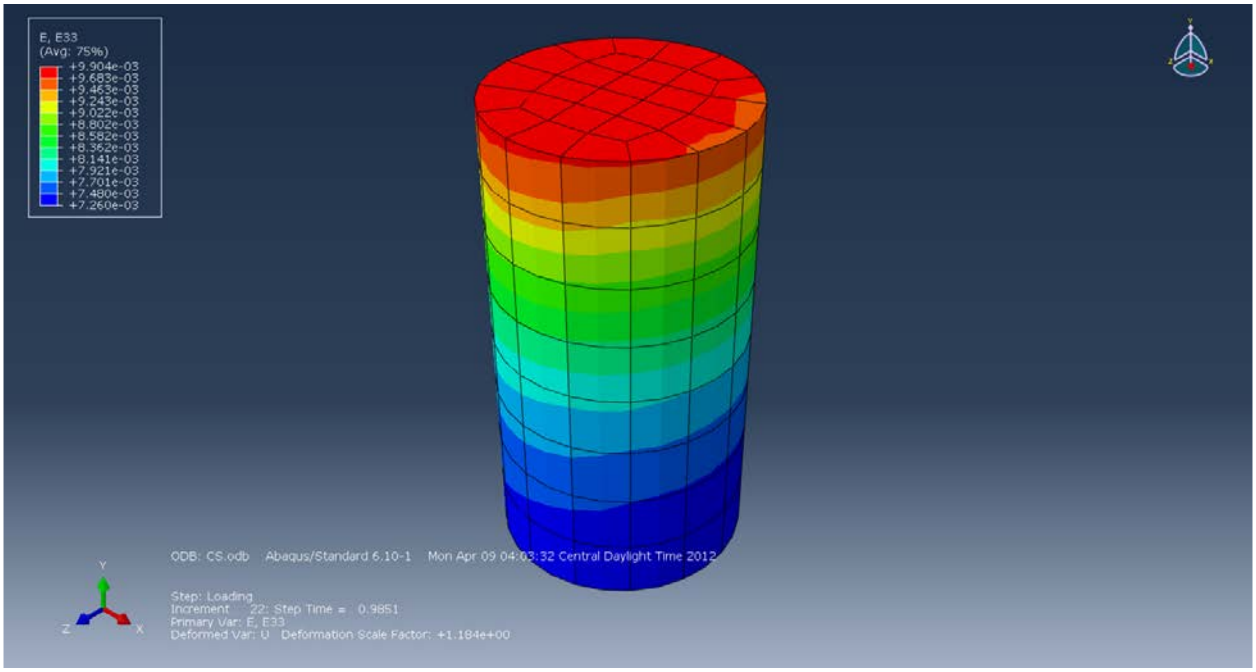

Figure B-142: Strain (E33) in the Z-axis.

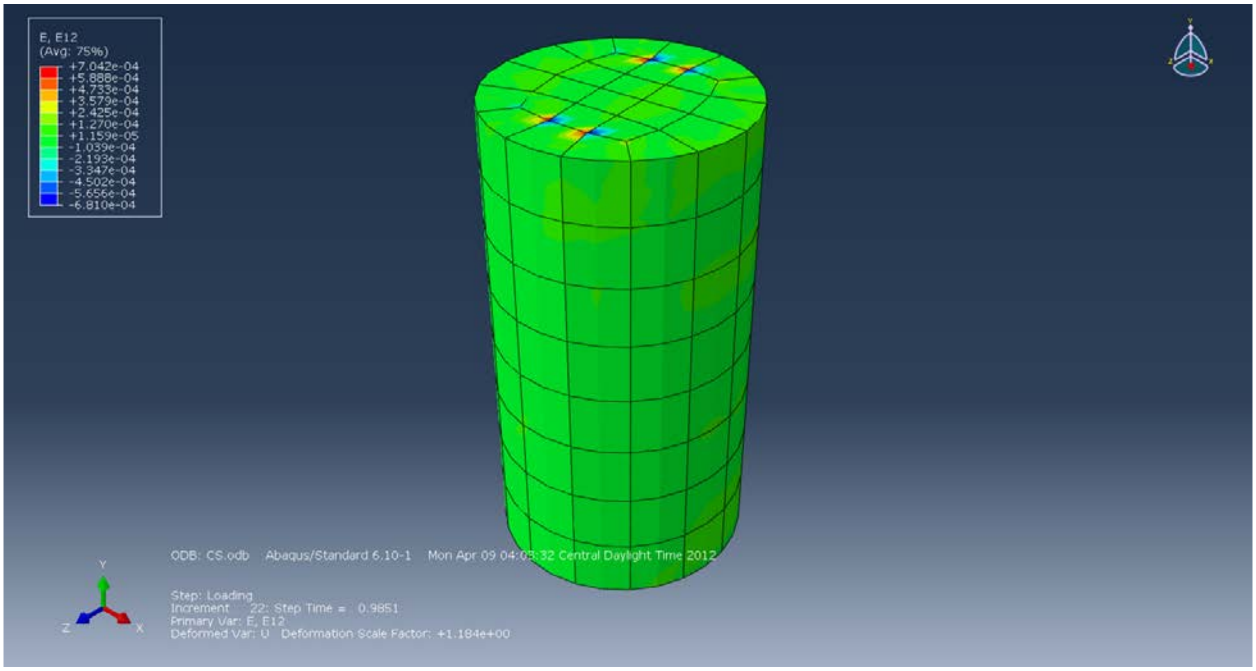

Figure B-143: Strain (E12) in the XY-Plane.

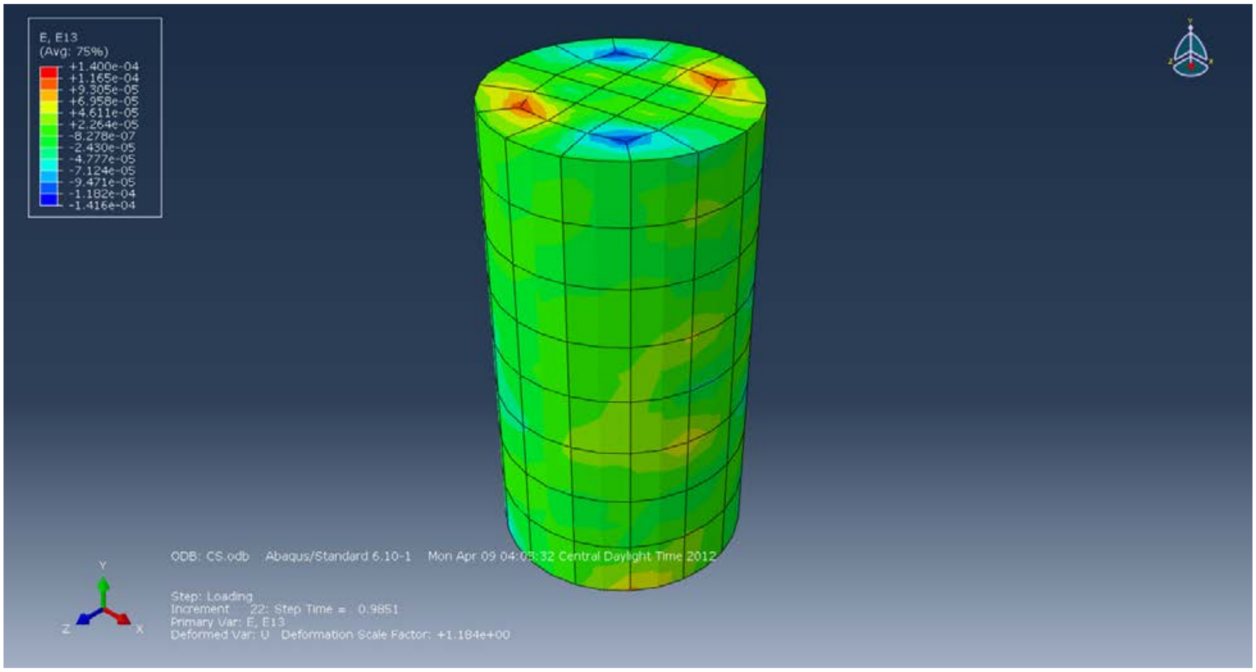

Figure B-144: Strain (E13) in the XZ-Plane.

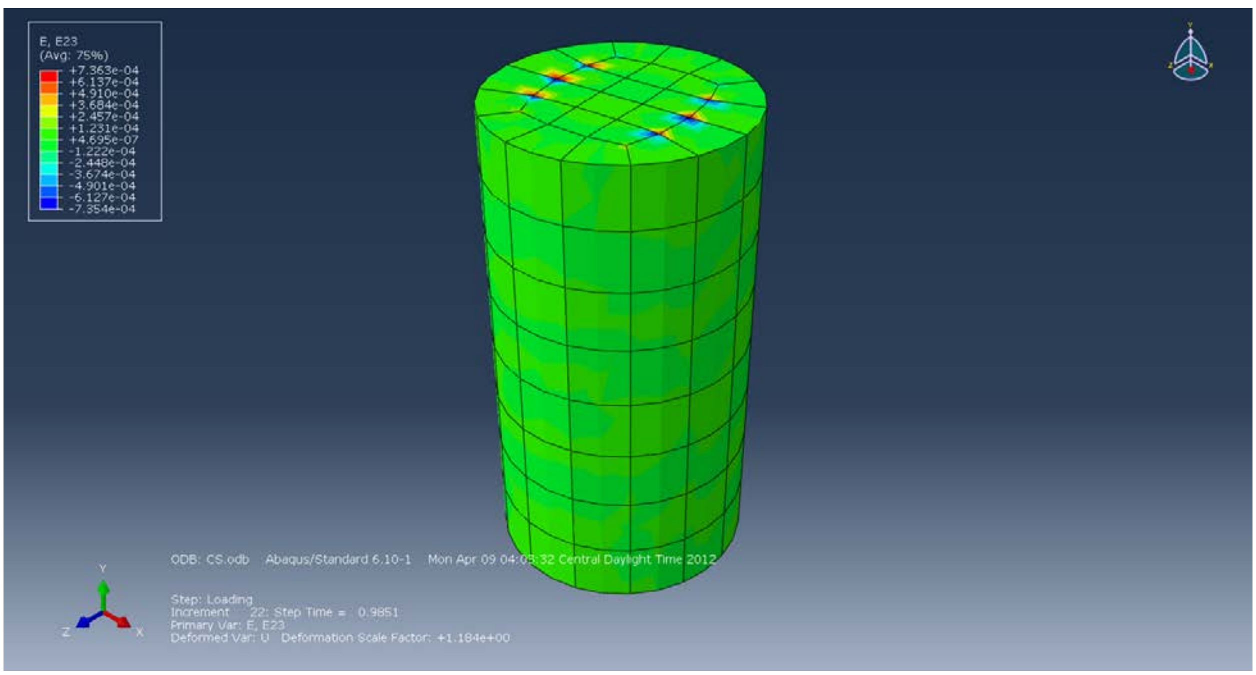

Figure B-145: Strain (E23) in the YZ-Plane.

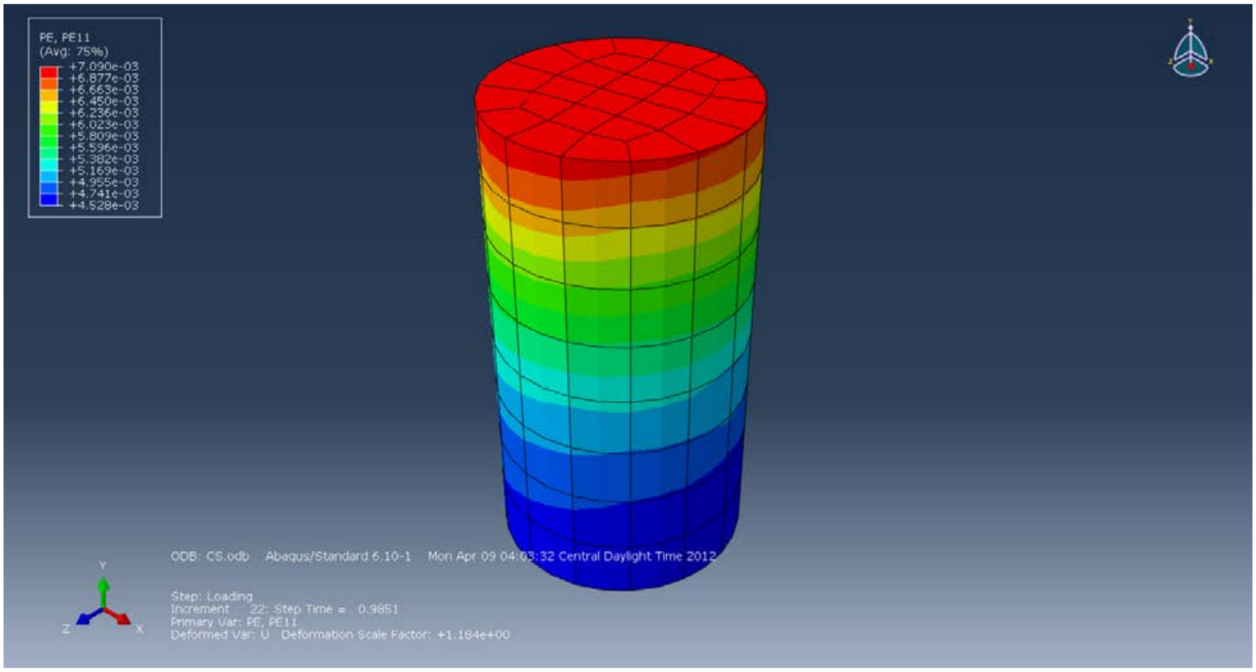

Figure B-146: Plastic Strain (PE11) in the X-axis.

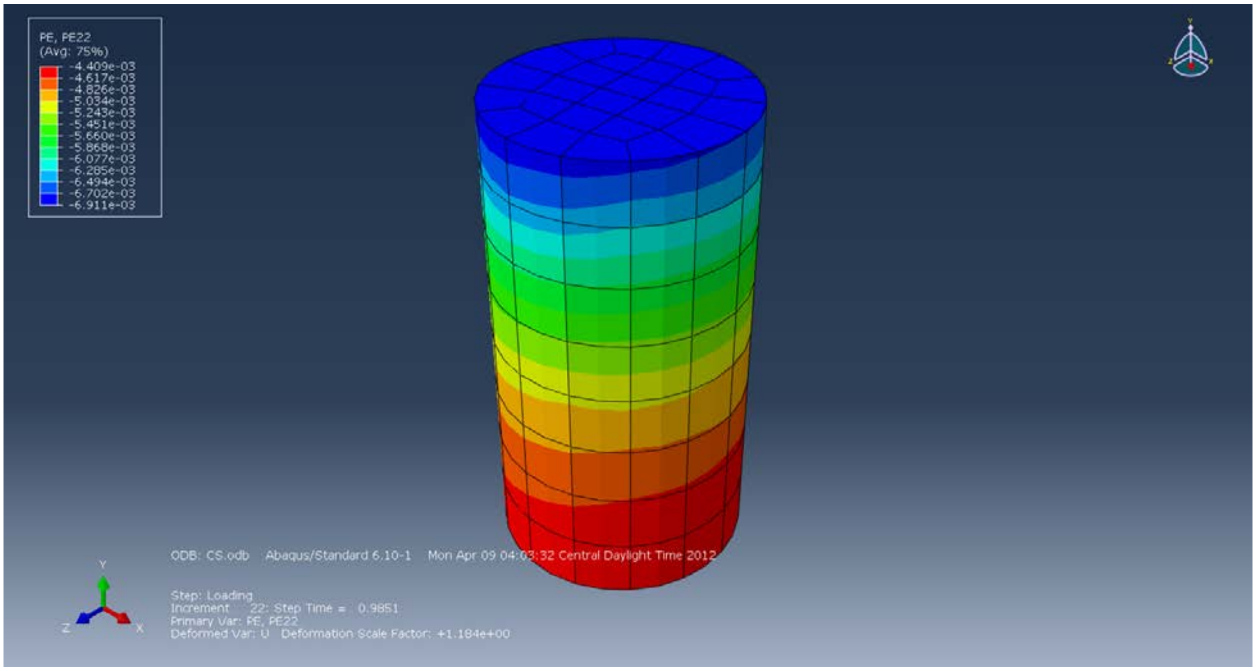

Figure B-147: Plastic Strain (PE22) in the Y-axis.

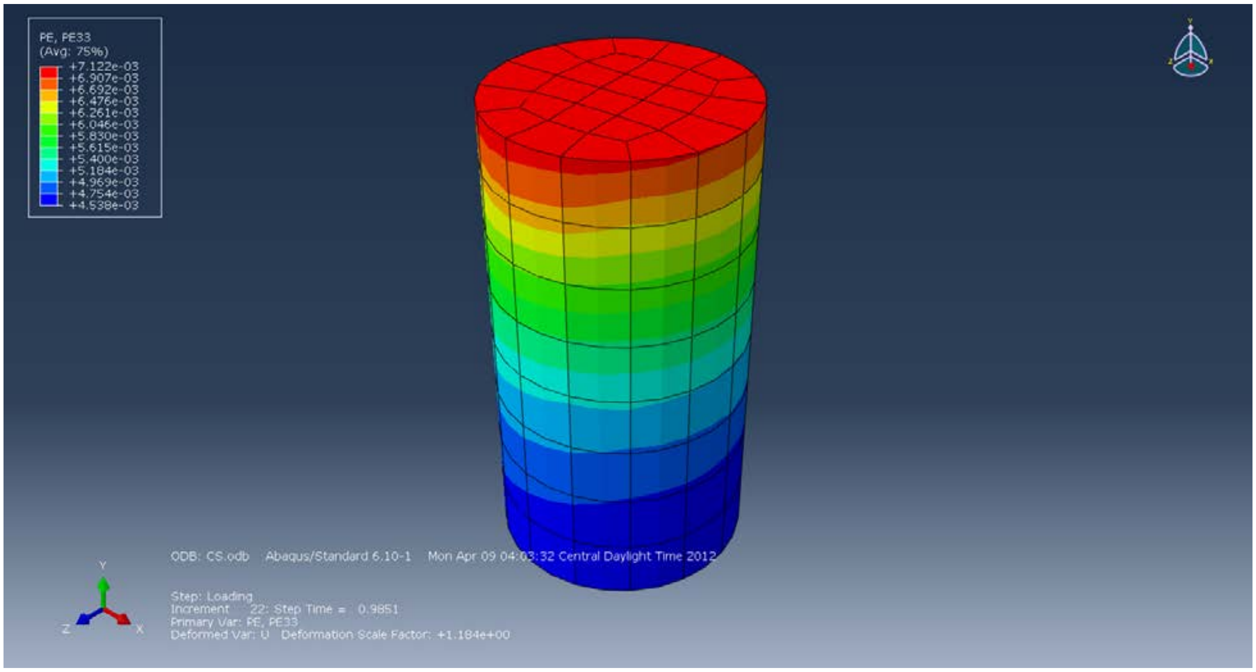

Figure B-148: Plastic Strain (PE33) in the Z-axis.

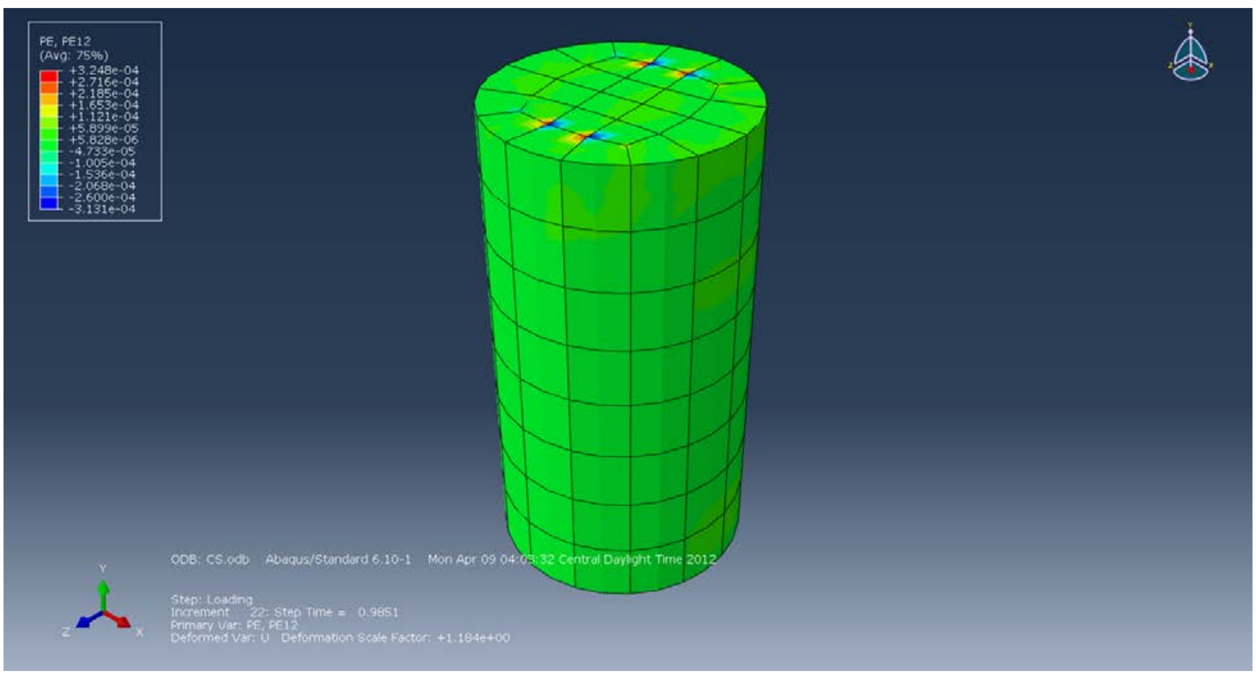

Figure B-149: Plastic Strain (PE12) in the XY-Plane.

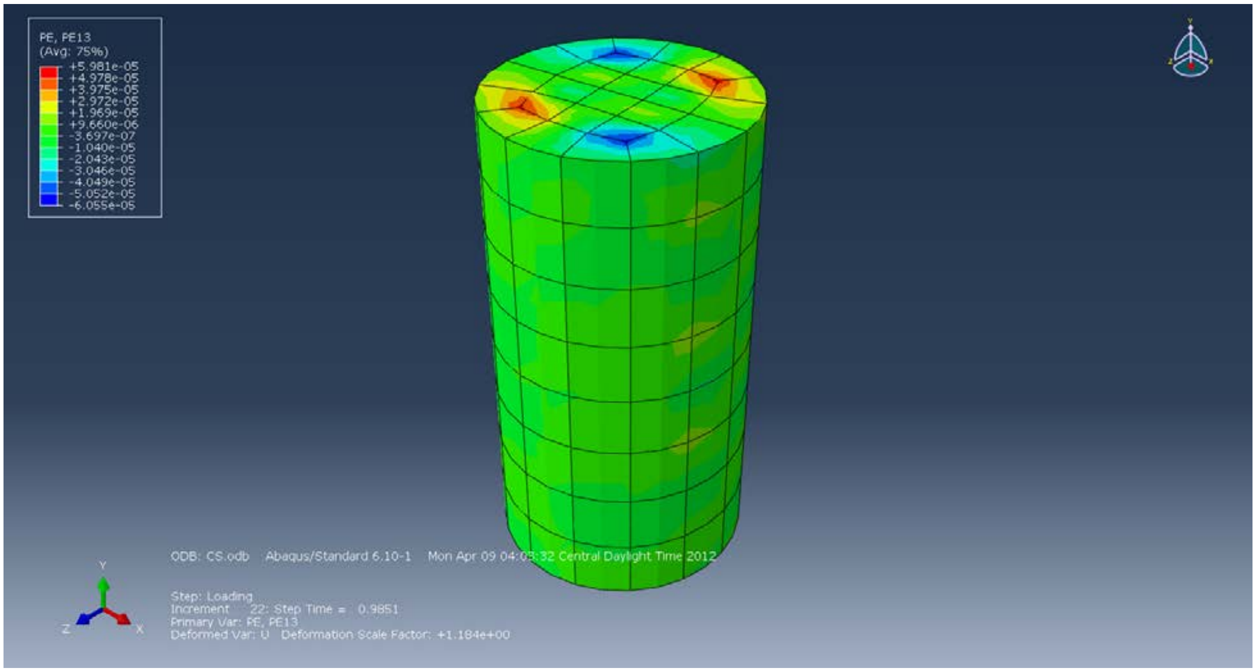

Figure B-150: Plastic Strain (PE13) in the XZ-Plane.

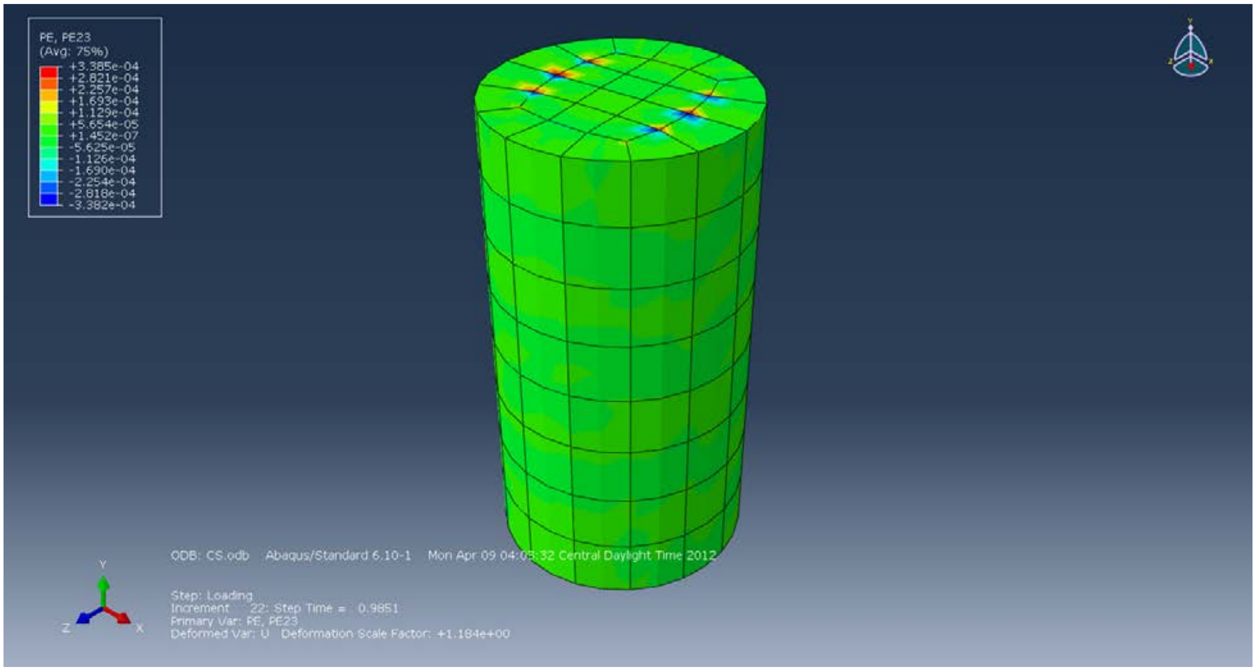

Figure B-151: Plastic Strain (PE23) in the YZ-Plane.

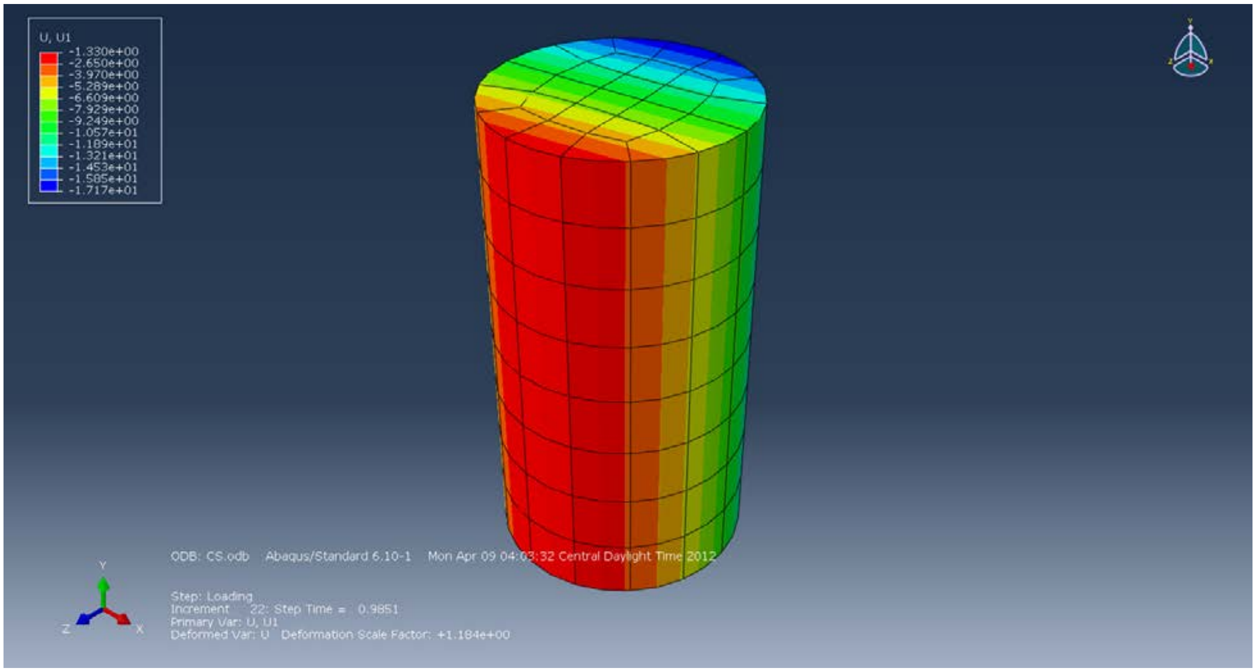

Figure B-152: Displacement (U1) in the X-axis (mm).

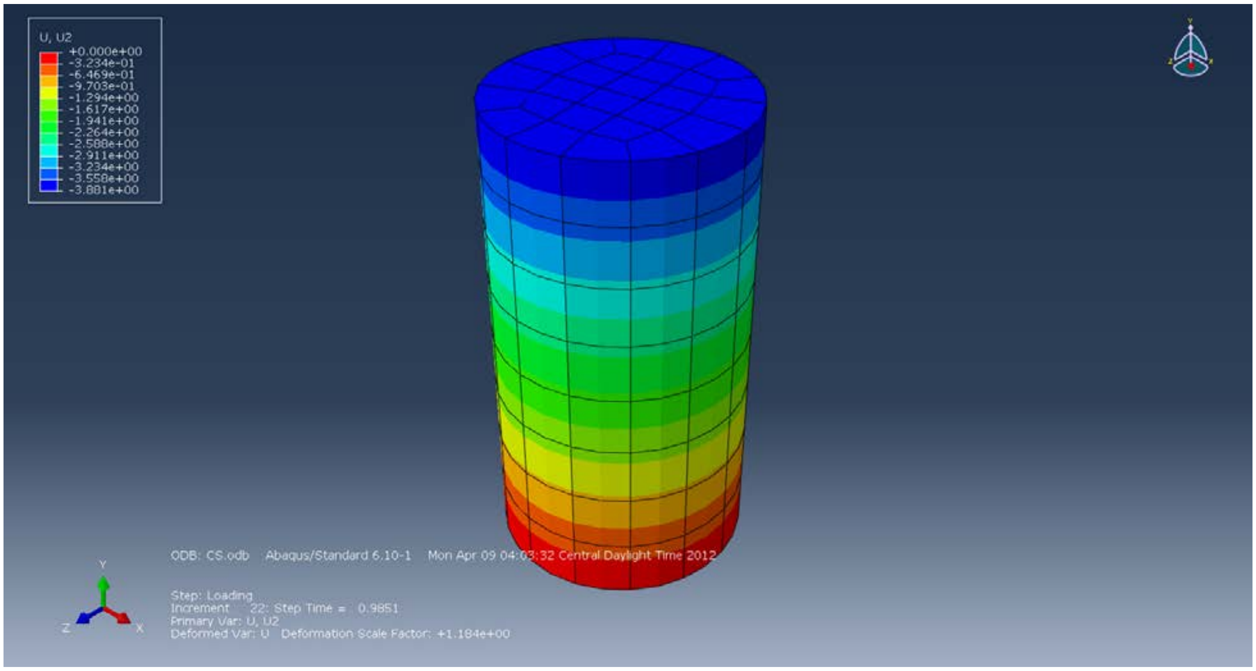

Figure B-153: Displacement (U2) in the Y-axis (mm).

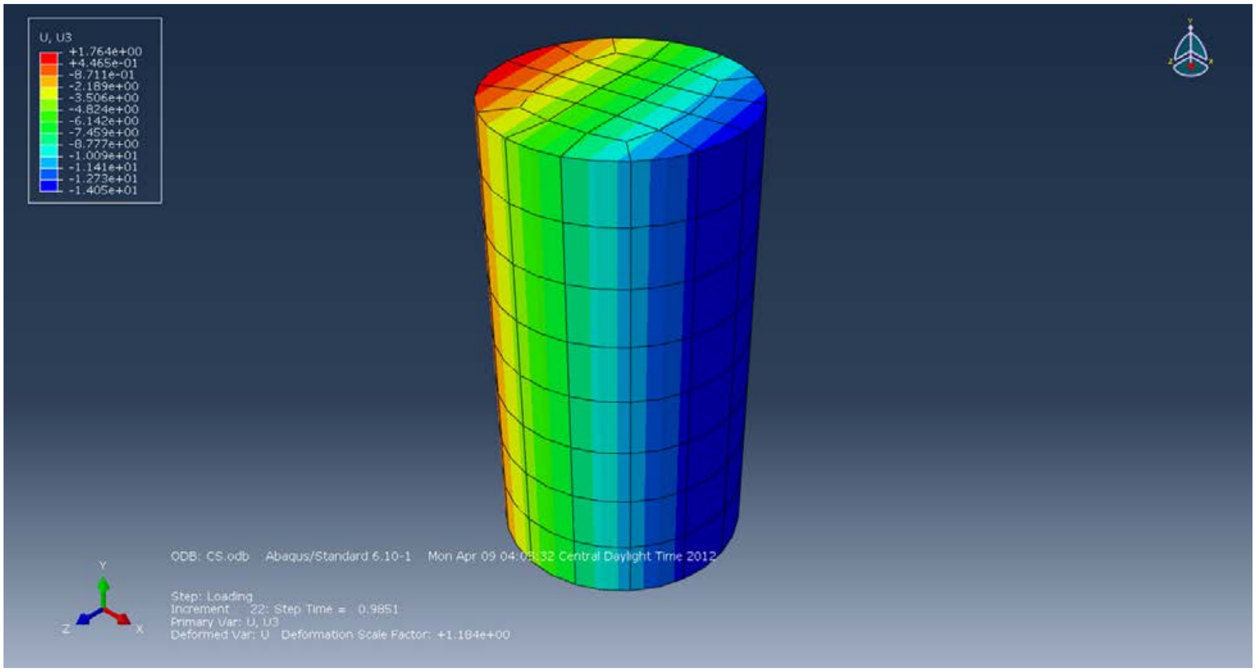

Figure B-154: Displacement (U3) in the Z-axis (mm).

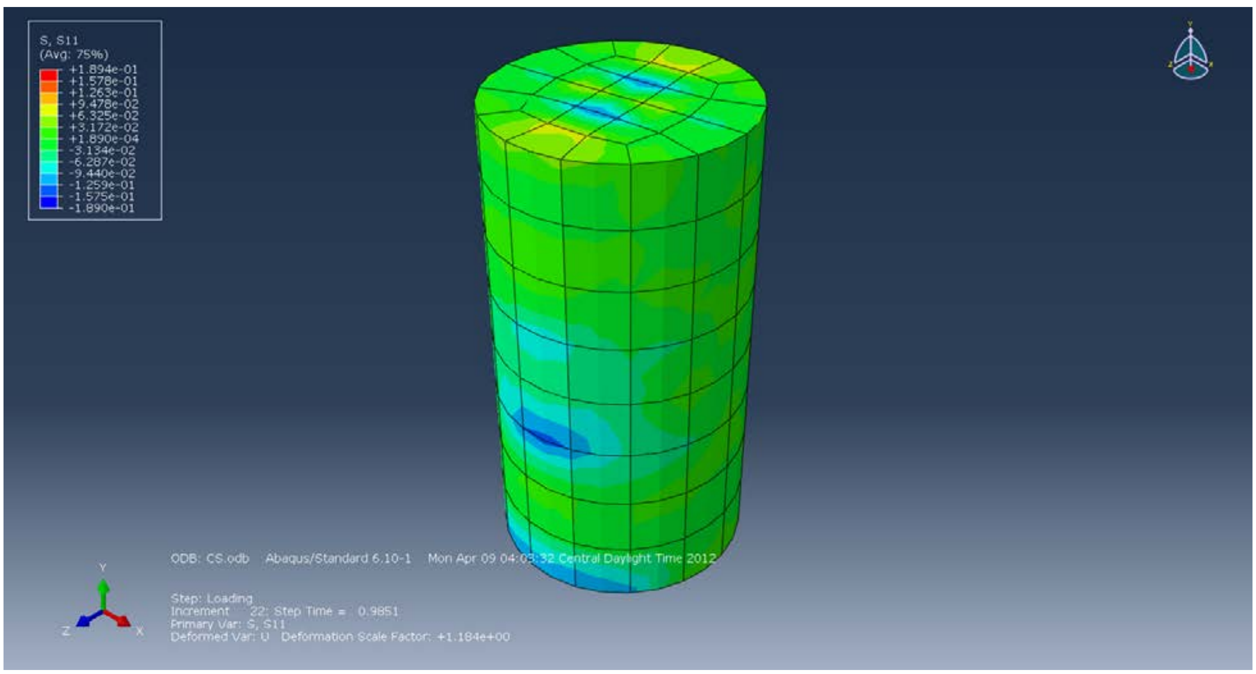

Figure B-155: Stress (S11) in the X-Direction (MPa).

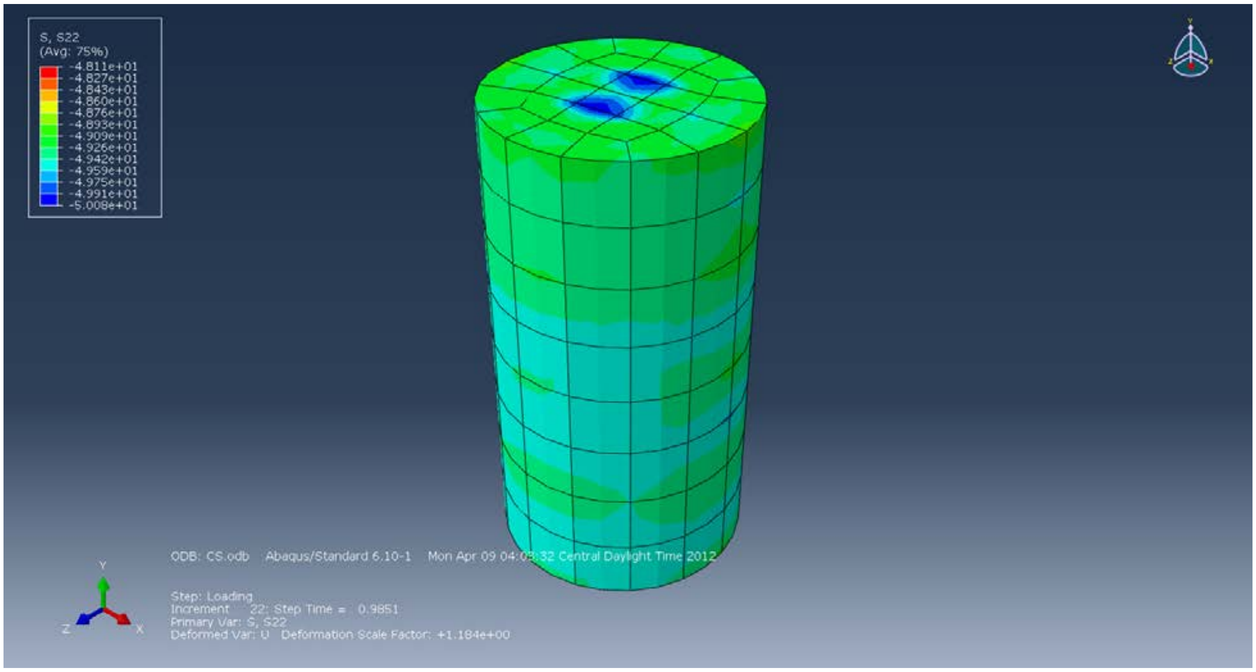

Figure B-156: Stress (S22) in the Y-Direction (MPa).

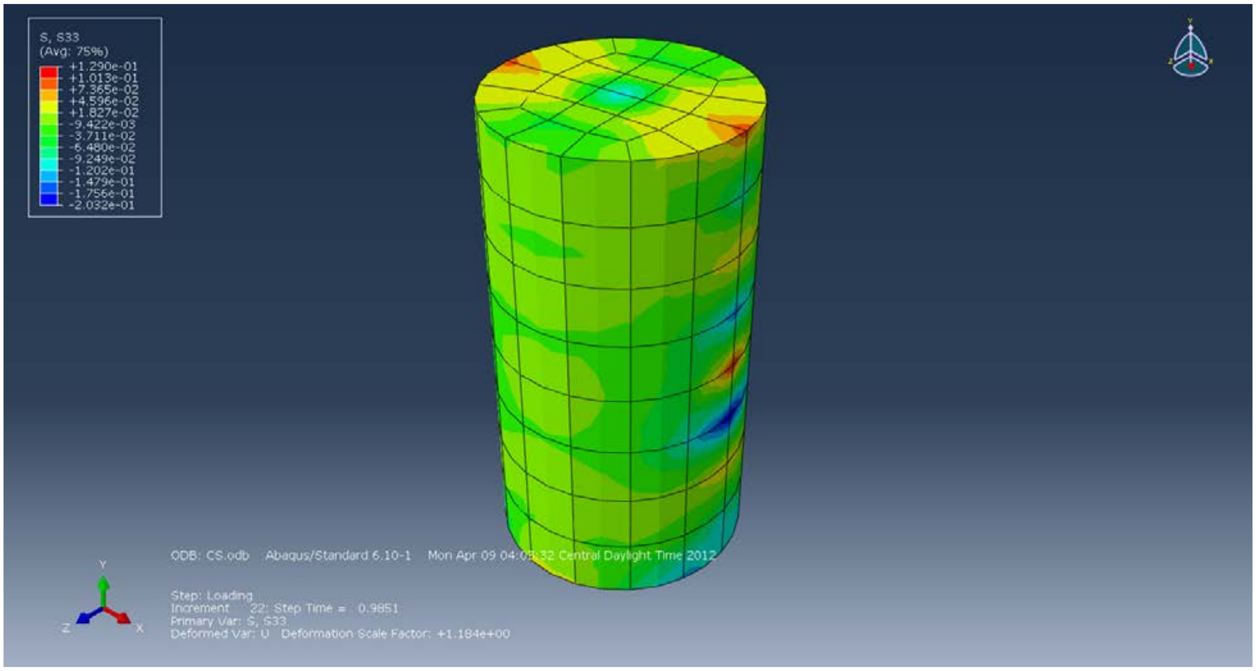

Figure B-157: Stress (S33) in the Z-Direction (MPa).

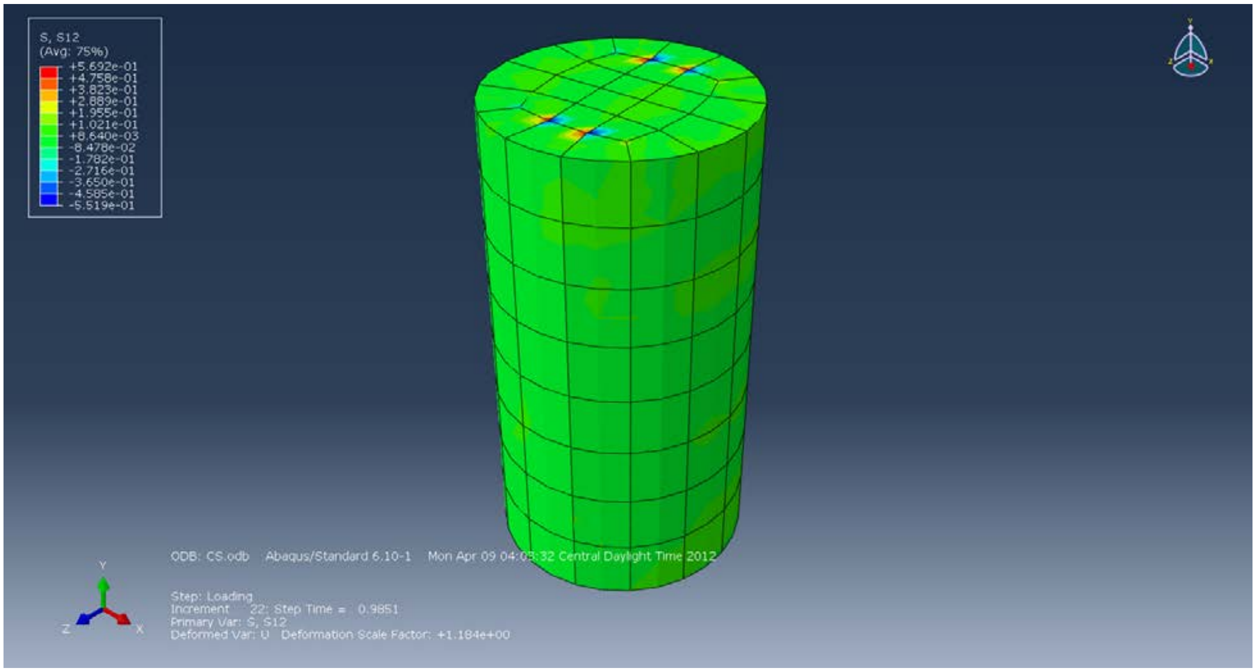

Figure B-158: Stress (S12) in the XY-Direction (MPa).

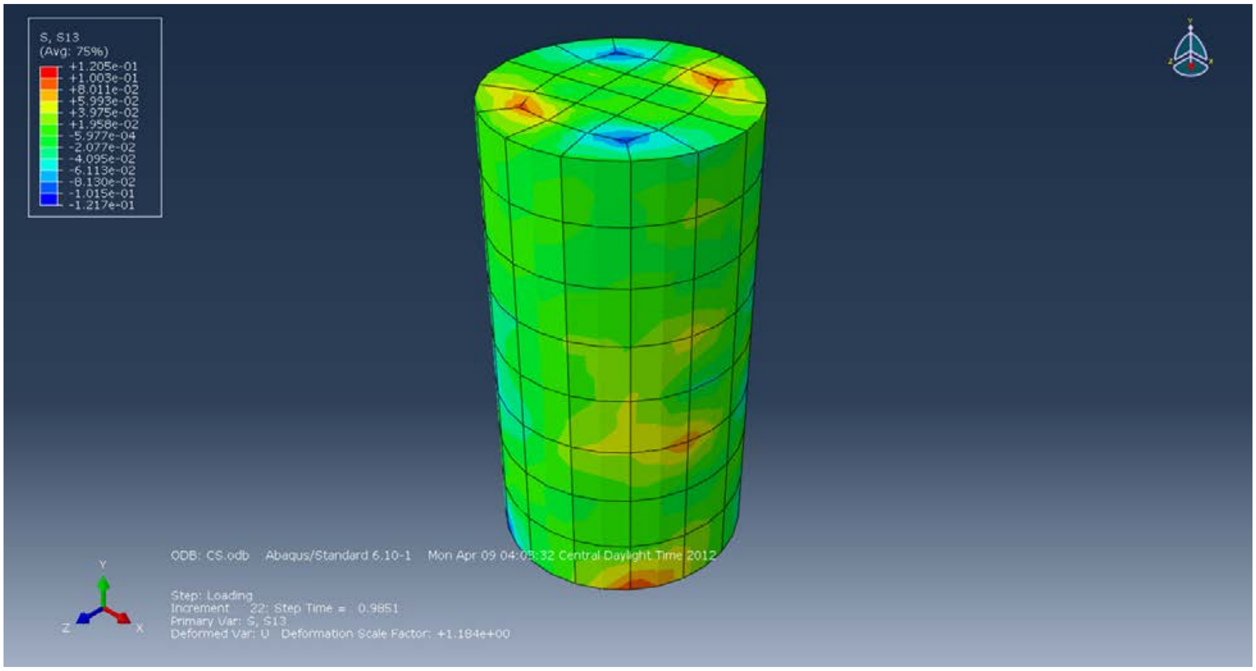

Figure B-159: Stress (S13) in the XZ-Direction (MPa).

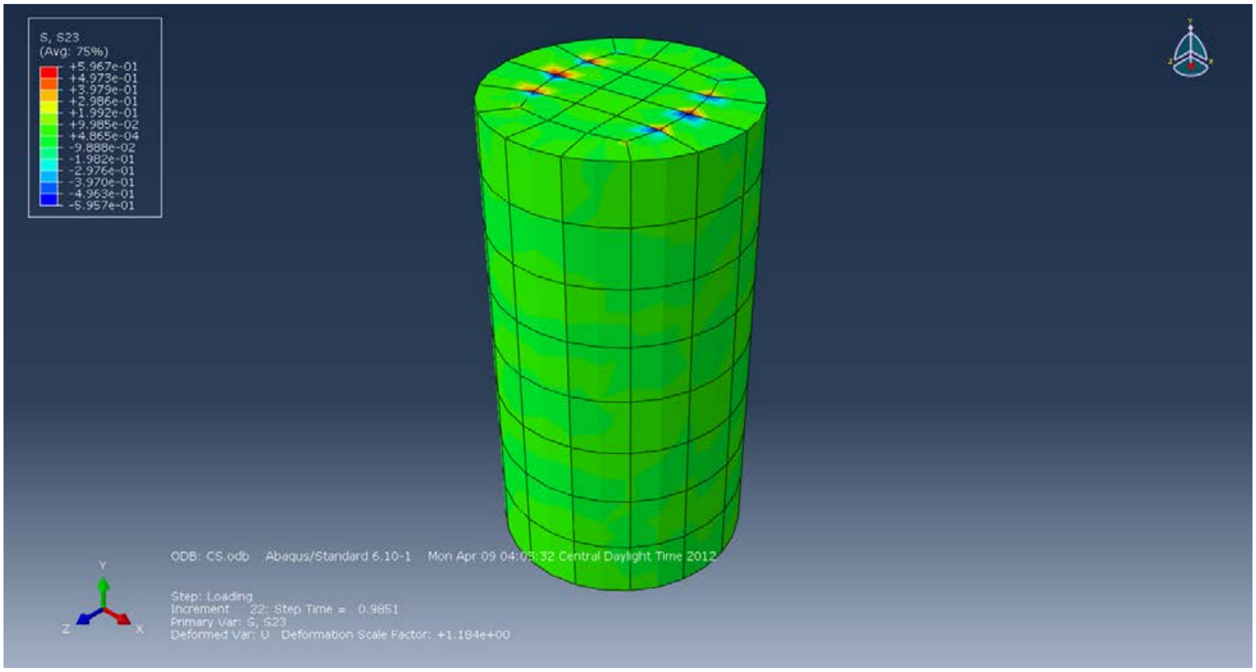

Figure B-160: Stress (S23) in the YZ-Direction (MPa).

Control Prisms:

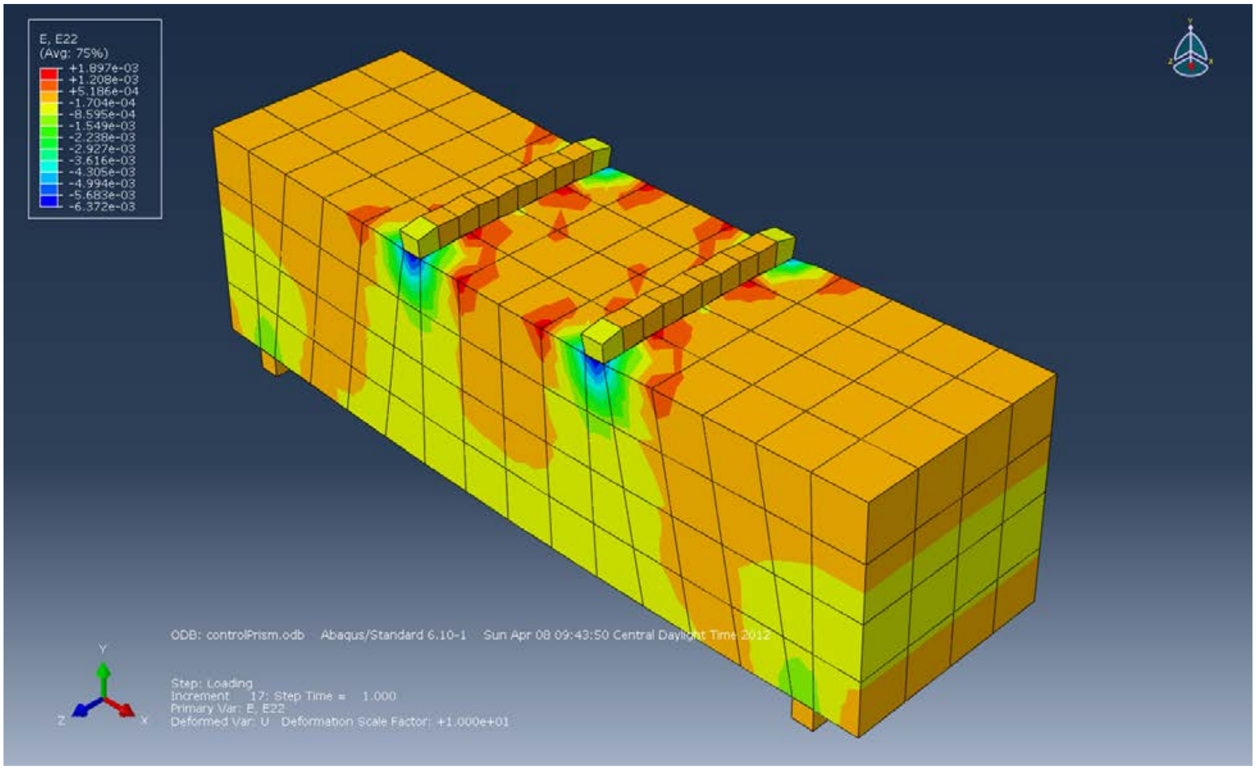

Figure B-161: Strain (E22) in the Y-axis.

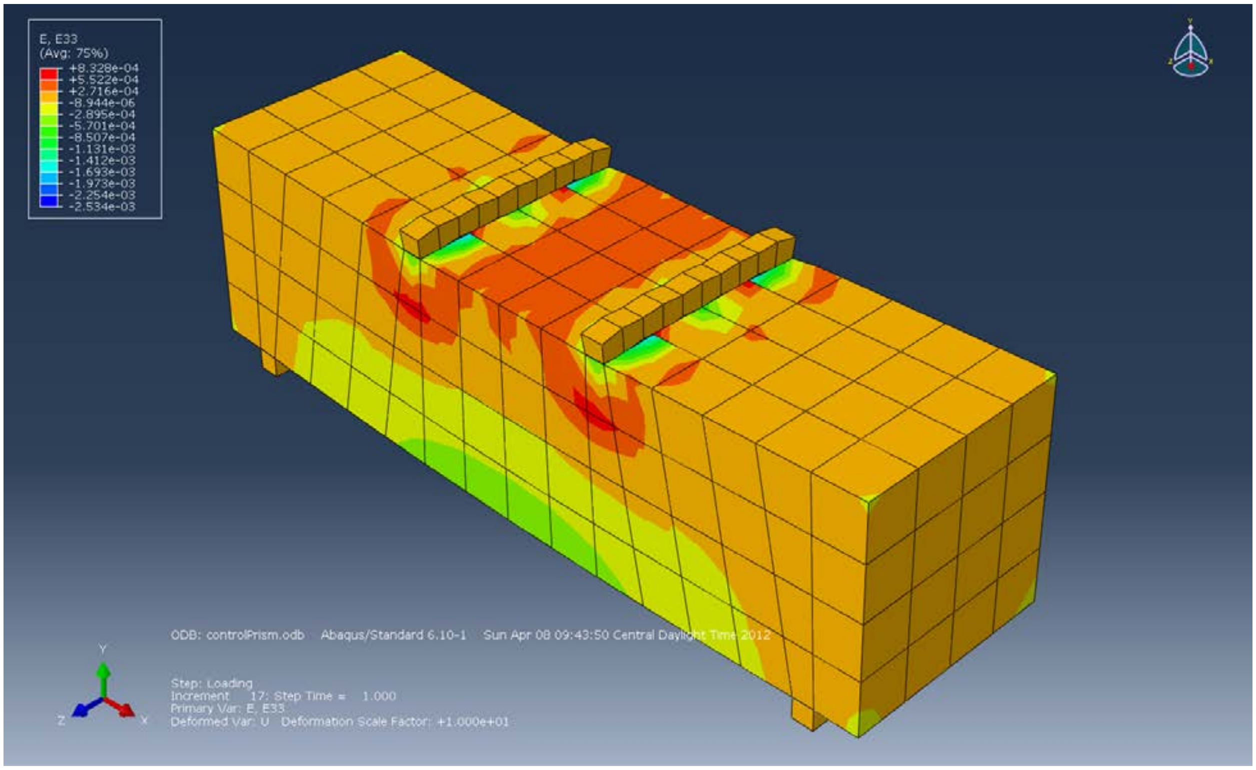

Figure B-162: Strain (E33) in the Z-axis.

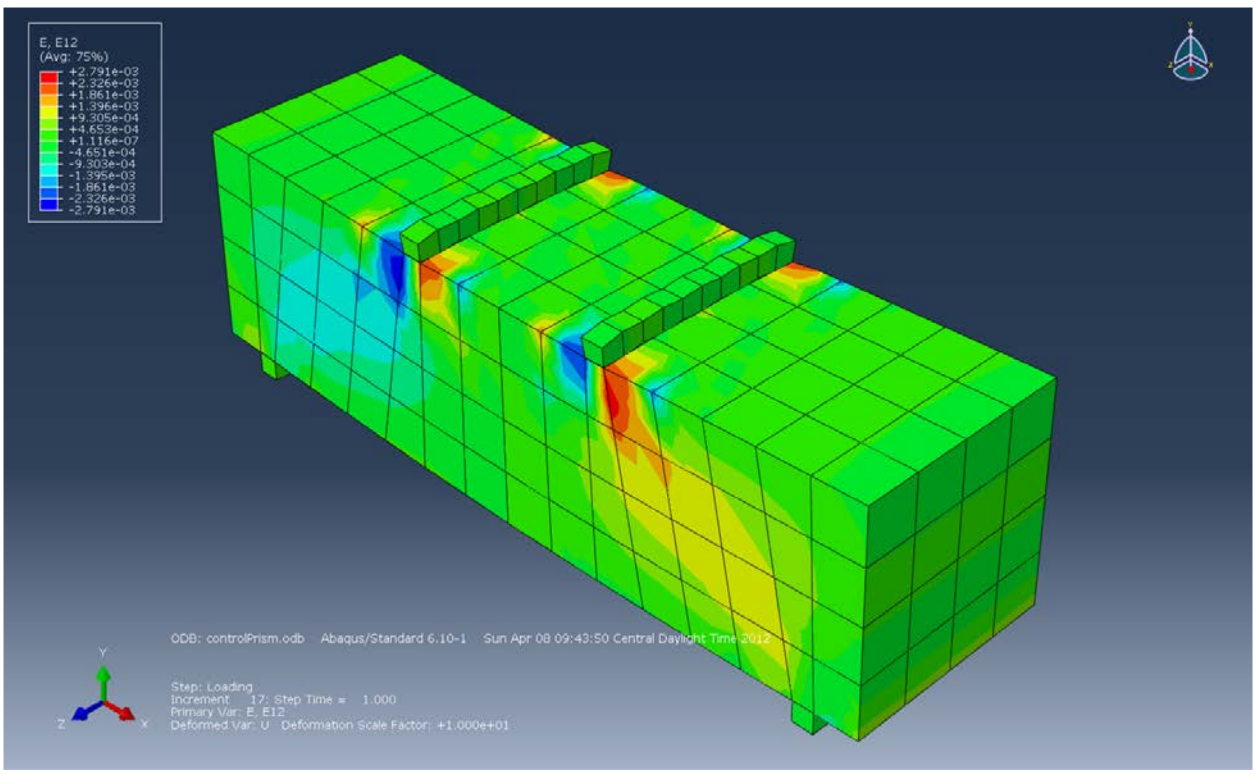

Figure B-163: Strain (E12) in the XY-Plane.

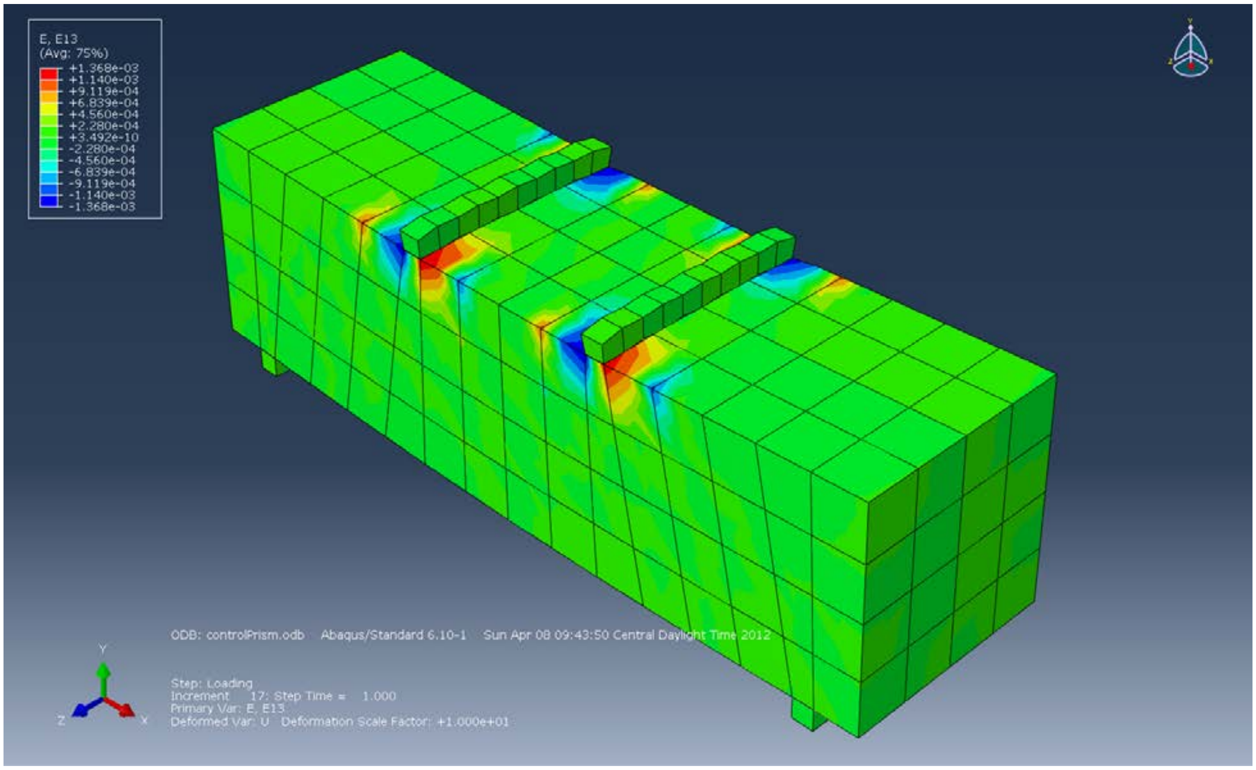

Figure B-164: Strain (E13) in the XZ-Plane.

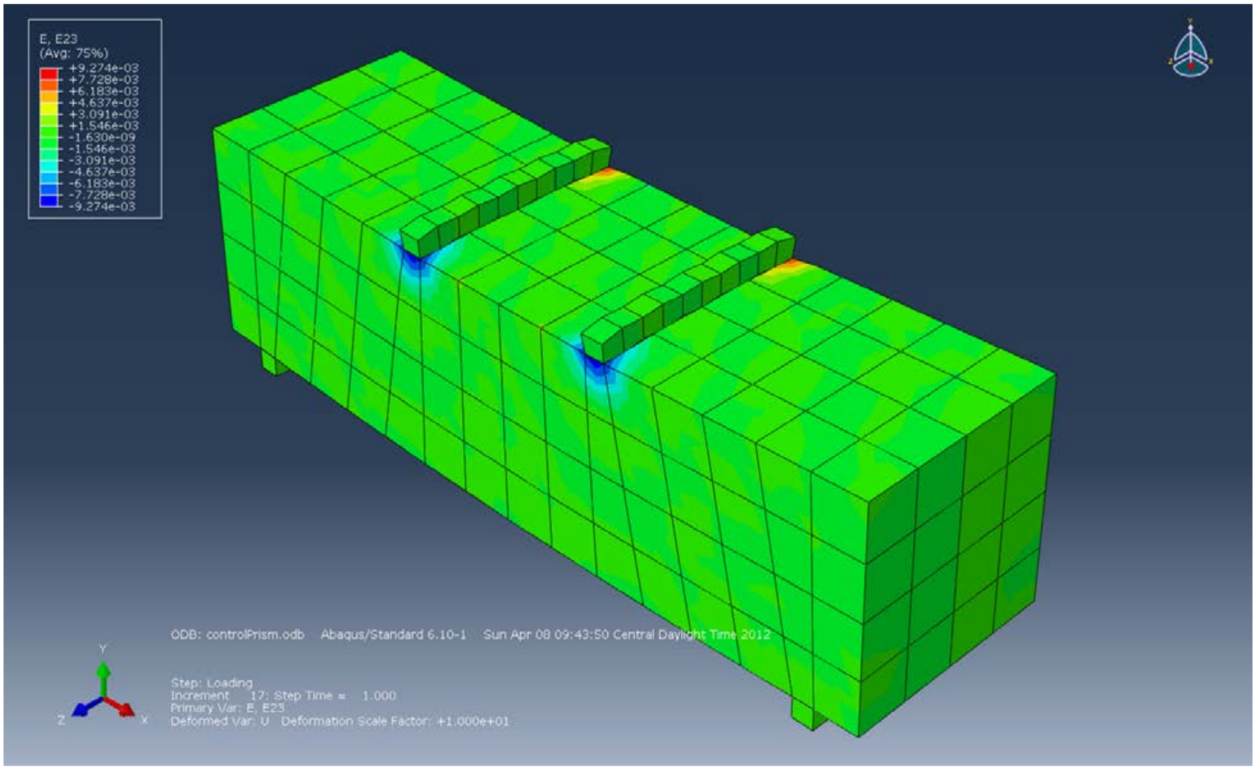

Figure B-165: Strain (E23) in the YZ-Plane.

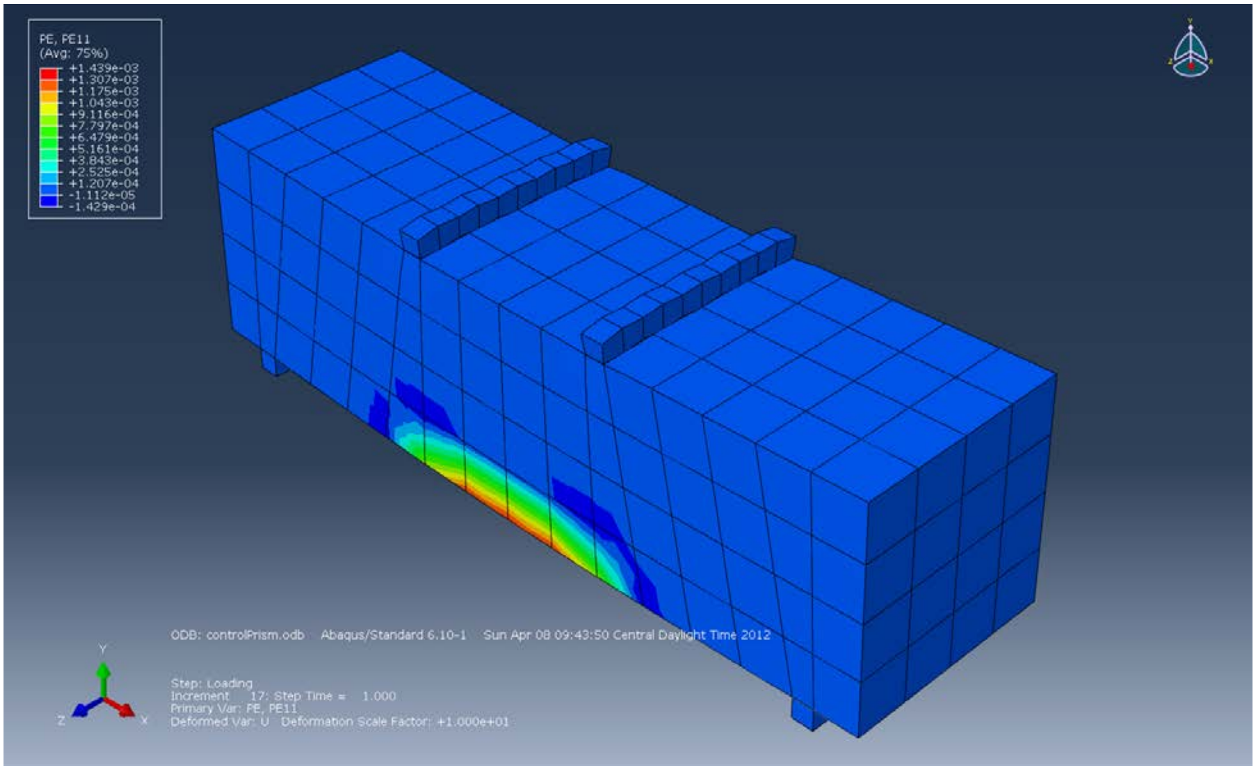

Figure B-166: Plastic Strain (PE11) in the X-axis.

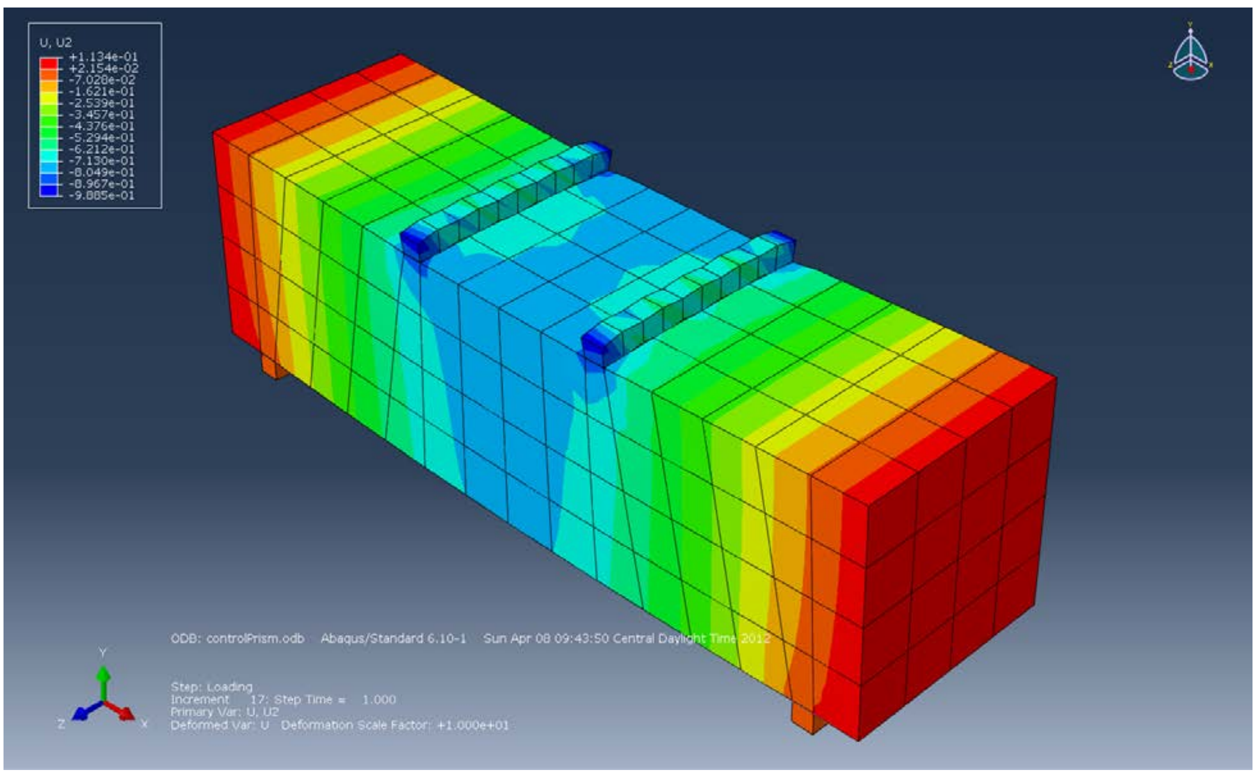

Figure B-167: Displacement (U2) in the Y-axis (mm).

Prisms with 0.5% Wheat Fibers:

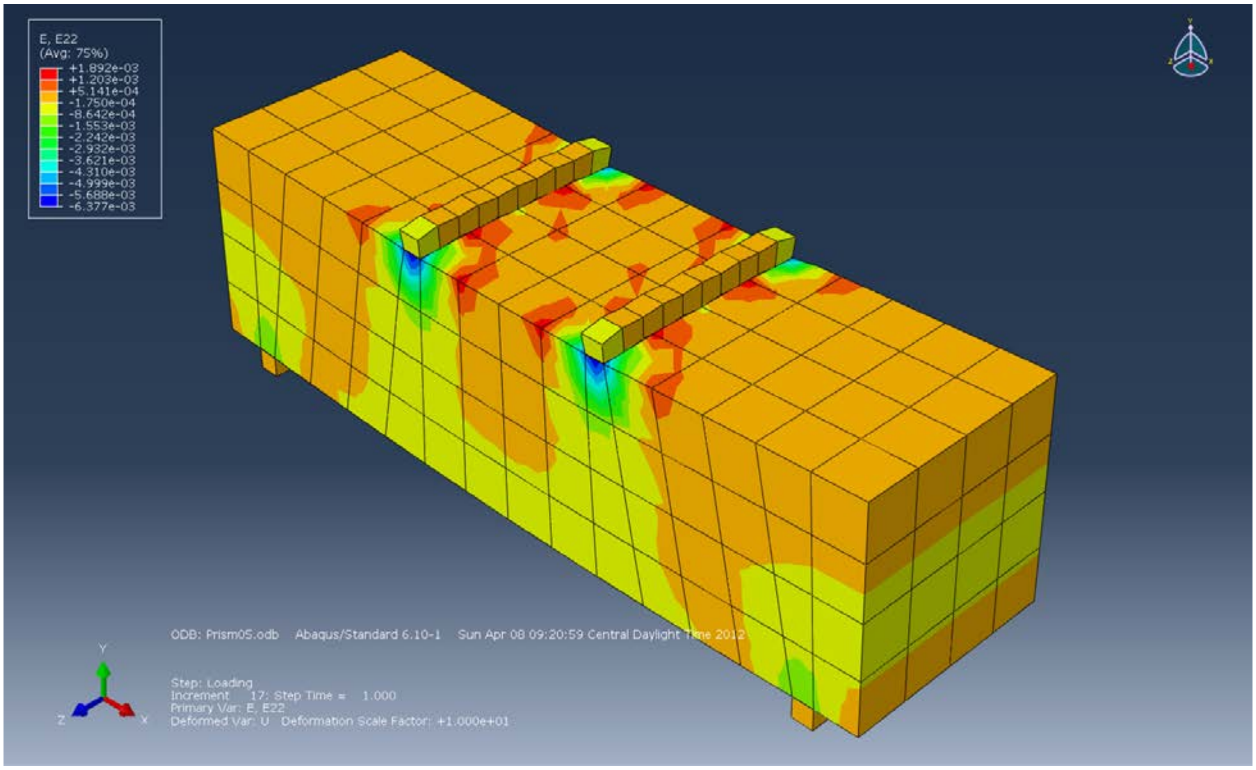

Figure B-168: Strain (E22) in the Y-axis.

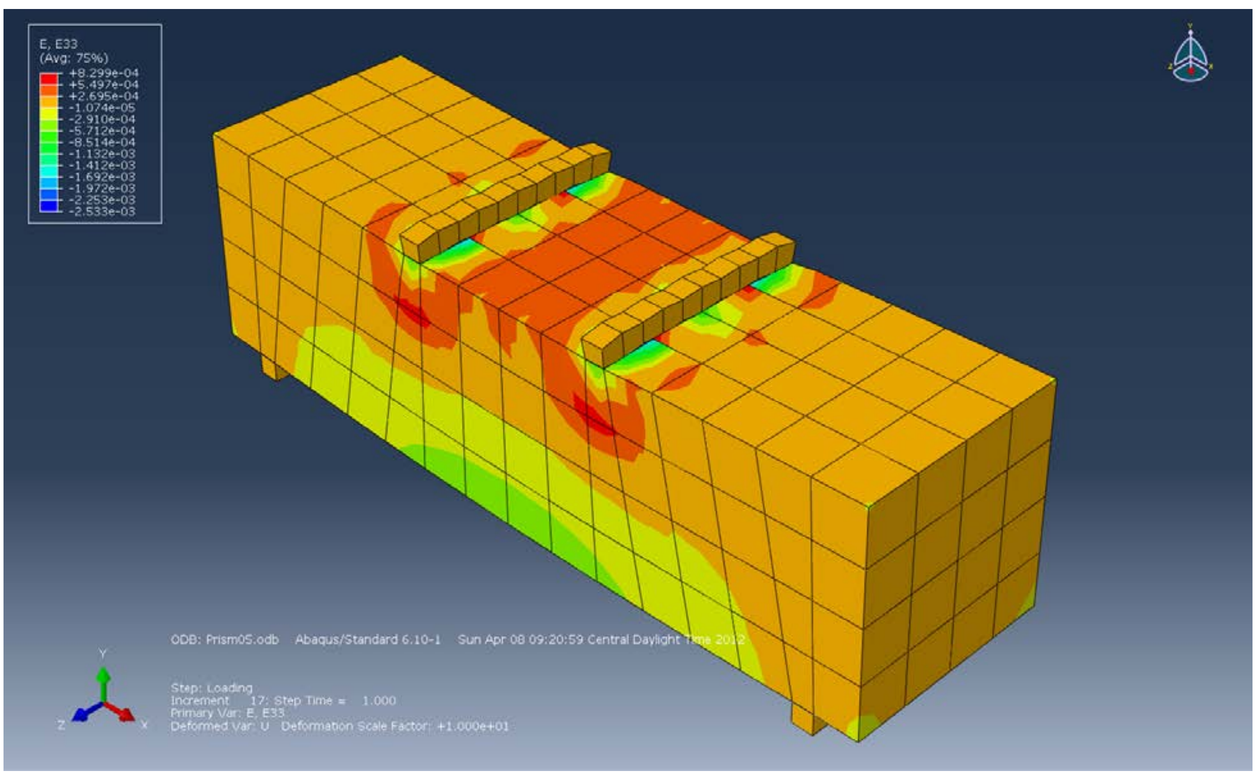

Figure B-169: Strain (E33) in the Z-axis.

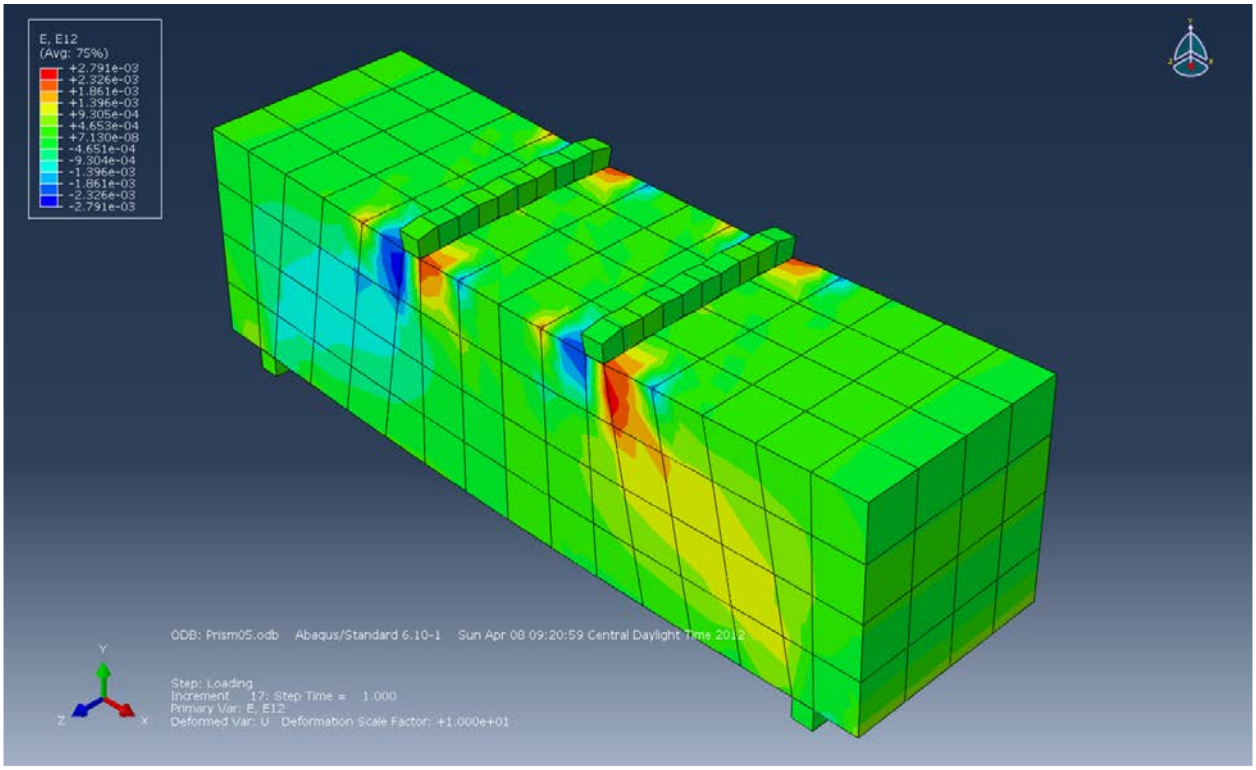

Figure B-170: Strain (E12) in the XY-Plane.

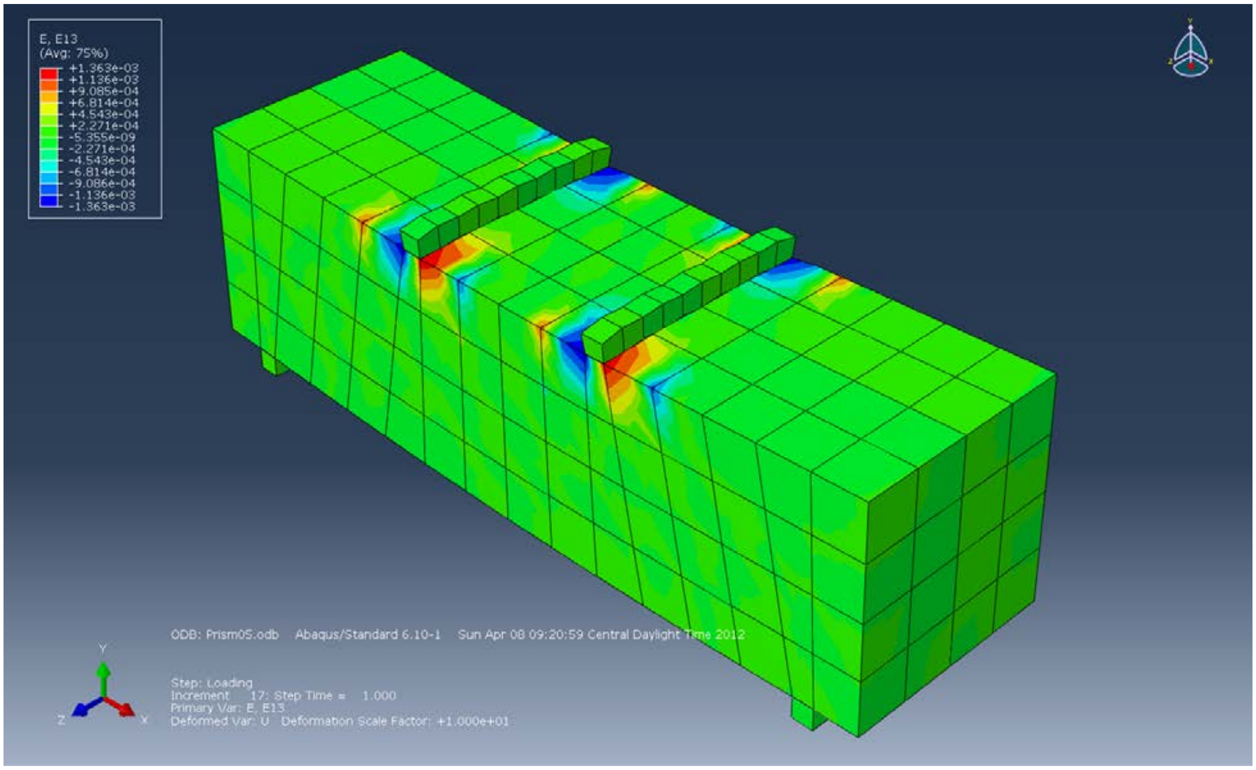

Figure B-171: Strain (E13) in the XZ-Plane.

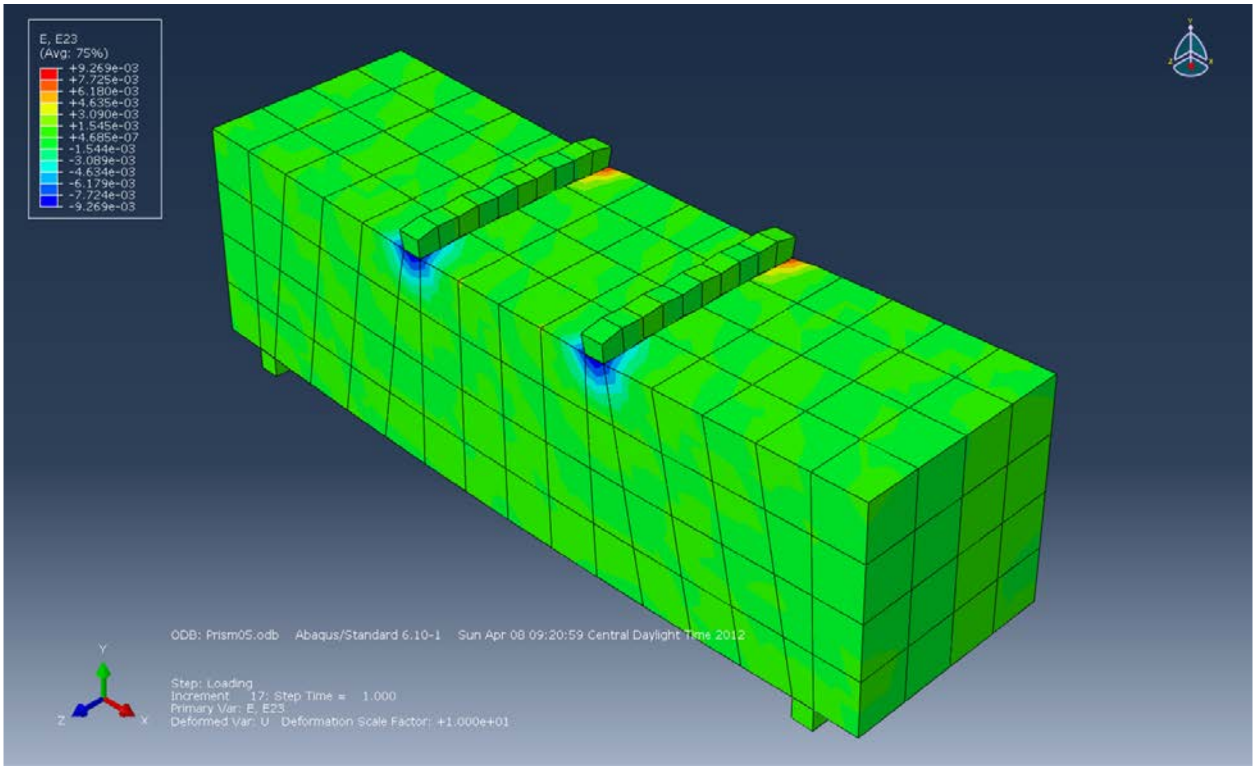

Figure B-172: Strain (E23) in the YZ-Plane.

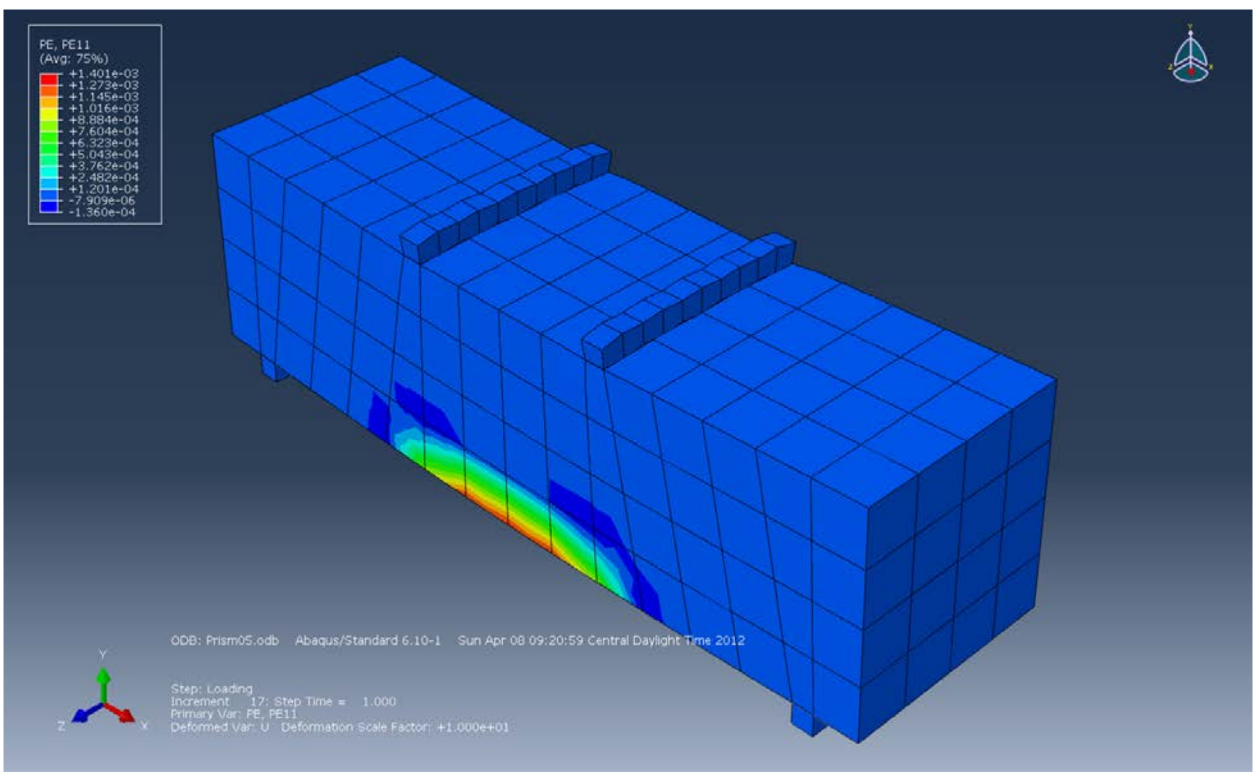

Figure B-173: Plastic Strain (PE11) in the X-axis.

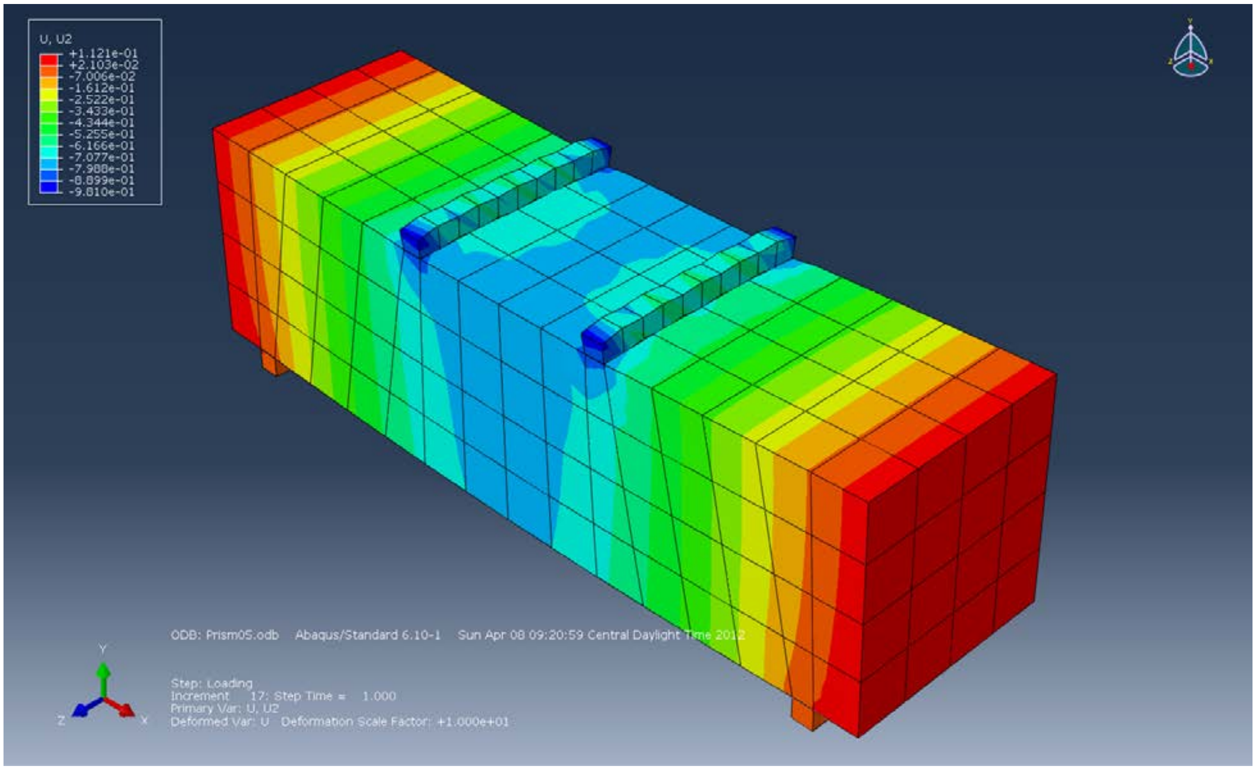

Figure B-174: Displacement (U2) in the Y-axis (mm).

Prisms with 0.75% Wheat Fibers:

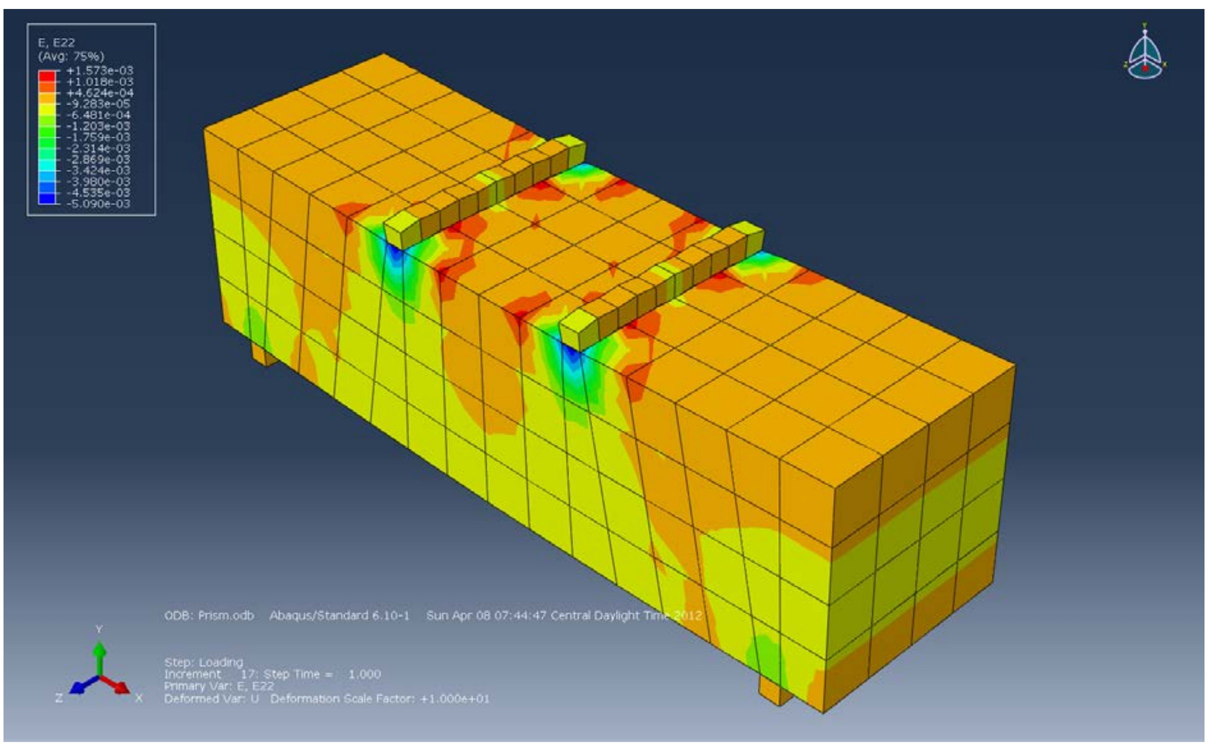

Figure B-175: Strain (E22) in the Y-axis.

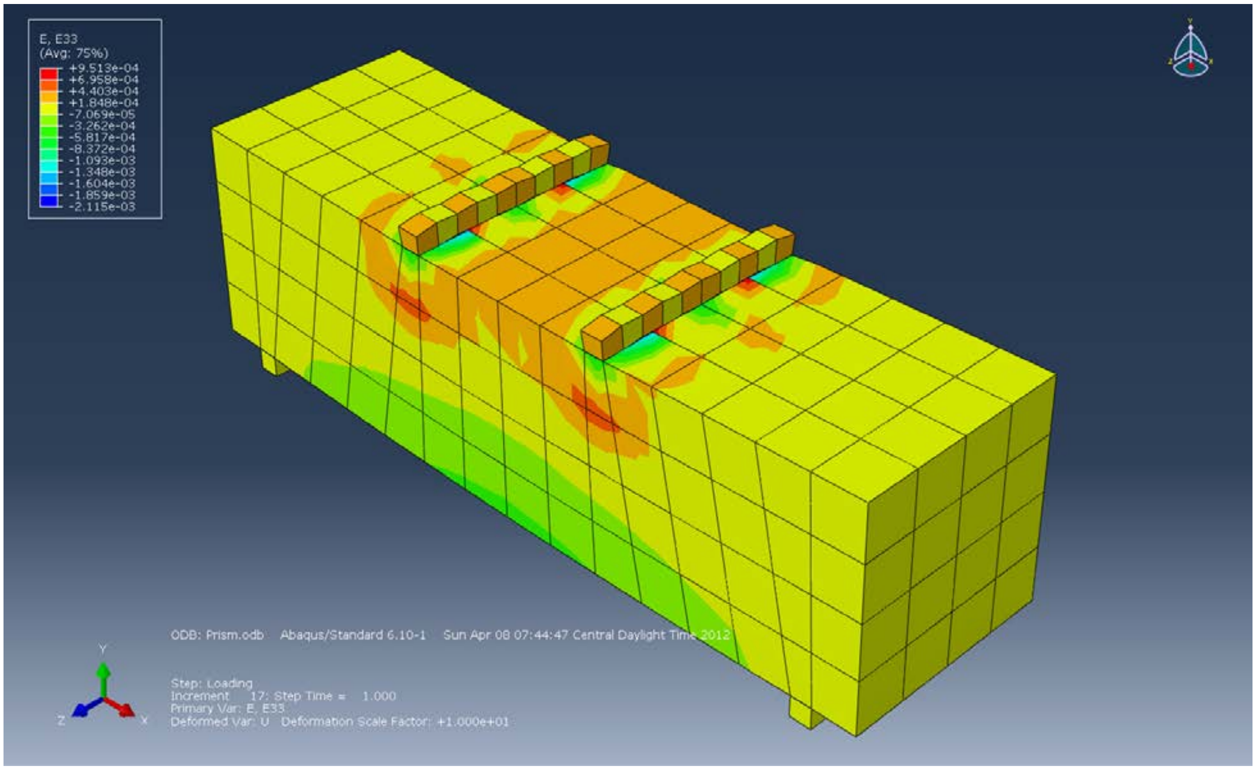

Figure B-176: Strain (E33) in the Z-axis.

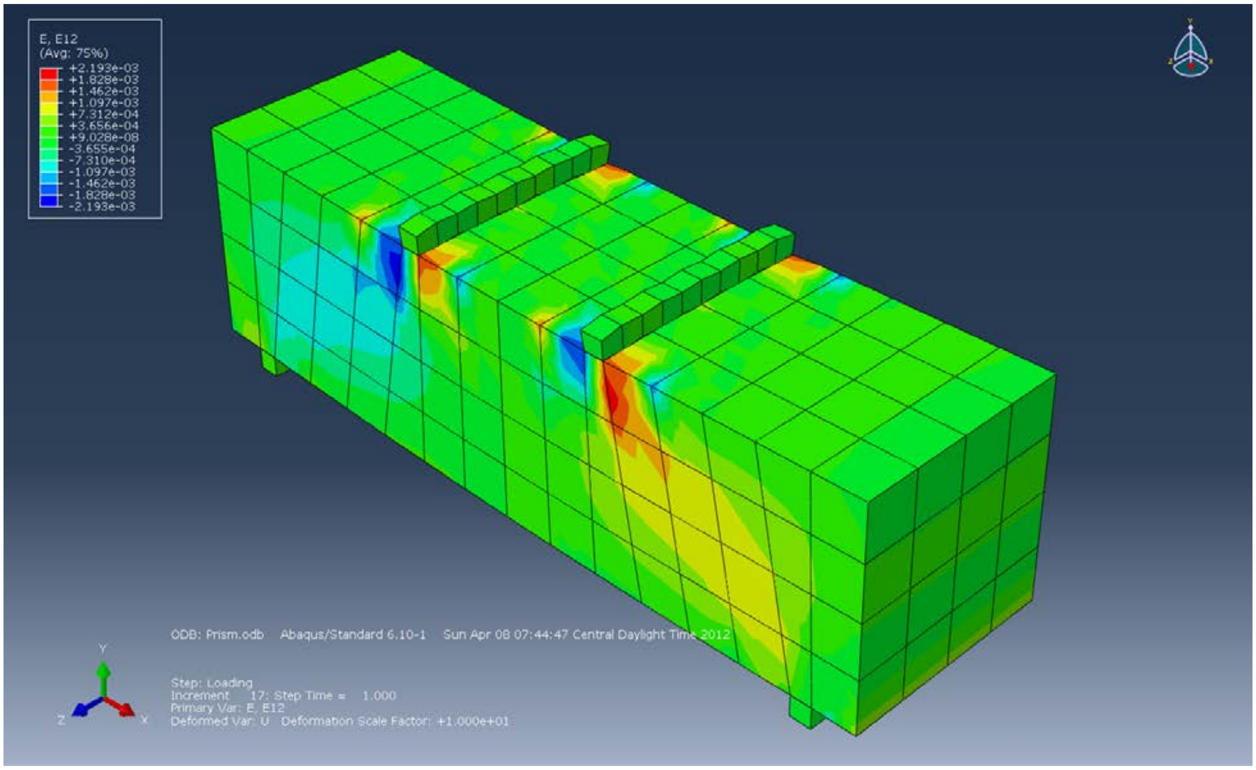

Figure B-177: Strain (E12) in the XY-Plane.

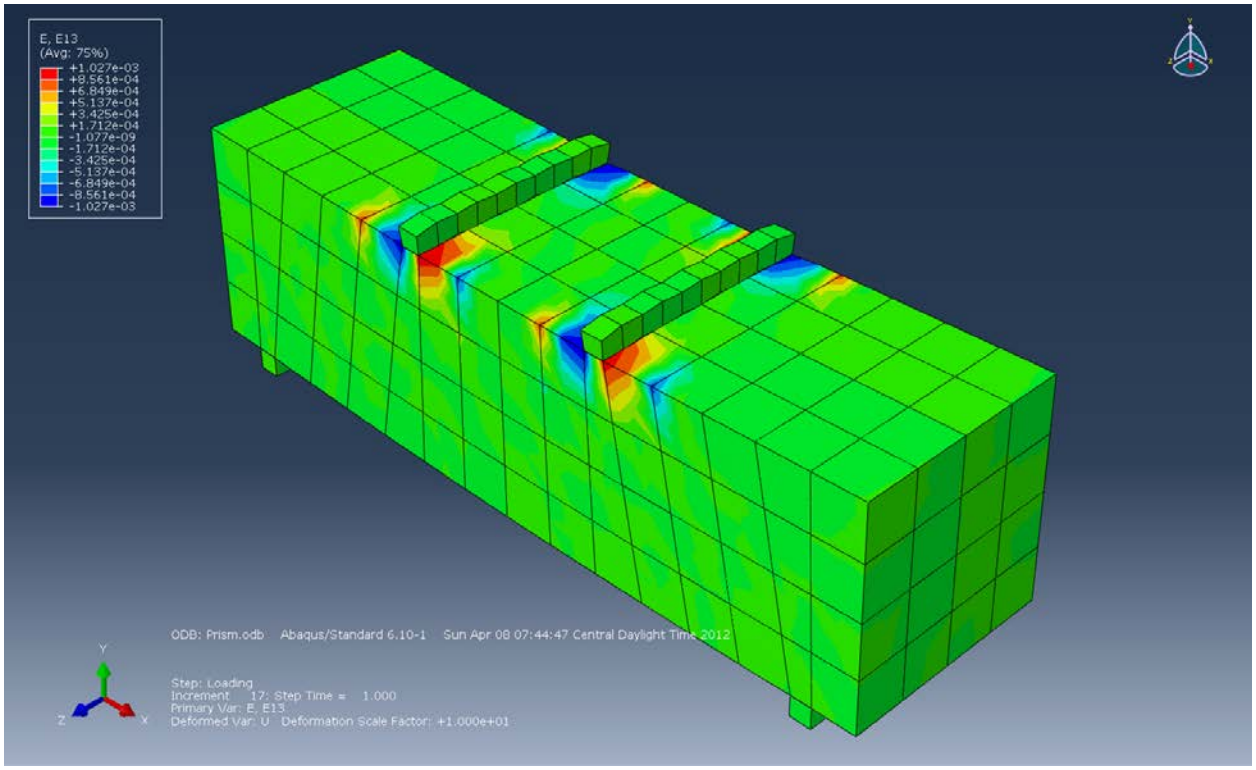

Figure B-178: Strain (E13) in the XZ-Plane.

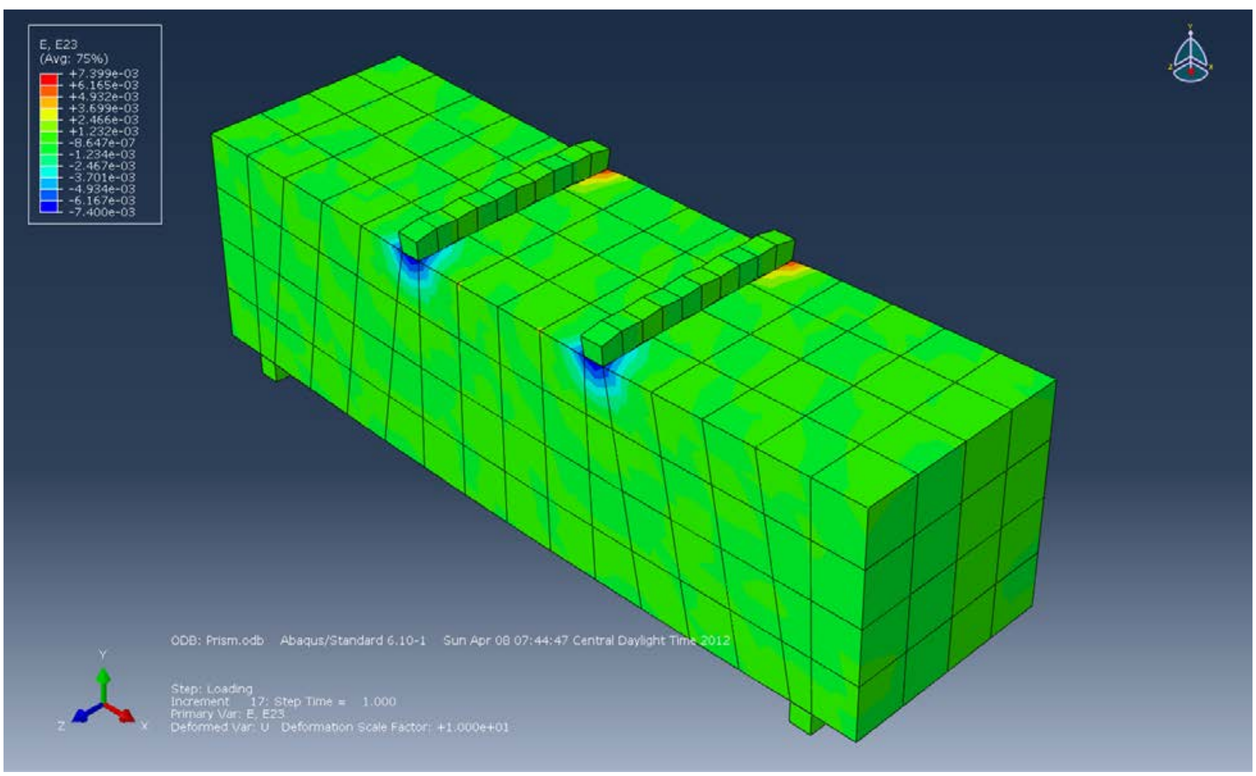

Figure B-179: Strain (E23) in the YZ-Plane.

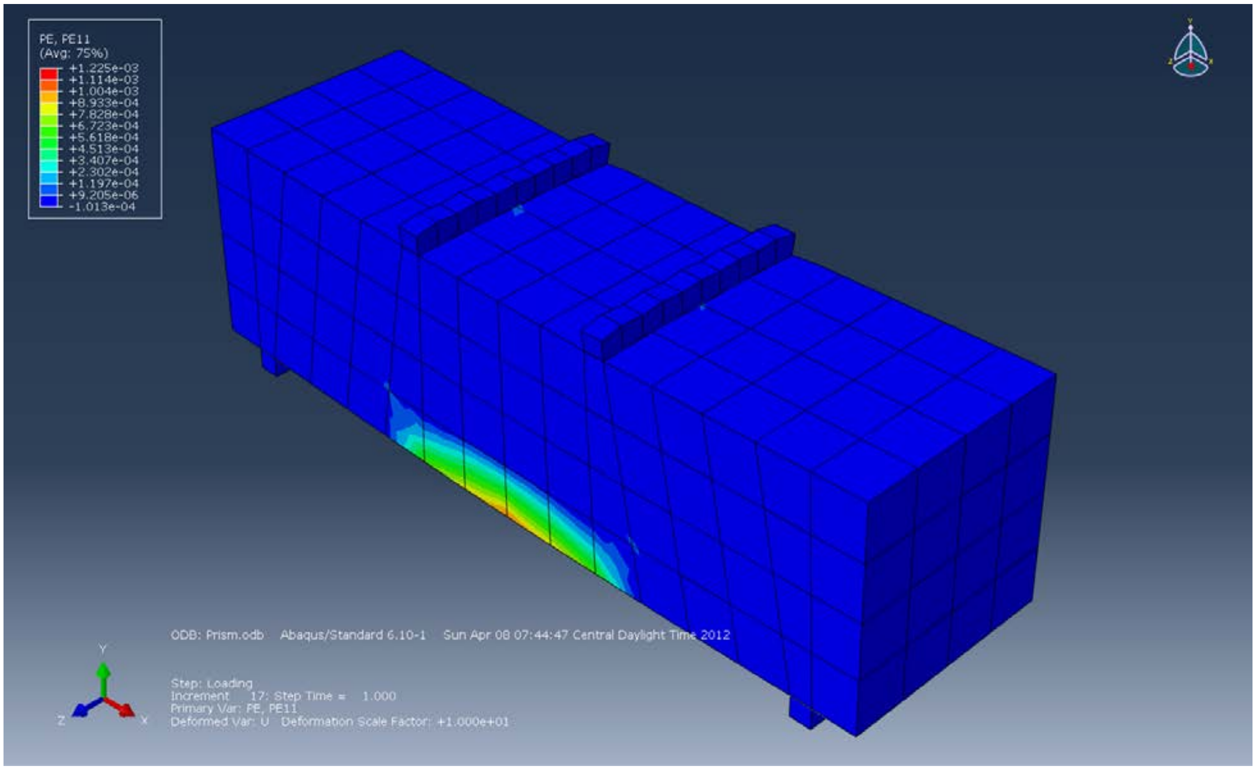

Figure B-180: Plastic Strain (PE11) in the X-axis.

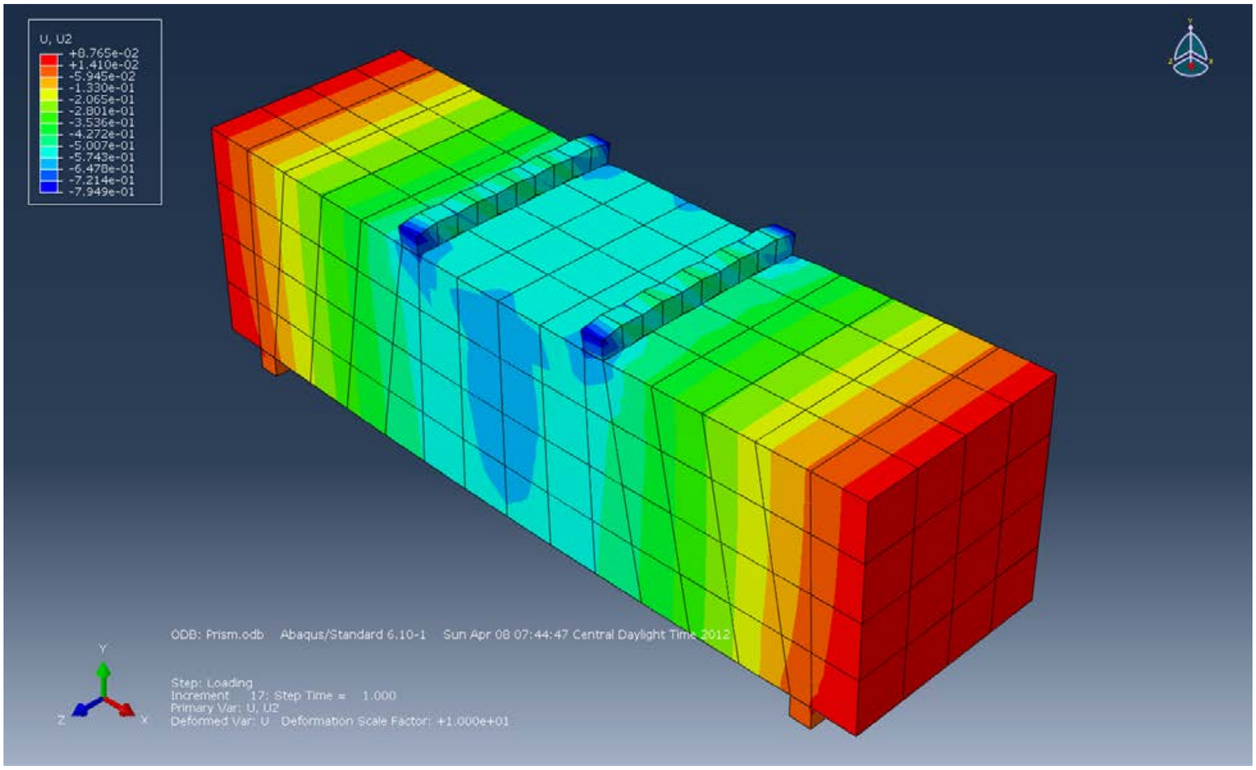

Figure B-181: Displacement (U2) in the Y-axis (mm).

Prisms with 1% Wheat Fibers:

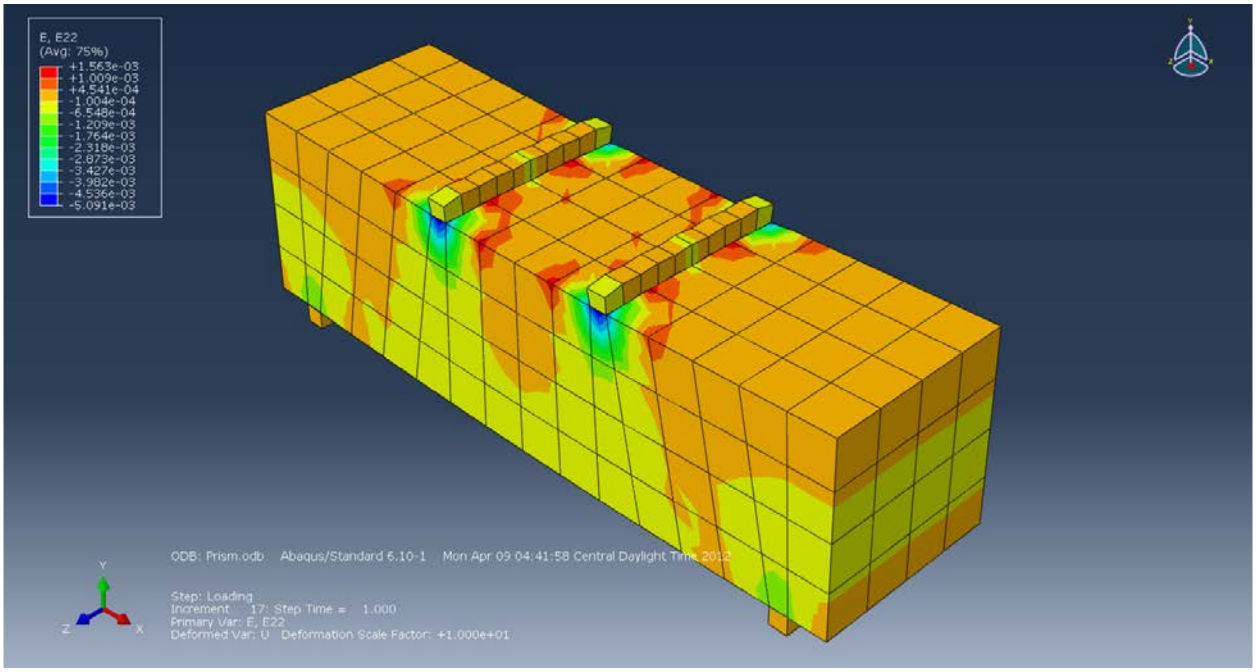

Figure B-182: Strain (E22) in the Y-axis.

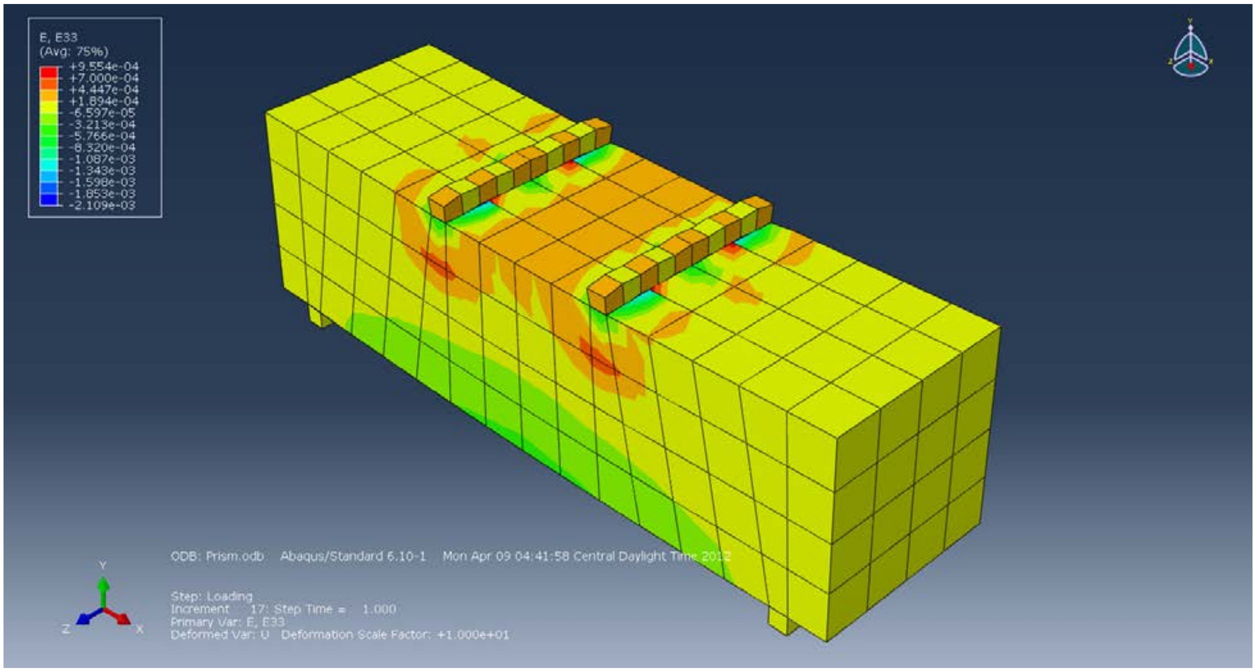

Figure B-183: Strain (E33) in the Z-axis.

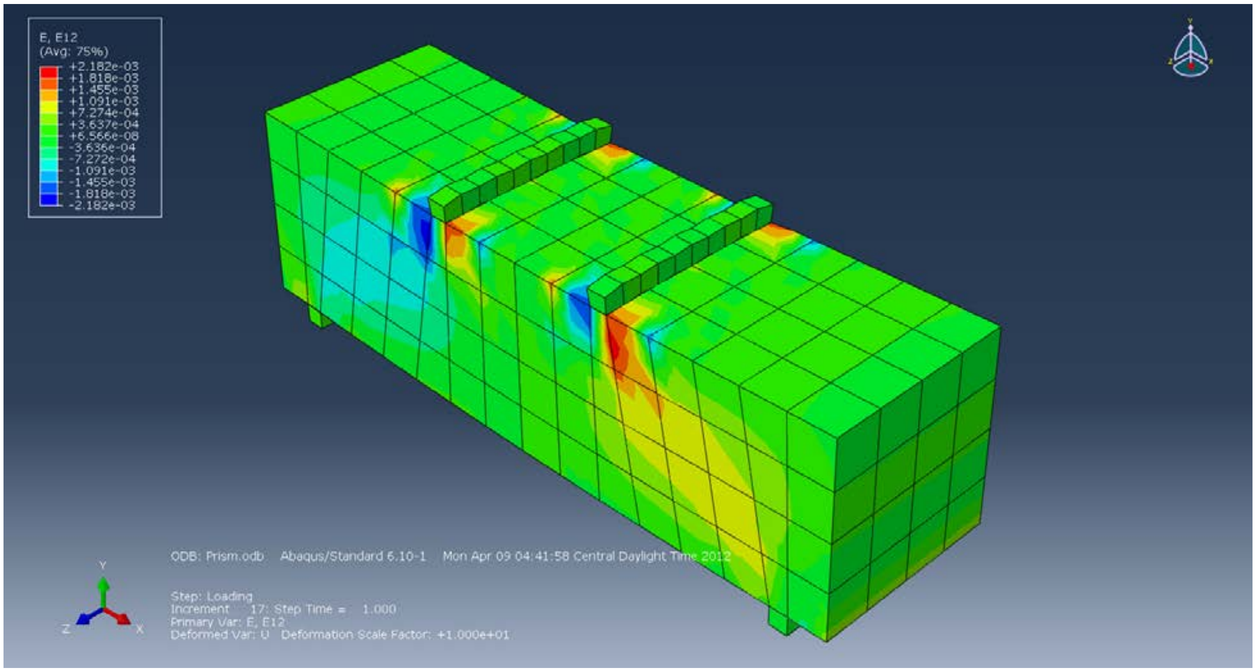

Figure B-184: Strain (E12) in the XY-Plane.

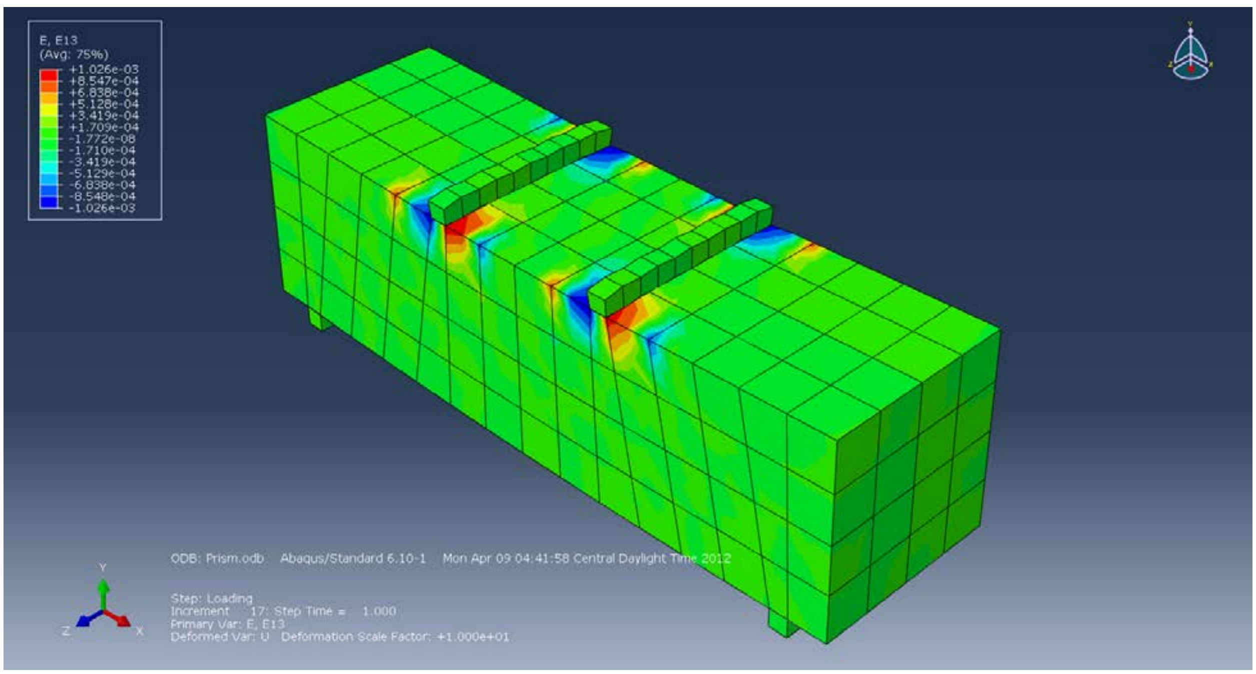

Figure B-185: Strain (E13) in the XZ-Plane.

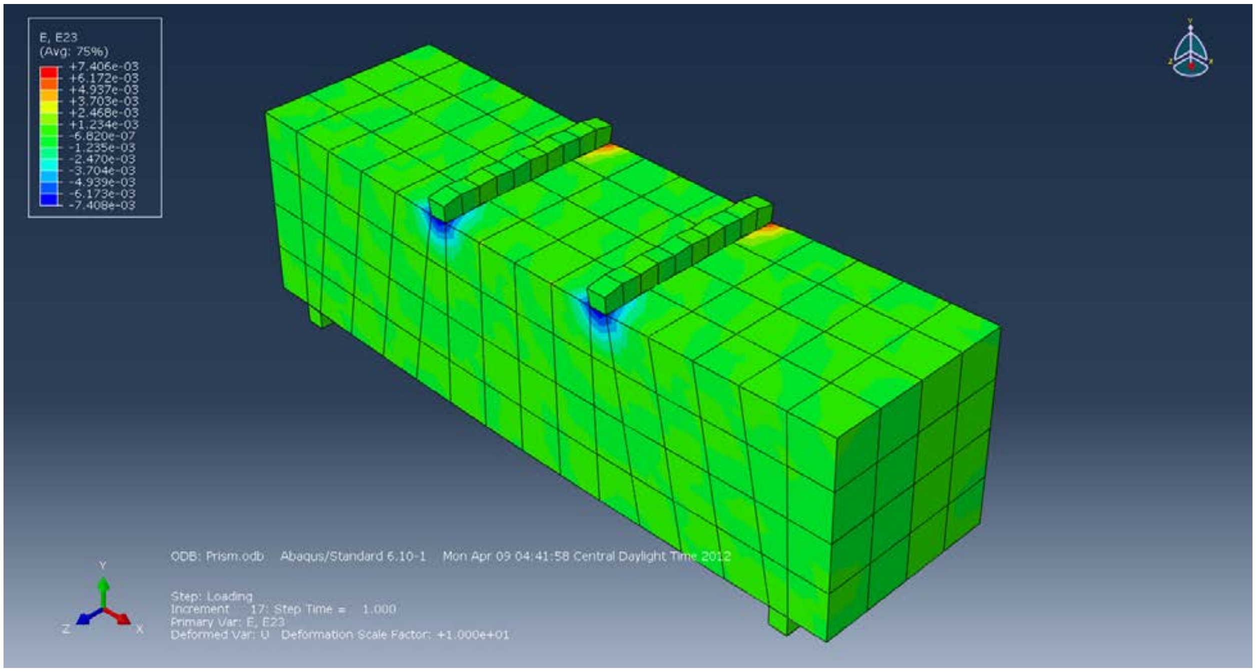

Figure B-186: Strain (E23) in the YZ-Plane.

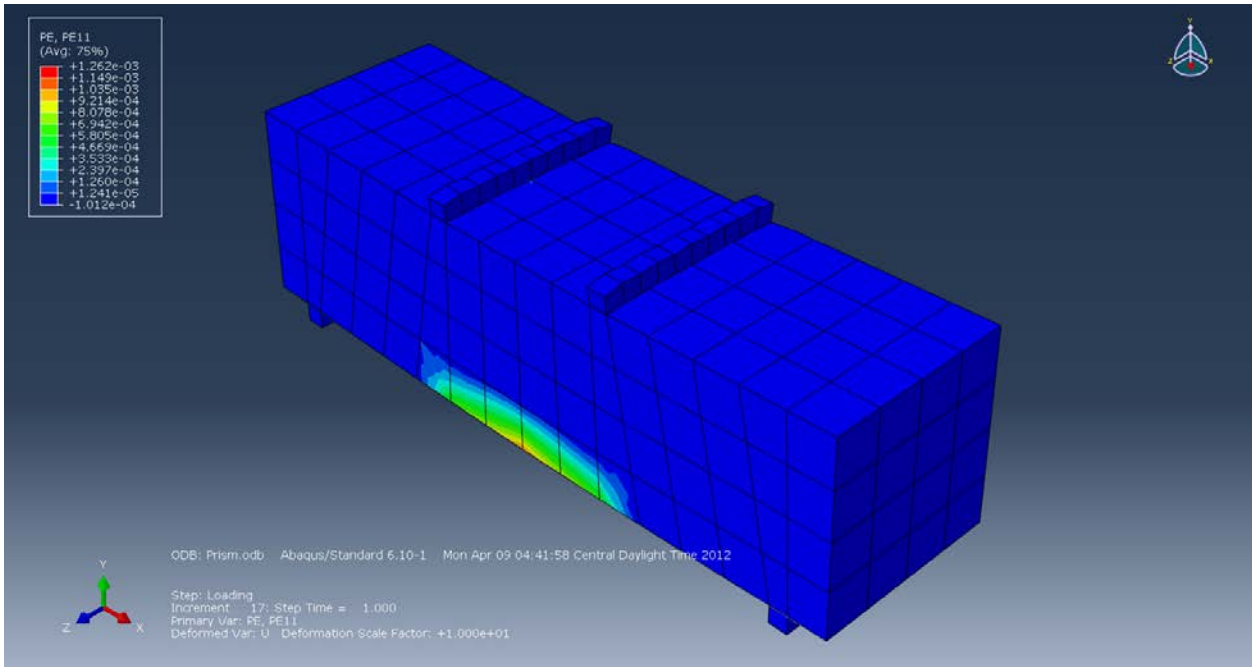

Figure B-187: Plastic Strain (PE11) in the X-axis.

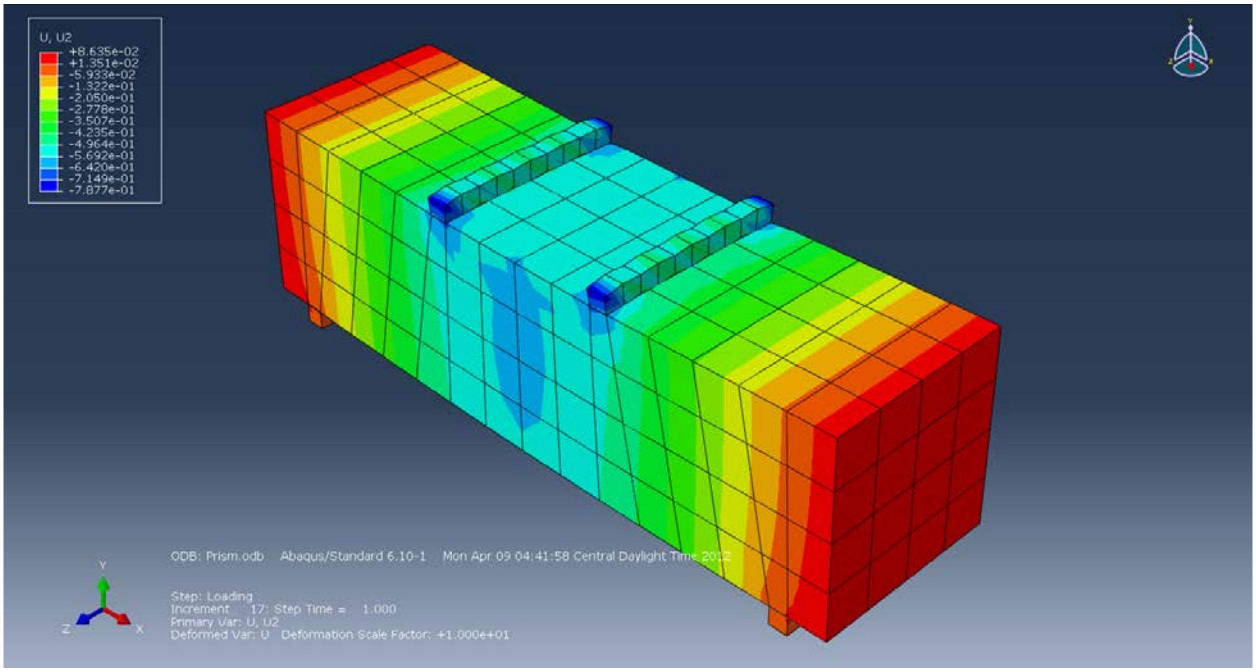

Figure B-188: Displacement (U2) in the Y-axis (mm).